frontiers | Research Topics

Neural control of immunity

Edited by
Maureen Ann Cox, Peder S. Olofsson and Michael D. Burton

Published in
Frontiers in Immunology

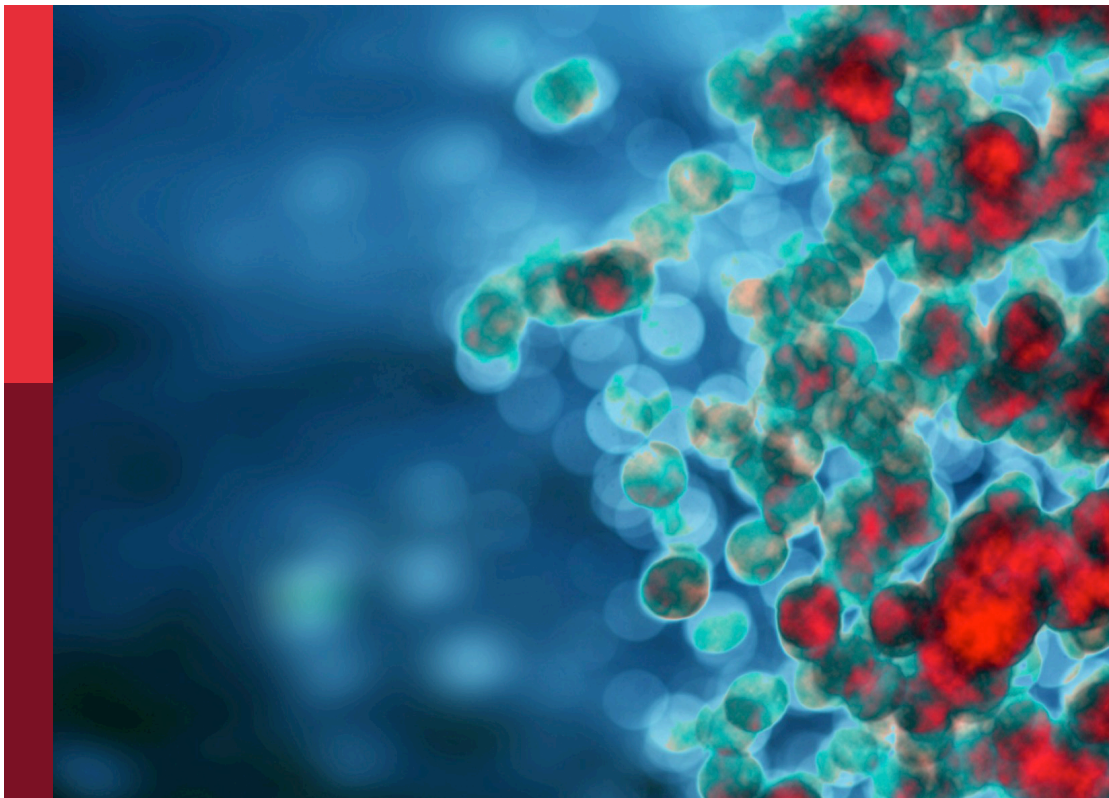

ISSN 1664-8714
ISBN 978-2-83251-797-0
DOI 10.3389/978-2-83251-797-0

About Frontiers

Frontiers is more than just an open access publisher of scholarly articles: it is a pioneering approach to the world of academia, radically improving the way scholarly research is managed. The grand vision of Frontiers is a world where all people have an equal opportunity to seek, share and generate knowledge. Frontiers provides immediate and permanent online open access to all its publications, but this alone is not enough to realize our grand goals.

Frontiers journal series

The Frontiers journal series is a multi-tier and interdisciplinary set of open-access, online journals, promising a paradigm shift from the current review, selection and dissemination processes in academic publishing. All Frontiers journals are driven by researchers for researchers; therefore, they constitute a service to the scholarly community. At the same time, the *Frontiers journal series* operates on a revolutionary invention, the tiered publishing system, initially addressing specific communities of scholars, and gradually climbing up to broader public understanding, thus serving the interests of the lay society, too.

Dedication to quality

Each Frontiers article is a landmark of the highest quality, thanks to genuinely collaborative interactions between authors and review editors, who include some of the world's best academicians. Research must be certified by peers before entering a stream of knowledge that may eventually reach the public - and shape society; therefore, Frontiers only applies the most rigorous and unbiased reviews. Frontiers revolutionizes research publishing by freely delivering the most outstanding research, evaluated with no bias from both the academic and social point of view. By applying the most advanced information technologies, Frontiers is catapulting scholarly publishing into a new generation.

What are Frontiers Research Topics?

Frontiers Research Topics are very popular trademarks of the *Frontiers journals series*: they are collections of at least ten articles, all centered on a particular subject. With their unique mix of varied contributions from Original Research to Review Articles, Frontiers Research Topics unify the most influential researchers, the latest key findings and historical advances in a hot research area.

Find out more on how to host your own Frontiers Research Topic or contribute to one as an author by contacting the Frontiers editorial office: frontiersin.org/about/contact

Neural control of immunity

Topic editors

Maureen Ann Cox — University of Oklahoma Health Sciences Center, United States
Peder S. Olofsson — Karolinska Institutet (KI), Sweden
Michael D. Burton — The University of Texas at Dallas, United Stateses

Citation

Cox, M. A., Olofsson, P. S., Burton, M. D., eds. (2023). *Neural control of immunity*. Lausanne: Frontiers Media SA. doi: 10.3389/978-2-83251-797-0

Table of contents

frontiers in Immunology

REVIEW
published: 29 October 2020
doi: 10.3389/fimmu.2020.576929

Neural Regulation of Interactions Between Group 2 Innate Lymphoid Cells and Pulmonary Immune Cells

Weiwei Chen[1,2], *Qiang Shu*[2] *and Jie Fan*[1,3,4]*

[1] Department of Surgery, University of Pittsburgh School of Medicine, Pittsburgh, PA, United States, [2] The Children's Hospital, Zhejiang University School of Medicine, National Clinical Research Center for Child Health, Hangzhou, China, [3] Research and Development, Veterans Affairs Pittsburgh Healthcare System, Pittsburgh, PA, United States, [4] McGowan Institute for Regenerative Medicine, University of Pittsburgh, Pittsburgh, PA, United States

Emerging evidence supports the involvement of nervous system in the regulation of immune responses. Group 2 innate lymphoid cells (ILC2), which function as a crucial bridge between innate and adaptive immunity, are present in large numbers in barrier tissues. Neuropeptides and neurotransmitters have been found to participate in the regulation of ILC2, adding a new dimension to neuroimmunity. However, a comprehensive and detailed overview of the mechanisms of neural regulation of ILC2, associated with previous findings and prospects for future research, is still lacking. In this review, we compile existing information that supports neurons as yet poorly understood regulators of ILC2 in the field of lung innate and adaptive immunity, focusing on neural regulation of the interaction between ILC2 and pulmonary immune cells.

Keywords: neuroimmunity, adaptive immunity, innate immunity, lung, group 2 innate lymphoid cells (ILC2)

OPEN ACCESS

Edited by:
Maureen Ann Cox, University of Oklahoma Health Sciences Center, United States

Reviewed by:
Chaofeng Han, Second Military Medical University, China
Cyril Seillet, Walter and Eliza Hall Institute of Medical Research, Australia

***Correspondence:**
Jie Fan
jif7@pitt.edu

Specialty section:
This article was submitted to Molecular Innate Immunity, a section of the journal Frontiers in Immunology

Received: *27 June 2020*
Accepted: *05 October 2020*
Published: *29 October 2020*

Citation:
Chen W, Shu Q and Fan J (2020) Neural Regulation of Interactions Between Group 2 Innate Lymphoid Cells and Pulmonary Immune Cells. Front. Immunol. 11:576929. doi: 10.3389/fimmu.2020.576929

INTRODUCTION

The past decade has witnessed an unprecedented interest in the neural modulation of immunity (1–4). The immune barrier consists of innate and adaptive components that adopt different strategies to perceive and respond to pathogen challenge. In the context of innate immunity, innate lymphoid cells (ILCs) have been demonstrated to be a crucial bridge between both immunity branches (5, 6).

ILCs are a heterogeneous family of lymphocytes that lack re-arranged antigen receptors present on B and T cells. In earlier studies, lymphoid tissue inducer (LTi) cells and natural killer (NK) cells were initially identified as the subgroups of the ILCs (7–10). In recent years, more subgroups of the ILCs were discovered and, based on the surface markers, cytokines, and transcription factors, categorized into three major types, ILC1, ILC2 and ILC3 (11, 12). These ILCs groups have distinct

Abbreviations: α7nAChR, α7 nicotinic acetylcholine receptor; Ach, Acetylcholine; AD, Atopic Dermatitis; Areg, Amphiregulin; CGRP, α-Calcitonin Gene-Related Peptide; CRTH2, Chemoattractant Receptor-homologous molecule expressed on Th2 cells; DCs, Dendritic Cells; PGD2, Prostaglandin D2; EGF, Epidermal Growth Factors; EGFR, EGF Receptor; HMGB1, High Mobility Group Box 1; ICOS, Inducible Costimulator; ILCs, Innate Lymphoid Cells; ILC2, Group 2 Innate Lymphoid Cells; KLRG1, Killer-cell Lectin Like Receptor G1; NMU, Neuromedin U; NMB, Neuromedin B; Nb, Nippostrongylus brasiliensis; PCTR1, Protectin Conjugates in Tissue Regeneration 1; PD-L1, Programmed Death-Ligand 1; PNECs, Pulmonary Neuroendocrine cells; PNS, Peripheral Nervous System; RAGE, Receptor for Advanced Glycation End products; RAMP1, Receptor Activity-Modifying Protein; TLRs, Toll-Like Receptors; Tregs, Regulatory T Cells; TSLP, Thymic Stromal Lymphopoietin; VIP, Vasoactive Intestinal Peptide.

phenotypic, developmental, and functional properties. They are the innate counterparts of T lymphocytes: ILC1, ILC2, and ILC3 mirror $CD4^+$ T helper (Th)1, Th2, and Th17 cells, respectively, based on cytokine secretion and transcription factor expression (11, 13, 14). ILC1 consists of conventional NK cells and ILC1s. T-bet, a T-box transcription factor, is indispensable for the differentiation and interferon-gamma (IFN-γ) secretion ability of ILC1. RORα and GATA3 are essential for the development of ILC2, which can be grouped into transient, circulating inflammatory ILC2 (iILC2) and tissue-resident natural ILC2 (nILC2) types (15, 16). ILC3 comprises the classical lymphoid inducer (LTi) cells and LTi-like ILC3 with or without natural cytotoxicity receptors (NCRs), all of which rely on the RORγt (transcription factor) for development and secrete IL-17 and/or IL-22. ILCs protect individuals against infectious agents, response to inflammatory stimuli, and orchestrate lymphoid organogenesis and tissue repair, at various tissues especially mucosal barriers (17–19).

Among all subsets, ILC2 are the center of numerous investigations. They are mainly localized at mucosal barriers, e.g. the small intestine, skin, and lung (19–21). ILC2 are a master regulator of immune and inflammatory responses, but their own regulatory mechanisms remain largely elusive.

ILC2 are activated by host-derived alarmins such as IL-25, IL-33, and thymic stromal lymphopoietin (TSLP), which are expressed during tissue injury (22–24). Once activation takes place, ILC2 release large quantities of cytokines such as IL-4, IL-5, IL-6, IL-9, IL-10, IL-13, IL-17, and amphiregulin (16, 25–28). Furthermore, ILC2 interact with other cells through surface-bound molecules, such as CD80/86, MHC class II, PD-L1, OX40L, and inducible costimulator ligand (ICOS-L), and participate in immune-regulatory functions (29–32). ILC2 play critical roles in the regulation of inflammation, allergic immunity, metabolic homeostasis, parasite rejection, and tissue repair. Dysregulation of ILC2 contributes to inflammatory responses, including allergen-induced lung inflammation (33, 34), airway hyperreactivity (35), and atopic dermatitis (36).

Currently, the nervous system is found to have complex dual functions to quickly stimulate or suppress immune cells to defend the body against various inflammatory responses. There are continuing advances in our knowledge of neural regulation of ILC2, these brilliant results provide a new dimension of immune regulation (37–47). Studies have shown that receptors for norepinephrine, acetylcholine (Ach), neuromedin U (NMU), neuromedin B (NMB), α-Calcitonin Gene-Related Peptide (CGRP), and other neurotransmitters are present on T cells, dendritic cells (DCs), macrophages, ILC2, and other immune cells (19, 37, 38, 44, 48–50), and pattern-recognition receptors (PRRs) and cytokine receptors are distributed on neurons (51–54). Interestingly, immune cells are also able to synthesize and secrete catecholamines, acetylcholine, CGRP, and other neurotransmitters (39, 48, 49, 55). Moreover, ILC subtypes express the nicotinic and muscarinic cholinergic receptor for Ach, β_2-adrenergic receptor (β_2AR) for epinephrine and norepinephrine, calcitonin receptor-like (CALCRL) for CGRP, neuromedin U receptor 1 (NMUR1) for NMU, neuromedin B receptor (NMBR) for NMB, and VPAC1/2 (vasoactive intestinal peptide receptor) for vasoactive intestinal peptide (VIP) (19, 39, 44, 50, 56). These findings suggest physical machinery for neuro-immune communications. Also, type I cytokines can also influence cells of the center nervous system (CNS) and mediate what is called "sickness behavior" (57, 58). In this review, we highlight existing information that describes neurons as novel regulators of ILC2 in the context of pulmonary innate and adaptive immunity.

MECHANISMS UNDERLYING ILC2 INTERACT WITH OTHER IMMUNE CELLS

ILC2 function both as initiator of adaptive immunity or as responder to signals produced by B and T cells. Using ILC2-targeted models, investigations have shown multiple mechanisms by which ILC2 regulate innate and adaptive immune system.

Many previous studies showed that "crosstalk" exist between T cells and ILC2 (**Figure 1**). For instance, ILC2 are the largest group of the cytokine-secreting leukocytes after ovalbumin or HDM treatment (59), and ILC2 activity is essential for the efficient differentiation of T_h2 cells (29, 60–63). In $Rag2^{-/-}$ mice, in which T cells and B cells are depleted due to *Rag* deficiency, the numbers of ILC2 also markedly decreased after helminth infection, indicating that T cells advance the survival of ILC2 (64). Epithelial cells derived cytokines and alarmins activate ILC2, which can be main producer of type 2 cytokines. Moreover, ILC2 can activate $CD4^+$T cells either in the priming phase or during the effector phase since they present major histocompatibility complex class II (MHCII) (65, 66). IL-33–activated ILC2 enhances DCs migration into cancer tissues *via* C-C motif chemokine ligand 5 (CCL5) and further improve $CD8^+$ T cell-mediated tumor immunity (67). Combination of anti-PD1 checkpoint blockade with rIL33 treatment collaborates to improve anti-tumor immunity by unleashing ILC2 activity (68). Activated ILC2 further facilitate the polarization of the anti-inflammatory M2 macrophages, which in turn stimulate Foxp3 regulatory T cells (Tregs) (69). Tregs are a subpopulation of T cells which modulate the adaptive immune responses through direct cell-cell interactions, as well as through the inhibitory functions of TGF-β and IL-10.

Through cytokines and interactions of ICOS with its ligand ICOS-L, ILC2 activate B cell to undergo isotype-switching, survival, and secrete IgG1 and IgE (64, 70, 71). IgE produced by B cells, together with type 2 cytokines released by T_h2 cells and ILC2, lead to further activation of smooth muscle contraction, mucus production, granulocyte effector cells, and, which in turn, result in the encapsulation or expulsion of inflammatory stimuli (72). B cell-derived IgE is an important effector of type 2 immunity, and the recognition of allergens by IgE on mast cells is responsible for induction of the cardinal features of classic allergic responses, including anaphylactic shock (70). ILC2-derived IL-5 is an important growth factor that contributes to B1 cell self-renewal (73, 74). ILC2 sorted from

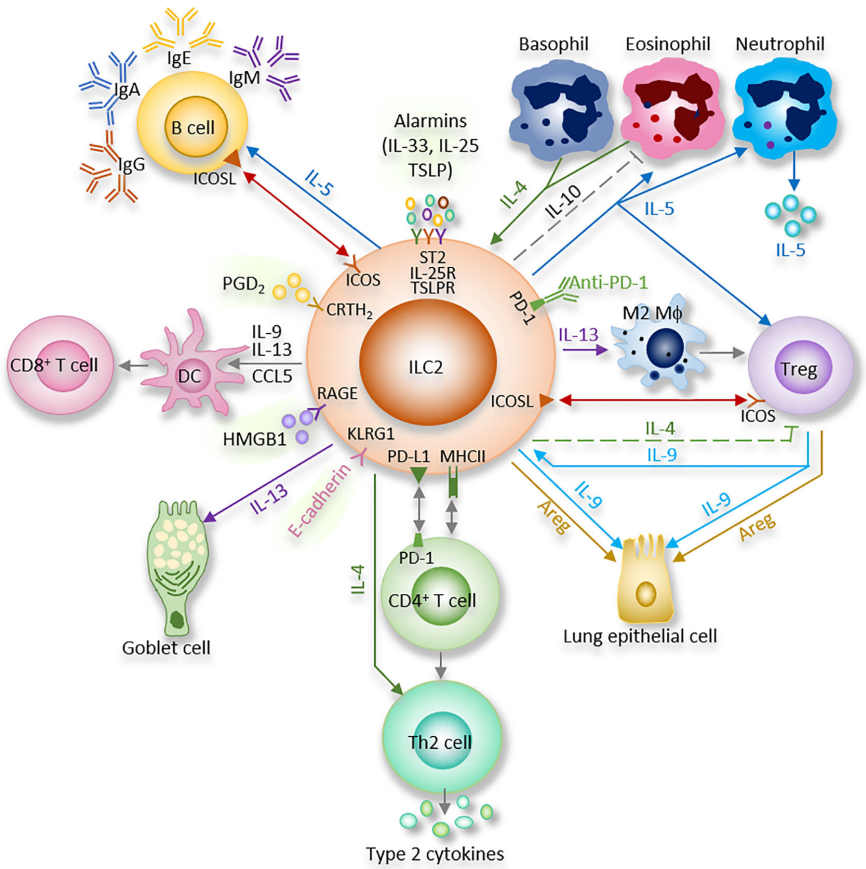

FIGURE 1 | ILC2 interacts with other immune and non-immune cells through a variety of cytokines and cell surface mediators. (1) After activation with alarmins, ILC2 produce type II cytokines and mediators; (2) ILC2 interact with T cells *via* MHCII, CCL5, PD-1/PD-L1, OX40/OX40L, CD86, CD80, IL-4, IL-5, and IL-13; (3) ILC2 activate B cells to undergo isotype-switching, survival, self-renewal, and secrete antibodies *via* ICOS/ICOS-L, IL-5; (4) ILC2 stimulate Tregs *via* IL-5, IL-9, ICOS/ICOS-L, while ILC2-released IL-4 suppress Tregs. Tregs are capable of inhibiting ILC2; (5) ILC2 prime macrophages into a type 2 immune cell phenotype *via* IL-13; (6) Epithelial cells derived alarmins activate ILC2. ILC2-released IL-9 and Areg protect lung endothelial cells. (7) ILC2 increase eosinophils *via* IL-5, HMGB1. ILC2 inhibit eosinophils *via* IL-10. Eosinophil- or basophil-released IL-4 activate ILC2; (8) ILC2 activate DCs *via* IL-9, IL-13, HMGB1.

mesenteric fat-associated lymphoid clusters are able to increase IgA production by peritoneal B cells *in vitro* (74).

Multiple indirect (cytokines) and direct (surface-bound molecules) mechanisms are involved in interactions between ILC2 and other cells as summarized below (**Figure 1**) (29, 75–77).

IL-4

IL-4 is expressed by activated ILC2 (78, 79). ILC2-released IL-4 participates in blocking the expansion of allergen-specific Tregs, thus involving in food allergy (80). ILC2-released IL-4 is also able to polarize T_H2 cells during helminth infection (81).

On the other hand, eosinophil- or basophil-released IL-4 is found to affect ILC2 by enhancing ILC2 lineage proliferation, function and stability (82, 83).

IL-5

ILC2 can coordinate adaptive and innate immune functions through IL-5. IL-5 is critical for B cell function (74) and eosinophil homeostasis (**Figure 1**) (84, 85). When splenic B cells co-culture with mesenteric ILC2, IL-5 from ILC2 plays a pivotal role in the release of IgA from B cells (74). Besides, peripheral ILC2 in pulmonary, peritoneal cavity, and spleen are able to elevate the secretion of IgA, IgE, IgG1, and IgM by B cells in *ex vivo* co-cultures (86). Furthermore, upon NP-Ficoll (primes for a high affinity IgM anti-NP response) treatment *in vivo*, IgM produced by B cells is selectively initiated by lung ILC2 in an IL-5–dependent pattern (86). IL-5–producing ILC2 are also essential for the Th2 and Th9 cytokine responses against Trichinella spiralis infection (87). In addition, lung $ICOS^+$ILC2 act a protective factor in a bleomycin model in an IL-5-dependent manner (88). Of note, the timing of IL-5 release by ILC2 seems important for the protective activity (88). Study showed that prostaglandin D_2 (PGD_2)-chemoattractant receptor-homologous molecule expressed on Th2 cells (CRTH2) signaling increases ILC2 and its production of IL-5, which promotes Tregs proliferation (89).

Our recent study discovered that high mobility group box 1 (HMGB1, a late mediator of sepsis) signals *via* receptor for

advanced glycation end products (RAGE) to increase lung ILC2 by enhancing ILC2 proliferation and suppressing ILC2 death. The activated ILC2 increase type 2 cytokines production and eosinophil infiltration in the lungs, both of which improve haemorrhagic shock-induced acute lung injury (85). Lung ILC2 activated by IL-33 secrete a large number of IL-5, which further up-regulate neutrophil and its IL-5 production (90).

IL-9

Price *et al*, reported in detail that ILC2 express IL-9 receptor (78). Using IL-9 reporter and subsequently IL-9 fate mapping mice, two studies delineated the autocrine signaling mechanism of IL-9 in ILC2 that enhances IL-13 and IL-5 release (**Figure 1**) (66, 91). In papain-induced pulmonary inflammation model, IL-9 was secreted for a short period by ILC2, then ILC2 changed to release IL-13 and IL-5. Furthermore, IL-33, but not IL-25, increased IL-9–producing ILC2 (91). Rauber *et al*, recently uncovered that IL-9 from ILC2 was necessary for Tregs activation and inflammation resolution in an arthritis model (92). HMGB1-activated ILC2 also secrete IL-9, which increase DCs (93). Moreover, our study discovered that ILC2-released IL-9 protects lung endothelial cells from pyroptosis by suppressing caspase-1 in a septic model (17).

IL-2 released by adaptive immune cells also play a crucial role in the IL-9 expression by ILC2, suggesting again the strong functional link between adaptive and innate lymphoid cells (94). Besides, IL-2 functions as a costimulator to ILC2 and promotes cell proliferation and survival by activating NF-κB pathway and gene transcription through p65 translocation (94). IL-9 and IL-2 work synergistically to direct ILC2 biology, and increased IL-9 production is related to an asthma-like phenotype in humans and mice highlighting the key role of these cytokines (95–98).

IL-13

IL-13 also mediates the interaction between ILC2 and immune and non-immune cells (**Figure 1**). During infection of helminth in mice, IL-13 released from ILC2 is more abundant than that from Th2 cells for restricting worm expulsion and immune response (23, 64, 78). IL-13 from ILC2 can induce goblet cell hyperplasia as well as mucus secretion (99). Yet the precise mechanism of IL-13 receptors on pulmonary cells at different states remains to be fully elucidated.

Pulmonary IL-13$^+$ ILC2 and CD4$^+$ T cells cooperate to suppress Nippostrongylus brasiliensis (*Nb*) infection. Immune-damaged larvae have a severe morphological defect that is due to the increase of CD4$^+$ T cells and IL-13$^+$ ILC2, as well as the activation of M2 macrophages (100). Besides, alveolar macrophages can be primed by ILC2-derived IL-13 into a type 2 immune cell phenotype (101). DCs are stimulated by IL-13 to convert to a type 2 chemokine-secreting phenotype. ILC2-derived IL-13 is also able to mediate DCs migration from the lungs to the LNs, thus impacting the differentiation of T_H2 cell (102). In addition, the number of IL-13$^+$ ILC2 was reported to be markedly upregulated in patients with uncontrolled asthma, and it was significantly decreased when these patients had their symptoms controlled by treatment, suggesting an important role for ILC2-derived IL-13 in asthma (103). In conclusion, ILC2-derived IL-13 can initiate and affect innate and adaptive type 2 immune responses.

Amphiregulin (Areg)

Areg is a member of the epidermal growth factors (EGF) family and acts *via* the EGF receptor (EGFR) (104). Both hematopoietic and non-hematopoietic cells in the lung present EGFR (105). ILC2 are a major cellular producer of Areg after activation with IL-33. ILC2-derived Areg is a critical component of effective pulmonary wound healing during influenza infection and restoring epithelial integrity and lung function (20). The initiation of mucus secretion and wound healing can prevent or ameliorate some respiratory diseases, although enhanced and excessive mucus may play a detrimental role in diseases, such as asthma (106, 107). Pulmonary Tregs are also capable of producing Areg without TCR signaling (**Figure 1**) (108). Thus, innate Areg released by ILC2 and Tregs is of high importance to restore tissue homeostasis and wound healing after pulmonary infection.

ICOS/ICOS-Ligand Interaction

Studies on helminth expulsion revealed ILC2-Tregs crosstalk (109). Tregs and ILC2 colocalize to similar regions within the lung tissues and visceral adipose tissue under homeostatic and inflammatory conditions (**Figure 1**) (31). Of note, ICOS$^+$ Tregs and ICOS-L$^+$ ILC2 were reported to accumulate in tissues after *Nb* infection or IL-33 administration, while Tregs accumulation in ICOS-L knock-out mice or after administration with neutralizing monoclonal antibody against ICOS-L was reduced, indicating that ICOS-L$^+$ ILC2 could improve Tregs expansion, thus establishing a pathway for Tregs to cooperate with ILC2 (31). On the other hand, Tregs are capable of inhibiting ILC2 to restrict allergic airway inflammation (110). Besides, ICOS/ICOS-L interaction on ILC2 affects STAT5 signaling, activating ILC2 function and proliferation in an allergic model (111).

PD-1/PD-L1 Interaction

ILC2 constitutively express the checkpoint inhibitor molecule programmed death-ligand 1 (PD-L1), which has been discovered to activate CD4$^+$ Th2 cell responses during type 2 pulmonary responses (**Figure 1**) (30). Conditional knockout of PD-L1 on ILC2 disrupted cytokine production and early Th2 polarization, resulting in delayed worm expulsion during infection with the gastrointestinal helminth *Nb* (30). Nevertheless, ILC2 can also express PD-1, which was reported to be upregulated on activated ILC2, and depletion of these PD-1$^+$ ILC2 resolves papain-induced lung inflammation (112).

E-Cadherin/KLRG1 Interaction

E-cadherin, a cell adhesion molecule, interacts with the mature ILC2 marker, killer-cell lectin like receptor G1 (KLRG1). The finding that E-cadherin-KLRG1 ligation on human ILC2 reveals a significant decrease in GATA3 expression and type 2 cytokine (such as IL-5 and IL-13) release and the discovery that E-cadherin expression is suppressed in keratinocytes propose that inhibited E-cadherin expression may activate ILC2, promoting atopic dermatitis (AD) immunopathogenesis (28).

Other Interactions

OX40 ligand (OX40L) expression on ILC2 can be enhanced by IL-33. OX40-OX40L ligation has been reported to increase Th2 cell survival and number (32, 113), thus promoting adaptive immunity (75).

A molecularly distinct subset of lung ILC2 can secrete IL-10 and suppress some pro-inflammatory genes. IL-2, IL-4, IL-27, IL-10, and NMU stimulate IL-10 production from ILC2 and are associated with decreased eosinophil recruitment to the lung, indicating that ILC2 have anti-inflammatory functions similar to Tregs (**Figures 1** and **3**) (26, 114).

The expression of CD86, CD80, and MHCII by mouse ILC2 is also involved in ILC2 interactions with $CD4^+$ T cells;

$MHCII^+$ ILC2 can drive the differentiation of naive $CD4^+$ T cells into T_h2 *in vitro*, whereas MHCII-deficient ILC2 upregulate T_h2 cell-driven helminth expulsion *in vivo* (29, 75).

PULMONARY NERVOUS SYSTEM AND ITS REGULATORY FUNCTION

Lung is densely innervated by peripheral nervous system (PNS), which is divided into motor and somatosensory nervous systems (**Figure 2**).

Motor Nervous System

The motor nervous system consists of the autonomic (sympathetic, parasympathetic, and enteric) and somatic branches.

Autonomic nervous system serves to regulate involuntary functions. Sympathetic branch comes from the upper six thoracic spinal cord segments; the synapse together with the sympathetic ganglia, and postganglionic fibers then innervate the airways. The sympathetic nervous system participates in the body response to stress and regulates bronchodilation and the production of mucous.

The cholinergic parasympathetic branch comes from the vagal nuclei of the medulla; the superior and recurrent laryngeal vagal nerves synapse at the parasympathetic ganglia to innervate the lung (115). The parasympathetic branch is mainly responsible for keeping homeostasis (116). It regulates bronchoconstriction, carbon dioxide and oxygen levels, as well as neural reflexes including coughing.

Somatosensory Nervous System

The somatosensory nervous system delivers sensory stimuli, such as proprioception, touch, and pain. Somatosensory neurons are further divided into pruriceptors and nociceptors responsible for sensing itch-inducing or noxious stimuli, respectively. These neurons are important because their activation is closely related to inflammation and immunity (**Figure 2**).

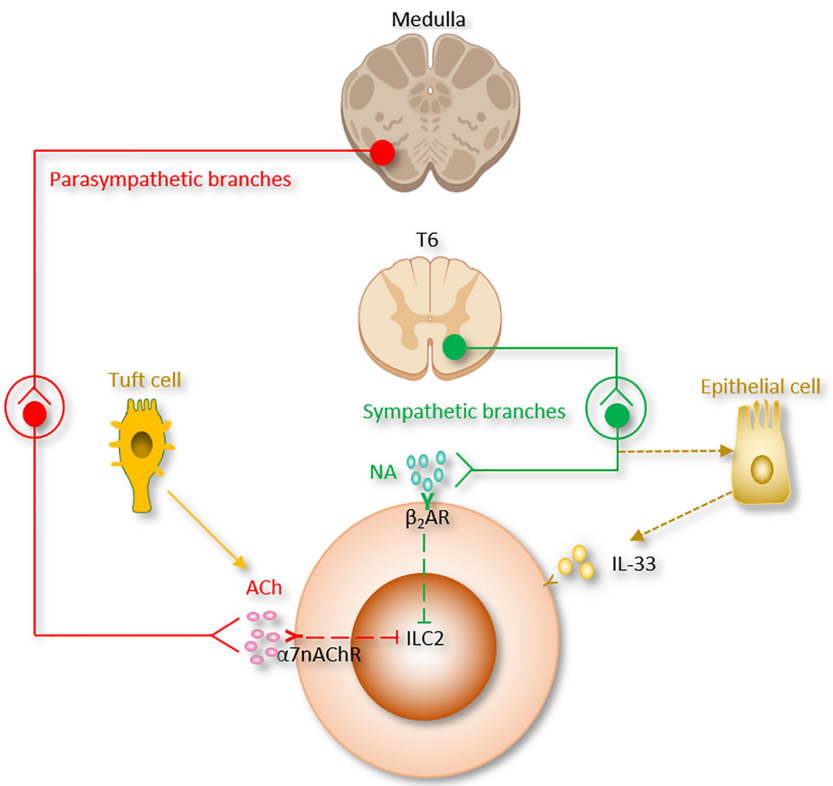

FIGURE 2 | The autonomic nervous system regulation of ILC2 function. Ach, Acetylcholine; α7nAChR, α7 nicotinic acetylcholine receptor; β_2AR, β_2-adrenergic receptor; NA, Norepinephrine.

All opponents of the PNS play a critical role in orchestrating immunity, inflammation, and tissue repair at host barrier tissues in response to stimuli and stressors. Primary evidence that neurotransmitters may regulate immune responses was that their release from nerves could lead to signaling through the surface receptors of lymphocyte cell (117). Leukocytes have receptors for the neurotransmitters such as dopamine, serotonin and glutamate (117), and also produce neurotransmitters that work as paracrine or autocrine signals (118). The neuronal reflex senses peripheral inflammation and coordinates the host response to injury and/or infection, regulating events within the initiation of inflammation (48, 119). Lung is heavily populated by resident immune cells, such as macrophages, DCs, γδ T cells mast cells and ILCs. It allows fast, integrated reactions to pathogens and noxious stimuli (120).

Sympathetic Nervous System

Sympathetic nervous system helps the center nervous system to control innate immune responses between antiviral and pro-inflammatory actions (**Figure 2**) (121, 122).

The nerves of the sympathetic nervous system distribute the neurotransmitter catecholamines into tissue microenvironments in which immune response gene transcription occurs, including all lymphoid organs, most musculoskeletal structures and visceral organs, and the vasculature and perivascular tissues (123).

Recent reports have revealed a sympathetic nervous system-mediated steering of innate immune response programs, which include enhanced transcription of pro-inflammatory cytokine genes (such as *Il6*, *tnf*, and *Il1β*) (121, 124) and inhibition of type I IFN-mediated antiviral responses (122).

Stimulation of the sympathetic nervous system has also been shown to change the production and trafficking of innate immune cells, for instance, through the upregulation of myelopoiesis and the mobilization of monocytes, splenic neutrophils, natural killer cells, and haematopoietic stem cells (123). A current study showed that the sympathetic nervous system stimulates IL-33 and then ILC2 in adipose tissue. Cold exposure stimulates IL-33 expression, ILC2 and eosinophils in adipose tissue. Furthermore, sympathetic denervation induced by 6-hydroxydopamine (6-OHDA) cancels this effect (125).

Catecholamines are monoamine neurotransmitters which are mainly released by the postganglionic fibers of the sympathetic nervous system and the chromaffin cells of the adrenal medulla. Included among catecholamines are dopamine, epinephrine (adrenaline), and norepinephrine (noradrenaline) (**Table 1** and **Figure 2**). Release of the epinephrine and norepinephrine from the adrenal glands and adrenergic nerves is part of the fight-or-flight response.

Catecholamines exert their effects *via* two classes of adrenergic receptors, α and β. Both groups could be functionally divided into subgroups (α_1 and α_2; β_1, β_2, and β_3).

Norepinephrine regulates leukocyte gene expression through β-adrenergic receptors (123). β-adrenergic receptor is expressed on most immune cells, such as B cells, T cells, and other innate cells (40, 126–128). It was initially thought to regulate adaptive immune responses by suppressing the expression of TH1-type genes, such as *Il12β* and *Ifnγ*, and activating the transcription of TH2-type cytokine genes, i.e. *Il4* and *Il5* (129–131).

Interestingly, β_2AR has an inhibitory effect on innate immune responses. β_2-agonists suppress cardiodepressant and inflammatory factors, including HMGB1 and TNF. Recently, ILC2 from the lung and the gut-related tissues (small intestinal lamina propria, colonic lamina propria and mesenteric lymph nodes) were found to express β_2AR. ILC2 were also shown to colocalize with adrenergic neurons in the mouse intestine (40).

β_2AR deficiency led to enhanced ILC2 proliferation and subsequent type 2 cytokine production in lung and intestinal tissues after infection with *Nb*. Lung eosinophilia was observed following enhanced IL-5 production from ILC2 in β_2AR-deficient mice. On the other aspect, β_2AR agonist administration disrupted ILC2 responses and suppressed inflammation *in vivo*. By using conditional β_2AR-deficient mice, or by transferring ILC2 progenitors from wild-type mice or β_2AR-deficient mice into ILC-deficient mice, the group generated ILC2-specific β_2AR-deficient mice and ensured that the β_2AR negatively controls ILC2 and type 2 inflammation (40). This study provides another evidence of neuronal regulatory circuit that regulates ILC2-dependent type 2 inflammation. β_2AR-agonists are the most effective medications for the treatment of asthma. β_2AR-mediated ILC2 regulation could be one of the pathways of β_2AR-agonists effect in asthma (33, 38, 44, 110, 132, 133). On the other hand, β_2AR is the first adrenergic receptor documented to participate in the "anti-inflammatory reflex" of the parasympathetic system which will be discussed in the next section (**Table 1** and **Figure 2**).

Parasympathetic Nervous System

Parasympathetic and sympathetic systems are usually considered to work in opposition to maintain physiological homeostasis. While current literatures suggested that both branches work together to restrain systemic inflammation in life-threatening illnesses, including arthritis, inflammatory bowel disease, sepsis and endotoxemia (46, 48, 134–138).

Nerve fibers of the parasympathetic nervous system arise from three primary areas: cranial nerves (facial nerve, oculomotor nerve, and glossopharyngeal nerve), vagus nerve, and pelvic splanchnic nerves (three spinal nerves in the sacrum, S2-4).

The parasympathetic nervous system mainly utilizes acetylcholine (ACh) as its neurotransmitter (**Table 1** and **Figure 2**). Tuft cells, capable of secreting the ILC2 activator IL-25, also secrete Ach (139, 140). The ACh has two kinds of receptors, the nicotinic and muscarinic cholinergic receptors. α7 nicotinic acetylcholine receptor (α7nAChR), one of the nicotinic acetylcholine receptors, is expressed by ILC2 at steady state, and this expression is further increased following alarmin-induced activation such as IL-33 (44). The α7nAChR is also present on B cells (141), T cells (142, 143), macrophages (144) and ILC3 (41).

$\alpha7nAChR^{-/-}$ mice were more susceptible to severe lung injury and higher mortality than $\alpha7nAChR^{+/+}$ mice. Increased $\alpha7nAChR^{+}$ alveolar neutrophils and macrophages were observed in the mice injured lungs. The immunomodulatory

TABLE 1 | Sources, receptors on ILC2, and relationships with ILC2 of several neurotransmitters.

Neurotransmitters		Sources		Relevant receptors on ILC2	Relationships with ILC2
Catecholamines	Epinephrine (Adrenaline) Norepinephrine	Autonomic (Involuntary)	Sympathetic nervous system;	β_2AR	• Adrenergic neurons colocalize with ILC2; • β_2AR agonist administration impairs ILC2 responses and reduces inflammation; • Mediator of the "anti-inflammatory reflex";
Acetylcholine			Parasympathetic nervous system; Also released by tuft cells;	α7nAChR	• α7nAChR agonist administration inhibits the proliferation of ILC2, but does not alter the death of ILC2; • α7nAChR agonist administration inhibits type 2 cytokine production from ILC2 and ameliorates ILC2-mediated lung inflammation; • Mediator of the "anti-inflammatory reflex";
CGRP		Somatic (Voluntary, afferent and efferent neurons)	Sensory neurons; Also released by PNECs and ILC2;	RAMP1 and CALCRL	• CGRP-secreting PNECs locate in close proximity to ILC2 near airway branch points; • ILC2 express both CGRP and its receptor CGRPR; • CGRP stimulates ILC2 proliferation; • CGRP suppresses KLRG1$^+$ILC2s proliferation but promotes IL-5 expression; • CGRP alone does not increase cytokine production from ILC2, a combination of (NMU + IL-33 + CGRP) stimulates IL-5 but limits IL-13 production and ILC2 proliferation;
VIP			Sensory neurons;	VPAC1 and VPAC2	• VIP stimulates IL-5 from ILC2, ILC2-derived IL-5 activates nociceptors on sensory neurons and upregulates the release of VIP, which in return acts *via* VPAC2 and leads ILC2 and subsequently T cells to release more IL-5 and thereby forming a type 2 inflammatory positive feedback loop mainly based on the neuro-immune axis;
NMU			Sensory neurons (released by cholinergic sensory neurons originating from DRG); Also secreted by some APCs (including monocytes, B cells, and dendritic cells);	NMUR1	• NMU-expressing neurons locate in close vicinity to ILC2; • NMU elevates ILC2 proliferation; • Stimulation of ILC2 with NMU leads to strong and immediate production of tissue protection and innate inflammatory cytokines in a NMUR1-dependent manner; • NMU increases IL-10 production in activated ILC2, IL-10 further stimulates IL-10 production in ILC2 through a positive feedback loop; • ILC2 activated by NMU increase the number of lung eosinophils and mast cells; • IL-13 enhance NMU production in DRG neurons, thus indicating the existence of a reciprocal neuron–ILC2 regulatory loop *via* ILC2-derived IL-13 and neuronal NMU expression;
NMB		CNS (olfactory bulb, dentate gyrus, amygdala, basal ganglia, brainstem); PNS (Gastrointestinal tract; Trigeminal and dorsal root ganglia (DRG));		NMBR	• Treatment with NMB inhibits ILC2 responses, eosinophilia and mucus production; • Basophils prime ILC2 for NMB-mediated inhibition;

cholinergic α7nAChR pathway of alveolar neutrophils and macrophages alleviated E. coli- and LPS-induced acute lung injury by inhibiting transalveolar neutrophil migration and chemokine production.

It was reported that the expression of HMGB1 protein was suppressed by α7nAChR agonist nicotine and the survival of post-sepsis acute lung injury was improved (145). In addition, administration of α7nAChR agonist inhibits type 2 cytokine production from ILC2 and ameliorates ILC2-mediated lung inflammation induced *via* IL-33 stimulation or Alternaria alternata inhalation. Mechanistically, α7nAChR agonist is reported to inhibit cellular markers for proliferation in ILC2 (Ki67, NF-κB and GATA3 signaling pathways) (27, 44, 146, 147) (**Table 1**). These findings indicate that α7nAChR may be a potential therapeutic target for acute lung injury (120).

On the other aspect, Bcl-2, an anti-apoptotic factor of ILC2, was unchanged by α7nAChR agonist treatment. These studies indicate that parasympathetic nervous system modulates ILC2 proliferation, but not death. The suppressive effects of α7nAChR on ILC2 may serve as the mechanism underlying the observed reduced pulmonary allergic inflammation induced by nicotine treatment (148). Moreover, in cancer immunity, nicotine treatment stimulates tumor growth by suppressing apoptosis and promoting cell proliferation (149–152).

Anti-Inflammatory Reflex

The vagus nerve is the main parasympathetic nerve connecting between the central nervous system and peripheral organs (128, 153). Pharmacological or electrical stimulation of the vagus nerve can restrain the systemic inflammation response, organ damage, and mortality in different experimental hemorrhage and resuscitation (43), pancreatitis (154), ischemia and reperfusion (43, 155, 156), colitis (157), endotoxemia (42, 155, 158, 159) and sepsis (145, 160).

Mechanically, the motor and sensory vagus nerve form a complex neural reflex circuit termed the "anti-inflammatory

reflex" which control spleen cytokine production through splenic nerve (42, 161–166). ACh released by the vagus nerve in the celiac mesenteric ganglia stimulates postsynaptic α7nAChR of splenic nerve (46). The adrenergic splenic nerve release norepinephrine to activate a discrete subset of spleen lymphocytes *via* β_2AR. Activated lymphocytes then release Ach (48, 167). Lymphocyte-derived Ach downregulates macrophage cytokine release, and switches them toward a tissue-protective, M2 anti-inflammatory phenotype. α7nAChR mediates Ach-induced signal transduction in macrophages and monocytes (144). α7nAChR inhibits the inflammasome activity (168), enhances the JAK2-STAT3 pathway (169), stabilizes mitochondrial membranes, and suppresses the nuclear translocation of NF-κB (119, 145, 168–170).

The eventual influence of inflammatory reflex on the spleen is the inhibition of cytokine release by spleen macrophages, which produce over 90% of the IL-1 and TNF during acute endotoxemia (159, 167). The anti-inflammatory reflex is a special instance of a functional network between the efferent parasympathetic vagus nerve, the splenic nerve (termed sympathetic) and T cells relaying neural signals. In depicting this cooperation, the use of the classical sympathetic-versus-parasympathetic neuronal designation should be modified.

Indirect studies suggested that anti-inflammatory reflex is involved in the regulation of ILC. Dalli *et al*, reported that dissection of the right vagus downregulated the number of peritoneal ILC3 and changed peritoneal macrophage responses. Right vagotomy led to decreased peritoneal levels of pro-resolving mediators, which include the protective immunoresolvent protectin conjugates in tissue regeneration 1 (PCTR1), as well as increased inflammation-initiating eicosanoids. Ach restored the PCTR1 production from ILC3. Treatment of PCTR1 or ILC3 repaired tissue and ameliorated *E. coli* infections in vagotomized mice (41). Another group studied the regulation of ILC2 using coding α7nAChR (Chrna7) knockout mice, pulmonary C fibre (PCF, which releases ACh and neuropeptides) degeneration mice, and vagotomized mice. Knockout of Chrna7 enhanced resident ILC2s and trafficking iILC2s in the lung, worsened allergic inflammation. However, PCF degeneration and vagotomy significantly reduced these two types of ILC2 and attenuated asthma responses (171). Although there is no direct evidence suggests that "anti-inflammatory reflex" regulates ILC2, it is promising to investigate since the number of ILC2 is significantly increased in spleen during inflammation or infection (172).

In sum, parasympathetic nervous system participates in the pathogenesis of various diseases, with a different role in each disease.

Sensory Neurons

The lung is innervated by a dense network of sensory neurons that mainly comes from vagal afferents whose cell bodies reside in the vagal ganglia (jugular and nodose ganglia); while other sensory nerve innervation originates from the dorsal root ganglion (DRG) (**Figure 3**) (115, 173–175). Nociceptive receptors are richly expressed in sensory neurons endings, which are abundantly present in the lung parenchyma and near the airways; this poises them to act as the first wall for host defense and these neurons interact directly with inflammatory stimuli such as ATP, pathogens, allergens, protons, heat, mechanical injury and chemical irritants like immune cells such as APCs, macrophages, and other phagocytes (116, 176–178).

Sensory neuronal action potentials evoked by this interaction are then transmitted into the CNS within milliseconds of the detection of inflammation or invasion. This action-potential signaling mechanism is significantly faster than immune cell. Once activated, nociceptive receptors induce coughing, pain and bronchoconstriction (173, 178–180). Neuropeptides emanating from nociceptor nerve terminals also participate in the nociceptors crosstalk with immune cells (173, 181–183).

Excitation of nociceptors increases the release of multiple neuropeptides, such as substance P, VIP and CGRP which regulate both innate and adaptive immune cells (184) (**Table 1** and **Figure 3**).

CGRP

CGRP, encoded by *Calca*, is a member of the calcitonin family peptides that not only secreted by peripheral nociceptive neurons but also found in central neurons (45, 185). CGRP binds to a heteromeric receptor composed of a receptor activity-modifying protein (RAMP1) and a G-protein coupled receptor termed CALCRL. CGRP *via* these receptors stimulates AC, which results in cAMP and PKA pathway activation and leads to the phosphorylation of several downstream pathways including NOS, MAPK, and CREB pathways (186).

In skin bacterial infection, lymph node hypertrophy and TNF-α production are found to be suppressed by CGRP (183, 187). CGRP levels markedly increased in the bronchoalveolar lavage fluid (BALF) after Staphylococcus aureus infection. S. aureus also increases cultured neuronal production of CGRP *in vitro*. CGRP could alleviate the symptoms of S. aureus-induced pneumonia by suppressing TNF-α, CXCL1, γδ T cells and neutrophils (188).

A recent study discovered the relationship between CGRP and pulmonary neuroendocrine cells (PNECs), which comprise ~1% of the airway cell population (189, 190). PNECs (locate in close proximity to ILC2 near airway branch points) could secrete CGRP, which aggravates allergen-induced asthma in mice by stimulating ILC2 proliferation and the secretion of IL-5 from ILC2 (133). On the other hand, *Il5*^{hi}ILC2 produce both CGRP and its receptor CGRPR following *Nb* infection. CGRP treatment alone does not increase cytokine production from ILC2, a combination of neuromedin U (NMU) + IL-33 with CGRP stimulates IL-5 but limits IL-13 production and ILC2 proliferation. Worm expulsion and ILC2 responses are augmented without CGRP signaling (39). Interestingly, Xu et al, reported that OVA-induced inflammation increased the expression of *Calca* in KLRG1$^+$ILC2. CGRP suppressed KLRG1$^+$ILC2s proliferation but promoted IL-5 expression (191). Collectively, these paradoxes point to both pro- and anti-inflammatory properties of CGRP on immune responses in the lung and warrant further investigation (**Table 1** and **Figure 3**).

VIP

The neuropeptide VIP also involves in the regulation of ILC2. It has been firstly characterized as a polypeptide isolated from the small intestine with multiple impacts on different systems such as respiratory and cardiovascular systems (192). VIP can be perceived by VIP receptor type 1 (VPAC1) or VIP receptor type 2 (VPAC2), which are differentially regulated according to cell type and activity conditions (193, 194). Similar to CGRP, VIP enhances the AC/cAMP/PKA pathway and phospholipase C, which causes the accumulation of intracellular Ca^{2+} (195).

Of note, pulmonary and intestinal ILC2 express VPAC1 and VPAC2 and produce IL-5 when they are incubated with IL-7 and VIP- or VPAC2-specific agonist (84). Talbot *et al*, discovered a critical relationship between ILC2, VIP, T cells, and nociceptive neurons (182). Reciprocally, ILC2-derived IL-5 activates nociceptors on afferent neurons and upregulates the release of VIP, which in return acts *via* VPAC2 and leads ILC2 and subsequently T cells to release more IL-5 and thereby forming a type 2 inflammatory positive feedback loop mainly based on the neuro-immune axis (**Table 1** and **Figure 3**) (182). Since the levels of blood eosinophils and type 2 cytokine release from ILC2 are regulated by circadian rhythm and food intake, this suggests that VIP might influence blood eosinophils *via* upregulation of ILC2 (84).

NMU

NMU is a neuropeptide mainly released by cholinergic sensory neurons originating from DRG, but not parasympathetic neurons in the vagal ganglion (196). The initial biological functions ascribed to NMU were food intake and body weight reduction, smooth muscle contraction of the uterus, pronociceptive effects promotion and circadian rhythm regulation (197, 198). In addition, NMU is also occasionally secreted by some APCs, including monocytes, B cells, and

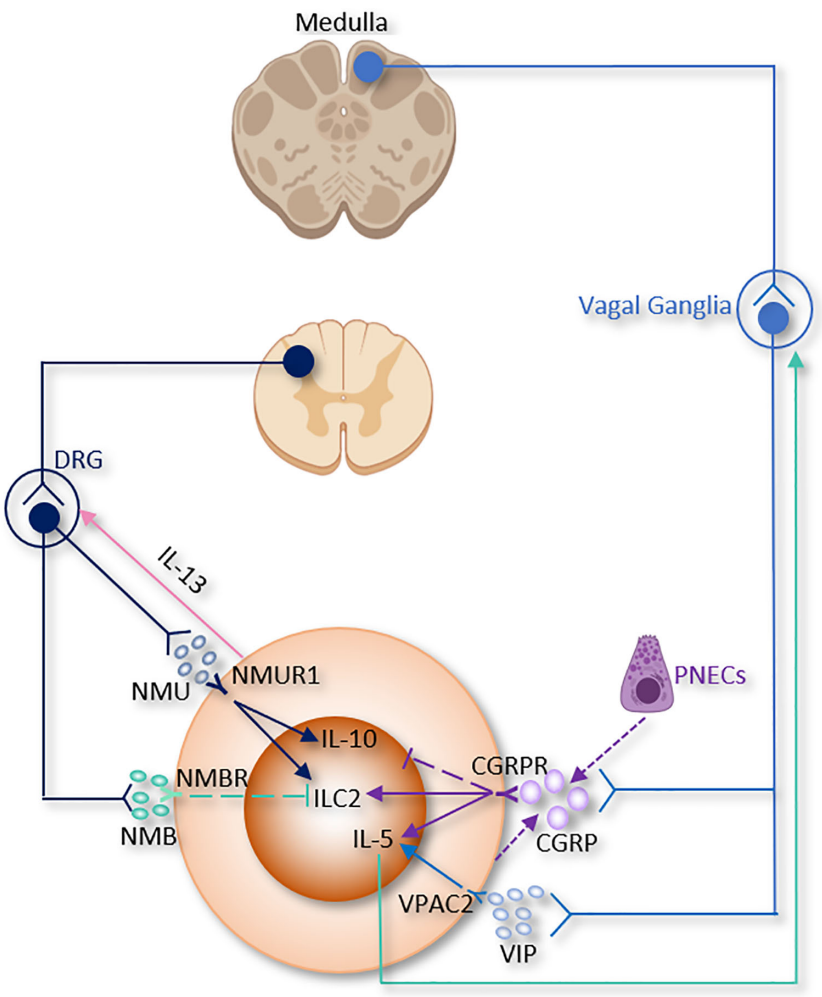

FIGURE 3 | The somatic nervous system regulation of ILC2 function. CGRP, α-calcitonin gene-related peptide; DRG, Dorsal root ganglion; NMB, neuromedin B; NMU, neuromedin U; PNECs, Pulmonary neuroendocrine cells; VIP, Vasoactive Intestinal Peptide.

dendritic cells (199). Thus, it is suggested to play an important role in the regulation of adaptive and innate immunity. In an allergen-induced asthma model, airway eosinophilia was shown to decrease in *nmu*$^{-/-}$ mice. NMU directly stimulated extracellular/signal-regulated kinase phosphorylation and Ca^{2+} mobilization. NMU also induced cell adhesion to components of the extracellular matrix, and chemotaxis *in vitro* (200).

Recent studies reported that NMU from lamina propria play a regulatory role in mice type 2 innate immunity through binding to the neuromedin U receptor 1 (Nmur1), which is selectively enriched in ILC2. Consistent with this idea, NMU-expressing neurons have been discovered in close vicinity to ILC2 in the lungs (19, 37, 38). Lung ILC2 present NMUR1 at steady state and upon IL-25 stimulation, however, NMUR1 was inhibited upon IL-33 exposure (38).

In a mice model of worm infection in the lungs and intestine, stimulation of ILC2 with NMU led to strong and immediate production of tissue protection and innate inflammatory cytokines in a NMUR1-dependent manner, thereby alleviating worm burden (37).

In a model of airway allergy, ILC2 were activated by NMU *in vitro*, and *in vivo* co-treatment of NMU with IL-25 significantly increased lung histopathology. Disruption of NMU-NMUR1 pathway decreased ILC2 number and effector function, and changed transcriptional programs following *in vivo* allergen exposure (38). NMU elevates pulmonary ILC2 proliferation and a selectively potent secretion of innate IL-5, IL-13, and amphiregulin (19, 37, 38). Furthermore, ILC2 activated by NMU increase the number of lung eosinophils and mast cells, thus alleviating antihelminth responses (19, 37, 38). Interestingly, IL-13 enhance NMU production in DRG neurons, thus indicating the existence of a reciprocal neuron–ILC2 regulatory loop *via* ILC2-derived IL-13 and neuronal NMU expression (38). IL-10, primarily secreted by Tregs, was increased by NMU in activated intestinal ILC2. IL-10 further stimulated IL-10 production in ILC2 through a positive feedback loop (**Table 1** and **Figure 3**) (114). These findings suggested that NMU treatment enhance inflammation-induced damage in the lungs and pointed to a double-edged sword of NMU-NMUR1 signaling.

NMB

NMB belongs to the neuromedin family that includes NMB, NMC, NMK, NML, NMN, NMU and NMS (201, 202). It is expressed widely in the CNS (olfactory bulb, dentate gyrus, amygdala, basal ganglia, and brainstem) and the PNS (gastrointestinal tract, trigeminal and dorsal root ganglia (DRG)) (203, 204).

NMB controls cell growth, blood glucose, body temperature, emotion, energy homeostasis, exocrine and endocrine secretion, food intake, grooming and scratching, nociception and smooth muscle contraction. Inclan-Rico, Juan M *et al*, found that administration of NMB suppressed ILC2 responses *via* NMU receptor (NMBR), eosinophilia and mucus production after *Nb* infection in the lung. In consistent with *in vivo* results, *in vitro* treatment of NMB inhibited the growth of sorted ILC2 (**Table 1** and **Figure 3**). Of note, ILC2 sorted from basophil-depleted mice were unchanged by NMB stimulation, indicating that basophils are indispensable for the inhibitory effects of NMB on ILC2 (50).

PROMISING DIRECTIONS FOR RESEARCH ON THE NEURAL REGULATION OF ILC2 IN THE LUNG

The discoveries of neural control of ILC2 have added a new dimension to neuroimmunity. All previously known findings of ILC2 in the lung could be re-examined from this perspective.

Previous studies on the lung ILC2 have been mainly performed in models of allergic disease (205–208), helminth infection (16, 50, 209, 210), and septic lung injury (17, 85, 211, 212). Multiple neural pathways have been reported to be involved in these disease models (4, 213, 214). Although recent studies have found some clues, the relationship between nervous system and ILC2 still remains contradictory and inconclusive. For example, CGRP shows opposite effects on different ILC2 subtypes. NMU is able to enhance the pro-inflammatory function of ILC2 as well as its anti-inflammatory function. Does the nervous system or neural mediators play ameliorating or worsening roles in these diseases by regulating ILC2? If future studies can prove this hypothesis, then ILC2 will not only be a bridge between innate and adaptive immunity, but also between the nervous system and the immune system.

The second promising research direction will be the effects of neural-regulated ILC2 on nervous system. Type I cytokines and their receptors (such as IL-1, IL-6, and TNFs) are expressed widely in CNS cells and are important for the development and function of the CNS (58). However, the impacts of ILC2-released type II cytokines and mediators on nervous system remains to be elucidated. Currently, a reciprocal DRG–ILC2 regulatory loop *via* ILC2-derived IL-13 and neuronal NMU expression has been found (38). Besides, ILC2-derived IL-5 activates nociceptors on afferent neurons and upregulates the release of VIP, which in return, acting *via* VPAC2 leads to ILC2 and T cells to release more IL-5 and, thereby, forming a type 2 inflammatory positive feedback loop (182). It would be important to explore unidentified neuron-ILC2 positive/negative regulatory loops.

The third area of interest will be the neural regulation of ILC1 and ILC3. Recent studies have shown that three ILCs are functionally plastic. For instance, plastic iILC2 can coproduce both type-2 cytokines and the ILC3-characteristic cytokine (IL-17A) (215). Under certain conditions, c-Kit^{+}ILC2 can convert to ILC3-like cells (216). Besides, IL-12 and IL-18 converted ILC2 into ILC1 in patients with chronic obstructive pulmonary disease (COPD) (217). Does neuromodulation affect the interconversion of ILC2 and two other cell subtypes? If these plastic properties can be elucidated, we can gain a comprehensive understanding of the relationship between ILC as a cell type and the nervous system.

Least but not last, these results have great therapeutic implications for precision medicine. For example, NMUR1 is selectively expressed by ILC2, while receptors for classical ILC2 activators, i.e. IL-25, IL-33, and TSLP, are widely expressed by

various cell types (19, 37, 38). Meanwhile, researchers have developed many methods to selectively stimulate and inhibit neurons (218, 219). Combining these advances will allow us to identify more effective clinical targets.

CONCLUSION

Emerging evidence from *in vivo* animal models, human studies, and *in vitro* experiments indicates that neuropeptides and neurotransmitters released from various neurons and non-neuronal cells are critical in regulation of immune responses in different tissues including the lung. This review article provides a comprehensive overview of the effects of novel neural mediators and pathways on ILC2 and underlying mechanisms as well as the insights into the direct and indirect interactions between ILC2 and other immune cells, highlighting ILC2 as the bridge between innate and adaptive immunity. However, the research in neuro-immune area is, in general, in a premature status, and numerous questions remain to be addressed. For examples, the most of signaling pathways that mediate neural regulation of ILC2 are yet clear; and the mechanisms, by which ILC2 selectively respond to neutral and non-neural signaling need to be elucidated as well. In addition, translational and clinical investigations are required to promote the application resulted from the studies in this area.

AUTHOR CONTRIBUTIONS

WC collected the data and drafted the manuscript. WC, QS, and JF conceived and designed the study. JF reviewed and finalized the manuscript. All authors contributed to the article and approved the submitted version.

FUNDING

This work was supported by the USA National Institutes of Health Grant R01-HL-079669 (JF), USA National Institutes of Health Grant R01HL076179 (JF), USA National Institutes of Health Grant R01-HL-139547 (JF), VA Merit Award 1I01BX002729 (JF), and VA BLR&D Award 1IK6BX004211 (JF).

REFERENCES

1. Chavan SS, Tracey KJ. Essential Neuroscience in Immunology. *J Immunol* (2017) 198:3389–97. doi: 10.4049/jimmunol.1601613
2. Irwin MR, Cole SW. Reciprocal regulation of the neural and innate immune systems. *Nat Rev Immunol* (2011) 11:625–32. doi: 10.1038/nri3042
3. Hoffman C, Aballay A. Role of neurons in the control of immune defense. *Curr Opin Immunol* (2019) 60:30–6. doi: 10.1016/j.coi.2019.04.005
4. Zhai Q, Lai D, Cui P, Zhou R, Chen Q, Hou J, et al. Selective Activation of Basal Forebrain Cholinergic Neurons Attenuates Polymicrobial Sepsis-Induced Inflammation via the Cholinergic Anti-Inflammatory Pathway. *Crit Care Med* (2017) 45:e1075–82. doi: 10.1097/CCM.0000000000002646
5. Zhong C, Zhu J. Transcriptional regulators dictate innate lymphoid cell fates. *Protein Cell* (2017) 8:242–54. doi: 10.1007/s13238-017-0369-7
6. Schuijs MJ, Halim TYF. Group 2 innate lymphocytes at the interface between innate and adaptive immunity. *Ann N Y Acad Sci* (2018) 1417:87–103. doi: 10.1111/nyas.13604
7. Kiessling R, Klein E, Wigzell H. "Natural" killer cells in the mouse. I. Cytotoxic cells with specificity for mouse Moloney leukemia cells. Specificity and distribution according to genotype. *Eur J Immunol* (1975) 5:112–7. doi: 10.1002/eji.1830050208
8. Pross HF, Jondal M. Cytotoxic lymphocytes from normal donors. A functional marker ofhuman non-T lymphocytes. *Clin Exp Immunol* (1975) 21:226–35. PMID: 810282
9. Kelly KA, Scollay R. Seeding of neonatal lymph nodes by T cells and identification of a novel population of CD3-CD4+ cells. *Eur J Immunol* (1992) 22:329–34. doi: 10.1002/eji.1830220207
10. Mebius RE, Rennert P, Weissman IL. Developing lymph nodes collect CD4 +CD3- LTbeta+ cells that can differentiate to APC, NK cells, and follicular cells but not T or B cells. *Immunity* (1997) 7:493–504. doi: 10.1016/S1074-7613(00)80371-4
11. Spits H, Artis D, Colonna M, Diefenbach A, Di Santo JP, Eberl G, et al. Innate lymphoid cells–a proposal for uniform nomenclature. *Nat Rev Immunol* (2013) 13:145–9. doi: 10.1038/nri3365
12. Vivier E, Artis D, Colonna M, Diefenbach A, Di Santo JP, Eberl G, et al. Innate Lymphoid Cells: 10 Years On. *Cell* (2018) 174:1054–66. doi: 10.1016/j.cell.2018.07.017
13. Eberl G, Colonna M, Di Santo JP, McKenzie AN. Innate lymphoid cells. Innate lymphoid cells: a new paradigm in immunology. *Science* (2015) 348: aaa6566. doi: 10.1126/science.aaa6566
14. Artis D, Spits H. The biology of innate lymphoid cells. *Nature* (2015) 517:293–301. doi: 10.1038/nature14189
15. Wong SH, Walker JA, Jolin HE, Drynan LF, Hams E, Camelo A, et al. Transcription factor RORalpha is critical for nuocyte development. *Nat Immunol* (2012) 13:229–36. doi: 10.1038/ni.2208
16. Huang Y, Guo L, Qiu J, Chen X, Hu-Li J, Siebenlist U, et al. IL-25-responsive, lineage-negative KLRG1(hi) cells are multipotential 'inflammatory' type 2 innate lymphoid cells. *Nat Immunol* (2015) 16:161–9. doi: 10.1038/ni.3078
17. Lai D, Tang J, Chen L, Fan EK, Scott MJ, Li Y, et al. Group 2 innate lymphoid cells protect lung endothelial cells from pyroptosis in sepsis. *Cell Death Dis* (2018) 9:369. doi: 10.1038/s41419-018-0412-5
18. Hammad H, Lambrecht BN. Barrier Epithelial Cells and the Control of Type 2 Immunity. *Immunity* (2015) 43:29–40. doi: 10.1016/j.immuni.2015.07.007
19. Klose CSN, Mahlakõiv T, Moeller JB, Rankin LC, Flamar AL, Kabata H, et al. The neuropeptide neuromedin U stimulates innate lymphoid cells and type 2 inflammation. *Nature* (2017) 549:282–6. doi: 10.1038/nature23676
20. Monticelli LA, Sonnenberg GF, Abt MC, Alenghat T, Ziegler CG, Doering TA, et al. Innate lymphoid cells promote lung-tissue homeostasis after infection with influenza virus. *Nat Immunol* (2011) 12:1045–54. doi: 10.1038/ni.2131
21. Halim TY, Krauss RH, Sun AC, Takei F. Lung natural helper cells are a critical source of Th2 cell-type cytokines in protease allergen-induced airway inflammation. *Immunity* (2012) 36:451–63. doi: 10.1016/j.immuni.2011.12.020
22. Fort MM, Cheung J, Yen D, Li J, Zurawski SM, Lo S, et al. IL-25 induces IL-4, IL-5, and IL-13 and Th2-associated pathologies in vivo. *Immunity* (2001) 15:985–95. doi: 10.1016/S1074-7613(01)00243-6
23. Fallon PG, Ballantyne SJ, Mangan NE, Barlow JL, Dasvarma A, Hewett DR, et al. Identification of an interleukin (IL)-25-dependent cell population that provides IL-4, IL-5, and IL-13 at the onset of helminth expulsion. *J Exp Med* (2006) 203:1105–16. doi: 10.1084/jem.20051615
24. Cording S, Medvedovic J, Aychek T, Eberl G. Innate lymphoid cells in defense, immunopathology and immunotherapy. *Nat Immunol* (2016) 17:755–7. doi: 10.1038/ni.3448
25. Monticelli LA, Osborne LC, Noti M, Tran SV, Zaiss DM, Artis D, et al. IL-33 promotes an innate immune pathway of intestinal tissue protection dependent on amphiregulin-EGFR interactions. *Proc Natl Acad Sci U S A* (2015) 112:10762–7. doi: 10.1073/pnas.1509070112
26. Seehus CR, Kadavallore A, Torre B, Yeckes AR, Wang Y, Tang J, et al. Alternative activation generates IL-10 producing type 2 innatelymphoid cells. *Nat Commun* (2017) 8:1900. doi: 10.1038/s41467-017-02023-z

27. Mjosberg J, Bernink J, Golebski K, Karrich JJ, Peters CP, Blom B, et al. The transcription factor GATA3 is essential for the function ofhuman type 2 innate lymphoid cells. *Immunity* (2012) 37:649–59. doi: 10.1016/j.immuni.2012.08.015
28. Salimi M, Barlow JL, Saunders SP, Xue L, Gutowska-Owsiak D, Wang X, et al. A role for IL-25 and IL-33-driven type-2 innate lymphoid cells inatopic dermatitis. *J Exp Med* (2013) 210:2939–50. doi: 10.1084/jem.20130351
29. Oliphant CJ, Hwang YY, Walker JA, Salimi M, Wong SH, Brewer JM, et al. MHCII-mediated dialog between group 2 innate lymphoid cells andCD4(+) T cells potentiates type 2 immunity and promotes parasitic helminth expulsion. *Immunity* (2014) 41:283–95. doi: 10.1016/j.immuni.2014.06.016
30. Schwartz C, Khan AR, Floudas A, Saunders SP, Hams E, Rodewald HR, et al. ILC2s regulate adaptive Th2 cell functions via PD-L1 checkpointcontrol. *J Exp Med* (2017) 214:2507–21. doi: doi: 10.1084/jem.20170051
31. Molofsky AB, Van Gool F, Liang HE, Van Dyken SJ, Nussbaum JC, Lee J, et al. Interleukin-33 and Interferon-γ Counter-Regulate Group 2 Innate Lymphoid Cell Activation during Immune Perturbation. *Immunity* (2015) 43:161–74. doi: 10.1016/j.immuni.2015.05.019
32. Webb GJ, Hirschfield GM, Lane PJ. OX40, OX40L and Autoimmunity: a Comprehensive Review. *Clin Rev Allergy Immunol* (2016) 50:312–32. doi: 10.1007/s12016-015-8498-3
33. Chang YJ, DeKruyff RH, Umetsu DT. The role of type 2 innate lymphoid cells in asthma. *J Leukoc Biol* (2013) 94:933–40. doi: 10.1189/jlb.0313127
34. Barlow JL, Bellosi A, Hardman CS, Drynan LF, Wong SH, Cruickshank JP, et al. Innate IL-13-producing nuocytes arise during allergic lunginflammation and contribute to airways hyperreactivity. *J Allergy ClinImmunol* (2012) 129:191–198.e191-194. doi: 10.1016/j.jaci.2011.09.041
35. Kim HY, Chang YJ, Subramanian S, Lee HH, Albacker LA, Matangkasombut P, et al. Innate lymphoid cells responding to IL-33 mediate airwayhyperreactivity independently of adaptive immunity. *J Allergy Clin Immunol* (2012) 129:216–227.e211-216. doi: 10.1016/j.jaci.2011.10.036
36. Imai Y, Yasuda K, Sakaguchi Y, Haneda T, Mizutani H, Yoshimoto T, et al. Skin-specific expression of IL-33 activates group 2 innate lymphoid cells and elicits atopic dermatitis-like inflammation in mice. *Proc Natl Acad Sci U S A* (2013) 110:13921–6. doi: 10.1073/pnas.1307321110
37. Cardoso V, Chesné J, Ribeiro H, García-Cassani B, Carvalho T, Bouchery T, et al. Neuronal regulation of type 2 innate lymphoid cells via neuromedin U. *Nature* (2017) 549:277–81. doi: 10.1038/nature23469
38. Wallrapp A, Riesenfeld SJ, Burkett PR, Abdulnour RE, Nyman J, Dionne D, et al. The neuropeptide NMU amplifies ILC2-driven allergic lung inflammation. *Nature* (2017) 549:351–6. doi: 10.1038/nature24029
39. Nagashima H, Mahlakõiv T, Shih HY, Davis FP, Meylan F, Huang Y, et al. Neuropeptide CGRP Limits Group 2 Innate Lymphoid Cell Responses andConstrains Type 2 Inflammation. *Immunity* (2019) 51:682-95.e6. doi: 10.1016/j.immuni.2019.06.009
40. Moriyama S, Brestoff JR, Flamar AL, Moeller JB, Klose CSN, Rankin LC, et al. β2-adrenergic receptor-mediated negative regulation of group 2 innate lymphoid cell responses. *Science* (2018) 359:1056–61. doi: 10.1126/science.aan4829
41. Dalli J, Colas RA, Arnardottir H, Serhan CN. Vagal Regulation of Group 3 Innate Lymphoid Cells and the Immunoresolvent PCTR1 Controls Infection Resolution. *Immunity* (2017) 46:92–105. doi: 10.1016/j.immuni.2016.12.009
42. Borovikova LV, Ivanova S, Zhang M, Yang H, Botchkina GI, Watkins LR, et al. Vagus nerve stimulation attenuates the systemic inflammatory response to endotoxin. *Nature* (2000) 405:458–62. doi: 10.1038/35013070
43. Cai B, Chen F, Ji Y, Kiss L, de Jonge WJ, Conejero-Goldberg C, et al. Alpha7 cholinergic-agonist prevents systemic inflammation and improves survival during resuscitation. *J Cell Mol Med* (2009) 13:3774–85. doi: 10.1111/j.1582-4934.2008.00550.x
44. Galle-Treger L, Suzuki Y, Patel N, Sankaranarayanan I, Aron JL, Maazi H, et al. Nicotinic acetylcholine receptor agonist attenuates ILC2-dependent airway hyperreactivity. *Nat Commun* (2016) 7:13202. doi: 10.1038/ncomms13202
45. Holzmann B. Modulation of immune responses by the neuropeptide CGRP. *Amino Acids* (2013) 45:1–7. doi: 10.1007/s00726-011-1161-2
46. Vida G, Peña G, Deitch EA, Ulloa L. α7-cholinergic receptor mediates vagal induction of splenic norepinephrine. *J Immunol* (2011) 186:4340–6. doi: 10.4049/jimmunol.1003722
47. Vida G, Peña G, Kanashiro A, Thompson-Bonilla Mdel R, Palange D, Deitch EA, et al. β2-Adrenoreceptors of regulatory lymphocytes are essential for vagal neuromodulation of the innate immune system. *FASEB J* (2011) 25:4476–85. doi: 10.1096/fj.11-191007
48. Rosas-Ballina M, Olofsson PS, Ochani M, Valdés-Ferrer SI, Levine YA, Reardon C, et al. Acetylcholine-synthesizing T cells relay neural signals in a vagus nerve circuit. *Science* (2011) 334:98–101. doi: 10.1126/science.1209985
49. Kawashima K, Fujii T, Moriwaki Y, Misawa H. Critical roles of acetylcholine and the muscarinic and nicotinic acetylcholine receptors in the regulation of immune function. *Life Sci* (2012) 91:1027–32. doi: 10.1016/j.lfs.2012.05.006
50. Inclan-Rico JM, Ponessa JJ, Valero-Pacheco N, Hernandez CM, Sy CB, Lemenze AD, et al. Basophils prime group 2 innate lymphoid cells for neuropeptide-mediated inhibition. *Nat Immunol* (2020) 21:1181–93. doi: 10.1038/s41590-020-0753-y
51. Hosoi T, Okuma Y, Matsuda T, Nomura Y. Novel pathway for LPS-induced afferent vagus nerve activation: possible role of nodose ganglion. *Auton Neurosci* (2005) 120:104–7. doi: 10.1016/j.autneu.2004.11.012
52. de Lartigue G, Barbier de la Serre C, Espero E, Lee J, Raybould HE. Diet-induced obesity leads to the development of leptin resistance in vagal afferent neurons. *Am J Physiol Endocrinol Metab* (2011) 301:E187–195. doi: 10.1152/ajpendo.00056.2011
53. Ma F, Zhang L, Westlund KN. Reactive oxygen species mediate TNFR1 increase after TRPV1 activation in mouse DRG neurons. *Mol Pain* (2009) 5:31. doi: 10.1186/1744-8069-5-31
54. Li M, Shi J, Tang JR, Chen D, Ai B, Chen J, et al. Effects of complete Freund's adjuvant on immunohistochemical distribution of IL-1beta and IL-1R I in neurons and glia cells of dorsal root ganglion. *Acta Pharmacol Sin* (2005) 26:192–8. doi: 10.1111/j.1745-7254.2005.00522.x
55. Cosentino M, Bombelli R, Ferrari M, Marino F, Rasini E, Maestroni GJ, et al. HPLC-ED measurement of endogenous catecholamines in human immune cells and hematopoietic cell lines. *Life Sci* (2000) 68:283–95. doi: 10.1016/S0024-3205(00)00937-1
56. Quatrini L, Vivier E, Ugolini S. Neuroendocrine regulation of innate lymphoid cells. *Immunol Rev* (2018) 286:120–36. doi: 10.1111/imr.12707
57. Schedlowski M, Engler H, Grigoleit JS. Endotoxin-induced experimental systemic inflammation in humans: a model to disentangle immune-to-brain communication. *Brain Behav Immun* (2014) 35:1–8. doi: 10.1016/j.bbi.2013.09.015
58. Mousa A, Bakhiet M. Role of cytokine signaling during nervous system development. *Int J Mol Sci* (2013) 14:13931–57. doi: 10.3390/ijms140713931
59. Klein Wolterink RG, Kleinjan A, van Nimwegen M, Bergen I, de Bruijn M, Levani Y, et al. Pulmonary innate lymphoid cells are major producers of IL-5 and IL-13 in murine models of allergic asthma. *Eur J Immunol* (2012) 42:1106–16. doi: 10.1002/eji.201142018
60. Van Dyken SJ, Nussbaum JC, Lee J, Molofsky AB, Liang HE, Pollack JL, et al. A tissue checkpoint regulates type 2 immunity. *Nat Immunol* (2016) 17:1381–7. doi: 10.1038/ni.3582
61. Guo L, Huang Y, Chen X, Hu-Li J, Urban JF Jr, Paul WE, et al. Innate immunological function of TH2 cells in vivo. *Nat Immunol* (2015) 16:1051–9. doi: 10.1038/ni.3244
62. Halim TY, MacLaren A, Romanish MT, Gold MJ, McNagny KM, Takei F, et al. Retinoic-acid-receptor-related orphan nuclear receptor alpha is required for natural helper cell development and allergic inflammation. *Immunity* (2012) 37:463–74. doi: 10.1016/j.immuni.2012.06.012
63. Gold MJ, et al. Group 2 innate lymphoid cells facilitate sensitization to local, but not systemic, TH2-inducing allergen exposures. *J Allergy Clin Immunol* (2014) 133:1142–8. doi: 10.1016/j.jaci.2014.02.033
64. Neill DR, Wong SH, Bellosi A, Flynn RJ, Daly M, Langford TK, et al. Nuocytes represent a new innate effector leukocyte that mediates type-2 immunity. *Nature* (2010) 464:1367–70. doi: 10.1038/nature08900
65. Saenz SA, Siracusa MC, Perrigoue JG, Spencer SP, Urban JF Jr, Tocker JE, et al. IL25 elicits a multipotent progenitor cell population that promotes T (H)2 cytokine responses. *Nature* (2010) 464:1362–6. doi: 10.1038/nature08901
66. Wilhelm C, Hirota K, Stieglitz B, Van Snick J, Tolaini M, Lahl K, et al. An IL-9 fate reporter demonstrates the induction of an innate IL-9 response in lung inflammation. *Nat Immunol* (2011) 12:1071–7. doi: 10.1038/ni.2133

67. Mattiola I, Diefenbach A. Enabling anti-tumor immunity by unleashing ILC2. *Cell Res* (2020) 30:461–2. doi: 10.1038/s41422-020-0330-9
68. Moral JA, Leung J, Rojas LA, Ruan J, Zhao J, Sethna Z, et al. ILC2s amplify PD-1 blockade by activating tissue-specific cancer immunity. *Nature* (2020) 579:130–5. doi: 10.1038/s41586-020-2015-4
69. Besnard AG, Guabiraba R, Niedbala W, Palomo J, Reverchon F, Shaw TN, et al. IL-33-mediated protection against experimental cerebral malaria is linked to induction of type 2 innate lymphoid cells, M2 macrophages and regulatory T cells. *PLoS Pathog* (2015) 11:e1004607. doi: 10.1371/journal.ppat.1004607
70. Licona-Limon P, Kim LK, Palm NW, Flavell RA. TH2, allergy and group 2 innate lymphoid cells. *Nat Immunol* (2013) 14:536–42. doi: 10.1038/ni.2617
71. Fukuoka A, Futatsugi-Yumikura S, Takahashi S, Kazama H, Iyoda T, Yoshimoto T, et al. Identification of a novel type 2 innate immunocyte with the ability to enhance IgE production. *Int Immunol* (2013) 25:373–82. doi: 10.1093/intimm/dxs160
72. Moriyama S, Artis D. Neuronal regulation of group 2 innate lymphoid cells and type 2 inflammation. *Adv Immunol* (2019) 143:1–9. doi: 10.1016/bs.ai.2019.08.001
73. Erickson LD, Foy TM, Waldschmidt TJ. Murine B1 B cells require IL-5 for optimal T cell-dependent activation. *J Immunol* (2001) 166:1531–9. doi: 10.4049/jimmunol.166.3.1531
74. Moro K, Yamada T, Tanabe M, Takeuchi T, Ikawa T, Kawamoto H, et al. Innate production of T(H)2 cytokines by adipose tissue-associated c-Kit(+) Sca-1(+) lymphoid cells. *Nature* (2010) 463:540–4. doi: 10.1038/nature08636
75. Drake LY, Iijima K, Kita H. Group 2 innate lymphoid cells and CD4+ T cells cooperate to mediate type 2 immune response in mice. *Allergy* (2014) 69:1300–7. doi: 10.1111/all.12446
76. Mirchandani AS, Besnard AG, Yip E, Scott C, Bain CC, Cerovic V, et al. Type 2 innate lymphoid cells drive CD4+ Th2 cell responses. *J Immunol* (2014) 192:2442–8. doi: 10.4049/jimmunol.1300974
77. von Burg N, Turchinovich G, Finke D. Maintenance of Immune Homeostasis through ILC/T Cell Interactions. *Front Immunol* (2015) 6:416. doi: 10.3389/fimmu.2015.00416
78. Price AE, Liang HE, Sullivan BM, Reinhardt RL, Eisley CJ, Erle DJ, et al. Systemically dispersed innate IL-13-expressing cells in type 2 immunity. *Proc Natl Acad Sci U S A* (2010) 107:11489–94. doi: 10.1073/pnas.1003988107
79. Doherty TA, Khorram N, Lund S, Mehta AK, Croft M, Broide DH. Lung type 2 innate lymphoid cells express cysteinyl leukotriene receptor 1, which regulates TH2 cytokine production. *J Allergy Clin Immunol* (2013) 132:205–13. doi: 10.1016/j.jaci.2013.03.048
80. Noval Rivas M, Burton OT, Oettgen HC, Chatila T. IL-4 production by group 2 innate lymphoid cells promotes foodallergy by blocking regulatory T-cell function. *J Allergy Clin Immunol* (2016) 138:801–811.e809. doi: 10.1016/j.jaci.2016.02.030
81. Pelly VS, Kannan Y, Coomes SM, Entwistle LJ, Rückerl D, Seddon B, et al. IL-4-producing ILC2s are required for the differentiation of T. *Mucosal Immunol* (2016) 9:1407–17. doi: 10.1038/mi.2016.4
82. Bal SM, Bernink JH, Nagasawa M, Groot J, Shikhagaie MM, Golebski K, et al. IL-1β, IL-4 and IL-12 control the fate of group 2 innate lymphoid cells in human airway inflammation in the lungs. *Nat Immunol* (2016) 17:636–45. doi: 10.1038/ni.3444
83. Motomura Y, Morita H, Moro K, Nakae S, Artis D, Endo TA, et al. Basophil-derived interleukin-4 controls the function of natural helper cells, a member of ILC2s, *in* lung inflammation. *Immunity* (2014) 40:758–71. doi: 10.1016/j.immuni.2014.04.013
84. Nussbaum JC, Van Dyken SJ, von Moltke J, Cheng LE, Mohapatra A, Molofsky AB, et al. Type 2 innate lymphoid cells control eosinophil homeostasis. *Nature* (2013) 502:245–8. doi: 10.1038/nature12526
85. Zhang K, Jin Y, Lai D, Wang J, Wang Y, Wu X, et al. RAGE-induced ILC2 expansion in acute lung injury due to haemorrhagic shock. *Thorax* (2020) 75:209–19. doi: 10.1136/thoraxjnl-2019-213613
86. Drake LY, Iijima K, Bartemes K, Kita H. Group 2 Innate Lymphoid Cells Promote an Early Antibody Response to a Respiratory Antigen in Mice. *J Immunol* (2016) 197:1335–42. doi: 10.4049/jimmunol.1502669
87. Angkasekwinai P, Sodthawon W, Jeerawattanawart S, Hansakon A, Pattanapanyasat K, Wang YH, et al. ILC2s activated by IL-25 promote antigen-specific Th2 and Th9 functions that contribute to the control of Trichinella spiralis infection. *PLoS One* (2017) 12:e0184684. doi: 10.1371/journal.pone.0184684
88. Hrusch CL, Manns ST, Bryazka D, Casaos J, Bonham CA, Jaffery MR, et al. ICOS protects against mortality from acute lung injury through activation of IL-5. *Mucosal Immunol* (2018) 11:61–70. doi: 10.1038/mi.2017.42
89. Wu L, Lin Q, Ma Z, Chowdhury FA, Mazumder MHH, Du W. Mesenchymal PGD2 activates an ILC2-Treg axis to promoteproliferation of normal and malignant HSPCs. *Leukemia* (2020) 360:eaan8546. doi: 10.1038/s41375-020-0843-8
90. Xu J, Guardado J, Hoffman R, Xu H, Namas R, Vodovotz Y, et al. IL33-mediated ILC2 activation and neutrophil IL5 production in the lung response after severe trauma: A reverse translation study from a human cohort to a mouse trauma model. *PLoS Med* (2017) 14:e1002365. doi: 10.1371/journal.pmed.1002365
91. Turner JE, Morrison PJ, Wilhelm C, Wilson M, Ahlfors H, Renauld JC, et al. IL-9-mediated survival of type 2 innate lymphoid cells promotes damage control in helminth-induced lung inflammation. *J Exp Med* (2013) 210:2951–65. doi: 10.1084/jem.20130071
92. Rauber S, Luber M, Weber S, Maul L, Soare A, Wohlfahrt T, et al. Resolution of inflammation by interleukin-9-producing type 2 innatelymphoid cells. *Nat Med* (2017) 23:938–44. doi: 10.1038/nm.4373
93. Wan J, Huang L, Ji X, Yao S, Hamed Abdelaziz M, Cai W, et al. HMGB1-induced ILC2s activate dendritic cells by producing IL-9 in asthmatic mouse model. *Cell Immunol* (2020) 352:104085. doi: 10.1016/j.cellimm.2020.104085
94. Roediger B, Kyle R, Tay SS, Mitchell AJ, Bolton HA, Guy TV, et al. IL-2 is a critical regulator of group 2 innate lymphoid cellfunction during pulmonary inflammation. *J Allergy Clin Immunol* (2015) 136:1653–1663.e1657. doi: 10.1016/j.jaci.2015.03.043
95. Erpenbeck VJ, Hohlfeld JM, Volkmann B, Hagenberg A, Geldmacher H, Braun A, et al. Segmental allergen challenge in patients with atopic asthma leads to increased IL-9 expression in bronchoalveolar lavage fluid lymphocytes. *J Allergy Clin Immunol* (2003) 111:1319–27. doi: 10.1067/mai.2003.1485
96. Temann UA, Geba GP, Rankin JA, Flavell RA. Expression of interleukin 9 in the lungs of transgenic mice causes airway inflammation, mast cell hyperplasia, and bronchial hyperresponsiveness. *J Exp Med* (1998) 188:1307–20. doi: 10.1084/jem.188.7.1307
97. Temann UA, Laouar Y, Eynon EE, Homer R, Flavell RA. IL9 leads to airway inflammation by inducing IL13 expression in airway epithelial cells. *Int Immunol* (2007) 19:1–10. doi: 10.1093/intimm/dxl117
98. Shimbara A, Christodoulopoulos P, Soussi-Gounni A, Olivenstein R, Nakamura Y, Levitt RC, et al. IL-9 and its receptor in allergic and nonallergic lung disease: increased expression in asthma. *J Allergy Clin Immunol* (2000) 105:108–15. doi: 10.1016/S0091-6749(00)90185-4
99. Sugita K, Steer CA, Martinez-Gonzalez I, Altunbulakli C, Morita H, Castro-Giner F, et al. Type 2 innate lymphoid cells disrupt bronchial epithelial barrierintegrity by targeting tight junctions through IL-13 in asthmatic patients. *J Allergy Clin Immunol* (2018) 141:300–310.e311. doi: 10.1016/j.jaci.2017.02.038
100. Bouchery T, Kyle R, Camberis M, Shepherd A, Filbey K, Smith A, et al. ILC2s and T cells cooperate to ensure maintenance of M2 macrophages for lung immunity against hookworms. *Nat Commun* (2015) 6:6970. doi: 10.1038/ncomms7970
101. Saluzzo S, Gorki AD, Rana BMJ, Martins R, Scanlon S, Starkl P, et al. First-Breath-Induced Type 2 Pathways Shape the Lung Immune Environment. *Cell Rep* (2017) 18:1893–905. doi: 10.1016/j.celrep.2017.01.071
102. Halim TY, Steer CA, Mathä L, Gold MJ, Martinez-Gonzalez I, McNagny KM, et al. Group 2 innate lymphoid cells are critical for the initiation of adaptive T helper 2 cell-mediated allergic lung inflammation. *Immunity* (2014) 40:425–35. doi: 10.1016/j.immuni.2014.01.011
103. Jia Y, Fang X, Zhu X, Bai C, Zhu L, Jin M, et al. IL-13. *Am J Respir Cell Mol Biol* (2016) 55:675–83. doi: 10.1165/rcmb.2016-0099OC
104. Zaiss DMW, Gause WC, Osborne LC, Artis D. Emerging functions of amphiregulin in orchestrating immunity, inflammation, and tissue repair. *Immunity* (2015) 42:216–26. doi: 10.1016/j.immuni.2015.01.020
105. Zaiss DM, van Loosdregt J, Gorlani A, Bekker CP, Gröne A, Sibilia M, et al. Amphiregulin enhances regulatory T cell-suppressive function via the

epidermal growth factor receptor. *Immunity* (2013) 38:275–84. doi: 10.1016/j.immuni.2012.09.023
106. Crosby LM, Waters CM. Epithelial repair mechanisms in the lung. *Am J Physiol Lung Cell Mol Physiol* (2010) 298:L715–731. doi: 10.1152/ajplung.00361.2009
107. Puddicombe SM, Polosa R, Richter A, Krishna MT, Howarth PH, Holgate ST, et al. Involvement of the epidermal growth factor receptor in epithelial repair in asthma. *FASEB J* (2000) 14:1362–74. doi: 10.1096/fj.14.10.1362
108. Arpaia N, Green JA, Moltedo B, Arvey A, Hemmers S, Yuan S, et al. A Distinct Function of Regulatory T Cells in Tissue Protection. *Cell* (2015) 162:1078–89. doi: 10.1016/j.cell.2015.08.021
109. Smith KA, Filbey KJ, Reynolds LA, Hewitson JP, Harcus Y, Boon L, et al. Low-level regulatory T-cell activity is essential for functional type-2 effector immunity to expel gastrointestinal helminths. *Mucosal Immunol* (2016) 9:428–43. doi: 10.1038/mi.2015.73
110. Rigas D, Lewis G, Aron JL, Wang B, Banie H, Sankaranarayanan I, et al. Type 2 innate lymphoid cell suppression by regulatory T cellsattenuates airway hyperreactivity and requires inducible T-cell costimulator-inducible T-cell costimulator ligand interaction. *J Allergy Clin Immunol* (2017) 139:1468–1477.e1462. doi: 10.1016/j.jaci.2016.08.034
111. Maazi H, Patel N, Sankaranarayanan I, Suzuki Y, Rigas D, Soroosh P, et al. ICOS: ICOS-ligand interaction is required for type 2 innate lymphoid cell function, homeostasis, and induction of airway hyperreactivity. *Immunity* (2015) 42:538–51. doi: 10.1016/j.immuni.2015.02.007
112. Yu Y, Tsang JC, Wang C, Clare S, Wang J, Chen X, et al. Single-cell RNA-seq identifies a PD-1. *Nature* (2016) 539:102–6. doi: 10.1038/nature20105
113. Croft M. Control of immunity by the TNFR-related molecule OX40 (CD134). *Annu Rev Immunol* (2010) 28:57–78. doi: 10.1146/annurev-immunol-030409-101243
114. Bando JK, Gilfillan S, Di Luccia B, Fachi JL, Sécca C, Cella M, et al. ILC2s are the predominant source of intestinal ILC-derived IL-10. *J Exp Med* (2020) 217(2):e20191520. doi: 10.1084/jem.20191520
115. Belvisi MG. Overview of the innervation of the lung. *Curr Opin Pharmacol* (2002) 2:211–5. doi: 10.1016/S1471-4892(02)00145-5
116. McMahon SB, La Russa F, Bennett DL. Crosstalk between the nociceptive and immune systems in host defence and disease. *Nat Rev Neurosci* (2015) 16:389–402. doi: 10.1038/nrn3946
117. Franco R, Schoneveld OJ, Pappa A, Panayiotidis MII. The central role of glutathione in the pathophysiology of human diseases. *Arch Physiol Biochem* (2007) 113:234–58. doi: 10.1080/13813450701661198
118. Papa I, Saliba D, Ponzoni M, Bustamante S, Canete PF, Gonzalez-Figueroa P, et al. TFH-derived dopamine accelerates productive synapses in germinal centres. *Nature* (2017) 547:318–23. doi: 10.1038/nature23013
119. Pavlov VA, Tracey KJ. The vagus nerve and the inflammatory reflex–linking immunity and metabolism. *Nat Rev Endocrinol* (2012) 8:743–54. doi: 10.1038/nrendo.2012.189
120. Su X, Matthay MA, Malik AB. Requisite role of the cholinergic alpha7 nicotinic acetylcholine receptor pathway in suppressing Gram-negative sepsis-induced acute lung inflammatory injury. *J Immunol* (2010) 184:401–10. doi: 10.4049/jimmunol.0901808
121. Cole SW, Arevalo JM, Takahashi R, Sloan EK, Lutgendorf SK, Sood AK, et al. Computational identification of gene-social environment interaction at the human IL6 locus. *Proc Natl Acad Sci U S A* (2010) 107:5681–6. doi: 10.1073/pnas.0911515107
122. Collado-Hidalgo A, Sung C, Cole S. Adrenergic inhibition of innate anti-viral response: PKA blockade of Type I interferon gene transcription mediates catecholamine support for HIV-1 replication. *Brain Behav Immun* (2006) 20:552–63. doi: 10.1016/j.bbi.2006.01.005
123. Nance DM, Sanders VM. Autonomic innervation and regulation of the immune system (1987-2007). *Brain Behav Immun* (2007) 21:736–45. doi: 10.1016/j.bbi.2007.03.008
124. Grebe KM, Takeda K, Hickman HD, Bailey AL, Embry AC, Bennink JR, et al. Cutting edge: Sympathetic nervous system increases proinflammatory cytokines and exacerbates influenza A virus pathogenesis. *J Immunol* (2010) 184:540–4. doi: 10.4049/jimmunol.0903395
125. Ding X, Luo Y, Zhang X, Zheng H, Yang X, Yang X, et al. IL-33-driven ILC2/eosinophil axis in fat is induced by sympathetic tone and suppressed by obesity. *J Endocrinol* (2016) 231:35–48. doi: 10.1530/JOE-16-0229
126. Elenkov IJ, Wilder RL, Chrousos GP, Vizi ES. The sympathetic nerve–an integrative interface between twosupersystems: the brain and the immune system. *Pharmacol Rev*(2000) 52:595–638.
127. Muller PA, Koscsó B, Rajani GM, Stevanovic K, Berres ML, Hashimoto D, et al. Crosstalk between Muscularis Macrophages and Enteric Neurons Regulates Gastrointestinal Motility. *Cell* (2014) 158:1210. doi: 10.1016/j.cell.2014.08.002
128. Sternberg EM. Neural regulation of innate immunity: a coordinated nonspecific host response to pathogens. *Nat Rev Immunol* (2006) 6:318–28. doi: 10.1038/nri1810
129. Lee HJ, Takemoto N, Kurata H, Kamogawa Y, Miyatake S, O'Garra A, et al. GATA-3 induces T helper cell type 2 (Th2) cytokine expression and chromatin remodeling in committed Th1 cells. *J Exp Med* (2000) 192:105–15. doi: 10.1084/jem.192.1.105
130. Panina-Bordignon P, Mazzeo D, Lucia PD, D'Ambrosio D, Lang R, Fabbri L, et al. Beta2-agonists prevent Th1 development by selective inhibition of interleukin 12. *J Clin Invest* (1997) 100:1513–9. doi: 10.1172/JCI119674
131. Cole SW, Korin YD, Fahey JL, Zack JA. Norepinephrine accelerates HIV replication via protein kinase A-dependent effects on cytokine production. *J Immunol* (1998) 161:610–6.
132. Cai T, Qiu J, Ji Y, Li W, Ding Z, Suo C, et al. IL-17-producing ST2. *J Allergy ClinImmunol* (2019) 143:229–244.e229. doi: 10.1073/pnas.0900591106
133. Sui P, Wiesner DL, Xu J, Zhang Y, Lee J, Van Dyken S, et al. Pulmonary neuroendocrine cells amplify allergic asthma responses. *Science* (2018) 360: eaan8546. doi: 10.1126/science.aan8546
134. Pavlov VA, Ochani M, Gallowitsch-Puerta M, Ochani K, Huston JM, Czura CJ, et al. Central muscarinic cholinergic regulation of the systemic inflammatory response during endotoxemia. *Proc Natl Acad Sci U S A* (2006) 103:5219–23. doi: 10.1073/pnas.0600506103
135. Rosas-Ballina M, Valdés-Ferrer SI, Dancho ME, Ochani M, Katz D, Cheng KF, et al. Xanomeline suppresses excessive pro-inflammatory cytokine responses through neural signal-mediated pathways and improves survival in lethal inflammation. *Brain Behav Immun* (2015) 44:19–27. doi: 10.1016/j.bbi.2014.07.010
136. Ji H, Rabbi MF, Labis B, Pavlov VA, Tracey KJ, Ghia JE. Central cholinergic activation of a vagus nerve-to-spleen circuit alleviates experimental colitis. *Mucosal Immunol* (2014) 7:335–47. doi: 10.1038/mi.2013.52
137. Miksa M, Das P, Zhou M, Wu R, Dong W, Ji Y, et al. Pivotal role of the alpha (2A)-adrenoceptor in producing inflammation and organ injury in a rat model of sepsis. *PLoS One* (2009) 4:e5504. doi: 10.1371/journal.pone.0005504
138. Levine YA, Koopman FA, Faltys M, Caravaca A, Bendele A, Zitnik R, et al. Neurostimulation of the cholinergic anti-inflammatory pathway ameliorates disease in rat collagen-induced arthritis. *PLoS One* (2014) 9:e104530. doi: 10.1371/journal.pone.0104530
139. von Moltke J, Ji M, Liang HE, Locksley RM. Tuft-cell-derived IL-25 regulates an intestinal ILC2-epithelial response circuit. *Nature* (2016) 529:221–5. doi: 10.1038/nature16161
140. Schneider C, O'Leary CE, Locksley RM. Regulation of immune responses by tuft cells. *Nat Rev Immunol* (2019) 19:584–93. doi: 10.1038/s41577-019-0176-x
141. Skok MV, Grailhe R, Agenes F, Changeux JP. The role of nicotinic receptors in B-lymphocyte development and activation. *Life Sci* (2007) 80:2334–6. doi: 10.1016/j.lfs.2007.02.005
142. Nizri E, Hamra-Amitay Y, Sicsic C, Lavon I, Brenner T. Anti-inflammatory properties of cholinergic up-regulation: A new role for acetylcholinesterase inhibitors. *Neuropharmacology* (2006) 50:540–7. doi: 10.1016/j.neuropharm.2005.10.013
143. Nizri E, Irony-Tur-Sinai M, Lory O, Orr-Urtreger A, Lavi E, Brenner T, et al. Activation of the cholinergic anti-inflammatory system by nicotine attenuates neuroinflammation via suppression of Th1 and Th17 responses. *J Immunol* (2009) 183:6681–8. doi: 10.4049/jimmunol.0902212
144. Wang H, Yu M, Ochani M, Amella CA, Tanovic M, Susarla S, et al. Nicotinic acetylcholine receptor alpha7 subunit is an essential regulator of inflammation. *Nature* (2003) 421:384–8. doi: 10.1038/nature01339
145. Wang H, Liao H, Ochani M, Justiniani M, Lin X, Yang L, et al. Cholinergic agonists inhibit HMGB1 release and improve survival in experimental sepsis. *Nat Med* (2004) 10:1216–21. doi: 10.1038/nm1124

146. Hoyler T, Klose CS, Souabni A, Turqueti-Neves A, Pfeifer D, Rawlins EL, et al. The transcription factor GATA-3 controls cell fate and maintenance of type 2 innate lymphoid cells. *Immunity* (2012) 37:634–48. doi: 10.1016/j.immuni.2012.06.020
147. Klein Wolterink RG, Serafini N, van Nimwegen M, Vosshenrich CA, de Bruijn MJ, Fonseca Pereira D, et al. Essential, dose-dependent role for the transcription factor Gata3 in the development of IL-5+ and IL-13+ type 2 innate lymphoid cells. *Proc Natl Acad Sci U S A* (2013) 110:10240–5. doi: 10.1073/pnas.1217158110
148. Mishra NC, Rir-Sima-Ah J, Langley RJ, Singh SP, Peña-Philippides JC, Koga T, et al. Nicotine primarily suppresses lung Th2 but not goblet cell and muscle cell responses to allergens. *J Immunol* (2008) 180:7655–63. doi: 10.4049/jimmunol.180.11.7655
149. Cesario A, Russo P, Nastrucci C, Granone P. Is alpha7-nAChR a possible target for lung cancer and malignant pleural mesothelioma treatment? *Curr Drug Targets* (2012) 13:688–94. doi: 10.2174/138945012800398900
150. West KA, Brognard J, Clark AS, Linnoila IR, Yang X, Swain SM, et al. Rapid Akt activation by nicotine and a tobacco carcinogen modulates the phenotype of normal human airway epithelial cells. *J Clin Invest* (2003) 111:81–90. doi: 10.1172/JCI200316147
151. Dasgupta P, Kinkade R, Joshi B, Decook C, Haura E, Chellappan S, et al. Nicotine inhibits apoptosis induced by chemotherapeutic drugs by up-regulating XIAP and survivin. *Proc Natl Acad Sci U S A* (2006) 103:6332–7. doi: 10.1073/pnas.0509313103
152. Schaal C, Chellappan SP. Nicotine-mediated cell proliferation and tumor progression in smoking-related cancers. *Mol Cancer Res* (2014) 12:14–23. doi: 10.1158/1541-7786.MCR-13-0541
153. Steinman L. Elaborate interactions between the immune and nervous systems. *Nat Immunol* (2004) 5:575–81. doi: 10.1038/ni1078
154. van Westerloo DJ, Giebelen IA, Florquin S, Bruno MJ, Larosa GJ, Ulloa L, et al. The vagus nerve and nicotinic receptors modulate experimental pancreatitis severity in mice. *Gastroenterology* (2006) 130:1822–30. doi: 10.1053/j.gastro.2006.02.022
155. Bernik TR, Friedman SG, Ochani M, DiRaimo R, Susarla S, Czura CJ, et al. Cholinergic antiinflammatory pathway inhibition of tumor necrosis factor during ischemia reperfusion. *J Vasc Surg* (2002) 36:1231–6. doi: 10.1067/mva.2002.129643
156. Altavilla D, Guarini S, Bitto A, Mioni C, Giuliani D, Bigiani A, et al. Activation of the cholinergic anti-inflammatory pathway reduces NF-kappab activation, blunts TNF-alpha production, and protects againts splanchic artery occlusion shock. *Shock* (2006) 25:500–6. doi: 10.1097/01.shk.0000209539.91553.82
157. Pullan RD, Rhodes J, Ganesh S, Mani V, Morris JS, Williams GT, et al. Transdermal nicotine for active ulcerative colitis. *N Engl J Med* (1994) 330:811–5. doi: 10.1056/NEJM199403243301202
158. Bernik TR, Friedman SG, Ochani M, DiRaimo R, Ulloa LR, Yang H, et al. Pharmacological stimulation of the cholinergic antiinflammatory pathway. *J Exp Med* (2002) 195:781–8. doi: 10.1084/jem.20011714
159. Huston JM, Ochani M, Rosas-Ballina M, Liao H, Ochani K, Pavlov VA, et al. Splenectomy inactivates the cholinergic antiinflammatory pathway during lethal endotoxemia and polymicrobial sepsis. *J Exp Med* (2006) 203:1623–8. doi: 10.1084/jem.20052362
160. van Westerloo DJ, Giebelen IA, Florquin S, Daalhuisen J, Bruno MJ, de Vos AF, et al. The cholinergic anti-inflammatory pathway regulates the host response during septic peritonitis. *J Infect Dis* (2005) 191:2138–48. doi: 10.1086/430323
161. Pavlov VA, Wang H, Czura CJ, Friedman SG, Tracey KJ. The cholinergic anti-inflammatory pathway: a missing link in neuroimmunomodulation. *Mol Med* (2003) 9:125–34. doi: 10.1007/BF03402177
162. Tracey KJ. Physiology and immunology of the cholinergic antiinflammatory pathway. *J Clin Invest* (2007) 117:289–96. doi: 10.1172/JCI30555
163. Tracey KJ. The inflammatory reflex. *Nature* (2002) 420:853–9. doi: 10.1038/nature01321
164. Tracey KJ. Reflex control of immunity. *Nat Rev Immunol* (2009) 9:418–28. doi: 10.1038/nri2566
165. Andersson U, Tracey KJ. Reflex principles of immunological homeostasis. *Annu Rev Immunol* (2012) 30:313–35. doi: 10.1146/annurev-immunol-020711-075015
166. Oke SL, Tracey KJ. From CNI-1493 to the immunological homunculus: physiology of the inflammatory reflex. *J Leukoc Biol* (2008) 83:512–7. doi: 10.1189/jlb.0607363
167. Rosas-Ballina M, Ochani M, Parrish WR, Ochani K, Harris YT, Huston JM, et al. Splenic nerve is required for cholinergic antiinflammatory pathway control of TNF in endotoxemia. *Proc Natl Acad Sci U S A* (2008) 105:11008–13. doi: 10.1073/pnas.0803237105
168. Lu B, Kwan K, Levine YA, Olofsson PS, Yang H, Li J, et al. alpha7 nicotinic acetylcholine receptor signaling inhibits inflammasome activation by preventing mitochondrial DNA release. *Mol Med* (2014) 20:350–8. doi: 10.2119/molmed.2013.00117
169. de Jonge WJ, van der Zanden EP, The FO, Bijlsma MF, van Westerloo DJ, Bennink RJ, et al. Stimulation of the vagus nerve attenuates macrophage activation by activating the Jak2-STAT3 signaling pathway. *Nat Immunol* (2005) 6:844–51. doi: 10.1038/ni1229
170. Guarini S, Altavilla D, Cainazzo MM, Giuliani D, Bigiani A, Marini H, et al. Efferent vagal fibre stimulation blunts nuclear factor-kappaB activation and protects against hypovolemic hemorrhagic shock. *Circulation* (2003) 107:1189–94. doi: 10.1161/01.CIR.0000050627.90734.ED
171. Feng X, Li L, Feng J, He W, Li N, Shi T, et al. Vagal-α7nAChR signalling attenuates allergic asthma responses and facilitates asthma tolerance by regulating inflammatory group 2 innate lymphoid cells. *Immunol Cell Biol* (2020). doi: 10.1111/imcb.12400
172. Zhou L. Striking similarity: GATA-3 regulates ILC2 and Th2 cells. *Immunity* (2012) 37:589–91. doi: 10.1016/j.immuni.2012.10.002
173. Trankner D, Hahne N, Sugino K, Hoon MA, Zuker C. Population of sensory neurons essential for asthmatic hyperreactivity of inflamed airways. *Proc Natl Acad Sci U S A* (2014) 111:11515–20. doi: 10.1073/pnas.1411032111
174. Chang RB, Strochlic DE, Williams EK, Umans BD, Liberles SD. Vagal Sensory Neuron Subtypes that Differentially Control Breathing. *Cell* (2015) 161:622–33. doi: 10.1016/j.cell.2015.03.022
175. Mazzone SB, Undem BJ. Vagal Afferent Innervation of the Airways in Health and Disease. *Physiol Rev* (2016) 96:975–1024. doi: 10.1152/physrev.00039.2015
176. Kollarik M, Ru F, Brozmanova M. Vagal afferent nerves with the properties of nociceptors. *Auton Neurosci* (2010) 153:12–20. doi: 10.1016/j.autneu.2009.08.001
177. Ni D, Gu Q, Hu HZ, Gao N, Zhu MX, Lee LY, et al. Thermal sensitivity of isolated vagal pulmonary sensory neurons: role of transient receptor potential vanilloid receptors. *Am J Physiol Regul Integr Comp Physiol* (2006) 291:R541–550. doi: 10.1152/ajpregu.00016.2006
178. Basbaum AII, Bautista DM, Scherrer G, Julius D. Cellular and molecular mechanisms of pain. *Cell* (2009) 139:267–84. doi: 10.1016/j.cell.2009.09.028
179. Canning BJ, Mori N, Mazzone SB. Vagal afferent nerves regulating the cough reflex. *Respir Physiol Neurobiol* (2006) 152:223–42. doi: 10.1016/j.resp.2006.03.001
180. Dubin AE, Patapoutian A. Nociceptors: the sensors of the pain pathway. *J Clin Invest* (2010) 120:3760–72. doi: 10.1172/JCI42843
181. Caceres AI, Brackmann M, Elia MD, Bessac BF, del Camino D, D'Amours M, et al. A sensory neuronal ion channel essential for airway inflammation and hyperreactivity in asthma. *Proc Natl Acad Sci U S A* (2009) 106:9099–104.
182. Talbot S, Abdulnour RE, Burkett PR, Lee S, Cronin SJ, Pascal MA, et al. Silencing Nociceptor Neurons Reduces Allergic Airway Inflammation. *Neuron* (2015) 87:341–54. doi: 10.1016/j.neuron.2015.06.007
183. Pinho-Ribeiro FA, Verri WA, Chiu IM. Nociceptor Sensory Neuron-Immune Interactions in Pain and Inflammation. *Trends Immunol* (2017) 38:5–19. doi: 10.1016/j.it.2016.10.001
184. Blake KJ, Jiang XR, Chiu IM. Neuronal Regulation of Immunity in the Skin and Lungs. *Trends Neurosci* (2019) 42:537–51. doi: 10.1016/j.tins.2019.05.005
185. Russell FA, King R, Smillie SJ, Kodji X, Brain SD. Calcitonin gene-related peptide: physiology and pathophysiology. *Physiol Rev* (2014) 94:1099–142. doi: 10.1152/physrev.00034.2013
186. Walker CS, Conner AC, Poyner DR, Hay DL. Regulation of signal transduction by calcitonin gene-related peptide receptors. *Trends Pharmacol Sci* (2010) 31:476–83. doi: 10.1016/j.tips.2010.06.006
187. Chiu IM, Heesters BA, Ghasemlou N, Von Hehn CA, Zhao F, Tran J, et al. Bacteria activate sensory neurons that modulate pain and inflammation. *Nature* (2013) 501:52–7. doi: 10.1038/nature12479

188. Baral P, Umans BD, Li L, Wallrapp A, Bist M, Kirschbaum T, et al. Nociceptor sensory neurons suppress neutrophil and γδ T cell responses in bacterial lung infections and lethal pneumonia. *Nat Med* (2018) 24:417–26. doi: 10.1038/nm.4501
189. Kuo CS, Krasnow MA. Formation of a Neurosensory Organ by Epithelial Cell Slithering. *Cell* (2015) 163:394–405. doi: 10.1016/j.cell.2015.09.021
190. Noguchi M, Sumiyama K, Morimoto M. Directed Migration of Pulmonary Neuroendocrine Cells toward Airway Branches Organizes the Stereotypic Location of Neuroepithelial Bodies. *Cell Rep* (2015) 13:2679–86. doi: 10.1016/j.celrep.2015.11.058
191. Xu H, Ding J, Porter CBM, Wallrapp A, Tabaka M, Ma S, et al. Transcriptional Atlas of Intestinal Immune Cells Reveals thatNeuropeptide α-CGRP Modulates Group 2 Innate Lymphoid Cell Responses. *Immunity* (2019) 51:696–708.e699. doi: 10.1016/j.immuni.2019.09.004
192. Said SII, Mutt V. Polypeptide with broad biological activity: isolation from small intestine. *Science* (1970) 169:1217–8. doi: 10.1126/science.169.3951.1217
193. Lara-Marquez M, O'Dorisio M, O'Dorisio T, Shah M, Karacay B. Selective gene expression and activation-dependent regulation of vasoactive intestinal peptide receptor type 1 and type 2 in human T cells. *J Immunol* (2001) 166:2522–30. doi: 10.4049/jimmunol.166.4.2522
194. Calvo JR, Pozo D, Guerrero JM. Functional and molecular characterization of VIP receptors and signal transduction in human and rodent immune systems. *Adv Neuroimmunol* (1996) 6:39–47. doi: 10.1016/S0960-5428(96)00005-8
195. Dickson L, Finlayson K. VPAC and PAC receptors: From ligands to function. *Pharmacol Ther* (2009) 121:294–316. doi: 10.1016/j.pharmthera.2008.11.006
196. Moriyama M, Furue H, Katafuchi T, Teranishi H, Sato T, Kano T, et al. Presynaptic modulation by neuromedin U of sensory synaptic transmission in rat spinal dorsal horn neurones. *J Physiol* (2004) 559:707–13. doi: 10.1113/jphysiol.2004.070110
197. Howard AD, Wang R, Pong SS, Mellin TN, Strack A, Guan XM, et al. Identification of receptors for neuromedin U and its role in feeding. *Nature* (2000) 406:70–4. doi: 10.1038/35017610
198. Nakahara K, Kojima M, Hanada R, Egi Y, Ida T, Miyazato M, et al. Neuromedin U is involved in nociceptive reflexes and adaptation to environmental stimuli in mice. *Biochem Biophys Res Commun* (2004) 323:615–20. doi: 10.1016/j.bbrc.2004.08.136
199. Hedrick JA, Morse K, Shan L, Qiao X, Pang L, Wang S, et al. Identification of a human gastrointestinal tract and immune system receptor for the peptide neuromedin U. *Mol Pharmacol* (2000) 58:870–5. doi: 10.1124/mol.58.4.870
200. Moriyama M, Fukuyama S, Inoue H, Matsumoto T, Sato T, Tanaka K, et al. The neuropeptide neuromedin U activates eosinophils and is involved in allergen-induced eosinophilia. *Am J Physiol Lung Cell Mol Physiol* (2006) 290:L971–977. doi: 10.1152/ajplung.00345.2005
201. Ohki-Hamazaki H, Neuromedin B. *Prog Neurobiol* (2000) 62:297–312. doi: 10.1016/S0301-0082(00)00004-6
202. Gajjar S, Patel BM. Neuromedin: An insight into its types, receptors and therapeutic opportunities. *Pharmacol Rep* (2017) 69:438–47. doi: 10.1016/j.pharep.2017.01.009
203. Krane IM, Naylor SL, Helin-Davis D, Chin WW, Spindel ER. Molecular cloning of cDNAs encoding the human bombesin-like peptideneuromedin B. Chromosomal localization and comparison to cDNAs encoding its amphibian homolog ranatensin. *J Biol Chem* (1988) 263:13317–23.
204. Wada E, Way J, Lebacq-Verheyden AM, Battey JF, Neuromedin B. and gastrin-releasing peptide mRNAs are differentially distributed in the rat nervous system. *J Neurosci* (1990) 10:2917–30. doi: 10.1523/JNEUROSCI.10-09-02917.1990
205. Khumalo J, Kirstein F, Hadebe S, Brombacher F. IL-4Rα signalling in CD4+CD25+FoxP3+ T regulatory cells restrain airway inflammation via limiting local tissue IL-33. *JCI Insight* (2020) 5:136206. doi: 10.1172/jci.insight.136206
206. Howard E, Lewis G, Galle-Treger L, Hurrell BP, Helou DG, Shafiei-Jahani P, et al. IL-10 production by ILC2s requires Blimp-1 and cMaf, modulatescellular metabolism and ameliorates airway hyperreactivity. *J Allergy ClinImmunol* (2020) 6:S0091-6749(20)31234-3. doi: 10.1016/j.jaci.2020.08.024
207. Xiao Q, He J, Lei A, Xu H, Zhang L, Zhou P, et al. PPARγ enhances ILC2 function during allergic airwayinflammation via transcription regulation of ST2. *Mucosal Immunol* (2020). doi: 10.1038/s41385-020-00339-6
208. Helou DG, Shafiei-Jahani P, Lo R, Howard E, Hurrell BP, Galle-Treger L, et al. PD-1 pathway regulates ILC2 metabolism and PD-1 agonist treatmentameliorates airway hyperreactivity. *Nat Commun* (2020) 11:3998. doi: 10.1038/s41467-020-17813-1
209. Miller MM, Patel PS, Bao K, Danhorn T, O'Connor BP, Reinhardt RL, et al. BATF acts as an essential regulator of IL-25-responsive migratoryILC2 cell fate and function. *Sci Immunol* (2020) 5(43):eaay3994. doi: 10.1126/sciimmunol.aay3994
210. Huang Y, Mao K, Chen X, Sun MA, Kawabe T, Li W, et al. S1P-dependent interorgan trafficking of group 2 innate lymphoidcells supports host defense. *Science* (2018) 359:114–9. doi: 10.1126/science.aam5809
211. Akama Y, Park EJ, Satoh-Takayama N, Gaowa A, Ito A, Kawamoto E, et al. Sepsis Induces Deregulation of IL-13 Production and PD-1 Expression in Lung Group 2 Innate Lymphoid Cells. *Shock* (2020). doi: 10.1097/SHK.0000000000001647
212. Xu H, Xu J, Xu L, Jin S, Turnquist HR, Hoffman R, et al. Interleukin-33 contributes to ILC2 activation and early inflammation-associated lung injury during abdominal sepsis. *Immunol Cell Biol* (2018) 96:935–47. doi: 10.1111/imcb.12159
213. Wang W, Cohen JA, Wallrapp A, Trieu KG, Barrios J, Shao F, et al. Age-Related Dopaminergic Innervation Augments T Helper 2-TypeAllergic Inflammation in the Postnatal Lung. *Immunity* (2019) 51:1102–1118.e1107. doi: 10.1016/j.immuni.2019.10.002
214. O'Leary CE, Schneider C, Locksley RM. Tuft Cells-Systemically Dispersed Sensory Epithelia Integrating Immune and Neural Circuitry. *Annu Rev Immunol* (2019) 37:47–72. doi: 10.1146/annurev-immunol-042718-041505
215. Zhang K, Xu X, Pasha MA, Siebel CW, Costello A, Haczku A, et al. Cutting Edge: Notch Signaling Promotes the Plasticity of Group-2 Innate Lymphoid Cells. *J Immunol* (2017) 198:1798–803. doi: 10.4049/jimmunol.1601421
216. Bernink JH, Ohne Y, Teunissen MBM, Wang J, Wu J, Krabbendam L, et al. c-Kit-positive ILC2s exhibit an ILC3-like signature that may contribute to IL-17-mediated pathologies. *Nat Immunol* (2019) 20:992–1003. doi: 10.1038/s41590-019-0423-0
217. Silver JS, Kearley J, Copenhaver AM, Sanden C, Mori M, Yu L, et al. Inflammatory triggers associated with exacerbations of COPD orchestrate plasticity of group 2 innate lymphoid cells in the lungs. *Nat Immunol* (2016) 17:626–35. doi: 10.1038/ni.3443
218. Wiegert JS, Mahn M, Prigge M, Printz Y, Yizhar O. Silencing Neurons: Tools, Applications, and Experimental Constraints. *Neuron* (2017) 95:504–29. doi: 10.1016/j.neuron.2017.06.050
219. Fenno L, Yizhar O, Deisseroth K. The development and application of optogenetics. *Annu Rev Neurosci* (2011) 34:389–412. doi: 10.1146/annurev-neuro-061010-113817

Conflict of Interest: The authors declare that the research was conducted in the absence of any commercial or financial relationships that could be construed as a potential conflict of interest.

frontiers in Immunology

ORIGINAL RESEARCH
published: 18 February 2021
doi: 10.3389/fimmu.2020.581911

The Cholinergic System Contributes to the Immunopathological Progression of Experimental Pulmonary Tuberculosis

Leon Islas-Weinstein[1], Brenda Marquina-Castillo[1], Dulce Mata-Espinosa[1], Iris S. Paredes-González[1], Jaime Chávez[2], Luciana Balboa[3], José Luis Marín Franco[3], Daniel Guerrero-Romero[4], Jorge Alberto Barrios-Payan[1] and Rogelio Hernandez-Pando[1]**

[1] Division of Experimental Pathology, Department of Pathology, National Institute of Medical Sciences and Nutrition Salvador Zubirán, México City, Mexico, [2] Department of Bronchial Hyperreactivity, National Institute of Respiratory Diseases (Mexico), Mexico City, Mexico, [3] Laboratorio de Inmunología de Enfermedades Respiratorias, Instituto de Medicina Experimental del National Scientific and Technical Research Council (CONICET), Academia Nacional de Medicina, Buenos Aires, Argentina, [4] Departamento de Matemáticas, Escuela Superior de Física y Matemáticas, Instituto Politécnico Nacional, Mexico City, Mexico

OPEN ACCESS

Edited by:
Maureen Ann Cox, University of Oklahoma Health Sciences Center, United States

Reviewed by:
Suraj Sable, Centers for Disease Control and Prevention (CDC), United States
Tobias Dallenga, Research Center Borstel (LG), Germany

***Correspondence:**
Jorge Alberto Barrios-Payan
qcjbp77@yahoo.com.mx
Rogelio Hernandez-Pando
rhdezpando@hotmail.com

Specialty section:
This article was submitted to Molecular Innate Immunity, a section of the journal Frontiers in Immunology

Received: *10 July 2020*
Accepted: *22 December 2020*
Published: *18 February 2021*

Citation:
Islas-Weinstein L, Marquina-Castillo B, Mata-Espinosa D, Paredes-González IS, Chávez J, Balboa L, Marín Franco JL, Guerrero-Romero D, Barrios-Payan JA and Hernandez-Pando R (2021) The Cholinergic System Contributes to the Immunopathological Progression of Experimental Pulmonary Tuberculosis. Front. Immunol. 11:581911. doi: 10.3389/fimmu.2020.581911

The cholinergic system is present in both bacteria and mammals and regulates inflammation during bacterial respiratory infections through neuronal and non-neuronal production of acetylcholine (ACh) and its receptors. However, the presence of this system during the immunopathogenesis of pulmonary tuberculosis (TB) *in vivo* and in its causative agent *Mycobacterium tuberculosis* (*Mtb*) has not been studied. Therefore, we used an experimental model of progressive pulmonary TB in BALB/c mice to quantify pulmonary ACh using high-performance liquid chromatography during the course of the disease. In addition, we performed immunohistochemistry in lung tissue to determine the cellular expression of cholinergic system components, and then administered nicotinic receptor (nAChR) antagonists to validate their effect on lung bacterial burden, inflammation, and pro-inflammatory cytokines. Finally, we subjected *Mtb* cultures to colorimetric analysis to reveal the production of ACh and the effect of ACh and nAChR antagonists on *Mtb* growth. Our results show high concentrations of ACh and expression of its synthesizing enzyme choline acetyltransferase (ChAT) during early infection in lung epithelial cells and macrophages. During late progressive TB, lung ACh upregulation was even higher and coincided with ChAT and α7 nAChR subunit expression in immune cells. Moreover, the administration of nAChR antagonists increased pro-inflammatory cytokines, reduced bacillary loads and synergized with antibiotic therapy in multidrug resistant TB. Finally, *in vitro* studies revealed that the bacteria is capable of producing nanomolar concentrations of ACh in liquid culture. In addition, the administration of ACh and nicotinic antagonists to *Mtb* cultures induced or inhibited bacterial proliferation, respectively. These results suggest that *Mtb* possesses a cholinergic system and upregulates the lung non-neuronal cholinergic system, particularly during late progressive TB. The upregulation of the cholinergic system during infection could aid both bacterial growth and immunomodulation within the lung to favor disease

progression. Furthermore, the therapeutic efficacy of modulating this system suggests that it could be a target for treating the disease.

Keywords: cholinergic, pulmonary inflammation, mycobacterium tuberculosis, acetylcholine, nAChR antagonism, immune response, tuberculosis, choline acetyltransferase

INTRODUCTION

The cholinergic system is responsible for the coordinated synthesis, effects, and degradation of acetylcholine (ACh), an endogenous nicotinic receptor (nAChR) and muscarinic receptor (mAChR) agonist (1). Although ACh is the primary parasympathetic neurotransmitter of the airways, non-neuronal cells are crucial sources of ACh production (2). Through nAChR and mAChR stimulation, ACh modulates airway inflammation in chronic inflammatory lung disease (3, 4) and in bacterial respiratory infection (5–9). However, its dynamics during pulmonary tuberculosis (TB) remain unknown.

Visceral afferent neurons monitor and transmit information from strategically located peripheral sites associated with infection and injury, and through a reflex fashion return efferent autonomic signals to regulate localized immune responses. In the lungs, vagal sensory neurons are activated during bacterial or viral infection, cellular damage, and in airway allergenic responses (10). Cholinergic modulation of the lung's immune response during normal conditions and in inflammatory conditions is partly mediated by the "pulmonary parasympathetic inflammatory reflex" (PPIR) (11), which is comparable to the spleen's inflammatory reflex (12). This reflex is initiated with stimulation of C-fiber receptors, cytokine receptors and toll-like receptors in pulmonary afferent vagus nerve fibers and neural signal relay to the solitary tract nuclei. Subsequent activation of the dorsal motor nucleus causes efferent vagus nerve activation and ensuing neuronal and non-neuronal ACh release within the lung. The released ACh downregulates local leukocyte proinflammatory cytokines output through NF-κB interference (11). Importantly, microorganisms may have developed strategies to hijack the PPIR to induce pulmonary immunomodulation and infection progression (5, 7, 11, 13).

Despite the widespread use of antibiotic combination therapy, TB remains the most lethal infectious disease worldwide and many aspects of its pathogenesis remain unknown (14). ACh has not been studied in a pulmonary TB context. However, several studies have demonstrated that nicotine, a major constituent of cigarette smoke, worsens disease outcomes through nAChR stimulation (15–17). Additionally, receptors involved in the PPIR are implicated in the pathogenesis of active TB (18, 19). Consequently, the purpose of our study was to determine if the cholinergic system is upregulated during pulmonary TB using an *in vivo* experimental model (20).

We found upregulation of the lung's extraneuronal cholinergic system during early infection and an even greater potentiation during advanced disease. Furthermore, administering nicotinic ACh receptor (nAChR) α7 and α4β2 antagonists reduced bacterial counts and presented synergism with second-line antibiotics. Finally, we demonstrated that *Mtb* produces ACh and that its growth is potentiated with nanomolar quantities of ACh and inhibited with nAChR antagonists.

MATERIALS AND METHODS

Mice

Pathogen-free, 6–8-week-old male BALB/c mice (aprox. weight 22g), were obtained from the animal facilities of the Salvador Zubirán National Institute of Medical Sciences and Nutrition (INCMNSZ). All work was done according to the guidelines of the Mexican Constitution law NOM 062–200-1999, and approval of the ethical committee for animal experimentation of the INCMNSZ under governmental permit 224. Animals were monitored daily and euthanasia with pentobarbital (Nembutal, 400 mg/kg) was carried out before sample obtainment, as well as on any animal that presented signs of respiratory insufficiency, accentuated cachexia or full immobilization. Mice euthanized for sample obtainment underwent exsanguination by bleeding out the axillary vein. All mouse and sample protocols were carried out in biosafety level III cabinets.

Induction of Experimental Pulmonary Tuberculosis

Bacterial cultures of the reference strain H37Rv and the multidrug resistant (MDR) isolate CIBIN-99 were prepared as previously described (19, 20). For infection assays, mid-log phases were used. Experimental pulmonary tuberculosis was induced as previously described (20, 21). Mice were anesthetized briefly before inoculation in acrylic lidded boxes through inhalation of 2% sevoflurane vapor (Abbott Laboratories, IL, USA) in 2 L of O_2. Mice were afterwards immobilized on a unicel cardboard covered by aluminum and infected by the non-invasive instillation (*via* the oro-tracheal route using a rigid stainless steel cannula [Thomas Scientific, Swedesboro, NJ] connected to an insulin syringe) of 2.5×10^5 H37Rv *Mtb* or 3.25×10^4 MDR *Mtb* live bacilli resuspended in 100 µl of sterile isotonic saline solution. Mice were grouped into five-mouse cages that were fitted with microisolators and connected to negative pressurizers within an animal biosafety level III facility.

Quantification of Lung Acetylcholine

Lungs from infected mice were obtained at 1, 3, 7, 14, 21, 28, and 60 days after infection with *Mtb* and stored at -80°C. Acetylcholine and choline concentrations in lung homogenates were measured by cation exchange HPLC-EC detection as described by Potter et al. (22). Briefly, an analytic column for ACh and choline (MF-6150; Bioanalytical Systems, West

Lafayette, IN) and an immobilized enzyme reactor (Bioanalytical Systems) attached in tandem were coupled to the HPLC (model 9012; Varian, Walnut Creek, CA) and connected to the electrochemical detector (Coulochem II; ESA, Chelmsford, MA). For this technique, the isocratic mobile phase (50 mM Tris/$NaClO_4$ plus 1% ProClin reagent, pH 8.5) was pumped at a rate of 1 ml/min. Standard curves for ACh and choline (1–100 nM) were used for calibration. The system's detection limit was ~0.1 nM for both molecules using 15-µl of the sample. Data were stored and analyzed using a data acquisition and analysis software (Star Chromatography Workstation v4.01, Varian). Total ACh was obtained by adding ACh and choline concentrations and adjusted to protein content (Bradford's method) and expressed as µmol/mg protein.

Immunohistochemistry

After removing the right lung for HPLC analysis, the left lungs of BALB/c mice were endotracheally perfused with absolute ethanol and embedded into paraffin blocks. Immunohistochemistry triplicate sections 5 µm thick belonging to three different mice per day of the infection kinetic were mounted on silane-coated slides, deparaffinized and rehydrated. Heat-induced epitope retrieval was carried out using 0.01 mol/L citrate buffer (pH 6.2) and immersing the slides for 10min into a 95°C water bath. The endogenous peroxidase was quenched using a rabbit polydetector peroxidase blocker (Bio SB). Slides were incubated overnight with 200 µl of rabbit anti-mouse polyclonal antibody [ChAT (Santa Cruz, sc-20672 1:250 dilution), α7 nAChR (Santa Cruz, sc-5544, 1:100 dilution). Afterwards, the slides were incubated for 30 mins with mouse/rabbit immunodetector biotin link and rabbit polydetector HRP Label (Bio SB) and bound antibodies were detected with the Rabbit Polydetector DAB kit (Bio SB, Santa Barbara California).

Treatment Administration

Mice infected with *Mtb* H37Rv were separated into three groups receiving treatment three times per week (Monday, Wednesday, and Friday). The first group received intragastric administration of the α7 nAChR antagonist methyllycaconitine (MLA, Sigma Aldrich - 3 mg/kg) (23). The second group received endotracheal administration, under anesthesia with sevoflurane, of the α4β2 nAChR antagonist dihydro-beta-erythroidine (24) (DHβE, Tocris Bioscience—0.19 mg/kg). The intratracheal dose determination of DHβE was obtained using Akhila et al's method (25). The third group received 100 µl of saline solution (vehicle) and served as the control group. The two nAChR antagonist treatment groups used for H37Rv infected mice were repeated for MDR *Mtb* infected mice.

To determine if the nAChR antagonists could have synergy with antibiotic treatment, MDR infected mice were additionally treated with an adjusted WHO-recommended regimen consisting of: 1.1 mg/kg of amikacin (A, Sigma Aldrich), 0.55 mg/kg of ethionamide (Et, Sigma Aldrich), 1.1 mg/kg of moxifloxacin (M, Bayer) and 1.65 mg/kg of pyrazinamide (Z, Sigma Aldrich) (26). AEtMZ was administered daily for 5 days per week (Monday–Friday) and served as the exclusive treatment of the control group of MDR TB treated mice. All pharmacological treatments received by mice were suspended in 100 µl of sterile isotonic saline solution, prepared on a weekly basis and stored at 4°C. Treatment schedules began 60 days after infection and continued for a 60-day period. Two independent experiments were performed.

Measuring Colony-Forming Units

Groups of four animals were euthanized 30 and 60 days after treatment initiation (see section above). In addition, groups of 4 mice infected with MDR *Mtb* were euthanized 7 and 14 days after commencing treatment. Following hilar lymph node and thymic tissue removal, right lungs were frozen and kept at −70°C for the subsequent measurement of CFUs as previously described (27, 28). In brief, lungs were exposed to 40-second cycles in a FastPrep homogenizer (MP biomedicals) within sterile tubes containing 1ml of isotonic saline solution (following the manufacturer's recommendations). Four serial 10-fold dilutions of each homogenate were spread onto duplicate plates containing Bacto Middle brook 7H10 agar (Difco Labs, Detroit MI, USA) enriched with oleic acid, albumin, catalase, and dextrose; CFU counting was done after a 21-day incubation period.

Morphometric Analysis

After removing the right lungs for CFU determination, the left lungs of three or four mice from each treatment group from two independent experiments were fixed with alcohol perfused through the intratracheal route. Sagittal lung sections were prepared for histological analysis and stained with hematoxylin and eosin. To determine pneumonic area percentage, each slide was photographed using a camera system (Olympus DP70, Milton Keynes) that obtained an image of the complete lung section, which corresponded to 100% of the lung area. Subsequently, pneumonic areas (foci of consolidation of leukocyte-rich infiltrate in airway walls and adjacent alveolar spaces) were delimited and quantified using an automated histology system (Q-Win Leica 500). Finally, the percentage of the lung surface area affected by pneumonia, was determined. Measurements were carried out blinded with respect to the experimental treatment to which each slide belonged.

Gene Expression of Lung Proinflammatory Molecules

These assays were performed as previously described (28). Briefly, after removing the right lungs for CFU determination, the left lungs of three or four mice from each treatment group were obtained from two independent experiments. Samples from the evaluated mice were stored in 1.5ml cryotubes containing 1ml of RLT plus, frozen immediately in liquid nitrogen and stored later at -80 degrees centigrade until processing. Each sample was homogenized with zirconia and flint beads (MP Biomedicals) in the FastPrep-24TM equipment for three cycles of 20 s. The RNA extraction was carried out using the commercial RNeasy Mini (Qiagen) kit, following the manufacturer's instructions. RNA concentration and purity were determined by spectrophotometry (EPOCH 2

spectrophotometer, A260/280). Subsequently, 100 ng of RNA from each lung were used for cDNA production by reverse transcription following the indications of the commercial OmniScript kit (Qiagen). From the complementary DNA (cDNA) obtained for each sample, real-time reverse transcription semi-quantitative PCR (RT-qPCR) was performed with the PCR-RT 7500 instrument (Applied Biosystems) and the QuantiTect SYBR Green Mastermix commercial kit (Qiagen). The expression of iNOS, TNF-α, IFN-γ, and IL-17A transcripts was determined, whose previously reported sequence is specified in **Supplementary Table 1**. The results were standardized with respect to the mRNA content of the β-actin housekeeping gene (whose primer sequence is also specified in **Supplementary Table 1**) of each sample. The appropriate standard curve was included in the individual gene detection, in addition to reverse transcription negative controls. The cycle conditions used were as follows: initial denaturation at 95°C for 15min, followed by 40 cycles at 95 degrees for 20 s, 60 degrees for 20 s, and 72 degrees for 34 s. Data analysis was calculated according to the rate of change in gene expression using the equation described by Livak and the method of 2-ΔΔCT occupying a minimum limit of 35 cycles of TC detection (29).

Minimum Growth and Inhibitory Concentration Assays

These assays were performed as previously described (28). Briefly, 3 x 10^5 CFUs (for the ACh assay) or 6 x 10^5 CFUs (for the nAChR antagonist assay) of the *Mtb* strain H37 Rv were placed in 100 µl of 7H9-OADC supplemented growth media in each well of a 96-well plate. Progressive concentrations of ACh [similar to those reported in human lungs (30)] or nAChR antagonists [in the range of the reported pharmacological dose (23, 24)] diluted in 100 µl of 7H9 medium were subsequently added. A well triplicate with bacteria in 7H9 medium without compounds was used as a positive (bacterial) control and a second triplicate without bacteria was used as a negative (medium) control. In addition, isoniazid (INH) at its minimum inhibitory concentration (0.5 µg/ml) and a solvent control containing saline solution and 7H9 medium were added. Plates were then placed in a humidified incubator at 37˚C with 5% CO2 for 7 days. Four hours prior to the end of the exposure period, MTS (Owen's reagent, 20 µl/well) was added and its conversion to formazan was tracked every hour spectrophotometrically at 492 nm (BioTek Instruments, ELX 800, USA) and used as an indirect measure of bacterial quantity. The number of bacteria was confirmed counting CFUs taken from 30 µl of the control wells, in addition to the wells exposed to the maximum and minimum concentrations of ACh and conducting four serial 10-fold dilutions into 7H-10 agar plates.

Macrophage Phagocytosis Assay

The assays were realized as previously described (27). Briefly, murine BALB/c alveolar macrophages (MHS cell line, ATCC CRL-2019) were incubated for 2h in duplicate wells (6 x 10^4 cells per well) containing 200 µl of RPMI medium supplemented with Fetal Bovine Serum within a 96-well plate with no *Mtb* strains (negative control) or at a multiplicity of infection (MOI) of 5:1 with the following *Mtb* strains (31): H37 Ra (non-virulent strain), 5186 (hypervirulent strain), live and heat-inactivated H37Rv strain. Subsequently, the supernatants were removed and cells were washed 3 times with Fetal Bovine Serum free RPMI supplemented with 1% streptomycin and once with PBS cell solution and were later incubated in 200 µl of Fetal Bovine Serum free RPMI for 2h. The well contents were then collected and MH-S cells were lysed through pipetting, after having added the assay buffer and were later centrifuged at 25,830 x g for 2 mins at 4°C to retrieve supernatants. The supernatants were later collected and kept on ice and subsequent CFU analysis was carried out as a control measure.

Determination of Acetylcholine in Mycobacteria Growth Culture Medium and in Macrophage Supernatants by Colorimetric Analysis

For colorimetric assays, 3 x 10^5 CFUs of freshly grown bacterial cultures were obtained, 2, 10, and 18 days after culture initiation (lag, log and stationary growth phases respectively). Each culture sample was diluted in 600 µl of 7H9 medium, centrifuged at 25,830 x g for 2min at 4°C and the bacterial supernatants collected and kept on ice. The remaining bacterial pellet was complemented with 500 µl of assay buffer (Colorimetric Acetylcholine Assay kit, Abcam, ab65345) and exposed to three 20-s cycles at 5500 RPMs in the Precellys 24 tissue homogenizer using the bacterial lysing CK01 kit (Bertin Instruments, France). The samples were then centrifuged at 25,830 x g for 2min at 4°C and the bacterial lysate supernatants collected and kept on ice. Standards, choline probe, acetylcholinesterase solution and the enzyme mix were prepared according to the manufacturer's instructions of the colorimetric acetylcholine assay kit (Abcam, ab65345). Duplicate wells containing 50 µl of standard curve, reaction mix (background wells), bacterial, and cell samples were prepared with and without acetylcholinesterase to determine total and free choline values respectively. Afterwards, 50 µl of the reaction mix was added to each well and the plate was left incubating at RT for 30min protected from light. A colorimetric reading at OD 570 nm was subsequently made and values were extrapolated from the standard curve. Acetylcholine concentrations were obtained by subtracting free choline from total choline values. In addition, a medium control consisting of 7H9 media without bacterial or cell samples was added and its colorimetric value was subtracted from the value of each sample.

Statistical Analysis

The data represented in **Figures 1** and **5**, **6** were analyzed using one way analysis of variance (ANOVA) followed by a Bonferroni correction for multiple comparisons and presented as either the median ± interquartile range or as the mean ± standard error of the mean (SEM) respectively. The data represented in **Figures 2**–**4** were analyzed using the Kruskal-Wallis test with Dunn's multiple comparison and presented as the median +

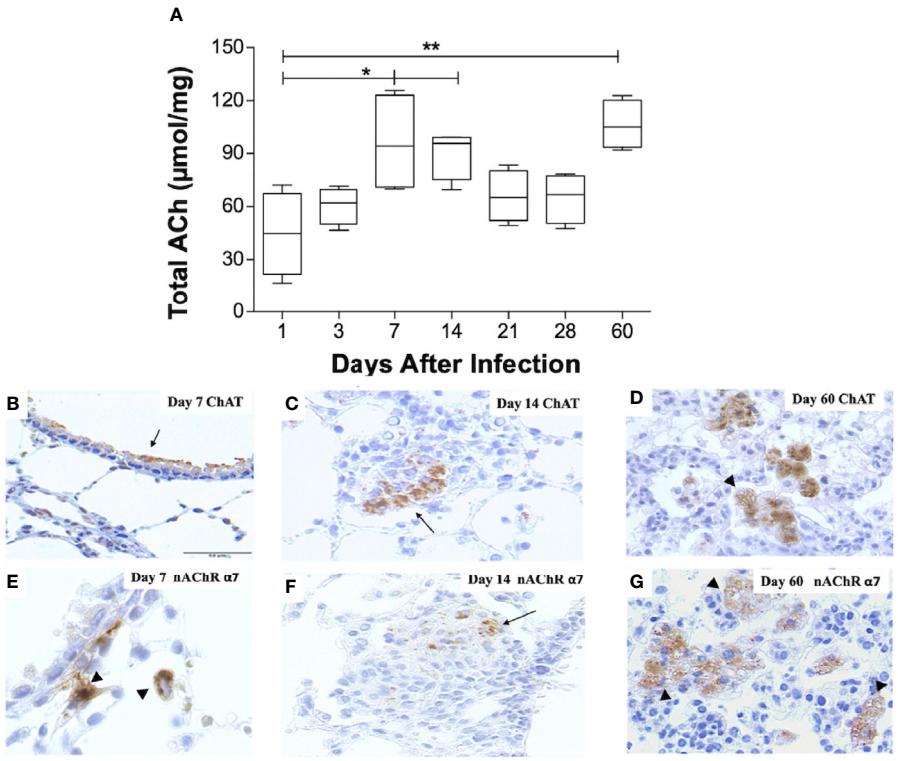

FIGURE 1 | Kinetics of ACh, ChAT, and the α7 nAChR subunit during pulmonary TB. Kinetics of ACh quantification determined by HPLC in BALB/C mice lung pairs infected with the Mtb strain H37Rv (box-and-whisker plots of ACh values). **(A)** Horizontal black lines within the boxes represent the median, while the lower and upper boundaries represent the 25th and 75th percentile, respectively. The upper and lower whiskers correspondingly outspread from the box toward the maximum and minimum values (n = 4 mice per time point/group). One-way ANOVA was used for significance testing, with Bonferroni's post-test for comparisons using lungs of mice from day 1 as the control group (*P < 0.05, **p < 0.01). Representative immunohistochemistry micrographs detecting ChAT and the nAChR α7 subunit **(B–G)**. Representative sections are shown by a 40x objective; bar, 50 um. At day 7 postinfection, there is mild ChAT immunostaining in the bronchial epithelium (arrow) **(B)**. Two weeks after infection, organized nodules constituted by inflammatory cells that correspond to granulomas showed some cells that exhibit ChAT immunostaining (arrow). **(C)**. After 60 days of infection, occasional macrophages with cytoplasmic vacuoles located in pneumonic areas show strong ChAT immunostaining (arrowheads) **(D)**. After one week of infection, some macrophages exhibit intense immunolabeling (arrowhead) of the α7 nAChR subunit **(E)**. Two weeks after infection, some cells in a granuloma show α7 nAChR immunostaining (arrow) **(F)**. After 60 days of infection, numerous vacuolated macrophages and lymphocytes located in pneumonic patches exhibit α7 nAChR immunostaining (arrowheads) **(G)**.

interquartile range. Tests were performed using GraphPad Prism Software, Inc. (version 8.0, La Jolla, USA).

RESULTS

Lung Acetylcholine Increases During Pulmonary Tuberculosis

To record pulmonary ACh concentrations during experimental TB, mouse lungs from representative days of the experimental kinetic underwent HPLC analysis (**Figure 1A**). ACh concentrations obtained during the first day after infection had a mean value of 45 µmol/mg, the lowest in all the kinetic. This mean value, therefore, served as a control to compare against other days. Comparison analysis revealed a two-fold increase ($P \leq 0.05$) in lung ACh concentrations 7 and 14 days after infection, which averaged a mean value of 93 µmol/mg. The highest ACh concentration ($P \leq 0.01$) was seen after 60 days of infection (106 µmol/mg). Thus, ACh concentrations were measurable during all the TB infection kinetic and showed two peaks, the first at early infection (days 7 and 14) and the highest concentration during late progressive disease (day 60).

Cholinergic Elements Are Upregulated During Disease Progression

To establish the expression of cholinergic elements (ChAT and α7 nAChR), during early (days 7 and 14) and late (day 60) infection with elevated ACh concentrations, lung tissue sections were studied by immunohistochemistry (**Figure 1**). Mice that had not received intratracheal inoculation of *Mtb* served as controls. Immunohistochemistry analysis of non-infected mice did not show ChAT or α7 nAChR staining (results not shown). However, bronchial epithelial cells and occasional scattered lung fibroblasts and alveolar macrophages in infected mice 7 days after infection display intense ChAT immune staining (**Figure 1B**). After 2 weeks of infection, the airway epithelium appears negative

to ChAT immunostaining, while scattered macrophages and macrophages in diffuse inflammatory infiltrates exhibit strong ChAT staining (**Figure 1C**). At these time points, macrophages show intracellular α7 nAChR staining (**Figures 1E, F**). During late disease (day 60 after infection), diffuse inflammatory infiltrates and particularly pneumonic patches reveal strong and widespread ChAT immunostaining (**Figure 1D**), while lung lymphocytes and macrophages express α7 nAChR immunostaining (**Figure 1G**).

Administration of nAChR Antagonists During Late Tuberculosis Reduces Lung Bacillary Burden but Not Inflammation

To gain insight into the impact of nAChR stimulation by ACh on bacterial burden and inflammation during pulmonary tuberculosis, mice received the α7 nAChR antagonist (MLA) and the α4β2 nAChR antagonist (DHβE) 60 days after infection. Compared with the control group, which only received vehicle treatment, MLA and DHβE administration produced a significant reduction in lung CFUs (**Figure 2A**) but not lung inflammation (**Figures 2B–E**).

Th1 and Th17 Associated Lung mRNA Transcripts Are Increased After the Administration of a nAChR Antagonist During Advanced Disease

To gain insight into the immunomodulatory effects generated by administering nAChR antagonists during pulmonary tuberculosis, mice were treated with the α4β2 antagonist DHβE, 60 days after infection. Compared with the control group, lung molecular transcripts of the Th1 cytokines TNF-α and IFN-γ and of inducible nitric oxide synthetase (iNOS), increased by more than two-fold, 60 days after the start of treatment (**Figures 3A–C**). Furthermore, administering the nAChR antagonist potentiated the transcription of IL-17A mRNA in the lungs, by approximately five times ($P \leq 0.001$) during the same time period (**Figure 3D**).

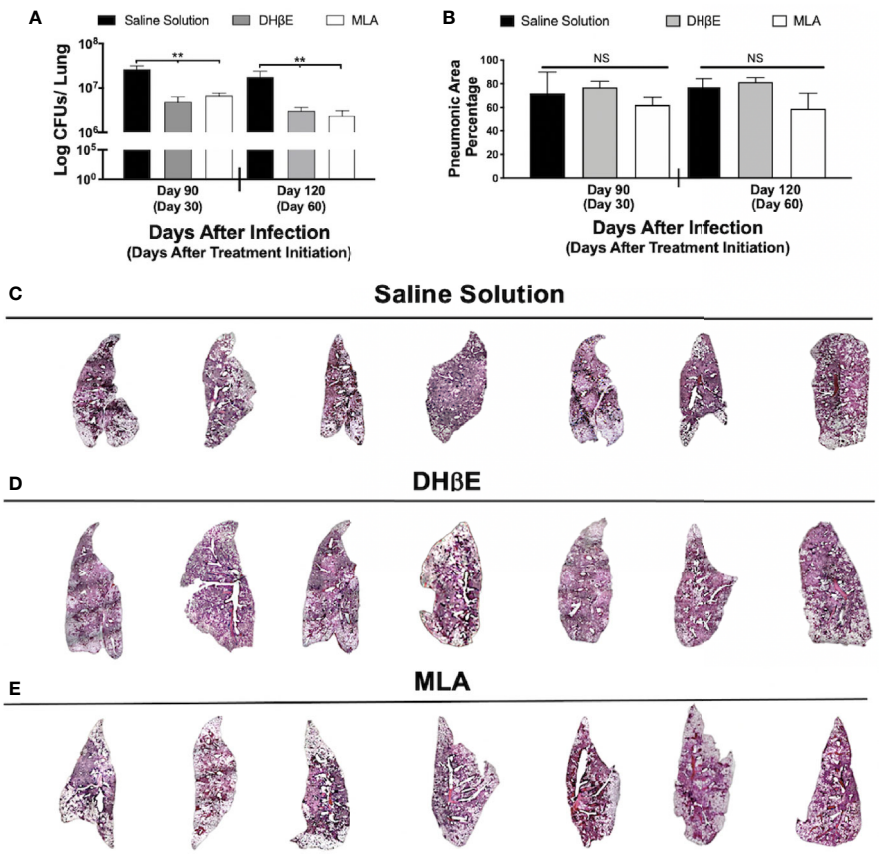

FIGURE 2 | Administration of nAChR antagonists during late infection with Mtb H37Rv reduces lung bacillary burden but does not reduce pneumonia. **(A)** After 60 days of infection with Mtb strain H37Rv BALB/c mice received saline solution (control mice, black bars) or a nAChR antagonist (dihydro-beta-erythroidine [DHβE] gray bars or methyllycaconitine [MLA] white bars). After 30 and 60 days of treatment initiation, quantification of colony forming units (CFU) determined bacilli load in the lungs. **(B)** Percentage of pneumonic areas of the mice infected lungs determined by automated morphometry. Automatized reconstruction of infected lungs after 60 days of treatment with saline solution **(C)**, DHβE **(D)**, or MLA **(E)**. Graphs represent pooled data from two experiments (N = 7 mice) and individual groups display median + interquartile range at each time-point. Significance testing was done using the Kruskal-Wallis test with Dunn's multiple comparison. NS refers to non-significant difference between groups (**$P < 0.01$).

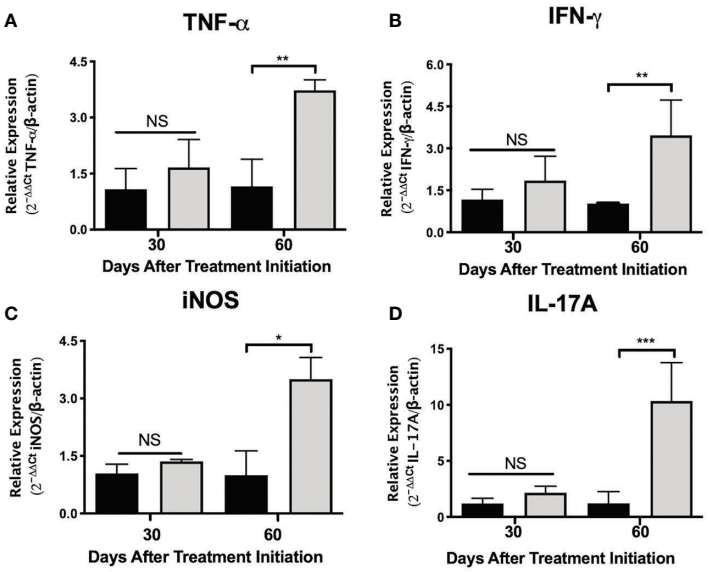

FIGURE 3 | Administration of nAChR antagonists during late tuberculosis infection increases the mRNA transcripts of proinflammatory mediators in the lungs. After 60 days of infection with the *Mtb* strain H37Rv, groups of BALB/c mice were treated with saline solution (control mice, black bars) or dihydro-beta-erythroidine (DHβE, a nAChR antagonist, gray bars). After 90 and 120 days of infection, the indicated gene expression of the proinflammatory molecules in the lungs was quantified by RT-PCR using the $2^{-\Delta\Delta CT}$method in relation to the expression of the β-actin housekeeping gene: TNG-α **(A)** IFN-γ **(B)** iNOS **(C)** and IL-17A **(D)**. Graphs represent pooled data from two experiments (N = 7 mice) and individual groups display mean + interquartile range at each time-point. Significance testing was done using the Kruskal-Wallis test with Dunn's multiple comparison. NS refers to a non-significant difference between groups (*P < 0.05, **P < 0.01, *** P < 0.001).

Blockade of Nicotinic Receptors During Late Tuberculosis Infection Synergizes With Antibiotic Therapy in MDR Infection by Reducing Lung Bacillary Burden and Lung Inflammation

To determine if nAChR antagonists could be useful in shortening the duration of second-line chemotherapy, 60 days after mice were infected with an MDR TB strain, treatment with second-line antibiotics alone or in combination with MLA and DHβE was initiated. After 14 days of treatment with MLA and antibiotics, a reduction in bacillary burden was observed compared with mice that received only antibiotics ($P \leq 0.01$, **Figure 4A**). Moreover, after 1 month, combined treatment with both nAChR antagonists and antibiotics produced a significant reduction in bacillary burden compared with mice that received only antibiotics ($P \leq 0.01$, **Figure 4A**) and additionally reduced pulmonary inflammation (**Figures 4B–E**).

Acetylcholine Stimulates *Mtb* Growth, While nAChR Antagonists Possess Bactericidal Activity

Mycobacterial incubation with ACh or nAChR antagonists determined the effect of bacterial growth to cholinergic agonism and antagonism; and this was assessed through colorimetric detection and CFU count. Nanomolar and micromolar concentrations of ACh increased optical density ($P \leq 0.01$ and $P \leq 0.05$ respectively, **Figure 5A**) and bacterial CFU numbers (**Figure 5B**). Conversely, the addition of incremental concentrations of nAChR antagonists reduced optical density (**Figure 5C**) and bacterial CFUs (**Figure 5D**). Thus, suggesting that ACh may function as a mycobacterial growth factor.

Diverse Acetylcholine Concentrations Are Present in *Mtb* Supernatants and Lysates During Its Growth Curve and in Supernatants of Infected Alveolar Macrophages

To determine if *Mtb* is capable of ACh production, supernatants and bacterial lysates of the *Mtb* strain H37Rv after 2, 10, and 18 days of culture initiation that corresponded to the lag, log, and stationary growth phases, respectively underwent ACh measurement using a colorimetric assay (**Figure 6A**). ACh was detected in supernatants (~35 nM) only during *Mtb*'s lag phase and in lysates predominantly during the logarithmic phase (~10 nM). Additionally, when murine alveolar macrophages of the MH-S cell line were infected with virulent (H37Rv and 5186) or avirulent (H37Ra) strains of *Mtb*, the virulent, but not the avirulent or heat-inactivated Mtb strains, induced ACh secretion in culture supernatants (**Figure 6B**).

DISCUSSION

The cholinergic system is present within the lungs where it aids in maintaining their proper physiological functioning. Altered lung cholinergic expression typically occurs in chronic

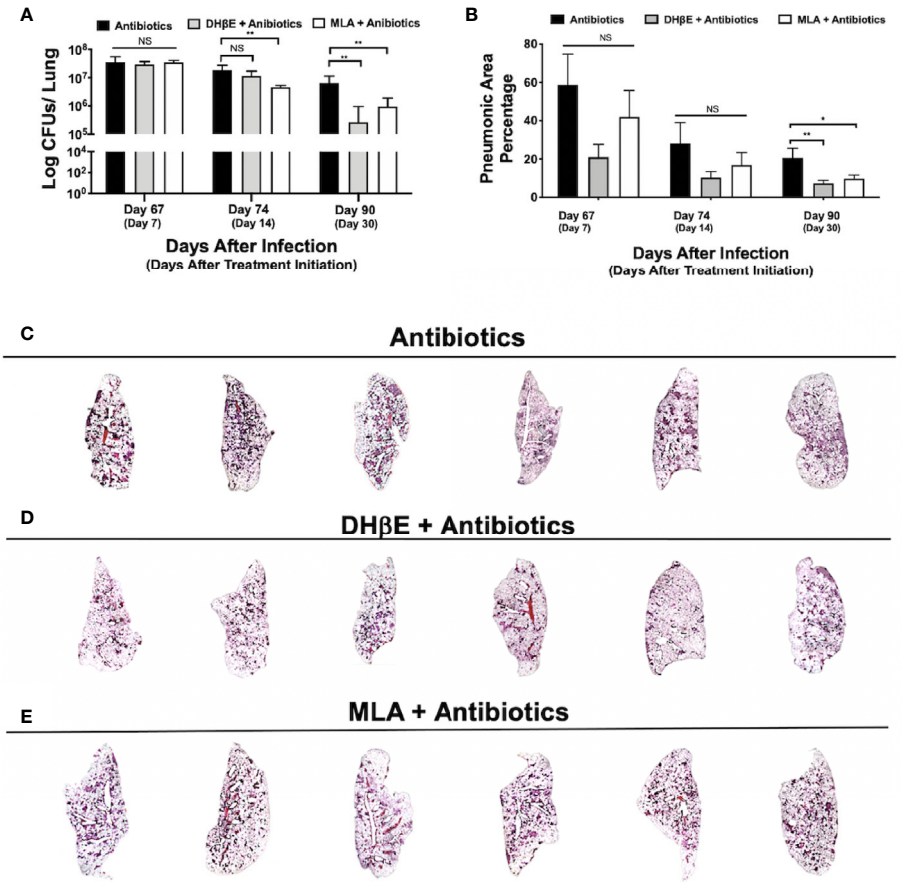

FIGURE 4 | Administration of nAChR antagonists synergizes with antibiotic therapy reducing bacillary burden and pneumonia. **(A)** Lung colony forming unit (CFU) determination in mice receiving the indicated treatments for 7, 14 and 30 days, following 60 days of infection with an MDR strain. **(B)** Percentage of lung area affected by pneumonia determined by automated morphometry. Graphs represent pooled data from two experiments (N = 6 mice) and individual groups display median + interquartile range at each time-point. Significance testing was done using the Kruskal-Wallis test with Dunn's multiple comparison. NS refers to a non-significant difference between groups (*P < 0.05, **P < 0.01). Lower panel **(C–E)** shows low power micrographs of the lungs after 90 days of the indicated treatment.

obstructive pulmonary disease (COPD) and results in pathological processes such as mucus hypersecretion and fibrosis (32, 33). Although alteration of the lung's cholinergic system has not previously been demonstrated in advanced pulmonary TB, pathological manifestations similar to those occurring in COPD are characteristically observed (33). Larcombe and colleagues previously demonstrated that basal cholinergic tone is completely absent in BALB/c mice (34). However, using a well-characterized BALB/c mouse TB model (20), we have shown for the first time that upregulation of the lung's non-neuronal cholinergic system occurs during experimental pulmonary TB. Our results suggest that cholinergic upregulation is generated as a consequence of *Mtb* infection favoring immunopathological progression and extensive lung inflammation partly due to the suppression of protective Th1 and Th17 immune responses.

Acetylcholine has generally been regarded as a classical neurotransmitter, despite the fact that it was first identified in the spleen, an immune organ (35). Currently, the capacity to synthesize ACh has been detected in both neuronal and non-neuronal cells, which release it in a rapid or slow fashion respectively (10, 36). ACh has been termed the 'universal cytotransmitter' in reference to its extensive expression (35) and almost every lung and airway cell is either a source or a potential cholinergic target. In fact, a myriad actions are regulated by ACh through stimulation of muscarinic and nicotinic ACh receptors (mAChRs and nAChRs), including bronchial epithelial cell growth, goblet cell secretion and regulation of mucosal surface barrier function (4, 37).

In our experimental model, we have observed substantial concentrations of lung ACh during the complete course of infection. Increased ACh concentrations in the lungs and other organs secondary to intracellular pathogen exposure have previously been described (38, 39). For example, the parainfluenza virus potentiates lung ACh concentrations through mRNA degradation and cleavage of sialic acid residues

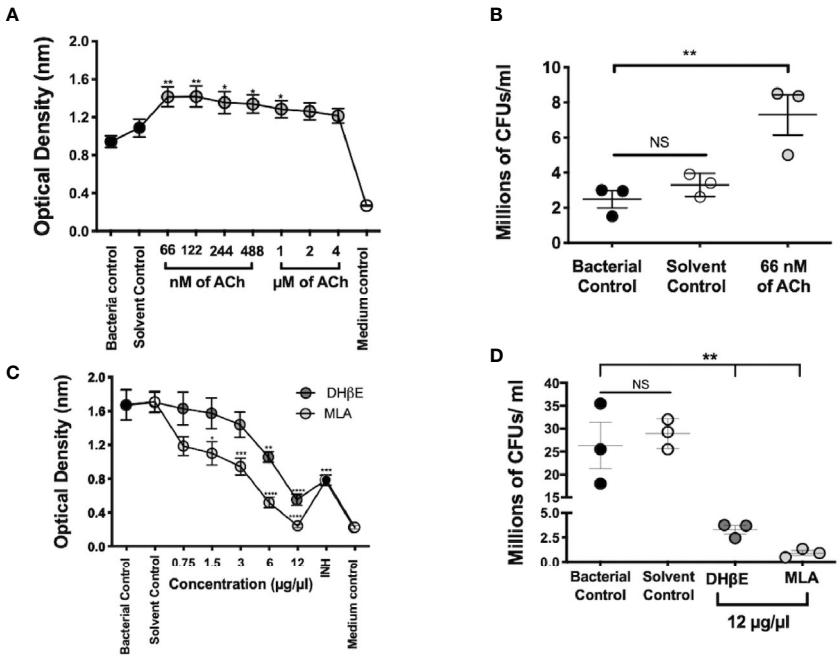

FIGURE 5 | Mtb growth is stimulated by ACh and is blocked by nAChR antagonists. Optical density served as a surrogate of the quantity of live bacteria after the addition of Owen's reagent and was confirmed by CFU counting. The optical density of 3×10^5 CFUs of the Mtb strain H37Rv in liquid culture increases after incubation with nanomolar and micromolar concentrations of ACh (gray circles). Bacteria exposed to nM concentrations and 1 µM concentrations of ACh showed a significant increase in optical density compared with bacterial and solvent controls, indicating bacterial proliferation **(A)**. Increase in mycobacterial CFU burden in bacteria incubated with the ACh concentration that presented the highest optical density (66 nM) compared with bacterial and solvent controls was confirmed through the determination and counting of CFUs **(B)**. Conversely, the incubation of 6×10^5 CFUs of the Mtb strain H37Rv after the addition of incremental concentrations of nAChR antagonists (gray circles) reduced their optical density **(C)** and CFU burden **(D)** compared with bacterial and solvent controls. Data expressed as the mean SEM of three wells and are representative of three independent experiments. ANOVA $P < 0.001$. Bonferroni's multiple comparison of values from the bacterial control (black circles), which was not exposed to any compound, with bacteria exposed to the solvent control (saline solution), isoniazid (INH), as well as different concentrations of ACh **(A)** or nicotinic antagonists **(B)** is shown (*$P < 0.05$, **$P < 0.01$ ***$P < 0.001$ ****$P < 0.0001$), NS refers to a non-significant difference between groups.

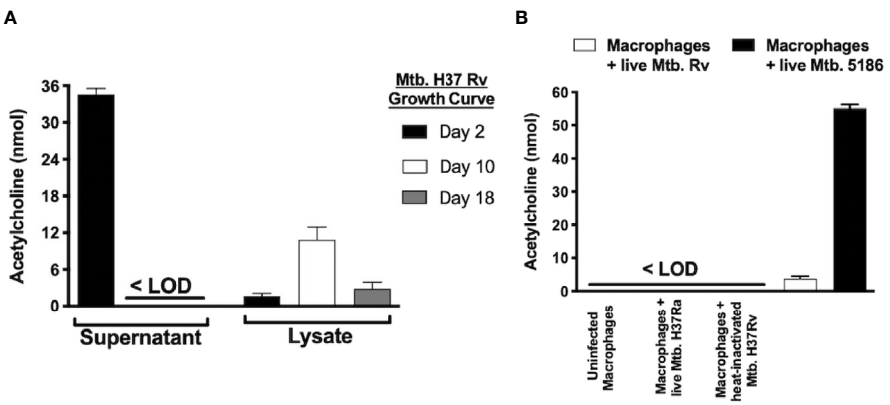

FIGURE 6 | Mycobacterium tuberculosis produces different acetylcholine concentrations during its growth curve and induces acetylcholine secretion in MH-S cells as measured in supernatants and lysates of Mtb H37Rv recovered during three different growth phases. Acetylcholine was detected in Mtb supernatants exclusively during its lag phase and was present in bacterial lysates during all three growth phases but predominated during the logarithmic phase (day 10). **(A)** Acetylcholine concentrations in supernatants of MH-S cells. Acetylcholine concentrations were below the limit of detection (<LOD) in the supernatants of uninfected MH-S cells and in supernatants of MH-S cells infected with avirulent or heat-inactivated Mtb strains. In contrast, infection with live Mtb virulent strains generated detectable acetylcholine concentrations in MH-S cell supernatants **(B)**. Data expressed as the mean + SEM of three wells and are representative of two independent experiments using 3×10^5 CFUs of Mtb. ANOVA $P < 0.001$. The limit of detection of acetylcholine for the assay was 3 nmol.

of the inhibitory mAChR2 which regulates both neuronal (38), and non-neuronal ACh secretion (38, 40). Although we did not measure mAChR2 expression, previous reports suggest that *Mtb* is capable of altering G-protein-coupled receptor expression during infection (41). Alternatively, cytokines such as TNF-α and IFN-γ which are induced under LPS challenge (39), and are also highly induced in our model (20) should be able to increase ACh availability through mechanisms such as the inhibition of acetylcholinesterase, the ACh degrading enzyme (38, 39). Finally, neurohormonal changes described in our model (27, 42–44) may also be responsible for potentiating lung ACh concentrations through non-neuronal ACh release during infection. This could occur through reported mechanisms which include the inhibition of organic cation transporters by steroids and noradrenaline (2, 37) and/or the stimulation of β2-adrenergic and cholecystokinin receptors (45). Importantly, these neurochemicals and their receptors are present in mammal lungs (42, 46). Our model has restrictive parameters including mouse strain, sex, and age, which may bias cholinergic expression and thus might not be representative of the cholinergic dynamics of human disease. However, the fact that pulmonary ACh concentrations vary during disease progression suggests that the lung cholinergic system might carry out different roles during early and late TB.

Immune cells have the capacity to synthesize, release, and respond to molecules classically classified as neurotransmitters (10). Indeed, CD4+ T lymphocytes are important non-neuronal sources of ACh (1), although almost all cell types within the lungs express ACh synthesizing enzymes (2, 47). Here we have documented the upregulation of ChAT, the main ACh synthesizing enzyme in peripheral tissues and non-neuronal cells (1, 2), during *in vivo* TB infection. Upregulation of ChAT during early disease occurs in lung epithelial cells, which are known to be directly devoid of neuronal ACh (4). While during advanced disease, ChAT upregulation occurs to an even greater extent within immune cells, particularly lymphocytes and macrophages. Moreover, our *in vivo* and *in vitro* results suggest that *Mtb* infection induces ACh production. Interestingly, when comparing the levels of ACh detected during infection of macrophages of the MH-S cell line with the standard Mtb H37Rv strain (31), ACh detection was either potentiated or nullified when the infection was carried out with the hypervirulent *Mtb* strain 5186 (31) or the hypovirulent Mtb strain H37Ra (15) respectively. This would suggest that the degree of virulence of the strain of mycobacteria correlates with the levels of ACh production induced during infection. Furthermore, heat-inactivation of the H37Rv strain also nullified ACh detection, suggesting that ACh production requires intact bacteria. It is therefore plausible that the bacilli might have either produced the measured ACh or alternatively, induced ACh production by MH-S cells during infection. Heat-killed and avirulent Mtb may therefore lack the biochemical machinery to either produce ACh or induce production of ACh by MH-S cells. Induction of ChAT through T cell receptor (48) and toll-like receptor (12, 39) stimulation has been demonstrated in several immune cell types including T cells, macrophages and dendritic cells (1, 36, 45). Moreover, the induction of ChAT in immune cells through neurohormonal receptor stimulation has also been suggested (45) and is especially relevant, as several neurohormonal alterations have been described in our experimental mouse model (27, 42–44). Importantly, we were unable to experimentally differentiate the source of ACh production during infection and therefore cannot conclude whether the ACh was produced by the mycobacteria, by cells during their infection or by both.

Cholinergic receptors are expressed on several immune cells including macrophages, monocytes and lymphocytes (1, 10, 36). Leukocytes express all nAChR subtypes and these help trigger mechanisms of action in these cells that are different from those triggered in neurons. Instead of forming voltage-activated gates, nAChRs release intracellular calcium stores after sequestering intracellular chains from neighboring receptors which modify second messenger, transcription factors and enzyme activity (1, 36, 49–52). The α7 nAChR is perhaps the most studied nAChR in the regulation of the immune response (10, 12). However, other receptors such as the α4β2, α9 or α10 nAChRs are known regulators (50, 53). Activation of nAChR receptors can alter cytokine production in alveolar macrophages (7, 54). Moreover, nicotine affects the migratory lung response of key leukocyte subpopulations (neutrophils, macrophages and lymphocytes) which are critical in regulating infection (55). This might explain the increased susceptibility of smokers or cultured leukocytes exposed to nicotine, to a long list of infections caused by microorganisms including *Streptococcus pneumoniae, Hemophilus influenza, Chlamydia pneumoniae, Legionella pneumophila, Pseudomonas aeruginosa, and Cryptococcus neoformans* (5–7, 13, 55, 56).

Previously, Matsunaga et al. used non-infected MH-S alveolar macrophages, a BALB/c mouse cell-line, to demonstrate the expression of α4β2 but not α7 nAChR transcripts by RT-PCR. A limitation of our study is that we did not measure other nAChR subunits such the α4β2 nAChR. However, in concordance with Matsunaga et al's findings, we did not observe the expression of the α7 nAChR subunit in alveolar macrophages of non-infected mice (7). Contrastingly, after *Mtb* infection lung macrophages showed intracellular nAChR α7 subunit expression during early TB and abundant membranal α7 nAChR expression in lymphocytes and during advanced disease in macrophages with foamy appearance present in pneumonic patches. We speculate that this effect could be caused by a product of the infecting bacilli, which could be directly inducing the observed α7 nAChR overexpression. This mechanism has been described in HIV infection, where it was mediated by gp-120 and resulted in the paradoxical potentiation of the inflammatory response (57). An alternative mechanism that could be responsible for nAChR α7 overexpression would be the interference of nAChR expression and function by host steroids (2, 37). The alteration of host steroid production and performance has previously been documented in our model (43, 44).

The previously mentioned study by Matsunaga et al. using a model of *Hemophilus influenza*, reported immunomodulatory

effects after general nAChR treatment but not after α7 selective treatment (7). In contrast, an *ex vivo* study of *Mtb* proliferation found that the α7, β2 and β4 nAChR subunits were crucial in regulating the effectiveness of macrophage containment of bacterial proliferation. The same authors concluded that nAChRs directly modulate macrophage autophagy and indirectly modulate Treg TGF-β and IL-10 production (16). While the α7 nAChR has a low affinity for acetylcholine and is rapidly desensitized, the α4β2 nAChR possesses high affinity for acetylcholine and is desensitized slowly (58). In our model, the administration of both α4β2 and α7 nAChRs nAChR antagonists to mice infected with drug susceptible *Mtb* decreased lung CFU burden but not inflammation. This suggests that immunomodulation secondary to cholinergic upregulation of α4β2 and α7 nAChRs might offer protection from excessive inflammation, but at the same time, decrease the proinflammatory protective immune response contributing to disease progression.

In our experimental model, several neurochemicals, their enzymes and receptors present variability in their concentrations during the course of disease. This variability is probably induced by the host or the bacteria, partly to regulate the immune response (27, 42, 43). Here, we have documented varying kinetics of ACh, ChAT and α7 nAChR expression throughout the disease's progression. During very early disease (days 1 and 3 after infection), we recorded the lowest lung concentrations of ACh and observed ChAT and α7 nAChR expression in bronchial epithelial cells and alveolar macrophages, respectively. This suggests that although ACh concentrations are not yet significantly measurable in a global manner within the lung, the cholinergic system begins to be expressed at a local level in the first cellular responders of the infection, where it might play an immunoregulatory role (15). However, during early disease (days 7 and 14 after infection), ACh concentrations increased significantly and the enzyme ChAT began to be expressed in macrophages and lymphocytes present in diffuse inflammatory infiltrates. Contrastingly, during this time period, the α7 nAChR appeared to be underexpressed in the lungs. We therefore believe that during this stage the transient upregulation of other cholinergic receptors, such as certain muscarinic receptor subtypes, might be taking place to promote protective innate cellular immune responses (47, 54). Further on, during advanced infection (days 21 and 28 after infection), when the Th1 and Th17 adaptive immune responses and M1 macrophages contain bacilli (20), we observed downregulation of ACh expression in the lung. A decrease in cholinergic activity at this stage might be orchestrated by the host to favor the development of a protective adaptive immune response. Contrastingly, during late disease (60 days after infection), when the Th2 and T regulatory responses facilitate bacilli replication and lung pneumonia ensues (20), there is a notable upregulation of lung ACh, ChAT, and α7 nAChR in lung immune cells. It is likely that cholinergic potentiation during advanced disease is induced by the host to downregulate the cellular immune response and avoid overt lung damage. Paradoxically, this strategy ends up favoring bacterial replication and disease progression.

Th1 cytokines, such as TNF-α and IFN-γ, have been classically regarded as correlates of protection during advanced pulmonary tuberculosis (59). In addition, the production of reactive oxygen species within the phagosome represents a crucial mechanism of *Mtb* eradication and is mainly regulated by the enzyme iNOS, which in turn is regulated by Th1 cytokines (60). We observed potentiated lung transcription of iNOS, TNF-α and IFNγ after the administration of the nAChR antagonist DHβE. Regulation of Th1 cytokines and reactive oxygen species by nAChR stimulation has in fact been described in several models (7, 49–51, 61). However, this is the first time that it has been reported in an *in vivo* model of TB. In addition, the administration of DHβE potentiated the transcription of Th17 cytokines in our model. The Th17 response has been associated as a correlate of protection in pulmonary TB and is characteristically represented by the cytokine IL-17A (62). Importantly, the regulation of the Th17 response by nAChRs has been previously described in a different disease model (52). Furthermore, in a recent report, the stimulation of nAChRs after *Mtb* infection of human monocyte-derived macrophages decreased the production of both Th1 and Th17 associated cytokines (IL-6, IL-8, and TNF-α) (17). While in an *ex vivo* TB infection model, nAChR stimulation appeared to potentiate Th2 and T regulatory cytokines, which are known to oppose protective Th1 and Th17 responses (16). In summary, the administration of an α4β2 nicotinic antagonist appears to counteract the immunomodulatory alterations caused by the bacilli, which are responsible for the disease's progression. A limitation of our study is that we did not measure MLA's effect on Th1 and Th17 cytokines or the effect of nAChR antagonists on Th2 and T-regulatory cytokines.

Currently, drug-sensitive TB can be cured using combination therapy. However, the therapeutic regimen requires an average intake of four antibiotics for at least 6 months resulting in significant adherence complications. Moreover, a recent meta-analysis concluded that patients that were taking first-line therapy for TB were significantly at risk for developing disease recurrence, as well as multidrug resistance (63). In the past year, approximately half a million cases and more than two hundred thousand deaths were attributed to MDR-TB (14). MDR-TB cases require treatment with second-line therapy, which is significantly more expensive, toxic, and less effective than first-line therapy (64). When given in addition to second-line antibiotic therapy, nAChR antagonists accelerated the reduction of both lung CFU burden and inflammation. Therefore, the administration of nicotinic antagonists could potentially reduce treatment duration if administered with antibiotic therapy, a goal proposed by the WHO (14).

Remarkably, the cholinergic system is phylogenetically ancient and its components have been reported in vertebrate and invertebrate organisms, including insects, plants, fungi, and even bacteria (2, 65). Pathogenic bacteria such as *E. coli* and *S. aureus* are capable of synthesizing ACh using an uncharacterized enzyme (65). Moreover, microorganisms such as T. *kodakaraensis*, an archaebacteria, can synthesize ACh through ChAT activity (66). Cholinergic stimulation has been implicated

in bacterial functions such as motility (67), and in growth regulation in plants and mammalian cells (65, 67, 68). Here we report that the addition of ACh potentiates the growth of *Mtb* and we also demonstrate that Mtb is capable of producing ACh *in vitro*. Importantly, the highest quantities of ACh in *Mtb* supernatants were found during its lag phase suggesting that during its initial growth phase, *Mtb* might secrete ACh as an autocrine or paracrine growth factor. Contrastingly, the highest quantities of ACh in *Mtb* lysates were found during the subsequent exponential growth phase. This is consistent with its role as a growth factor, as this phase is associated with the highest bacterial growth and bacterial uptake or internal production of a growth factor would be anticipated to take place at this stage (69). Other secreted growth factors produced by *Mtb* that are active at very low concentrations and which regulate its virulence have in fact already been isolated (70, 71). Therefore, the existence of additional secreted growth factors produced by *Mtb* which impact its virulence remains viable.

Furthermore, previous studies confirmed increased *Mtb* growth when exposed to nicotine supplemented medium (72), which would insinuate that the potentiating and hindering effects of ACh and nAChR antagonists respectively on *Mtb* growth that we have shown might be due to their interaction with an ancestral bacterial nAChR. In fact, two ancestral nAChR members of the pentameric ligand-gated ion channel (pLGIC) family have already been described in other bacteria, the homologous protein from *Gloeobacter violaceus* (GLIC) and *Erwinia chrysanthemi* (ELIC) (73). Predictive phylogenetic analysis found bacterial pLGIC genes in many taxons and importantly they were present in several bacterial pathogens. These pentameric receptors mediate chemo-electric signal transduction and are constituted by homologous subunits and an extracellular domain with five agonist binding sites. Despite homology in sequence and structure, significant phylogenetic divergence exists between prokaryotic and eukaryotic pentameric receptors and their properties and form of functioning in bacteria remain unclear (74).

In conclusion, our findings suggest that cholinergic upregulation during pulmonary TB favors *Mtb* infection not only by altering the protective immune response but also by aiding bacterial proliferation. Further investigations must, therefore, explore the mechanisms that favor upregulation of the cholinergic elements discussed here as well as the role of other cholinergic factors during disease progression.

DATA AVAILABILITY STATEMENT

The raw data supporting the conclusions of this article will be made available by the authors, without undue reservation.

ETHICS STATEMENT

The animal study was reviewed and approved by Ethical Committee of Animal Experimentation (CICUAL).

AUTHOR CONTRIBUTIONS

RH-P and LI-W contributed to the theoretical background and design of the experiments. LI-W performed all of the experiments. LI-W and DG-R performed the data analysis. JB-P performed the Mtb infections and supervised the animal experiments. BM-C performed and supervised the molecular biology, immunohistochemistry, and acetylcholine-colorimetric experiments. DM-S performed and supervised the Mtb culture preparations and minimum inhibitory concentration experiments. JC performed and supervised the HPLC analysis. LB, JLMF and ISP-G performed and supervised the cell-culture experiments. LI-W and RH-P wrote the manuscript. JB-P provided the funds. All authors contributed to the article and approved the submitted version.

FUNDING

This work was financed by CONACYT, through the convocation of basic science support CB-2015-01; project # 255209. LI-W is a doctoral student from Programa de Doctorado en Ciencias Biomédicas, Universidad Nacional Autónoma de México (UNAM) and received fellowship 587041 from CONACYT. This manuscript is part of his Ph.D. thesis under the aforementioned program and university.

SUPPLEMENTARY MATERIAL

The Supplementary Material for this article can be found online at: https://www.frontiersin.org/articles/10.3389/fimmu.2020.581911/full#supplementary-material

REFERENCES

1. Kawashima K, Fujii T, Moriwaki Y, Misawa H, Horiguchi K. International Immunopharmacology Non-neuronal cholinergic system in regulation of immune function with a focus on α 7 nAChRs. *Int Immunopharmacol* (2015) 29:127–34. doi: 10.1016/j.intimp.2015.04.015. Elsevier B.V.
2. Wessler I, Kirkpatrick CJ. Acetylcholine beyond neurons: The non-neuronal cholinergic system in humans. *Br J Pharmacol* (2008) 154:1558–71. doi: 10.1038/bjp.2008.185
3. Kistemaker LEM, Gosens R. Acetylcholine beyond bronchoconstriction: Roles in inflammation and remodeling. *Trends Pharmacol Sci* (2015) 36:164–71. doi: 10.1016/j.tips.2014.11.005. Elsevier Ltd.
4. Racké K, Matthiesen S. The airway cholinergic system: Physiology and pharmacology. *Pulm Pharmacol Ther* (2004) 17:181–98. doi: 10.1016/j.pupt.2004.03.001
5. Lafargue M, Xu L, Carlès M, Serve E, Anjum N, Iles KE, et al. Stroke-induced activation of the α7 nicotinic receptor increases Pseudomonas aeruginosa lung injury. *FASEB J* (2012) 26:2919–29. doi: 10.1096/fj.11-197384
6. Giebelen IAJ, Leendertse M, Florquin S, Van Der Poll T. Stimulation of acetylcholine receptors impairs host defence during pneumococcal pneumonia. *Eur Respir J* (2009) 33:375–81. doi: 10.1183/09031936.00103408
7. Matsunaga K, Klein TW, Friedman H, Yamamoto Y. Involvement of Nicotinic Acetylcholine Receptors in Suppression of Antimicrobial Activity and Cytokine Responses of Alveolar Macrophages to Legionella pneumophila

Infection by Nicotine. *J Immunol* (2001) 167:6518–24. doi: 10.4049/jimmunol.167.11.6518
8. Enioutina EY, Myers EJ, Tvrdik P, Hoidal JR, Rogers SW, Gahring LC. The Nicotinic Receptor Alpha7 Impacts the Mouse Lung Response to LPS through Multiple Mechanisms. *PLoS One* (2015) 10:1–20. doi: 10.1371/journal.pone.0121128
9. Engel O, Akyüz L, Da Costa Goncalves AC, Winek K, Dames C, Thielke M, et al. Cholinergic Pathway Suppresses Pulmonary Innate Immunity Facilitating Pneumonia after Stroke. *Stroke* (2015). doi: 10.1161/STROKEAHA.115.008989
10. Pavlov VA, Chavan SS, Tracey KJ. Molecular and Functional Neuroscience in Immunity. *Annu Rev Immunol* (2018) 36:783–812. doi: 10.1146/annurev-immunol-042617-053158
11. Wu H, Li L, Su X. Vagus Nerve through α 7 nAChR Modulates Lung Infection and Inflammation: Models, Cells, and Signals. *BioMed Res Int* (2014) 2014:1–20. doi: 10.1155/2014/283525
12. Tracey KJ. The inflammatory reflex. *Nature* (2002) 420:853–9. doi: 10.1038/nature01321
13. Richter K, Koch C, Perniss A, Wolf PM, Schweda EKH, Wichmann S, et al. Phosphocholine-modified lipooligosaccharides of Haemophilus influenzae inhibit ATP-induced IL-1β release by pulmonary epithelial cells. *Molecules* (2018) 23:8–23. doi: 10.3390/molecules23081979
14. Baddeley A, Bartens M-C, Dean A, Dias HM, Falzon D, Floyd K, et al. *Global Tuberculosis Report 2020*. Geneva (2020).
15. López-Hernández Y, Rivas-Santiago CE, López JA, Mendoza-Almanza G, Hernandez-Pando R. Tuberculosis and cigarette smoke exposure: An update of in vitro and in vivo studies. *Exp Lung Res* (2018) 44:113–26. doi: 10.1080/01902148.2018.1444824
16. Bai X, Stitzel JA, Bai A, Zambrano CA, Phillips M, Marrack P, et al. Nicotine impairs macrophage control of mycobacterium tuberculosis. *Am J Respir Cell Mol Biol* (2017) 57:324–33. doi: 10.1165/rcmb.2016-0270OC
17. Valdez-Miramontes CE, Trejo Martínez LA, Torres-Juárez F, Rodríguez Carlos A, Marin-Luévano SP, de Haro-Acosta JP, et al. Nicotine modulates molecules of the innate immune response in epithelial cells and macrophages during infection with M. tuberculosis. *Clin Exp Immunol* (2020) 199:230–43. doi: 10.1111/cei.13388
18. Bai W, Liu H, Ji Q, Zhou Y, Liang L, Zheng R, et al. TLR3 regulates mycobacterial RNA-induced IL-10 production through the PI3K/AKT signaling pathway. *Cell Signal* (2014) 26:942–50. doi: 10.1016/j.cellsig.2014.01.015. Elsevier Inc.
19. Lai YF, Lin TM, Wang CH, Su PY, Wu JT, Lin MC, et al. Functional polymorphisms of the TLR7 and TLR8 genes contribute to Mycobacterium tuberculosis infection. *Tuberculosis* (2016) 98:125–31. doi: 10.1016/j.tube.2016.03.008. Elsevier Ltd.
20. Hernández-Pando R, Orozcoe H, Sampieri A, Pavon L, Velasquillo C, Larriva-Sahd J, et al. Correlation between the kinetics of Th1, Th2 cells and pathology in a murine model of experimental pulmonary tuberculosis. *Immunology* (1996) 89:26–33.
21. van Soolingen D, Hernandez-Pando R, Orozco H, Aguilar D, Magis-Escurra C, Amaral L, et al. The antipsychotic thioridazine shows promising therapeutic activity in a mouse model of multidrug-resistant tuberculosis. *PLoS One* (2010) 5:1–6. doi: 10.1371/journal.pone.0012640
22. Potter PE, Meek JL, Neff NH. Acetylcholine and Choline in Neuronal Tissue Measured by HPLC with Electrochemical Detection. *J Neurochem* (1983) 41:188–94. doi: 10.1111/j.1471-4159.1983.tb13668.x
23. Marrero MB, Lucas R, Salet C, Hauser TA, Mazurov A, Lippiello PM, et al. An 7 Nicotinic Acetylcholine Receptor-Selective Agonist Reduces Weight Gain and Metabolic Changes in a Mouse Model of Diabetes. *J Pharmacol Exp Ther* (2010) 332:173–80. doi: 10.1124/jpet.109.154633
24. Damaj MI, Welch SP, Martin BR. In vivo pharmacological effects of dihydro-β-erythroidine, a nicotinic antagonist, in mice. *Psychopharmacol (Berl)* (1995) 117:67–73. doi: 10.1007/BF02245100
25. Akhila JS, Shyamjith, Deepa, Alwar MC. Acute toxicity studies and determination of median lethal dose. *Curr Sci* (2007).
26. Veziris N, Ibrahim M, Lounis N, Andries K, Jarlier V. Sterilizing activity of second-line regimens containing TMC207 in a murine model of tuberculosis. *PLoS One* (2011) 6:1–6. doi: 10.1371/journal.pone.0017556
27. Zetter M, Barrios-Payán J, Mata-Espinosa D, Marquina-Castillo B, Quintanar-Stephano A, Hernández-Pando R. Involvement of Vasopressin in the Pathogenesis of Pulmonary Tuberculosis: A New Therapeutic Target? *Front Endocrinol (Lausanne)* (2019) 10:1–11. doi: 10.3389/fendo.2019.00351/full
28. Mata-espinosa D, Barrios-payan J, Herna R, Marquina-castillo B. A significant therapeutic effect of silymarin administered alone , or in combination with chemotherapy, in experimental pulmonary tuberculosis caused by drug-sensitive or drug- resistant strains : In vitro and in vivo studies. *PLoS One* (2019) 14:1–20 doi: 10.1371/journal.pone.0217457
29. Schmittgen TD, Livak KJ. Analyzing real-time PCR data by the comparative CT method. *Nat Protoc* (2008) 3:1101–8. doi: 10.1038/nprot.2008.73
30. Wessler I, Bender H, Harle P, Hohle KD, Kirdorf G, Klapproth H, et al. Release of [3H]acetylcholine in human isolated bronchi: Effect of indomethacin on muscarinic autoinhibition. *Am J Respir Crit Care Med* (1995) 151:1040–6. doi: 10.1164/ajrccm.151.4.7697228
31. Marquina-Castillo B, García-García L, Ponce-De-León A, Jimenez-Corona ME, Bobadilla-Del Valle M, Cano-Arellano B, et al. Virulence, immunopathology and transmissibility of selected strains of Mycobacterium tuberculosis in a murine model. *Immunology* (2009) 128:123–33. doi: 10.1111/j.1365-2567.2008.03004.x
32. Kummer W, Lips KS. Non-neuronal acetylcholine release and its contribution to COPD pathology. *Drug Discov Today Dis Mech* (2006). doi: 10.1016/j.ddmec.2006.02.008
33. Chakrabarti B, Calverley PMA, Davies PDO. Tuberculosis and its incidence, special nature, and relationship with chronic obstructive pulmonary disease. *Int J COPD* (2007) 2:263–72.
34. Larcombe AN, Zosky GR, Bozanich EM, Turner DJ, Hantos Z, Sly PD. Absence of cholinergic airway tone in normal BALB/c mice. *Respir Physiol Neurobiol* (2008) 161:223–9. doi: 10.1016/j.resp.2008.01.009
35. Wessler I, Kirkpatrick CJ, Racké K. The cholinergic "pitfall": Acetylcholine, a universal cell molecule in biological systems, including humans. *Clin Exp Pharmacol Physiol* (1999) 26:198–205. doi: 10.1046/j.1440-1681.1999.03016.x
36. Fujii T, Mashimo M, Moriwaki Y, Misawa H, Ono S, Horiguchi K, et al. Physiological functions of the cholinergic system in immune cells. *J Pharmacol Sci* (2017) 134:1–21. doi: 10.1016/j.jphs.2017.05.002
37. Reinheimer T, Münch M, Bittinger F, Racké K, Kirkpatrick CJ, Wessler I. Glucocorticoids mediate reduction of epithelial acetylcholine content in the airways of rats and humans. *Eur J Pharmacol* (1998) 349:277–84. doi: 10.1016/S0014-2999(98)00185-X
38. Jacoby DB, Xiao HQ, Lee NH, Chan-Li Y, Fryer AD. Virus- and interferon-induced loss of inhibitory M2 muscarinic receptor function and gene expression in cultured airway parasympathetic neurons. *J Clin Invest* (1998) 102:242–8. doi: 10.1172/JCI1114
39. Shi X, Wang L, Zhou Z, Liu R, Li Y, Song L. Acetylcholine modulates the immune response in Zhikong scallop Chlamys farreri. *Fish Shellfish Immunol* (2014) 38:204–10. doi: 10.1016/j.fsi.2014.03.008
40. Bjur D, Danielson P, Alfredson H, Forsgren S. Presence of a non-neuronal cholinergic system and occurrence of up- and down-regulation in expression of M2 muscarinic acetylcholine receptors: New aspects of importance regarding Achilles tendon tendinosis (tendinopathy). *Cell Tissue Res* (2008). doi: 10.1007/s00441-007-0524-1
41. Alaridah N, Lutay N, Tenland E, Rönnholm A, Hallgren O, Puthia M, et al. Mycobacteria Manipulate G-Protein-Coupled Receptors to Increase Mucosal Rac1 Expression in the Lungs. *J Innate Immun* (2017) 9:318–29. doi: 10.1159/000453454
42. Barrios-Payán J, Revuelta A, Mata-Espinosa D, Marquina-Castillo B, Villanueva EB, Gutiérrez MEH, et al. The contribution of the sympathetic nervous system to the immunopathology of experimental pulmonary tuberculosis. *J Neuroimmunol* (2016) 298:98–105. doi: 10.1016/j.jneuroim.2016.07.012
43. Bini EI, Mata Espinosa D, Marquina Castillo B, Barrios Payán J, Colucci D, Cruz AF, et al. The influence of sex steroid hormones in the immunopathology of experimental pulmonary tuberculosis. *PLoS One* (2014) 9:2–10. doi: 10.1371/journal.pone.0093831
44. Hernandez-Pando R. Emergent immunoregulatory properties of combined glucocorticoid and anti-glucocorticoid steroids in a model of tuberculosis. *QJM* (1998) 91:755–66. doi: 10.1093/qjmed/91.11.755

45. Reardon C, Duncan GS, Brüstle A, Brenner D, Tusche MW, Olofsson PS, et al. Lymphocyte-derived ACh regulates local innate but not adaptive immunity. *Proc Natl Acad Sci* (2013) 110:1410–5. doi: 10.1073/pnas.1221655110
46. Barnes PJ. The third nervous system in the lung: Physiology and clinical perspectives. *Thorax* (1984) 39:561–7. doi: 10.1136/thx.39.8.561
47. Lips KS, Lührmann A, Tschernig T, Stoeger T, Alessandrini F, Grau V, et al. Down-regulation of the non-neuronal acetylcholine synthesis and release machinery in acute allergic airway inflammation of rat and mouse. *Life Sci* (2007) 80:2263–9. doi: 10.1016/j.lfs.2007.01.026
48. Vijayaraghavan S, Karami A, Aeinehband S, Behbahani H, Grandien A, Nilsson B, et al. Regulated Extracellular Choline Acetyltransferase Activity-The Plausible Missing Link of the Distant Action of Acetylcholine in the Cholinergic Anti-Inflammatory Pathway. *PLoS One* (2013) 8:1–15. doi: 10.1371/journal.pone.0065936
49. de Jonge WJ, van der Zanden EP, The FO, Bijlsma MF, van Westerloo DJ, Bennink RJ, et al. Stimulation of the vagus nerve attenuates macrophage activation by activating the Jak2-STAT3 signaling pathway. *Nat Immunol* (2005) 6:844–51. doi: 10.1038/ni0905-954b
50. Nordman JC, Muldoon P, Clark S, Damaj MI, Kabbani N. The α4 nicotinic receptor promotes CD4+ T-Cell proliferation and a helper T-cell immune response. *Mol Pharmacol* (2014). doi: 10.1124/mol.113.088484
51. Takahashi HK, Iwagaki H, Hamano R, Yoshino T, Tanaka N, Nishibori M. Effect of nicotine on IL-18-initiated immune response in human monocytes. *J Leukoc Biol* (2006). doi: 10.1189/jlb.0406236
52. Nizri E, Irony-Tur-Sinai M, Lory O, Orr-Urtreger A, Lavi E, Brenner T. Activation of the Cholinergic Anti-Inflammatory System by Nicotine Attenuates Neuroinflammation via Suppression of Th1 and Th17 Responses. *J Immunol* (2009). doi: 10.4049/jimmunol.0902212
53. Koval L, Lykhmus O, Zhmak M, Khruschov A, Tsetlin V, Magrini E, et al. Differential involvement of α4β2, α7 and α9α10 nicotinic acetylcholine receptors in B lymphocyte activation in vitro. *Int J Biochem Cell Biol* (2011). doi: 10.1016/j.biocel.2010.12.003
54. Kummer W, Krasteva-Christ G. Non-neuronal cholinergic airway epithelium biology. *Curr Opin Pharmacol* (2014). doi: 10.1016/j.coph.2014.03.001
55. Razani-Boroujerdi S, Singh SP, Knall C, Hahn FF, Peña-Philippides JC, Kalra R, et al. Chronic nicotine inhibits inflammation and promotes influenza infection. *Cell Immunol* (2004). doi: 10.1016/j.cellimm.2004.07.007
56. Yamaguchi H, Friedman H, Yamamoto Y. Involvement of nicotinic acetylcholine receptors in controlling Chlamydia pneumoniae growth in epithelial HEp-2 cells. *Infect Immun* (2003) 71:3645–7. doi: 10.1128/IAI.71.6.3645-3647.2003
57. Delgado-Vélez M, Báez-Pagán CA, Gerena Y, Quesada O, Santiago-Pérez LI, Capó-Vélez CM, et al. The α7-nicotinic receptor is upregulated in immune cells from HIV-seropositive women: consequences to the cholinergic anti-inflammatory response. *Clin Transl Immunol* (2015) 4:e53. doi: 10.1038/cti.2015.31
58. Cordero-Erausquin M, Marubio LM, Klink R, Changeux JP. Nicotinic receptor function: New perspectives from knockout mice. *Trends Pharmacol Sci* (2000) 21:211–7. doi: 10.1016/S0165-6147(00)01489-9
59. Keane J, Shurtleff B, Kornfeld H. TNF-dependent BALB/c murine macrophage apoptosis following Mycobacterium tuberculosis infection inhibits bacillary growth in an IFN-γ independent manner. *Tuberculosis* (2002). doi: 10.1054/tube.2002.0322
60. Fenton MJ, Vermeulen MW. Immunopathology of tuberculosis: Roles of macrophages and monocytes. *Infect Immun* (1996). doi: 10.1128/IAI.64.3.683-690.1996
61. Tsoyi K, Jang HJ, Kim JW, Chang HK, Lee YS, Pae HO, et al. Stimulation of Alpha7 nicotinic acetylcholine receptor by nicotine attenuates inflammatory response in macrophages and improves survival in experimental model of sepsis through heme oxygenase-1 induction. *Antioxid Redox Signal* (2011). doi: 10.1089/ars.2010.3555
62. Shen H, Chen ZW. The crucial roles of Th17-related cytokines/signal pathways in M.Tuberculosis infection. *Cell Mol Immunol* (2018). doi: 10.1038/cmi.2017.128
63. Pasipanodya JG. Gumbo T. A meta-analysis of self-administered vs directly observed therapy effect on microbiologic failure, relapse, and acquired drug resistance in tuberculosis patients. *Clin Infect Dis* (2013). doi: 10.1093/cid/cit167
64. Suárez PG, Floyd K, Portocarrero J, Alarcón E, Rapiti E, Ramos G, et al. Feasibility and cost-effectiveness of standardised second-line drug treatment for chronic tuberculosis patients: A national cohort study in Peru. *Lancet* (2002) 359:1980–9. doi: 10.1016/S0140-6736(02)08830-X
65. Horiuchi Y, Kimura R, Kato N, Fujii T, Seki M. Evolutional study on acetylcholine expression. *Life Sciences* (2003) 72:1745–56. doi: 10.1016/S0024-3205(02)02478-5
66. Yamada T, Fujii T, Kanai T, Amo T, Imanaka T, Nishimasu H, et al. Expression of acetylcholine (ACh) and ACh-synthesizing activity in Archaea. *Life Sci* (2005) 77:1935–44. doi: 10.1016/j.lfs.2005.01.026
67. Faust MA, Doetsch RN. Effect of drugs that alter excitable membranes on the motility of Rhodospirillum rubrum and Thiospirillum jenense. *Can J Microbiol* (1971) 17:191–6. doi: 10.1139/m71-033
68. Klapproth H, Reinheimer T, Metzen J, Münch M, Bittinger F, Kirkpatrick CJ, et al. Non-neuronal acetylcholine, a signalling molecule synthezised by surface cells of rat and man. *Naunyn Schmiedebergs Arch Pharmacol* (1997) 355:515–23. doi: 10.1007/PL00004977
69. Monod J. The Growth of Bacterial Cultures. *Annu Rev Microbiol* (1949) 3:371–94. doi: 10.1146/annurev.mi.03.100149.002103
70. Mukamolova GV, Turapov OA, Young DI, Kaprelyants AS, Kell DB. Young M. A family of autocrine growth factors in Mycobacterium tuberculosis. *Mol Microbiol* (2002). doi: 10.1046/j.1365-2958.2002.03184.x
71. Rosser A, Stover C, Pareek M, Mukamolova GV. Resuscitation-promoting factors are important determinants of the pathophysiology in Mycobacterium tuberculosis infection. *Crit Rev Microbiol* (2017) 43:621–30. doi: 10.1080/1040841X.2017.1283485
72. Sir D, Sir D, Kotian FM, Col L. Book reviews. *J R Soc Med* (1983) 76:530–1. doi: 10.1177/014107688307601224
73. Zimmermann I, Dutzler R. Ligand Activation of the Prokaryotic Pentameric Ligand- Gated Ion Channel ELIC. *PLoS Biol* (2011) 9(6):e1001101 doi: 10.1371/journal.pbio.1001101
74. Jaiteh M, Taly A, Hénin J. Evolution of pentameric ligand-gated ion channels: Pro-loop receptors. *PLoS One* (2016) 11:1–24. doi: 10.1371/journal.pone.0151934

Conflict of Interest: The authors declare that the research was conducted in the absence of any commercial or financial relationships that could be construed as a potential conflict of interest.

frontiers in Immunology

MINI REVIEW
published: 22 February 2021
doi: 10.3389/fimmu.2021.641588

Role of Peripheral Immune Cells for Development and Recovery of Chronic Pain

John R. Bethea[1] *and Roman Fischer*[2,3]*

[1] Department of Biology, Drexel University, Philadelphia, PA, United States, [2] Institute of Cell Biology and Immunology, University Stuttgart, Stuttgart, Germany, [3] Stuttgart Research Center Systems Biology, University of Stuttgart, Stuttgart, Germany

Chronic neuropathic pain (CNP) is caused by a lesion or disease of the somatosensory nervous system. It affects ∼8% of the general population and negatively impacts a person's level of functioning and quality of life. Its resistance to available pain therapies makes CNP a major unmet medical need. Immune cells have been shown to play a role for development, maintenance and recovery of CNP and therefore are attractive targets for novel pain therapies. In particular, in neuropathic mice and humans, microglia are activated in the dorsal horn and peripheral immune cells infiltrate the nervous system to promote chronic neuroinflammation and contribute to the initiation and progression of CNP. Importantly, immunity not only controls pain development and maintenance, but is also essential for pain resolution. In particular, regulatory T cells, a subpopulation of T lymphocytes with immune regulatory function, and macrophages were shown to be important contributors to pain recovery. In this review we summarize the interactions of the peripheral immune system with the nervous system and outline their contribution to the development and recovery of pain.

Keywords: chronic neuropathic pain, immune cells, T cells, Tregs, recovery, macrophages

OPEN ACCESS

Edited by:
Michael D. Burton, The University of Texas at Dallas, United States

Reviewed by:
Temugin Berta, University of Cincinnati, United States
Prapti Mody, The University of Texas at Dallas, United States

***Correspondence:**
Roman Fischer
roman.fischer@izi.uni-stuttgart.de

Specialty section:
This article was submitted to Molecular Innate Immunity, a section of the journal Frontiers in Immunology

Received: *14 December 2020*
Accepted: *03 February 2021*
Published: *22 February 2021*

Citation:
Bethea JR and Fischer R (2021) Role of Peripheral Immune Cells for Development and Recovery of Chronic Pain. Front. Immunol. 12:641588. doi: 10.3389/fimmu.2021.641588

INTRODUCTION

Chronic pain is defined as a more than 12 weeks lasting pain that is characterized by irregular somatosensory processing in the peripheral nervous system (PNS) or the central nervous system (CNS) (1). Chronic neuropathic pain (CNP) is a specific form of chronic pain that is caused by damage to or disease of the somatosensory nervous system (2, 3) and affects up to 8% of the general population (4). CNP can result as a consequence of a large number of medical conditions, such as injuries to the PNS or CNS, metabolic, autoimmune or neurodegenerative diseases as well as cancer and chemotherapy (4, 5). In this review, we will mainly focus on CNP due to peripheral nerve injuries and discuss results from chemotherapy-induced pain. Individuals suffering from CNP exhibit stimulus-independent pain that is often characterized by abnormal sensations or hypersensitivity in the affected area. Patients often describe the pain as a burning and/or stabbing sensation (6). Allodynia, pain elicited by a usually non-painful stimulus, and hyperalgesia, an increased pain response due to painful stimulus, are frequent symptoms described by CNP patients (7). CNP can have a dramatic impact on a person's level of functioning and quality of life and is resistant to conservative pain management (7). Therefore, effective therapies that either prevent or reverse CNP are critical for both public health and clinical practice (5).

Research from the last two decades has demonstrated that a robust neuroimmune response and bidirectional signaling between the sensory and immune system contribute to development and maintenance of CNP. Indeed, increased levels of soluble pro-inflammatory mediators and recruitment of immune cells to the site of nerve injury, the dorsal root ganglion (DRG) and the spinal cord after PNS/CNS injury are well-characterized in rodent models of CNP (8–15). In addition, immune cells also contribute to recovery of CNP (16–18), indicating that modulation of immunity has therapeutic potential to treat CNP. Therefore, a detailed understanding of the contribution of immune responses to the development, maintenance and resolution of CNP may result in novel therapeutic approaches that are superior to current pain-relieving therapies.

DEVELOPMENT AND MAINTENANCE OF CNP IS CONTROLLED BY $CD4^+$ EFFECTOR T CELLS

T cells were identified as important contributors to CNP development and maintenance in animal models and human patients. Early on, the general importance of T cells for pain development was demonstrated by several independent studies showing that immunodeficient mice without functional lymphocytes in contrast to control mice do not develop pain hypersensitivity after nerve injury (9, 19, 20). Reconstitution of immunodeficient nude rats (9), and mice (19) with $CD4^+$ T helper cells resulted in reestablishment of the pain phenotype, suggesting that pro-inflammatory T helper cells promote pain responses. T cells were shown to infiltrate into the lumbar spinal cord post-injury (19). Similar, the Th1 cytokine interferon-γ (IFN-γ) is upregulated in the dorsal horn after nerve injury and functional IFN-γ signaling is required for full development of neuropathic hypersensitivity (20), indicating that Th1 responses in the spinal cord contribute to pain hypersensitivity. The important role of T cell infiltration for development of pain was further confirmed by a recent study demonstrating that intrathecal injection of a T cell receptor (TCR) specific antibody that depletes functional $CD4^+$ T cells resulted in alleviation of mechanical allodynia, indicating that CNS infiltrating T cells directly contribute to pain responses. Once treatment was terminated, mechanical allodynia returned to levels comparable to control mice, presumably due to repopulation of functional T cells in the CNS (21).

Next to IFN-γ expressing Th1 cells, IL17-expressing T helper cells were detected in peripheral nerves, indicating that Th17 cells may also contribute to pain development (22). Indeed, intrathecal and intraneural injection of recombinant IL-17A induced pain hypersensitivity (23), indicating a role of IL-17A for pain development. A recent study further confirmed that IL-17A regulates neuron-glial communications, synaptic transmission, and neuropathic pain after chemotherapy (24). Additional mechanistic data showed that DRG-infiltrating T lymphocytes release leukocyte elastase after nerve injury. Confirming that leukocyte elastase promotes T cell-dependent pain responses, adoptive transfer of leukocyte elastase deficient T cells did not restore pain development in immunodeficient $Rag2^{-/-}$ mice (25). This indicated that T cells may also directly contribute to nerve damage.

Interestingly, MHC class II knockout (k/o) mice that lack MHC class II-restricted T helper cells displayed an impaired chronification of mechanical allodynia after peripheral nerve injury (26), indicating the general importance of $CD4^+$ T helper cells for pain chronification in rodents. This was confirmed by a recent study showing that MHC class II-restricted $CD4^+$ T helper cells contribute to the transition from acute to chronic mechanical allodynia in a rat model of peripheral nerve injury (21). Clinical studies have shown that a human major histocompatibility complex (MHC) class II gene polymorphism (DQB1*03:02 HLA haplotype) is associated with an increased risk to develop CNP after inguinal hernia surgery and lumbar disc herniation (27). The importance of MHC class II genes for CNP development indicates that, similar to the animal models, $CD4^+$ Th cells contribute to CNP development in human patients. The relevance of MHCII-restricted T helper cells as an important trigger for chronic hypersensitivity after nerve injuries has been recently discussed by Ding et al. (28), where they indicate that there is a growing body of clinical evidences showing that increased blood Th cell numbers and changes in subset patterns are correlated with neuropathic pain intensities after nerve injuries. Other clinical data indicate that an emergent T-helper 2 profile with high interleukin-6 levels correlates with the appearance of bortezomib-induced neuropathic pain (29). Interestingly, Luchting et al. (30) found a disrupted Th17/Treg balance with significantly increased anti-inflammatory Tregs and decreased pro-inflammatory Th17 cells in patients suffering from chronic unspecific low back pain compared to healthy controls, indicating an anti-inflammatory T cell shift in the patients they analyzed. Altogether, these clinical data indicate that there is a considerable impact of the T cell compartment in neuropathic pain. However, the role of pro- and anti-inflammatory T cell subsets in CNP patients seems to differ depending on the pain condition of the patients.

T CELL SUBSETS CONTRIBUTE TO PAIN RECOVERY

In 2004 Moalem et al. (9) showed that adoptive transfer of Th2 polarized T helper cells in athymic nude rats further reduced pain hypersensitivity, indicating that anti-inflammatory responses mediated by Th2 cells may counteract inflammatory processes that promote pain development and maintenance. Indeed, higher circulating levels of the anti-inflammatory interleukins IL-10 and IL-4 were detected in patients with painless neuropathy compared to patients with painful neuropathy and controls (31), indicating that anti-inflammatory responses may be necessary to control pain development. Indeed, Leger et al. (32) demonstrated that glatiramer acetate treatment, an approved MS therapy, inhibited microglia activation and increased IL-10 and IL-4 expressing T cells in the dorsal horn after peripheral nerve injury resulting

in alleviation of neuropathic allodynia. This indicates that next to their pathologic role for development and maintenance of CNP, T cells may also contribute to the resolution of pain.

$CD8^+$ T CELLS CONTRIBUTE TO PAIN RECOVERY

Whereas, $CD4^+$ Th1 cells promote pain development and maintenance, several reports indicate that $CD8^+$ T cells may contribute to pain resolution. Krukowski et al. (33) showed that chemotherapy-induced mechanical hypersensitivity was prolonged in T-cell-deficient $Rag1^{-/-}$ mice compared to wild type mice. Adoptive transfer of $CD8^+$, but not $CD4^+$ T cells to neuropathic $Rag1^{-/-}$ mice restored pain resolution. Mechanistically, this study indicated that $CD8^+$ T Cells and endogenous IL-10 were required for resolution of CNP (33). Other studies have also reported a role of IL-10 for pain resolution and functional recovery after peripheral nerve injury (34), indicating the general importance of anti-inflammatory responses for pain resolution. Laumet et al. (35) recently confirmed that resolution of chemotherapy-induced mechanical allodynia is dependent on presence of $CD8^+$ T cells. They showed that adoptive transfer of $CD8^+$ T cells from naïve wildtype mice to T-cell-deficient neuropathic $Rag2^{-/-}$ mice failed to promote pain resolution. In contrast, adoptive transfer of cisplatin-educated $CD8^+$ T cells prevented the development of chemotherapy-induced CNP (35). Importantly, this T cell education appeared to be independent of antigen recognition by the T cell receptor because cisplatin-educated $CD8^+$ T cells did also promote pain resolution in a model of paclitaxel-induced CNP and reconstitution of T cell deficient mice with ovalbumin-specific $CD8^+$ T cells also restored CNP resolution (35). This study indicates that $CD8^+$ T cells need to be activated to acquire the capacity to promote resolution of CNP, but their therapeutic activity seems to be independent of their antigen-specific education. However, the role of $CD8^+$ T cells for CNP seems to be complex. Using a model of paclitaxel-induced CNP, Liu et al. (36) showed that blocking of functional $CD8^+$ T cells at the level of the spinal cord and the DRG, reversed chemotherapy induced mechanical hypersensitivity. Similar, adoptive transfer of $CD8^+$ T cells exacerbated neuropathic pain in this model (36), suggesting that cytotoxic T cells contribute to pain progression.

TREGS CONTROL IMMUNITY TO PROMOTE PAIN RESOLUTION

Another important T cell subset that plays a role for pain recovery are regulatory T cells (Tregs), immunomodulatory T lymphocytes that control the activity of innate and adaptive immune cells (37). After peripheral nerve injury, Tregs are recruited to the site of injury, the DRG and the spinal cord (16, 17, 38). Systemic expansion of Tregs was shown to alleviate peripheral CNP following nerve injury and experimental autoimmune neuritis-associated central CNP (16). Similar, anti-$CD25$ antibody-dependent depletion of $CD25^+$ cells prolonged mechanical hypersensitivity after peripheral nerve injury (16, 18), indicating a role of $CD25^+$ Tregs for pain recovery. In another study DEREG mice, where FoxP3-expressing Tregs can be depleted by injection of diphtheria toxin, were used to specifically assess Treg contribution to pain recovery. Indeed, following toxin application DEREG mice developed increased mechanical pain hypersensitivity after peripheral nerve injury (17), confirming that Tregs are important for pain recovery. The analgesic role of Tregs was further confirmed in a model of chemotherapy-induced CNP, where adoptive transfer of a population of $CD4^+CD25^+$ T cells, which largely are composed of Tregs, alleviated CNP (36).

In a recent study it was shown that nerve-infiltrating Tregs suppress the development of neuropathic pain mainly through the inhibition of the Th1 response by $CD4^+$ T helper cells following nerve injury (38). This resulted indirectly in reduced neuronal damage and neuroinflammation at the level of the sensory ganglia. The authors further identified IL-10 signaling as an intrinsic mechanism by which Treg cells counteract neuropathic pain development (38). Indeed, in a previous study the neuroprotective effect of IL-10 secretion by CNS infiltrating Tregs was demonstrated in an ischemia model (39). Another recent study by Duffy et al. (40) showed that adoptive transfer of activated Tregs or intrathecal delivery of the Treg cytokine IL-35 alleviated spontaneous and facial stimulus-evoked pain behaviors in mice with experimental autoimmune encephalomyelitis (EAE). The effects of intrathecal IL-35 therapy were dependent on presence of Tregs and associated with reduced monocyte infiltration in the trigeminal afferent pathway and upregulated IL-10 expression in CNS-infiltrating lymphocytes (40). Interestingly, intrathecal injection of plasmids encoding IL-10 at the onset of clinical EAE suppressed disease development and alleviated pain behaviors (41, 42), indicating that the upregulated IL-10 expression observed in the study of Duffy et al. (40) may be responsible for the observed pain alleviating effect of Tregs.

All these data point toward a critical role of IL-10 for pain resolution. Indeed, additional research showed that central activation of anti-inflammatory cytokines such as IL-10 and TGFβ suppresses allodynia after peripheral nerve injury (43) and in a model of chemotherapy-induced neuropathic pain (44). Mechanistically, *in vitro* studies showed that in addition to its master anti-inflammatory role, IL-10 reverses voltage-gated sodium currents to reduce neuronal excitability (45), indicating a possible immune cell independent mechanism of IL-10 mediated pain recovery. Therefore, therapies that promote Treg activity and IL-10 signaling in the CNS may prove beneficial for pain therapies.

Over the last decade, we and others showed that tumor necrosis factor receptor 2 (TNFR2) is critical for Treg function and that selective agonism of TNFR2 results in Treg expansion and is therapeutic in inflammatory conditions such as experimental arthritis (46, 47) and graft vs. host disease (48). We recently demonstrated that treatment of neuropathic mice with a TNFR2 agonist promoted long-term pain recovery

after peripheral nerve injury (18) and in neuropathic EAE mice (49). Mechanistically, our study revealed that systemic TNFR2 agonist application promoted expansion of Tregs resulting in alleviation of peripheral and central inflammation. We further detected increased Treg and IL-10 levels in the spinal cord after TNFR2 agonist treatment (18), indicating that Treg-mediated IL-10 signaling in the CNS may contribute to the pain alleviating effect of TNFR2 agonists too. Interestingly, next to their anti-inflammatory functions, Tregs were shown to directly promote tissue regeneration in the CNS (50). Confirming, we observed upregulation of various proteins associated with neuroregeneration after TNFR2 agonist treatment in neuropathic mice (18), indicating that TNFR2-dependent expansion of Tregs may promote pain recovery not only by modulation of immunity, but also via enhanced tissue regeneration. Indeed, previous studies showed that TNFR2 directly contributes to neuroprotection (51–53).

MACROPHAGES CONTRIBUTE TO THE DEVELOPMENT OF CNP

Next to T lymphocytes, peripheral monocytes that differentiate into macrophages upon tissue infiltration were shown to play a role for pain development. These cells were shown to infiltrate around injured sensory neurons and in the DRG. Inhibition of monocyte infiltration into the DRG prevented the development of pain hypersensitivity in rodent models of CNP (54, 55), indicating the importance of peripheral macrophages for pain development. In a model of chemotherapy-induced CNP, nerve infiltrating monocytes were activated by the chemokine fractalkine (CX3CL1) resulting in the production of reactive oxygen species that in turn activated the receptor TRPA1 in sensory neurons and evoked the pain response (56). Additional data indicate an interaction between the fractalkine receptor CX3CR1 and the chemokine receptor CCR2 in monocytes that may constitute an underlying mechanism for persistent chemotherapy-induced pain (57).

Monocytes/macrophages were shown to act synergistically with microglia to initiate hypersensitivity and promote the transition from acute to chronic pain after peripheral nerve injury (58). A recent study demonstrated that DRG macrophages, but not macrophages that had infiltrated at the site of injury contribute to initiation and maintenance of mechanical hypersensitivity (59). Indeed, depletion of DRG macrophages, but not at the site of injury, prevented the development of pain and reversed ongoing nerve injury-induced hypersensitivity (59). Macrophages that invade the DRG, release excitatory agents that generate ectopic activity in sensory neurons thereby contributing to neuropathology responsible for pain development (60, 61).

MACROPHAGES ALLEVIATE PAIN VIA THE OPIOID SYSTEM AND ANTI-INFLAMMATORY RESPONSES

Macrophage infiltration into the nerve is an essential step to allow nerve regeneration. In particular, anti-inflammatory/reparative M2 macrophages have been indicated to play a role for repair processes after nerve injury (62). Indeed, perineural transplantation of M2 macrophages resulted in attenuated neuropathy-induced mechanical hypersensitivity (63, 64). Similar, injection of IL-4, a cytokine responsible for M2 macrophage differentiation, at the site of nerve injury promoted repolarization of macrophages into an anti-inflammatory M2 state, and ameliorated mechanic and thermal hypersensitivity (65). Recently, it was shown that local sympathectomy relieves chemotherapy-induced allodynia in mice via anti-inflammatory responses. Depletion of monocytes/macrophages and blockade of transforming growth factor-β (TGF-β) signaling reversed the relief of mechanical allodynia by sympathectomy (66). Importantly, TGF-β induces M2-like macrophage polarization (67), indicating that TGF-β-induced M2 macrophage polarization might be responsible for the therapeutic effect of local sympathectomy in the aforementioned study.

Interestingly, cultured M2 macrophages contained and released higher amounts of opioid peptides (63). Similar, a recent study demonstrated that IL-4 application at injured nerves shifted macrophage polarization from a proinflammatory M1 to an anti-inflammatory M2 phenotype. These M2 macrophages continuously synthesized opioid peptides. IL-4 administration further resulted in a long-lasting attenuation of neuropathy-induced mechanical hypersensitivity after discontinuing treatment. Confirming the importance of M2 macrophage-secreted opioids, IL-4-induced analgesia was decreased after neutralizing opioid peptides or blocking opioid receptors at the injured nerves (68). These studies indicate that M2 polarized macrophages may regulate pain perception by modulation of the opioid system. A key observation of our study showing that TNFR2 agonist treatment promotes long-lasting pain recovery was a repolarization of CNS-infiltrating macrophages into an anti-inflammatory M2-like phenotype (18). However, the contribution of M2 polarized macrophages in the spinal cord to pain alleviation and a potential role of the opioid system is not clear yet.

IMMUNE-MEDIATED SEX DIFFERENCES IMPACT CNP DEVELOPMENT

Next to social and psychological factors, functional differences in the immune system contribute to a higher female prevalence for CNP development (69, 70). Using rodent models of injury-induced CNP, it was shown that male and female mice use different immune cells to initiation and maintain CNP. In particular, microglia were shown to be the driver of male neuroinflammation and CNP, whereas T cells primarily drive neuroinflammation and CNP in females (71). These differences seem to be dependent on cell populations, differences in suppression by hormones, and disparate cellular responses in males and females (72). Interestingly, in the absence of adaptive immune cells, e.g., in $Rag1^{-/-}$ mice, female mice use the male, glial-dependent pathway (71). Since sex differences may impact the effectivity of analgesic therapeutics, the different impact of immune cells to pain responses

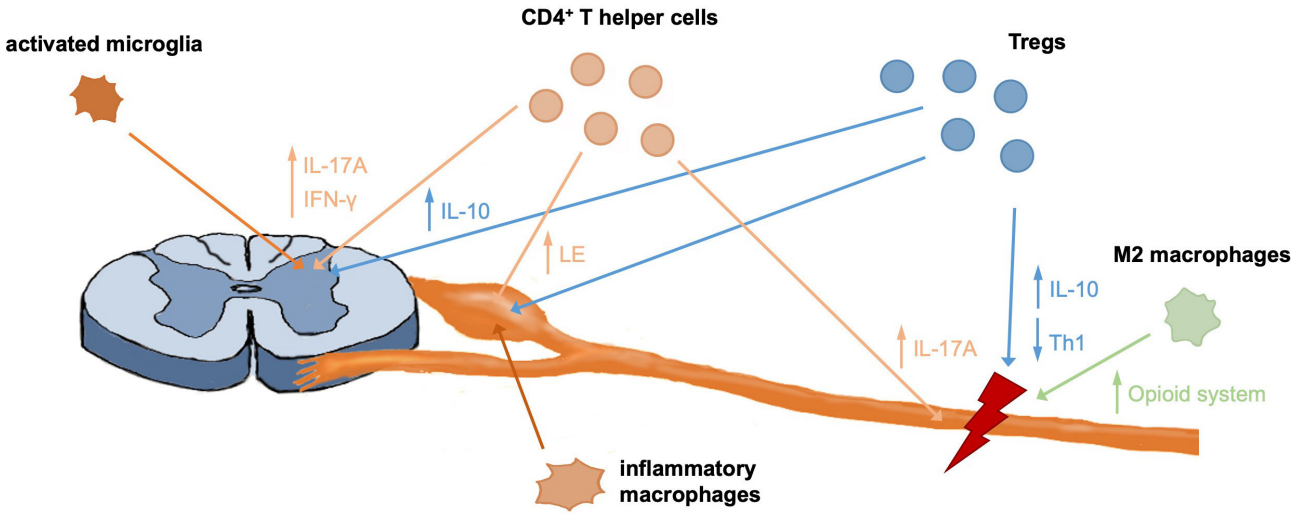

FIGURE 1 | Contribution of different immune cells to pain development and recovery. $CD4^+$ T helper cells were shown to infiltrate the spinal cord, DRG and injured nerve, where they contribute to pain responses through different mechanisms. Further, DRG invading macrophages were shown to be important mediators of pain. Like T effector cells, Tregs infiltrate the nerve, DRG, and spinal cord in neuropathic mice and contribute to immunomodulation and tissue regeneration through different mechanisms, including secretion of anti-inflammatory IL-10. M2 macrophages were shown to initiate analgesic responses in the nerve through upregulation of the endogenous opioid system and anti-inflammatory responses.

TABLE 1 | Overview of peripheral immune cell contribution to pain development and recovery.

Immune cell	Role	Mediators (Therapeutic target)
$CD4^+$ Th1 cells	Promote pain development and maintenance	IL17A, leukocyte elastase
$CD4^+$ Th2 cells	Promote pain recovery	IL-10, IL-4
$CD8^+$ T cells (educated)	Promote pain recovery	IL-10
Tregs	Promote pain recovery	IL-10, IL-35, TGF-β, TNFR2
Inflammatory macrophages	Promote pain development and maintenance	CX3CL1, ROS
Anti-inflammatory macrophages	Alleviate pain	Endogenous opioids, TGF-β, IL-10

needs to be considered in therapeutics development. Indeed, we observed different responsiveness of male and female mice in a preclinical trial for a novel TNF modulating compound (73). Therefore, it is important to study the therapeutic responses in males and females during preclinical evaluation, in particular if they address T cell or microglial responses. Therapies based on Treg modulation work across sexes (18) indicating that they may interfere with microglial and adaptive immune cell contribution to CNP development and maintenance.

CONCLUSION AND OUTLOOK

The contribution of immunity to development and maintenance of CNP are well-established and a complex interaction of different immune cells contributes to CNP development (**Figure 1**). Over the last years a growing body of literature on the protective and regenerative role of the immune system for pain has been published, including contributions of $CD8^+$ T cells, Tregs and M2 macrophages (**Figure 1**). Modulation of immune responses, e.g., by targeting inflammatory or anti-inflammatory mediators of peripheral immune cells, therefore is a promising therapeutic approach to alleviate neuropathic pain (**Table 1**). Concluding, a detailed understanding of immune-mediated tissue regeneration in pain may promote the development of novel immunotherapies for pain alleviation and ultimately may translate into novel non-opioid therapies.

AUTHOR CONTRIBUTIONS

RF wrote the review and generated the figure. JB reviewed and revised the manuscript. Both authors contributed to the article and approved the submitted version.

FUNDING

RF was supported by a grant from the Michael J. Fox Foundation (MJFF18334) and JB was supported by grants from the NIH (R01NS051709, R01NS111761, R01NS106908, R01NS096971).

REFERENCES

1. Fasick V, Spengler RN, Samankan S, Nader ND, Ignatowski TA. The hippocampus and TNF: Common links between chronic pain and depression. *Neurosci Biobehav Rev.* (2015) 53:139–59. doi: 10.1016/j.neubiorev.2015.03.014
2. Costigan M, Scholz J, Woolf CJ. Neuropathic pain: a maladaptive response of the nervous system to damage. *Annu Rev Neurosci.* (2009) 32:1–32. doi: 10.1146/annurev.neuro.051508.135531
3. Jensen TS, Baron R, Haanpää M, Kalso E, Loeser JD, Rice ASC, et al. A new definition of neuropathic pain. *Pain.* (2011) 152:2204–5. doi: 10.1016/j.pain.2011.06.017
4. Murphy KL, Bethea JR, Fischer R. *Multiple Sclerosis: Perspectives in Treatment and Pathogenesis: Neuropathic Pain in Multiple Sclerosis—Current Therapeutic Intervention and Future Treatment Perspectives*. Brisbane, QLD: Codon Publications. (2017). doi: 10.15586/codon.multiplesclerosis.2017.ch4
5. Colloca L, Ludman T, Bouhassira D, Baron R, Dickenson AH, Yarnitsky D, et al. Neuropathic pain. *Nat Rev Dis Primers.* (2017) 3:17002. doi: 10.1038/nrdp.2017.2
6. Woolf CJ, Mannion RJ. Neuropathic pain: aetiology, symptoms, mechanisms, and management. *Lancet.* (1999) 353:1959–64. doi: 10.1016/S0140-6736(99)01307-0
7. Jensen TS, Finnerup NB. A brief history of pain. *Lancet Neurol.* (2014) 13:872. doi: 10.1016/S1474-4422(14)70187-5
8. Sweitzer SM, Hickey WF, Rutkowski MD, Pahl JL, DeLeo JA. Focal peripheral nerve injury induces leukocyte trafficking into the central nervous system: potential relationship to neuropathic pain. *Pain.* (2002) 100:163–70. doi: 10.1016/S0304-3959(02)00257-9
9. Moalem G, Xu K, Yu L. T lymphocytes play a role in neuropathic pain following peripheral nerve injury in rats. *Neuroscience.* (2004) 129:767–77. doi: 10.1016/j.neuroscience.2004.08.035
10. Moalem G, Grafe P, Tracey DJ. Chemical mediators enhance the excitability of unmyelinated sensory axons in normal and injured peripheral nerve of the rat. *Neuroscience.* (2005) 134:1399–411. doi: 10.1016/j.neuroscience.2005.05.046
11. Moalem G, Tracey DJ. Immune and inflammatory mechanisms in neuropathic pain. *Brain Res Rev.* (2006) 51:240–64. doi: 10.1016/j.brainresrev.2005.11.004
12. Austin PJ, Moalem-Taylor G. The neuro-immune balance in neuropathic pain: involvement of inflammatory immune cells, immune-like glial cells and cytokines. *J Neuroimmunol.* (2010) 229:26–50. doi: 10.1016/j.jneuroim.2010.08.013
13. Grace PM, Hutchinson MR, Maier SF, Watkins LR. Pathological pain and the neuroimmune interface. *Nat Rev Immunol.* (2014) 14:217–31. doi: 10.1038/nri3621
14. Chavan SS, Ma P, Chiu IM. Neuro-immune interactions in inflammation and host defense: Implications for transplantation. *Am J Transplant.* (2018) 18:556–63. doi: 10.1111/ajt.14515
15. Laumet G, Ma J, Robison AJ, Kumari S, Heijnen CJ, Kavelaars A. T cells as an emerging target for chronic pain therapy. *Front Mol Neurosci.* (2019) 12:216. doi: 10.3389/fnmol.2019.00216
16. Austin PJ, Kim CF, Perera CJ, Moalem-Taylor G. Regulatory T cells attenuate neuropathic pain following peripheral nerve injury and experimental autoimmune neuritis. *Pain.* (2012) 153:1916–31. doi: 10.1016/j.pain.2012.06.005
17. Lees JG, Duffy SS, Perera CJ, Moalem-Taylor G. Depletion of Foxp3$^+$ regulatory T cells increases severity of mechanical allodynia and significantly alters systemic cytokine levels following peripheral nerve injury. *Cytokine.* (2015) 71:207–14. doi: 10.1016/j.cyto.2014.10.028
18. Fischer R, Sendetski M, del Rivero T, Martinez GF, Bracchi-Ricard V, Swanson KA, et al. TNFR2 promotes Treg-mediated recovery from neuropathic pain across sexes. *Proc Natl Acad Sci USA.* (2019) 116:17045–50. doi: 10.1073/pnas.1902091116
19. Cao L, DeLeo JA. CNS-infiltrating CD4$^+$ T lymphocytes contribute to murine spinal nerve transection-induced neuropathic pain. *Eur J Immunol.* (2008) 38:448–58. doi: 10.1002/eji.200737485
20. Costigan M, Moss A, Latremoliere A, Johnston C, Verma-Gandhu M, Herbert TA, et al. T-cell infiltration and signaling in the adult dorsal spinal cord is a major contributor to neuropathic pain-like hypersensitivity. *J Neurosci.* (2009) 29:14415–22. doi: 10.1523/JNEUROSCI.4569-09.2009
21. Du B, Ding YQ, Xiao X, Ren HY, Su BY, Qi JG. CD4$^+$ αβ T cell infiltration into the leptomeninges of lumbar dorsal roots contributes to the transition from acute to chronic mechanical allodynia after adult rat tibial nerve injuries. *J Neuroinflammation.* (2018) 15:81. doi: 10.1186/s12974-018-1115-7
22. Kleinschnitz C, Hofstetter HH, Meuth SG, Braeuninger S, Sommer C, Stoll G. T cell infiltration after chronic constriction injury of mouse sciatic nerve is associated with interleukin-17 expression. *Exp Neurol.* (2006) 200:480–5. doi: 10.1016/j.expneurol.2006.03.014
23. Kim CF, Moalem-Taylor G. Interleukin-17 contributes to neuroinflammation and neuropathic pain following peripheral nerve injury in mice. *J Pain.* (2011) 12:370–83. doi: 10.1016/j.jpain.2010.08.003
24. Luo H, Liu HZ, Zhang WW, Matsuda M, Lv N, Chen G, et al. Interleukin-17 regulates neuron-glial communications, synaptic transmission, and neuropathic pain after chemotherapy. *Cell Rep.* (2019) 29:2384–97.e5. doi: 10.1016/j.celrep.2019.10.085
25. Vicuña L, Strochlic DE, Latremoliere A, Bali KK, Simonetti M, Husainie D, et al. The serine protease inhibitor SerpinA3N attenuates neuropathic pain by inhibiting T cell-derived leukocyte elastase. *Nat Med.* (2015) 21:518–23. doi: 10.1038/nm.3852
26. Sweitzer S. The differential role of spinal MHC class II and cellular adhesion molecules in peripheral inflammatory versus neuropathic pain in rodents. *J Neuroimmunol.* (2002) 125:82–93. doi: 10.1016/S0165-5728(02)00036-X
27. Dominguez CA, Kalliomäki M, Gunnarsson U, Moen A, Sandblom G, Kockum I, et al. The DQB1 *03:02 HLA haplotype is associated with increased risk of chronic pain after inguinal hernia surgery and lumbar disc herniation. *Pain.* (2013) 154:427–33. doi: 10.1016/j.pain.2012.12.003
28. Ding YQ, Luo H, Qi JG. MHCII-restricted T helper cells: an emerging trigger for chronic tactile allodynia after nerve injuries. *J Neuroinflammation.* (2020) 17:3. doi: 10.1186/s12974-019-1684-0
29. Mangiacavalli S, Corso A, Amici M, de Varettoni M, Alfonsi E, Lozza A, et al. Emergent T-helper 2 profile with high interleukin-6 levels correlates with the appearance of bortezomib-induced neuropathic pain. *Br J Haematol.* (2010) 149:916–8. doi: 10.1111/j.1365-2141.2010.08138.x
30. Luchting B, Rachinger-Adam B, Heyn J, Hinske LC, Kreth S, Azad SC. Anti-inflammatory T-cell shift in neuropathic pain. *J Neuroinflammation.* (2015) 12:12. doi: 10.1186/s12974-014-0225-0
31. Uçeyler N, Rogausch JP, Toyka KV, Sommer C. Differential expression of cytokines in painful and painless neuropathies. *Neurology.* (2007) 69:42–9. doi: 10.1212/01.wnl.0000265062.92340.a5
32. Leger T, Grist J, D'Acquisto F, Clark AK, Malcangio M. Glatiramer acetate attenuates neuropathic allodynia through modulation of adaptive immune cells. *J Neuroimmunol.* (2011) 234:19–26. doi: 10.1016/j.jneuroim.2011.01.005
33. Krukowski K, Eijkelkamp N, Laumet G, Hack CE, Li Y, Dougherty PM, et al. CD8$^+$ T cells and endogenous IL-10 are required for resolution of chemotherapy-induced neuropathic pain. *J Neurosci.* (2016) 36:11074–83. doi: 10.1523/JNEUROSCI.3708-15.2016
34. Siqueira Mietto B, Kroner A, Girolami EI, Santos-Nogueira E, Zhang J, David S. Role of IL-10 in resolution of inflammation and functional recovery after peripheral nerve injury. *J Neurosci.* (2015) 35:16431–42. doi: 10.1523/JNEUROSCI.2119-15.2015
35. Laumet G, Edralin JD, Dantzer R, Heijnen CJ, Kavelaars A. Cisplatin educates CD8$^+$ T cells to prevent and resolve chemotherapy-induced peripheral neuropathy in mice. *Pain.* (2019) 160:1459–68. doi: 10.1097/j.pain.0000000000001512
36. Liu XJ, Zhang Y, Liu T, Xu ZZ, Park CK, Berta T, et al. Nociceptive neurons regulate innate and adaptive immunity and neuropathic pain through MyD88 adapter. *Cell Res.* (2014) 24:1374–7. doi: 10.1038/cr.2014.106
37. Sakaguchi S, Yamaguchi T, Nomura T, Ono M. Regulatory T cells and immune tolerance. *Cell.* (2008) 133:775–87. doi: 10.1016/j.cell.2008.05.009
38. Davoli-Ferreira M, Lima KA, de, Fonseca MM, Guimarães RM, Gomes FI, Cavallini MC, et al. Regulatory T cells counteract neuropathic pain through inhibition of the Th1 response at the site of peripheral nerve injury. *Pain.* (2020) 161:1730–43. doi: 10.1097/j.pain.0000000000001879
39. Liesz A, Suri-Payer E, Veltkamp C, Doerr H, Sommer C, Rivest S, et al. Regulatory T cells are key cerebroprotective immunomodulators in acute experimental stroke. *Nat Med.* (2009) 15:192–9. doi: 10.1038/nm.1927

40. Duffy SS, Keating BA, Perera CJ, Lees JG, Tonkin RS, Makker PGS, et al. Regulatory T cells and their derived cytokine, interleukin-35, reduce pain in experimental autoimmune encephalomyelitis. *J Neurosci.* (2019) 39:2326–46. doi: 10.1523/JNEUROSCI.1815-18.2019
41. Sloane E, Ledeboer A, Seibert W, Coats B, van Strien M, Maier SF, et al. Anti-inflammatory cytokine gene therapy decreases sensory and motor dysfunction in experimental multiple sclerosis: MOG-EAE behavioral and anatomical symptom treatment with cytokine gene therapy. *Brain Behav Immun.* (2009) 23:92–100. doi: 10.1016/j.bbi.2008.09.004
42. Grace PM, Loram LC, Christianson JP, Strand KA, Flyer-Adams JG, Penzkover KR, et al. Behavioral assessment of neuropathic pain, fatigue, and anxiety in experimental autoimmune encephalomyelitis (EAE) and attenuation by interleukin-10 gene therapy. *Brain Behav Immun.* (2017) 59:49–54. doi: 10.1016/j.bbi.2016.05.012
43. Milligan ED, Langer SJ, Sloane EM, He L, Wieseler-Frank J, O'Connor K, et al. Controlling pathological pain by adenovirally driven spinal production of the anti-inflammatory cytokine, interleukin-10. *Eur J Neurosci.* (2005) 21:2136–48. doi: 10.1111/j.1460-9568.2005.04057.x
44. Ledeboer A, Jekich BM, Sloane EM, Mahoney JH, Langer SJ, Milligan ED, et al. Intrathecal interleukin-10 gene therapy attenuates paclitaxel-induced mechanical allodynia and proinflammatory cytokine expression in dorsal root ganglia in rats. *Brain Behav Immun.* (2007) 21:686–98. doi: 10.1016/j.bbi.2006.10.012
45. Shen KF, Zhu HQ, Wei XH, Wang J, Li YY, Pang RP, et al. Interleukin-10 down-regulates voltage gated sodium channels in rat dorsal root ganglion neurons. *Exp Neurol.* (2013) 247:466–75. doi: 10.1016/j.expneurol.2013.01.018
46. Fischer R, Proske M, Duffey M, Stangl H, Martinez GF, Peters N, et al. Selective activation of tumor necrosis factor receptor II induces antiinflammatory responses and alleviates experimental arthritis. *Arthritis Rheumatol.* (2018) 70:722–35. doi: 10.1002/art.40413
47. Lamontain V, Schmid T, Weber-Steffens D, Zeller D, Jenei-Lanzl Z, Wajant H, et al. Stimulation of TNF receptor type 2 expands regulatory T cells and ameliorates established collagen-induced arthritis in mice. *Cell Mol Immunol.* (2019) 16:65–74. doi: 10.1038/cmi.2017.138
48. Chopra M, Biehl M, Steinfatt T, Brandl A, Kums J, Amich J, et al. Exogenous TNFR2 activation protects from acute GvHD via host T reg cell expansion. *J Exp Med.* (2016) 213:1881–900. doi: 10.1084/jem.20151563
49. Fischer R, Padutsch T, Bracchi-Ricard V, Murphy KL, Martinez GF, Delguercio N, et al. Exogenous activation of tumor necrosis factor receptor 2 promotes recovery from sensory and motor disease in a model of multiple sclerosis. *Brain Behav Immun.* (2019) 81:247–59. doi: 10.1016/j.bbi.2019.06.021
50. Dombrowski Y, O'Hagan T, Dittmer M, Penalva R, Mayoral SR, Bankhead P, et al. Regulatory T cells promote myelin regeneration in the central nervous system. *Nat Neurosci.* (2017) 20:674–80. doi: 10.1038/nn.4528
51. Marchetti L, Klein M, Schlett K, Pfizenmaier K, Eisel ULM. Tumor necrosis factor (TNF)-mediated neuroprotection against glutamate-induced excitotoxicity is enhanced by N-methyl-D-aspartate receptor activation. Essential role of a TNF receptor 2-mediated phosphatidylinositol 3-kinase-dependent NF-kappa B pathway. *J Biol Chem.* (2004) 279:32869–81. doi: 10.1074/jbc.M311766200
52. Fischer R, Maier O, Siegemund M, Wajant H, Scheurich P, Pfizenmaier K. A TNF receptor 2 selective agonist rescues human neurons from oxidative stress-induced cell death. *PLoS ONE.* (2011) 6:e27621. doi: 10.1371/journal.pone.0027621
53. Dong Y, Fischer R, Naudé PJW, Maier O, Nyakas C, Duffey M, et al. Essential protective role of tumor necrosis factor receptor 2 in neurodegeneration. *Proc Natl Acad Sci USA.* (2016) 113:12304–9. doi: 10.1073/pnas.1605195113
54. Abbadie C, Lindia JA, Cumiskey AM, Peterson LB, Mudgett JS, Bayne EK, et al. Impaired neuropathic pain responses in mice lacking the chemokine receptor CCR2. *Proc Natl Acad Sci USA.* (2003) 100:7947–52. doi: 10.1073/pnas.1331358100
55. Huang ZZ, Li D, Liu CC, Cui Y, Zhu HQ, Zhang WW, et al. CX3CL1-mediated macrophage activation contributed to paclitaxel-induced DRG neuronal apoptosis and painful peripheral neuropathy. *Brain Behav Immun.* (2014) 40:155–65. doi: 10.1016/j.bbi.2014.03.014
56. Old EA, Nadkarni S, Grist J, Gentry C, Bevan S, Kim K-W, et al. Monocytes expressing CX3CR1 orchestrate the development of vincristine-induced pain. *J Clin Invest.* (2014) 124:2023–36. doi: 10.1172/JCI71389
57. Montague K, Simeoli R, Valente J, Malcangio M. A novel interaction between CX3CR1 and CCR2 signalling in monocytes constitutes an underlying mechanism for persistent vincristine-induced pain. *J Neuroinflammation.* (2018) 15:101. doi: 10.1186/s12974-018-1116-6
58. Peng J, Gu N, Zhou L, B, Eyo U, Murugan M, Gan WB, et al. Microglia and monocytes synergistically promote the transition from acute to chronic pain after nerve injury. *Nat Commun.* (2016) 7:12029. doi: 10.1038/ncomms12029
59. Yu X, Liu H, Hamel KA, Morvan MG, Yu S, Leff J, et al. Dorsal root ganglion macrophages contribute to both the initiation and persistence of neuropathic pain. *Nat Commun.* (2020) 11:264. doi: 10.1038/s41467-019-13839-2
60. Hu P, McLachlan EM. Macrophage and lymphocyte invasion of dorsal root ganglia after peripheral nerve lesions in the rat. *Neuroscience.* (2002) 112:23–38. doi: 10.1016/S0306-4522(02)00065-9
61. Hu P, Bembrick AL, Keay KA, McLachlan EM. Immune cell involvement in dorsal root ganglia and spinal cord after chronic constriction or transection of the rat sciatic nerve. *Brain Behav Immun.* (2007) 21:599–616. doi: 10.1016/j.bbi.2006.10.013
62. Liu P, Peng J, Han GH, Ding X, Wei S, Gao G, et al. Role of macrophages in peripheral nerve injury and repair. *Neural Regen Res.* (2019) 14:1335–42. doi: 10.4103/1673-5374.253510
63. Pannell M, Labuz D, Celik MÖ, Keye J, Batra A, Siegmund B, et al. Adoptive transfer of M2 macrophages reduces neuropathic pain via opioid peptides. *J Neuroinflammation.* (2016) 13:262. doi: 10.1186/s12974-016-0735-z
64. Takahashi Y, Hasegawa-Moriyama M, Sakurai T, Inada E. The macrophage-mediated effects of the peroxisome proliferator-activated receptor-gamma agonist rosiglitazone attenuate tactile allodynia in the early phase of neuropathic pain development. *Anesth Analg.* (2011) 113:398–404. doi: 10.1213/ANE.0b013e31821b220c
65. Kiguchi N, Kobayashi Y, Saika F, Sakaguchi H, Maeda T, Kishioka S. Peripheral interleukin-4 ameliorates inflammatory macrophage-dependent neuropathic pain. *Pain.* (2015) 156:684–93. doi: 10.1097/j.pain.0000000000000097
66. Tonello R, Xie W, Lee SH, Wang M, Liu X, Strong JA, et al. Local sympathectomy promotes anti-inflammatory responses and relief of paclitaxel-induced mechanical and cold allodynia in mice. *Anesthesiology.* (2020) 132:1540–53. doi: 10.1097/ALN.0000000000003241
67. Zhang F, Wang H, Wang X, Jiang G, Liu H, Zhang G, et al. TGF-β induces M2-like macrophage polarization via SNAIL-mediated suppression of a pro-inflammatory phenotype. *Oncotarget.* (2016) 7:52294–306. doi: 10.18632/oncotarget.10561
68. Celik MÖ, Labuz D, Keye J, Glauben R, Machelska H. IL-4 induces M2 macrophages to produce sustained analgesia via opioids. *JCI Insight.* (2020) 5:e133093. doi: 10.1172/jci.insight.133093
69. Berkley KJ. Sex differences in pain. *Behav Brain Sci.* (1997) 20:371–80; discussion 435–513. doi: 10.1017/S0140525X97221485
70. Fillingim RB, King CD, Ribeiro-Dasilva MC, Rahim-Williams B, Riley JL. Sex, gender, and pain: a review of recent clinical and experimental findings. *J Pain.* (2009) 10:447–85. doi: 10.1016/j.jpain.2008.12.001
71. Sorge RE, Mapplebeck JCS, Rosen S, Beggs S, Taves S, Alexander JK, et al. Different immune cells mediate mechanical pain hypersensitivity in male and female mice. *Nat Neurosci.* (2015) 18:1081–3. doi: 10.1038/nn.4053
72. Sorge RE, Totsch SK. Sex differences in pain. *J Neurosci Res.* (2017) 95:1271–81. doi: 10.1002/jnr.23841
73. del Rivero T, Fischer R, Yang F, Swanson KA, Bethea JR. Tumor necrosis factor receptor 1 inhibition is therapeutic for neuropathic pain in males but not in females. *Pain.* (2019) 160:922–31. doi: 10.1097/j.pain.0000000000001470

Conflict of Interest: JB and RF are named inventors on patent applications covering the use of TNFR2 agonists. RF is a named inventor on patent applications covering the TNFR2 agonist technology.

frontiers in Immunology

ORIGINAL RESEARCH
published: 12 April 2021
doi: 10.3389/fimmu.2021.642420

Neuroimmune Consequences of eIF4E Phosphorylation on Chemotherapy-Induced Peripheral Neuropathy

Nilesh M. Agalave[†], *Prapti H. Mody*[†], *Thomas A. Szabo-Pardi*, *Han S. Jeong and Michael D. Burton*[*]

Neuroimmunology and Behavior Laboratory, Department of Neuroscience, School of Behavioral and Brain Sciences, Center for Advanced Pain Studies, University of Texas at Dallas, Richardson, TX, United States

OPEN ACCESS

Edited by:
Junji Xing, Houston Methodist Research Institute, United States

Reviewed by:
Michaela Semeraro, Assistance Publique Hopitaux De Paris, France
Temugin Berta, University of Cincinnati, United States

***Correspondence:**
Michael D. Burton
Michael.Burton@UTDallas.edu

[†]*These authors have contributed equally to this work*

Specialty section:
This article was submitted to Molecular Innate Immunity, a section of the journal Frontiers in Immunology

Received: *16 December 2020*
Accepted: *18 March 2021*
Published: *12 April 2021*

Citation:
Agalave NM, Mody PH, Szabo-Pardi TA, Jeong HS and Burton MD (2021) Neuroimmune Consequences of eIF4E Phosphorylation on Chemotherapy-Induced Peripheral Neuropathy. Front. Immunol. 12:642420. doi: 10.3389/fimmu.2021.642420

Chemotherapy-induced peripheral neuropathy (CIPN) is a major dose-limiting side effect that occurs in up to 63% of patients and has no known effective treatment. A majority of studies do not effectively assess sex differences in the onset and persistence of CIPN. Here we investigated the onset of CIPN, a point of therapeutic intervention where we may limit, or even prevent the development of CIPN. We hypothesized that cap-dependent translation mechanisms are important in early CIPN development and the bi-directional crosstalk between immune cells and nociceptors plays a complementary role to CIPN establishment and sex differences observed. In this study, we used wild type and eIF4E-mutant mice of both sexes to investigate the role of cap-dependent translation and the contribution of immune cells and nociceptors in the periphery and glia in the spinal cord during paclitaxel-induced peripheral neuropathy. We found that systemically administered paclitaxel induces pain-like behaviors in both sexes, increases helper T-lymphocytes, downregulates cytotoxic T-lymphocytes, and increases mitochondrial dysfunction in dorsal root ganglia neurons; all of which is eIF4E-dependent in both sexes. We identified a robust paclitaxel-induced, eIF4E-dependent increase in spinal astrocyte immunoreactivity in males, but not females. Taken together, our data reveals that cap-dependent translation may be a key pathway that presents relevant therapeutic targets during the early phase of CIPN. By targeting the eIF4E complex, we may reduce or reverse the negative effects associated with chemotherapeutic treatments.

Keywords: Dorsal Root Ganglia, astrocyte, microglia, T-cell, mitochondrial respiration, eIF4E, sex differences, neuroimmune

INTRODUCTION

Chemotherapy-induced peripheral neuropathy (CIPN) is one of the most prevalent and dose-limiting complications in chemotherapy patients. It is characterized by pain and numbness or a "pins and needles" feeling in the extremities (1–4). Approximately 70% of patients report the development of peripheral neuropathy during administration of chemotherapy, which leads to early

treatment cessation and substandard regimens (5, 6). Additionally, over 30% of patients experience persistent neuropathy for months or years after treatment cessation, making CIPN a long-term morbidity in patients that survive cancer and other diseases (7).

There is limited data on sex differences in neuroimmune effects during CIPN. Both clinical and preclinical investigations have reported conflicting observations ranging from marked sexual dimorphisms to no sex differences during CIPN (8–11). There are few studies that investigate sex differences and the mechanisms involved in the development of CIPN. These findings necessitate a comprehensive and fully powered assessment of sex differences in the development of CIPN. Considering the recent interest in sex differences in chronic pain development and immune cell activation, it is purported that neuroimmune mechanisms vary between sexes. A benchmark paper in the pain field suggests sexual dimorphisms in the role of T-cells in pain initiation in females (12). Moreover, recent studies have shown that cytotoxic T-cells ($CD8^+$) contribute to the resolution of CIPN (13, 14). A more recent study showed that "primed" $CD8^+$ T-cells, previously exposed to a chemotherapy agent, could prevent CIPN development when transferred to a new host (15). Based on these previous studies, we decided to assess the role of discrete T-cell subtypes: $CD4^+$(Th1, Th2), T regulatory (T_{regs}), Effector (T_{eff}), and activated cytotoxic T-lymphocytes ($CD8^+$) in the draining lymph nodes of male and female mice after induction of CIPN.

Immune cells recruited to the dorsal root ganglion (DRG) in turn can influence the activity of nociceptors through the release of inflammatory mediators (16, 17). This signaling could happen in tandem, in real-time, and this bi-directional crosstalk could be directly responsible for changes in nociceptors and immune cells, leading to changes in pain behaviors. These reciprocal interactions may contribute to maladaptive nociceptor plasticity if the homeostatic functioning of the cell-mediated immune response is dysregulated and has been shown to contribute to the development of CIPN (18–21)

Eukaryotic translation initiation factor 4E (eIF4E) is a cytosolic regulator that directs ribosomes to the cap structure of a subset of mRNAs to induce translation of proteins involved in inflammation and pain (22, 23). Cellular signaling cascades responsive to external stimuli such as the mitogen-associated protein kinase (MAPK) pathway and the mammalian target of rapamycin (mTOR) pathway directly feed into central cap-dependent translation in all cell types (24, 25). Regulation of eIF4E activation affects downstream signaling for production of a subset of pro-inflammatory cytokines involved in T-cell subsets activation, cellular metabolic pathways of nociceptors, and other components that regulate pain, inflammation, and behavior (26–33). While we have begun to assess the role of eIF4E phosphorylation in sensory neuron populations (34), a complete breakdown of sex and sensory neuron metabolic phenotyping has yet to occur along with phenotyping of immune cell subtypes during the development of CIPN. It is known that sensory neuron metabolism is exceptionally responsive to nerve injury and inflammation (35–37). CIPN is accompanied with changes in mitochondrial bioenergetics and an energy deficit in DRG neurons (38, 39). These changes can also alter ion signaling and other downstream metabolic processes to contribute to long-term development of nociceptor sensitivity and pain (40). The metabolic effect(s) paclitaxel has in late CIPN, has been assessed in sensory neurons from male rats only (38).

Therefore, we sought to elucidate the role of cap-dependent protein translation in CIPN-induced alterations that may be mediated by neuroimmune communication between activated immune cells and sensory neurons. We used eIF4E mice that harbor a point mutation at the serine 209 site on the eIF4E complex that codes alanine instead, designated as $eIF4E^{S209A}$ (41). This point mutation prevents phosphorylation of eIF4E, thus inhibiting its activation and consequently inhibiting cap-dependent protein translation (42, 43). Paclitaxel is one of many chemotherapeutics used in rodent models to mimic clinical CIPN (44). Given that CIPN has an elusive etiology and the diverse array of cell types that could participate in CIPN development, we investigated whether there was a sex-dependent role of eIF4E phosphorylation in DRG sensory neuron metabolism, local immune cell populations, peripheral T-cell subpopulations, and spinal microglia and astrocytes. We hypothesized that eIF4E phosphorylation regulates activation of specific macrophage and T-cell subpopulations, alters nociceptor metabolism, and glial activation during the early phase of paclitaxel-induced peripheral neuropathy.

MATERIALS AND METHODS

Animals

Adult mice of both sexes (9-12 weeks old, 20-25g weight) were used for all experiments. $eIF4E^{S209A}$ mice were generated on a C57BL/6 background in the Sonenberg laboratory at McGill University as previously described (41). These were a gift and further bred to maintain genotypes at the University of Texas at (UT) Dallas vivarium to generate our experimental cohorts. In-house animals were weaned between 21 and 28 days of age and tail-clipped to verify genotypes. Both wild-type (WT) and $eIF4E^{S209A}$ gift mice were bred with breeder animals purchased from Jackson laboratory (WT). We used only homozygous $eIF4E^{S209A}$ mutant animals and WT littermates for experiments. All animals were housed at the UT Dallas vivarium with standard temperature (20-25°C) and a 12-hour light/dark cycle (lights on from 6 AM to 6 PM). Mice were group housed in polypropylene ventilated cages with 4-5 animals per cage and provided *ad libitum* access to food and water. All behavioral experiments and data analysis were carried out from 9am to 12pm during the light cycle. All experiments were performed in accordance with protocols and standard operating procedures (SOPs) approved by the University of Texas at Dallas Institutional Animal Care and Use Committee (IACUC) and the Institution Biosafety and Chemical Safety Committee. The experimenters were blinded to animal

genotypes and treatment groups for all assays. A timeline of experiments and dosing regimen is shown in **Figure 1**.

Induction of Chemotherapy-Induced Peripheral Neuropathy (CIPN) With Administration of Paclitaxel

Paclitaxel (European pharmacopoeia (EP) Reference standard purchased from Sigma, Y0000698) was dissolved in a vehicle (1:1 ratio of Kolliphor oil (Sigma, C5135) and 100% ethanol), to prepare stock paclitaxel solution (5mg/mL stored at 4°C). Working stock was freshly prepared on injection days by diluting stock solution with sterile 1× PBS. Paclitaxel injections were administered intraperitoneally every other day for four (4mg/kg/day) injections to induce peripheral neuropathy (16mg/kg total dose per animal, **Figure 1**) as previously described (44, 45), these studies show little to no differences of 2mg/kg versus 4mg/kg in the development of painful CIPN.

Behavioral Experiments

Baseline readings for all behavior assays were taken twice, a day apart (days -1 and -3) before administration of the 1st paclitaxel injection on day 0. Behavioral assessment for spontaneous pain using the grimace scale, mechanical hypersensitivity, grip strength, and thermal hyperalgesia were performed on days 1, 3, 5, 7, and 9, in that order. This was important to maintain non-confounding observations of evoked pain behavior using touch or heat stimuli after noting spontaneous pain. All behavior datasets are additionally represented as effect size. Effect size here is determined by calculating the cumulative difference between the value for each time point and the baseline value. All effect values were added to get effect size represented as an absolute number for each of the animal groups (46).

Assessment of Spontaneous Pain by Grimace Scale

Grimace is assessment of spontaneous pain using the observation of facial expression (47–49). Five parameters for facial grimace behavior were assessed: orbital tightening, ear position, cheek bulge, nose bulge, and whisker position. Each component was scored as follows: not present was given a score of "0", moderately present was given a score of "1", and obviously present was given a score of "2". The score of the five components was averaged to give a mean grimace score (MGS).

Assessment of Mechanical Hypersensitivity by von Frey Filaments

Mechanical hypersensitivity was assessed using the previously described von Frey assay (50). Von Frey acrylic chamber (11cm long, 10 cm wide, and 4.5 cm height) with mesh floor, elevated 4.25 feet off the ground, were used for this assay. Animals were acclimated to the testing room and habituated to the von Frey apparatus and test environment for at least 1 hour prior to baseline and testing measurements. After 2 baseline recordings (one day rest in between the recordings), animals were randomly

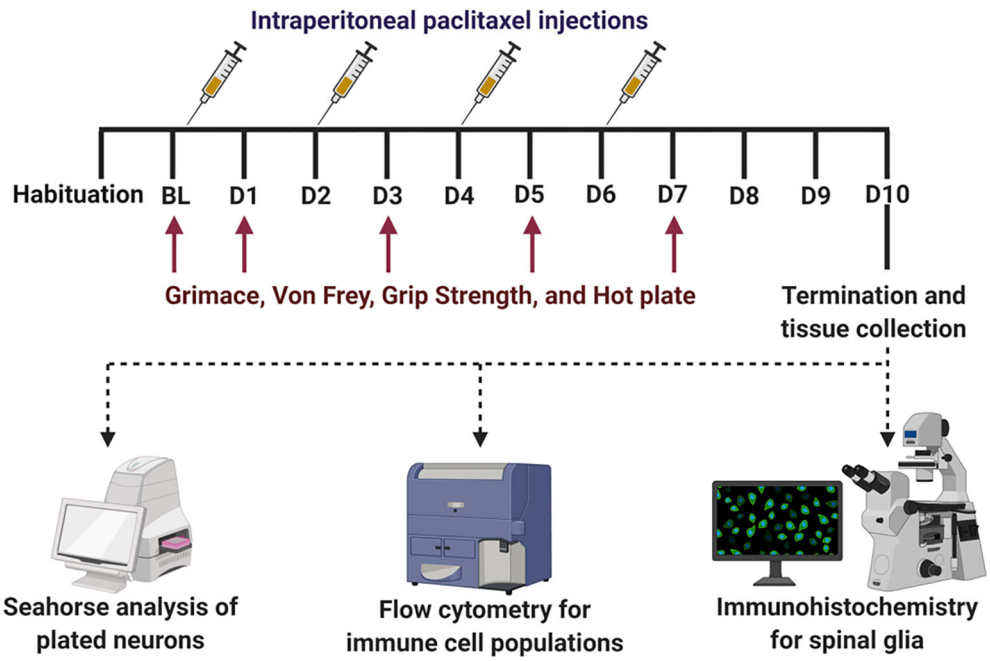

FIGURE 1 | Experimental timeline with dosing regimen and terminal analysis. After habituation and baseline (BL) measures for behavior, all mice were subjected to intraperitoneal injection of paclitaxel (4 mg/kg per mouse) after BL i.e. on day 0, D2, D4, and D6 to induce peripheral neuropathy. Behavioral assays (mechanical hypersensitivity, grimace, grip strength, and thermal hypersensitivity) were measured on BL, D1, D3, D5, D7, and D9. On D10, animals were terminated and spinal cord, popliteal and inguinal lymph nodes, and DRG (L3 to T13) were collected. The lumbar portion of the spinal cord was used for immunohistochemical analyses for glia reactivity. The lymph nodes and DRG were used for flow cytometry analyses of immune cell populations. DRG neurons were plated and used for Seahorse analyses of bioenergetics.

assigned to the different treatment groups. Mechanical hypersensitivity was determined by assessment of paw withdrawal threshold in response to the application of calibrated von Frey filaments (Stoelting, Illinois, USA) using the up-down method. A series of filaments with logarithmically incremental stiffness of 2.83, 3.22, 3.61, 3.84, 4.08, and 4.17 (converted to the 0.07, 0.16, 0.4, 0.6, 1, and 1.4 grams, respectively) were applied to the plantar surface of the hind paw and held for 2-3 seconds. A positive response was counted if there was a brisk withdrawal of the paw, paw shaking, and paw licking, or holding the paw in the air more than 2 seconds. The withdrawal threshold of both hind paws was measured and averaged.

Assessment of Muscle Dexterity by Grip Strength

Grip strength is a measure of functional pain in laboratory rodents and is measured with a grip strength test meter (IITC, California, USA). All animals were habituated to the apparatus for 5 minutes per animal, and were trained to grip the mesh wire surface prior to baseline or experiment. To measure, animals were gently placed on the rectangular wire meshed surface connected to the transducer in the grip strength meter and gently pulled away until they let go of the mesh. The maximal grip force was automatically measured by the transducer and recorded. Three trials were performed and averaged for both baseline measures and all experiments.

Assessment of Thermal Hyperalgesia by Hot Plate

Thermal sensitivity was assessed using the hot plate apparatus (IITC, California, USA). Animals were individually placed onto a surface maintained at 52°C, with their locomotion restricted by a Plexiglas chamber. Hind paw licking, shaking, and jumping was recorded as a positive response. Total time spent on the hot plate surface until a positive response was detected was measured and recorded as latency to response. The heating time cutoff was restricted to maximum 30 seconds to prevent tissue injury.

Immunohistochemistry

Animals were anesthetized with intraperitoneal injection of Ketamine/Xylazine (100 mg/kg) and intracardially perfused with 1x PBS solution followed by 4% paraformaldehyde (PFA). Lumbar spinal cord tissue was collected, post fixed in 4% PFA for 4 hours at 4°C and cryoprotected in 30% sucrose for 48 hours at 4°C. Tissues were embedded in optimal cutting temperature (OCT) (Fisher Scientific; 23-730-571) followed by cryo-sectioning into 20 µm sections that were mounted on positively charged glass slides (VWR, 48311-703). Mounted sections were treated with 1M HCL for 30 minutes followed by neutralization with 0.1 M sodium borate (pH 8.5) for 10 minutes. The slides were washed with 1x PBS and pre-incubated with 5% normal goat serum in 0.2% Triton X-100 in 1x PBS solution to block nonspecific binding. Subsequently, sections were incubated with the primary antibodies overnight at 4°C (see **Table 1**). The next day, sections were incubated in respective secondary antibodies and treated with DAPI solution (1:5000 dilution, Sigma-Aldrich D9542). Stained sections were covered with Gelvatol mounting medium and cover slips (51) and images were taken on a Zeiss Axio-observer 7 microscope (Jena, Germany) for quantitative analysis. Representative images were taken on an Olympus FV3000RS confocal laser scanning microscope (Shinjuku, Tokyo, Japan). Images acquired for quantitative analysis were taken using identical exposure times and representative images at identical laser power. Image analysis was done using FIJI (ImageJ) and Cell Sens version 3.1 (Olympus, Japan) software.

TABLE 1 | Antibodies used for IHC and flow cytometry.

Antibody	Company	Catalog number	Working dilution
Antibodies used for IHC			
Anti-Iba1	WAKO	019-19741	1:1000
Anti-GFAP	DAKO	Z-0331	1:1000
Anti-NeuN	EMD Millipore	MAB377	1:1000
Anti-ATF3	Abcam	ab207434	1:1000
Goat anti-mouse Alexa Fluor 488	Invitrogen	A21121	1:500
Goat anti-rabbit Alexa Fluor 647	Invitrogen	A21245	1:500
Antibodies used for flow cytometry			
Anti-CD16/32	eBioscience	16016185	1:2000
Anti-CD3 Alexa fluor 700 conjugate	eBioscience	56003280	1:200
Anti-CD4 Fluorescein isothiocyanate conjugate	eBioscience	11004185	1:200
Anti-CD8 Phycoerythrin conjugate	eBioscience	12-0081-83	1:200
Anti-CD25 eFluor 450 conjugate	eBioscience	48025182	1:200
Anti-CD44 eFluor780 conjugate	eBioscience	47044182	1:200
Anti-CCR7 Allophycocyanin conjugate	eBioscience	17197942	1:200
Anti-CD11b Allophycocyanin-Cy7 conjugate	Life Technologies	A15390	1:200
Anti-CD45 Brilliant violet 421 conjugate	Biolegend	103133	1:200
Anti-MHCII Alexa fluor 488 conjugate	eBioscience	11532282	1:2000
Anti-CD40 Phycoerythrin conjugate	eBioscience	120401-82	1:200

Flow Cytometry

Flow cytometric analysis of isolated immune cells from lymph node and dissociated DRG was performed based on previous protocols with few modifications (52). In brief, lymph nodes (popliteal and inguinal) and DRG (lumbar and thoracic, T13 to L5) were collected in ice cold sterile DPBS (Hyclone, Logan, UT). Lymph nodes were passed through a 70 micron nylon mesh with flow buffer (0.5% bovine serum albumin with 0.02% glucose) while DRG were first digested with enzymes (details described in section 2.6) and then passed through 70 micron nylon mesh. Resultant cell suspensions were centrifuged at 400 × g for 6 minutes at 4 °C. Cell pellets were washed with cold 1x PBS and resuspended in pre-chilled flow buffer. Fc receptors were blocked by anti-CD16/CD32 purified antibody. Cells from lymph nodes were incubated with anti-CD3-Alexa Flour 700, anti-CD4-Fluorescein isothiocyanate, anti-CD8 Phycoerythrin, anti-CD25-eFluor 450, anti-CD44-eFluor780, and anti-CCR7-Allophycocyanin (see **Table 1** for antibody details). Cells from DRG were incubated with anti-CD11b-Allophycocyanin-Cy7, anti-CD45-Brillient violet 421, anti-MHCII-Alexa Fluor 488, and anti-CD40 Phycoerythrin antibodies. Appropriate compensation controls and isotypes were used for determination

and gating. Cells were washed twice in ice cold flow buffer and resuspended in ice cold flow buffer. T_{helper} T-cells were initially identified with gating CD3 and CD4 cell surface markers, whereas cytotoxic T-cells were identified by gating for CD3 and CD8. These populations were further gated to identify activation and polarization (T_{h1} vs. T_{h2}) with CD44 and CD25. CCR7 was also used to identify T-effector cells. Tissue activated macrophages were identified from CD45 separated cells with cell surface markers CD11b, MHC-II, and CD40. Stained samples were analyzed using a Becton-Dickinson Fortessa analyzer (Red Oaks, CA) and data were analyzed using FlowJo software (De Novo Software, Los Angeles, CA). For a complete list of antibodies used, please refer **Table 1**.

Primary Dorsal Root Ganglia (DRG) Culture and Cellular Energetics

On day 10, animals were deeply anesthetized with isoflurane and decapitated. DRG were dissected bilaterally starting from T13 to L5 and transferred to pre-chilled 1x PBS containing 1% penicillin/streptomycin (ThermoFisher Scientific, 15070063). Samples were centrifuged at 400 x g for 4 minutes. Supernatants were removed and DRG were treated with Collagenase A (Sigma, 10103586001) and incubated in water bath at 37°C for 20 minutes, followed with treatment of Collagenase D (Sigma, 1188866001) for another 20 minutes. Cells were centrifuged at 400 x g and pellet was resuspended in Enzyme T (soybean trypsin inhibitor made up in 1 part bovine serum albumin and 1 part DMEM/F12 media) to stop the enzymatic reaction. Digested tissues were triturated approximately 30 times using a 1 ml pipette tip and passed through the 70 micron nylon mesh, with a subsequent wash with DMEM/F12 media (supplemented with 10% Fetal bovine serum and 1% penicillin/streptomycin). Resultant suspension was centrifuged at 400 x g for 5 minutes and resuspended in DMEM/F12 medium. The number of cells was counted using a hemocytometer with trypan blue dye exclusion. For bioenergetic profile, 70,000 cells were seeded directly in respective XFp Cell Culture Miniplates (Agilent, 103025-100) coated with poly-D-Lysine (Millipore Sigma, P0899). Next day, XF Assay media (Seahorse Bioscience) supplemented with 2 mM GlutaMAX, 5 mM glucose (Sigma), 1 mM sodium pyruvate (Fisher Scientific, Loughborough, United Kingdom), and pH adjusted to pH 7.4, was warmed to 37°C. Cells were incubated with this Seahorse media for 1 hour at 37°C, 0% CO2 incubator. The media was replaced with the Seahorse XF calibrant solution for another hour before running the Mito Stress according to manufacturer's recommended protocol (53).

Statistical Analysis

Data were analyzed using GraphPad Prism software (version 8.4) and expressed as mean ± standard error of the mean (SEM). For behavior, flow cytometry, and Seahorse datasets, two-way ANOVAs were performed followed by Tukey's *post-hoc* for multiple comparisons. For Seahorse divided into phases of mitochondrial respiration, one-way ANOVA was performed with Sidak's multiple comparison test. For IHC datasets, two-way ANOVA followed by Bonferroni's *post-hoc* was performed for glia reactivity and Sidak's *post-hoc* was used for ATF3. A p value of ≤ 0.05 was considered significant.

RESULTS

Paclitaxel Induces Pain Like Behavior in Male and Female Mice, Which Is Mediated *via* eIF4E

Previously, it has been shown that an intraperitoneal injection regimen of paclitaxel leads to development of long-lasting mechanical hypersensitivity in WT male and female mice during later stages of CIPN (45, 54). We investigated whether cap-dependent translation was involved in earlier stages of CIPN development after intraperitoneal paclitaxel administration. We found a significant paclitaxel-dependent increase in mechanical hypersensitivity in WT mice of both sexes, compared to vehicle treatment (**Figures 2A–D** and **Table 2**). In the absence of eIF4E phosphorylation, this increase was observed only in females (**Figures 2C, D** and **Table 2**), not male mice (**Figures 2A, B** and **Table 2**). Compared to WT paclitaxel-treated mice, the $eIF4E^{S209A}$ paclitaxel-treated mice had significantly lower mechanical hypersensitivity (**Figures 2B, D** and **Table 2**) in both sexes. These findings indicate that eIF4E phosphorylation plays a protective role in the development of mechanical hypersensitivity after paclitaxel administration, but this protection is to a lesser extent in females. We assessed spontaneous pain by grimace and grip strength. Paclitaxel treatment induced more grimacing in male mice in an eIF4E-dependent manner (**Figures 2E, F** and **Table 2**). For females, spontaneous pain was higher with paclitaxel administration, but $eIF4E^{S209A}$ females had lower grimacing compared to WT (**Figures 2G, H**). This indicates that eIF4E affects pain perception associated with paclitaxel-induced peripheral neuropathy. There were no changes in the grip strength for either sex, genotype, or treatment (**Figures 2I–L**). Male WT mice showed the maximum latency of response to hot plate with paclitaxel treatment, with no difference in $eIF4E^{S209A}$ male mice (**Figures 2M** and **Table 2**), indicating that eIF4E is required for mediating response to thermal stimuli after paclitaxel. On the other hand, females of both genotypes did not show significant changes in latency with paclitaxel treatment compared to vehicle (**Figures 2O, P** and **Table 2**). Interestingly, $eIF4E^{S209A}$ females treated with paclitaxel had a significantly reduced latency of response to heat stimuli compared to their WT counterparts (**Figure 2P** and **Table 2**). Taken together, our data suggests that eIF4E is important for mechanisms involved in CIPN development early in both sexes.

Paclitaxel Dysregulates $CD4^+$ and $CD8^+$ T-Cell Subpopulations in an eIF4E-Dependent Manner

An obvious early contribution of adaptive immune cells in the development of paclitaxel-induced peripheral neuropathy has not been shown till date. Given that the paclitaxel was

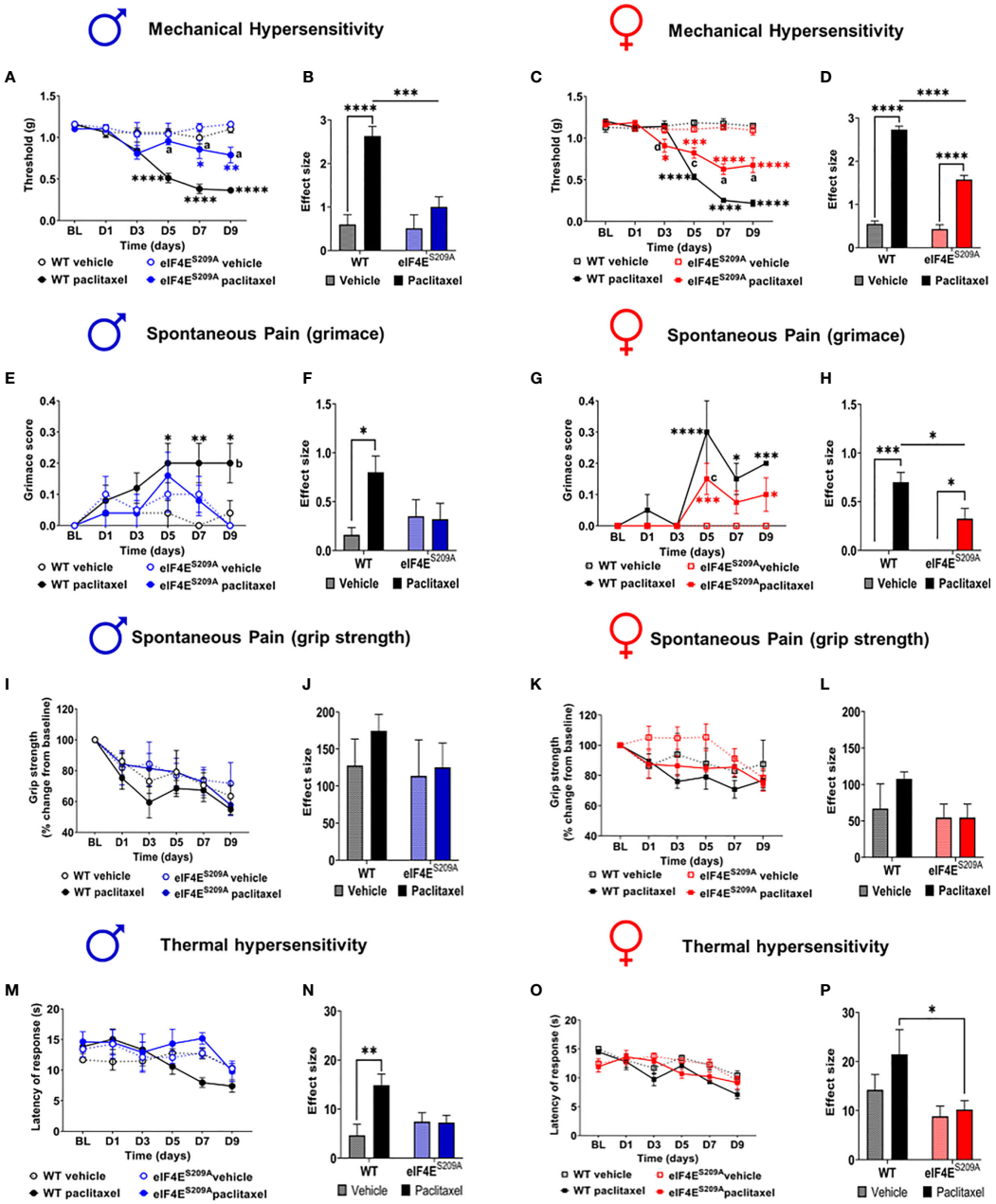

FIGURE 2 | Paclitaxel induces pain like behavior in male and female mice, which is eIF4E dependent. **(A)** Mechanical hypersensitivity in male WT and eIF4E^{S209A} mice. Blue asterisks *p 0.0475, ** p 0.0014 for eIF4E vehicle VS paclitaxel, Black asterisks ****p<0.0001 for WT vehicle VS paclitaxel, a=p<0.0001 for WT paclitaxel VS eIF4E paclitaxel. **(B)** Effect size here is determined by calculating the cumulative difference between the value for each time point and the baseline value. Data for male mice shown as effect size, ****p<0.0001, ***p 0.0004. **(C)** Mechanical hypersensitivity in female WT and eIF4E^{S209A} mice. Red asterisks *p 0.0261 , ***p 0.003 for eIF4E vehicle VS paclitaxel, Black asterisks ****p<0.0001 for WT vehicle VS paclitaxel, a=p<0.0001, c=p 0.0029, d=p 0.0286 for WT paclitaxel VS eIF4E paclitaxel. **(D)** Data for female mice shown as effect size, ****p<0.0001. **(E)** Spontaneous pain assessment by grimace score in male mice. *p 0.0495, **p 0.008 for WT vehicle VS paclitaxel. **(F)** Grimace scores shown as effect size for male mice, *p 0.0302. **(G)** Grimace scores for female mice. *p 0.0153 for D7 WT vehicle VS paclitaxel, 0.0328 for D9 for eIF4E vehicle VS paclitaxel, ***p 0.0004 for D5 for eIF4E vehicle VS paclitaxel, 0.0009 for D9 for WT vehicle VS paclitaxel, ****p<0.0001 for WT vehicle VS paclitaxel. **(H)** Grimace scores shown as effect size for female mice, *p 0.0249 compared for treatment, *p 0.0293 compared for genotype, ***p 0.0005. **(I)** Grip strength for male mice. **(J)** Grip strength for males shown as effect size. **(K)** Grip strength for female mice. **(L)** Grip strength in females shown as effect size. **(M)** Thermal hypersensitivity in male mice. **(N)** Thermal hypersensitivity in males shown as effect size. **p 0.0072. **(O)** Thermal hypersensitivity in female mice. **(P)** Thermal hypersensitivity in females shown as effect size, *p 0.0453. All data are presented as mean ± standard error of the mean, males: n = 6 mice per group; females: n = 12 mice per group. Two-way ANOVA was performed with Tukey's *post*-hoc for multiple comparisons. For all line graphs, asterisks indicate significant differences between vehicle VS paclitaxel-treated for each genotype at indicated time points. "a" (p < 0.0001), "b" (p < 0.001), "c" (p < 0.01), and "d" (p < 0.05) depict significant difference between paclitaxel-treated WT and eIF4E^{S209A} mice at indicated time points.

TABLE 2 | Statistical values for behavior data analysis.

Dataset	Main effect		Interactions		Multiple comparisons		
	F (DFn,DFd)	*p*-value	F (DFn,DFd)	*p*-value	Effect	Groups	*p*-value
Mechanical hypersensitivity male mice	Treatment: F (1, 25) = 12.26	**0.0018**	F (1, 25) = 9.797	**0.0044**	Treatment	Vehicle	0.9938
						Paclitaxel	**0.0004**
	Genotype: F (1, 25) = 26.48	**<0.0001**			Genotype	WT	**<0.0001**
						eIF4E^{S209A}	0.5380
Mechanical hypersensitivity female mice	Treatment: F (1, 19) = 251.1	**<0.0001**	F (1, 19) = 24.49	**<0.0001**	Treatment	Vehicle	0.8600
						Paclitaxel	**<0.0001**
	Genotype: F (1, 19) = 36.87	**<0.0001**			Genotype	WT	**<0.0001**
						eIF4E^{S209A}	**<0.0001**
Grimace male mice	Treatment: F (1, 15) = 4.236	**0.0574**	F (1, 15) = 5.111	**0.0391**	Treatment	Vehicle	0.8146
						Paclitaxel	0.1282
	Genotype: F (1, 15) = 0.9575	0.3433			Genotype	WT	**0.0302**
						eIF4E^{S209A}	0.9990
Grimace female mice	Treatment: F (1, 19) = 34.43	**<0.0001**	F (1, 19) = 4.609	**0.0449**	Treatment	Vehicle	>0.9999
						Paclitaxel	**0.0293**
	Genotype: F (1, 19) = 4.609	**0.0449**			Genotype	WT	**0.0005**
						eIF4E^{S209A}	**0.0249**
Grip strength male mice	Treatment: F (1, 18) = 0.6734	0.4226	F (1, 18) = 0.2471	0.6251	N/A		
	Genotype: F (1, 18) = 0.7916	0.3854					
Grip strength female mice	Treatment: F (1, 16) = 0.8995	0.3570	F (1, 16) = 0.8995	0.3570	N/A		
	Genotype: F (1, 16) = 2.349	0.1449					
Thermal hypersensitivity male mice	Treatment: F (1, 24) = 6.294	**0.0193**	F (1, 24) = 6.743	**0.0158**	Treatment	Vehicle	0.7602
						Paclitaxel	**0.0579**
	Genotype: F (1, 24) = 1.455	0.2395			Genotype	WT	**0.0072**
						eIF4E^{S209A}	>0.9999
Thermal hypersensitivity female mice	Treatment: F (1, 19) = 2.332	0.1432	F (1, 19) = 1.090	0.3097	Treatment	Vehicle	0.5527
						Paclitaxel	**0.0453**
	Genotype: F (1, 19) = 8.729	**0.0081**			Genotype	WT	0.4059
						eIF4E^{S209A}	0.9762

Two-way ANOVA was performed followed by Tukey's post-hoc for multiple comparisons between genotypes and treatments for each sex. $p \leq 0.05$ was considered significant (bolded).

administered peripherally, T-cells are activated in the lymph nodes, and neuropathy develops in the limbs, we chose to study subpopulations of T-cells from the draining (popliteal and inguinal) lymph nodes that are $CD4^+$ (T_{helper}) $CD8^+$, $CD25^{+/-}$ and $CD44^{+/-}$ (activated T-cells), $CCR7^+$ (effector T-cells) (**Figures 3A–F**). We found a significant increase in $CD4^+$ T-cells in WT female mice injected with paclitaxel, but not males (**Figures 3A, B, E** and **Table 3**). The $CD4^+$ subset was further analyzed for CCR7, the marker for lymphocyte homing to lymph nodes as well as T-cell priming (55, 56). The CD4+CD25-CD44+ subset was significantly reduced in eIF4E^{S209A} females treated with paclitaxel compared to WT (**Figure 3G**, **Table 3**). The $CD4^+CCR7^+$ subpopulation was significantly higher in eIF4E^{S209A} mice of both sexes independent of paclitaxel treatment (**Figures 3C, F** and **Table 3**). This suggests that inhibiting cap-dependent translation upregulates T-cell priming and activation of T cells. We found significant downregulation of $CD8^+$ T-cells in female eIF4E^{S209A} mice compared to WT, irrespective of treatment (**Figures 3G–L**, **Table 3**). This population was unchanged in male mice (**Figure 3H**). $CD8^+CCR7^+$ T-cells, i.e. activated memory T-cells were higher in eIF4E^{S209A} mice (**Figures 3I, L** and **Table 3**) regardless of sex or treatment. $CD8^+CD44^+CD25^-$ T-cells were increased in paclitaxel-treated eIF4E^{S209A} male mice compared to WT males treated with paclitaxel (**Figure 3J** and **Table 3**). There were no differences in female mice for this subpopulation (**Figure 3M** and **Table 3**). Overall, our data shows that paclitaxel induces activation and/or expansion of T-helper, memory T, and effector T-cells, which is modulated in an eIF4E-dependent manner.

Paclitaxel Induces Increased Infiltration of Activated Myeloid Cells in DRG in Absence of eIF4E Phosphorylation

We further investigated if peripheral neuropathy leads to the recruitment of macrophages into the DRG. No studies to date have shown the recruitment of the macrophages and the activation state of macrophages in DRG after CIPN. We looked for the infiltration and activation of macrophages using the $CD11b^+$-$CD45^+$ and $MHCII^+$-$CD40^+$ cells respectively in male and female mice. We identified macrophages within DRG by gating for $CD11b^+$ and $CD45^+$ cells. This population was further gated for $MHCII^+$ and $CD40^+$ to assess activated macrophage subsets (**Figure 4A**). We found that $CD11b^+$-$CD45^+$-$CD40^+$-MHC-II^- and $CD11b^+$-$CD45^+$-$CD40^-$-MHC-II^+ populations were unchanged in both sexes with paclitaxel or lack of eIF4E (**Figures 4B, C** and **Table 3**), indicative of no effect on dendritic cells or tissue-resident macrophages. We found a significant increase in $CD11b^+$-$CD45^+$-$CD40^+$-MHC-II^+ cells in male and female eIF4E^{S209A} mice treated with paclitaxel compared to vehicle. Additionally, in female mice, this subpopulation was significantly higher in paclitaxel-treated

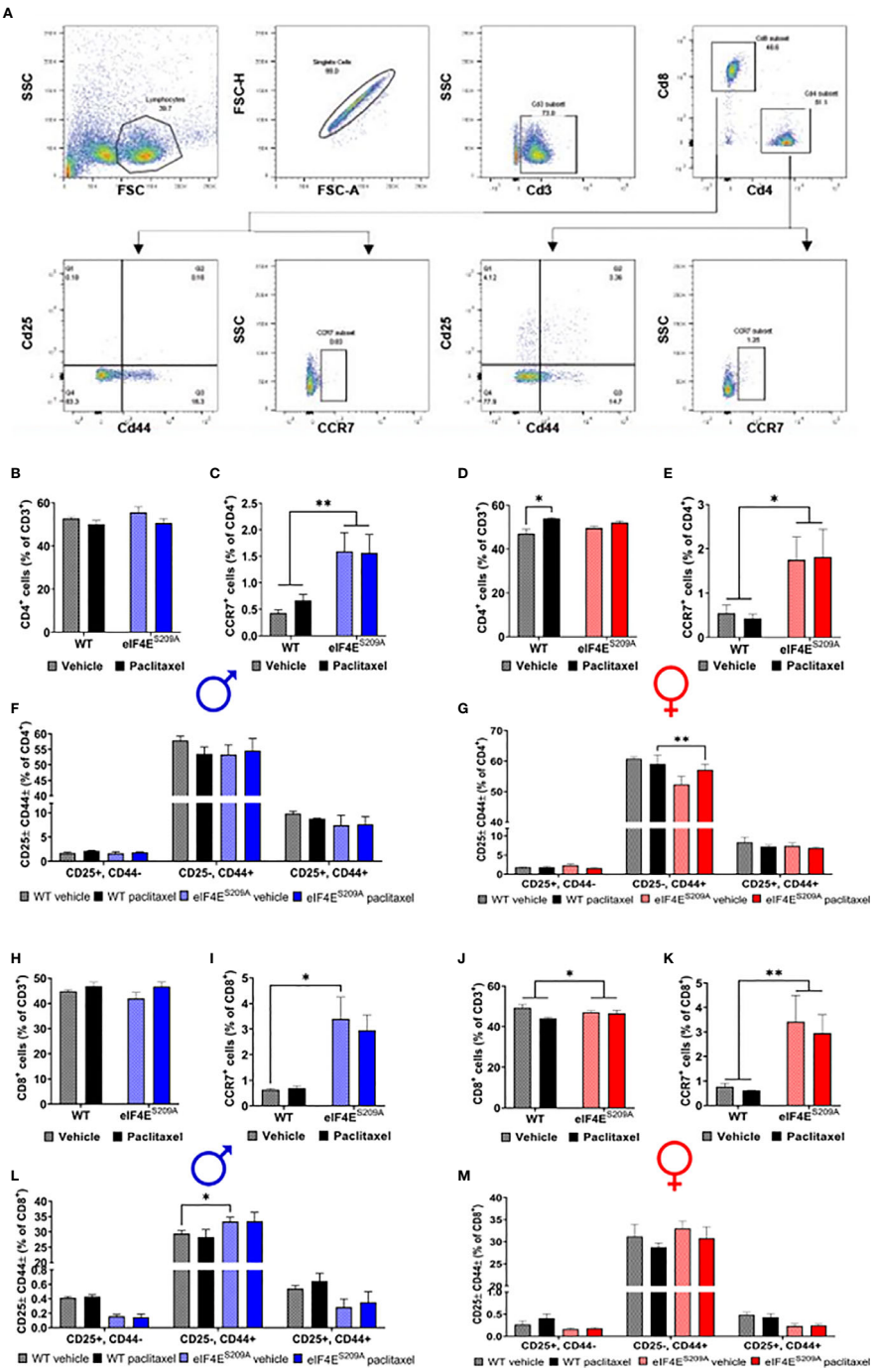

FIGURE 3 | Paclitaxel dysregulates $CD4^+$ and $CD8^+$ T-cell subpopulations in an eIF4E-dependent manner. **(A)** Gating strategy used for flow cytometry of lymphocytes from popliteal and inguinal lymph nodes. T-cells were separated from the whole lymphoid cells population using CD3. $CD3^+$ cells were then gated for $CD4^+$ T-cell and $CD8^+$ T-cells. For each of these subsets, cells were further gated for CCR7 or CD25 and CD44. **(B)** Quantification of $CD4^+$ T-cells from the CD3 population from male mice. **(C)** $CCR7^+$ T-cells from isolated $CD4^+$ population in males, $^{**}p$ 0.0063. **(D)** $CD4^+$ cells gated for CD25 and/or CD44 in males. **(E)** Quantification of $CD4^+$ T-cells from the $CD3^+$ population from female mice, $^{*}p$ 0.0101. **(F)** $CCR7^+$ T-cells from isolated $CD4^+$ population in female mice, $^{*}p$ 0.0250. **(G)** $CD4^+$ cells gated for CD25 and/or CD44 in female mice, $^{**}p$ 0.0011. **(H)** Quantification of $CD8^+$ T-cells from the $CD3^+$ population from male mice. **(I)** $CCR7^+$ T-cells from isolated $CD8^+$ population in males, $^{*}p$ 0.0433. **(J)** $CD8^+$ cells gated for CD25 and/or CD44 in males, $^{*}p$ 0.0396. **(K)** Quantification of $CD8^+$ T-cells from the CD3 population from female mice, $^{*}p$ 0.041. **(L)** $CCR7^+$ T-cells from isolated $CD8^+$ population in female mice, $^{**}p$ 0.0097. **(M)** $CD8^+$ cells gated for CD25 and/or CD44 in female mice. All data are presented as mean ± standard error of the mean, n = 3 mice each for male/female WT vehicle-treated and WT paclitaxel groups, n = 4 mice each for male/female $eIF4E^{S209A}$ vehicle-treated and paclitaxel. Two-way ANOVA was performed with Tukey's *post*-hoc for multiple comparisons.

TABLE 3 | Statistical values for flow cytometry data analysis.

Dataset	Main effect		Interactions		Multiple comparisons		
	F (DFn,DFd)	*p*-value	F (DFn,DFd)	*p*-value	Effect	Groups	*p*-value
Flow cytometry data analysis for T-cells from popliteal and inguinal lymph nodes							
$CD4^+$ males	Treatment: F (1, 10) = 3.139	0.1069	F (1, 10) = 0.3061	0.5922	N/A		
	Genotype: F (1, 10) = 0.6463	0.4401					
$CD4^+CCR7^+$ males	Treatment: F (1, 10) = 0.1196	0.7367	F (1, 10) = 0.1991	0.6650	Treatment	Vehicle	0.0814
						Paclitaxel	0.2116
	Genotype: F (1, 10) = 11.86	**0.0063**			Genotype	WT	0.9514
						$eIF4E^{S209A}$	0.9998
$CD4^+CD44^{\pm}CD25^{\pm}$ males	Cell populations: F (2, 30) = 809.1	**<0.0001**	F (6, 30) = 0.2916	0.9362	No genotype or treatment difference within $CD4^+CD44^+CD25^-$, $CD4^+CD44^-CD25^+$, or $CD4^+CD44^+CD25^+$ populations.		
	Genotype-treatment: F (3, 30) = 0.6686	0.5780					
$CD4^+$ females	Treatment: F (1, 10) = 17.44	**0.0019**	F (1, 10) = 3.920	0.0759	Treatment	Vehicle	0.3920
						Paclitaxel	0.6742
	Genotype: F (1, 10) = 0.1340	0.7219			Genotype	WT	**0.0101**
						$eIF4E^{S209A}$	0.3831
$CD4^+CCR7^+$ females	Treatment: F (1, 10) = 0.0027	0.9591	F (1, 10) = 0.0341	0.8571	Treatment	Vehicle	0.3583
						Paclitaxel	0.2532
	Genotype: F (1, 10) = 6.933	**0.0250**			Genotype	WT	0.9985
						$eIF4E^{S209A}$	0.9996
$CD4^+CD44^{\pm}CD25^{\pm}$ females	Cell populations: F (2, 30) = 1893	**<0.0001**	F (6, 30) = 2.406	0.0512	$CD4^+CD44^+CD25^-$ Genotype ns		
	Genotype-treatment: F (3, 30) = 2.452	0.0827			$CD4^+CD44^+CD25^-$ Treatment	Vehicle	**0.0011**
						Paclitaxel	0.7767
$CD8^+$ males	Treatment: F (1, 10) = 3.180	0.1049	F (1, 10) = 0.5157	0.4891	N/A		
	Genotype: F (1, 10) = 0.6004	0.4564					
$CD8^+CCR7^+$ males	Treatment: F (1, 10) = 0.0917	0.7681	F (1, 10) = 0.1555	0.7016	Treatment	Vehicle	**0.0433**
						Paclitaxel	0.1044
	Genotype: F (1, 10) = 16.48	**0.0023**			Genotype	WT	>0.9999
						$eIF4E^{S209A}$	0.9491
$CD8^+CD44^{\pm}CD25^{\pm}$ males	Cell populations: F (2, 30) = 772.5	**<0.0001**	F (6, 30) = 1.591	0.1842	$CD8^+CD44^+CD25^-$ Genotype ns		
	Genotype-treatment: F (3, 30) = 1.096	0.3660			$CD8^+CD44^+CD25^-$Treatment	Vehicle	0.1579
						Paclitaxel	**0.0396**
$CD8^+$ females	Treatment: F (1, 10) = 5.496	**0.0410**	F (1, 10) = 3.684	0.0839	Treatment	Vehicle	0.6174
						Paclitaxel	0.4863
	Genotype: F (1, 10) = 0.0273	0.8720			Genotype	WT	0.0730
						$eIF4E^{S209A}$	0.9875
$CD8^+CCR7^{\pm}$ females	Treatment: F (1, 10) = 0.1574	0.6999	F (1, 10) = 0.0371	0.8510	Treatment	Vehicle	0.1422
						Paclitaxel	0.2125
	Genotype: F (1, 10) = 10.15	**0.0097**			Genotype	WT	0.9991
						$eIF4E^{S209A}$	0.9681
$CD8^+CD44^{\pm}CD25^{\pm}$ females	Cell populations: F (2, 30) = 788.2	**<0.0001**	F (6, 30) = 0.7166	0.6392	No genotype or treatment difference within $CD8^+CD44^+CD25^-$, $CD8^+CD44^-CD25^+$, or $CD8^+CD44^+CD25^+$ populations.		
	Genotype-treatment: F (3, 30) = 0.5383	0.6597					
Flow cytometry data analysis for myeloid cells from DRG							
Males $CD11b^+CD45^+CD40^{\pm}MHCII^{\pm}$	Cell populations: F (2, 24) = 84.59	**<0.0001**	F (6, 24) = 1.803	0.1410	$CD40^+MHCII^+$ Treatment ns		
	Genotype-treatment: F (3, 24) = 1.139	0.3535			$CD40^+MHCII^+$ Genotype	WT	0.4651
						$eIF4E^{S209A}$	**0.0275**
Females $CD11b^+CD45^+CD40^{\pm}MHCII^{\pm}$	Cell populations: F (2, 24) = 141.3	**<0.0001**	F (6, 24) = 4.720	**0.0026**	$CD40^+MHCII^+$ Treatment	Vehicle	**0.0140**
						Paclitaxel	**0.0055**
	Genotype-treatment: F (3, 24) = 5.042	**0.0075**			$CD40^+MHCII^+$ Genotype	WT	0.5182
						$eIF4E^{S209A}$	**<0.0001**

Two-way ANOVA was performed followed by Tukey's post-hoc for multiple comparisons between genotypes and treatments for each sex. $p \leq 0.05$ was considered significant (bolded).

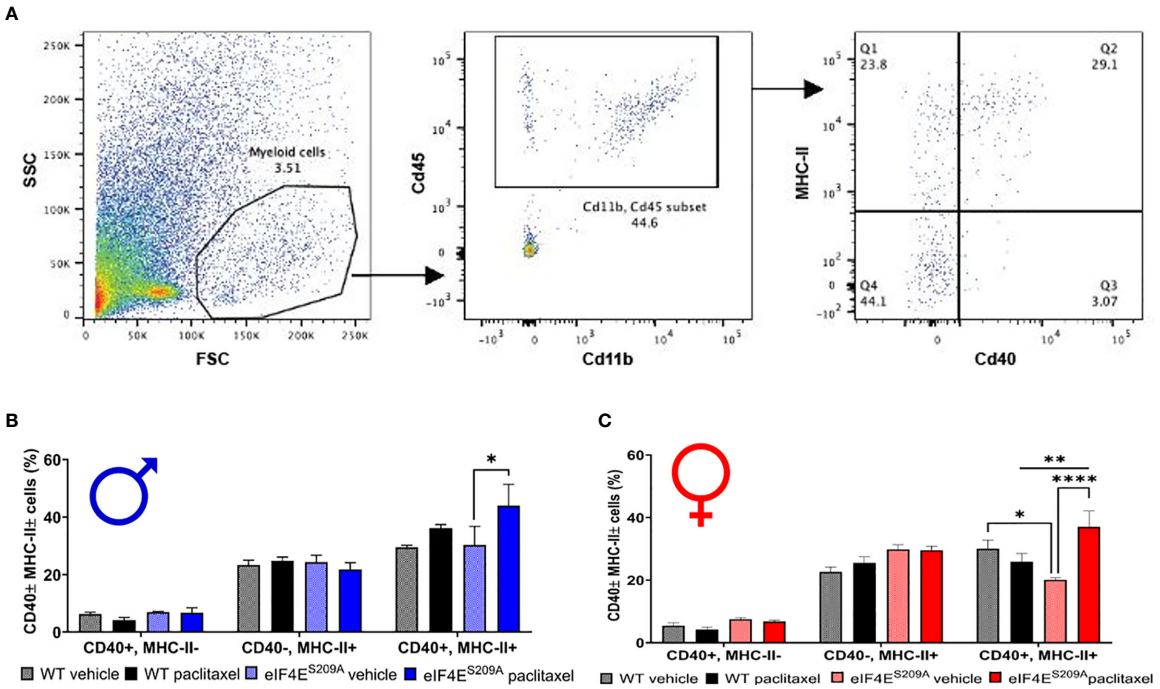

FIGURE 4 | Paclitaxel induces activation of antigen-presenting myeloid cells in eIF4E^{S209A} mice DRG. **(A)** Gating strategy for isolating myeloid APCs from mouse DRG. Total cells were gated for CD11b and CD45 to separate out immune cells. The CD11b^{+} CD45^{+} subset was then gated for MHC-II^{+} and/or CD40^{+} cells. **(B)** Quantification of CD40^{+} and/or MHC-II^{+} cells from male mice, *p 0.0275. **(C)** Quantification of CD40^{+} and/or MHC-II^{+} cells from female mice, *p 0.014, **p 0.0055, ****p<0.0001. All data are presented as mean ± standard error of the mean, n = 3 mice each for male/female WT vehicle-treated and WT paclitaxel groups, n = 4 mice each for male/female eIF4E^{S209A} vehicle-treated and paclitaxel. Two-way ANOVA was performed with Tukey's *post*-hoc for multiple comparisons.

eIF4E^{S209A} animals compared to paclitaxel-treated WT (**Figure 4C** and **Table 3**). This indicates that antigen-presenting cells (APCs) are upregulated with paclitaxel treatment in absence of eIF4E. Interestingly, female eIF4E^{S209A} vehicle-treated mice had a significantly lower proportion of activated APCs compared to WT (**Table 3**). This shows that cap-dependent translation may be facilitating the recruitment of activated myeloid cells as a result of paclitaxel treatment, which in turn could be activating or expanding the T-cell populations.

Paclitaxel Alters Mitochondrial Function of DRG Neurons in an eIF4E-Dependent Manner

We investigated mitochondrial function in DRG neurons to examine if paclitaxel changed the bioenergetic profiles (**Figures 5A–Q** and **Table 4**) in an eIF4E-dependent manner. The overall oxygen consumption rate (OCR) was lower in paclitaxel-treated eIF4E^{S209A} males and females compared to paclitaxel-treated WT (**Figures 5B, C, J, K** and **Table 4**) whereas the overall extracellular acidification rate (ECAR) was higher with paclitaxel treatment in both sexes and lower in paclitaxel-treated eIF4E^{S209A} males compared to paclitaxel-treated WT males (**Figures 5H, I, P, Q** and **Table 4**). This suggests that lack of eIF4E causes a shift in mitochondrial respiration with paclitaxel treatment. We divided the different phases of the OCR bioenergetic profile into basal respiration (before oligomycin treatment), ATP production (after oligomycin treatment and before FCCP – 2-[2-[4-(trifluoromethoxy)phenyl] hydrazinylidene]-propanedinitrile treatment), maximal respiration (after FCCP and before antimycin A and rotenone), and non-mitochondrial respiration or reserve capacity (**Figure 5A**). For males, we found a significant increase in the basal respiration and non-mitochondrial respiration after paclitaxel treatment in WT, but not eIF4E^{S209A} mice (**Figures 5D, G** and **Table 4**), but no change in ATP turnover or maximal respiration (**Figures 5E, F** and **Table 4**). For female mice, we found that basal respiration and non-mitochondrial respiration was increased after paclitaxel treatment for both genotypes (**Figures 5L, O** and **Table 4**). ATP turnover and maximal respiration was also higher in WT females treated with paclitaxel compared to vehicle and in eIF4E^{S209A} females compared to paclitaxel-treated WT (**Figures 5M, N** and **Table 4**). Taken together, our data shows that sensory neurons in the DRG undergo an excited mitochondrial shift with paclitaxel treatment in an eIF4E-dependent manner in both sexes. Paclitaxel increased all aspects of mitochondrial respiration in females but did not affect ATP turnover and maximal respiration in males, which indicates divergent effects of paclitaxel in eIF4E absence in both sexes.

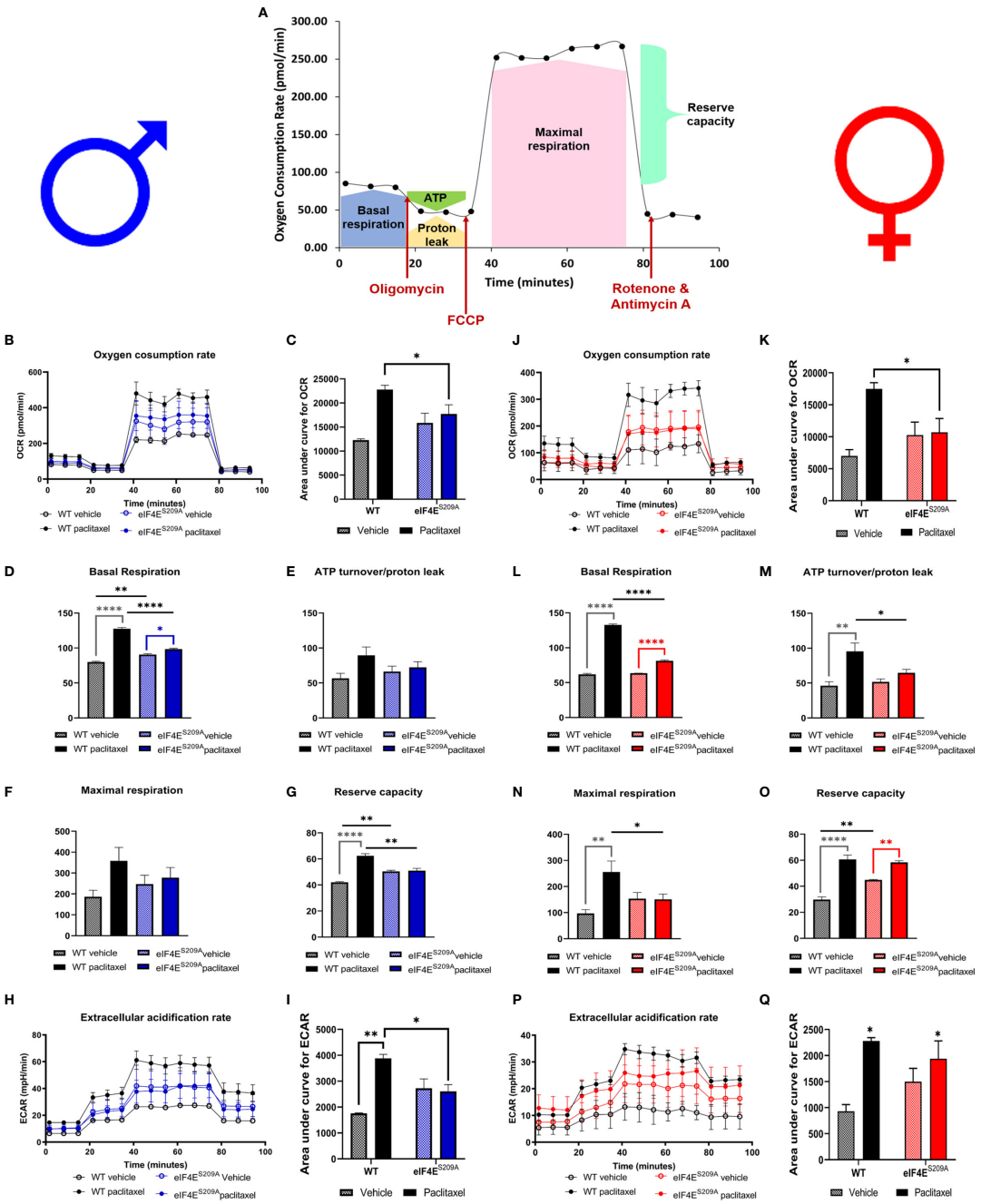

FIGURE 5 | Paclitaxel alters mitochondrial function of DRG neurons in an eIF4E-dependent manner. Dissociated dorsal root ganglion (DRG) neurons from WT and eIF4E^{S209A} male and female mice were analyzed by the Seahorse Mito Stress test. **(A)** Graphic showing different phases of mitochondrial respiration. Adapted from the Agilent Seahorse XFp Cell Mito Test Kit User Guide published by Agilent Technologies. **(B)** Oxygen consumption rate (OCR) through phases of the Mito Stress test for male mice. **(C)** OCR data in male mice shown as area under the curve (AUC), *p 0.0136. **(D-G)** OCR data for male mice broken down into phases of mitochondrial respiration. Basal respiration: *p 0.0134, **p 0.0018, ****p<0.0001. Reserve capacity: **p 0.0063 for WT vs eIF4E^{S209A} vehicle, **p 0.001 for WT vs eIF4E^{S209A} paclitaxel. **(H)** Extracellular acidification rate (ECAR) for male mice. **(I)** ECAR data in male mice shown as AUC, *p 0.0303 for WT vs eIF4E^{S209A} vehicle, **p 0.0021 for WT vehicle vs WT paclitaxel groups. **(J)** OCR through phases of the Mito Stress test for female mice. **(K)** OCR data in female mice shown as AUC, *p 0.0455. **(L–O)** OCR data for female mice broken down into phases of mitochondrial respiration. Basal respiration: ****p<0.0001, ATP turnover: *p 0.0481, **p 0.0021, maximal respiration: *p 0.0417, **p 0.0011, reserve capacity: **p 0.0037 for WT vs eIF4E^{S209A} vehicle, **p 0.074 for eIF4E^{S209A} vehicle vs eIF4E^{S209A} paclitaxel, ****p<0.0001. **(P)** ECAR for female mice. **(Q)** ECAR data in female mice shown as AUC, *p 0.0116 for both genotypes vehicle vs paclitaxel-treated groups. All data are presented as mean ± standard error of the mean, n = 3-4 mice each for male/female WT vehicle-treated and WT paclitaxel groups, n = 4-7 mice each for male/female eIF4E^{S209A} vehicle-treated and paclitaxel. For analyzing AUC data, two-way ANOVA was performed with Tukey's *post*-hoc for multiple comparisons. For analyzing each phase of mitochondrial respiration, an ordinary one-way ANOVA was used with Sidak's *post-hoc* for multiple comparisons.

TABLE 4 | Statistical values for DRG neuron mitochondrial respiration.

Dataset	Main effect		Interaction		Multiple comparisons		
	F (DFn,DFd)	p-value	F (DFn,DFd)	p-value	Effect	Groups	p-value
Males OCR AUC	Treatment: F (1, 11) = 11.85	**0.0055**	F (1, 11) = 5.817	**0.0345**	Treatment	Vehicle	0.5347
						Paclitaxel	0.2303
	Genotype: F (1, 11) = 0.1714	0.6868			Genotype	WT	**0.0136**
						eIF4E^{S209A}	0.8475
Females OCR AUC	Treatment: F (1, 17) = 6.074	**0.0247**	F (1, 17) = 5.158	**0.0364**	Treatment	Vehicle	0.7519
						Paclitaxel	0.1426
	Genotype: F (1, 17) = 0.6271	0.4393			Genotype	WT	**0.0455**
						eIF4E^{S209A}	0.9982
Males ECAR AUC	Treatment: F (1, 11) = 13.04	**0.0041**	F (1, 11) = 16.26	**0.0020**	Treatment	Vehicle	0.1313
						Paclitaxel	**0.0303**
	Genotype: F (1, 11) = 0.2927	0.5993			Genotype	WT	**0.0021**
						eIF4E^{S209A}	0.9866
Females ECAR AUC	Treatment: F (1, 17) = 7.989	**0.0116**	F (1, 17) = 2.068	0.1686	Treatment	Vehicle	0.6269
						Paclitaxel	0.8523
	Genotype: F (1, 17) = 0.1287	0.7242			Genotype	WT	0.0792
						eIF4E^{S209A}	0.6287
Breakdown datasets for OCR	**Interaction**	**p-value**	**Multiple comparisons - groups compared**				**p-value**
Males basal respiration	F (3, 8) = 233.2	**<0.0001**	WT vehicle		WT paclitaxel		**<0.0001**
			eIF4E^{S209A} vehicle		eIF4E^{S209A} paclitaxel		**0.0134**
			WT vehicle		eIF4E^{S209A} vehicle		**0.0018**
			WT paclitaxel		eIF4E^{S209A} paclitaxel		**<0.0001**
Females basal respiration	F (3, 8) = 838.7	**<0.0001**	WT vehicle		WT paclitaxel		**<0.0001**
			eIF4E^{S209A} vehicle		eIF4E^{S209A} paclitaxel		**<0.0001**
			WT vehicle		eIF4E^{S209A} vehicle		0.8413
			WT paclitaxel		eIF4E^{S209A} paclitaxel		**<0.0001**
Males ATP turnover	F (3, 12) = 2.384	0.1203	WT vehicle		WT paclitaxel		0.0905
			eIF4E^{S209A} vehicle		eIF4E^{S209A} paclitaxel		0.9832
			WT vehicle		eIF4E^{S209A} vehicle		0.9188
			WT paclitaxel		eIF4E^{S209A} paclitaxel		0.5864
Females ATP turnover	F (3, 12) = 8.828	**0.0023**	WT vehicle		WT paclitaxel		0.0021
			eIF4E^{S209A} vehicle		eIF4E^{S209A} paclitaxel		0.6736
			WT vehicle		eIF4E^{S209A} vehicle		0.9766
			WT paclitaxel		eIF4E^{S209A} paclitaxel		0.0481
Males maximal respiration	F (3, 28) = 2.233	0.1064	WT vehicle		WT paclitaxel		0.0661
			eIF4E^{S209A} vehicle		eIF4E^{S209A} paclitaxel		0.9857
			WT vehicle		eIF4E^{S209A} vehicle		0.8539
			WT paclitaxel		eIF4E^{S209A} paclitaxel		0.6683
Females maximal respiration	F (3, 28) = 5.986	**0.0028**	WT vehicle		WT paclitaxel		**0.0011**
			eIF4E^{S209A} vehicle		eIF4E^{S209A} paclitaxel		>0.9999
			WT vehicle		eIF4E^{S209A} vehicle		0.4836
			WT paclitaxel		eIF4E^{S209A} paclitaxel		**0.0417**
Males non-mitochondrial respiration (reserve capacity)	F (3, 8) = 42.18	**<0.0001**	WT vehicle		WT paclitaxel		**<0.0001**
			eIF4E^{S209A} vehicle		eIF4E^{S209A} paclitaxel		0.9978
			WT vehicle		eIF4E^{S209A} vehicle		**0.0063**
			WT paclitaxel		eIF4E^{S209A} paclitaxel		**0.0010**
Females non-mitochondrial respiration (reserve capacity)	F (3, 8) = 46.31	**<0.0001**	WT vehicle		WT paclitaxel		**<0.0001**
			eIF4E^{S209A} vehicle		eIF4E^{S209A} paclitaxel		**0.0074**
			WT vehicle		eIF4E^{S209A} vehicle		**0.0037**
			WT paclitaxel		eIF4E^{S209A} paclitaxel		0.9212

Two-way ANOVA was performed on AUC values for OCR and ECAR followed by Tukey's post-hoc for multiple comparisons between genotypes and treatments for each sex. For breakdown data of mitochondrial respiration, ordinary one-way ANOVAs were used to analyze mean values of four groups (WT vehicle, WT paclitaxel, eIF4E^{S209A} vehicle, and eIF4ES^{209A} paclitaxel), followed by Sidak's post-hoc for multiple comparisons between genotypes and treatments for each sex. $p \leq 0.05$ was considered significant (bolded). OCR, oxygen consumption rate; ECAR, extracellular acidification rate.

Sensory Neuron Damage by Paclitaxel Is Similar for Both Sexes and Genotypes

Previous studies have shown no association between sickness behavior or change in the body weight of the animal with 16mg/Kg dose of paclitaxel. Moreover, other researchers have used even higher doses of paclitaxel to induce peripheral neuropathy (57, 58). We assessed number of DRG neurons positive for activating transcription factor 3 (ATF3). The number of ATF3^{+} neurons were significantly higher in the DRG of paclitaxel-treated animals indicating damage; however, there were no sex-based or genotype differences observed (**Figure 6** and **Table 5**). The increase is similar to previously published literature, albeit at a later time point (59, 60), thus we conclude that this higher dose does not comparatively alter DRG neurons at day 10 after our regimen.

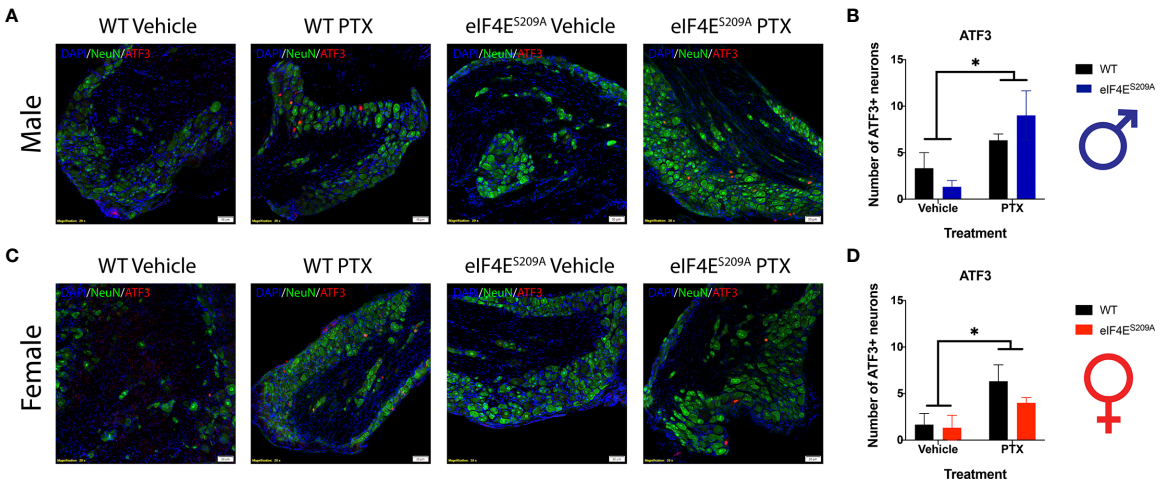

FIGURE 6 | ATF3+ neurons are observed in DRG of all animals subjected to Paclitaxel. **(A, B)** Representative composite images showing ATF3^{+} cells (red) and NeuN^{+} cells (green) for male mice and their quantitation, respectively. *p 0.0114 for males' vehicle vs paclitaxel groups. **(C, D)** Representative composite images showing ATF3^{+} cells (red) and NeuN^{+} cells (green) for female mice and their quantitation, respectively. *p 0.0218 for females for vehicle vs paclitaxel groups. All sections were counterstained with DAPI (blue). Data represented as mean and SEM. Two-way ANOVA was performed with Sidak's post-hoc for multiple comparisons; n=3 for all groups. Magnification 20X, scale bar 50μm. PTX – paclitaxel.

TABLE 5 | Statistical values for IHC data analysis.

Dataset	Main effect		Interaction		Multiple comparisons		
	F (DFn,DFd)	p-value	F (DFn,DFd)	p-value	Effect	Groups	p-value
Male mice ATF3^{+} cells	Treatment: F (1, 8) = 10.67	**0.0114**	F (1, 8) = 2.042	0.1909	Treatment	Vehicle	0.6539
						Paclitaxel	0.4838
	Genotype: F (1, 8) = 0.04	0.8434			Genotype	WT	0.4073
						eIF4E^{S209A}	**0.0210**
Female mice ATF3^{+} cells	Treatment: F (1, 8) = 8.067	**0.0218**	F (1, 8) = 0.600	0.4609	Treatment	Vehicle	0.9803
						Paclitaxel	0.4179
	Genotype: F (1, 8) = 1.067	0.3319			Genotype	WT	0.0666
						eIF4E^{S209A}	0.3313
Male mice Iba1	Treatment: F (1, 8) = 10.06	**0.0132**	F (1, 8) = 6.556	**0.0336**	Treatment	Vehicle	>0.9999
						Paclitaxel	**0.0140**
	Genotype: F (1, 8) = 13.24	**0.0066**			Genotype	WT	**0.0220**
						eIF4E^{S209A}	>0.9999
Female mice Iba1	Treatment: F (1, 6) = 7.540	**0.0335**	F (1, 6) = 18.22	**0.0053**	Treatment	Vehicle	0.9194
						Paclitaxel	**0.0029**
	Genotype: F (1, 6) = 40.14	**0.00071**			Genotype	WT	**0.0153**
						eIF4E^{S209A}	>0.9999
Male mice GFAP	Treatment: F (1, 8) = 12.90	**0.0071**	F (1, 8) = 7.104	**0.0286**	Treatment	Vehicle	**0.0133**
						Paclitaxel	>0.9999
	Genotype: F (1, 8) = 1.075	0.3301			Genotype	WT	>0.9999
						eIF4E^{S209A}	0.1845
Female mice GFAP	Treatment: F (1, 6) = 40.81	**0.0007**	F (1, 6) = 0.1627	0.7007	Treatment	Vehicle	**0.0180**
						Paclitaxel	**0.0329**
	Genotype: F (1, 6) = 2.078	0.1995			Genotype	WT	>0.9999
						eIF4E^{S209A}	>0.9999

Two-way ANOVA was performed followed by Sidak's post-hoc for ATF3^{+} cell number and Bonferroni's post-hoc for Iba1 and GFAP for multiple comparisons between genotypes and treatments for each sex. $p \leq 0.05$ was considered significant (bolded).

Spinal Glia Reactivity Is Altered in a Sex-Dependent Manner With Paclitaxel Treatment

Previous data has shown activation of microglia and astrocytes at different phases of CIPN (61–63). Here, we investigated whether the eIF4E complex plays a role in the activation of microglia and astrocytes in the spinal cord. We found a significant increase in immunoreactivity of microglia and astrocytes in both male and female WT mice (**Figure 7**). Iba1 fluorescence was significantly higher in paclitaxel-treated WT mice of both sexes compared to

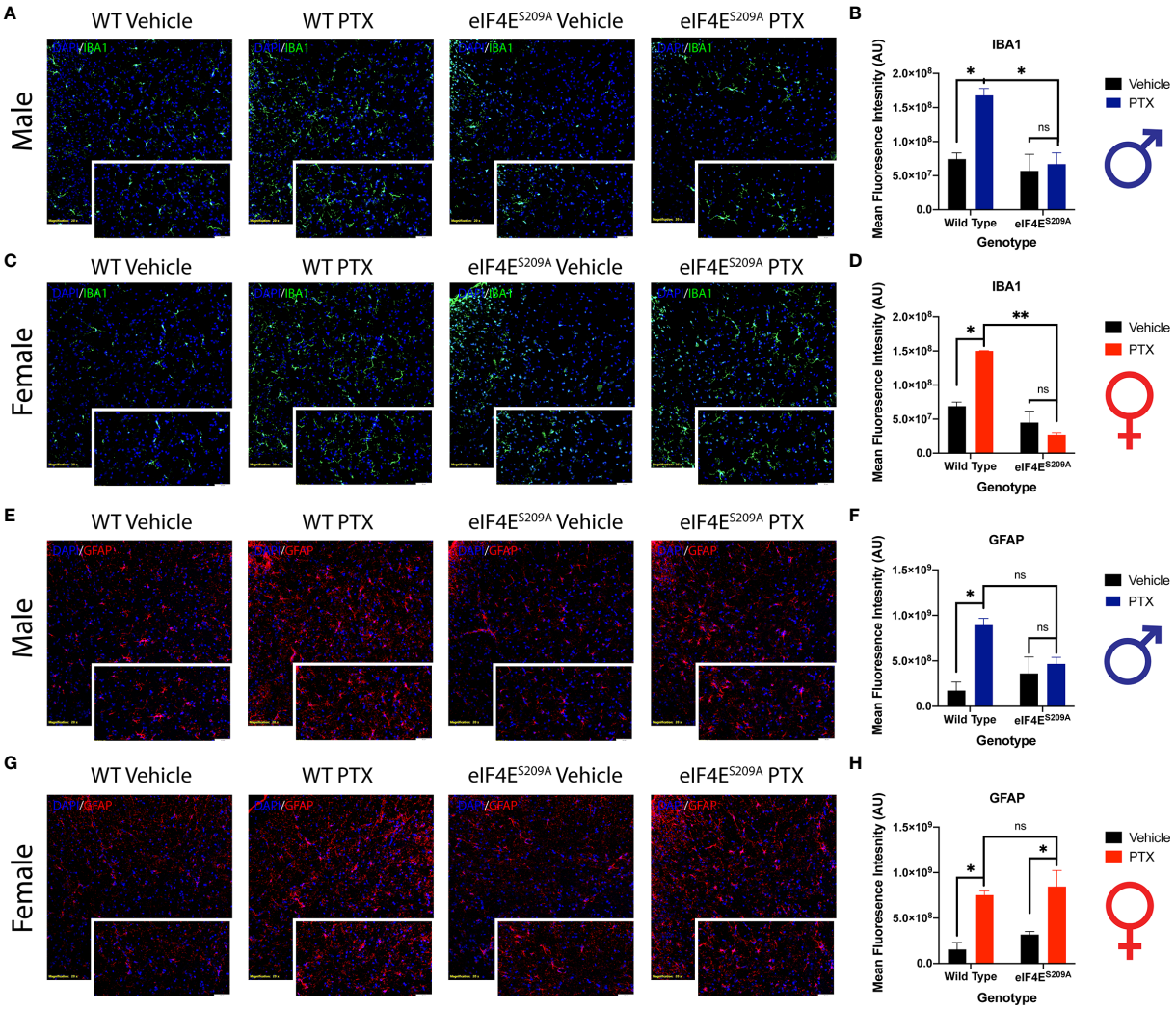

FIGURE 7 | Spinal glia reactivity is altered in a sex-dependent manner with paclitaxel treatment. **(A)** Immunohistochemistry for male microglia on lumbar spinal cord. Blue represents DAPI for cell nuclei, green represents Iba1 for microglia. Magnification 20X, scale bar 50μm. **(B)** Quantification of Iba1 fluorescence intensity from male mice, *p 0.022 for WT vehicle vs WT paclitaxel groups, *p 0.014 for WT paclitaxel vs eIF4E^{S209A} paclitaxel groups. **(C)** Immunohistochemistry for female microglia on lumbar spinal cord. Blue represents DAPI for cell nuclei, green represents Iba1 for microglia. Magnification 20X, scale bar 50μm. **(D)** Quantification of Iba1 fluorescence intensity from female mice, *p 0.0153, **p 0.0029. **(E)** Immunohistochemistry for male astrocytes on lumbar spinal cord. Blue represents DAPI for cell nuclei, red represents GFAP for astrocytes. Magnification 20X, scale bar 50μm. **(F)** Quantification of GFAP fluorescence intensity from male mice, *p 0.0133. **(G)** Immunohistochemistry for female astrocytes on lumbar spinal cord. Blue represents DAPI for cell nuclei, red represents GFAP for astrocytes. Magnification 20X, scale bar 50μm. **(H)** Quantification of GFAP fluorescence intensity from female mice, *p 0.018 for WT vehicle vs WT paclitaxel groups, *p 0.0329 for eIF4E^{S209A} vehicle vs eIF4E^{S209A} paclitaxel groups. Data are presented as mean ± standard error of the mean, males: n = 3 mice per group; females n = 3 mice per group. Two-way ANOVA was performed with Bonferroni's *post-hoc* for multiple comparisons. ns, not significant.

vehicle (**Figures 7A–C** and **Table 5**), indicating that paclitaxel induced microglial activation. This increase was lacking for eIF4E^{S209A} animals for whom the Iba1 immunoreactivity stayed at WT vehicle levels. In eIF4E^{S209A} females, there was a decrease in Iba1 fluorescence with paclitaxel treatment compared to vehicle (**Figure 7C**). For astrocytes, females lacking cap-dependent translation had increased GFAP fluorescence after paclitaxel compared to vehicle (**Figures 7D, F, G, and H,** and **Table 5**), which was different from the males where the GFAP fluorescence was at the same level as seen for the WT vehicle group (**Figures 7D, E**). This data shows that paclitaxel may mediate activation of astrocytes via an eIF4E-independent pathway in females but modulates microglia activation via eIF4E in both sexes and astrocyte activation in males.

DISCUSSION

The current study begins to uncover the importance of eIF4E phosphorylation in the development of CIPN and associated

neuroimmune consequences in male and female mice. In our study, we found an eIF4E-dependent increase of mechanical and thermal hypersensitivity in both sexes, upregulated T-helper and reduced cytotoxic T-lymphocytes in draining lymph nodes in female but not male mice, whereas activated macrophages in DRG were significantly increased in eIF4E but not WT mice of both sexes. In addition to this, DRG neuronal mitochondrial function was significantly higher in WT mice but not in eIF4E mice of both sexes. Microglia were significantly activated in an eIF4E-dependent manner with paclitaxel treatment in WT mice of both sexes; however, astrocytes were activated in an eIF4E-dependent manner with paclitaxel treatment only in male mice. Female eIF4E mice showed significant astrocyte activation.

Our study was designed and powered with the intent to appropriately assess sex differences in neuroimmune interactions during CIPN development—a question left unanswered in previous literature. We found an eIF4E-dependent increase in spontaneous pain as well as mechanical and thermal hypersensitivity after paclitaxel. This suggests that the pain-like behavior changes due to paclitaxel are mediated via the central cap-dependent translation pathway that is common across diverse cell types, with more pronounced effects in female mice.

The cell bodies of primary afferent neurons reside in the dorsal root ganglia. The persistent signals from nerve terminals activate the machinery and signaling cascades in the nucleus and cytoplasm of the neuronal soma (64–66). Hyper-excited nociceptor neurons recruit immune cells by secreting chemokines, neurotransmitters, and/or other neuropeptides (16, 67). It has been shown that paclitaxel treatment recruits macrophages into the DRG (20). Our findings corroborate this finding at an earlier time point and add to this knowledge by characterizing the macrophage population as $CD45^+CD11b^+CD40^+MHC\text{-}II^+$ i.e. activated APCs. It has been shown that such infiltration may be beneficial to recruit Th2 anti-inflammatory cells at later time points (62, 68). We have presented evidence that paclitaxel injection leads to a significant increase in the activated APC population in eIF4E males and females, but not in WT mice. Thus, a lack of eIF4E phosphorylation or cap-dependent translation exacerbates the immune cell response and DRG infiltration during CIPN development.

A prior study performed only in male mice showed an increase in $CD4^+$ T-cells at paclitaxel post-injection day 7 (14). We found a similar increase of $CD4^+$ T-cells in female WT mice with paclitaxel treatment. Additionally, a novel finding was that $CD8^+$ T-cells were decreased in female but not in male WT mice during early phase of CIPN development. This indicates sex differences in T-cell activation in the lymph nodes, which would affect the subsets of T-cells that would infiltrate other tissues such as DRG (69). A previously published study showed increased numbers of $CD3^+$, helper T-cells, and cytotoxic T-lymphocytes after paclitaxel on day 7 in mice DRG (70). Our dataset adds niche T-cell population characterization to this previously published literature. T-cell subset activation in the lymph nodes is highly dependent upon the antigen-presenting cells naïve T-cells encounter (71). Once activated, these subsets follow their divergent fates of redistribution to tissues in need of immune response. Thus, characterizing different subsets of T-cells in the lymph nodes allows us to determine what populations we can expect in interfaces where neuroimmune communication can occur, such as the meninges or DRG. T-cells are also important in the transition from acute to chronic pain (15). By showing alterations in specialized T-cell subsets, our study raises important questions about the implications for establishment of CIPN and its resolution. Animals lacking eIF4E had higher proportion of memory T-cells in both sexes. There were no changes in the effector T-cell population for the lymph nodes. These alterations in the activation and proportion of T-cell subsets and APCs suggest that although affective pain behavior is similar in male and female mice after development of CIPN, the mechanism driving the pain phenotypes in both sexes involves varied contribution from innate and adaptive immune cells.

Basal respiration and non-mitochondrial respiration were higher in male DRG neurons treated with paclitaxel compared to vehicle, which is contrary to a previous report for rats (38). We have further shown that the lack of eIF4E does not change this trend, even though oxygen consumption is lower, suggesting that paclitaxel may induce mitochondrial function independent of cap-dependent translation regulation. In females, while the effects on basal respiration follow the same trend as the males, paclitaxel seems to mediate an increase in non-mitochondrial respiration independent of eIF4E. Female DRG neurons also had significantly higher ATP turnover and maximal respiration with paclitaxel treatment in WT. Considering that eIF4E female mice show higher mechanical hypersensitivity with paclitaxel and that their DRG neuron ATP turnover and maximal respiration is higher, this may be indicative of the severity of the pain phenotype. Whereas for males, the increased basal respiration may reflect the pain phenotype in general. To our knowledge, this is the first study to show sex differences in mitochondrial bioenergetics in the premise of cap-dependent translation for paclitaxel-induced peripheral neuropathy. These differences seen early during CIPN development, may be important for identifying strategies to prevent its establishment in both sexes. Thus, it is necessary to understand the particular mitochondrial pathways downstream of eIF4E to identify potential targets to prevent CIPN. Alternatively, therapies that address restoration of normal mitochondrial function and morphology are also promising for either sex.

Previously published data has shown that paclitaxel leads to spinal activation of astrocytes but not microglia at different phases of paclitaxel-induced peripheral neuropathy in mouse and rat models (72, 73). In contrast, we found that both microglia and astrocytes are significantly activated after paclitaxel injection in male mice, which is eIF4E dependent. However, the astrocyte reactivity increase in female mice was independent of eIF4E, suggesting that paclitaxel may have alternate mechanisms of astrocyte activation in females. Activated glia are known to secrete a number of pro-inflammatory mediators that act directly on CNS neurons, which can sensitize them if subjected to constant stimulation over extended periods (64). This has implications for the

establishment of pain phenotypes post paclitaxel treatment. It has also been shown that intraperitoneal paclitaxel can activate astrocytes and mediate mechanical allodynia in the 1st hour, possibly by miniscule amounts crossing the blood-brain barrier (62). Thus, the glia activation seen 10 days post our paclitaxel regimen may be important for onset as well as establishment of CIPN through cap-dependent translation in males but via other pathways in females.

Regulation of cap-dependent translation happens via multiple different pathways. This is partly related to the expression of cell-specific surface receptors such as TrkA/B, gp130, mGLuR1/5, and insulin receptors and this influences which pathway is activated in response to which stimuli (74–76). In behavioral experiments, we assessed the role of eIf4E for regulation of brain behaviors i.e the interaction of all cells in the body after insult, but in the molecular experiments, we target specific populations of cells to understand how they individually change as a result of eIF4E manipulation and paclitaxel treatment. Our study provides novel insight into how cap-dependent translation dysregulation of immune or neuronal cells may be important for sex-divergent mechanisms of early CIPN. But comprehensive future studies would still be required to further deduce the cell-specific responses after paclitaxel treatment in the absence of cap-dependent translation.

Overall, our data suggest that although pain-like behavior during the early development of the CIPN are similar, the mechanisms and cell types involved in engendering these behaviors are different in males and females. The differences in immune cell populations and activation of glia indicate that separate upstream pathways may regulate cap-dependent translation in both sexes and thus lead to changed downstream outcomes. The central player i.e. the eIF4E complex can thus be a valuable target for preventing establishment of CIPN and limiting associated pain.

DATA AVAILABILITY STATEMENT

The raw data supporting the conclusions of this article will be made available by the authors, without undue reservation.

ETHICS STATEMENT

The animal study was reviewed and approved by University of Texas at Dallas Institute for Animal Care and Use Committee (IACUC).

AUTHOR CONTRIBUTIONS

Methodology, NA. Data analysis and curation, NA, PM, TS-P, and HJ. Writing manuscript and drawing figures, NA, PM, TS-P, and HJ. MB conceptualized the study and participated and supervised in all aspects of the study and manuscript preparation. All authors contributed to the article and approved the submitted version.

FUNDING

This research was funded by the NIH/NINDS, grant number K22NS096030 (MB), the University of Texas System STARS program research support grant (MB), the American Pain Society Future Leaders Grant (MB), and the Rita Allen Foundation Grant (MB).

ACKNOWLEDGMENTS

We would like to thank Luz R. Barron, Brandon T. Lane, and Carlos Salinas for their technical contributions. We would also like to thank all current and former lab members for the assistance and input on this manuscript. Graphics created with Biorender.com.

SUPPLEMENTARY MATERIAL

The Supplementary Material for this article can be found online at: https://www.frontiersin.org/articles/10.3389/fimmu.2021.642420/full#supplementary-material

REFERENCES

1. Cata J, Weng H R, Lee NB, Reuben J, Dougherty MP. Clinical and experimental finding in humans and animals with chemotherapy-induced peripheral neuropathy. *Minerva Anestesiol* (2006) 72(3):151–69.
2. Quasthoff S, Hartung HP. Chemotherapy-induced peripheral neuropathy. *J Neurol* (2002) 249(1):9–17. doi: 10.1007/pl00007853
3. Windebank AJ, Grisold W. Chemotherapy-induced neuropathy. *J Peripher Nerv Syst* (2008) 13(1):27–46. doi: 10.1111/j.1529-8027.2008.00156.x
4. Kannarkat G, Lasher EE, Schiff D. Neurologic complications of chemotherapy agents. *Curr Opin Neurol* (2007) 20(6):719–25. doi: 10.1097/WCO.0b013e3282f1a06e
5. Pachman DR, Barton DL, Swetz KM, Loprinzi CL. Troublesome symptoms in cancer survivors: fatigue, insomnia, neuropathy, and pain. *J Clin Oncol* (2012) 30(30):3687–96. doi: 10.1200/JCO.2012.41.7238
6. Seretny M, Currie GL, Sena ES, Ramnarine S, Grant R, MacLeod MR, et al. Incidence, prevalence, and predictors of chemotherapy-induced peripheral neuropathy: A systematic review and meta-analysis. *Pain* (2014) 155 (12):2461–70. doi: 10.1016/j.pain.2014.09.020
7. Ibrahim EY, Ehrlich BE. Prevention of chemotherapy-induced peripheral neuropathy: A review of recent findings. *Crit Rev Oncol Hematol* (2020) 145:102831. doi: 10.1016/j.critrevonc.2019.102831
8. Hwang BY, Kim ES, Kim CH, Kwon JY, Kim HK. Gender differences in paclitaxel-induced neuropathic pain behavior and analgesic response in rats. *Korean J Anesthesiol* (2012) 62(1):66–72. doi: 10.4097/kjae.2012.62.1.66
9. Naji-Esfahani H, Vaseghi G, Safaeian L, Pilehvarian AA, Abed A, Rafieian-Kopaei M. Gender differences in a mouse model of chemotherapy-induced neuropathic pain. *Lab Anim* (2016) 50(1):15–20. doi: 10.1177/0023677215575863
10. Gewandter JS, Kleckner AS, Marshall JH, Brown JS, Curtis LH, Bautista J, et al. Chemotherapy-induced peripheral neuropathy (CIPN) and its treatment: an NIH Collaboratory study of claims data. *Supportive Care Cancer* (2020) 28 (6):2553–62. doi: 10.1007/s00520-019-05063-x

11. Ferrari LF, Araldi D, Green PG, Levine JD. Marked sexual dimorphism in neuroendocrine mechanisms for the exacerbation of paclitaxel-induced painful peripheral neuropathy by stress. *Pain* (2020) 161(4):865–74. doi: 10.1097/j.pain.0000000000001798
12. Sorge RE, Mapplebeck JCS, Rosen S, Beggs S, Taves S, Alexander JK, et al. Different immune cells mediate mechanical pain hypersensitivity in male and female mice. *Nat Neurosci* (2015) 18(8):1081–3. doi: 10.1038/nn.4053
13. Krukowski K, Eijkelkamp N, Laumet G, Hack CE, Li Y, Dougherty PM, et al. CD8+ T Cells and Endogenous IL-10 Are Required for Resolution of Chemotherapy-Induced Neuropathic Pain. *J Neurosci* (2016) 36(43):11074–83. doi: 10.1523/JNEUROSCI.3708-15.2016
14. Makker PG, Duffy SS, Lees JG, Perera CJ, Tonkin RS, Butovsky O, et al. Characterisation of Immune and Neuroinflammatory Changes Associated with Chemotherapy-Induced Peripheral Neuropathy. *PloS One* (2017) 12(1): e0170814. doi: 10.1371/journal.pone.0170814
15. Laumet G, Edralin JD, Dantzer R, Heijnen CJ, Kavelaars A. Cisplatin educates CD8+ T cells to prevent and resolve chemotherapy-induced peripheral neuropathy in mice. *Pain* (2019) 160(6):1459–68. doi: 10.1097/j.pain.0000000000001512
16. Pinho-Ribeiro FA, Verri WAJr, Chiu IM. Nociceptor Sensory Neuron-Immune Interactions in Pain and Inflammation. *Trends Immunol* (2017) 38 (1):5–19. doi: 10.1016/j.it.2016.10.001
17. McMahon SB, La Russa F, Bennett DL. Crosstalk between the nociceptive and immune systems in host defence and disease. *Nat Rev Neurosci* (2015) 16 (7):389–402. doi: 10.1038/nrn3946
18. Moalem G, Xu K, Yu L. T lymphocytes play a role in neuropathic pain following peripheral nerve injury in rats. *Neuroscience* (2004) 129(3):767–77. doi: 10.1016/j.neuroscience.2004.08.035
19. Siau C, Xiao W, Bennett GJ. Paclitaxel- and vincristine-evoked painful peripheral neuropathies: loss of epidermal innervation and activation of Langerhans cells Vol. 201. *Experimental Neurology* (2006) p. 507–14. doi: 10.1016/j.expneurol.2006.05.007
20. Zhang H, Li Y, de Carvalho-Barbosa M, Kavelaars A, Heijnen CJ, Albrecht PJ, et al. Dorsal Root Ganglion Infiltration by Macrophages Contributes to Paclitaxel Chemotherapy-Induced Peripheral Neuropathy. *J Pain* (2016) 17 (7):775–86. doi: 10.1016/j.jpain.2016.02.011
21. Luo X, Huh Y, Bang S, He Q, Zhang L, Matsuda M, et al. Macrophage Toll-like Receptor 9 Contributes to Chemotherapy-Induced Neuropathic Pain in Male Mice. *J Neurosci* (2019) 39(35):6848–64. doi: 10.1523/jneurosci.3257-18.2019
22. Sonenberg N, Hinnebusch AG. Regulation of translation initiation in eukaryotes: mechanisms and biological targets. *Cell* (2009) 136(4):731–45. doi: 10.1016/j.cell.2009.01.042
23. Khoutorsky A, Price TJ. Translational Control Mechanisms in Persistent Pain. *Trends Neurosci* (2018) 41(2):100–14. doi: 10.1016/j.tins.2017.11.006
24. Shveygert M, Kaiser C, Bradrick SS, Gromeier M. Regulation of Eukaryotic Initiation Factor 4E (eIF4E) Phosphorylation by Mitogen-Activated Protein Kinase Occurs through Modulation of Mnk1-eIF4G Interaction▽. *Mol Cell Biol* (2010) 30(21):5160–7. doi: 10.1128/mcb.00448-10
25. Thoreen CC, Chantranupong L, Keys HR, Wang T, Gray NS, Sabatini DM. A unifying model for mTORC1-mediated regulation of mRNA translation. *Nature* (2012) 485(7396):109–13. doi: 10.1038/nature11083
26. Nikolcheva T, Pyronnet S, Chou SY, Sonenberg N, Song A, Clayberger C, et al. A translational rheostat for RFLAT-1 regulates RANTES expression in T lymphocytes. *J Clin Invest* (2002) 110(1):119–26. doi: 10.1172/jci15336
27. Herdy B, Jaramillo M, Svitkin YV, Rosenfeld AB, Kobayashi M, Walsh D, et al. Translational control of the activation of transcription factor NF-κB and production of type I interferon by phosphorylation of the translation factor eIF4E. *Nat Immunol* (2012) 13(6):543–50. doi: 10.1038/ni.2291
28. Pashenkov MV, Balyasova LS, Dagil YA, Pinegin BV. The Role of the p38-MNK-eIF4E Signaling Axis in TNF Production Downstream of the NOD1 Receptor. *J Immunol* (2017) 198(4):1638–48. doi: 10.4049/jimmunol.1600467
29. Moy JK, Khoutorsky A, Asiedu MN, Black BJ, Kuhn JL, Barragán-Iglesias P, et al. The MNK–eIF4E Signaling Axis Contributes to Injury-Induced Nociceptive Plasticity and the Development of Chronic Pain. *J Neurosci* (2017) 37(31):7481–99. doi: 10.1523/jneurosci.0220-17.2017
30. Amorim IS, Kedia S, Kouloulia S, Simbriger K, Gantois I, Jafarnejad SM, et al. Loss of eIF4E Phosphorylation Engenders Depression-like Behaviors via Selective mRNA Translation. *J Neurosci* (2018) 38(8):2118–33. doi: 10.1523/JNEUROSCI.2673-17.2018
31. Amorim IS, Lach G, Gkogkas CG. The Role of the Eukaryotic Translation Initiation Factor 4E (eIF4E) in Neuropsychiatric Disorders. *Front Genet* (2018) 9:1–9. doi: 10.3389/fgene.2018.00561
32. Moy JK, Kuhn JL, Szabo-Pardi TA, Pradhan G, Price TJ. eIF4E phosphorylation regulates ongoing pain, independently of inflammation, and hyperalgesic priming in the mouse CFA model. *Neurobiol Pain* (2018) 4:45–50. doi: 10.1016/j.ynpai.2018.03.001
33. Mody PH, Dos Santos NL, Barron LR, Price TJ, Burton MD. eIF4E phosphorylation modulates pain and neuroinflammation in the aged. *Geroscience* (2020) 42(6):1663–74. doi: 10.1007/s11357-020-00220-1
34. Megat S, Ray PR, Moy JK, Lou TF, Barragan-Iglesias P, Li Y, et al. Nociceptor Translational Profiling Reveals the Ragulator-Rag GTPase Complex as a Critical Generator of Neuropathic Pain. *J Neurosci* (2019) 39(3):393–411. doi: 10.1523/JNEUROSCI.2661-18.2018
35. Munoz FM, Gao R, Tian Y, Henstenburg BA, Barrett JE, Hu H. Neuronal P2X7 receptor-induced reactive oxygen species production contributes to nociceptive behavior in mice. *Sci Rep* (2017) 7(1):3539. doi: 10.1038/s41598-017-03813-7
36. de Campos Lima T, Santos D, Lemes JBP, Chiovato LM, Lotufo C. Hyperglycemia induces mechanical hyperalgesia and depolarization of the resting membrane potential of primary nociceptive neurons: Role of ATP-sensitive potassium channels. *J Neurol Sci* (2019) 401:55–61. doi: 10.1016/j.jns.2019.03.025
37. Luu W, Bjork J, Salo E, Entenmann N, Jurgenson T, Fisher C, et al. Modulation of SUR1 KATP Channel Subunit Activity in the Peripheral Nervous System Reduces Mechanical Hyperalgesia after Nerve Injury in Mice. *Int J Mol Sci* (2019) 20(9):1–17. doi: 10.3390/ijms20092251
38. Duggett NA, Griffiths LA, Flatters SJL. Paclitaxel-induced painful neuropathy is associated with changes in mitochondrial bioenergetics, glycolysis, and an energy deficit in dorsal root ganglia neurons. *Pain* (2017) 158(8):1499–508. doi: 10.1097/j.pain.0000000000000939
39. Singhmar P, Huo X, Li Y, Dougherty PM, Mei F, Cheng X, et al. Orally active Epac inhibitor reverses mechanical allodynia and loss of intraepidermal nerve fibers in a mouse model of chemotherapy-induced peripheral neuropathy. *Pain* (2018) 159(5):884–93. doi: 10.1097/j.pain.0000000000001160
40. Yilmaz E, Watkins SC, Gold MS. Paclitaxel-induced increase in mitochondrial volume mediates dysregulation of intracellular Ca2+ in putative nociceptive glabrous skin neurons from the rat. *Cell Calcium* (2017) 62:16–28. doi: 10.1016/j.ceca.2017.01.005
41. Furic L, Rong L, Larsson O, Koumakpayi IH, Yoshida K, Brueschke A, et al. eIF4E phosphorylation promotes tumorigenesis and is associated with prostate cancer progression. *Proc Natl Acad Sci U.S.A.* (2010) 107 (32):14134–9. doi: 10.1073/pnas.1005320107
42. Moy JK, Khoutorsky A, Asiedu MN, Dussor G, Price TJ. eIF4E Phosphorylation Influences Bdnf mRNA Translation in Mouse Dorsal Root Ganglion Neurons. *Front Cell Neurosci* (2018) 12:29:29. doi: 10.3389/fncel.2018.00029
43. Hershey JW, Sonenberg N, Mathews MB. Principles of translational control: an overview. *Cold Spring Harb Perspect Biol* (2012) 4(12):1–10. doi: 10.1101/cshperspect.a011528
44. Toma W, Kyte SL, Bagdas D, Alkhlaif Y, Alsharari SD, Lichtman AH, et al. Effects of paclitaxel on the development of neuropathy and affective behaviors in the mouse. *Neuropharmacology* (2017) 117:305–15. doi: 10.1016/j.neuropharm.2017.02.020
45. Smith SB, Crager SE, Mogil JS. Paclitaxel-induced neuropathic hypersensitivity in mice: responses in 10 inbred mouse strains. *Life Sci* (2004) 74(21):2593–604. doi: 10.1016/j.lfs.2004.01.002
46. Hassler SN, Kume M, Mwirigi JM, Ahmad A, Shiers S, Wangzhou A, et al. The cellular basis of protease-activated receptor 2-evoked mechanical and affective pain. *JCI Insight* (2020) 5(11):1–17. doi: 10.1172/jci.insight.137393
47. Langford DJ, Bailey AL, Chanda ML, Clarke SE, Drummond TE, Echols S, et al. Coding of Facial Expressions of Pain in the Laboratory Mouse. *Nat Methods* (2010) 7(6):447–9. doi: 10.1038/nmeth.1455
48. Matsumiya LC, Sorge RE, Sotocinal SG, Tabaka JM, Wieskopf JS, Zaloum A, et al. Using the Mouse Grimace Scale to reevaluate the efficacy of postoperative analgesics in laboratory mice. *J Am Assoc Lab Anim Sci* (2012) 51(1):42–9.

49. Avona A, Burgos-Vega C, Burton MD, Akopian AN, Price TJ, Dussor G. Dural Calcitonin Gene-Related Peptide Produces Female-Specific Responses in Rodent Migraine Models. *J Neurosci* (2019) 39(22):4323–31. doi: 10.1523/jneurosci.0364-19.2019
50. Chaplan SR, Bach FW, Pogrel JW, Chung JM, Yaksh TL. Quantitative assessment of tactile allodynia in the rat paw. *J Neurosci Methods* (1994) 53 (1):55–63. doi: 10.1016/0165-0270(94)90144-9
51. Harlow E, Lane D. Mounting samples in gelvatol or mowiol. *CSH Protoc* (2006) 2006(1). doi: 10.1101/pdb.prot4461
52. Johnson SD, Young MR. Indomethacin Treatment of Mice with Premalignant Oral Lesions Sustains Cytokine Production and Slows Progression to Cancer. *Front Immunol* (2016) 7:379. doi: 10.3389/fimmu.2016.00379
53. Rogers GW, Burroughs SE, Dranka BP. Direct Cellular Metabolism Measurements. *Genet Eng Biotechnol News* (2019) 39(3):48–50. doi: 10.1089/gen.39.03.12
54. Inyang KE, McDougal TA, Ramirez ED, Williams M, Laumet G, Kavelaars A, et al. Alleviation of paclitaxel-induced mechanical hypersensitivity and hyperalgesic priming with AMPK activators in male and female mice. *Neurobiol Pain* (2019) 6:100037. doi: 10.1016/j.ynpai.2019.100037
55. Korbecki J, Grochans S, Gutowska I, Barczak K, Baranowska-Bosiacka I. CC Chemokines in a Tumor: A Review of Pro-Cancer and Anti-Cancer Properties of Receptors CCR5, CCR6, CCR7, CCR8, CCR9, and CCR10 Ligands. *Int J Mol Sci* (2020) 21(20):1–34. doi: 10.3390/ijms21207619
56. Trebst C, Brunhorn K, Lindner M, Windhagen A, Stangel M. Expression of chemokine receptors on peripheral blood mononuclear cells of patients with immune-mediated neuropathies treated with intravenous immunoglobulins. *Eur J Neurol* (2006) 13(12):1359–63. doi: 10.1111/j.1468-1331.2006.01521.x
57. Galmarini CM, Bouchet BP, Falette N, Vila L, Lamblot C, Audoynaud C, et al. Weekly administration of paclitaxel induces long-term aneugenicity in nude mice. *Cancer Biol Ther* (2007) 6(3):377–82. doi: 10.4161/cbt.6.3.3713
58. Huehnchen P, Boehmerle W, Springer A, Freyer D, Endres M. A novel preventive therapy for paclitaxel-induced cognitive deficits: preclinical evidence from C57BL/6 mice. *Trans Psychiatry* (2017) 7(8):1–11. doi: 10.1038/tp.2017.149
59. Peters CM, Jimenez-Andrade JM, Jonas BM, Sevcik MA, Koewler NJ, Ghilardi JR, et al. Intravenous paclitaxel administration in the rat induces a peripheral sensory neuropathy characterized by macrophage infiltration and injury to sensory neurons and their supporting cells. *Exp Neurol* (2007) 203(1):42–54. doi: 10.1016/j.expneurol.2006.07.022
60. Li Y, Yin C, Liu B, Nie H, Wang J, Zeng D, et al. Transcriptome profiling of long noncoding RNAs and mRNAs in spinal cord of a rat model of paclitaxel-induced peripheral neuropathy identifies potential mechanisms mediating neuroinflammation and pain. *J Neuroinflamm* (2021) 18(1):1–22. doi: 10.1186/s12974-021-02098-y
61. Robinson CR, Zhang H, Dougherty PM. Astrocytes, but not microglia, are activated in oxaliplatin and bortezomib-induced peripheral neuropathy in the rat. *Neuroscience* (2014) 274:308–17. doi: 10.1016/j.neuroscience.2014.05.051
62. Liu X, Tonello R, Ling Y, Gao YJ, Berta T. Paclitaxel-activated astrocytes produce mechanical allodynia in mice by releasing tumor necrosis factor-alpha and stromal-derived cell factor 1. *J Neuroinflamm* (2019) 16(1):209. doi: 10.1186/s12974-019-1619-9
63. Ochi-ishi R, Nagata K, Inoue T, Tozaki-Saitoh H, Tsuda M, Inoue K. Involvement of the chemokine CCL3 and the purinoceptor P2X7 in the spinal cord in paclitaxel-induced mechanical allodynia. *Mol Pain* (2014) 10:53. doi: 10.1186/1744-8069-10-53
64. Matsuda M, Huh Y, Ji RR. Roles of inflammation, neurogenic inflammation, and neuroinflammation in pain. *J Anesth* (2019) 33(1):131–9. doi: 10.1007/s00540-018-2579-4
65. Ren K, Dubner R. Interactions between the immune and nervous systems in pain. *Nat Med* (2010) 16(11):1267–76. doi: 10.1038/nm.2234
66. Weyer AD, Zappia KJ, Garrison SR, O'Hara CL, Dodge AK, Stucky CL. Nociceptor Sensitization Depends on Age and Pain Chronicity. *Eneuro* (2016) 3(1):26. doi: 10.1523/eneuro.0115-15.2015
67. Kandasamy R, Price TJ. The Pharmacology of Nociceptor Priming. *Handb Exp Pharmacol* (2015) 227:15–37. doi: 10.1007/978-3-662-46450-2_2
68. Tonello R, Xie W, Lee SH, Wang M, Liu X, Strong JA, et al. Local Sympathectomy Promotes Anti-inflammatory Responses and Relief of Paclitaxel-induced Mechanical and Cold Allodynia in Mice. *Anesthesiology* (2020) 132(6):1540–53. doi: 10.1097/ALN.0000000000003241
69. Huang S, Ziegler CGK, Austin J, Mannoun N, Vukovic M, Ordovas-Montanes J, et al. Lymph nodes are innervated by a unique population of sensory neurons with immunomodulatory potential. *Cell* (2021) 184(2):441–59. doi: 10.1016/j.cell.2020.11.028
70. Liu X-J, Zhang Y, Liu T, Xu Z-Z, Park C-K, Berta T, et al. Nociceptive neurons regulate innate and adaptive immunity and neuropathic pain through MyD88 adapter. *Cell Res* (2014) 24(11):1374–7. doi: 10.1038/cr.2014.106
71. Bousso P. T-cell activation by dendritic cells in the lymph node: lessons from the movies. *Nat Rev Immunol* (2008) 8(9):675–84. doi: 10.1038/nri2379
72. Li Y, Zhang H, Zhang H, Kosturakis AK, Jawad AB, Dougherty PM. Toll-like receptor 4 signaling contributes to Paclitaxel-induced peripheral neuropathy. *J Pain* (2014) 15(7):712–25. doi: 10.1016/j.jpain.2014.04.001
73. Zhang H, Yoon SY, Zhang H, Dougherty PM. Evidence that spinal astrocytes but not microglia contribute to the pathogenesis of Paclitaxel-induced painful neuropathy. *J Pain* (2012) 13(3):293–303. doi: 10.1016/j.jpain.2011.12.002
74. Uttam S, Wong C, Price TJ, Khoutorsky A. eIF4E-Dependent Translational Control: A Central Mechanism for Regulation of Pain Plasticity. *Front Genet* (2018) 9:1–10. doi: 10.3389/fgene.2018.00470
75. Mamane Y, Petroulakis E, Rong L, Yoshida K, Ler LW, Sonenberg N. eIF4E–from translation to transformation. *Oncogene* (2004) 23(18):3172–9. doi: 10.1038/sj.onc.1207549
76. Mody PH, Lucia Dos Santos N, Lenert ME, Barron LR, Nottingham BA, Burton MD. The role of cap-dependent translation in aged-related changes in neuroimmunity and affective behaviors. *Neurobiol Aging* (2020) 98:173–84. doi: 10.1016/j.neurobiolaging.2020.10.014

Conflict of Interest: The authors declare that the research was conducted in the absence of any commercial or financial relationships that could be construed as a potential conflict of interest.

frontiers in Immunology

ORIGINAL RESEARCH
published: 28 April 2021
doi: 10.3389/fimmu.2021.637845

Physiological Sympathetic Activation Reduces Systemic Inflammation: Role of Baroreflex and Chemoreflex

*Fernanda Brognara[1], Jaci Airton Castania[1], Alexandre Kanashiro[2], Daniel Penteado Martins Dias[3] and Helio Cesar Salgado[1]**

[1] Department of Physiology, Ribeirão Preto Medical School, University of São Paulo, Ribeirão Preto, Brazil, [2] Department of Neuroscience and Behavior, Ribeirão Preto Medical School, University of São Paulo, Ribeirão Preto, Brazil, [3] Barão de Mauá University Center, Ribeirão Preto, Brazil

Baroreflex and chemoreflex act through the autonomic nervous system, which is involved with the neural regulation of inflammation. The present study reports the effects of reflex physiological sympathetic activation in endotoxemic rats using bilateral carotid occlusion (BCO), a physiological approach involving the baroreflex and chemoreflex mechanisms and the influence of the baroreceptors and peripheral chemoreceptors in the cardiovascular and systemic inflammatory responses. After lipopolysaccharide (LPS) administration, the arterial pressure was recorded during 360 min in unanesthetized rats, and serial blood samples were collected to analyze the plasma cytokine levels. BCO elicited the reflex activation of the sympathetic nervous system, providing the following outcomes: (I) increased the power of the low-frequency band in the spectrum of the systolic arterial pressure during the BCO period; (II) reduced the levels of pro-inflammatory cytokines in plasma, including the tumor necrosis factor (TNF) and the interleukin (IL)-1β; (III) increased the plasma levels of anti-inflammatory cytokine IL-10, 90 min after LPS administration. Moreover, selective baroreceptor or chemoreceptor denervation deactivated mechanosensitive and chemical sensors, respectively, and decreased the release of the LPS-induced cytokine but did not alter the BCO modulatory effects. These results show, for the first time, that physiological reflex activation of the sympathetic circuit decreases the inflammatory response in endotoxemic rats and suggest a novel function for the baroreceptors as immunosensors during the systemic inflammation.

Keywords: baroreceptors, bilateral carotid occlusion, chemoreceptors, inflammation, neuroimmune interactions, sympathetic activation

OPEN ACCESS

Edited by:
Michael D. Burton, The University of Texas at Dallas, United States

Reviewed by:
Edward Sherwood, Vanderbilt University Medical Center, United States
Eva Bartok, Institute of Tropical Medicine Antwerp, Belgium

***Correspondence:**
Helio Cesar Salgado
hcsalgado@fmrp.usp.br

Specialty section:
This article was submitted to Molecular Innate Immunity, a section of the journal Frontiers in Immunology

Received: *04 December 2020*
Accepted: *06 April 2021*
Published: *28 April 2021*

Citation:
Brognara F, Castania JA, Kanashiro A, Dias DPM and Salgado HC (2021) Physiological Sympathetic Activation Reduces Systemic Inflammation: Role of Baroreflex and Chemoreflex. Front. Immunol. 12:637845. doi: 10.3389/fimmu.2021.637845

INTRODUCTION

The interaction between the central nervous system and the immune system has been studied since the 19th century (1). Of note, this interaction plays a fundamental role in the regulation of inflammation *via* activation of neuroendocrine circuits including the hypothalamic–pituitary–adrenal axis (2, 3), the "cholinergic anti-inflammatory pathway" (4, 5), and the "splanchnic anti-inflammatory pathway" (6). The autonomic nervous system has been the focus of studies involving

control of the immune system (6–12). These neuroimmune circuits have been described in endotoxemia, the most known model of inflammation. Lipopolysaccharide (LPS), also known as endotoxin, is a molecule present in the cell wall of Gram-negative bacteria and, when administrated, can stimulate innate immunity *via* activation of Toll-like receptor 4 (TLR-4) expressed on the surface of macrophages, for example, inducing the release of pro-inflammatory cytokines (13–15). Besides, in rodents, the outer membrane LPS of Gram-negative bacteria can also activate the noncanonical inflammasome pathway and stimulate the release of IL-1β *via* caspase-11 (16, 17). Briefly, intracellular LPS is recognized by the CARD domain of caspase-11, which cleaves the pore-forming protein gasdermin D (17–19). Through a K^+ efflux-dependent process, the N-terminal domain of gasdermin D activates NLRP3 inflammasome, which triggers the release of IL-1β by active caspase-1, increasing the inflammation (18).

The body has physiological reflex mechanisms to activate or deactivate both the sympathetic and/or the parasympathetic branches. Among these mechanisms are: (I) the baroreflex, which provides the moment-to-moment control of arterial pressure mediated primarily by the arterial baroreceptors, which, when stimulated, activate the parasympathetic branch and inhibit the sympathetic branch; and (II) the chemoreflex, which maintains the cardiorespiratory homeostasis in response to changes in blood gas concentrations (such as oxygen or carbon dioxide) due to the presence of the peripheral chemoreceptors, which, when stimulated, activate both branches of the autonomic nervous system, *i.e.*, the sympathetic and the parasympathetic. Thus, physiological methods able to activate or deactivate the autonomic nervous system reflexively could be useful to mimic the authentic role of this system during inflammation. However, to the best of our knowledge, no previous study has used a methodological approach that activates the autonomic nervous system reflexively, during a reliable physiological context, so as to investigate the importance of the nervous system during an immune challenge.

The bilateral carotid occlusion (BCO) is one of the techniques used to elicit global reflex activation of the sympathetic nervous system in both unanesthetized (20–23) and anesthetized animals (24, 25). Moreover, when the common carotids arteries are occluded temporarily, there is a significant reduction in the arterial pressure and blood flow inside the carotid sinus region, culminating with the deactivation of the carotid baroreceptors. This inactivation of the carotid baroreceptors induces an increase in sympathetic activity to the blood vessels, increasing the global peripheral resistance, combined with a concomitant reduction in cardiac parasympathetic activity, determining the increase in arterial pressure (26, 27). In addition, there is the activation of the carotid chemoreceptors, due to the hypoxia caused by the reduction of blood flow into the carotid sinus, contributing to the increase in sympathetic activity (26, 27).

Because the BCO is a methodological approach that promotes reflex sympathetic activation, it could be used to study the influence of the autonomic nervous system in the control of systemic inflammation. Furthermore, taking into account that the baroreceptors and the chemoreceptors are involved in the pressor response to BCO, it is also necessary to examine the individual participation of these receptors during an inflammatory process. Thus, the present study aimed to investigate in unanesthetized LPS-induced endotoxemic rats: (I) the effect of BCO-induced sympathetic reflex activation; (II) the importance of both the baroreflex and the chemoreflex in this procedure; and (III) the influence of the baroreceptors and the peripheral chemoreceptors, through their specific surgical denervation, in the systemic inflammatory response.

METHODS

Experimental Animals and Groups

Male Wistar-Hannover rats (250–320 g) obtained from the Main Animal Facility of the University of São Paulo (Campus of Ribeirão Preto; Ribeirão Preto, SP, Brazil) were used. The animals were maintained in individual cages under controlled temperature (22°C), and a constant 12-hour light–dark cycle, with free access to water and food. All procedures were reviewed and approved by the Committee of Ethics in Animal Research of the Ribeirão Preto Medical School - University of São Paulo (Protocol # 194/2016). The rats were divided into seven experimental groups:

I. **Saline (n = 9):** fictitious surgery and saline administration.
II. **LPS (n = 8):** bilateral implantation of the pneumatic cuffs, without BCO, with the administration of LPS.
III. **BCO + LPS (n = 8):** bilateral implantation of the pneumatic cuffs and, BCO during 20 s, with the administration of LPS.
IV. **BARO-X + LPS (n = 7):** selective denervation of the aortic and carotid baroreceptors, bilateral implantation of the pneumatic cuffs, without BCO, with the administration of LPS.
V. **BARO-X + BCO + LPS (n = 9):** selective denervation of the aortic and carotid baroreceptors, bilateral implantation of the pneumatic cuffs and BCO during 20 s, with the administration of LPS.
VI. **CHEMO-X + LPS (n = 7):** selective denervation of the carotid chemoreceptors, bilateral implantation of the pneumatic cuffs, without BCO, with the administration of LPS.
VII. **CHEMO-X + BCO + LPS (n = 9):** selective denervation of the carotid chemoreceptors, bilateral implantation of the pneumatic cuffs and BCO during 20 s, with the administration of LPS.

Surgical Procedures

The animals were anesthetized with a mixture of Ketamine and Xylazine (50 mg/kg and 10 mg/kg, i.p.) and then subjected to the surgical procedure for cannulation of the left femoral artery and vein for arterial pressure recording and LPS (or saline) administration, respectively. Briefly, polyethylene tubes (PE-50 soldered to PE-10 polyethylene tube; Intramedic, Clay Adams, Parsippany, NJ, USA) were implanted into the femoral artery

and vein and pulled up through a subcutaneous track to the rat's neck and exteriorized in the nape. The catheter inserted into the femoral artery was filled with 100 IU/ml heparin in saline. In the same surgery, except for the saline group, all other animals had pneumatic cuffs implanted, bilaterally, around the common carotid arteries. For this procedure, an anterior median cervicotomy was carried out, while the sternohyoid and sternocleidomastoid muscles were identified and retracted, exposing the common carotid artery and the carotid sinus. To implant the pneumatic cuffs, the common carotid arteries were carefully isolated, and the pneumatic cuffs fixed around them with cotton threads. The catheters for filling the balloons were exteriorized and fixed onto the back of the neck, as well as the vascular catheters. In the saline group, the animals were subjected to the same surgical procedures, but the pneumatic cuffs were not implanted around the common carotid arteries. The surgical incisions were properly sutured and, immediately after the surgery, an analgesic was administered (tramadol hydrochloride, 2 mg/kg, s.c.). Pneumatic cuffs (**Supplementary Figures 1A–C**) were made following the technique described by Maio et al. (28).

Concerning the groups IV and V, in the same surgery for the pneumatic cuff implantation, the rats were submitted to procedures for baroreceptor denervation. This approach was undertaken to prevent the attenuation of the sympathetic activity by the baroreceptors during the elevation of the arterial pressure resulting from the BCO, and also to eliminate a possible influence of the baroreflex in the anti-inflammatory response caused by sympathetic activation. For this purpose, the denervation of the aortic and carotid baroreceptors was performed bilaterally. The carotid baroreceptor denervation was performed according to the technique described by Castania et al. (29). Briefly, the common carotid region and the carotid bifurcation were exposed. Next to the glossopharyngeal nerve, two branches were identified, usually separated by a small artery. With the aid of a magnifying glass one of these branches, which carries the afferent fibers of the carotid baroreceptors, was carefully sectioned. The aortic baroreceptor denervation, on the other hand, was carried out following the technique described by Krieger (30), in which the superior laryngeal nerve and the superior cervical ganglion were isolated and sectioned. The cervical sympathetic trunk was also sectioned caudally to the superior cervical ganglion, which was dissected and removed. The procedure was performed on both sides. On the other hand, groups VI and VII were submitted to the denervation of the carotid chemoreceptors so as to study their influences in the inflammatory response during the BCO. The technique was also performed bilaterally, following the method described by Franchini and Krieger (31). For this procedure, the common carotid artery and its bifurcation were exposed. With the aid of a magnifying glass, the carotid body was identified, and the carotid body artery was carefully isolated and sectioned distally to the ligature.

Arterial Pressure Recording

After recovering from the surgery, which took 24 h, the unanesthetized rats were connected to the arterial pressure recording system. Briefly, the arterial catheter was connected to a pressure transducer (MLT844; ADInstruments, Bella Vista, Australia), and the signal was amplified (ML224; ADInstruments, Bella Vista, Australia) and sampled at 2 kHz by an IBM/PC computer (Core 2 Duo, 2.2 GHz, 4 GB RAM) attached to an analog-to-digital interface (PowerLab, ADInstruments, Bella Vista, Australia). The experiment was conducted with the animals moving freely in their own cage, and silence was maintained to minimize environmental stress. Arterial pressure recordings were processed with computer software (LabChart 7.0, ADInstruments, Bella Vista, Australia) capable of detecting inflection points and generate mean arterial pressure, systolic arterial pressure, diastolic arterial pressure, and heart rate beat-by-beat time series. In the case of groups with BCO, the two catheters for filling the balloons were connected to a syringe with water through a personalized Y-shaped polyethylene tubing to perform the occlusion simultaneously on both sides.

Following the basal recording of pulsatile arterial pressure during 30 min, both common carotid arteries were occluded for 20 s, decreasing the blood flow above the carotid region (**Supplementary Figures 1D, E**). Next, the balloons were deflated to re-establish the blood flow. Immediately after the end of the occlusion, LPS [0.06 mg/kg (i.v.); *Escherichia coli*-0111: B4 purified by phenol extraction; Sigma-Aldrich, St. Louis, MO, USA] was administered (**Supplementary Figure 1F**). For the other groups not subjected to BCO, saline or LPS was administered immediately after the end of the basal recordings. Arterial pressure was recorded continuously during 360 min after the administration of LPS or saline, in all groups (**Supplementary Figure 1F**). During this period, serial blood samples (250 μl per sample) were taken at 90, 180, 270, and 360 min after the administration of LPS or saline, through the catheter placed into the left femoral artery (**Supplementary Figure 1F**). Blood samples were collected with heparin and kept on ice until centrifuged at 4°C for 15 min at 5,000 rpm. Subsequently, the plasma was collected and stored at −80°C until processing. In the groups with denervation (baroreceptor or chemoreceptor), at the end of the last blood collection, tests were performed with phenylephrine (2 μg in 0.1 ml, i.v.) and potassium cyanide (40 μg in 0.1 ml, i.v.) to confirm the correct denervation of each animal. Subjects that were not adequately denervated were not included in the study.

Cardiocirculatory Variability Analysis

Beat-by-beat time series with systolic arterial pressure and cardiac interval values were extracted from periods of approximately 10 min for each moment (basal, 90, 180, 270, and 360 min after LPS or saline) from pulsatile arterial pressure tracings. For the analysis during the BCO period, data points from the first 60 s after BCO was initiated (20 s of the BCO period plus the next 40 s after BCO ending) were used. The time series were analyzed in the frequency domain by means of spectral analysis using an open-access custom computer software (CardioSeries v2.7, www.danielpenteado.com). Briefly, the beat-by-beat time series were resampled using cubic spline interpolation (10 Hz), and the interpolated series were split into half-overlapping sequential segments of 512 data points. All segments were visually inspected by a highly experienced

researcher looking for transients that could affect the calculation of the power spectral density. To ensure that visual inspection of the time series was properly performed, a Hanning window was used to diminish side effects, and the spectrum was calculated for all segments using a direct Fast Fourier Transform (FFT) algorithm for discrete-time series. Finally, all spectra were visually inspected for abnormalities and were integrated into low- (LF: 0.20–0.75 Hz) and high-frequency (HF: 0.75–3.00 Hz) bands. Results are expressed in absolute (ms^2 and $mmHg^2$) and normalized (nu) units. LF/HF ratio was also calculated. It is worth noting that cardiac interval and arterial pressure variability measured by spectral analysis are useful tools to evaluate the autonomic modulation of the cardiovascular system (32, 33) and have been used in the study of cardiovascular and inflammatory diseases, revealing a strong association between the levels of cytokines and autonomic modulation (34–36). What is more, the HF oscillations of the cardiac interval correspond to the vagal modulation of the heart (37–39) and the LF oscillations of both the cardiac interval and systolic arterial pressure reflect sympathetic modulation of the heart and vessels, respectively (32, 37, 40, 41).

Cytokine Measurements

Plasma levels of cytokines (TNF, IL-1β, IL-6, and IL-10) were measured by the immune-enzymatic ELISA method using Duo set kits from R&D Systems (Minneapolis, MN, USA) according to the manufacturer's instructions.

Statistical Analysis

The results are presented as mean ± standard error of the mean (SEM). The hemodynamic and cardiocirculatory variability parameters were analyzed by two-way analysis of variance (ANOVA) for repeated measurements followed by the Tukey post-test when indicated and also by one-way ANOVA followed by the Tukey post-test when indicated. The data obtained from plasma were analyzed by one-way ANOVA, followed by the Student–Newman–Keuls post-test when indicated and also by the two-way ANOVA for repeated measures followed by the Student–Newman–Keuls post-test. Interrelations between systolic arterial pressure variability and IL-6 and IL-10 levels were examined by Pearson's correlation after being classified as normally distributed by the Shapiro–Wilk normality test. Interrelations between systolic arterial pressure variability and TNF and IL-1β levels were examined by Spearman's correlation after not being classified as normally distributed by the Shapiro-Wilk normality test. Differences were considered statistically significant if $p < 0.05$. Statistical analysis was performed using SigmaPlot 12.0 software (Systat Software, San Jose, CA, USA) and GraphPad Prism 6.0 software (GraphPad Software, San Diego, CA, USA).

RESULTS

Hemodynamic and Autonomic Responses to Bilateral Carotid Occlusion

BCO promoted an increase in systolic, diastolic, and mean arterial pressure (**Figures 1A–C**), in intact animals and in those with selective denervation of baroreceptors (BARO-X) or chemoreceptors (CHEMO-X), indicating an increase in peripheral resistance due to the sympathetic activation. However, the hypertensive response to BCO was lower in the CHEMO-X than in the intact and BARO-X animals (mean arterial pressure: Intact, Δ 61 ± 3 mmHg; BARO-X, Δ 61 ± 3 mmHg; CHEMO-X, Δ 47 ± 3 mmHg; Intact *vs.* BARO-X, $p = 0.998$; Intact *vs.* CHEMO-X, $p = 0.005$; BARO-X *vs.* CHEMO-X, $p = 0.005$; **Figure 1E**), indicating the importance of the integrity of the chemoreceptors for the peak of hypertensive response during BCO as previously described (26). In addition, while BCO did not change the heart rate of intact and BARO-X animals, it did promote bradycardia in the CHEMO-X subjects (**Figure 1D**), indicating a reflex response involving the aortic baroreceptors activating the parasympathetic function in the heart.

It is worth mentioning that the increase in sympathetic modulation of the vessels, resulting from the BCO maneuver, was in line with the increase of the power of the LF band in the spectrum of the systolic arterial pressure during the BCO period (**Figure 1F**), in both intact and denervated animals (BARO-X and CHEMO-X).

Time Course of Hemodynamic and Autonomic Responses

The analysis of the hemodynamic parameters from animals with BARO-X showed higher mean arterial pressure than the intact rats under basal conditions (**Figure 2A**). Regarding the other periods evaluated, no difference was observed in the mean arterial pressure among groups at each time frame evaluated (**Figures 2B–E**). Concerning the heart rate under basal conditions, the subjects with BARO-X exhibited higher levels of heart rate than intact—an outcome already described in the literature (42, 43)—and CHEMO-X animals (**Figure 2F**). Ninety min after LPS, the subjects with BARO-X still showed higher heart rate levels than intact rats (**Figure 2G**). Over time, the rats that received LPS showed an increase in heart rate compared to the animals that received saline, starting from 180 min after LPS administration (**Figure 2H**). Moreover, this response was similar at 270 min after LPS injection (**Figures 2I**). In addition, this tachycardia was maintained until the end of the protocol (360 min) in the animals exhibiting endotoxemia (**Figure 2J**).

The analysis of cardiac interval variability did not reveal any difference in the power of the LF band between the groups evaluated over time (**Figures 2K–O**). The same was observed for the LF/HF ratio (**Figures 2U–Y**). Regarding the power of the HF band, a reduction in this parameter was observed in the basal period in the animals with BARO-X compared to the intact control rats (**Figure 2P**). The group with CHEMO-X also showed lower values of the power of the HF band during the basal period (**Figure 2P**). However, the group with CHEMO-X associated with BCO showed an increase in the HF band compared to the BARO-X + BCO + LPS group under basal and 90 min (**Figures 2P, Q**). Over time, the groups that received LPS showed a reduction in the power of the HF band compared to the saline group, as displayed at 180, 270 and 360 min (**Figures 2R–T**).

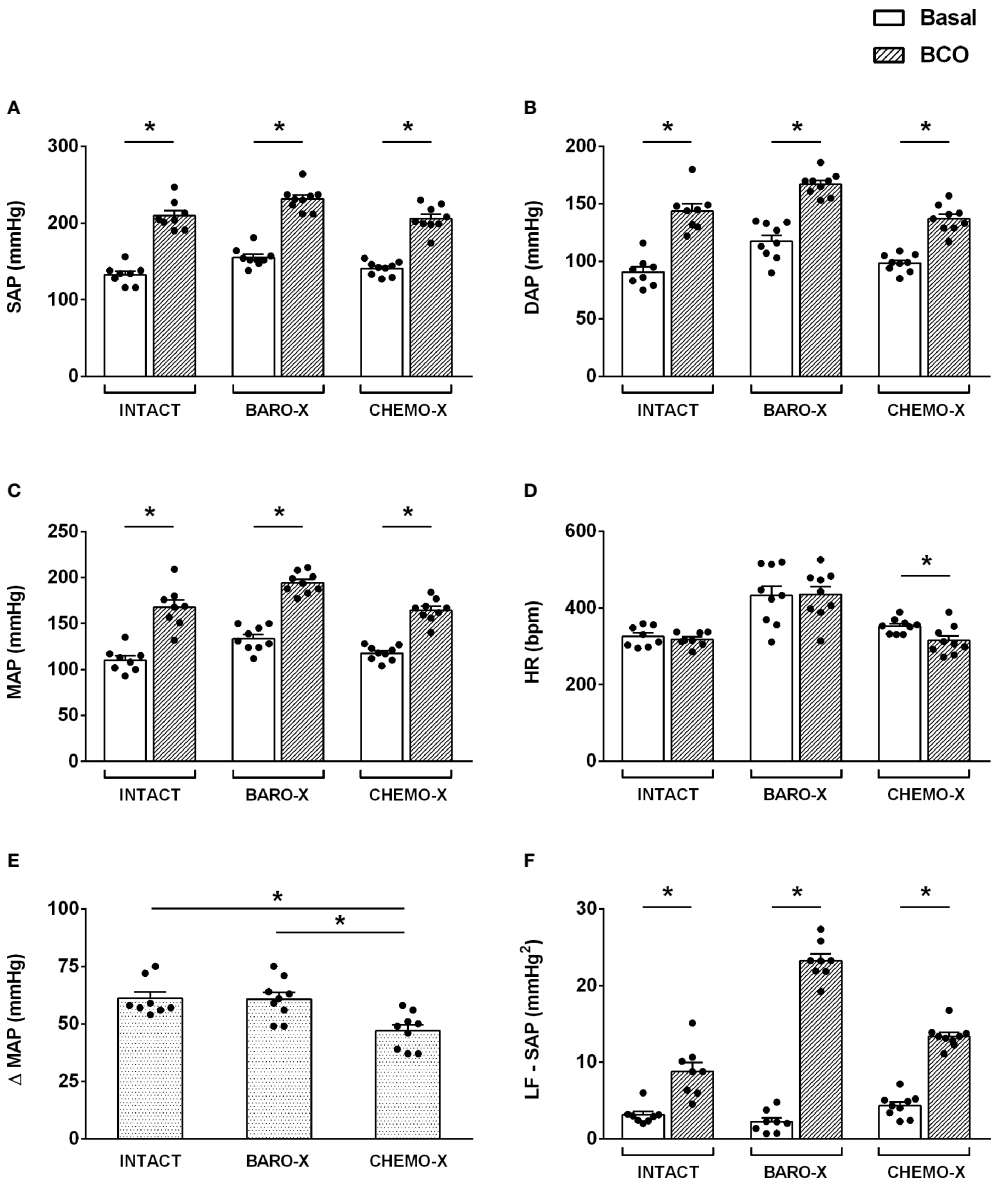

FIGURE 1 | Hemodynamic and autonomic responses to bilateral carotid occlusion (BCO) in intact animals and with denervation of baroreceptors (BARO-X) or chemoreceptors (CHEMO-X). SAP, systolic arterial pressure **(A)**; DAP, diastolic arterial pressure **(B)**; MAP, mean arterial pressure **(C)**; HR, heart rate **(D)**; Δ MAP: the difference between basal and BCO values of MAP **(E)**; LF-SAP: low frequency band in the spectrum of the systolic arterial pressure **(F)**. Panels **(A–D)**: basal period (white bars) and BCO peak response period (period of 5 s within the peak response during BCO; gray bars). Panel **(F)**: basal (white bars) and BCO period (period of 20 s of the BCO plus the next 40 s after BCO ending; gray bars). Bars represent mean ± SEM. *p < 0.05.

Bilateral Carotid Occlusion Reduced Systemic Inflammation

BCO reduced the plasma levels of TNF ($p < 0.001$) and IL-1β ($p < 0.001$) in intact animals 90 min after LPS administration (**Figures 3A, B**, **Table 1**). However, in those animals with BARO-X, BCO did not change the levels of TNF ($p = 0.061$) or IL-1β ($p = 0.946$), and in CHEMO-X rats BCO increased TNF levels ($p < 0.001$), but not modified IL-1β ($p = 0.862$) 90 min after LPS administration (**Table 1**). For IL-1β, in intact rats, this effect was maintained until 180 min after LPS administration (**Table 1**). In addition, BCO increased the levels of IL-10 in the plasma of intact animals ($p = 0.001$) at 90 min and those with CHEMO-X up to 270 min ($p < 0.001$) (**Figure 3D**, **Table 1**). In other words, the anti-inflammatory cytokine levels increased in plasma when the carotid baroreceptors were deactivated since when the BCO was performed in intact and CHEMO-X rats, there was reflexive deactivation of the carotid baroreceptors due to a significant

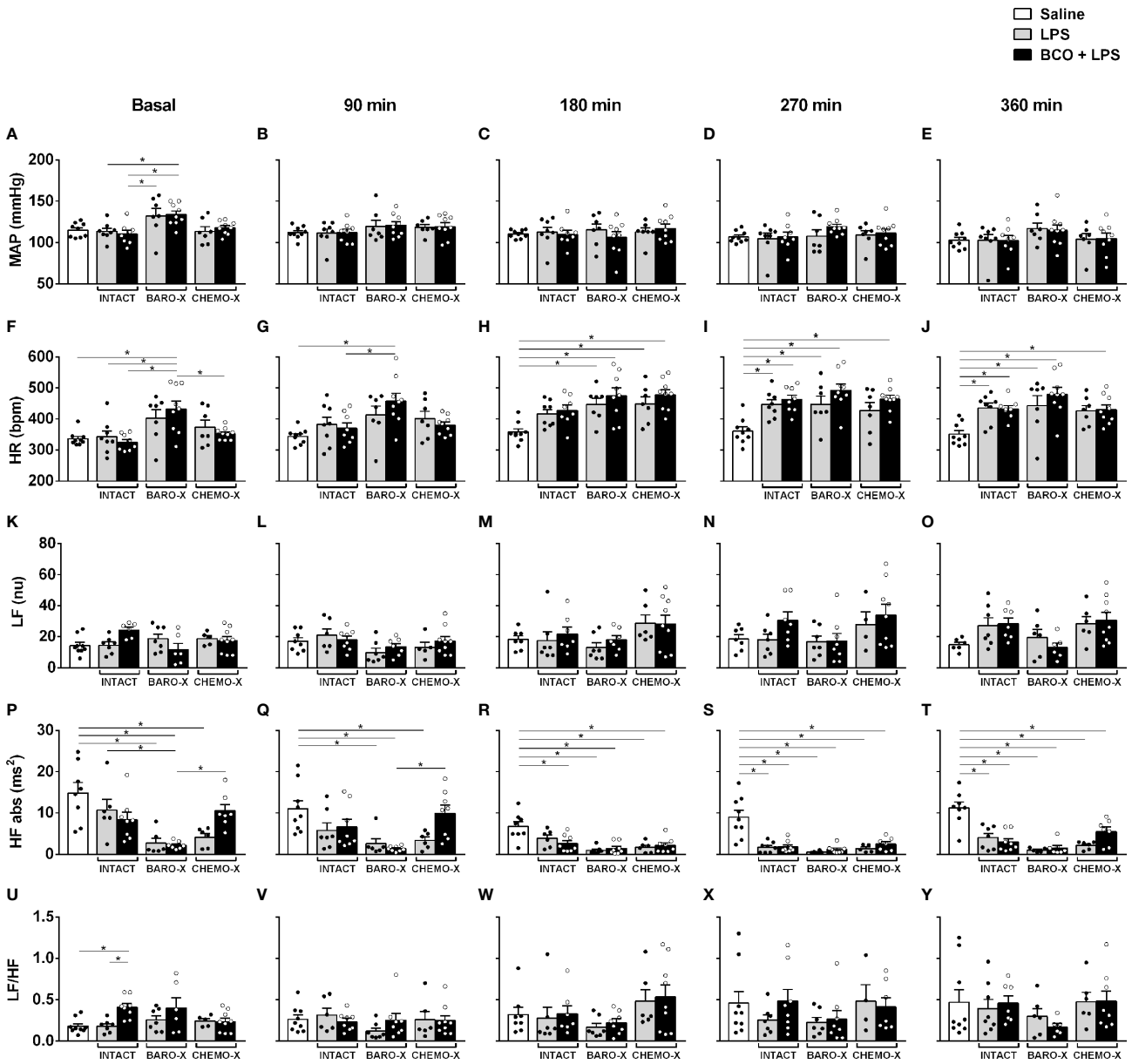

FIGURE 2 | Time course of hemodynamic and cardiac interval variability responses. Mean arterial pressure (MAP; panels **A–E**), heart rate (HR; panels **F–J**), low-frequency band (LF; panels **K–O**), and high-frequency band (HF; panels **P–T**) in the spectrum of the cardiac interval, and LF/HF ratio (panels **U–Y**) at different times: baseline, 90, 180, 270, and 360 min after LPS or saline. BARO-X, selective denervation of baroreceptors; BCO, bilateral carotid occlusion; CHEMO-X, selective denervation of chemoreceptors; LPS, lipopolysaccharide. Bars represent mean ± SEM. *$p < 0.05$.

reduction in the arterial pressure and blood flow inside the carotid sinus region. However, in BARO-X animals, the BCO decreased the plasma levels of IL-10 at 90 min ($p = 0.007$), 270 min ($p = 0.049$), and 360 min ($p = 0.024$), but not at 180 min ($p = 0.194$) (**Table 1**). This data shows that the IL-10 levels decreased in plasma when only the carotid chemoreceptors were activated by BCO. Of note, these results from IL-10 due to BCO performed in different animals (intact, BARO-X and CHEMO-X) confirm that surgical denervation is not the same as the deactivation of a sensory receptor by a physiological mechanism. Finally, BCO was not effective in reducing the plasma IL-6 in intact animals at any of the evaluated time frames (90 min: $p = 0.816$; 180 min: $p = 0.916$; 270 min: $p = 0.990$; 360 min: $p = 1$) (**Table 1**). Nevertheless, BCO increased IL-6 in BARO-X ($p < 0.001$) and CHEMO-X ($p = 0.037$) rats 90 min after LPS administration (**Table 1**). Moreover, for BARO-X subjects this effect was also observed 180 min after LPS ($p < 0.001$) (**Table 1**).

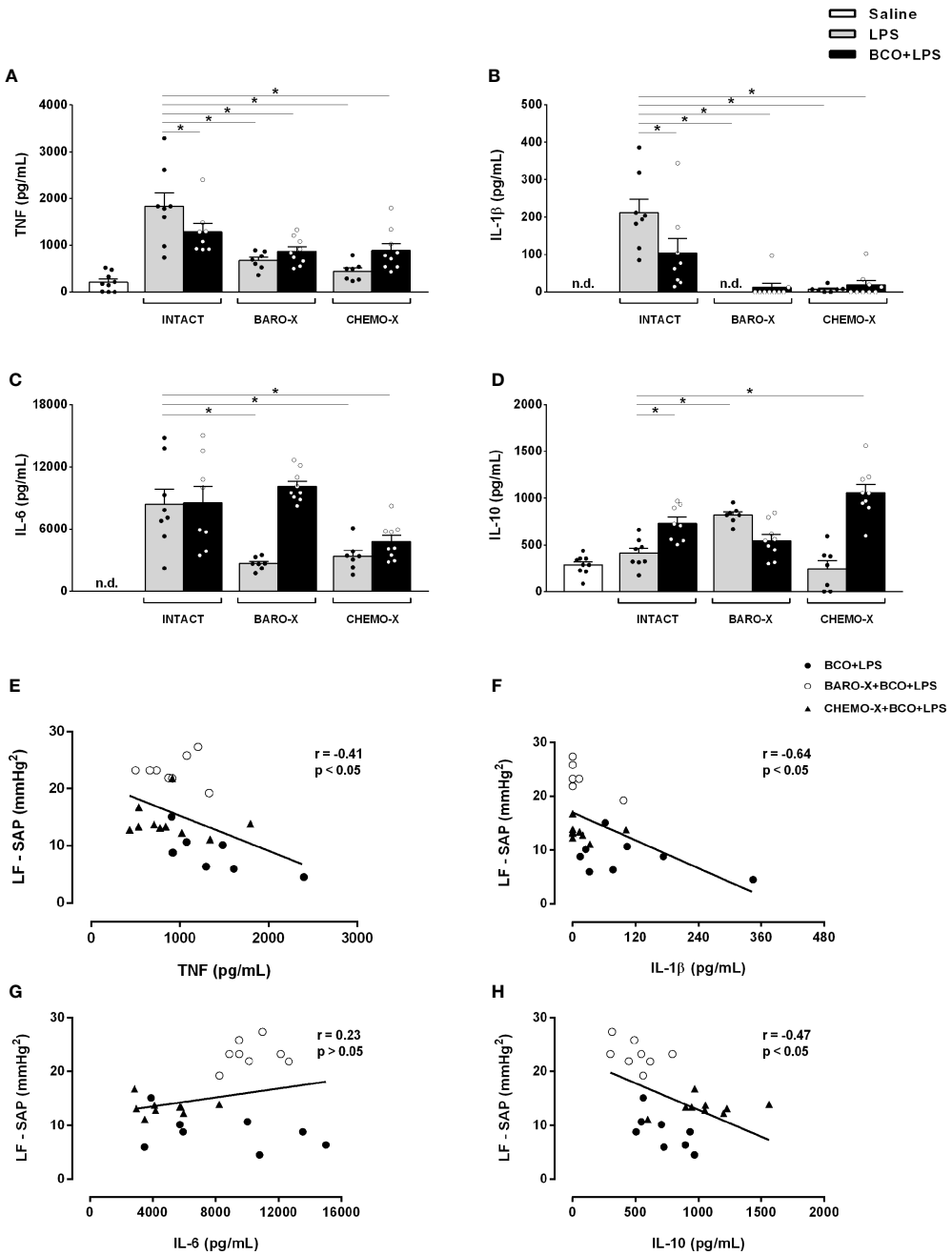

FIGURE 3 | Plasma cytokine levels 90 min after saline or LPS and correlation of systolic arterial pressure variability and cytokine levels. Plasma levels of TNF **(A)**, IL-1β **(B)**, IL-6 **(C)** and IL-10 **(D)** 90 min after administration of LPS or saline, and Pearson's and Spearman's correlation between the power of the low-frequency band of the systolic arterial pressure (LF-SAP) during the BCO period and the cytokines plasma levels [TNF **(E)**, IL-1β **(F)**, IL-6 **(G)**, and IL-10 (**H**)] at 90 min after the administration of LPS. BARO-X, selective denervation of baroreceptors; BCO, bilateral carotid occlusion; CHEMO-X, selective denervation of chemoreceptors; LPS, lipopolysaccharide; n.d., not detected. Bars represent mean ± SEM. *p < 0.05.

Denervation of the Baroreceptors or Chemoreceptors Modulates Systemic Inflammatory Response

Surprisingly, the surgical denervation of the aortic and carotid baroreceptors attenuated the release of TNF, IL-6, and IL-1β into the plasma 90 min after LPS administration (**Figures 3A–C**, **Table 1**). This effect remained until 180 min after triggering the immune challenge for IL-6, and until 270 min for IL-1β (**Table 1**). The same outcome was observed in animals that underwent CHEMO-X (**Figures 3A–C**, **Table 1**), suggesting a possible communication

TABLE 1 | Time Course of Plasma Cytokines.

	Saline (n = 9)	LPS (n = 8)	BCO + LPS (n = 8)	BARO-X + LPS (n = 7)	BARO-X + BCO + LPS (n = 9)	CHEMO-X + LPS (n = 7)	CHEMO-X+ BCO + LPS (n = 9)
TNF (pg/ml)							
90 min	207 ± 66	1831 ± 290*	1326 ± 180*#	671 ± 72*#†	873 ± 96*#†	442 ± 75*#†$§	889 ± 146*#†‡
180 min	117 ± 36	275 ± 40	206 ± 19	222 ± 15	299 ± 21	69 ± 9	213 ± 22
270 min	105 ± 25	120 ± 18	100 ± 8	114 ± 18	226 ± 18	30 ± 7	121 ± 8
360 min	89 ± 20	99 ± 12	76 ± 5	92 ± 14	181 ± 12	24 ± 8	97 ± 9
IL-6 (pg/ml)							
90 min	0 ± 0	8389 ± 1480*	8546 ± 1560*	2684 ± 225*#†	10120 ± 502*#†$	3398 ± 533*#†§	4810 ± 587*#†$§‡
180 min	0 ± 0	2977 ± 588*	3048 ± 1191*	252 ± 92#†	3888 ± 695*$	0 ± 0#†§	398 ± 49#†§
270 min	0 ± 0	14 ± 12	22 ± 19	0 ± 0	0 ± 0	0 ± 0	0 ± 0
360 min	0 ± 0	0 ± 0	0 ± 0	0 ± 0	0 ± 0	0 ± 0	0 ± 0
IL-1β (pg/ml)							
90 min	0 ± 0	212 ± 35*	104 ± 39*#	0 ± 0#†	12 ± 11#†	7 ± 3#†	19 ± 11#†
180 min	2 ± 1	178 ± 26*	116 ± 50*#	18 ± 12#†	0 ± 0#†	4 ± 2#†	19 ± 11#†
270 min	0 ± 0	82 ± 18*	47 ± 20	0 ± 0#	23 ± 14#	0 ± 0#	8 ± 5#
360 min	0 ± 0	39 ± 35	11 ± 7	0 ± 0	2 ± 1	0 ± 0	3 ± 2
IL-10 (pg/ml)							
90 min	287 ± 34	410 ± 55	730 ± 66*#	819 ± 33*#	546 ± 63*†$	245 ± 86†$§	1057 ± 88*#†$§‡
180 min	198 ± 18	474 ± 51*	523 ± 56*	989 ± 173*#†	730 ± 70*#†	307 ± 94$§	900 ± 108*#†‡
270 min	105 ± 12	229 ± 38	295 ± 39	539 ± 49*#†	328 ± 40*$	14 ± 13†$§	349 ± 48*$‡
360 min	43 ± 11	122 ± 31	137 ± 13	415 ± 50*#†	222 ± 42$	0 ± 0$	188 ± 29$

*Data are expressed as mean ± SEM. TNF, tumor necrosis factor; IL-6, interleukin 6; IL-1β, interleukin 1β; IL-10, interleukin 10. *p < 0.05 vs. Saline at the same moment; #p < 0.05 vs. LPS at the same moment; † p < 0.05 vs. BCO + LPS at the same moment; $p < 0.05 vs. BARO-X + LPS at the same moment; § p < 0.05 vs. BARO-X + BCO + LPS at the same moment; ‡p < 0.05 vs. CHEMO-X + LPS at the moment. BARO-X, selective denervation of baroreceptors; BCO, bilateral carotid occlusion; CHEMO-X, selective denervation of chemoreceptors; LPS, lipopolysaccharide.*

among both baroreceptors and chemoreceptors that modulated the inflammatory response. Considering the plasma levels of IL-10, compared to the LPS group, the BARO-X stimulated its release during the basal period (**Table 1**) and maintained the same response 90 min after the administration of LPS (**Figure 3D**, **Table 1**), as well as in the other periods evaluated (**Table 1**). On the other hand, no difference was observed in IL-10 plasma levels in any time frame periods in the CHEMO-X + LPS group compared to the LPS group (**Table 1**).

Correlation of Sympathetic Modulation and Cytokines Levels Release

Negative correlations between the sympathetic modulation and TNF (**Figure 3E**), IL-1β (**Figure 3F**) and IL-10 (**Figure 3H**) plasma levels were found. These results can be interpreted as follows: the higher the reflex sympathetic modulation, the lower the cytokine release in unanesthetized endotoxemic rats. In contrast, no correlation was found between the sympathetic modulation and IL-6 plasma level (**Figure 3G**).

DISCUSSION

The present study shows for the first time that a reflex physiological activation of the sympathetic nervous system reduces the systemic LPS-induced inflammatory response. In addition, it was also demonstrated that surgical denervation of the aortic and carotid baroreceptors, as well as of the peripheral chemoreceptors, by themselves decrease the plasma cytokines levels in endotoxemic rats.

Previous studies have highlighted the role of the autonomic nervous system branches controlling the immune system (6–12). However, taking into account that the body uses fine regulatory mechanisms to preserve homeostasis, this is the first study showing that a conspicuous physiological reflex activation controls an inflammatory response. The BCO technique promotes a reduction of the perfusion pressure and the blood flowing into the carotid sinus region, culminating, therefore, in the deactivation of the carotid baroreceptors and activation of the peripheral chemoreceptors. These outcomes determine the increase in sympathetic activity, particularly upon the arterioles, increasing the global peripheral resistance, combined with a concomitant reduction in parasympathetic activity to the heart, thus increasing arterial pressure (26, 27).

The BCO promoted an increase in arterial pressure in both intact and denervated (BARO-X or CHEMO-X) groups. However, compared to the baseline values, BCO promoted a smaller rise of the mean arterial pressure in the CHEMO-X than with the intact and BARO-X animals. Overall, in intact animals, when the common carotid arteries are occluded temporarily, there is the inactivation of the carotid baroreceptors and the carotid activation chemoreceptors contribute to an increase in sympathetic activity. When the BCO is performed in the absence of peripheral chemoreceptors (CHEMO-X), there is only the effect from the inactivation of carotid baroreceptors, which can partly explain the smaller increase in mean arterial pressure in the CHEMO-X compared to other groups. Moreover, this data suggests that chemoreflex activation plays a more significant role in increasing arterial pressure during BCO than baroreflex deactivation. Regarding the heart rate, the effect promoted by BCO was different between the groups. Intact rats and those with

denervated baroreceptors did not show a change in heart rate. In contrast, the animals with denervated chemoreceptors exhibited bradycardia during BCO. We have to consider that during BCO in the intact animals there is a combination of the different mechanisms at the same time (1. activation of peripheral chemoreceptors; 2. deactivation of carotid baroreceptors; and 3. activation of aortic baroreceptors). This combination of mechanisms, especially involving central interaction, can result in many responses. In this case, no change in heart rate. In the CHEMO-X group, the decrease in heart rate during BCO could be due to a reflex response involving the aortic baroreceptors induced by the increase in arterial pressure, activating the parasympathetic branch to the heart. In the BARO-X group, the chemoreflex activation during BCO may have augmented the sympathetic activation to the vessels, increasing the arterial pressure, but it may not have been enough to change the heart rate.

In the present study, the sympathetic activation elicited by BCO decreased pro-inflammatory plasma cytokines (TNF and IL-1β) and increased the anti-inflammatory cytokine (IL-10) in intact rats, contributing to the control of the systemic inflammatory response. Moreover, a negative correlation was found between the sympathetic modulation, assessed by the power of the LF band of systolic arterial pressure spectra and cytokine production, suggesting that the higher the sympathetic modulation of the resistance vessels during the BCO, the lower the pro-inflammatory cytokine release induced by LPS. Of note, an increase in the sympathetic modulation of the resistance vessels during the BCO approach was shown by the rise of the power of the LF band of the systolic arterial pressure spectra, since this parameter is related to the peripheral resistance from blood vessels (41). Thus, taking into account that BCO determines a significant sympathetic activation, and given that the spleen, an organ known as the main source of cytokines, is innervated by the sympathetic nervous system, it is suggested that BCO can stimulate the celiac ganglion, inhibiting the release of pro-inflammatory cytokines by the splenic macrophages (4, 11, 44).

The selective denervation of aortic and carotid baroreceptors reduced the plasma levels of TNF and IL-6 compared to intact animals (LPS group). Moreover, the IL-1β release induced by LPS was abolished in animals without baroreceptors. The same response was observed in animals that had only their carotid chemoreceptors denervated. These exciting data suggest that both baroreceptors and chemoreceptors have an essential role in the signaling of the inflammatory response in endotoxemic rats, favoring the release of cytokines. Regarding the role of the chemoreceptors in the inflammatory response, several studies have shown that glomus cells from the carotid body have receptors for pro-inflammatory cytokines (TNF, IL-6, and IL-1), expressing TLR-4, responsible for LPS recognition (45–51). Moreover, the administration of LPS increased the expression of TNF and TNF receptor in the carotid body, increasing the immune response (46, 47). Thus, the findings of the current study, as well as those from the literature (47) suggest an immunosensory function of the carotid body as a peripheral sensor for the presence of immunogenic agents from the blood.

Little is known about the role of the baroreceptors influencing the signaling of the inflammatory response. Since some studies have proposed that sympathetic neurons are the efferent arm of the inflammatory reflex (52) and the activation of the baroreceptors promotes inhibition of the sympathetic nervous system (53), it is plausible to propose that in the absence of the baroreceptors the sympathetic nervous system would act on the spleen, inhibiting the release of cytokines by the splenic macrophages. In addition, it is also known that both TLR-4 and cytokine receptors are expressed in neurons and the nodose ganglion (54–58), suggesting, therefore, that LPS and peripheral cytokines could inform the brain about a peripheral inflammatory response *via* baroreceptor nerve endings. Moreover, a recent study showed that sinoaortic denervation attenuated the release of plasma IL-6 and IL-10 in endotoxemic rats (59). However, since sinoaortic denervation includes the removal of the carotid chemoreceptors (30, 31, 60, 61), it is possible that the response observed in the aforementioned study occurred due to the absence of the chemoreceptors, but not baroreceptors. Nevertheless, it is clear that the baroreceptors play a role in modulating the immune response, and additional investigations of the mechanism involved are required.

In animals that had their baroreceptors denervated, the IL-1β release induced by LPS was abolished. In rats subjected to the carotid chemoreceptors' denervation, there was also a substantial reduction of this cytokine in plasma compared to the LPS group (intact animals). The IL-1β release depends on the process intermediated by caspase-11 and the NLRP3 inflammasome in which the cytokine precursor pro-IL-1β is cleaved into mature IL-1β. Of note, two steps are needed for NLRP3 inflammasome activation: (1) a priming step, which is provided by an inflammatory stimulus such as TLR-4 agonists, and (2) an activation step, which is stimulated by pathogen-associated molecular patterns (PAMPs) and danger-associated molecular patterns (DAMPs) (62). However, intracellular LPS can also activate the NLRP3 inflammasome by the caspase-11 route and stimulate IL-1β release (18, 19). Thus, the absence of baroreceptors or chemoreceptors may affect both the caspase-11/NLRP3 pathway, which is responsible for releasing the mature IL-1β, and the transcription of pro-IL-1β by TLR-4 stimulus, contributing together to the reduction of this cytokine in plasma. A limitation of our study has to be mentioned. Given that we did not use ultrapure LPS isolated from *Escherichia coli*, some contaminants could activate other receptors from TLR-4 and release the cytokines investigated.

Over time, the administration of LPS decreased the power of the HF band, but not the LF band, in the cardiac interval spectrum. Likewise, none of the techniques used in the present study (BCO, BARO-X or CHEMO-X) changed the power of the LF band in the spectrum of the cardiac interval over time. Of note, the groups with BARO-X already showed a decrease in the power of the HF band of the cardiac interval spectrum in the baseline period, confirming a reduction of vagal modulation when the aortic and carotid baroreceptors are absent. Corroborating previous studies (59, 63, 64), the data from the current study indicate that during systemic inflammation, the absence of the aortic and carotid baroreceptors, or the peripheral chemoreceptors, does not significantly affect the sympathetic modulation of the heart, but decreases its vagal modulation. It is essential to highlight that the analysis of

cardiocirculatory variability is a remarkable tool for understanding the autonomic modulation of the heart and vessels in a number of situations (41, 65, 66). Moreover, the assessment of the autonomic balance is an important analytical tool that is reliably useful under different clinical conditions, including infectious and autoimmune diseases (67, 68). Furthermore, the heart rate variability parameters are used for the diagnosis and monitoring of patients with sepsis (69, 70). Furthermore, this non-invasive approach does not promote additional stress and hemodynamic alterations in patients and experimental animals.

In conclusion, these results show, for the first time in the literature, that the reflex physiological activation of the sympathetic circuit decreases the inflammatory response in endotoxemic rats. In addition, the data indicate that the baroreceptors (aortic and carotid) and the peripheral chemoreceptors contribute to the development of the systemic inflammatory response induced by LPS since their absence attenuates the release of pro-inflammatory cytokines.

DATA AVAILABILITY STATEMENT

The raw data supporting the conclusions of this article will be made available by the authors without undue reservation.

ETHICS STATEMENT

The animal study was reviewed and approved by Committee of Ethics in Animal Research of the Ribeirão Preto Medical School - University of São Paulo (Protocol # 194/2016).

AUTHOR CONTRIBUTIONS

FB conceived and designed the research study, performed experiments, analyzed data, interpreted results, prepared figures and the table, and wrote the manuscript. JC performed experiments and interpreted results. AK interpreted the results, commented and edited the manuscript. DD analyzed data, commented and edited the manuscript. HS conceived and designed the research study, commented and edited the manuscript. All authors contributed to the article and approved the submitted version.

FUNDING

Supported by The São Paulo Research Foundation (FAPESP) process #2013/20549-7 and #2017/05163-6, by The Academic Excellence Program (PROEX) from Coordination for the Improvement of Higher Education Personnel (CAPES) process #88887.505419/2020-00, and by Foundation to Support Teaching, Research, and Assistance (FAEPA).

SUPPLEMENTARY MATERIAL

The Supplementary Material for this article can be found online at: https://www.frontiersin.org/articles/10.3389/fimmu.2021.637845/full#supplementary-material

REFERENCES

1. Salomonsen CJ, Madsen T. Influence De Quelques Poisons Sur Le Pouvoir Antitoxiquen Du Sang. *Comt Rend Acad Sci* (1898) 125:1229–33.
2. Hench PS, Kendall EC, Slocumb CH, Polley HF. The Effect of a Hormone of the Adrenal Cortex (17-hydroxy-11-dehydrocorticosterone: Compound E) and of Pituitary Adrenocortical Hormone in Arthritis: Preliminary Report. *Ann Rheum Dis* (1949) 8:97–104. doi: 10.1136/ard.8.2.97
3. Selye H. Stress and Disease. *Science* (1955) 122:625–31. doi: 10.1126/science.122.3171.625
4. Rosas-Ballina M, Tracey KJ. The Neurology of the Immune System: Neural Reflexes Regulate Immunity. *Neuron* (2009) 64:28–32. doi: 10.1016/j.neuron.2009.09.039
5. Tracey KJ. The Inflammatory Reflex. *Nature* (2002) 420:853–9. doi: 10.1038/nature01321
6. Martelli D, Yao ST, McKinley MJ, McAllen RM. Reflex Control of Inflammation by Sympathetic Nerves, Not the Vagus. *J Physiol* (2014) 592:1677–86. doi: 10.1113/jphysiol.2013.268573
7. Bassi GS, Brognara F, Castania JA, Talbot J, Cunha TM, Cunha FQ, et al. Baroreflex Activation in Conscious Rats Modulates the Joint Inflammatory Response Via Sympathetic Function. *Brain Behav Immun* (2015) 49:140–7. doi: 10.1016/j.bbi.2015.05.002
8. Borovikova LV, Ivanova S, Zhang M, Yang H, Botchkina GI, Watkins LR, et al. Vagus Nerve Stimulation Attenuates the Systemic Inflammatory Response to Endotoxin. *Nature* (2000) 405:458–62. doi: 10.1038/35013070
9. Brognara F, Castania JA, Dias DPM, Lopes AH, Fazan R, Kanashiro A, et al. Baroreflex Stimulation Attenuates Central But Not Peripheral Inflammation in Conscious Endotoxemic Rats. *Brain Res* (2018) 1682:54–60. doi: 10.1016/j.brainres.2018.01.003
10. Koopman FA, Chavan SS, Miljko S, Grazio S, Sokolovic S, Schuurman PR, et al. Vagus Nerve Stimulation Inhibits Cytokine Production and Attenuates Disease Severity in Rheumatoid Arthritis. *Proc Natl Acad Sci USA* (2016) 113:8284–9. doi: 10.1073/pnas.1605635113
11. Vida G, Peña G, Deitch EA, Ulloa L. A7-Cholinergic Receptor Mediates Vagal Induction of Splenic Norepinephrine. *J Immunol (Baltimore Md : 1950)* (2011) 186:4340–6. doi: 10.4049/jimmunol.1003722
12. Caravaca AS, Centa M, Gallina AL, Tarnawski L, Olofsson PS. Neural Reflex Control of Vascular Inflammation. *Bioelectron Med* (2020) 6:3. doi: 10.1186/s42234-020-0038-7
13. Akira S, Takeda K, Kaisho T. Toll-Like Receptors: Critical Proteins Linking Innate and Acquired Immunity. *Nat Immunol* (2001) 2:675–80. doi: 10.1038/90609
14. Beutler B, Rietschel ET. Innate Immune Sensing and its Roots: The Story of Endotoxin. *Nat Rev Immunol* (2003) 3:169–76. doi: 10.1038/nri1004
15. Raetz CRH, Whitfield C. Lipopolysaccharide Endotoxins. *Annu Rev Biochem* (2002) 71:635–700. doi: 10.1146/annurev.biochem.71.110601.135414
16. Kayagaki N, Warming S, Lamkanfi M, Vande Walle L, Louie S, Dong J, et al. Dixit VM non-Canonical Inflammasome Activation Targets Caspase-11. *Nature* (2011) 479(7371):117–21. doi: 10.1038/nature10558
17. Kayagaki N, Stowe IB, Lee BL, O'Rourke K, Anderson K, Warming S, et al. Caspase-11 Cleaves Gasdermin D for non-Canonical Inflammasome Signalling. *Nature* (2015) 526(7575):666–71. doi: 10.1038/nature15541
18. Yang Y, Wang H, Kouadir M, Song H, Shi F. Recent Advances in the Mechanisms of NLRP3 Inflammasome Activation and its Inhibitors. *Cell Death Dis* (2019) 10(2):128. doi: 10.1038/s41419-019-1413-8
19. Yang J, Zhao Y, Shao F. Non-Canonical Activation of Inflammatory Caspases by Cytosolic LPS in Innate Immunity. *Curr Opin Immunol* (2015) 32:78–83. doi: 10.1016/j.coi.2015.01.007

20. DiCarlo SE, Stahl LK, Hasser EM, Bishop VS. The Role of Vasopressin in the Pressor Response to Bilateral Carotid Occlusion. *J Auton Nerv Syst* (1989) 27:1–10. doi: 10.1016/0165-1838(89)90122-7
21. Lataro RM, Castania JA, Chapleau MW, Salgado HC, Fazan R. Baroreceptor and Chemoreceptor Contributions to the Hypertensive Response to Bilateral Carotid Occlusion in Conscious Mice. *Am J Physiol Heart Circ Physiol* (2010) 299:H1990–5. doi: 10.1152/ajpheart.00315.2010
22. Parra RS, Mendes LAF, Fazan R, Salgado HC. Pressure Response to Carotid Occlusion in Diabetic Rats: Effect of Insulin Therapy. *Diabetes Res Clin Pract* (2005) 68:12–7. doi: 10.1016/j.diabres.2004.08.010
23. Salgado HC, Salgado MC, Krieger EM. Cardiovascular Reflexes in Conscious Sodium-Depleted Rats. *Braz J Med Biol Res* (1986) 19:319–25.
24. Reison DS, Oliver JA, Sciacca RR, Cannon PJ. Release of Norepinephrine From Sympathetic Nerve Efferents by Bilateral Carotid Occlusion. *Am J Physiol* (1983) 245:H635–639. doi: 10.1152/ajpheart.1983.245.4.H635
25. Wang HH, Chai CY, Kuo JS. Wang SC. Participation of Cardiac and Peripheral Sympathetics in Carotid Occlusion Response. *Am J Physiol* (1970) 218:1548–54. doi: 10.1152/ajplegacy.1970.218.6.1548
26. Bedran-de-castro MT, Moreira ED, Krieger EM. Reflex and Central Components of Carotid Occlusion in Conscious Rats Effect of Lesion of the Medial Forebrain Bundle. *Hypertension* (1986) 8(4):I-47–51.
27. Krieger EM. Carotid Occlusion in the Rat: Circulatory and Respiratory Effects. *Acta Physiol Lat Am* (1963) 13:350–7.
28. Maio A, Moreira ED, Salgado HC, Krieger EM. Cardiovascular Responses of Conscious Rats Due to Arterial Occlusion. *Braz J Med Biol Res* (1981) 14:115.
29. Castania JA, Katayama PL, Brognara F, Moraes DJA, Sabino JPJ, Salgado HC. Selective Denervation of the Aortic and Carotid Baroreceptors in Rats. *Exp Physiol* (2019) 104:1335–42. doi: 10.1113/EP087764
30. Krieger EM. Neurogenic Hypertension in the Rat. *Circ Res* (1964) 15:511–21. doi: 10.1161/01.RES.15.6.511
31. Franchini KG, Krieger EM. Carotid Chemoreceptors Influence Arterial Pressure in Intact and Aortic-Denervated Rats. *Am J Physiol* (1992) 262: R677–683. doi: 10.1152/ajpregu.1992.262.4.R677
32. Cerutti C, Gustin MP, Paultre CZ, Lo M, Julien C, Vincent M, et al. Autonomic Nervous System and Cardiovascular Variability in Rats: A Spectral Analysis Approach. *Am J Physiol* (1991) 261:H1292–9. doi: 10.1152/ajpheart.1991.261.4.H1292
33. Task Force. Heart Rate Variability: Standards of Measurement, Physiological Interpretation and Clinical Use. Task Force of the European Society of Cardiology and the North American Society of Pacing and Electrophysiology. *Circulation* (1996) 93:1043–65. doi: 10.1161/01.CIR.93.5.1043
34. Fairchild KD, Saucerman JJ, Raynor LL, Sivak JA, Xiao Y, Lake DE, et al. Endotoxin Depresses Heart Rate Variability in Mice: Cytokine and Steroid Effects. *Am J Physiol Regul Integr Comp Physiol* (2009) 297:R1019–27. doi: 10.1152/ajpregu.00132.2009
35. Aronson D, Mittleman MA, Burger AJ. Interleukin-6 Levels are Inversely Correlated With Heart Rate Variability in Patients With Decompensated Heart Failure. *J Cardiovasc Electrophysiol* (2001) 12:294–300. doi: 10.1046/j.1540-8167.2001.00294.x
36. Hamaad A, Sosin M, Blann AD, Patel J, Lip GYH, MacFadyen RJ. Markers of Inflammation in Acute Coronary Syndromes: Association With Increased Heart Rate and Reductions in Heart Rate Variability. *Clin Cardiol* (2005) 28:570–6. doi: 10.1002/clc.4960281207
37. Akselrod S, Gordon D, Ubel FA, Shannon DC, Berger AC, Cohen RJ. Power Spectrum Analysis of Heart Rate Fluctuation: A Quantitative Probe of Beat-to-Beat Cardiovascular Control. *Science* (1981) 213:220–2. doi: 10.1126/science.6166045
38. Japundzic N, Grichois ML, Zitoun P, Laude D, Elghozi JL. Spectral Analysis of Blood Pressure and Heart Rate in Conscious Rats: Effects of Autonomic Blockers. *J Auton Nerv Syst* (1990) 30:91–100. doi: 10.1016/0165-1838(90)90132-3
39. Julien C, Zhang ZQ, Cerutti C, Barrès C. Hemodynamic Analysis of Arterial Pressure Oscillations in Conscious Rats. *J Auton Nerv Syst* (1995) 50:239–52. doi: 10.1016/0165-1838(94)00095-2
40. Elghozi J-L, Julien C. Sympathetic Control of Short-Term Heart Rate Variability and its Pharmacological Modulation. *Fundam Clin Pharmacol* (2007) 21:337–47. doi: 10.1111/j.1472-8206.2007.00502.x
41. Julien C. The Enigma of Mayer Waves: Facts and Models. *Cardiovasc Res* (2006) 70:12–21. doi: 10.1016/j.cardiores.2005.11.008
42. Fazan Júnior R, Machado BH, Salgado HC. Hemodynamic Responses to Acute Aortic Coarctation in Conscious Sinoaortic Denervated Rats. *Braz J Med Biol Res* (1997) 30:1249–55. doi: 10.1590/s0100-879x1997001000018
43. Vasques E, Krieger E. Regulatory, Integrative and Comparative Physiology Sequence of Tachycardia Following Baroreceptor Denervation in the Rat. *Oxford Univ Press Oxford Engl* (1980) 413–7.
44. Rosas-Ballina M, Olofsson PS, Ochani M, Valdés-Ferrer SI, Levine YA, Reardon C, et al. Acetylcholine-Synthesizing T Cells Relay Neural Signals in a Vagus Nerve Circuit. *Science* (2011) 334:98–101. doi: 10.1126/science.1209985
45. Fernandez R, Nardocci G, Navarro C, Reyes EP, Acuña-Castillo C, Cortes PP. Neural Reflex Regulation of Systemic Inflammation: Potential New Targets for Sepsis Therapy. *Front Physiol* (2014) 5:489. doi: 10.3389/fphys.2014.00489
46. Fernández R, Nardocci G, Simon F, Martin A, Becerra A, Rodríguez-Tirado C, et al. Lipopolysaccharide Signaling in the Carotid Chemoreceptor Pathway of Rats With Sepsis Syndrome. *Respir Physiol Neurobiol* (2011) 175:336–48. doi: 10.1016/j.resp.2010.12.014
47. Fung ML. Pathogenic Roles of the Carotid Body Inflammation in Sleep Apnea. *Mediators Inflamm* (2014) 2014:354279. doi: 10.1155/2014/354279
48. Lam S-Y, Tipoe GL, Liong EC, Fung M-L. Chronic Hypoxia Upregulates the Expression and Function of Proinflammatory Cytokines in the Rat Carotid Body. *Histochem Cell Biol* (2008) 130:549–59. doi: 10.1007/s00418-008-0437-4
49. Wang X, Wang B-R, Duan X-L, Zhang P, Ding Y-Q, Jia Y, et al. Strong Expression of Interleukin-1 Receptor Type I in the Rat Carotid Body. *J Histochem Cytochem* (2002) 50:1677–84. doi: 10.1177/002215540205001213
50. Kåhlin J, Mkrtchian S, Ebberyd A, Hammarstedt-Nordenvall L, Nordlander B, Yoshitake T, et al. The Human Carotid Body Releases Acetylcholine, ATP and Cytokines During Hypoxia. *Exp Physiol* (2014) 8:1–23. doi: 10.1113/expphysiol.2014.078873
51. Mkrtchian S, Kåhlin J, Ebberyd A, Gonzalez C, Sanchez D, Balbir A, et al. The Human Carotid Body Transcriptome With Focus on Oxygen Sensing and Inflammation–a Comparative Analysis. *J Physiol (Lond)* (2012) 590:3807–19. doi: 10.1113/jphysiol.2012.231084
52. Martelli D, Farmer DGS, Yao ST. The Splanchnic Anti-Inflammatory Pathway: Could it be the Efferent Arm of the Inflammatory Reflex? *Exp Physiol* (2016) 101:1245–52. doi: 10.1113/EP085559
53. Chapleau MW, Hajduczok G, Abboud FM. Mechanisms of Resetting of Arterial Baroreceptors: An Overview. *Am J Med Sci* (1988) 295:327–34. doi: 10.1097/00000441-198804000-00019
54. Chavan SS, Pavlov VA, Tracey KJ. Mechanisms and Therapeutic Relevance of Neuro-immune Communication. *Immunity* (2017) 46:927–42. doi: 10.1016/j.immuni.2017.06.008
55. de Lartigue G, Barbier de la Serre C, Espero E, Lee J, Raybould HE. Diet-Induced Obesity Leads to the Development of Leptin Resistance in Vagal Afferent Neurons. *Am J Physiol Endocrinol Metab* (2011) 301:E187–195. doi: 10.1152/ajpendo.00056.2011
56. Hosoi T, Okuma Y, Matsuda T, Nomura Y. Novel Pathway for LPS-induced Afferent Vagus Nerve Activation: Possible Role of Nodose Ganglion. *Auton Neurosci* (2005) 120:104–7. doi: 10.1016/j.autneu.2004.11.012
57. Li M, Shi J, Tang J-R, Chen D, Ai B, Chen J, et al. Effects of Complete Freund's Adjuvant on Immunohistochemical Distribution of IL-1beta and IL-1R I in Neurons and Glia Cells of Dorsal Root Ganglion. *Acta Pharmacol Sin* (2005) 26:192–8. doi: 10.1111/j.1745-7254.2005.00522.x
58. Ma F, Zhang L, Westlund KN. Reactive Oxygen Species Mediate TNFR1 Increase After TRPV1 Activation in Mouse DRG Neurons. *Mol Pain* (2009) 5:31. doi: 10.1186/1744-8069-5-31
59. Amorim MR, de Deus JL, Pereira CA, da Silva LEV, Borges GS, Ferreira NS, et al. Baroreceptor Denervation Reduces Inflammatory Status But Worsens Cardiovascular Collapse During Systemic Inflammation. *Sci Rep* (2020) 10:6990. doi: 10.1038/s41598-020-63949-x
60. Silva EF, Sera CTN, Mourão AA, Lopes PR, Moreira MCS, Ferreira-Neto ML, et al. Involvement of Sinoaortic Afferents in Renal Sympathoinhibition and Vasodilation Induced by Acute Hypernatremia. *Clin Exp Pharmacol Physiol* (2015) 42:1135–41. doi: 10.1111/1440-1681.12475

61. Zhang ZQ, Barrès C, Julien C. Involvement of Vasodilator Mechanisms in Arterial Pressure Lability After Sino-Aortic Baroreceptor Denervation in Rat. *J Physiol (Lond)* (1995) 482(Pt 2):435–48. doi: 10.1113/jphysiol.1995.sp020530
62. Bauernfeind FG, Horvath G, Stutz A, Alnemri ES, MacDonald K, Speert D, et al. Cutting Edge: NF-kappaB Activating Pattern Recognition and Cytokine Receptors License NLRP3 Inflammasome Activation by Regulating NLRP3 Expression. *J Immunol (Baltimore Md: 1950)* (2009) 183(2):787–91. doi: 10.4049/jimmunol.0901363
63. Brognara F, Castania JA, Dias DPM, Kanashiro A, Salgado HC. Time Course of Hemodynamic Responses to Different Doses of Lipopolysaccharide in Unanesthetized Male Rats. *Front Physiol* (2019) 10:771. doi: 10.3389/fphys.2019.00771
64. Amorim MR, de Deus JL, Cazuza RA, Mota CMD, da Silva LEV, Borges GS, et al. Neuroinflammation in the NTS is Associated With Changes in Cardiovascular Reflexes During Systemic Inflammation. *J Neuroinflamm* (2019) 16:125. doi: 10.1186/s12974-019-1512-6
65. Cygankiewicz I, Zareba W. Heart Rate Variability. *Handb Clin Neurol* (2013) 117:379–93. doi: 10.1016/B978-0-444-53491-0.00031-6
66. ChuDuc H, NguyenPhan K, NguyenViet D. A Review of Heart Rate Variability and its Applications. *APCBEE Proc* (2013) 7:80–5. doi: 10.1016/j.apcbee.2013.08.016
67. Pongratz G, Straub RH. Role of Peripheral Nerve Fibres in Acute and Chronic Inflammation in Arthritis. *Nat Rev Rheumatol* (2013) 9:117–26. doi: 10.1038/nrrheum.2012.181
68. Zubcevic J, Jun JY, Kim S, Perez PD, Afzal A, Shan Z, et al. Altered Inflammatory Response is Associated With an Impaired Autonomic Input to the Bone Marrow in the Spontaneously Hypertensive Rat. *Hypertension* (2014) 63:542–50. doi: 10.1161/HYPERTENSIONAHA.113.02722
69. Bohanon FJ, Mrazek AA, Shabana MT, Mims S, Radhakrishnan GL, Kramer GC, et al. Heart Rate Variability Analysis is More Sensitive At Identifying Neonatal Sepsis Than Conventional Vital Signs. *Am J Surg* (2015) 210:661–7. doi: 10.1016/j.amjsurg.2015.06.002
70. Bravi A, Green G, Longtin A, Seely AJE. Monitoring and Identification of Sepsis Development Through a Composite Measure of Heart Rate Variability. *PloS One* (2012) 7:e45666. doi: 10.1371/journal.pone.0045666

Conflict of Interest: The authors declare that the research was conducted in the absence of any commercial or financial relationships that could be construed as a potential conflict of interest.

frontiers in Immunology

REVIEW
published: 31 May 2021
doi: 10.3389/fimmu.2021.644664

Herpes Simplex Virus 1 Infection of Neuronal and Non-Neuronal Cells Elicits Specific Innate Immune Responses and Immune Evasion Mechanisms

*Amanda L. Verzosa[1], Lea A. McGeever[1], Shun-Je Bhark[2], Tracie Delgado[2], Nicole Salazar[1] and Erica L. Sanchez[1]**

[1] Biology Department, College of Science and Engineering, San Francisco State University, San Francisco, CA, United States, [2] Biology Department, Seattle Pacific University, Seattle, WA, United States

OPEN ACCESS

Edited by:
Maureen Ann Cox,
University of Oklahoma Health Sciences Center, United States

Reviewed by:
Gyorgy Fejer,
University of Plymouth, United Kingdom
Paramananda Saikia,
Cleveland Clinic, United States

***Correspondence:**
Erica L. Sanchez
elsanchez09@sfsu.edu

Specialty section:
This article was submitted to Molecular Innate Immunity, a section of the journal Frontiers in Immunology

Received: 21 December 2020
Accepted: 07 May 2021
Published: 31 May 2021

Citation:
Verzosa AL, McGeever LA, Bhark SJ, Delgado T, Salazar N and Sanchez EL (2021) Herpes Simplex Virus 1 Infection of Neuronal and Non-Neuronal Cells Elicits Specific Innate Immune Responses and Immune Evasion Mechanisms. Front. Immunol. 12:644664. doi: 10.3389/fimmu.2021.644664

Alphaherpesviruses (α-HV) are a large family of double-stranded DNA viruses which cause many human and animal diseases. There are three human α-HVs: Herpes Simplex Viruses (HSV-1 and HSV-2) and Varicella Zoster Virus (VZV). All α-HV have evolved multiple strategies to suppress or exploit host cell innate immune signaling pathways to aid in their infections. All α-HVs initially infect epithelial cells (primary site of infection), and later spread to infect innervating sensory neurons. As with all herpesviruses, α-HVs have both a lytic (productive) and latent (dormant) stage of infection. During the lytic stage, the virus rapidly replicates in epithelial cells before it is cleared by the immune system. In contrast, latent infection in host neurons is a life-long infection. Upon infection of mucosal epithelial cells, herpesviruses immediately employ a variety of cellular mechanisms to evade host detection during active replication. Next, infectious viral progeny bud from infected cells and fuse to neuronal axonal terminals. Here, the nucleocapsid is transported *via* sensory neuron axons to the ganglion cell body, where latency is established until viral reactivation. This review will primarily focus on how HSV-1 induces various innate immune responses, including host cell recognition of viral constituents by pattern-recognition receptors (PRRs), induction of IFN-mediated immune responses involving toll-like receptor (TLR) signaling pathways, and cyclic GMP-AMP synthase stimulator of interferon genes (cGAS-STING). This review focuses on these pathways along with other mechanisms including autophagy and the complement system. We will summarize and discuss recent evidence which has revealed how HSV-1 is able to manipulate and evade host antiviral innate immune responses both in neuronal (sensory neurons of the trigeminal ganglia) and non-neuronal (epithelial) cells. Understanding the innate immune response mechanisms triggered by HSV-1 infection, and the mechanisms of innate immune evasion, will impact the development of future therapeutic treatments.

Keywords: alphaherpesvirus, HSV-1, innate immunity, neuronal, latency, TLR - toll-like receptor, cGAS-STING pathway, IFN - interferon

INTRODUCTION

Herpesviruses

The *Herpesviridae* family is a large family of viruses that infects both humans and animals. Herpesviridae is derived from the Greek "*herpein*" meaning "*to creep*" (1). Structurally, herpesviruses contain four layers. First, the herpesvirus *genome* consists of linear double-stranded DNA (dsDNA), ranging in size between ~120-250 kilobases (2, 3). Second, the viral DNA genome is enclosed by a protein icosahedral *capsid*, approximately 100 to 110 nanometers in diameter (4). Third, *tegument* proteins, an amorphous viral protein matrix of 30 or more proteins, surrounds the capsid and is poorly defined (5). Fourth, herpesviruses are encapsulated by a lipid *envelope* which contains both viral glycoproteins and some host cellular proteins (6, 7).

The Herpesviridae family consists of eight types of human herpesviruses (HHVs), belonging to three subfamilies: Alphaherpesvirinae (α–HV), Betaherpesvirinae (β–HV) and Gammaherpesvirinae (γ–HV) (8). Their characteristics are summarized in **Table 1**.

Each herpesvirus is classified based on their biological characteristics and tissue tropism during primary (lytic) and latent infections (8). α–HV lytic infections have a short reproductive cycle, leading to rapid destruction of infected host cells. While α–HV's have a broad host range, they primarily infect mucosal epithelial cells during initial infection and neuronal ganglia during latent infection (9). β–HV lytic infections have a relatively longer reproductive cycle, with a large host range and the ability to latently persist in monocytes or hematopoietic stem cells (10). γ–HVs have a variable reproductive cycle length and a narrow host range, which is restricted to the family or order to which the natural host belongs (8, 11). γ–HVs traditionally establish latent infection in lymphoid tissues and are associated with lymphoproliferative diseases (8).

Herpesviruses exhibit both lytic (productive) and latent (dormant) infection life cycles (1, 12). During primary lytic herpesvirus infection, the virus replicates and produces new viral progeny in host cells, often resulting in cellular death (**Figure 1**). During primary lytic infection, there is symptomatic and asymptomatic shedding of virus. Once the host immune response is elicited, HHVs characteristically establish latency and hide in secondary host cells in order to prevent detection by the immune system (13). During latency, the viral DNA can either integrate to the host genome or tether to host DNA as a circular episome, and expresses very few viral genes (14–16). The virus can persist in the latent form forever. Periodically, the virus can reactivate from latency due to various related host factors (17). During reactivation, the virus typically returns to the primary site of infection and undergoes lytic replication until the host immune response forces it back into latency (18) (**Figure 2**).

TABLE 1 | Human Herpesviruses.

HHV	Virus Name	Subfamily	Abbreviation(s)
HHV–1	Herpes simplex–1 virus	α	HHV–1/HSV–1
HHV–2	Herpes simplex–2 virus	α	HHV–2/HSV–2
HHV–3	Varicella zoster virus	α	HHV–3/VZV
HHV–4	Epstein–Barr virus	γ	HHV–4/EBV
HHV–5	Cytomegalovirus	β	HHV–5/CMV
HHV–6	N/A	β	HHV–6
HHV–7	N/A	β	HHV–7
HHV–8	Kaposi's Sarcoma Herpesvirus	γ	HHV–8/KSHV

Human Herpesviruses: Clinical Manifestations and Epidemiology

Alphaherpesviruses

Human Herpesviruses cause a wide variety of diseases, which are most often manifested during primary lytic infection. Herpes Simplex Virus 1 (HSV–1) and Herpes Simplex Virus 2 (HSV–2) cause primary infections in epithelial cells and establish latency in neuronal ganglia (9, 12). Both HSV–1 and HSV–2 infections are widespread among humans globally and clinically manifest as skin ulcerations and flu–like discomfort in infected individuals. HSV–1 infection is primarily transmitted by oral–to–oral contact and commonly causes oral cold sores (19). HSV–1 can also be transmitted sexually *via* oral–to–genital contact and subsequently cause genital sores. HSV–1 is a life–long and persistent infection with ~55% of the US population infected in 2018 (20). In approximately 1 in 250,000 to 1 in 500,000 individuals per year, HSV–1 reactivates backwards towards the brain, and causes herpes simplex encephalitis, leading to inflammation, necrosis, and liquefaction of brain tissue (21). Children and adolescents account for approximately one third of all cases and result in a greater than 70% mortality rate. In 10 out of every 100,000 births globally, infants exposed to HSV–1 or HSV–2 in the genital tract during delivery develop neonatal herpes, which results in severe neurological disability or death (22). The risk of neonatal herpes transmission is highest when the mother is infected for the first time during her pregnancy (23). HSV–2 infection is almost entirely sexually transmitted and causes genital sores (24). In 2015, approximately 10–20% of people aged 18–49 in the USA were infected with HSV–2 (25). HSV–1 and HSV–2 have a greater transmission rate when there are active sores present (26). However, most infections are asymptomatic despite active shedding of viruses, leading to undetected infections and spread (26).

Varicella–Zoster Virus (VZV) causes varicella (chickenpox) during primary infection of epithelial cells and establishes latency in neuronal dorsal root ganglia. The clinical manifestations of VZV infection includes skin rash, blisters, fever, pain, sore throat, and headache (27). VZV typically infects children but can infect people at any age and is transmitted by droplets. Children infected with VZV typically have minor symptoms, while adults have more severe symptoms (28). VZV's reactivation from latency, and subsequent transport down sensory neurons, causes herpesvirus zoster (shingles): a very painful rash (29). Risk of shingles increases as an individual gets older, with almost 1 out of 3 people in the United States developing shingles during their lifetime (30). Before the VZV vaccine was introduced in 1995, greater than 95% of individuals were naturally infected with VZV by adulthood (31).

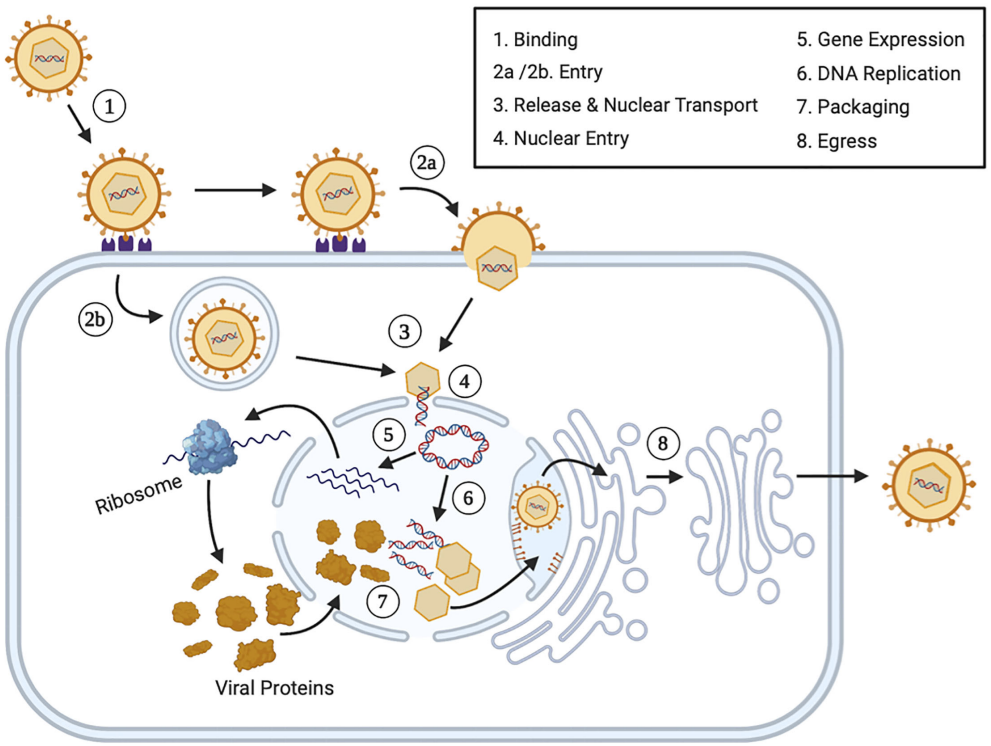

FIGURE 1 | The Lytic Human Herpesvirus Life Cycle. Step 1 (*Binding*): During primary lytic infection, HHVs bind extracellular host cells receptors using specific envelope viral glycoproteins. Step 2 (*Entry*): HHVs enters the cell *via* fusion through receptor mediated endocytosis (2a) or endosome formation (2b). Step 3 (*Release and Nuclear Transport*): After viral uncoating, both the nucleocapsid and tegument proteins are released into the cytoplasm. The nucleocapsids are transported *via* cytoskeletal structures or diffusion to the nucleus. Step 4 (*Nuclear Entry*): The viral genome plus some associated viral proteins, including some tegument proteins, enter the nucleus *via* nuclear pores and the viral genome circularizes. Step 5 (*Gene Expression*): Immediately early (IE) viral genes, early (E) viral genes and late (L) viral genes are expressed in a temporal fashion. Each set of mRNAs are transported to the cytoplasm and translated into protein before returning to the nucleus and before initiating the next set of viral genes. Step 6 (*DNA Replication*): Early viral gene expression initiates viral DNA replication. Step 7 (*Packaging*): Late viral structural proteins assemble into viral capsids and they are packaged with DNA. Step 8 (*Egress*): Viral progeny bud through the inner nuclear membrane and enter the intermembrane space. Virions are transported to the nuclear associated endoplasmic reticulum and are transported to the cellular plasma membrane, where they are released *via* cell fusion, exocytosis or cellular lysis.

However, since vaccination, the primary VZV disease incidence has been reduced by 80–90% (32).

Betaherpesviruses

Cytomegalovirus (CMV) infection causes "mononucleosis–like syndrome" (fever, rash, sore throat, nausea, muscle aches, swollen glands, and fatigue) during primary infection (12). CMV infection is a significant cause of congenital disease. In mothers, first–time infection or latent CMV reactivation during pregnancy, particularly during their first trimester, can lead to congenital defects, mental retardation, hearing and vision loss in their infants (33). While most people are infected with CMV at some point during their lifetime, it typically results in no symptoms. Immunocompromised patients are most susceptible to CMV and often have severe and life threatening outcomes (34, 35). Estimates of seroprevalence of CMV in the US ranges from 40% to 83%, with lower socioeconomic status correlating with higher infection rates (36). CMV primarily infects epithelial cells of the respiratory tract, salivary glands, and kidneys and undergoes latency in monocytes or hematopoietic stem cells (37, 38). CMV is primarily transmitted by saliva and urine (39, 40).

HHV–6 and HHV–7 are the least characterized human herpesviruses. HHV–6 and HHV–7 typically infect children during their early years of life (12). Primary HHV–6 and HHV–7 infections are associated with roseola (exanthem subitum) and fever, with most infections being minor or asymptomatic. HHV–7 infection is less virulent than HHV–6, with HHV–7 rarely causing symptomatic disease. Both HHV–6 and HHV–7 have universal prevalence in persons 6 years old and older (41). Both HHV–6 and HHV–7 infect T–lymphocytes, with the latent infection target site and mechanism of spread still under investigation (42, 43).

Gammaherpesviruses

Epstein–Barr Virus (EBV) causes infectious mononucleosis and is associated with Burkitt's lymphoma. Primary EBV infection can cause fever, rash, sore throat, nausea, muscle aches, pain, swollen lymph nodes, fatigue, weight loss, and vomiting (44). Over 90% of the human population is infected with EBV,

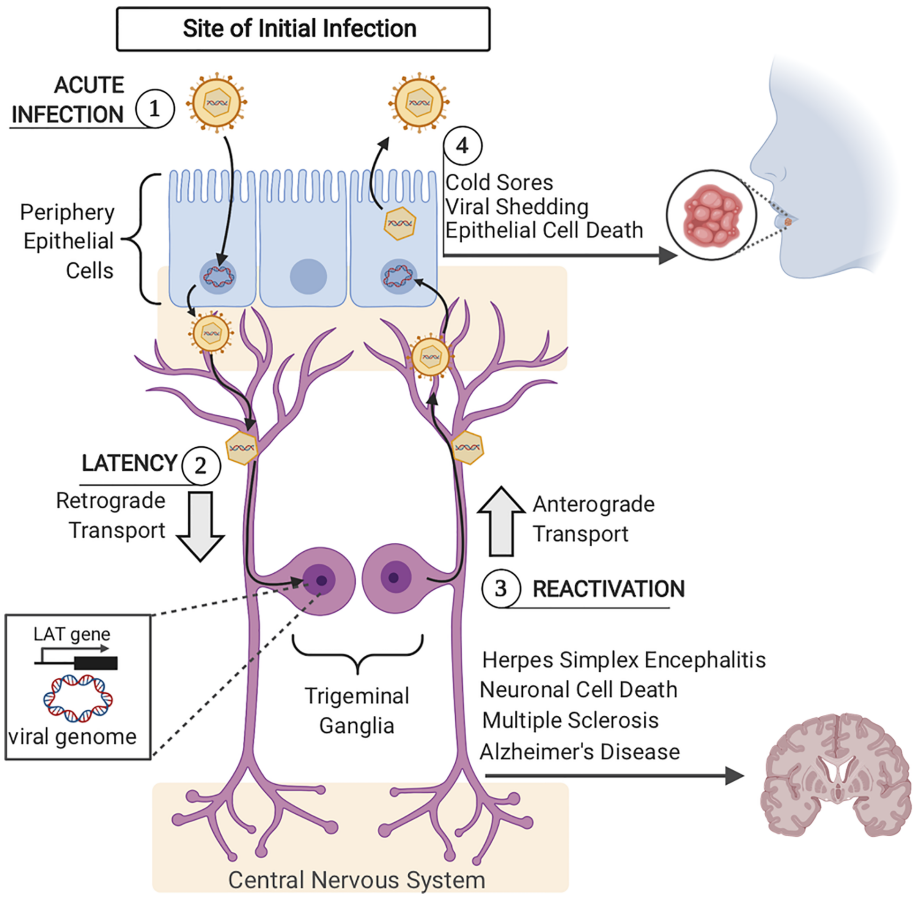

FIGURE 2 | Acute and Latent HSV–1 Infection (1). Acute HSV–1 infection is initiated when infectious virions enter epithelial cells *via* viral envelope fusion with the plasma membrane. The viral nucleocapsid reaches the epithelial cells nucleus and the viral genome enters. In the nucleus, viral genome replication and viral gene expression occur to produce more infectious virions. Newly formed viral particles are released, some of which infect nearby innervating sensory neurons. (2) Via retrograde trafficking, HSV–1 capsids reach the neuronal cell body in the sensory ganglia (trigeminal ganglia). In the neuronal nucleus, the viral DNA circularizes, causing the host cell to silence viral genome transcription, except for the latency– associated transcript (LAT) gene. If viral progeny reach the central nervous system, this can lead to herpes simplex encephalitis, neuronal cell death, and has more recently been connected to long–term pathogenesis including Multiple Sclerosis and Alzheimer's Disease. (3) Upon viral reactivation, viral nucleocapsids leave the neuronal nucleus and travel back to epithelial cells *via* anterograde trafficking. (4) Once virions arrive at the epithelial cells, viral replication is once again initiated, viral progeny are assembled and released, causing epithelial cell death and orofacial sores.

resulting in 200,000 cancer cases a year (45). EBV primarily infects and replicates in epithelial cells of the oropharynx and parotid gland and establishes latency in lymphocytes (46–49).

Kaposi's Sarcoma Herpesvirus (KSHV) causes Kaposi's Sarcoma, an endothelial cell derived vascular tumor that is common in acquired immunodeficiency (AIDS) patients and organ transplant recipients (50). KSHV is also associated with two B cell lymphoproliferative diseases, primary effusion lymphoma (PEL) and Multicentric Castleman's disease (MCD). KSHV infections cause Kaposi's Sarcoma (KS) in 1 out of every 200 transplant patients in the US (51). In the US, KSHV seroprevalence is estimated to be less than 10% and incidences of KS are usually below 0.1% (41). The primary modes of KSHV transmission include saliva, seminal fluid, nasal secretions, transplant of infected organs and blood transfusions (52).

Alphaherpesvirus Infection of Neuronal and Non–Neuronal Cells

All alphaherpesviruses (α–HVs) cause primary infection in epithelial cells and establish latency in neuronal ganglia (12). Upon reactivation, HSV–1 and HSV–2 virions travel back to oral or genital epithelial cells where a new stage of productive infection initiates cutaneous and/or mucosal lesions. Both primary HSV infection, as well as reactivation events can lead to infection of the central nervous system (CNS) (53).

HSV–1 infection involves multiple cell types throughout the life–cycle of the virus. This review will primarily compare and contrast the immune response elicited by HSV–1 infected epithelial cells (non–neuronal) and sensory neurons, while also reviewing immune evasion mechanisms used by the virus at these same sites. HSV–1 infection is most often initiated *via* an orofacial route, entering the mucosal epithelium of the mouth,

nose, or eyes (8). Upon infection, HSV–1 establishes lytic infection and undergoes multiple rounds of viral replication in epithelial cells. Infectious virions released from epithelial cells gain access to innervating sensory neurons, entering at axonal termini. HSV–1 virions traffic in a retrograde manner along neuronal axons to reach neuronal cell bodies in trigeminal ganglia (TG). While acute infection of epithelial cells will be cleared, virions that migrate to the cell bodies of sensory neurons and establish latent infections for the life of the host. Virions that reach neuronal nuclei enter the latency stage of infection, characterized by viral DNA circularization and episomal genome formation, resulting in limited expression of HSV–1 genes. Of the over 70 genes encoded by the HSV–1 genome, the non–coding latency–associated transcript (LAT) is the only viral RNA transcript highly expressed during HSV–1 latent infection in human dorsal root ganglia (54–56). HSV–1 LAT represses lytic gene expression and suppresses virus reactivation from latently infected neurons (55). LAT derived viral miRNAs have been shown to silence the expression of viral genes and prevent productive infection. Nonetheless, as with all herpesviruses, all latently infected cells hold the potential to reactivate to lytic replication and produce infectious virus (57). Upon reactivation, infectious virions are produced, which travel to axonal termini *via* anterograde trafficking to return to the initial site of infection. Subsequently, skin epithelial cells are infected and productive infection is established again, often resulting in epithelial cell death and the formation of recurrent blisters. Virus shedding during these reactivation events is a critical step in viral spread to new hosts.

Evidence has shown that the host immune response mounted during acute infection of epithelial cells is quite different from the immunological response at neuronal sites of infection. α–HV infections become latent in collaboration with immune suppression mechanisms. To evade host innate responses, HSV–1 has developed multiple mechanisms that attenuate host antiviral elements and facilitate its infection.

Innate Immune Response and Immune Evasion

Overview of Innate Immunity and Mechanisms Herpesviruses Evade Effectively

Herpesviruses persist in human hosts by hiding from immune responses, which involve both innate and adaptive immune mechanisms. In this review, we focus on innate antiviral responses as they determine the outcome of viral load before the adaptive immune response can be activated. In the *immediate* response to infection, resident macrophages which are present in tissues without infection, represent the first line of defense against invading pathogens, while during active HSV–1 replication, macrophages can continue to infiltrate the TG (58, 59). In the *induced* innate response to infection, neutrophils are the first white blood cells recruited to sites of inflammation or areas of viral infection. Although a recent study of herpesvirus infection that caused neuroinflammation demonstrated neutrophils were not induced (60). The phagocytic process in neutrophils and macrophages is initiated through recognition of opsonized microbes by Fc receptors or complement receptors expressed on these phagocytes. Macrophages can engulf HSV–1 infected cells, and ubiquitinate the HSV–1 capsid to degrade it in a proteasome–dependent manner to expose the viral DNA to cytosolic DNA sensors and induce innate responses such as IFNβ (61). Here, we introduce innate immune mechanisms which herpesviruses evade effectively and we describe each of these processes with detailed examples from recent literature.

Interferon Response

The innate immune response to viral infection primarily consists of the induction of type I interferons (IFN–α and IFN–β). Interferons are a subgroup of cytokines released by host cells in response to viruses (and some bacteria) to help regulate the activity of the immune system. Interferons interfere with the propagation of viruses by producing proteins from IFN stimulated genes (ISGs) that create an antiviral state in infected cells and cells nearby (62). Release of IFN–α and IFN–β can induce an antiviral response by inducing IFN–responsive genes on neighboring cells that bind to the IFNα/β receptor and activate the JAK–STAT pathway to inhibit viral replication.

Plasmacytoid Dendritic Cells and Natural Killer Cells

Plasmacytoid dendritic cells (pDCs) and Natural Killer (NK) cells contribute to the innate immune response against HSV. pDCs can detect herpesvirus DNA in endosomes *via* Toll–Like–Receptors 9 and secrete massive amounts of type I interferon to prevent systemic spread of infection (61, 62). Interferon binding to receptors on circulating NK cells activate the NK cells to kill virus–infected cells (63). Yet, NK cells do not only depend on IFN to mediate anti–HSV immunity, as evidenced by patients that have functional IFN production, but absence of NK cell function, that are unable to clear severe HSV infections (62).

Toll–Like–Receptors (TLRs)

Toll–Like–Receptors are pattern recognition receptors (PRRs) that do not promote phagocytosis, but rather initiate intracellular signaling cascades that activate various cellular responses. TLRs recognize PAMPs from bacteria, fungi, and viruses. TLRs are present either on the plasma membrane or on endosomal membranes (64). Two major PRR families activate innate immunity in the central nervous system (CNS): the Toll–Like–Receptors (TLRs) and the Nod–like–receptors (NLRs). Since the first discovery report of a TLR4 in 1998, 10 human TLRs have been identified. TLRs are expressed in intracellular endosomal compartments (TLR3, TLR7, TLR8 and TLR9) or as transmembrane cell–surface receptors (all other TLRs). TLR3 activation increases type I IFN from microglia and monocyte–derived macrophages. TLR7 and TLR8 activation in CNS macrophages triggers canonical TLR signaling, leading to inflammation *via* NFkB and inflammatory cytokine production, including pro–IL–1β, which can trigger neuron death (65).

Cyclic GMP-AMP Synthase Stimulator of Interferon Genes (cGAS–STING)

The cyclic GMP-AMP synthase stimulator of interferon genes (cGAS–STING) is a cytosolic DNA sensor involved in the innate

response to infection. cGAS generates cyclic dinucleotides (CDNs), including cGAMP that bind STING, leading to the activation of IFN regulatory factor 3 (IRF3) and resulting in IFN–β production (66).

The Complement System

Complement was initially established as the necessary blood serum component that completed antibody–mediated cell lysis. The complement system plays an important role bridging both innate and adaptive immune response to pathogens. The complement system can recognize and destroy pathogens based on PAMPs in addition to helping antibody–mediated lysis. The complement system is made of a cascade of proteins activated *via* three major pathways: the classical, alternative, and mannose–binding lectin pathway. The basic function of the complement system is to clear microbes and damaged cells from an organism, which promotes phagocytosis of particulate antigens, inflammatory responses, and immune clearance (67). HSV–1 and 2 evade complement–mediated destruction by expressing glycoprotein C, which binds to the C3b complement component, inhibiting both the classical and alternative complement pathways (68).

Autophagy

Autophagy is a cell death program activated when cells suffer nutrient starvation. During autophagy activation, cells digest their own cytoplasmic components and organelles in cytoplasmic lysosomes in order to recycle and scavenge various chemical species that may prolong their survival. Host cells can clear cytosol invading pathogens (viruses, bacteria, and protozoa) *via* autophagic degradation (69). Autophagy is important in viral antigen processing and presentation, mediating MHC class I or II presentation during the adaptive immune response. Selective viral autophagy plays a crucial role in antiviral host defense, for example, HSV–1 neurovirulence protein ICP34.5 binds the mammalian autophagy protein Beclin 1, inhibiting Beclin–1 dependent autophagy, as an innate immunity evasion mechanism (70).

Immune Evasion Strategies

Immune evasion is essential for the acute and chronic phases of herpesviruses infection (71). Viruses can encode for cytokine receptor genes acquired by the viral genome from the host to bind cytokines with high affinity and block their inflammatory response activity (72–75). Because less is known about innate immunity than adaptive immunity, understanding how herpesviruses manipulate mechanisms of innate immunity, as we describe below, can impact the development of improved therapeutic management of viral infections in order to prevent long term disorders and pathology of the central nervous system.

IFN–MEDIATED IMMUNE RESPONSE DURING HSV–1 INFECTION

The interferon response is induced during HSV–1 infection when PRRs in epithelial cells sense HSV–1 associated PAMPs (e.g., viral particles or viral replication products) (76). When IFNs are produced, they bind to their cognate receptors and activate IFN signaling cascades, resulting in the induction of IFN–stimulated genes (ISGs). ISG products create an antiviral state in the infected cells and neighboring uninfected cells to control the infection (77, 78).

Human myxovirus resistance protein B (MxB), an ISG product, is shown to restrict HSV–1 infection by inhibiting the delivery of incoming HSV–1 DNA to the nucleus, which is specified by its amino terminus and requires GTPase function (79). Human myxovirus resistance protein 1 (MxA) is an IFN–α/β induced antiviral protein that also inhibits replication of HSV–1, however the antiviral mechanism is not fully understood. A variant MxA (varMxA) isoform stimulated by HSV–1 infected cells in the absence of IFN–α induction enhanced production of infectious virus progeny in HSV-1 infected cells (80). The VarMxA protein is expressed as a smaller 56 kDa variant and is alternatively spliced in HSV-1-infected cells. In contrast to IFN-induced human MxA, which remains cytoplasmic, the varMxA protein is translocated into the nuclei of infected cells where it is associated with viral replication compartments and virions. This suggests that humans code for two MxA isoforms which is produced from alternative splicing (80, 81).

Three major classes of IFNs: IFN–1, IFN–2, and IFN–3 have been elucidated. These classes of IFNs compose the systematic response generated to combat HSV–1 infection. IFN–I limits the replication, spread, and cytopathic effect of HSV–1 (82–84). Studies show that increased viral replication, severe pathogenesis, and reduced survival rates are observed in mice lacking interferon–alpha/beta receptors (IFNAR) compared to WT controls (85, 86). IFN regulatory factor 3 (IRF3) and IFN regulatory factor 7 (IRF7), factors required for the induction of IFN–I production, are also both critical in controlling HSV–1 infection. Humans with IRF3 deficiencies are shown to be associated with Herpes simplex encephalitis (HSE) (87). An additional regulatory factor, IFN regulatory factor 1, is known to bind to the promoter of IFNβ and induce IFN–I response (88). To combat IFN–I response, microRNA–373 targets IRF1 which results in the suppression of ISG expression and promotion of HSV–1 replication. This suggests that HSV–1 can hijack the most miRNAs to promote replication by negatively regulating IFN–I production (89).

The IFN–II (i.e. IFNγ, or IFN–gamma) signaling pathway plays crucial roles in controlling and minimizing the pathogenesis of HSV–1 lytic infection (90). Mice lacking interferon–gamma receptors (IFNGR) were more susceptible to HSV–1 infection and had a higher mortality rate than WT mice (91–93). Furthermore, mice lacking both IFNGR and IFNAR had increased susceptibility to HSV–1 infection compared to mice lacking a single receptor (86). IFNγ can also directly inhibit the replication of HSV–1 through synergizing with IFNα and IFNβ (84, 94). IFNγ is also known to link the host innate and adaptive immune responses through stimulating the expression of major histocompatibility complex class I to enhance antigen presentation to CD8+ T cells. This linkage plays a key role in the maintenance of viral latency (92).

IFN–III (i.e. IFNλ, or IFN–lambda) utilizes the same signaling cascade as IFN–I. Studies have addressed the role of IFNλ during HSV–1 infection (95, 96). IFN–λ rapidly primes an IFN–I antiviral response in HSV–1–infected plasmacytoid dendritic cells (97). pDCs producing IFNλ during HSV–1 infection show a more efficient antiviral response in comparison to cells that don't produce IFNλ (97). The underlying mechanism(s) of IFN–III during HSV–1 infection has yet to be elucidated.

IFN–Mediated Immune Response During HSV–1 Infection in Neuronal Cells

Neuronal IFN signaling and its role in controlling acute and latent HSV–1 infection has recently been investigated. Neuronal antiviral response to HSV–1 is driven by IFN–β signaling (98). Sensory neurons respond to IFN–β, which then stimulates innate immunity and inhibits viral spread (99). However, multiple IFN types are involved in stimulating innate immunity. IFN–λ inhibits HSV–1 replication and viral protein synthesis in primary human astrocytes and neurons when exogenously treated (100).

HSV–1 replication is dependent upon autophagy. Specifically, HSV–1 is known to use the host endosomal sorting complexes required for transport (ESCRT) machinery for viral production and transportation (101, 102). As a defense mechanism, IFN–β and IFN–λ interfere with neuronal autophagy by subverting vacuolar protein sorting 4 (Vps4), a key protein involved in the ESCRT pathway. This is observed *in vivo* and in primary neurons where HSV–1 infection causes a decrease in Vps4 RNA and protein (103). Sensory ganglia also shows an accumulation of IFN–dependent LC3–decorated autophagic structures (LCS clusters) in result to HSV–1 infection (104). LC3 clusters appear to be associated with a delay in autophagy maturation, and resemble accumulations of autophagosomes and oversized autolysosomes *in vivo* (105).

IFN–β treatment in primary neurons and in other cell types is sufficient to transiently decrease Vsp4 RNA and protein levels. However, combined IFN–β and IFN–λ treatment recapitulate sustained LC3 clustering observed *in vivo*. Neighboring HSV–1 antigen–negative neurons also have decreased Vsp4 RNA and protein expression. It is speculated these neighboring neurons may be receiving IFN paracrine signaling, resulting in Vps4 reduction (105). Although HSV–1 downregulates IFN response and establishes lifelong latent infection in sensory neurons of the host, many studies show IFN response is critical for controlling HSV–1infection in neuronal and non–neuronal cells.

TOLL–LIKE RECEPTOR (TLR) SIGNALING AND HSV–1 INFECTION

The major TLRs activated during HSV–1 recognition that lead to the production of IFNs are summarized in **Figure 3**. TLRs are critical in controlling HSV–1 replication and dissemination by mediating antiviral activities during acute and latent infection. When TLRs bind to HSV–1 proteins or viral nucleic acid, they activate the innate immune response by inducing the production of chemokines and proinflammatory cytokines. This is accomplished through the signaling pathways of nuclear factor kappa–light–chain–enhancer of activated B cells (NF–κB), or p38 mitogen–activated protein kinase (MAPK) and c–Jun NH2–terminal kinase (Jnk) activation of activator protein–1 (AP–1), a transcription factor (106, 107). TLR expression varies among cell types such as macrophages and dendritic cells. TLRs are expressed differentially in the epithelial cells in HSV–targeted oral, ocular and genital mucosa (108) as well as in the central nervous system (CNS) resident cells (109, 110). Other studies show human neuronal cells express TLR family members 1–10 and IFN-α/β during HSV–1 infection (64). The following expands on the role of important TLRs expressed during HSV–1 infection, primarily in neuronal cells. Relevant TLRs are listed and described in **Table 2**.

TLR2

TLR2 is a plasma membrane receptor that recognizes HSV–1 glycoprotein B (gB), promoting NF–κB activation and the secretion of interleukin (IL)–8 through the MyD88/TRAF6–dependent signaling pathway as shown in **Figure 3** (111). Induction of the degradation of I–κBα (an inhibitor of NF–κB) is followed after NF–κB activation, which allows NF–κB to translocate to the nucleus. This leads to the expression of several pro–inflammatory cytokines and chemokines in several human and mouse cell types, including epithelial, immune, and neuronal cells (78, 112–115). TLR2 also induces the IL–15 gene in response to HSV–1 infection (116). Additionally, IL–15 with IL–21 elicits proliferation of naive and memory CD8+ T Cells which contributes to controlling virus replication and spread (117). TLR2 is also found on the cell surface of microglia and astrocytes in the CNS, indicating that TLR2 plays a role in CNS autoimmunity, neurodegeneration, and tissue injury (118, 119). TLR2 mediates the inflammatory cytokine response to HSV–1 infection. Furthermore, TLR2 deficient mice have a blunted cytokine and chemokine response to HSV–1 infection (112). Furthermore, TLR2 synergizes with TLR9, which together controls viral replication and dissemination to the CNS (112, 120–122). TLR2 activation is also required to reduce the viral load in trigeminal ganglia and the brain during HSV–1 infection (122, 123). In TLR2 knockout mice, neuronal CCL2 levels were decreased, in association with reduced macrophage recruitment into the enteric nervous system after intragastric HSV–1 infection (124). TLR2's role in the production of cytokines results in viral containment in response to HSV–1 infection.

TABLE 2 | Toll–Like Receptors Activated During HSV–1 Infection.

Toll–like receptor	Cellular Location	PAMP	Associated Factor
TLR2	Cell surface	Glycoprotein B	MyD88, TRAF6
TLR3	Endosome	dsRNA	TRIF, TRAF6
TLR9	Endosome	dsDNA	MyD88, TRAF6

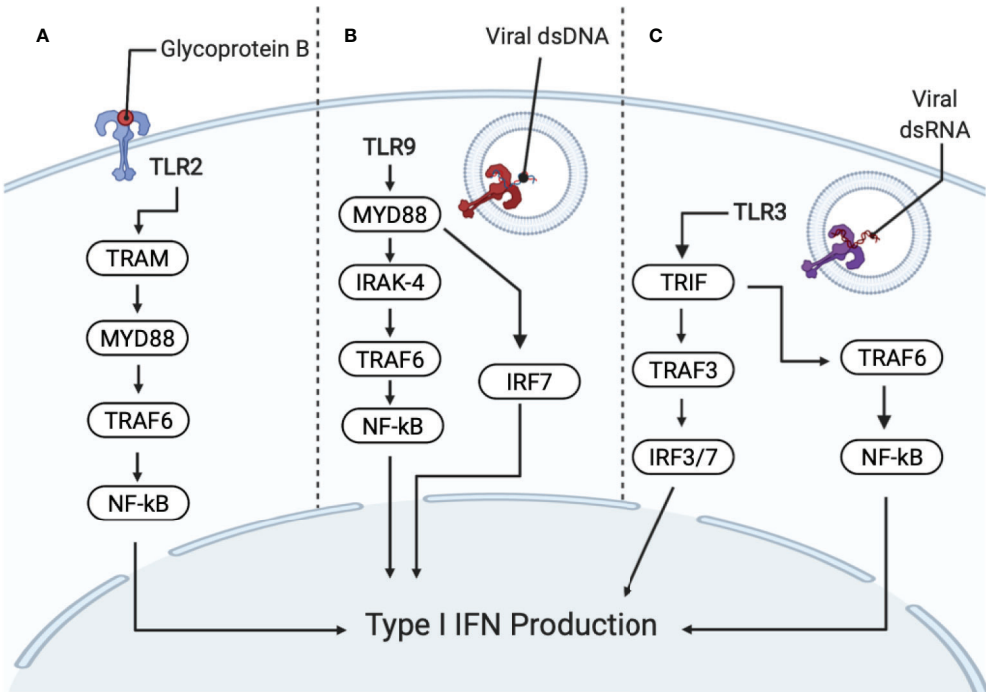

FIGURE 3 | Recognition of HSV–1 by PRRs (pattern recognition receptors) activates interferon (IFN) and cytokine production. PRRs include toll–like receptors TLR2, TLR9 and TLR3. **(A)** TLR2 recognizes HSV–1 glycoprotein B (gB), promoting NF–κB activation and the secretion of interleukin (IL)–8 through the MyD88/TRAF6–dependent signaling pathway. Subsequent degradation of I–κBα (an inhibitor of NF–κB) allows NF–κB to translocate to the nucleus. TLR2 also signals through TRIF–related adaptor molecule (TRAM) and MyD88 for IFN production. **(B)** TLR9 senses viral DNA, which contains unmethylated CpG motifs. TLR9 is dependent on IRAK–4 and MyD88–dependent pathways. MyD88 and TRAF6 resulting in the activation of the NF–κB pathway for downstream cytokine secretion. TLR9 activation also signals IRF7, which produces type I IFNs. **(C)** TLR3 recognizes dsRNA, which are produced during viral replication. TLR3 activates MyD88–independent signaling cascade through the Toll/IL1 receptor domain, containing adaptor inducing IFNβ (TRIF) and TRAF3, resulting in IRF3/7 translocating to the nucleus, for the production of type I IFNs. TLR3 also signals TRIF and TRAF6, resulting in NF–κB activation.

TLR3

TLR3 is found in cell compartments of microglia, astrocytes, oligodendrocytes, and neurons (58, 125–128). During HSV–1 infection, TLR3 is important for an efficient antiviral response. TLR3 recognizes double–stranded RNA (dsRNA) and induces the expression of type 1 IFNs and inflammatory cytokines upon activation of MyD88–independent signaling cascade (97, 106, 129–131). TLR3 localizes in endosomes and is TRIF and TRAF3–dependent for downstream signaling (132) (see **Figure 3**). TLR3 also signals through TRIF and TRAF6 for NF–κB and IRF–3 activation (132). Multiple studies suggest that TLR3 has an important role against HSV–1 in the CNS, supporting a model that the TLR3 axis, consisting of UBC93B, TRIF, TRAF3 and TBK1, exerts protective immunity to HSV–1 in the CNS (133–136). Furthermore, patients with TLR3 deficiencies or mutations are more susceptible to developing HSE (134, 137–139). TLR3 activation in neuronal cells is associated with increased resistance to HSV–1 infection and an increase in the production of IFNs and strengthened response to IFNs (64, 128, 140, 141). These studies reinforce the central role of type I IFNs and TLR3 as necessary components to contain viruses within the CNS (141).

TLR9

TLR9 is found in endosomes/vacuolar compartments of microglia, astrocytes, dendritic cells and other antigen presenting cells. TLR9 recognizes dsDNA containing un–methylated CpG motifs (58, 125, 142, 143). During HSV–1 infection, TLR9 mediates an early and rapid production of type I IFNs and cytokine secretion through an IRAK–4 and MyD88–dependent pathway as shown in **Figure 3** (144–147). Interaction between TLR9 and other TLRs seems to be essential when mounting an effective immune response to HSV–1. In mice, defense against HSV–1 appears to be concentrated primarily in the TG (148). If the immune response to HSV–1 in the TG fails, a weak immune response is then seen in the brain. In WT mice, increased expression of TLR9 and TLR2 is seen in the TG, but not in the brain. Increased TLR expression in the brain is only observed in TLR2 deficient mice. TLR9 deficient mice are unable to mount an effective immune response in either location and die, despite the expression of other TLRs in the TG and brain (148). This indicates that in mice, TLR9 is important in coordinating the innate immune response with other TLRs. Further research is necessary to determine if the same is true in humans. TLR9 is required for IFN–α production in plasmacytoid dendritic cells (149). Furthermore, HSV–1 infection in human neurons was shown to

be suppressed by IFN–λ, which upregulates TLR9 expression and subsequent TLR9–mediated antiviral responses involving the transcription factor IRF7 (150). This result remains to be validated as IFN–λ has been shown to be secreted during HSV–1 infection in the vaginal mucosa, mainly by dendritic cells (151).

Interestingly, TLR9 also coordinates with DNA sensors other than TLRs. The cGAS–STING pathway is a cytosolic DNA sensor (specific details on the mechanism of cGAS–STING signaling is provided in the next section). Like TLR9, cGAS–STING is also expressed in pDCs. Signaling through both the TLR9 pathway and the cGAS–STING pathway results in the induction of IFNs. Without modulation, this overlapping activation of IFN production could potentially lead to overproduction of IFN, which can have negative consequences. Crosstalk between the cGAS–STING pathway and the TLR9 pathway has recently been elucidated. Specifically, activation of the cGAS–STING pathway results in inhibitory signals that dampen the IFN production by the TLR9 pathway (152). The modulation of the TLR9 pathway by cGAS–STING is thought to be facilitated by two signals: suppressor of cytokine signaling 1 (SOCS1) and SOCS3. However, more research is required to determine the exact identity of the signal molecule.

TLR9 is a complex DNA sensor. Although its essential role in IFN production in pDCs is well established, more research in elucidating the role that TLR9 plays in coordinating with other TLRs and DNA sensors to coordinate an effective innate immune response to HSV–1 is necessary.

cGAS–STING PATHWAY AND HSV–1 INFECTION

TLRs are an important mechanism for sensing HSV–1 and other viral infections. However, TLRs are not the only PRRs that can sense viral DNA. Another important PRR is cGAS–STING, a signaling pathway that detects cytosolic DNA and triggers a myriad of downstream immune responses. cGAS–STING has been the target of intense study as it has been identified as a potential universal cytoplasmic DNA sensor (153), and cGAS has also been implicated as the target of several strategies utilized by herpesviruses to evade the immune system (154). Due to the importance of cGAS–STING in responding to HSV–1 infection, the mechanism of cGAS-STING will be described further (see **Figure 4**). One of the outcomes of cGAS–STING signaling is the expression of Type I IFN genes, which help trigger the innate immune response. Upon cytosolic dsDNA detection, cGAS catalyzes the production of cyclic GMP–AMP (cGAMP), which serves as a second messenger and activator of STING (155). STING binding to cGAMP triggers ubiquitination of STING by TRIM56, inducing the dimerization of STING. The dimerized STING then translocates from the endoplasmic reticulum, where it usually resides, and moves to the golgi complex. Next, STING is poly–ubiquitinated by TRIM32, and serves as an anchor for the attachment of Tank binding kinase–1 (TBK1). Upon TBK1 binding to STING, TBK1 phosphorylates serine–365 (S365) on STING, facilitating the binding of IRF3 to STING. Subsequently, STING is phosphorylated by TBK1, leading to activation of IRF3 (154), a transcription factor whose activation leads to the transcription of IFN-1 Overall, phosphorylation of STING results in the induction of IFN-1.

HSV–1 Mechanisms to Evade cGAS–STING Pathway

Coevolution of HSV–1 with humans has resulted in several mechanisms to bypass the immune response, resulting in HSV–1 circumventing or suppressing the cGAS–STING signaling pathway (see **Figure 4**). One mechanism is the expression of HSV–1 protein UL41, which reduces the expression of cGAS by degrading cGAS mRNA, and inhibits downstream activation of the IFN response (66) (**Table 3**). Additionally, HSV–1 protein VP22 interacts directly with cGAS and inhibits its enzymatic activity, preventing cGAMP production and STING activation (156). However, bypassing signaling by cGAS is not the only mechanism by which this pathway can be inhibited. HSV–1 protein UL46 has been shown to interfere with dimerization of TBK1, interfering with TBK1's ability to interact with IRF3, ultimately resulting in a diminished IFN response (157). Interestingly, in addition to suppressing aspects of cGAS–STING signaling, there is some evidence that STING is required for optimal growth of HSV–1 (158). When HeLa cells were infected with a strain of HSV–1 lacking viral proteins ICP0 or ICP4, STING degradation was observed. These results suggest ICP0 and ICP4 are involved in stabilizing STING (158). Overall, STING has been shown to be both detrimental and required for HSV–1 replication (158). More research is needed to elucidate the exact relationship between STING degradation and HSV–1 replication.

IFN–Independent cGAS-STING Signaling

The myriad of mechanisms that HSV–1 has developed to bypass or inhibit DNA sensing *via* the cGAS–STING pathway indicates that this pathway is essential to coordinate an effective innate immune response. Interestingly, STING–deficient mice demonstrated an increased susceptibility to HSV–1 infection (159). Previously, it was assumed that increased susceptibility to HSV–1 infection resulting from cGAS–STING deficiency was solely the result of an impaired IFN response. However, recent work suggests that IFN production is one of multiple mechanisms triggered by cGAS–STING signaling pathway that combines to create an effective immune response (160). Mice with a serine 365–to–alanine mutation in STING, which renders STING unable to activate downstream IFN, demonstrates an increased resistance to HSV–1 infection when compared to mice with a STING–null phenotype (160). This raises the possibility that STING activation results in a series of IFN–independent signaling events that are also important in mounting an antiviral response. This activation does not involve S365, which is necessary for activating the IFN response, and instead relies on other STING domains. The evolutionary history of cGAS–STING supports this possibility. The cGAS–STING signaling pathway is demonstrably ancient, in fact,

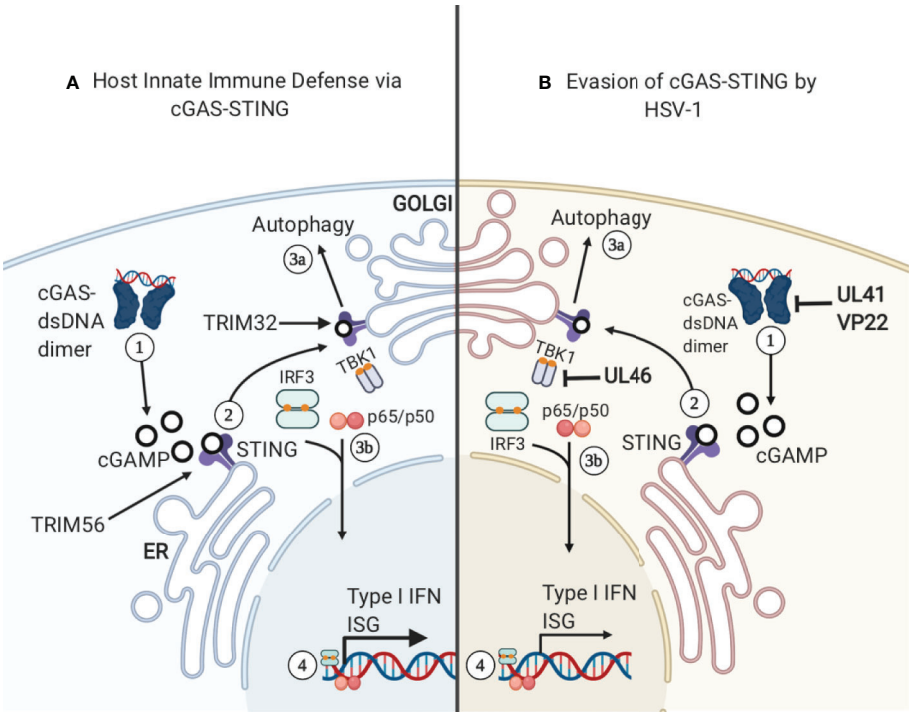

FIGURE 4 | cGAS–STING. **(A)** 1) cGAS binds cytosolic dsDNA and they form a dimer. The cGAS–dsDNA dimer catalyzes the production of cGAMP, a ligand and secondary messenger for STING. 2) STING binds cGAMP and is ubiquitinated by TRIM56, inducing STING dimerization and translocation from the ER to the golgi. STING is then further ubiquitinated by TRIM32, allowing TBK1 to bind the complex. 3A) STING relocation to the golgi complex can activate autophagy in a pathway that is separate from the activation of IFN–related genes. 3B) TBK1 binding to STING triggers STING phosphorylation of S365 and the binding and activation of IRF3. Subsequently, IRF3 translocates to the nucleus and activates the transcription of IFN–1 and Interferon Stimulatory Genes (ISG). **(B)** HSV–1 has developed several mechanisms to sabotage cGAS-STING signaling. 1) Viral proteins UL41 and VP22 interact with cGAS, preventing the synthesis of cGAMP. 2) UL46 acts on TBK1 and prevents autophagy induction.

TABLE 3 | HSV–1 Proteins and Innate Immune Evasion.

Viral Protein	Action	Citation
UL41	Degrades cGAS mRNA	Su and Zheng (66)
VP22	Interacts directly with cGAS, suppressing cGAMP production	Huang et al. (156)
UL46	Inhibits dimerization TBK1	You et al. (157)

cGAS–STING homologs have been identified in the sea anemone *Nematostella vectensis*, which is divergent from humans by ~500 million years (161). Thus, it is possible that the role of STING in induction of IFN–based immunity is something that was taken up by the cGAS–STING pathway at a later point, as IFN–based immunity is likely a vertebrate evolutionary trait (162). More recent work indicates that the IFN–independent axis of cGAS–STING signaling contributes more to the immune response than previously thought (160). Although the exact details of this IFN–independent signaling pathway have yet to be fully elucidated, some evidence suggests that the function of the IFN–independent signaling pathway may be the induction of autophagy (163). A key event in autophagy induction is the conversion of the LC3 protein into its lipidated form, LC3–II, which takes place prior to the formation of autophagosomes (163). While LC3 lipidation can be induced by different mechanisms, cGAS production of cGAMP is sufficient to induce LC3 lipidation (163). When STING binds cGAMP, STING buds from the ER. After budding, STING interacts with protein transport protein SEC24C, allowing STING to bud into COP–II vesicles, forming the ERGIC complex (163). ERGIC acts as a locus for LC3 lipidation, leading to the formation of autophagosomes that clear cytosolic DNA or RNA (163). The involvement of STING in autophagosome formation supports the possibility that signaling through the cGAS–STING pathway also activates the autophagy response. Although this aspect of cGAS–STING signaling has only recently been elucidated in mammalian cells, autophagy induction is likely an ancient and evolutionarily conserved function of this pathway (163). The same motif for LC3 lipidation can be found in the STING homolog of *N. vectensis*, while the C–terminal domain which is essential for IFN signaling is absent (163). Taken together, these findings suggest that autophagy induction is indeed the ancient, evolutionarily conserved function of STING, and the induction of the IFN response was added in addition to the autophagy induction response.

cGAS–STING Signaling in Non–Neuronal Cells

cGAS–STING is a key pathway in the CNS which senses and responds to HSV–1 infection (164). However, high viral load in the CNS produces an interesting phenotype in non–neuronal cells that is mediated by cGAS–STING signaling. More specifically, mice with herpes simplex encephalitis (HSE) exhibited increased apoptosis of microglia (brain–specific immune cells) (165). The apoptotic response appears to be independent of IFN–1 signaling, as IFNAR–deficient mice demonstrate an increased susceptibility to HSV–1, while not demonstrating less apoptosis of immune cells. In addition, apoptosis appears to be specific to microglia and other immune cells, as neurons and other neuronal cell types do not demonstrate the same degree of apoptosis as immune cells (165). Although this apoptotic response was initially observed in mice, apoptosis of immune cells was also observed in human organotypic cell culture and in tissue obtained from patients who had succumbed from HSE (165). The exact mechanism responsible for activation of apoptosis through cGAS–STING signaling is yet to be elucidated. It is thought that the apoptotic response in immune cells may function as a regulator of IFN–1 expression by the cGAS–STING signaling pathway (165). When the viral load during HSV–1 infection is low, local immune cells can produce IFN–1 *via* DNA sensing through cGAS–STING. However, prolonged expression of IFN–1 can lead to immunopathologies, especially in the brain, where prolonged inflammation can cause irreversible damage. To protect against damage from prolonged inflammation, it appears that cGAS–STING signaling is shut off by triggering local immune cells to initiate apoptosis, decreasing IFN–1 expression, despite elevated viral load (165). This represents a potential negative regulation of cGAS–STING signaling, and appears to be unique to non–neuronal cells, however more research is necessary to determine if this is truly unique to non–neuronal cells.

COMPLEMENT SYSTEM AND HSV–1 INFECTION

Complement System and HSV–1 Infection of Non–Neuronal Cells

HSV–1 has evolved multiple strategies to avoid immune evasion, many of which include inhibiting the complement system, whose proteins are found in serum and is part of the host innate immune response. The complement system is a cascade of proteins whose activation results in the formation of the membrane attack complex (MAC), a protein complex which penetrates the cell membranes of microbes by forming cytotoxic pores. In defense, HSV–1 encodes glycoprotein C (gC), a 511–amino–acid protein that plays several roles in host immune evasion (68, 166). More specifically, gC binds to the complement component C3b by interfering with the binding of C5 and properdin, thereby blocking alternative pathways that otherwise lead to the formation of a MAC on the pathogen surface, or the surface of virus–infected cells (see **Figure 5**) (167–169). Additionally, gC is able to accelerate the decay of the alternative pathway C3 convertase. Interestingly, HSV–1 lacking gC was more sensitive to complement–independent neutralization (170). These results suggest that HSV–1 gC is involved in immune invasion as it protects other viral envelope glycoproteins, including gB, which are essential for viral host cell entry and shielding these glycoproteins from neutralization as a potential mechanism of immune evasion (170).

Complement System and HSV–1 Infection in Neuronal Cells

HSV–1 infection of human brain cells induces changes in gene expression, favorable to HSV–1 propagation and detrimental to the function of the host cells. Mechanistically, HSV–1 infection downregulates complement factor H (CFH), a complement regulator essential for controlling the complement pathway in blood and on cell surfaces (171, 172). When downregulated, CFH

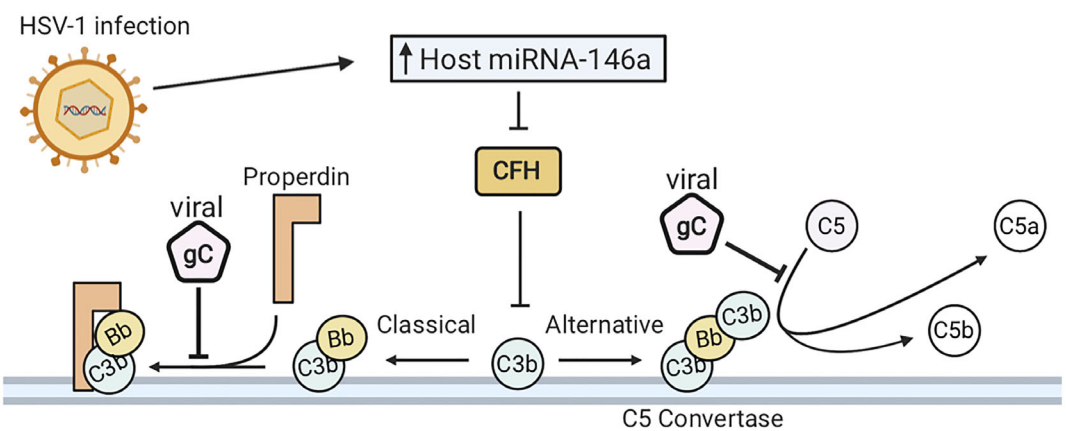

FIGURE 5 | HSV–1 infection evades the complement system. (A) HSV–1 glycoprotein C (gC) binds complement component C3b. This inhibits the interaction of C5 and properdin with C3b, blocking activation of both the classical and alternative complement pathways. HSV–1 downregulates complement factor H (CFH), which is concurrent with elevated expression of host microRNA (miRNA) –146a.

inhibits the amplification of the alternative pathway of complement activation (173). Downregulation of CFH is synchronous with elevated expression of host microRNA (miRNA) –146a (172). Furthermore, human primary neural cells infected with HSV–1 upregulate a brain–enriched miRNA–146a. Alterations in miR–146a expression levels can lead to pathogenesis of numerous neurological diseases. Furthermore, miRNA–146a is associated with proinflammatory signaling in stressed brain cells and Alzheimer's Disease (AD) (174). HSV–1 DNA has also been detected in brain tissue from patients with AD (175–177). Overall, HSV–1 infection has developed strategies to evade the complement system in infected cells and human primary neural cells and can induce pathogenesis of AD.

CONCLUSIONS AND FUTURE PERSPECTIVES

In this review, we summarized and discussed recent evidence of HSV–1 manipulating and evading host antiviral innate immune responses in both neuronal and non–neuronal cells. We described how HSV–1 induces IFN, TLR, and cGAS–STING mediated immune responses and overviewed mechanisms of how HSV–1 evades the innate immune response. The neuronal antiviral response to HSV–1 is driven by IFN signaling, which stimulates innate immunity and inhibits viral spread. The IFN response is critical for controlling HSV–1 infections in neuronal and non–neuronal cells as the IFN response establishes lifelong latent infection in sensory neurons of the host. Additionally, TLRs are critical in controlling HSV–1 replication and dissemination by mediating antiviral activities during acute and latent infection. TLRs bind to HSV–1 proteins or viral nucleic acid and activate the innate immune response by inducing the production of chemokines and proinflammatory cytokines. Previously, it was thought that cGAS–STING signaling only had IFN–1 expression as its most important function. However, new evidence indicates that cGAS–STING signaling also activates non–IFN related responses which are also important to mounting an effective immune response. Because cGAS–STING signaling is an important mechanism for controlling HSV–1 infection, HSV–1 has developed many ways to sabotage this pathway. Additionally, we reviewed the strategies HSV–1 utilizes to evade the complement system in infected cells and human primary neural cells, which can induce pathogenesis of Alzheimer's Disease.

Most of the world's population is infected by at least one α–HV, with ~90% of the world's population infected with HSV–1 or HSV–2, or both (178). After initial α–HV infection, the host immune response plays a crucial role in clearing α–HVs from primary epithelial cells. As a result, α–HVs undergo latency in host neuronal cells in order to avoid immune system detection. Therefore it is crucial to consider that most normal immune responses likely involve latent herpesvirus infection and the virus plays important roles in patient's responses to subsequent infections and predispositions to neurodegenerative as well as other chronic diseases (71). Thus, understanding how α–HV manipulates mechanisms of immunity can have major impacts for the development of improved therapeutic management of viral infections and improved quality of life.

Furthermore, as we continue to learn more about how HSV–1 can infiltrate the CNS, we will better understand how this life–long infection can impact neurological diseases such as Herpes Simplex Encephalitis (HSE), Multiple Sclerosis (MS) and Alzheimer's disease (AD). While rare, HSE occurs in an estimated one in 250,000 to 500,000 HSV–1 infected individuals and can be life–threatening. Interestingly, the vast majority of adult cases of HSE are caused by HSV–1 infection (53, 179, 180). Furthermore, HSV–1 has been detected in the brains of both MS and AD patients more frequently than healthy controls (181–183). While the direct mechanisms by which HSV–1 may be contributing to the development of these diseases is controversial, several recent studies have pointed to the immune response during HSV–1 infection in the brain as a critical factor (53). These studies are extremely important, especially given the high prevalence of HSV–1 infection in humans worldwide. Overall, understanding the immune response and evasion mechanisms involved in both acute and latent HSV–1 infection may illuminate potential therapeutic targets to prevent long term neurological pathology.

AUTHOR CONTRIBUTIONS

AV, LM, S-JB, TD, NS and ES conceptualized and drafted the manuscript, as well as created the figures and tables. AV, LM, S-JB, TD, NS and ES all reviewed and edited the manuscript. All authors contributed to the article and approved the submitted version.

FUNDING

AV is supported by NIH MBRS–RISE: R25–GM059298. LM is supported by Genentech Foundation Scholarship at SFSU. TD is funded by SPU Faculty Research and Scholarship Grant. NS is funded by NIH NIGMS 1SC2GM135135–01. ES is funded by the California State University Program for Education and Research in Biotechnology (CSUPERB).

REFERENCES

1. Rechenchoski DZ, Faccin–Galhardi LC, Linhares REC, Nozawa C. Herpesvirus: An Underestimated Virus. *Folia Microbiol (Praha)* (2017) 62:151–6. doi: 10.1007/s12223–016–0482–7
2. Falke D, Siegert R, Vogell W. Electron Microscopic Findings on the Problem of Double Membrane Formation in Herpes Simplex Virus. *Arch Gesamte Virusforsch* (1959) 9:484–96. doi: 10.1007/BF01242855
3. Furlong D, Swift H, Roizman B. Arrangement of Herpesvirus Deoxyribonucleic Acid in the Core. *J Virol* (1972) 10:1071–4. doi: 10.1128/JVI.10.5.1071-1074.1972
4. Booy FP, Trus BL, Davison AJ, Steven AC. The Capsid Architecture of Channel Catfish Virus, an Evolutionarily Distant Herpesvirus, Is Largely Conserved in the Absence of Discernible Sequence Homology With Herpes Simplex Virus. *Virology* (1996) 215:134–41. doi: 10.1006/viro.1996.0016

5. Morgan C, Rose HM, Holden M, Jones EP. Electron Microscopic Observations on the Development of Herpes Simplex Virus. *J Exp Med* (1959) 110:643–56. doi: 10.1084/jem.110.4.643
6. Asher Y, Heller M, Becker Y. Incorporation of Lipids Into Herpes Simplex Virus Particles. *J Gen Virol* (1969) 4:65–76. doi: 10.1099/0022–1317–4–1–65
7. Wildy P, Watson DH. Electron Microscopic Studies on the Architecture of Animal Viruses. *Cold Spring Harb Symp Quant Biol* (1962) 27:25–47. doi: 10.1101/sqb.1962.027.001.006
8. Roizman B. The Family Herpesviridae: General Description, Taxonomy, and Classification. In: B Roizman, editor. *The Herpesviruses the Viruses*. Boston, MA: Springer US. (1982). p. 1–23. doi: 10.1007/978–1–4684–4163–5_1
9. Baringer JR, Swoveland P. *Recovery of Herpes–Simplex Virus From Human Trigeminal Ganglions* (2010). Available at: http://dx.doi.org/101056/NEJM197303292881303.
10. Schwartz M, Stern–Ginossar N. The Transcriptome of Latent Human Cytomegalovirus. *J Virol* (2019) 93:1–5. doi: 10.1128/JVI.00047–19
11. Roizman B, Carmichael LE, Deinhardt F, de–The G, Nahmias AJ, Plowright W, et al. Herpesviridae. Definition, Provisional Nomenclature, and Taxonomy. The Herpesvirus Study Group, The International Committee on Taxonomy of Viruses. *Intervirology* (1981) 16:201–17. doi: 10.1159/000149269
12. Grinde B. Herpesviruses: Latency and Reactivation – Viral Strategies and Host Response. *J Oral Microbiol* (2013) 5:1–9. doi: 10.3402/jom.v5i0.22766
13. Cohen JI. Herpesvirus Latency. *J Clin Invest* (2020) 130:3361–9. doi: 10.1172/JCI136225
14. Juillard F, De León Vázquez E, Tan M, Li S, Kaye KM. Kaposi's Sarcoma–Associated Herpesvirus LANA–Adjacent Regions With Distinct Functions in Episome Segregation or Maintenance. *J Virol* (2019) 93:1–15. doi: 10.1128/JVI.02158–18
15. Arthur JL, Scarpini CG, Connor V, Lachmann RH, Tolkovsky AM, Efstathiou S. Herpes Simplex Virus Type 1 Promoter Activity During Latency Establishment, Maintenance, and Reactivation in Primary Dorsal Root Neurons In Vitro. *J Virol* (2001) 75:3885–95. doi: 10.1128/JVI.75.8.3885–3895.2001
16. King W, Thomas–Powell AL, Raab–Traub N, Hawke M, Kieff E. Epstein–Barr Virus RNA. V. Viral RNA in a Restringently Infected, Growth–Transformed Cell Line. *J Virol* (1980) 36:506–18. doi: 10.1128/JVI.36.2.506-518.1980
17. Stoeger T, Adler H. "Novel" Triggers of Herpesvirus Reactivation and Their Potential Health Relevance. *Front Microbiol* (2019) 9:3207. doi: 10.3389/fmicb.2018.03207
18. Roizman B, Whitley RJ. An Inquiry Into the Molecular Basis of HSV Latency and Reactivation. *Annu Rev Microbiol* (2013) 67:355–74. doi: 10.1146/annurev–micro–092412–155654
19. Higgins CR, Schofield JK, Tatnall FM, Leigh IM. Natural History, Management and Complications of Herpes Labialis. *J Med Virol* (1993) Suppl 1:22–6. doi: 10.1002/jmv.1890410506
20. Ayoub HH, Chemaitelly H, Abu–Raddad LJ. Characterizing the Transitioning Epidemiology of Herpes Simplex Virus Type 1 in the USA: Model–Based Predictions. *BMC Med* (2019) 17:57. doi: 10.1186/s12916–019–1285–x
21. Whitley RJ. Herpes Simplex Encephalitis: Adolescents and Adults. *Antiviral Res* (2006) 71:141–8. doi: 10.1016/j.antiviral.2006.04.002
22. Looker KJ, Magaret AS, May MT, Turner KME, Vickerman P, Newman LM, et al. First Estimates of the Global and Regional Incidence of Neonatal Herpes Infection. *Lancet Glob Health* (2017) 5:e300–9. doi: 10.1016/S2214–109X(16)30362–X
23. Brown ZA, Vontver LA, Benedetti J, Critchlow CW, Sells CJ, Berry S, et al. *Effects on Infants of a First Episode of Genital Herpes During Pregnancy* (2010). Available at: http://dx.doi.org/101056/NEJM198711123172002.
24. Sacks SL, Griffiths PD, Corey L, Cohen C, Cunningham A, Dusheiko GM, et al. HSV–2 Transmission. *Antiviral Res* (2004) 63:S27–35. doi: 10.1016/j.antiviral.2004.06.005
25. Chemaitelly H, Nagelkerke N, Omori R, Abu–Raddad LJ. Characterizing Herpes Simplex Virus Type 1 and Type 2 Seroprevalence Declines and Epidemiological Association in the United States. *PloS One* (2019) 14:e0214151. doi: 10.1371/journal.pone.0214151
26. Tronstein E, Johnston C, Huang M–L, Selke S, Magaret A, Warren T, et al. Genital Shedding of Herpes Simplex Virus Among Symptomatic and Asymptomatic Persons With HSV–2 Infection. *JAMA* (2011) 305:1441–9. doi: 10.1001/jama.2011.420
27. Steiner I, Kennedy PG, Pachner AR. The Neurotropic Herpes Viruses: Herpes Simplex and Varicella–Zoster. *Lancet Neurol* (2007) 6:1015–28. doi: 10.1016/S1474–4422(07)70267–3
28. Tunbridge AJ, Breuer J, Jeffery KJM. Chickenpox in Adults – Clinical Management. *J Infect* (2008) 57:95–102. doi: 10.1016/j.jinf.2008.03.004
29. Hope–Simpson RE. The Nature of Herpes Zoster: A Long–Term Study and a New Hypothesis. *Proc R Soc Med* (1965) 58:9–20. doi: 10.1177/003591576505800106
30. *Shingles | Surveillance, Trends, Deaths | Herpes Zoster | Cdc* (2020). Available at: https://www.cdc.gov/shingles/surveillance.html (Accessed December 11, 2020).
31. Pergam S, Limaye A. Varicella Zoster Virus (VZV). *Am J Transplant Off J Am Soc Transplant Am Soc Transpl Surg* (2009) 9:S108–15. doi: 10.1111/j.1600–6143.2009.02901.x
32. Marin M, Meissner HC, Seward JF. Varicella Prevention in the United States: A Review of Successes and Challenges. *Pediatrics* (2008) 122:e744–751. doi: 10.1542/peds.2008–0567
33. Yinon Y, Farine D, Yudin MH. Screening, Diagnosis, and Management of Cytomegalovirus Infection in Pregnancy. *Obstet Gynecol Surv* (2010) 65:736–43. doi: 10.1097/OGX.0b013e31821102b4
34. Weller TH. The Cytomegaloviruses: Ubiquitous Agents With Protean Clinical Manifestations. *N Engl J Med* (1971) 285:203–14. doi: 10.1056/NEJM197107222850406
35. Weller TH. The Cytomegaloviruses: Ubiquitous Agents With Protean Clinical Manifestations. *N Engl J Med* (1971) 285:267–74. doi: 10.1056/NEJM197107292850507
36. Stockdale L, Nash S, Nalwoga A, Painter H, Asiki G, Fletcher H, et al. Human Cytomegalovirus Epidemiology and Relationship to Tuberculosis and Cardiovascular Disease Risk Factors in a Rural Ugandan Cohort. *PloS One* (2018) 13:e0192086. doi: 10.1371/journal.pone.0192086
37. Taylor–Wiedeman J, Sissons JG, Borysiewicz LK, Sinclair JH. Monocytes Are a Major Site of Persistence of Human Cytomegalovirus in Peripheral Blood Mononuclear Cells. *J Gen Virol* (1991) 72(Pt 9):2059–64. doi: 10.1099/0022–1317–72–9–2059
38. Sindre H, Tjoonnfjord G, Rollag H, Ranneberg–Nilsen T, Veiby O, Beck S, et al. Human Cytomegalovirus Suppression of and Latency in Early Hematopoietic Progenitor Cells. *Blood* (1996) 88:4526–33. doi: 10.1182/blood.V88.12.4526.bloodjournal88124526
39. Navti OB, Al–Belushi M, Konje JC. Cytomegalovirus Infection in Pregnancy – An Update. *Eur J Obstet Gynecol Reprod Biol* (2021) 258:216–22. doi: 10.1016/j.ejogrb.2020.12.006
40. Amin MM, Stowell JD, Hendley W, Garcia P, Schmid DS, Cannon MJ, et al. CMV on Surfaces in Homes With Young Children: Results of PCR and Viral Culture Testing. *BMC Infect Dis* (2018) 18:391. doi: 10.1186/s12879–018–3318–z
41. Wolz MM, Sciallis GF, Pittelkow MR. Human Herpesviruses 6, 7, and 8 From a Dermatologic Perspective. *Mayo Clin Proc* (2012) 87:1004–14. doi: 10.1016/j.mayocp.2012.04.010
42. Frenkel N, Schirmer EC, Wyatt LS, Katsafanas G, Roffman E, Danovich RM, et al. Isolation of a New Herpesvirus From Human CD4+ T Cells. *Proc Natl Acad Sci* (1990) 87:748–52. doi: 10.1073/pnas.87.2.748
43. Takahashi K, Sonoda S, Higashi K, Kondo T, Takahashi H, Takahashi M, et al. Predominant CD4 T–Lymphocyte Tropism of Human Herpesvirus 6–Related Virus. *J Virol* (1989) 63:3161–3. doi: 10.1128/JVI.63.7.3161–3163.1989
44. Grotto I, Mimouni D, Huerta M, Mimouni M, Cohen D, Robin G, et al. Clinical and Laboratory Presentation of EBV Positive Infectious Mononucleosis in Young Adults. *Epidemiol Infect* (2003) 131:683–9. doi: 10.1017/s0950268803008550
45. Cohen JI, Fauci AS, Varmus H, Nabel GJ. Epstein–Barr Virus: An Important Vaccine Target for Cancer Prevention. *Sci Transl Med* (2011) 3:107fs7. doi: 10.1126/scitranslmed.3002878
46. Sixbey JW, Nedrud JG, Raab–Traub N, Hanes RA, Pagano JS. Epstein–Barr Virus Replication in Oropharyngeal Epithelial Cells. *N Engl J Med* (1984) 310:1225–30. doi: 10.1056/NEJM198405103101905

47. Wolf H, Haus M, Wilmes E. Persistence of Epstein–Barr Virus in the Parotid Gland. *J Virol* (1984) 51:795–8. doi: 10.1128/JVI.51.3.795-798.1984
48. Klein G, Klein E, Kashuba E. Interaction of Epstein–Barr Virus (EBV) With Human B–Lymphocytes. *Biochem Biophys Res Commun* (2010) 396:67–73. doi: 10.1016/j.bbrc.2010.02.146
49. Kaye KM, Izumi KM, Kieff E. Epstein–Barr Virus Latent Membrane Protein 1 is Essential for B–Lymphocyte Growth Transformation. *Proc Natl Acad Sci USA* (1993) 90:9150–4. doi: 10.1073/pnas.90.19.9150
50. Ensoli B, Sgadari C, Barillari G, Sirianni MC, Stürzl M, Monini P. Biology of Kaposi's Sarcoma. *Eur J Cancer Oxf Engl 1990* (2001) 37:1251–69. doi: 10.1016/s0959–8049(01)00121–6
51. *Key Statistics About Kaposi Sarcoma*. Available at: https://www.cancer.org/cancer/kaposi–sarcoma/about/what–is–key–statistics.html (Accessed December 11, 2020).
52. Dukers NH, Renwick N, Prins M, Geskus RB, Schulz TF, Weverling GJ, et al. Risk Factors for Human Herpesvirus 8 Seropositivity and Seroconversion in a Cohort of Homosexual Men. *Am J Epidemiol* (2000) 151:213–24. doi: 10.1093/oxfordjournals.aje.a010195
53. Gnann JW, Whitley RJ. Herpes Simplex Encephalitis: An Update. *Curr Infect Dis Rep* (2017) 19:13. doi: 10.1007/s11908-017-0568-7
54. Wilson AC, Mohr I. A Cultured Affair: HSV Latency and Reactivation in Neurons. *Trends Microbiol* (2012) 20:604–11. doi: 10.1016/j.tim.2012.08.005
55. Nicoll MP, Hann W, Shivkumar M, Harman LER, Connor V, Coleman HM, et al. The HSV–1 Latency–Associated Transcript Functions to Repress Latent Phase Lytic Gene Expression and Suppress Virus Reactivation From Latently Infected Neurons. *PloS Pathog* (2016) 12:e1005539. doi: 10.1371/journal.ppat.1005539
56. Mador N, Goldenberg D, Cohen O, Panet A, Steiner I. Herpes Simplex Virus Type 1 Latency–Associated Transcripts Suppress Viral Replication and Reduce Immediate–Early Gene mRNA Levels in a Neuronal Cell Line. *J Virol* (1998) 72:5067–75. doi: 10.1128/JVI.72.6.5067–5075.1998
57. Rao DKB. Herpes Viruses – An Overview. *J Pharm* (2014) 4:39–41. doi: 10.9790/3013-04010039041
58. Olson JK, Miller SD. Microglia Initiate Central Nervous System Innate and Adaptive Immune Responses Through Multiple Tlrs. *J Immunol* (2004) 173:3916–24. doi: 10.4049/jimmunol.173.6.3916
59. Kodukula P, Liu T, Rooijen NV, Jager MJ, Hendricks RL. Macrophage Control of Herpes Simplex Virus Type 1 Replication in the Peripheral Nervous System. *J Immunol* (1999) 162:2895–905.
60. Laval K, Van Cleemput J, Vernejoul JB, Enquist LW. Alphaherpesvirus Infection of Mice Primes PNS Neurons to an Inflammatory State Regulated by TLR2 and Type I IFN Signaling. *PloS Pathog* (2019) 15:e1008087. doi: 10.1371/journal.ppat.1008087
61. Horan KA, Hansen K, Jakobsen MR, Holm CK, Søby S, Unterholzner L, et al. Proteasomal Degradation of Herpes Simplex Virus Capsids in Macrophages Releases DNA to the Cytosol for Recognition by DNA Sensors. *J Immunol Baltim Md 1950* (2013) 190:2311–9. doi: 10.4049/jimmunol.1202749
62. Chew T, Taylor KE, Mossman KL. Innate and Adaptive Immune Responses to Herpes Simplex Virus. *Viruses* (2009) 1:979–1002. doi: 10.3390/v1030979
63. Danastas K, Miranda–Saksena M, Cunningham AL. Herpes Simplex Virus Type 1 Interactions With the Interferon System. *Int J Mol Sci* (2020) 21:5150. doi: 10.3390/ijms21145150
64. Zhou Y, Ye L, Wan Q, Zhou L, Wang X, Li J, et al. Activation of Toll–Like Receptors Inhibits Herpes Simplex Virus–1 Infection of Human Neuronal Cells. *J Neurosci Res* (2009) 87:2916–25. doi: 10.1002/jnr.22110
65. Kigerl KA, de Rivero Vaccari JP, Dietrich WD, Popovich PG, Keane RW. Pattern Recognition Receptors and Central Nervous System Repair. *Exp Neurol* (2014) 258:5–16. doi: 10.1016/j.expneurol.2014.01.001
66. Su C, Zheng C. Herpes Simplex Virus 1 Abrogates the Cgas/STING–Mediated Cytosolic DNA–Sensing Pathway *Via* Its Virion Host Shutoff Protein, Ul41. *J Virol* (2017) 91:1–9. doi: 10.1128/JVI.02414–16
67. Kindt TJ, Goldsby RA, Osborne BA, Kuby J. *Kuby Immunology. 6th ed*. New York: W.H. Freeman (2007).
68. Kostavasili I, Sahu A, Friedman HM, Eisenberg RJ, Cohen GH, Lambris JD. Mechanism of Complement Inactivation by Glycoprotein C of Herpes Simplex Virus. *J Immunol Baltim Md 1950* (1997) 158:1763–71.
69. Tang D, Kang R, Coyne CB, Zeh HJ, Lotze MT. Pamps and DAMPs: Signal 0s That Spur Autophagy and Immunity. *Immunol Rev* (2012) 249:158–75. doi: 10.1111/j.1600–065X.2012.01146.x
70. Orvedahl A, Alexander D, Tallóczy Z, Sun Q, Wei Y, Zhang W, et al. Hsv–1 ICP34.5 Confers Neurovirulence by Targeting the Beclin 1 Autophagy Protein. *Cell Host Microbe* (2007) 1:23–35. doi: 10.1016/j.chom.2006.12.001
71. White DW, Beard RS, Barton ES. Immune Modulation During Latent Herpesvirus Infection. *Immunol Rev* (2012) 245:189–208. doi: 10.1111/j.1600–065X.2011.01074.x
72. Upton C, Macen JL, Schreiber M, McFadden G. Myxoma Virus Expresses a Secreted Protein With Homology to the Tumor Necrosis Factor Receptor Gene Family That Contributes to Viral Virulence. *Virology* (1991) 184:370–82. doi: 10.1016/0042–6822(91)90853–4
73. Upton C, Mossman K, McFadden G. Encoding of a Homolog of the IFN–gamma Receptor by Myxoma Virus. *Science* (1992) 258:1369–72. doi: 10.1126/science.1455233
74. Murphy PM. Molecular Mimicry and the Generation of Host Defense Protein Diversity. *Cell* (1993) 72:823–6. doi: 10.1016/0092–8674(93)90571–7
75. Alcamí A, Smith GL. A Soluble Receptor for Interleukin–1 Beta Encoded by Vaccinia Virus: A Novel Mechanism of Virus Modulation of the Host Response to Infection. *Cell* (1992) 71:153–67. doi: 10.1016/0092–8674(92)90274–g
76. Paludan SR, Bowie AG, Horan KA, Fitzgerald KA. Recognition of Herpesviruses by the Innate Immune System. *Nat Rev Immunol* (2011) 11:143–54. doi: 10.1038/nri2937
77. Conwell SE, White AE, Harper JW, Knipe DM. Identification of TRIM27 as a Novel Degradation Target of Herpes Simplex Virus 1 ICP0. *J Virol* (2015) 89:220–9. doi: 10.1128/JVI.02635–14
78. Kurt–Jones EA, Orzalli MH, Knipe DM. Innate Immune Mechanisms and Herpes Simplex Virus Infection and Disease. *Adv Anat Embryol Cell Biol* (2017) 223:49–75. doi: 10.1007/978–3–319–53168–7_3
79. Crameri M, Bauer M, Caduff N, Walker R, Steiner F, Franzoso FD, et al. Mxb is an Interferon–Induced Restriction Factor of Human Herpesviruses. *Nat Commun* (2018) 9:1980. doi: 10.1038/s41467–018–04379–2
80. Ku C–C, Che X–B, Reichelt M, Rajamani J, Schaap–Nutt A, Huang K–J, et al. Herpes Simplex Virus–1 Induces Expression of a Novel MxA Isoform That Enhances Viral Replication. *Immunol Cell Biol* (2011) 89:173–82. doi: 10.1038/icb.2010.83
81. Staeheli P, Haller O. Human MX2/MxB: A Potent Interferon–Induced Postentry Inhibitor of Herpesviruses and HIV–1. *J Virol* (2018) 92:1–9. doi: 10.1128/JVI.00709–18
82. Domke–Opitz I, Straub P, Kirchner H. Effect of Interferon on Replication of Herpes Simplex Virus Types 1 and 2 in Human Macrophages. *J Virol* (1986) 60:37–42. doi: 10.1128/JVI.60.1.37–42.1986
83. Rosato PC, Leib DA. Intrinsic Innate Immunity Fails to Control Herpes Simplex Virus and Vesicular Stomatitis Virus Replication in Sensory Neurons and Fibroblasts. *J Virol* (2014) 88:9991–10001. doi: 10.1128/JVI.01462–14
84. Sainz B, Halford WP. Alpha/Beta Interferon and Gamma Interferon Synergize to Inhibit the Replication of Herpes Simplex Virus Type 1. *J Virol* (2002) 76:11541–50. doi: 10.1128/jvi.76.22.11541–11550.2002
85. Leib DA, Harrison TE, Laslo KM, Machalek MA, Moorman NJ, Virgin HW. Interferons Regulate the Phenotype of Wild–Type and Mutant Herpes Simplex Viruses *In Vivo*. *J Exp Med* (1999) 189:663–72. doi: 10.1084/jem.189.4.663
86. Luker GD, Prior JL, Song J, Pica CM, Leib DA. Bioluminescence Imaging Reveals Systemic Dissemination of Herpes Simplex Virus Type 1 in the Absence of Interferon Receptors. *J Virol* (2003) 77:11082–93. doi: 10.1128/jvi.77.20.11082–11093.2003
87. Andersen LL, Mørk N, Reinert LS, Kofod–Olsen E, Narita R, Jørgensen SE, et al. Functional IRF3 Deficiency in a Patient With Herpes Simplex Encephalitis. *J Exp Med* (2015) 212:1371–9. doi: 10.1084/jem.20142274
88. Fujita T, Kimura Y, Miyamoto M, Barsoumian EL, Taniguchi T. Induction of Endogenous IFN–α and IFN–β Genes by a Regulatory Transcription Factor, IRF–1. *Nature* (1989) 337:270–2. doi: 10.1038/337270a0

89. Xie Y, He S, Wang J. MicroRNA–373 Facilitates HSV–1 Replication Through Suppression of Type I IFN Response by Targeting IRF1. *BioMed Pharmacother* (2018) 97:1409–16. doi: 10.1016/j.biopha.2017.11.071
90. Bigley NJ. Complexity of Interferon–γ Interactions With HSV–1. *Front Immunol* (2014) 5:15. doi: 10.3389/fimmu.2014.00015
91. Cantin EM, Hinton DR, Chen J, Openshaw H. Gamma Interferon Expression During Acute and Latent Nervous System Infection by Herpes Simplex Virus Type 1. *J Virol* (1995) 69:4898–905. doi: 10.1128/JVI.69.8.4898–4905.1995
92. Cantin E, Tanamachi B, Openshaw H. Role for Gamma Interferon in Control of Herpes Simplex Virus Type 1 Reactivation. *J Virol* (1999) 73:3418–23. doi: 10.1128/JVI.73.4.3418–3423.1999
93. Minami M, Kita M, Yan X–Q, Yamamoto T, Iida T, Sekikawa K, et al. Role of IFN–gamma and Tumor Necrosis Factor–Alpha in Herpes Simplex Virus Type 1 Infection. *J Interferon Cytokine Res Off J Int Soc Interferon Cytokine Res* (2002) 22:671–6. doi: 10.1089/10799900260100150
94. Vollstedt S, Arnold S, Schwerdel C, Franchini M, Alber G, Santo JPD, et al. Interplay Between Alpha/Beta and Gamma Interferons With B, T, and Natural Killer Cells in the Defense Against Herpes Simplex Virus Type 1. *J Virol* (2004) 78:3846–50. doi: 10.1128/JVI.78.8.3846–3850.2004
95. Zanoni I, Granucci F, Broggi A. Interferon (IFN)–λ Takes the Helm: Immunomodulatory Roles of Type III IFNs. *Front Immunol* (2017) 8:1661. doi: 10.3389/fimmu.2017.01661
96. Lazear HM, Schoggins JW, Diamond MS. Shared and Distinct Functions of Type I and Type III Interferons. *Immunity* (2019) 50:907–23. doi: 10.1016/j.immuni.2019.03.025
97. Yin Z, Dai J, Deng J, Sheikh F, Natalia M, Shih T, et al. Type III IFNs Are Produced by and Stimulate Human Plasmacytoid Dendritic Cells. *J Immunol Baltim Md 1950* (2012) 189:2735–45. doi: 10.4049/jimmunol.1102038
98. Low–Calle AM, Prada–Arismendy J, Castellanos JE. Study of Interferon–β Antiviral Activity Against Herpes Simplex Virus Type 1 in Neuron–Enriched Trigeminal Ganglia Cultures. *Virus Res* (2014) 180:49–58. doi: 10.1016/j.virusres.2013.12.022
99. Rosato PC, Leib DA. Neuronal Interferon Signaling Is Required for Protection Against Herpes Simplex Virus Replication and Pathogenesis. *PloS Pathog* (2015) 11:e1005028. doi: 10.1371/journal.ppat.1005028
100. Li J, Hu S, Zhou L, Ye L, Wang X, Ho J, et al. Interferon Lambda Inhibits Herpes Simplex Virus Type I Infection of Human Astrocytes and Neurons. *Glia* (2011) 59:58–67. doi: 10.1002/glia.21076
101. Crump CM, Yates C, Minson T. Herpes Simplex Virus Type 1 Cytoplasmic Envelopment Requires Functional Vps4. *J Virol* (2007) 81:7380–7. doi: 10.1128/JVI.00222–07
102. Schöneberg J, Lee I–H, Iwasa JH, Hurley JH. Reverse–Topology Membrane Scission by the ESCRT Proteins. *Nat Rev Mol Cell Biol* (2017) 18:5–17. doi: 10.1038/nrm.2016.121
103. Rusten TE, Vaccari T, Lindmo K, Rodahl LMW, Nezis IP, Sem–Jacobsen C, et al. ESCRTs and Fab1 Regulate Distinct Steps of Autophagy. *Curr Biol* (2007) 17:1817–25. doi: 10.1016/j.cub.2007.09.032
104. Katzenell S, Leib DA. Herpes Simplex Virus and Interferon Signaling Induce Novel Autophagic Clusters in Sensory Neurons. *J Virol* (2016) 90:4706–19. doi: 10.1128/JVI.02908–15
105. Cabrera JR, Manivanh R, North BJ, Leib DA. The ESCRT–Related Atpase Vps4 Is Modulated by Interferon During Herpes Simplex Virus 1 Infection. *mBio* (2019) 10:1–19. doi: 10.1128/mBio.02567–18
106. Akira S, Takeda K, Kaisho T. Toll–Like Receptors: Critical Proteins Linking Innate and Acquired Immunity. *Nat Immunol* (2001) 2:675–80. doi: 10.1038/90609
107. Karin M. The Regulation of AP–1 Activity by Mitogen–Activated Protein Kinases. *J Biol Chem* (1995) 270:16483–6. doi: 10.1074/jbc.270.28.16483
108. Herbst–Kralovetz M, Pyles R. Toll–Like Receptors, Innate Immunity and HSV Pathogenesis. *Herpes J IHMF* (2006) 13:37–41.
109. Konat GW, Kielian T, Marriott I. The Role of Toll–Like Receptors in CNS Response to Microbial Challenge. *J Neurochem* (2006) 99:1–12. doi: 10.1111/j.1471–4159.2006.04076.x
110. Aravalli RN, Peterson PK, Lokensgard JR. Toll–Like Receptors in Defense and Damage of the Central Nervous System. *J Neuroimmune Pharmacol Off J Soc NeuroImmune Pharmacol* (2007) 2:297–312. doi: 10.1007/s11481–007–9071–5
111. Cai M, Li M, Wang K, Wang S, Lu Q, Yan J, et al. The Herpes Simplex Virus 1–Encoded Envelope Glycoprotein B Activates NF–κb Through the Toll–Like Receptor 2 and MyD88/TRAF6–dependent Signaling Pathway. *PloS One* (2013) 8:e54586. doi: 10.1371/journal.pone.0054586
112. Kurt–Jones EA, Chan M, Zhou S, Wang J, Reed G, Bronson R, et al. Herpes Simplex Virus 1 Interaction With Toll–like Receptor 2 Contributes to Lethal Encephalitis. *Proc Natl Acad Sci* (2004) 101:1315–20. doi: 10.1073/pnas.0308057100
113. Kurt–Jones EA, Belko J, Yu C, Newburger PE, Wang J, Chan M, et al. The Role of Toll–Like Receptors in Herpes Simplex Infection in Neonates. *J Infect Dis* (2005) 191:746–8. doi: 10.1086/427339
114. Lucinda N, Figueiredo MM, Pessoa NL, Santos BSÁ da S, Lima GK, Freitas AM, et al. Dendritic Cells, Macrophages, NK and CD8+ T Lymphocytes Play Pivotal Roles in Controlling HSV–1 in the Trigeminal Ganglia by Producing IL1–beta, iNOS and Granzyme B. *Virol J* (2017) 14:37. doi: 10.1186/s12985–017–0692–x
115. Wang JP, Bowen GN, Zhou S, Cerny A, Zacharia A, Knipe DM, et al. Role of Specific Innate Immune Responses in Herpes Simplex Virus Infection of the Central Nervous System. *J Virol* (2012) 86:2273–81. doi: 10.1128/JVI.06010–11
116. Ahmad R, El Bassam S, Cordeiro P, Menezes J. Requirement of TLR2–mediated Signaling for the Induction of IL–15 Gene Expression in Human Monocytic Cells by HSV–1. *Blood* (2008) 112:2360–8. doi: 10.1182/blood–2008–02–137711
117. Rodrigues L, Nandakumar S, Bonorino C, Rouse BT, Kumaraguru U. Il–21 and IL–15 Cytokine DNA Augments HSV Specific Effector and Memory CD8+ T Cell Response. *Mol Immunol* (2009) 46:1494–504. doi: 10.1016/j.molimm.2008.12.033
118. Kielian T. Toll–Like Receptors in Central Nervous System Glial Inflammation and Homeostasis. *J Neurosci Res* (2006) 83:711–30. doi: 10.1002/jnr.20767
119. Aravalli RN, Hu S, Rowen TN, Palmquist JM, Lokensgard JR. Cutting Edge: Tlr2–Mediated Proinflammatory Cytokine and Chemokine Production by Microglial Cells in Response to Herpes Simplex Virus. *J Immunol* (2005) 175:4189–93. doi: 10.4049/jimmunol.175.7.4189
120. Sarangi PP, Kim B, Kurt–Jones E, Rouse BT. Innate Recognition Network Driving Herpes Simplex Virus–Induced Corneal Immunopathology: Role of the Toll Pathway in Early Inflammatory Events in Stromal Keratitis. *J Virol* (2007) 81:11128–38. doi: 10.1128/JVI.01008–07
121. Uyangaa E, Choi JY, Patil AM, Hossain FMA, Park SO, Kim B, et al. Dual TLR2/9 Recognition of Herpes Simplex Virus Infection Is Required for Recruitment and Activation of Monocytes and NK Cells and Restriction of Viral Dissemination to the Central Nervous System. *Front Immunol* (2018) 9:905. doi: 10.3389/fimmu.2018.00905
122. Sørensen LN, Reinert LS, Malmgaard L, Bartholdy C, Thomsen AR, Paludan SR. TLR2 and TLR9 Synergistically Control Herpes Simplex Virus Infection in the Brain. *J Immunol* (2008) 181:8604–12. doi: 10.4049/jimmunol.181.12.8604
123. Lima GK, Zolini GP, Mansur DS, Freire Lima BH, Wischhoff U, Astigarraga RG, et al. Toll–Like Receptor (TLR) 2 and TLR9 Expressed in Trigeminal Ganglia Are Critical to Viral Control During Herpes Simplex Virus 1 Infection. *Am J Pathol* (2010) 177:2433–45. doi: 10.2353/ajpath.2010.100121
124. Brun P, Scarpa M, Marchiori C, Conti J, Kotsafti A, Porzionato A, et al. Herpes Simplex Virus Type 1 Engages Toll Like Receptor 2 to Recruit Macrophages During Infection of Enteric Neurons. *Front Microbiol* (2018) 9:2148. doi: 10.3389/fmicb.2018.02148
125. Bsibsi M, Ravid R, Gveric D, van Noort JM. Broad Expression of Toll–Like Receptors in the Human Central Nervous System. *J Neuropathol Exp Neurol* (2002) 61:1013–21. doi: 10.1093/jnen/61.11.1013
126. Carpentier PA, Begolka WS, Olson JK, Elhofy A, Karpus WJ, Miller SD. Differential Activation of Astrocytes by Innate and Adaptive Immune Stimuli. *Glia* (2005) 49:360–74. doi: 10.1002/glia.20117
127. Farina C, Krumbholz M, Giese T, Hartmann G, Aloisi F, Meinl E. Preferential Expression and Function of Toll–Like Receptor 3 in Human Astrocytes. *J Neuroimmunol* (2005) 159:12–9. doi: 10.1016/j.jneuroim.2004.09.009

128. Préhaud C, Mégret F, Lafage M, Lafon M. Virus Infection Switches TLR–3–Positive Human Neurons to Become Strong Producers of Beta Interferon. *J Virol* (2005) 79:12893–904. doi: 10.1128/JVI.79.20.12893–12904.2005
129. Alexopoulou L, Holt AC, Medzhitov R, Flavell RA. Recognition of Double–Stranded RNA and Activation of NF–κb by Toll–Like Receptor 3. *Nature* (2001) 413:732–8. doi: 10.1038/35099560
130. Doyle SE, Vaidya SA, O'Connell R, Dadgostar H, Dempsey PW, Wu T–T, et al. Irf3 Mediates a TLR3/TLR4–Specific Antiviral Gene Program. *Immunity* (2002) 17:251–63. doi: 10.1016/S1074–7613(02)00390–4
131. Boehme KW, Compton T. Innate Sensing of Viruses by Toll–Like Receptors. *J Virol* (2004) 78:7867–73. doi: 10.1128/JVI.78.15.7867–7873.2004
132. Yamamoto M, Sato S, Hemmi H, Hoshino K, Kaisho T, Sanjo H, et al. Role of Adaptor TRIF in the MyD88–Independent Toll–Like Receptor Signaling Pathway. *Science* (2003) 301:640–3. doi: 10.1126/science.1087262
133. Pérez de Diego R, Sancho–Shimizu V, Lorenzo L, Puel A, Plancoulaine S, Picard C, et al. Human TRAF3 Adaptor Molecule Deficiency Leads to Impaired Toll–Like Receptor 3 Response and Susceptibility to Herpes Simplex Encephalitis. *Immunity* (2010) 33:400–11. doi: 10.1016/j.immuni.2010.08.014
134. Guo Y, Audry M, Ciancanelli M, Alsina L, Azevedo J, Herman M, et al. Herpes Simplex Virus Encephalitis in a Patient With Complete TLR3 Deficiency: TLR3 Is Otherwise Redundant in Protective Immunity. *J Exp Med* (2011) 208:2083–98. doi: 10.1084/jem.20101568
135. Herman M, Ciancanelli M, Ou Y–H, Lorenzo L, Klaudel–Dreszler M, Pauwels E, et al. Heterozygous TBK1 Mutations Impair TLR3 Immunity and Underlie Herpes Simplex Encephalitis of Childhood. *J Exp Med* (2012) 209:1567–82. doi: 10.1084/jem.20111316
136. Sancho–Shimizu V, Pérez de Diego R, Lorenzo L, Halwani R, Alangari A, Israelsson E, et al. Herpes Simplex Encephalitis in Children With Autosomal Recessive and Dominant TRIF Deficiency. *J Clin Invest* (2011) 121:4889–902. doi: 10.1172/JCI59259
137. Zhang S–Y, Jouanguy E, Ugolini S, Smahi A, Elain G, Romero P, et al. Tlr3 Deficiency in Patients With Herpes Simplex Encephalitis. *Science* (2007) 317:1522–7. doi: 10.1126/science.1139522
138. Zhang S–Y, Casanova J–L. Inborn Errors Underlying Herpes Simplex Encephalitis: From TLR3 to IRF3. *J Exp Med* (2015) 212:1342–3. doi: 10.1084/jem.2129insight4
139. Mielcarska MB, Bossowska–Nowicka M, Toka FN. Functional Failure of TLR3 and its Signaling Components Contribute to Herpes Simplex Encephalitis. *J Neuroimmunol* (2018) 316:65–73. doi: 10.1016/j.jneuroim.2017.12.011
140. Boivin N, Sergerie Y, Rivest S, Boivin G. Effect of Pretreatment With Toll–like Receptor Agonists in a Mouse Model of Herpes Simplex Virus Type 1 Encephalitis. *J Infect Dis* (2008) 198:664–72. doi: 10.1086/590671
141. Delhaye S, Paul S, Blakqori G, Minet M, Weber F, Staeheli P, et al. Neurons Produce Type I Interferon During Viral Encephalitis. *Proc Natl Acad Sci* (2006) 103:7835–40. doi: 10.1073/pnas.0602460103
142. Bowman CC, Rasley A, Tranguch SL, Marriott I. Cultured Astrocytes Express Toll–Like Receptors for Bacterial Products. *Glia* (2003) 43:281–91. doi: 10.1002/glia.10256
143. Jack CS, Arbour N, Manusow J, Montgrain V, Blain M, McCrea E, et al. Tlr Signaling Tailors Innate Immune Responses in Human Microglia and Astrocytes. *J Immunol* (2005) 175:4320–30. doi: 10.4049/jimmunol.175.7.4320
144. Krug A, Luker GD, Barchet W, Leib DA, Akira S, Colonna M. Herpes Simplex Virus Type 1 Activates Murine Natural Interferon–Producing Cells Through Toll–Like Receptor 9. *Blood* (2004) 103:1433–7. doi: 10.1182/blood–2003–08–2674
145. Kawai T, Sato S, Ishii KJ, Coban C, Hemmi H, Yamamoto M, et al. Interferon–α Induction Through Toll–like Receptors Involves a Direct Interaction of IRF7 With MyD88 and TRAF6. *Nat Immunol* (2004) 5:1061–8. doi: 10.1038/ni1118
146. Yang K, Puel A, Zhang S, Eidenschenk C, Ku C–L, Casrouge A, et al. Human TLR–7–, –8–, and –9–Mediated Induction of IFN–α/β and –λ Is Irak–4 Dependent and Redundant for Protective Immunity to Viruses. *Immunity* (2005) 23:465–78. doi: 10.1016/j.immuni.2005.09.016
147. Rasmussen SB, Sørensen LN, Malmgaard L, Ank N, Baines JD, Chen ZJ, et al. Type I Interferon Production During Herpes Simplex Virus Infection Is Controlled by Cell–Type–Specific Viral Recognition Through Toll–Like Receptor 9, the Mitochondrial Antiviral Signaling Protein Pathway, and Novel Recognition Systems. *J Virol* (2007) 81:13315–24. doi: 10.1128/JVI.01167–07
148. Zolini GP, Lima GK, Lucinda N, Silva MA, Dias MF, Pessoa NL, et al. Defense Against HSV–1 in a Murine Model is Mediated by iNOS and Orchestrated by the Activation of TLR2 and TLR9 in Trigeminal Ganglia. *J Neuroinflamm* (2014) 11:20. doi: 10.1186/1742–2094–11–20
149. Sakata K, Nakayamada S, Miyazaki Y, Kubo S, Ishii A, Nakano K, et al. Up–Regulation of TLR7–Mediated Ifn–α Production by Plasmacytoid Dendritic Cells in Patients With Systemic Lupus Erythematosus. *Front Immunol* (2018) 9:1957. doi: 10.3389/fimmu.2018.01957
150. Zhou L, Li J, Wang X, Ye L, Hou W, Ho J, et al. Il–29/IL–28A Suppress HSV–1 Infection of Human NT2–N Neurons. *J Neurovirol* (2011) 17:212–9. doi: 10.1007/s13365–011–0031–8
151. Iversen MB, Ank N, Melchjorsen J, Paludan SR. Expression of Type Iii Interferon (IFN) in the Vaginal Mucosa Is Mediated Primarily by Dendritic Cells and Displays Stronger Dependence on NF–κb Than Type I IFNs. *J Virol* (2010) 84:4579–86. doi: 10.1128/JVI.02591–09
152. Deb P, Dai J, Singh S, Kalyoussef E, Fitzgerald–Bocarsly P. Triggering of the Cgas–STING Pathway in Human Plasmacytoid Dendritic Cells Inhibits Tlr9–Mediated IFN Production. *J Immunol* (2020) 94(5):e01852–19. doi: 10.4049/jimmunol.1800933
153. Lin Y, Zheng C. A Tug of War: Dna–Sensing Antiviral Innate Immunity and Herpes Simplex Virus Type I Infection. *Front Microbiol* (2019) 10:2627. doi: 10.3389/fmicb.2019.02627
154. Stempel M, Chan B, Brinkmann MM. Coevolution Pays Off: Herpesviruses Have the License to Escape the DNA Sensing Pathway. *Med Microbiol Immunol (Berl)* (2019) 208:495–512. doi: 10.1007/s00430–019–00582–0
155. Ma Z, Damania B. The Cgas–STING Defense Pathway and Its Counteraction by Viruses. *Cell Host Microbe* (2016) 19:150–8. doi: 10.1016/j.chom.2016.01.010
156. Huang J, You H, Su C, Li Y, Chen S, Zheng C. Herpes Simplex Virus 1 Tegument Protein VP22 Abrogates Cgas/STING–Mediated Antiviral Innate Immunity. *J Virol* (2018) 92:1–11. doi: 10.1128/JVI.00841–18
157. You H, Zheng S, Huang Z, Lin Y, Shen Q, Zheng C. Herpes Simplex Virus 1 Tegument Protein UL46 Inhibits TANK–Binding Kinase 1–Mediated Signaling. *mBio* (2019) 10:1–10. doi: 10.1128/mBio.00919–19
158. Kalamvoki M, Roizman B. HSV–1 Degrades, Stabilizes, Requires, or is Stung by STING Depending on ICP0, the US3 Protein Kinase, and Cell Derivation. *Proc Natl Acad Sci USA* (2014) 111:E611–617. doi: 10.1073/pnas.1323414111
159. Ishikawa H, Ma Z, Barber GN. STING Regulates Intracellular DNA–mediated, Type I Interferon–Dependent Innate Immunity. *Nature* (2009) 461:788–92. doi: 10.1038/nature08476
160. Yamashiro LH, Wilson SC, Morrison HM, Karalis V, Chung J–YJ, Chen KJ, et al. Interferon–Independent STING Signaling Promotes Resistance to HSV–1 *In Vivo*. *Nat Commun* (2020) 11:3382. doi: 10.1038/s41467–020–17156–x
161. Kranzusch PJ, Wilson SC, Lee ASY, Berger JM, Doudna JA, Vance RE. Ancient Origin of Cgas–STING Reveals Mechanism of Universal 2',3' cGAMP Signaling. *Mol Cell* (2015) 59:891–903. doi: 10.1016/j.molcel.2015.07.022
162. Secombes CJ, Zou J. Evolution of Interferons and Interferon Receptors. *Front Immunol* (2017) 8:209. doi: 10.3389/fimmu.2017.00209
163. Gui X, Yang H, Li T, Tan X, Shi P, Li M, et al. Autophagy Induction *Via* STING Trafficking is a Primordial Function of the cGAS Pathway. *Nature* (2019) 567:262–6. doi: 10.1038/s41586–019–1006–9
164. Reinert LS, Lopušná K, Winther H, Sun C, Thomsen MK, Nandakumar R, et al. Sensing of HSV–1 by the cGAS–STING Pathway in Microglia Orchestrates Antiviral Defence in the CNS. *Nat Commun* (2016) 7:13348. doi: 10.1038/ncomms13348
165. Reinert LS, Rashidi AS, Tran DN, Katzilieris–Petras G, Hvidt AK, Gohr M, et al. Brain Immune Cells Undergo cGAS–STING–dependent Apoptosis During Herpes Simplex Virus Type 1 Infection. *J Clin Invest* (2020) 131(1):e136824. doi: 10.1172/JCI136824
166. Fries LF, Friedman HM, Cohen GH, Eisenberg RJ, Hammer CH, Frank MM. Glycoprotein C of Herpes Simplex Virus 1 is an Inhibitor of the Complement Cascade. *J Immunol Baltim Md 1950* (1986) 137:1636–41.

167. Friedman HM, Wang L, Pangburn MK, Lambris JD, Lubinski J. Novel Mechanism of Antibody–Independent Complement Neutralization of Herpes Simplex Virus Type 1. *J Immunol* (2000) 165:4528–36. doi: 10.4049/jimmunol.165.8.4528
168. Friedman HM, Cohen GH, Eisenberg RJ, Seidel CA, Cines DB. Glycoprotein C of Herpes Simplex Virus 1 Acts as a Receptor for the C3b Complement Component on Infected Cells. *Nature* (1984) 309:633–5. doi: 10.1038/309633a0
169. McNearney TA, Odell C, Holers VM, Spear PG, Atkinson JP. Herpes Simplex Virus Glycoproteins gC–1 and gC–2 Bind to the Third Component of Complement and Provide Protection Against Complement–Mediated Neutralization of Viral Infectivity. *J Exp Med* (1987) 166:1525–35. doi: 10.1084/jem.166.5.1525
170. Sari TK, Gianopulos KA, Nicola AV. Glycoprotein C of Herpes Simplex Virus 1 Shields Glycoprotein B From Antibody Neutralization. *J Virol* (2020) 94:1–9 doi: 10.1128/JVI.01852–19
171. Ferreira VP, Pangburn MK, Cortés C. Complement Control Protein Factor H: The Good, the Bad, and the Inadequate. *Mol Immunol* (2010) 47:2187–97. doi: 10.1016/j.molimm.2010.05.007
172. Cokarić Brdovčak M, Zubković A, Jurak I. Herpes Simplex Virus 1 Deregulation of Host Microrna. *Non–Coding RNA* (2018) 4:1–21. doi: 10.3390/ncrna4040036
173. Makou E, Herbert AP, Barlow PN. Functional Anatomy of Complement Factor H. *Biochemistry* (2013) 52:3949–62. doi: 10.1021/bi4003452
174. Hill JM, Zhao Y, Clement C, Neumann DM, Lukiw WJ. HSV–1 Infection of Human Brain Cells Induces miRNA–146a and Alzheimer–type Inflammatory Signaling. *Neuroreport* (2009) 20:1500–5. doi: 10.1097/WNR.0b013e3283329c05
175. Jamieson GA, Maitland NJ, Wilcock GK, Craske J, Itzhaki RF. Latent Herpes Simplex Virus Type 1 in Normal and Alzheimer's Disease Brains. *J Med Virol* (1991) 33:224–7. doi: 10.1002/jmv.1890330403
176. Jamieson GA, Maitland NJ, Wilcock GK, Yates CM, Itzhaki RF. Herpes Simplex Virus Type 1 DNA is Present in Specific Regions of Brain From Aged People With and Without Senile Dementia of the Alzheimer Type. *J Pathol* (1992) 167:365–8. doi: 10.1002/path.1711670403
177. Gordon L, McQuaid S, Cosby SL. Detection of Herpes Simplex Virus (Types 1 and 2) and Human Herpesvirus 6 DNA in Human Brain Tissue by Polymerase Chain Reaction. *Clin Diagn Virol* (1996) 6:33–40. doi: 10.1016/0928–0197(95)00203–0
178. Wald A, Corey L. Persistence in the Population: Epidemiology, Transmission, in: *Human Herpesviruses: Biology, Therapy, and Immunoprophylaxis* . Cambridge: Cambridge University Press. Available at: http://www.ncbi.nlm.nih.gov/books/NBK47447/ (Accessed December 18, 2020).
179. Hjalmarsson A, Blomqvist P, Sköldenberg B. Herpes Simplex Encephalitis in Sweden, 1990–2001: Incidence, Morbidity, and Mortality. *Clin Infect Dis Off Publ Infect Dis Soc Am* (2007) 45:875–80. doi: 10.1086/521262
180. George BP, Schneider EB, Venkatesan A. Encephalitis Hospitalization Rates and Inpatient Mortality in the United States, 2000–2010. *PloS One* (2014) 9: e104169. doi: 10.1371/journal.pone.0104169
181. Carter CJ. Susceptibility Genes are Enriched in Those of the Herpes Simplex Virus 1/Host Interactome in Psychiatric and Neurological Disorders. *Pathog Dis* (2013) 69:240–61. doi: 10.1111/2049–632X.12077
182. Wozniak MA, Mee AP, Itzhaki RF. Herpes Simplex Virus Type 1 DNA is Located Within Alzheimer's Disease Amyloid Plaques. *J Pathol* (2009) 217:131–8. doi: 10.1002/path.2449
183. Duarte LF, Farías MA, Álvarez DM, Bueno SM, Riedel CA, González PA. Herpes Simplex Virus Type 1 Infection of the Central Nervous System: Insights Into Proposed Interrelationships With Neurodegenerative Disorders. *Front Cell Neurosci* (2019) 13:46. doi: 10.3389/fncel.2019.00046

Conflict of Interest: The authors declare that the research was conducted in the absence of any commercial or financial relationships that could be construed as a potential conflict of interest.

frontiers in Immunology

ORIGINAL RESEARCH
published: 03 August 2021
doi: 10.3389/fimmu.2021.642373

Nociceptive Sensory Neurons Mediate Inflammation Induced by *Bacillus Anthracis* Edema Toxin

*Nicole J. Yang[1], Dylan V. Neel[1], Liwen Deng[1], Michelle Heyang[1], Angela Kennedy-Curran[1], Victoria S. Tong[1], Jin Mo Park[2] and Isaac M. Chiu[1]**

[1] Department of Immunology, Harvard Medical School, Boston, MA, United States, [2] Cutaneous Biology Research Center, Massachusetts General Hospital and Harvard Medical School, Charlestown, MA, United States

Bacterial products are able to act on nociceptive neurons during pathogenic infection. Neurogenic inflammation is an active part of pain signaling and has recently been shown to impact host-pathogen defense. *Bacillus anthracis* Edema Toxin (ET) produces striking edema in peripheral tissues, but the cellular mechanisms involved in tissue swelling are not completely understood. Here, we find that nociceptive neurons play a role in ET-induced edema and inflammation in mice. Subcutaneous footpad infection of *B. anthracis* Sterne caused ET-dependent local mechanical allodynia, paw swelling and body weight gain. Subcutaneous administration of ET induced paw swelling and vascular leakage, the early phases of which were attenuated in the absence of Trp_v1^+ or $Na_v1.8^+$ nociceptive neurons. Nociceptive neurons express the anthrax toxin receptor ANTXR2, but this did not mediate ET-induced edema. ET induced local cytokine expression and neutrophil recruitment, which were dependent in part on Trp_v1^+ nociceptive neurons. Ablation of Trp_v1^+ or $Na_v1.8^+$ nociceptive neurons also attenuated early increases in paw swelling and body weight gain during live *B. anthracis* infection. Our findings indicate that nociceptive neurons play an active role in inflammation caused by *B. anthracis* and Edema Toxin to potentially influence bacterial pathogenesis.

Keywords: *Bacillus anthracis*, edema toxin, nociceptors, neurogenic inflammation, neuron

OPEN ACCESS

Edited by:
Michael D Burton, The University of Texas at Dallas, United States

Reviewed by:
Man-Kyo Chung, University of Maryland, Baltimore, United States
Jean-Nicolas Tournier, Institut Pasteur, France

***Correspondence:**
Isaac M. Chiu
Isaac_Chiu@hms.harvard.edu

Specialty section:
This article was submitted to Molecular Innate Immunity, a section of the journal Frontiers in Immunology

Received: *15 December 2020*
Accepted: *19 July 2021*
Published: *03 August 2021*

Citation:
Yang NJ, Neel DV, Deng L, Heyang M, Kennedy-Curran A, Tong VS, Park JM and Chiu IM (2021) Nociceptive Sensory Neurons Mediate Inflammation Induced by Bacillus Anthracis Edema Toxin. Front. Immunol. 12:642373. doi: 10.3389/fimmu.2021.642373

INTRODUCTION

Nociceptive sensory neurons densely innervate barrier tissues such as the skin, lung and gut, and detect physical and chemical stimuli that are potentially damaging, which initiates pain signaling. Recent work has shown that nociceptive neurons can also detect bacterial products and respond by secreting neuropeptides and initiating pain behavior (1–3). Nociceptor activation triggers neurogenic inflammation, an axonal reflex that leads to rapid release of neural mediators from peripheral nerve terminals that in turn act on the vasculature and immune system to drive tissue inflammation (4). Major nociceptive neuron mediators include the neuropeptides calcitonin gene-related peptide (CGRP) and substance P (SP). CGRP acts on vascular smooth muscle cells to promote vasodilation and SP acts on vascular endothelial cells to increase vascular permeability, leading to edema (4). However, the role of the nervous system in mediating tissue inflammation in response to pathogen exposure is only beginning to be understood. Recent work demonstrated that

during bacterial infection, neuropeptides can additionally act on innate immune or epithelial cells to influence antimicrobial immunity (3, 5, 6). These findings suggest that nociceptive neurons may play a broader role in modulating host defense against pathogenic insults.

Bacillus anthracis is a gram-positive, spore-forming bacterium which is the etiologic agent of anthrax. Infection is classified based on the entry route of spores, and can produce cutaneous, inhalational and gastrointestinal disease. Cutaneous anthrax is characterized by extensive soft tissue edema which may extend beyond the local site of infection, and the formation of a black, painless eschar (7). Fluid accumulation in the chest or abdomen are also typical of inhalational and gastrointestinal anthrax (7), making edema a key feature of *B. anthracis* infection. However, the cellular and molecular mechanisms leading to local and systemic edema are not well understood.

Anthrax toxins are the key virulence factors of *B. anthracis*, and consist of Protective antigen (PA), Edema Factor (EF) and Lethal Factor (LF). PA binds to its cognate receptors ANTXR1 and ANTXR2, with higher affinity to the latter, and oligomerizes into a pore that translocates EF and LF into the cytoplasm. EF is an adenylyl cyclase that generates cAMP and LF is a protease that cleaves MAPK kinase kinases (MAPKKs), and they collectively produce potent alterations in host intracellular signaling. We recently reported that nociceptive neurons express ANTXR2 and can be targeted by anthrax toxins to alter cAMP levels and alter pain behavior (8). This finding suggested that these neurons may potentially be involved in pathogenesis during *B. anthracis* infection.

Administration of Edema Toxin (ET), the combination of PA and EF, produces striking edema and vascular leakage in laboratory animals (9, 10). Previous studies have suggested direct and indirect actions of ET on the vasculature to mediate tissue swelling. EF reduces cadherin expression and weakens intercellular junctions in endothelial cell lines, potentially contributing to the vascular effusion observed *in vivo* (11). In addition, chemical inhibition of prostanoid, neurokinin and histamine pathways attenuated ET-induced edema in rabbits, suggesting a potential role for mast cells and sensory neurons (12). Overall, the molecular and cellular interactions induced by ET remain incompletely defined.

Here, we report that nociceptive neurons contribute to ET-induced edema and inflammation. In a subcutaneous footpad infection model of *B. anthracis* Sterne in mice, we found that bacterial infection produces significant swelling accompanied by mechanical allodynia, both of which are dependent on EF, the effector component of ET. Nociceptor ablation by chemical or genetic methods significantly attenuated early tissue swelling, vascular leakage, and neutrophil recruitment induced by ET. Nociceptors also contributed to the early phase of *B. anthracis* induced edema. Edema was independent of ANTXR2 on nociceptive neurons, suggesting that nociceptors respond indirectly to infection and modulate tissue edema. Our findings highlight a novel regulatory role for nociceptive neurons in driving edema and inflammation during *B. anthracis* infection.

MATERIALS AND METHODS

Animals

All animal experiments were approved by the Institutional Animal Care and Use Committee (IACUC) at Harvard Medical School. C57BL/6J mice were purchased from Jackson Laboratory (Bar Harbor, ME) and bred at Harvard Medical School. All mice were housed in individually ventilated microisolator cages within a full barrier, specific pathogen-free animal facility at Harvard Medical School. Mice were kept on a 12 hr light/dark cycle and provided *ad libitum* access to food and water. $Na_v1.8$-lineage neuron-depleted mice ($Na_v1.8^{cre/+}/DTA^{+/-}$) and control littermates ($Na_v1.8^{+/+}/DTA^{+/-}$) were generated by breeding $Na_v1.8$-cre knock-in mice (provided by J. Wood, University College London) with B6.Rosa26-stop(flox)-DTA mice (Jackson Laboratory) as previously described (6). $Na_v1.8$ neuron-specific conditional ANTXR2 mice ($Na_v1.8^{cre/+}/Antxr2^{fl/fl}$) were generated by breeding Nav1.8-cre knock-in mice with a conditionally targeted allele of Antxr2 in the transmembrane region ($Antxr2^{fl/fl}$, Jackson Laboratory) as previously described (8). Experiments were performed with age- and sex-matched mice between 7 to 14 weeks of age unless otherwise noted.

Drug Treatment

For chemical ablation of Trp_v1^+ neurons with systemically administered resiniferatoxin (RTX, Sigma Aldrich), 4-week-old C57BL/6 mice were injected subcutaneously in the flank with escalating doses of RTX (30, 70, 100 μg/kg on consecutive days) or vehicle (2% DMSO/0.15% Tween-80 in PBS). For chemical ablation of Trp_v1^+ neurons with intrathecally administered RTX, 4-week-old C57BL/6 mice were injected intrathecally near the iliac crest with two daily doses of RTX (25 ng) or vehicle (0.25% DMSO/0.02% Tween-80 in PBS). BIBN 4096 (Tocris; 50 pmol in 10 μL) and its vehicle (0.05% DMSO in saline), Spantide I (Tocris; 5 nmol in 10 μL) and its vehicle (water) were injected subcutaneously into the ipsilateral footpad using a 100 μL Hamilton syringe and 32-gauge needle under isoflurane anesthesia. The antagonists and vehicle controls were administered 15 min prior to ET.

Recombinant Anthrax Toxins

Protective antigen (PA) was obtained through BEI Resources (#NR-140, recombinant from *B. anthracis*). The Edema Factor (EF) clone used in this study contains an extra alanine at the N-terminus compared to the native sequence (**Supplementary Figure 5**), which enhances intracellular stability and activity (13). EF was expressed in Rosetta 2 (DE3) *E. coli* (Novagen) using the Champion pET SUMO expression system (ThermoFisher Scientific) and purified as previously described (8). Endotoxin levels in the final product measured using the Pierce LAL Chromogenic Endotoxin Quantitation Kit (ThermoFisher Scientific) was 0.93 EU/mg.

B. anthracis Culture and Infection

The *Bacillus anthracis* Sterne 7702 strain (BA663, #NR-9396) and its isogenic mutant lacking EF (BA695, #NR-9398) were

obtained from ATCC. Spores for both strains were prepared as previously described (14) and stored at 4°C. All procedures were approved by the Committee on Microbiological Safety (COMS) at Harvard Medical School and conducted under Biosafety Level 2 protocols and guidelines. For infection, *B. anthracis* spores were streaked on BHI agar plates and grown overnight at 37°C. A day prior to infection, bacterial colonies were picked and inoculated into 2x SG medium and grown overnight at 37°C, 250 rpm. The overnight culture was diluted 50-fold into fresh 2x SG medium and grown for approximately 2 hr until mid-log phase was reached, then washed twice with PBS and stored in PBS on ice until injection. Mice were anesthetized with 3% isoflurane (Patterson Veterinary) with oxygen using a precision vaporizer, after which the indicated dose of bacteria was injected subcutaneously into the left hind paw in a 20 µL volume using a 100 µL Hamilton syringe and 31-gauge needle. The inoculum was also plated on BHI agar plates and incubated overnight to confirm dosages. Survival, paw thickness and body weight were monitored daily post-infection.

Tissue Bacterial Load Measurements

Mice were infected *via* subcutaneous footpad injection of vegetative *Bacillus anthracis* Sterne 7702 at a dosage of 1×10^7 CFUs, following procedures described in *B. anthracis* culture and infection. At 5 or 48 hr post-infection, mice were euthanized by CO_2 asphyxiation and the ipsilateral foot was harvested below the ankle. The ipsilateral popliteal lymph node, liver and spleen were also harvested. The organs were immediately transferred into pre-weighed 2 mL microcentrifuge tubes containing 1 mL of cold PBS and stored on ice. After organ weights were measured, foot samples were minced with scissors to facilitate homogenization. All samples were homogenized by bead beating at 25 Hz for 10 min using a TissueLyser (Qiagen). The tissue lysate was serially diluted in PBS and plated on BACARA agar (Biomerieux), a chromogenic media selective for the *Bacillus cereus* group (15). Plates were incubated overnight at 37°C and the number of resulting colonies were counted to calculate bacterial loads. Total CFU counts were normalized to organ weight.

Intraplantar Injection of Edema Toxin

2 µg of PA and 2 µg of EF were mixed with PBS to a volume of 20 µL. Injection was performed with a 100 µL Hamilton syringe and 32-gauge needle under isoflurane anesthesia.

Paw Thickness Measurements

Paw thicknesses were measured under isoflurane anesthesia using digital calipers (VWR International) and normalized to initial values measured prior to injection of bacteria or toxin.

Measurement of Mechanical Sensitivity

All behavioral tests were performed by observers blinded to the treatment groups or genotypes. Treatment groups were randomized and evenly distributed across cages and sex. Mechanical sensitivity thresholds were measured using von Frey filaments and the up/down method as previously described (8). Briefly, mice were habituated on the behavior apparatus for 2 consecutive days for 1 hr each. After habituation, baseline measurements were obtained on 3 separate days and averaged prior to infection. After infection, measurements were made at the indicated timepoints up to 48 hr post-infection.

Hot Plate Test

Mice were placed on a temperature-controlled metal plate (IITC Life Science) at 55°C, and the latency to response (jumping or hind paw licking) was recorded. A 90 s cut-off was imposed to avoid tissue injury.

Fluid Content Measurements

C57BL/6 mice were given subcutaneous footpad injection of 1×10^7 CFU *Bacillus anthracis* Sterne as described in *B. anthracis* culture and infection. At 48 hr post-infection, the indicated organs were harvested and weighed to measure their wet weight. Following incubation at 70°C for 40 min and 55°C for 48 hr with open lids, dry weights were recorded. Fluid weight was calculated as wet weight – dry weight, then normalized to dry weight.

Evans Blue Extravasation (Miles Assay)

Evans Blue dye (Sigma Aldrich) dissolved in 0.9% saline was administered retro-orbitally (25 mg/kg) and allowed to circulate for 30 min, after which mice were given intraplantar injection of ET. At 5 hr post-injection, animals were put under terminal anesthesia with Avertin (500 mg/kg, i.p) and perfused with 10 mL of cold PBS. The glabrous skin of the ipsilateral footpad was collected using a razor blade and minced with scissors in 500 µL of 50% TCA in 0.9% saline. The tissue was further homogenized in a TissueLyser II (Qiagen) for 10 min at 30 Hz, and centrifuged at 18,000 xg for 10 min. 100 µL of the supernatant was transferred to a 96-well plate and the absorbances at 620 nm were measured using a Synergy Mx multi-mode microplate reader (BioTek), along with a standard curve of Evans Blue prepared in 50% TCA. Values were fitted using GraphPad Prism.

Neutrophil Influx

Mice were given intraplantar injection of ET 5 hr prior to analysis. The glabrous skin of the ipsilateral footpad was collected using a razor blade and minced with scissors in 5 mL of PBS. The tissue was pelleted and resuspended in 2 mL of HEPES-buffered saline (Sigma) containing collagenase A (1 mg/kg, Roche Applied Sciences) and dispase II (2.4 U/mL, Roche Applied Sciences) for 2 hr at 37°C. After incubation, cells were dissociated using a 16-gauge needle attached to a 10 mL syringe, filtered through a 70 µm strainer, and washed with 20 mL of HBSS (Thermo Fisher Scientific) with 0.5% BSA (Sigma). Cells were resuspended in 500 µL of washing buffer and incubated on ice with mouse FcR Blocking Reagent (Miltenyi Biotec) for 10 min, then for 30 min on ice with the following antibodies: anti-CD45-APC/Cy7 (1:200, Biolegend), anti-Ly6G-A488 (1:200, Biolegend), anti-CD11b-BV605 (1:200, Biolegend), and Fixable Viability Dye eFluor-506 (1:1,200, Thermo Fisher). Cells were centrifuged for 5 min at 300 xg and resuspended in 500 µL of washing buffer with 2% PFA. Flow cytometry was performed on a LSR II flow cytometer (BD Biosciences) using BD FACSDiva software (BD Biosciences). Data was analyzed and plotted using FlowJo software (FlowJo LLC).

Cytokine Analysis

Mice were given intraplantar injection of ET 5 hr prior to analysis. The glabrous skin of the ipsilateral footpad was collected using a razor blade and minced with scissors in 500 uL of PBS. The tissue was further homogenized in a TissueLyser II (Qiagen) for 10 min at 30 Hz, and centrifuged at 18,000 xg for 10 min at 4°C. The supernatant was stored at -80°C until multiplex analysis of cytokine levels, performed by Eve Technologies.

Statistical Analysis

Statistical tests and significance levels are reported in figure legends. Data are represented as mean ± standard error (SEM). All statistical analyses were performed using GraphPad Prism 8 and 9. All t-tests were performed as two-tailed.

RESULTS

Subcutaneous Footpad Infection of *B. anthracis* Sterne Produces Mortality, Edema, and Body Weight Gain

To determine whether nociceptive neurons play a role during *B. anthracis* infection, we utilized a subcutaneous infection model in the footpad of C57BL/6 mice. This model was previously reported to induce robust edema and host immune response at the site of infection (14). We used the attenuated Sterne strain, which lacks the virulent capsule of *B. anthracis* but expresses all components of anthrax toxin, and is widely used for laboratory research (16). Vegetative bacteria were used to take advantage of active toxin production.

Subcutaneous *B. anthracis* infection caused a severe phenotype including mortality, with higher doses of bacteria inducing greater lethality (**Figure 1A**). Infection was accompanied by significant local swelling in the footpad and rapid increase in body weight during the first 2 days post-infection (**Figures 1B, C**). Given the severe edema observed in the footpad and adjacent hind limb, we hypothesized that the body weight gain was driven by accumulation of fluid. We thus measured the dry *vs.* wet weight of tissues post-infection to determine fluid weights. While we did not observe significant changes in the fluid content of most internal organs following infection (**Figure 1D**), the ipsilateral footpad gained fluid that accounted for approximately 400 mg in weight at the day 2 time point (**Figure 1E**). We observed a slight decrease in fluid content in the lungs, consistent with a previous study which performed systemic injection of ET (17). These data indicated major tissue

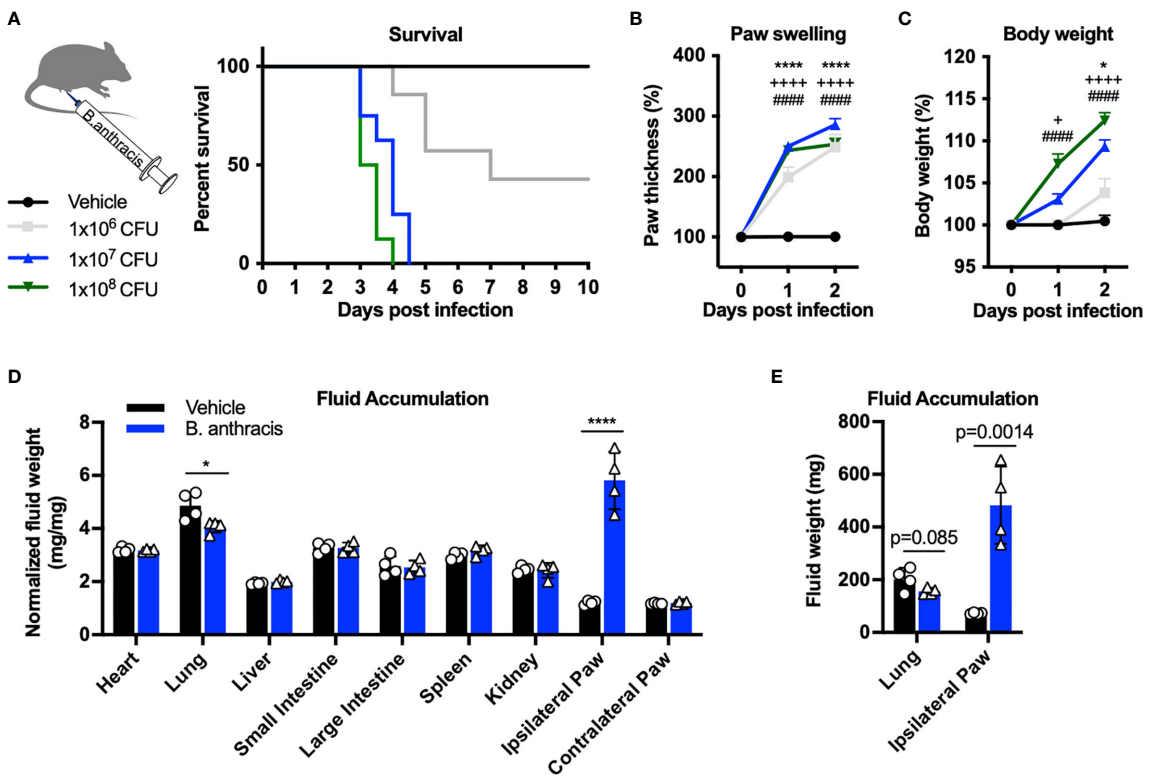

FIGURE 1 | Subcutaneous footpad infection of *Bacillus anthracis* induces significant paw swelling and body weight gain. **(A–C)** C57BL/6 mice received subcutaneous footpad injection of Vehicle (PBS) (n=7) or 1×10^6, 1×10^7 or 1×10^8 CFUs of *(B) anthracis* Sterne (n=7-8). Survival, thickness of the ipsilateral paw and body weight were measured daily. **(D, E)** Fluid weight in internal organs, normalized to the respective dry weights **(D)** or in absolute values **(E)**, following subcutaneous infection with Vehicle (PBS) (n=4) or 1×10^7 CFU of B. anthracis Sterne (n=4). Statistical analysis: **(A, F)** Log-rank (Mantel-Cox) test, $^{****}p < 0.0001$. **(B, C)** Two-way ANOVA with Dunnett's post-test. Vehicle *vs.* 1×10^6 CFUs, $^{+}p < 0.05$, $^{*}p < 0.05$, $^{****}p < 0.0001$. Vehicle *vs.* 1×10^7 CFUs, $^{++++}p < 0.0001$. Vehicle *vs.* 1×10^8 CFUs, $^{\#\#\#\#}p < 0.0001$. **(D, E)** Two-way ANOVA with Sidak's post-test. $^{*}p < 0.05$, $^{****}p < 0.0001$.

edema and fluid accumulation occurring in the site of infection in the first 48 hours.

B. anthracis-Induced Mortality, Tissue Swelling and Allodynia Is Mediated by Edema Factor

Edema Toxin (ET), which consists of Protective Antigen (PA) and Edema Factor (EF), is a major virulence factor of *B. anthracis* and known to cause severe swelling, edema, tissue damage and death in experimental animals (9, 10). To determine whether ET is responsible for pathogenesis and localized swelling during *B. anthracis* infection, we performed subcutaneous infection with an isogenic mutant *B. anthracis* strain lacking EF (ΔEF). Deficiency in EF led to significantly increased survival following infection compared to WT *B. anthracis* (**Figure 2A**). Furthermore, ΔEF mutant bacteria caused significantly less paw swelling in the footpad and body weight accumulation in mice compared to WT bacteria (**Figures 2B, C**). These results show that EF is a major virulence factor that mediates mortality, edema, and weight gain during *B. anthracis* infection.

We next measured whether infection induced changes in mechanical pain hypersensitivity and allodynia (sensitivity to normally innocuous stimuli) using von Frey filaments. Subcutaneous infection in mice induced mechanical allodynia over the first 48 hours of infection, prior to the lethal time points (**Figure 3A**). Mechanical allodynia was significantly reduced in ΔEF *B. anthracis* infected mice compared to WT bacteria-infected mice (**Figure 3B**), indicating that EF contributes to the pain-like behaviors during infection. The partial attenuation of pain suggested that additional factors were induced which work to sensitize nociceptive neurons, such as other damage-associated signals or inflammatory mediators.

Edema Toxin Is Sufficient to Induce Tissue Swelling, Vascular Leakage, Neutrophil Recruitment and Inflammatory Cytokine Production

Given the contribution of ET to tissue swelling during *B. anthracis* infection, we wished to interrogate its direct and independent effects on edema and localized inflammatory

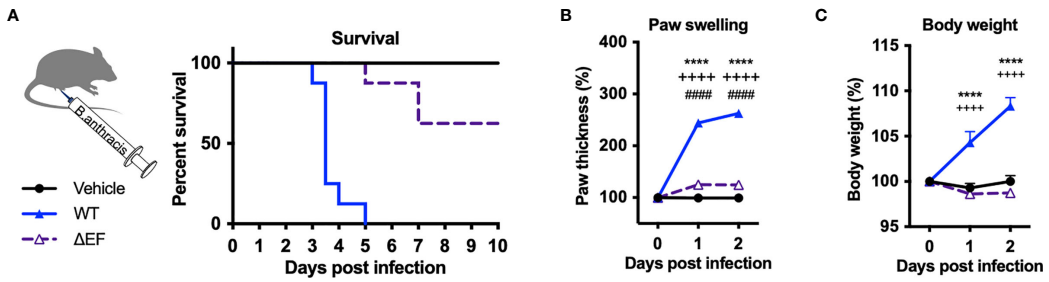

FIGURE 2 | Edema factor mediates *B. anthracis*-induced lethality, paw swelling and body weight gain. **(A–C)** C57BL/6 mice received subcutaneous footpad injection of Vehicle (PBS) (n=8), wild-type *B. anthracis* Sterne (1×10^7 CFUs; n=8), or an isogenic mutant lacking EF (ΔEF, 1×10^7 CFUs; n=8). Survival, thickness of the ipsilateral paw and body weight were measured daily. Statistical analysis: **(A)** Log-rank (Mantel-Cox) test, ****p < 0.0001. **(B, C)** Two-way ANOVA with Tukey's post-test. Vehicle *vs.* WT, ****p < 0.0001; WT *vs.* ΔEF, $^{++++}$p < 0.0001; Vehicle *vs.* ΔEF, $^{\#\#\#\#}$p < 0.0001.

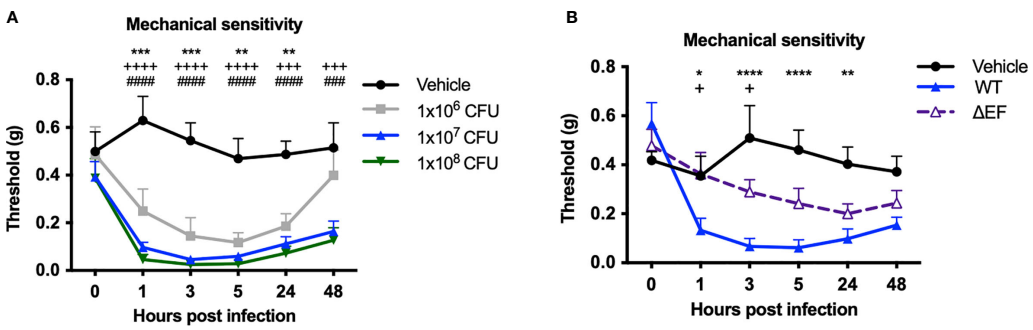

FIGURE 3 | Edema Factor contributes to mechanical sensitivity induced by *Bacillus anthracis* infection. **(A)** C57BL/6 mice received subcutaneous footpad injection of Vehicle (PBS) (n=7) or 1×10^6, 1×10^7 or 1×10^8 CFUs of *B. anthracis* Sterne (n=7-8). **(B)** C57BL/6 mice received subcutaneous footpad injection of Vehicle (PBS) (n=8), wild-type *B. anthracis* Sterne (1×10^7 CFUs; n=8), or an isogenic mutant lacking EF (ΔEF, 1×10^7 CFUs; n=8). Mechanical sensitivity of the ipsilateral footpad was measured using von Frey filaments. Statistical analysis: **(A)** Two-way ANOVA with Dunnett's post-test. Vehicle *vs.* 1×10^6 CFUs, **p < 0.01, ***p < 0.001. Vehicle *vs.* 1×10^7 CFUs, $^{+++}$p < 0.0001, $^{++++}$p < 0.0001. Vehicle *vs.* 1×10^8 CFUs, $^{\#\#\#}$p < 0.0001, $^{\#\#\#\#}$p < 0.0001. **(B)** Two-way ANOVA with Tukey's post-test. Vehicle *vs.* WT, *p < 0.05, **p < 0.01, ***p < 0.001,****p < 0.0001. WT *vs.* ΔEF, $^{+}$p < 0.05.

processes. We thus performed subcutaneous injection of ET into the footpad of mice. Subcutaneous ET produced significant swelling of the paw (**Figure 4A**) as previously reported (17), consistent with our observations during *B. anthracis* infection. We observed two distinct phases of paw swelling: an early phase lasting for several hours post-injection (hpi), where the thickness of the paw increased by 50%, followed by a late phase at 24 hpi, where a 200% increase in paw thickness was observed. In contrast to bacterial infection, we did not observe changes in body weight, suggesting that the effects of ET injection are locally confined. We also found that ET induces vascular effusion at the injection site, measured by extravasation of Evans Blue dye at 5 hpi (**Figures 4B, C**). This observation was consistent with previous reports (11, 12).

We next wished to determine the cellular components of ET-induced swelling. ET is known to inhibit host innate and adaptive immune responses in concert with LT (18), and has been observed to induce neutrophil infiltration in rabbits (12). We found that subcutaneous injection of ET induces significant influx of $CD45^+Ly6G^+$ neutrophils to the footpad of mice at 5 hpi, which continued to increase by 24 hpi (**Figure 4D**). To determine potential molecular mediators of this effect, we screened for cytokine expression in the footpad at 5 hpi. We found that ET injection induces high levels of CXCL1 and CXCL2 (**Figure 4E**), consistent with influx of neutrophils. We also observed that ET induces significant levels of IL-3, IL-6, MCP-1, G-CSF, LIF and MIG compared to vehicle injection, but to smaller magnitudes. Altogether, our results indicated that ET is sufficient to elicit a potent host immune response with both vascular and cellular components.

Nociceptive Neurons Mediate Edema and Vascular Leakage Induced by Edema Toxin

We next wished to determine whether nociceptive neurons contribute to ET-induced swelling and vascular leakage in the

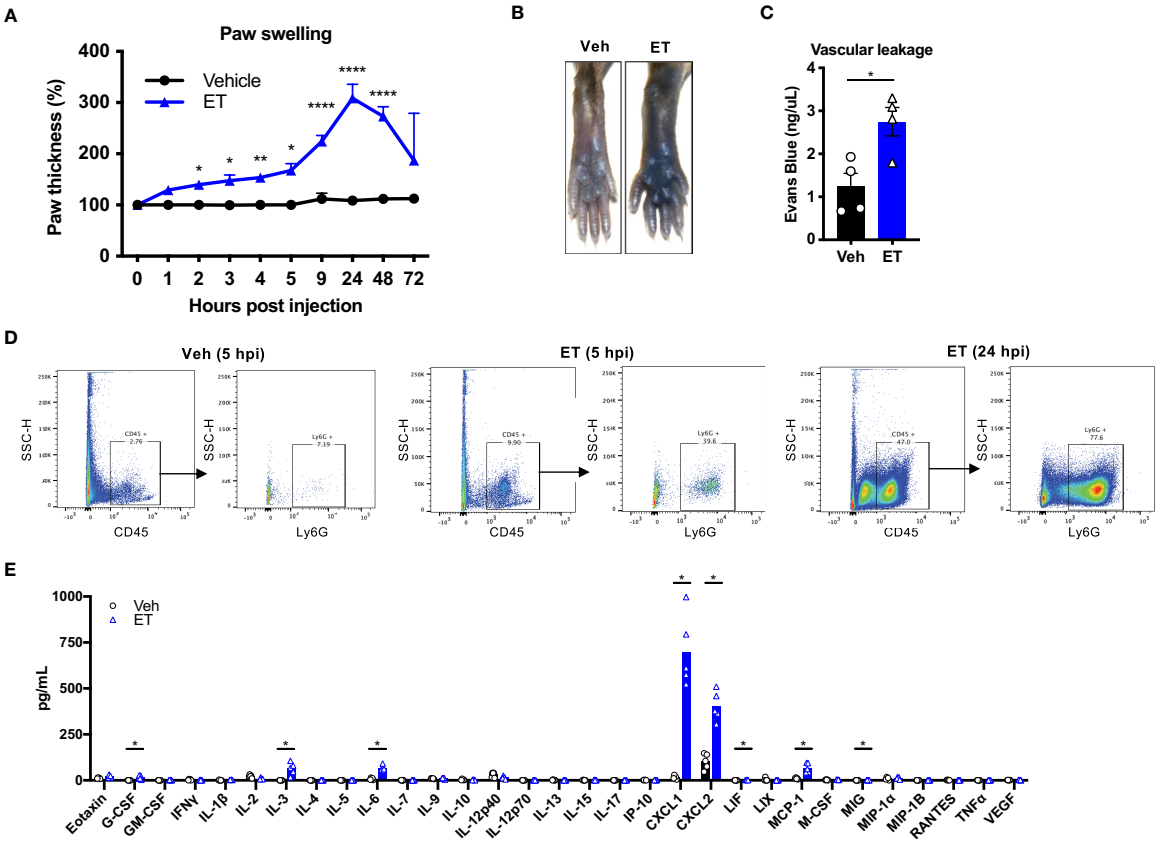

FIGURE 4 | Edema toxin drives significant edema and inflammatory cytokine production. **(A)** Mice received subcutaneous footpad injection of Vehicle (PBS) (n=6) or ET (2 μg PA + 2 μg EF) (n=6). Paw thicknesses were measured at the indicated time points. **(B, C)** Mice received retro-orbital injection of Evans Blue (25 mg/kg) 30 min prior to subcutaneous footpad injection of Vehicle (PBS) (n=4) or ET (2 μg PA + 2 μg EF) (n=4). **(B)** Representative images of ipsilateral footpads at 5 hpi. **(C)** The concentration of Evans Blue dye in clarified tissue lysate of the footpad at 5 hpi. **(D)** Mice received subcutaneous footpad injection of Vehicle (PBS) or ET (2 μg PA + 2 μg EF). Infiltration of $CD45^+Ly6G^+$ neutrophils in the footpad was measured at 5 or 24 hpi by flow cytometry. Data is from tissue combined from 3 different animals. **(E)** Mice received subcutaneous footpad injection of Vehicle (PBS) or ET (2 μg PA + 2 μg EF). Multiplex cytokine analysis was performed in clarified lysate of the footpad harvested at 5 hpi (n=5). Statistical analysis: **(A)** Two-way ANOVA with Sidak's post-test. *p < 0.05, **p < 0.01, ****p < 0.0001. **(C)** Unpaired t-test. *p < 0.05. **(E)** Mann-Whitney test with the two-stage linear step-up procedure of Benjamini, Krieger, and Yekutieli, 5% FDR. Discoveries are marked by asterisks.

footpad. To this end, we chemically ablated nociceptive neurons using Resiniferatoxin (RTX), a potent analog of capsaicin which induces calcium overload and death of Trp_v1^+ nociceptive neurons (19). Trp_v1 is the major ion channel responsible for detecting heat. RTX-treated mice showed significantly attenuated responses on a hot plate test (**Figure 5A**), indicating ablation of Trp_v1^+ nociceptive neurons. RTX and vehicle-treated mice were rested for 4 weeks before injection with ET. Nociceptor ablation by RTX significantly attenuated paw swelling hours after ET injection, but not at later time points (**Figure 5B**). RTX treatment also significantly reduced ET-induced vascular effusion of Evans Blue dye at 5 hpi (**Figures 5C, D**).

To further confirm the contribution of nociceptive neurons, we used an orthogonal, genetic method to ablate nociceptors by conditionally expressing the A chain of Diphtheria toxin (DTA) in $Na_v1.8^+$ neurons. DTA inhibits protein translation in mammalian cells through inactivation of eukaryotic elongation factor 2 (eEF-2), causing cell death. We bred $Na_v1.8^{cre/+}$ mice with ROSA-DTA mice containing a floxed-STOP cassette, selectively killing $Na_v1.8^+$ nociceptive neurons during development (herein referred to as $Na_v1.8^{cre/+}$/DTA mice). Genetic ablation of $Na_v1.8^+$ nociceptive neurons significantly attenuated ET-induced paw swelling during the early phase but not the late phase (**Figure 5E**), phenocopying our results with RTX-treated animals. Trp_v1 and $Na_v1.8$ mark distinct but overlapping subsets of nociceptive sensory neurons.

ET-Induced Edema Is Independent of Neuronal ANTXR2, CGRP Signaling and Substance P Signaling

Previously, we found that nociceptive sensory neurons express ANTXR2 and are susceptible to intoxication by ET (8). We thus wished to determine whether direct targeting of nociceptors by ET through ANTXR2 played a role in mediating edema and swelling. To this end, we utilized conditional ANTXR2 KO mice ($Na_v1.8^{cre/+}$/$Antxr2^{fl/fl}$) lacking receptor function from $Nav1.8^+$ nociceptive neurons. We did not observe a difference in ET-induced paw swelling between $Na_v1.8^{cre/+}$/$Antxr2^{fl/fl}$ mice and their control $Na_v1.8^{+/+}$/$Antxr2^{fl/fl}$ littermates at any time point (**Supplementary Figure 1**), suggesting that ET induces edema independent of targeting neuronal ANTXR2.

The neuropeptides Calcitonin gene-related peptide (CGRP) and Substance P (SP) are major mediators of neurogenic inflammation. To determine whether CGRP or SP are involved in ET-induced edema, we utilized BIBN 4096, a small molecule antagonist of the CGRP receptor RAMP1, and Spantide I, a peptide antagonist of the SP receptor NK1R. Intraplantar administration of BIBN 4096 or Spantide I 15 min prior to ET did not significantly affect paw

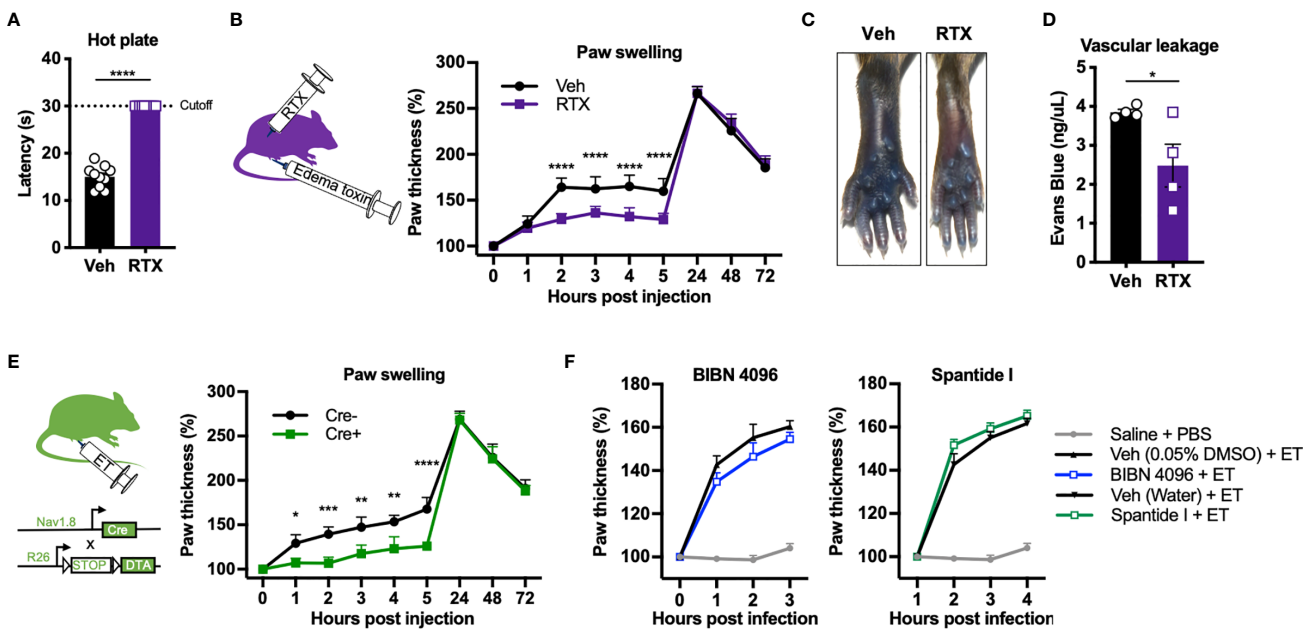

FIGURE 5 | Nociceptive neurons mediate acute edema and vascular leakage caused by Edema toxin injection. **(A)** Responses to the hot plate test was measured in mice treated with RTX or Vehicle (n=10). **(B)** Mice treated with RTX or Vehicle received subcutaneous footpad injection of ET (2 μg PA + 2 μg EF) (n=8-9). Paw thicknesses were measured at the indicated timepoints. **(C, D)** RTX- or Vehicle-treated mice received retro-orbital injection of Evans Blue (25 mg/kg) 30 min prior to subcutaneous footpad injection of ET (2 μg PA + 2 μg EF) (n=4). **(C)** Representative images of ipsilateral footpads at 5 hpi. **(D)** The concentration of Evans Blue dye in clarified tissue lysate of the footpad at 5 hpi. **(E)** $Na_v1.8^{cre/+}$/DTA (Cre+) or $Na_v1.8^{+/+}$/DTA littermate controls (Cre-) received subcutaneous footpad injection of ET (2 μg PA + 2 μg EF) (n=3-4). Paw thicknesses were measured at the indicated timepoints. **(F)** Wild-type mice received intraplantar injection of Saline, BIBN 4096 (50 pmol), the vehicle for BIBN 4096 (0.05% DMSO), Spantide I (5 nmol), or the vehicle for Spantide I (water), 15 min prior to PBS or ET (2 μg PA + 2 μg EF). The Saline + PBS group is identical in the two panels. No significant differences were detected between the respective antagonist and vehicle treatment. Statistical analysis: **(A, D)** Unpaired t-test. *$p < 0.05$. **(B, E)** Two-way ANOVA with Sidak's post-test. *$p < 0.05$, **$p < 0.01$, ***$p < 0.001$, ****$p < 0.0001$.

swelling (**Figure 5F**), suggesting that alternative neural mediators are involved in regulating the edema.

Nociceptive Neurons Modulate Neutrophil Influx Induced by Subcutaneous ET Injection

To determine whether nociceptive neurons play a role in the inflammatory response induced by ET, we administered ET into the footpad of nociceptor-ablated mice. We found that RTX treatment significantly attenuated infiltration of $CD45^+$ leukocytes and $CD45^+Ly6G^+CD11b^+$ neutrophils into the footpad at 5 hpi (**Figures 6A, B**). Levels of CXCL1 and CXCL2 were not significantly attenuated, while trending towards a decrease (**Figure 6C**). Collectively, our results suggested that nociceptive neurons regulate processes downstream of cytokine expression to impact vascular permeability, edema and cellular influx in response to ET.

Nociceptor Ablation Attenuates the Early Phase of Paw Swelling and Overall Body Weight Gain Induced by *B. anthracis* Infection

We wished to confirm whether nociceptive neurons modulate edema in a physiologically relevant context during *B. anthracis* infection. To this end, we performed subcutaneous footpad infection of *B. anthracis* in mice that underwent chemical ablation of nociceptors *via* systemic injection of RTX or genetic ablation using $Na_v1.8^{cre/+}$/DTA mice. Consistent with our observation with ET injection, paw swelling induced by *B. anthracis* was attenuated during the early hours of injection in nociceptor ablated mice (**Figures 7A, C**). *B. anthracis*-induced body weight gain was also significantly attenuated (**Figures 7B, D**) and notably beyond the early hours of infection. This observation suggested that nociceptive neurons may play a broader role in regulating body weight beyond regulating local edema during early timeframes. Nociceptor ablation did not significantly affect survival post infection (**Supplementary Figures 2A, B**). Nociceptor ablation also did not significantly affect bacterial load in the footpad or dissemination to the popliteal lymph node, liver or spleen at 5 and 48 hpi, time points at which differences in local edema in the footpad and body weight were visible, respectively (**Supplementary Figures 3A, B**).

Next, we sought to investigate whether $Trpv1^+$ dorsal root ganglia (DRG) neurons or vagal neurons specifically mediated the observed phenotype in regulating *B. anthracis*-induced edema. While DRG neurons mediate skin neurogenic inflammation, vagal ganglia neurons may also influence body fluid accumulation and sympathetic tone (20). To this end, we performed intrathecal injections of RTX to specifically ablate $Trpv1^+$ nociceptive neurons in the DRG without affecting vagal $Trpv1^+$ neurons (6). Treatment with intrathecal RTX significantly attenuated the footpad response to noxious heat (**Supplementary Figure 4**), confirming successful ablation. Paw swelling during the early hours of footpad infection with *B. anthracis* was significantly attenuated in mice treated with intrathecal RTX compared to vehicle (**Figure 7E**). We also

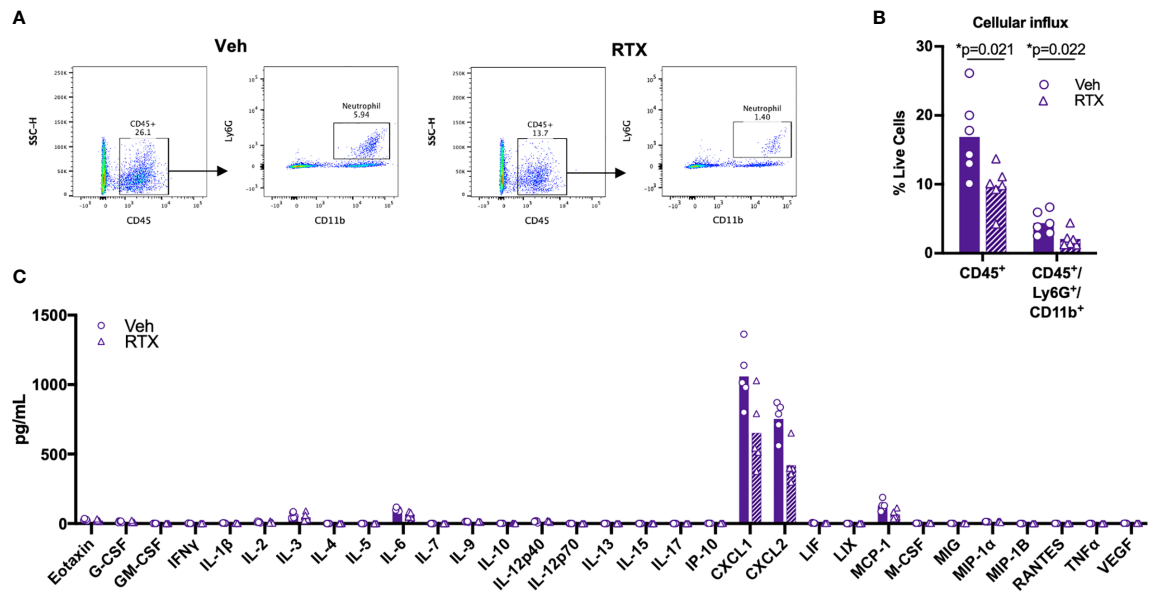

FIGURE 6 | Nociceptors contribute to Edema Toxin-induced neutrophil influx. **(A, B)** RTX- or Vehicle-treated mice received subcutaneous footpad injection of ET (2 μg PA + 2 μg EF). Infiltration of $CD45^+Ly6G^+CD11b^+$ neutrophils in the footpad was measured at 5 hpi by flow cytometry (n=6). **(A)** Representative dot plots. **(B)** Quantification of $CD45^+$ or $CD45^+Ly6G^+CD11b^+$ cells as a fraction of live cells. **(C)** RTX- or Vehicle-treated mice received subcutaneous footpad injection of ET (2 μg PA + 2 μg EF). Multiplex cytokine analysis was performed in footpad lysate harvested at 5 hpi (n=5). Statistical analysis: **(B)** Unpaired t-test with Holm-Sidak correction. *p < 0.05. **(C)** Mann-Whitney test with the two-stage linear step-up procedure of Benjamini, Krieger, and Yekutieli, 5% FDR. Discoveries are marked by asterisks.

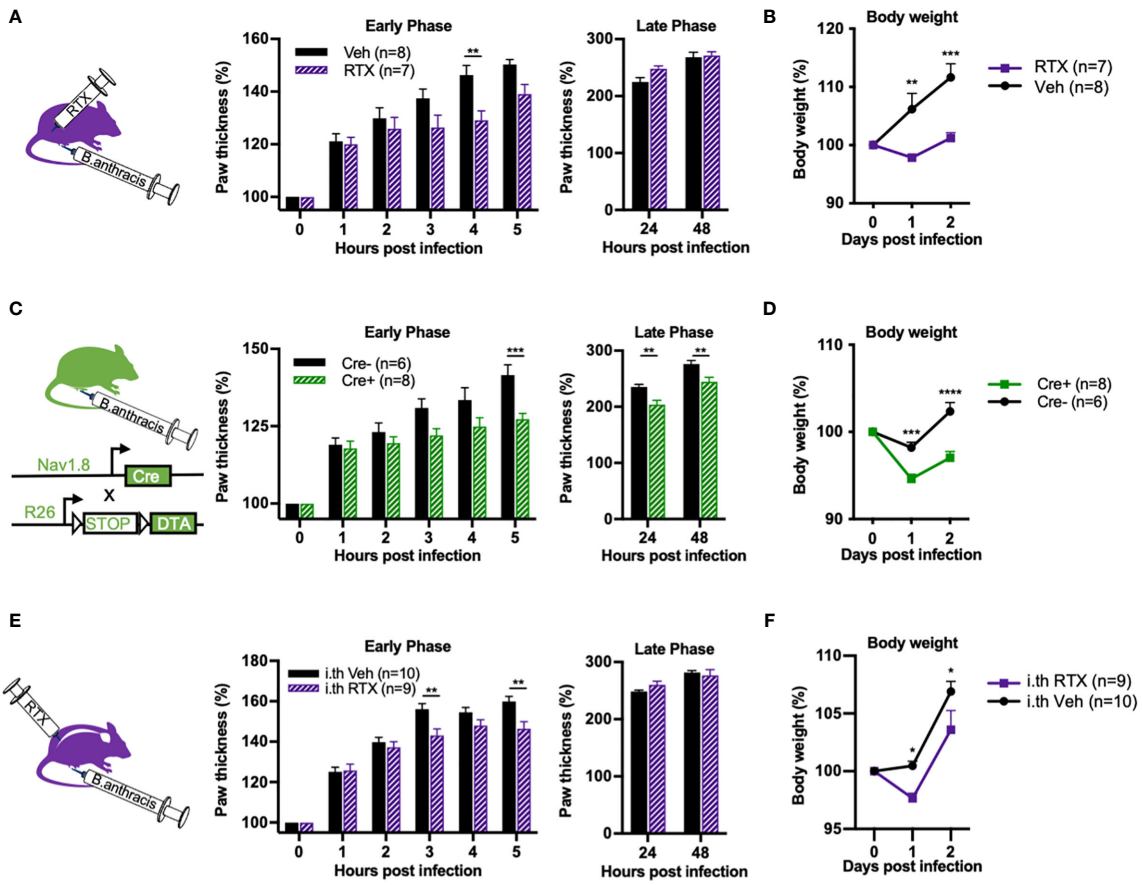

FIGURE 7 | Nociceptor ablation attenuates *Bacillus anthracis*-induced body weight gain and early phase of paw swelling. **(A, B)** Mice treated with subcutaneously administered RTX or Vehicle received subcutaneous footpad injection of 1×10^7 CFUs of *B. anthracis* Sterne. Thickness of the ipsilateral paw and body weight were measured at the indicated time points. **(C, D)** $Na_v1.8^{cre/+}$/DTA (Cre+) or $Na_v1.8^{+/+}$/DTA littermate controls (Cre-) received subcutaneous footpad injection of 1×10^7 CFUs of *B. anthracis* Sterne. Thickness of the ipsilateral paw and body weight were measured at the indicated time points. **(E, F)** Mice treated with intrathecally administered RTX or Vehicle received subcutaneous footpad injection of 1×10^7 CFUs of *B. anthracis* Sterne. Thickness of the ipsilateral paw and body weight were measured at the indicated time points. Statistical analysis: **(A–F)** Two-way ANOVA with Sidak's post-test. *p < 0.05, **p < 0.01, ***p < 0.001, ****p < 0.0001.

observed attenuation of body weight gain (**Figure 7F**), albeit to a lesser degree compared with systemic administration of RTX. Thus, while we cannot completely rule out potential contributions from vagal sensory neurons, our results indicate that $Trpv1^+$ DRG neurons play a significant role in regulating paw swelling and body weight during *B. anthracis* infection.

Altogether, our results demonstrate that nociceptor neurons modulate local tissue swelling during the early phases of *B. anthracis* infection, and also exert potentially longer lasting effects to modulate the infection-induced gain in body weight.

DISCUSSION

Beyond their role in detecting danger and signaling pain, nociceptive neurons can modulate host immune responses to bacterial infection. Here, we find that nociceptor neurons contribute to driving the immediate vascular effusion and neutrophil influx induced by ET, promoting rapid and local swelling of tissue within hours. We also found that subcutaneous infection of *B. anthracis* in mice produces mechanical allodynia, partially mediated by ET.

B. anthracis is the causative agent of anthrax. Although anthrax primarily afflicts domestic and wild herbivores, it remains a public health concern as an endemic disease in parts of the developing world and as a potential weapon of biological warfare. However, the pathogenic mechanisms by which *B. anthracis* impacts host physiology and produces major phenotypes such as edema are still being elucidated. The nervous system and neurogenic inflammation have not been previously linked to anthrax pathogenesis. One interesting observation we made was that *B. anthracis* infection led to a rapid increase in body weight, and that this phenotype was dependent on nociceptive neurons. It is interesting to note that in many other types of bacterial infections, body weight decreases rather than increases due to sickness behaviors. While the local

edema and fluid accumulation in the footpad contributed to this increase in body weight, it did not completely account for the body weight gain during infection. It is possible that nociceptive neurons innervating other organ systems could be controlling both fluid accumulation and immune cell influx in a dispersed manner.

While Edema Toxin has been long known to contribute to local tissue swelling and edema, the exact mechanisms leading to the vascular and immune changes related to this phenotype is still not completely known. We observed that ET induces significant tissue swelling, vascular leakage and cytokine production. Neurons in particular contributed to the early phase of tissue swelling and vascular leakage as well as the recruitment of neutrophils. The cellular and molecular mechanisms of how nociceptive neurons regulate ET-induced edema and immune cell influx remains to be determined. We found that blockade of CGRP signaling *via* RAMP1 using BIBN 4096, or blockade of SP signaling *via* NK1 receptors using Spantide I did not affect ET-induced swelling. However, pharmacological blockade (rather than genetic ablation) may be insufficient, or alternative receptors may be involved. Recently, SP has been found to act on MRGPRB2 in mast cells to induce neurogenic inflammation (21), and this pathway may be pursued in future studies. Vascular smooth muscle cells and vascular endothelial cells are also known targets of ET given their expression of ANTXR2 (17). Neurons may signal directly or indirectly to these cells, concurrent with ET-induced signaling, to modulate vascular inflammation. Neurons could also act on these cells to induce expression of chemokines, adhesion molecules or other factors important for recruitment of neutrophils (22).

The signals that drive nociceptive activation during *B. anthracis* infection remain to be determined. The modeling of subcutaneous footpad infection in mice showed that mechanical allodynia was induced, which could relate to the major tissue swelling that occurs locally due to the edema, or to other damage-associated signals released at the site of infection. This indicates potential pain hypersensitivity, which is in contrast to clinical reports that cutaneous anthrax in humans produce characteristically painless lesions (23, 24). This difference in pain phenotype may be due to disparate sites of infection, as our infection model was established using *B. anthracis* subcutaneous injections in mice, unlike cutaneous anthrax infections which occur through barrier-disrupted skin in humans. Different sites of infection also produce divergent pain symptoms in human, as gastrointestinal anthrax produces ulcerative lesions and abdominal pain (25). Here, we found that subcutaneous injection of ET induces expression of various cytokines including IL6, CXCL1, and CXCL2. CXCL1 in particular can directly activate DRG sensory neurons and produce hyperalgesia (26), and has been shown to contribute to the development of hyperalgesia in a model of inflammatory pain (27). ET may induce expression of these cytokines during *B. anthracis* infection in mice, which may contribute to the development of mechanical hypersensitivity. The mechanisms of pain and role of nociceptors during *B. anthracis* infection in humans remain to be further investigated.

In summary, we report a novel role for nociceptive neurons in the early phase of local edema and cellular influx induced by ET injection and *B. anthracis* infection. Therefore, neurogenic inflammation could play a key part of pathology and inflammation during infection. However, many open questions remain. The overall role of early and later stage edema in driving *B. anthracis* infection remains to be defined, despite it being a common feature of anthrax and the known importance of ET as a critical virulence factor. We did not find evidence that the edema regulated by nociceptors significantly influences bacterial dissemination or infection-induced mortality. Alternatively, *B. anthracis* may be taking advantage of the increase in nutrient availability that results from the increasing leakiness of the vasculature, which is partially mediated through nociceptive neurons. Altogether, our findings highlight nociceptors as a key modulator of early inflammation and edema induced by ET, and suggest a complex interplay between nociceptive neurons, immune cells and bacterial toxins in anthrax pathogenesis.

DATA AVAILABILITY STATEMENT

The raw data supporting the conclusions of this article will be made available by the authors, without undue reservation.

ETHICS STATEMENT

The animal study was reviewed and approved by Institutional Animal Care and Use Committee (IACUC) at Harvard Medical School.

AUTHOR CONTRIBUTIONS

NY and IC conceived the project. NY, DN, LD, MH, AK-C, and VT performed experiments and data analysis. JP advised experiments and provided *B. anthracis* strains. NY and IC wrote the manuscript with input from all authors. All authors contributed to the article and approved the submitted version.

FUNDING

This study was supported by the National Institutes of Health (NIH) (DP2AT009499, R01AI130019), the Burroughs Wellcome Fund to IC, and an NIH T32 training grant (5T32AG000222) to NY.

SUPPLEMENTARY MATERIAL

The Supplementary Material for this article can be found online at: https://www.frontiersin.org/articles/10.3389/fimmu.2021.642373/full#supplementary-material

REFERENCES

1. Chiu IM, Heesters BA, Ghasemlou N, Von Hehn CA, Zhao F, Tran J, et al. Bacteria Activate Sensory Neurons That Modulate Pain and Inflammation. *Nature* (2013) 501:52–7. doi: 10.1038/nature12479
2. Blake KJ, Baral P, Voisin T, Lubkin A, Pinho-Ribeiro FA, Adams KL, et al. Staphylococcus Aureus Produces Pain Through Pore-Forming Toxins and Neuronal TRPV1 That is Silenced by QX-314. *Nat Commun* (2018) 9:1–15. doi: 10.1038/s41467-017-02448-6
3. Pinho-Ribeiro FA, Baddal B, Haarsma R, O'Seaghdha M, Yang NJ, Blake KJ, et al. Blocking Neuronal Signaling to Immune Cells Treats Streptococcal Invasive Infection. *Cell* (2018) 173:1083–97. doi: 10.1016/j.cell.2018.04.006
4. Pinho-Ribeiro FA, Verri WA, Chiu IM. Nociceptor Sensory Neuron–Immune Interactions in Pain and Inflammation. *Trends Immunol* (2017) 38:5–19. doi: 10.1016/j.it.2016.10.001
5. Baral P, Umans BD, Li L, Wallrapp A, Bist M, Kirschbaum T, et al. Nociceptor Sensory Neurons Suppress Neutrophil and γδ T Cell Responses in Bacterial Lung Infections and Lethal Pneumonia. *Nat Med* (2018) 24:417–26. doi: 10.1038/nm.4501
6. Lai NY, Musser MA, Pinho-Ribeiro FA, Baral P, Jacobson A, Ma P, et al. Gut-Innervating Nociceptor Neurons Regulate Peyer's Patch Microfold Cells and SFB Levels to Mediate Salmonella Host Defense. *Cell* (2019) 180:33–49. doi: 10.1016/j.cell.2019.11.014
7. Sweeney DA, Hicks CW, Cui X, Li Y, Eichacker PQ. Anthrax Infection. *Am J Respir Crit Care Med* (2011) 184:1333–41. doi: 10.1164/rccm.201102-0209CI
8. Yang NJ, Isensee J, Neel D, Liu SM, Zhang HXB, Belu A, et al. Anthrax Toxin as a Molecular Platform to Target Nociceptive Neurons and Modulate Pain. *bioRxiv* (2020). doi: 10.1101/2020.03.28.004150
9. Leppla SH. Anthrax Toxin Edema Factor: A Bacterial Adenylate Cyclase That Increases Cyclic AMP Concentrations of Eukaryotic Cells. *PNAS* (1982) 79:3162–6. doi: 10.1073/pnas.79.10.3162
10. Firoved AM, Miller GF, Moayeri M, Kakkar R, Shen Y, Wiggins JF, et al. Bacillus Anthracis Edema Toxin Causes Extensive Tissue Lesions and Rapid Lethality in Mice. *Am J Pathol* (2005) 167:1309–20. doi: 10.1016/S0002-9440(10)61218-7
11. Guichard A, McGillivray SM, Cruz-Moreno B, van Sorge NM, Nizet V, Bier E. Anthrax Toxins Cooperatively Inhibit Endocytic Recycling by the Rab11/Sec15 Exocyst. *Nature* (2010) 467:854–8. doi: 10.1038/nature09446
12. Tessier J, Green C, Padgett D, Zhao W, Schwartz L, Hughes M, et al. Contributions of Histamine, Prostanoids, and Neurokinins to Edema Elicited by Edema Toxin From Bacillus Anthracis. *Infect Immun* (2007) 75:1895–903. doi: 10.1128/IAI.01632-06
13. Leysath CE, Phillips DD, Crown D, Fattah RJ, Moayeri M, Leppla SH. Anthrax Edema Factor Toxicity Is Strongly Mediated by the N-end Rule. *PloS One* (2013) 8:e74474. doi: 10.1371/journal.pone.0074474
14. Choo M-K, Sano Y, Kim C, Yasuda K, Li X-D, Lin X, et al. TLR Sensing of Bacterial Spore-Associated RNA Triggers Host Immune Responses With Detrimental Effects. *J Exp Med* (2017) 214:1297–311. doi: 10.1084/jem.20161141
15. Tallent SM, Kotewicz KM, Strain EA, Bennett RW. Efficient Isolation and Identification of Bacillus Cereus Group. *J AOAC Int* (2012) 95:446–51. doi: 10.5740/jaoacint.11-251
16. Staab A, Plaut RD, Pratt C, Lovett SP, Wiley MR, Biggs TD, et al. Whole-Genome Sequences of Variants of Bacillus Anthracis Sterne and Their Toxin Gene Deletion Mutants. *Genome Announc* (2017) 5(45):e01231–17. doi: 10.1128/genomeA.01231-17
17. Liu S, Zhang Y, Moayeri M, Liu J, Crown D, Fattah RJ, et al. Key Tissue Targets Responsible for Anthrax-Toxin-Induced Lethality. *Nature* (2013) 501:63–8. doi: 10.1038/nature12510
18. Baldari CT, Tonello F, Paccani SR, Montecucco C. Anthrax Toxins: A Paradigm of Bacterial Immune Suppression. *Trends Immunol* (2006) 27:434–40. doi: 10.1016/j.it.2006.07.002
19. Szallasi A, Blumberg PM. Vanilloid (Capsaicin) Receptors and Mechanisms. *Pharmacol Rev* (1999) 51:159–212.
20. Chen H, Hu B, Lv X, Zhu S, Zhen G, Wan M, et al. Prostaglandin E2 Mediates Sensory Nerve Regulation of Bone Homeostasis. *Nat Commun* (2019) 10:181. doi: 10.1038/s41467-018-08097-7
21. Green DP, Limjunyawong N, Gour N, Pundir P, Dong X. A Mast-Cell-Specific Receptor Mediates Neurogenic Inflammation and Pain. *Neuron* (2019) 101:412–20.e3. doi: 10.1016/j.neuron.2019.01.012
22. Kim ND, Luster AD. The Role of Tissue Resident Cells in Neutrophil Recruitment. *Trends Immunol* (2015) 36:547–55. doi: 10.1016/j.it.2015.07.007
23. Karahocagil MK, Akdeniz N, Akdeniz H, Calka O, Karsen H, Bilici A, et al. Cutaneous Anthrax in Eastern Turkey: A Review of 85 Cases. *Clin Exp Dermatol* (2008) 33:406–11. doi: 10.1111/j.1365-2230.2008.02742.x
24. Denk A, Tartar AS, Ozden M, Demir B, Akbulut A. Cutaneous Anthrax: Evaluation of 28 Cases in the Eastern Anatolian Region of Turkey. *Cutan Ocul Toxicol* (2016) 35:177–80. doi: 10.3109/15569527.2015.1067818
25. Dixon TC, Meselson M, Guillemin J, Hanna PC. Anthrax. *N Engl J Med* (1999) 341:815–26. doi: 10.1056/NEJM199909093411107
26. Qin X, Wan Y, Wang X. CCL2 and CXCL1 Trigger Calcitonin Gene-Related Peptide Release by Exciting Primary Nociceptive Neurons. *J Neurosci Res* (2005) 82:51–62. doi: 10.1002/jnr.20612
27. Cao D-L, Qian B, Zhang Z-J, Gao Y-J, Wu X-B. Chemokine Receptor CXCR2 in Dorsal Root Ganglion Contributes to the Maintenance of Inflammatory Pain. *Brain Res Bull* (2016) 127:219–25. doi: 10.1016/j.brainresbull.2016.09.016

Conflict of Interest: The authors declare that the research was conducted in the absence of any commercial or financial relationships that could be construed as a potential conflict of interest.

frontiers in Immunology

ORIGINAL RESEARCH
published: 27 August 2021
doi: 10.3389/fimmu.2021.650176

Prevention of Diabetes-Associated Cognitive Dysfunction Through Oral Administration of Lipopolysaccharide Derived From *Pantoea agglomerans*

Haruka Mizobuchi[1]*, *Kazushi Yamamoto*[1], *Masashi Yamashita*[1], *Yoko Nakata*[2], *Hiroyuki Inagawa*[1,2,3], *Chie Kohchi*[1,2] and *Gen-Ichiro Soma*[1,2,3]

[1] Control of Innate Immunity, Collaborative Innovation Partnership, Kagawa, Japan, [2] Research and Development Department Macrophi Inc., Kagawa, Japan, [3] Research Institute for Healthy Living, Niigata University of Pharmacy and Applied Life Sciences, Niigata, Japan

OPEN ACCESS

Edited by:
Michael D. Burton,
The University of Texas at Dallas,
United States

Reviewed by:
Gyorgy Fejer,
University of Plymouth,
United Kingdom
Zhongcheng Xin,
Second Hospital of Tianjin Medical University, China

***Correspondence:**
Haruka Mizobuchi
mizobuchi@shizenmeneki.org
orcid.org/0000-0002-6667-4820

Specialty section:
This article was submitted to Molecular Innate Immunity, a section of the journal Frontiers in Immunology

Received: 06 January 2021
Accepted: 13 August 2021
Published: 27 August 2021

Citation:
Mizobuchi H, Yamamoto K, Yamashita M, Nakata Y, Inagawa H, Kohchi C and Soma G-I (2021) Prevention of Diabetes-Associated Cognitive Dysfunction Through Oral Administration of Lipopolysaccharide Derived From Pantoea agglomerans. Front. Immunol. 12:650176. doi: 10.3389/fimmu.2021.650176

Diabetes-related cognitive dysfunction (DRCD) is a serious complication induced by diabetes. However, there are currently no specific remedies for DRCD. Here, we show that streptozotocin-induced DRCD can be prevented without causing side effects through oral administration of lipopolysaccharide (LPS) derived from *Pantoea agglomerans*. Oral administration of LPS (OAL) prevented the cerebral cortex atrophy and tau phosphorylation induced by DRCD. Moreover, we observed that neuroprotective transformation of microglia (brain tissue-resident macrophages) is important for preventing DRCD through OAL. These findings are contrary to the general recognition of LPS as an inflammatory agent when injected systemically. Furthermore, our results strongly suggest that OAL promotes membrane-bound colony stimulating factor 1 (CSF1) expression on peripheral leukocytes, which activates the CSF1 receptor on microglia, leading to their transformation to the neuroprotective phenotype. Taken together, the present study indicates that controlling innate immune modulation through the simple and safe strategy of OAL can be an innovative prophylaxis for intractable neurological diseases such as DRCD. In a sense, for modern people living in an LPS-depleted environment, OAL is like a time machine that returns microglia to the good old LPS-abundant era.

Keywords: microglia, lipopolysaccharide, oral administration, neuroprotection, cognitive dysfunction, dementia

INTRODUCTION

Diabetes affects 463 million people worldwide, and one of its more serious complications is diabetes-related cognitive dysfunction (DRCD) (1). However, there is still no radical preventive or curative treatment for DRCD. Accordingly, its prevention is a crucial to sustained global health.

To address this problem, we focused on oral administration of lipopolysaccharide (LPS) derived from *Pantoea agglomerans*. Our previous study showed that oral administration of LPS derived

from *P. agglomerans* (OAL) prevents high fat diet-induced cognitive dysfunction (2). In addition, *P. agglomerans* is reportedly used as a food preservative (3, 4), and the safety of OAL is objectively guaranteed based on Organization for Economic Co-operation and Development standards (5–7). Based on these findings, we hypothesized that OAL could prevent DRCD.

Here, we demonstrate the effect of OAL on preventing DRCD using an intracerebroventricular injection model of the diabetes inducer, streptozotocin (STZ), which has already been established as a DRCD model (8–10). Furthermore, in order to elucidate the DRCD prevention mechanism utilized by OAL, we depleted microglia, which are brain tissue macrophages, and performed genetic analysis of isolated microglia. The results revealed that transformation to neuroprotective microglia is required for DRCD prevention by OAL. Importantly, it is strongly suggested that signal activation of colony stimulating factor 1 receptor (CSF1R) by the membrane-bound form CSF1 is involved in this transformation to neuroprotective microglia.

MATERIALS AND METHODS

Animals and Tissue Sample Preparation

Six-week-old male C57BL/6 mice (20–22 g) were purchased from SLC, Inc., Shizuoka, Japan, and were acclimated for 1 week. All mice (3–5 mice per cage) were maintained under specific pathogen-free conditions in a temperature- and humidity-controlled room under a 12-h light/dark cycle with unrestricted access to food and water. Mouse diet D12450B was purchased from Research Diets, Inc., New Brunswick, NJ, USA. At the end of the experiments, mice were anaesthetized under 4% isoflurane vapor using the simple inhalation anesthesia device NARCOBIT-E (Natsume Seisakusho Co., Ltd., Tokyo, Japan) and euthanized by cardiac puncture whole blood collection. The animal experiments were reviewed and approved by the Animal Care and Use Committee of the Control of Innate Immunity CIP (Approval No. 18-04, 18-12, 18-13, and 20-01).

The experiment was carried out according to the Law for the Humane Treatment and Management of Animals Standards Relating to the Care and Management of Laboratory Animals and Relief of Pain (Ministry of the Environment, Japan), the Fundamental Guidelines for Proper Conduct of Animal Experiments and Related Activities in Academic Research Institutions (Ministry of Education, Culture, Sports, Science and Technology, Japan), and the Guidelines for Proper Conduct of Animal Experiments (the Science Council of Japan). Animal health and well-being was also assessed in accordance with the guidelines described above.

At the end of the experiment, whole blood was collected by cardiac puncture under anesthesia with 4% isoflurane vapor. Plasma/serum were collected after centrifugation for 10 min at 500 ×*g* for cytokine analysis and limulus amebocyte lysate (LAL) assay. Peripheral white blood cells were collected for RNA analysis. Bone marrows (BMs) were collected for isolation of $CD11b^+$ cells, RNA analysis, and primary culture. Hippocampuses were collected and frozen at -80°C for cytokine analysis. Brains were collected for histopathological analysis and isolation of microglia.

LPS Treatment

Purified LPS derived from *P. agglomerans* (Macrophi Inc., Kagawa, Japan) was used in this study. LPS derived from *P. agglomerans* was purified to over 99% according to the methods described previously (11). LPS derived from *P. agglomerans* has very low nucleic acid and protein contamination [protein contamination was 0.5%, nucleic acid contamination was less than 0.35% (w/w)] and activates macrophages in very small amounts (1.6 ng/ml) (11). It was confirmed that the LPS content of the D12450B diet was lower than that of the common mouse diet MF (Oriental Yeast Co., Ltd, Tokyo, Japan) or CE-2 (CLEA Japan Inc., Tokyo, Japan) (**Supplementary Table 1**). For oral LPS administration, LPS was dissolved in drinking water (sterile distilled water) and applied at 1 mg/kg body weight (BW)/day. The dose of LPS was determined to be the sufficient dose required to achieve preventive effects as estimated from previous studies (2, 12). The drinking water was changed weekly and the concentration of LPS was adjusted according to the average body weight and amount of water consumption. We previously confirmed that the LPS in drinking water was not significantly degraded in a week (12).

For the DRCD model, LPS was orally administrated to mice 1 week before STZ-injection until the end of the experiment (n = 17–19). For OAL without intracerebroventricular STZ injection, naïve mice were orally administered LPS (1 mg/kg/day, for 1 week) (n = 5). For intraperitoneal administration of LPS, naïve mice were intraperitoneally injected with LPS (4 mg/kg BW, single-dose) (n = 5), and samples were collected 4 h after LPS injection.

Intracerebroventricular STZ Injection

STZ was purchased from Sigma-Aldrich, St Louis, MO, USA. Under anesthesia with 4% isoflurane vapor, mice were fixed using the brain stereotaxic apparatus SR-5M-HT (Narishige, Tokyo, Japan) and administrated a single injection of STZ (6.6 mg/kg, dissolved in saline 5 μl) into the right lateral ventricle with the microinjector, IMS-20, and micromanipulator SMM-100 (Narishige). The stereotaxic coordinates were + 0.3 mm anterior, + 1.0 mm lateral (right) and + 2.5 mm ventral from bregma. After the skin suture, antibiotic ointment (20 mg/g Chloramphenicol, 5 mg/g Fradiomycin, 100,000 U/g Nystatin, Daiichi Sankyo Healthcare Co., Ltd, Tokyo, Japan) was dabbed on the wound. Control sham mice were administrated 5 μl saline into the right lateral ventricle. After the surgery, mice were monitored daily for pain/discomfort and infections in accordance with the guidelines described above. We checked for proper placement of the needle by delivering 7 μl of 5% Trypan Blue Dye (Nacalai, Kyoto, Japan) (**Supplementary Figure 1**).

Microglia Depletion

The CSF1R inhibitor PLX3397 (Pexidartinib) was purchased from Chemgood, Glen Allen, VA, USA. PLX3397 was formulated based on the D12450B diet (Research Diets) at a concentration of 400 mg/kg chow. The components of the PLX3397-containing diet are shown in **Supplementary**

Table 2. Mice were orally administered PLX3397 and LPS 1 week before STZ-injection until the end of the experiment.

Morris Water Maze (MWM) Test

To assess spatial learning and memory, the MWM test was carried out 3 weeks after STZ-injection as previously described (2), with minor modifications. Briefly, the experimental apparatus consisted of a circular tank 100 cm in diameter and 40 cm in height filled with water to 30 cm, maintained at 23 ± 1°C and rendered opaque with white ink. The area of the pool was conceptually divided into four equal quadrants, and cards with different shapes (circle, square, triangle or cross) were placed on the wall of each quadrant. A removable circular platform 10 cm in diameter was submerged 1 cm below the water surface and placed approximately in the midpoint of one quadrant, defined as the target quadrant. Each mouse consecutively received a pre-training session (1 day), training session (4 days), and probe session (1 day).

One day before the first training session, each mouse received a pre-training session to make it aware of the escape platform. The mouse was put on the platform for 20 s, given a 30 s free swim, and then assisted in swimming back to the platform. The next day, the first training session was conducted to assess spatial learning ability. From the next day, training session continued for four consecutive days. One each trial, the mouse was released into the water at a randomly assigned starting position, facing the pool's wall. The mouse was given 60 s to find the platform and was allowed to stay on it for 20 s after reaching the escape platform. The spatial learning ability of each mouse was identified as the time elapsed between releasing and locating the platform, defined as escape latency. If the mouse failed to find the platform within 60 s, it was gently guided to the platform and kept there for 20 s, and the escape latency was recorded as 60 s. Each mouse underwent four trials per day, and the average value of the escape latency was calculated. One day after the last training session, the probe test was performed to assess the spatial reference memory ability of the mice. The platform was removed from the pool, and each mouse was placed in the pool at a starting position located opposite the target quadrant and allowed to swim freely for 60 s. The time spent swimming in the target quadrant was recorded. A video camera was hung above the center of the pool to record the swimming paths of the mice. The swimming trajectory was visualized and the swimming distance/velocity was measured using AnimalTracker software (13).

Histochemical Analysis

Brains were fixed with 4% paraformaldehyde and embedded in paraffin. The cut surface was unified at the same position of the hippocampal dentate gyrus. Klüver-Barrera staining, Gallyas-Braak staining, and immunostaining of Iba1 were performed with the standard procedure. Briefly, Klüver-Barrera staining was performed as follows. The tissues were stained with 0.1% Luxol fast blue at 56°C overnight and differentiated in 0.05% lithium carbonate solution for 30 s. Then, the tissues were counterstained with 0.1% cresyl violet acetate for 10 min. For Gallyas-Braak staining, the tissues were placed in 5% periodic acid for 5 min and incubated in silver iodide solution for 1 min. After washing in 0.5% acetic acid, the tissues were placed in developer solution for 10–20 min. After washing in 0.5% acetic acid, the tissues were incubated in 0.1% gold chloride for 5 min. Then, the tissues were fixed in 1% sodium thiosulfate for 5 min and counterstained with 0.1% nuclear fast red for 2 min.

For immunostaining of Iba1, the tissues were incubated with anti-Iba1 antibody at room temperature (RT) for 15 min (Wako, Osaka, Japan) after blocking. Then, the tissues were incubated with HRP-conjugated anti-rabbit IgG antibody at 4°C for 1 h (Leica Biosystems, Buffalo Grove, IL, USA). Enzymatic color development was performed using DAB (Leica Biosystems).

To evaluate cerebral atrophy, the thickness of the cerebral cortex was measured using imaging software NIS-Element (Nikon, Tokyo, Japan) in the Klüver-Barrera stained brains. For quantitative analysis of tau inclusion, argyrophilic grains were counted in Gallyas-Braak stained brains.

Isolation of Primary Microglia From Adult Mouse

Primary microglial cells were isolated from adult mouse brain by enzymatic digestion as described previously (14), with minor modifications. Briefly, the brain was removed and kept in ice cold PBS. The brain tissue was chopped finely with a fine sharp razor. The whole brain homogenate was then incubated in DMEM containing 1.2 units/ml dispase II, 1 mg/ml papain (Sigma-Aldrich), 100 units/ml penicillin and 100 μg/ml streptomycin (Thermo Fisher Scientific, Waltham, MA, USA), 20 units/ml RNase inhibitor (Promega, Madison, WI, USA) and 10 units/ml DNase I (Takara Bio, Shiga, Japan) for 30 min at 37°C. The digestion was terminated by the addition of PBS containing 10% fetal bovine serum (FBS; Invitrogen, Carlsbad, CA, USA), and the cells were then centrifuged for 5 min at 300 ×*g* at RT. The pellets were resuspended in PBS containing 0.5% bovine serum albumin (BSA; Sigma-Aldrich) and 2 mM EDTA (Wako), then centrifuged for 5 min at 300 ×*g* at RT. The cell suspension was passed through a 70-μm cell strainer (Corning, Durham, NC, USA) and myelin was removed using the debris removal solution (Miltenyi Biotec, Bergisch Gladbach, Germany). After myelin removal, the cells were incubated with anti-CD11b antibodies conjugated to magnetic beads (20 μl/brain; Miltenyi Biotec) in PBS containing 0.5% BSA and 2 mM EDTA for 15 min at 4°C. After washing, the $CD11b^+$ cells were separated using autoMACS® proseparator (Miltenyi Biotec) and used as microglia. As a control, $CD11b^+$ cells were isolated from BM in a similar manner.

Flow-Cytometric Analysis of Iba1

Isolated $CD11b^+$ cells from brain or BM were fixed and permeabilized using fixation/permeabilization solution (BD Biosciences, San Jose, CA, USA) for 20 min at 4°C. After washing, the cells were incubated with anti-Iba1 antibody (Wako) for 30 min at 4°C followed by incubation with Alexa Fluor 555-conjugated anti-rabbit IgG (Thermo Fisher Scientific) for 30 min at 4°C. The median of fluorescent intensity (MFI) was measured in total 5,000-count cells using a Beckman Coulter Gallios flow cytometer and Kaluza for Gallios software version 1.3 (Beckman Coulter, Indianapolis, IN, USA).

Determination of $A\beta_{1\text{-}42}$ and Cytokines (ELISA)

The levels of $A\beta_{1\text{-}42}$ in isolated microglia were determined using a commercial ELISA kit (Wako). Protein was extracted from isolated microglia in ice-cold 70% (v/v) formic acid (Wako, Tokyo, Japan) followed by centrifugation at 20,000 ×*g* for 1 h at 4°C. The supernatant was neutralized with a 20-fold dilution in 1M Tris buffer, and used for $A\beta_{1\text{-}42}$ ELISA. The concentration of $A\beta_{1\text{-}42}$ was normalized against the number of isolated microglia.

The levels of IL-6 and TNF-α in plasma were determined using a commercial ELISA kit (BioLegend, San Diego, CA, USA). The levels of CSF1 in plasma and brain were determined using a commercial ELISA kit (R&D systems, Minneapolis, MN, USA). The snap-frozen brain tissues were homogenized in ice-cold PBS containing 1% protease inhibitor cocktail (GE Healthcare UK Ltd., Buckinghamshire, UK) and 1% phosphatase inhibitor cocktail (Nacalai), followed by sonication for 5 min and centrifugation at 12,000 ×*g* for 10 min at 4°C. The supernatant was used for CSF1 ELISA. The total protein concentration in each sample was determined by a BCA assay kit (Thermo Fisher Scientific) and the concentration of target protein in tissues were reported as pictograms of cytokine relative to the protein content. Absorbance was measured using the iMark microplate reader (BIO RAD, Hercules, CA, USA), and data was analyzed using the Microplate Manager 6 software (BIO RAD).

Microarray Analysis

Microarray analysis was performed at the Cell Innovator, Fukuoka, Japan. Briefly, the RNA samples of microglia were quantified with Agilent 2200 TapeStation (Agilent Technologies, Santa Clara, CA, USA). Each 50 ng of total RNA was labeled using a Low-Input QuickAmp Labeling Kit (Agilent Technologies). The RNA was hybridized with SurePrint G3 Mouse GE microarray 8 × 60K v2 (Agilent Technologies) using pooled sample (n = 4), and the signals were detected using a DNA microarray scanner (Agilent Technologies). Data was quantified by Feature Extraction software (Agilent Technologies). Normalization was performed by a quantile algorithm with statistical processing software R [R Core Team (2019). *R: A Language and Environment for Statistical Computing.* R Foundation for Statistical Computing, Vienna, Austria].

The ratio (non-log-scaled fold change) and Z scores (15) were calculated from the normalized signal intensities of each probe for comparison between control and experimental samples. Then, the criteria for regulated genes were defined as follows: for upregulated genes, Z score ≧ 2.0 and ratio ≧ 1.5-fold; for downregulated genes, Z score ≦ 2.0 and ratio ≦ 0.66 (16). The heat map was created by using the distance from the median of the log2 converted signal value with MultiExperiment Viewer (MeV) (17, 18).

Quantitative RT-PCR

RNA was extracted using the RNeasy micro kit (QIAGEN, Hilden, Germany) and cDNA was synthesized using the reverse transcription using ReverTra Ace qPCR RT Master Mix (TOYOBO, Osaka, Japan), according to the manufacturer's instructions. Real-time PCR assay was carried out using 2 μl of cDNA as the template and 10 μl of Power SYBR Green PCR Master Mix (Thermo Fisher Scientific) on the Stratagene Mx 3005P QPCR System (Agilent Technologies, Santa Clara, CA, USA).

The primers are listed in **Supplementary Table 3**. *m-CSF1* and *s-CSF1* were distinguished by specific primers (19). The data was analyzed based on $2^{-\Delta\Delta Ct}$ method and normalized by GADPH expression using the MxPro software version 4.10 (Agilent Technologies). The thermal cycling conditions for the PCR were 95°C for 10 min for polymerase activation, followed by 45 cycles of 95°C for 15 s for denaturation, and 60°C for 1 min for extension.

LAL Assay

The total abundance of LPS in serum was analyzed as described previously (2) using a kinetic turbidimetric assay with the Limulus Amebocyte Lysate (LAL) assay kit and a Toxinometer ET-6000 computer operated kinetic incubating tube reader (Wako). The serum was diluted 1:10 in pyrogen-free water (Otsuka Pharmaceutical Factory, Inc., Tokushima, Japan) and preheated to 70°C for 10 min prior to analysis. Data was analyzed using the Toximaster QC7 software.

Cell Culture

Bone marrows were collected from femurs by flushing with PBS. After RBC lysis, BMC (1×10^7 cells/ml) were seeded in 96-well tissue culture plates (n = 5) and cultured in Dulbecco's modified Eagle's medium (Wako, Osaka, Japan) supplemented with 10% fetal bovine serum (Sigma-Aldrich, St Louis, MO, USA), 100 U/ml penicillin and 100 μg/ml streptomycin (Life Technologies, Carlsbad, CA, USA), at 37°C in 5% CO_2. To evaluate CSF1 production by LPS, BMC were treated with or without LPS (1–10^4 pg/ml, purified LPS derived from *Pantoea agglomerans*, Macrophi Inc., Kagawa, Japan). RNA and culture supernatants were collected at 4 h and 24 h after the last LPS treatment, respectively.

The murine microglial cell line C8-B4 microglia, which was established from brain cerebella, was purchased from the American Type Culture Collection, Manassas, VA, USA. C8-B4 microglia (2×10^5 cells/ml) were seeded in 12-well tissue culture plates (n = 3, in triplicate) and cultured in Dulbecco's modified Eagle's medium (Wako) supplemented with 10% fetal bovine serum (Sigma-Aldrich), 100 U/ml penicillin and 100 μg/ml streptomycin (Life Technologies), at 37°C in 5% CO_2. C8-B4 microglia were treated with or without 80 ng/ml CSF1 (Promega). After 16 h of incubation, the culture supernatant was collected and RNA was extracted from the C8-B4 microglia.

For the phagocytosis assay, C8-B4 microglia were incubated with HiLyte Fluor 488-labeled $A\beta_{1\text{-}42}$ (1 μg/ml; AnaSpec, Fremont, CA, USA) or fluorescent latex beads (Fluoresbrite YG Microspheres 2.0 μm; Polysciences, Warrington, PA, USA) at a cell/bead ratio of 1:5 for 3 h after 16 h of treatment with CSF1. After washing with PBS, C8-B4 microglia were detached by 0.25% trypsin treatment (Life Technologies), and the MFI of phagocytosed beads in the cells were measured using a Beckman

Coulter Gallios flow cytometer with Kaluza software (Beckman Coulter).

To evaluate the neuroprotective effect of MCS, a murine neuroblast cell line Neuro-2a, which was established from brain neuroblastoma, was cultured with CSF1-treated MCS. Neuro-2a cells were provided from the Japanese Collection of Research Bioresources Cell Bank, Osaka, Japan. Neuro-2a cells were seeded in 24-well tissue culture plates (4×10^5 cells/ml) and pre-cultured in Eagle's minimal essential medium with non-essential amino acids (Wako) supplemented with 10% fetal bovine serum (Sigma-Aldrich), 100 U/ml penicillin and 100 µg/ml streptomycin (Life Technologies), at 37°C in 5% CO_2 for 24 h (n = 3). Then, the medium was replaced by CSF1-treated MCS. After culturing with CSF-1 treated MCS for 24 h, 400 µM STZ (Sigma-Aldrich) was added to the culture medium, and Neuro-2a cells were cultured for another 24 h. Finally, the cell number was counted after detachment by treatment with 0.25% trypsin for 2 min, and the survival rate was calculated by staining with Trypan Blue Dye (Nacalai).

Statistical Analysis

Statistical analysis was performed using the GraphPad Prism 6.0 software package (GraphPad Software Inc., San Diego, CA). Results were presented as the mean ± standard error of the mean (SE). The differences between the groups of mice were analyzed by one-way ANOVA followed by Tukey's multiple comparisons test or two-way ANOVA followed by Sidak multiple comparisons test. Student's t test was used to compare differences from two independent groups. A p-value < 0.05 was considered significantly different. Representative experiments were conducted at least twice, independently.

RESULTS

Prevention of DRCD by OAL

To demonstrate DRCD prevention through OAL, spatial learning memory was evaluated using the Morris water maze (MWM) procedure with the STZ-induced DRCD model (**Figure 1A**). In training session, STZ-injected mice showed reduced learning ability as their escape latency was significantly longer than saline-injected controls and LPS-treated mice. By contrast, the loss of learning ability was prevented by OAL. The escape latency of LPS-treated mice was comparable to saline-injected controls (**Figure 1B**). In probe test, the time spent in the target quadrant of STZ-injected mice was significantly shorter than saline-injected controls, indicating the declined memory performance. On the contrary, LPS-treated mice did not decline memory ability as they exhibited significantly longer time spent in the target quadrant than STZ-injected mice (**Figure 1C**). As shown in **Figure 1C**, it

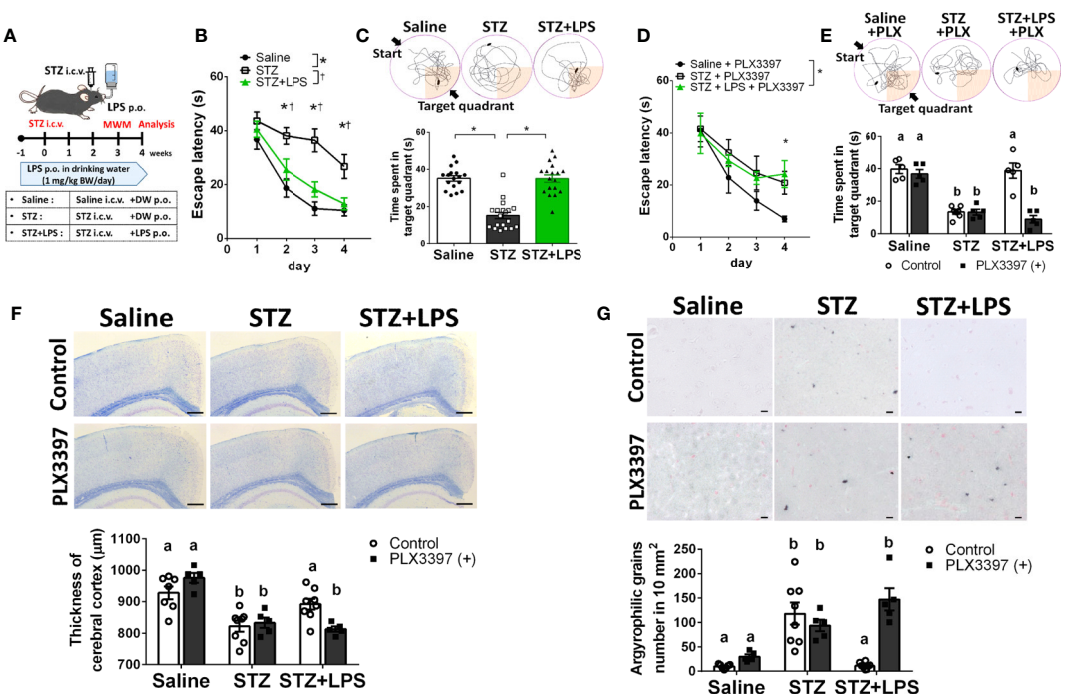

FIGURE 1 | Microglia are indispensable for preventing diabetes-related cognitive dysfunction (DRCD) through oral administration of LPS (OAL). **(A)** The experimental schedule of DRCD and OAL. **(B, C)** Prevention of deterioration of the learning ability and memory performance induced by OAL (n = 17–19). **(D, E)** PLX3397 reversed the prevention of DRCD by OAL (n = 5–7). **(F)** Prevention of cerebral cortex atrophy by OAL (n = 5–8). Bars, 200 µm. **(G)** Prevention of accumulation of argyrophilic grains by OAL (n = 5–8). Bars, 10 µm. Means ± SE are presented. $^{*,\dagger}p$ or $^{a,b}p$ < 0.05 for one-way ANOVA with Tukey's multiple comparisons or two-way ANOVA with Sidak multiple comparisons. DW, distilled water; i.c.v., intracerebroventricular; p.o., per os.

was evident from the swimming trajectory that LPS-treated mice memorized the target location. Furthermore, the athletic ability such as velocity and total swimming distance did not significantly vary between the groups (**Supplementary Figure 2**). Therefore, these results indicate that OAL prevents DRCD.

Microglia Are Indispensable for Preventing DRCD Through OAL

To investigate whether microglia are necessary for DRCD prevention through OAL, we depleted microglia using the PLX3397 (20, 21). Microglia depletion by PLX3397 was confirmed by reduced number of cells expressing Iba1 (**Supplementary Figure 3**). It was demonstrated that microglia depletion reversed the preventive effect of OAL on DRCD (**Figures 1D, E**). Furthermore, microglial depletion did not reduce the spatial learning memory of saline-injected healthy controls

Next, to investigate the pathological mechanism of DRCD prevention through OAL, a histological analysis of the brain was performed. STZ injection induced cerebral cortex atrophy, whereas OAL prevented diabetes-induced cerebral atrophy, which was ablated by microglial depletion (**Figure 1F**). As shown in **Figure 1G**, Gallyas-Braak staining revealed diabetes-induced accumulation of argyrophilic grains, which are mainly composed of hyperphosphorylated tau protein (22). Contrarily, the argyrophilic grains were hardly observed in the brains of saline-injected controls and LPS-treated mice. The prevention of argyrophilic grain accumulation by OAL was cancelled by PLX3397 administration. These results indicate that suppression of cerebral atrophy and tau phosphorylation *via* microglia are the preventive mechanisms of DRCD through OAL.

OAL-Microglia Are Distinct From Inflammatory Microglia Induced by Systemic Injection of LPS

The characteristics of microglia transformed by OAL (OAL-microglia) in naïve mice were compared to that of inflammatory microglia induced by intraperitoneal injection with LPS (LPS i.p.). First, the systemic effects of LPS administration were evaluated. As shown in **Figures 2A, B**, OAL did not induce weight loss and systemic elevation of inflammatory cytokines, unlike LPS i.p. (4 mg/kg). In addition, LPS was not detected in the blood of mice that received OAL unlike LPS i.p. (**Figure 2C**).

Second, gene expression analysis of OAL-microglia in naïve mice showed that OAL-microglia did not promote inflammatory mediators (IL-1β, IL-6, TNF-α, and NOS2) nor suppress anti-inflammatory mediator (PPARγ), unlike microglia of mice that received LPS i.p. (**Figure 2D**). These results indicate that OAL-microglia are distinct from inflammatory microglia transformed by LPS i.p. These results indicate that the characteristics of OAL-microglia are fundamentally different from those of inflammatory microglia induced by systemic LPS injection.

Characterization of Neuroprotective Microglia Transformed Through OAL

We next performed further characterization of OAL-microglia in the DRCD model. First, it was confirmed that isolated microglia, not peripheral monocytes, highly express Iba1 (microglia marker), indicating that the contamination of peripheral monocytes was extremely low (**Figure 3A**). In addition, the number of microglia was not significantly different between STZ-injected and LPS-treated mice (**Figure 3B**).

As shown in **Figure 3C**, Aβ contained in isolated microglia was declined in STZ-injected mice, but was not declined in LPS-treated mice as well as in saline-injected controls. whereas the diabetes-induced suppression of Aβ phagocytosis by microglia was prevented by OAL. The result indicates that OAL promotes Aβ phagocytosis of microglia.

Second, comprehensive gene analysis by microarray was used to extract the notable differentially expressed genes from the overall tendency of gene expression. Microarray analysis using pooled sample provided 1,061 candidate genes upregulated in OAL-microglia (**Supplementary Material 1** and **Supplementary Figure 4A**), showing that the gene expression patterns of OAL-microglia are distinct from healthy microglia and microglia in DRCD-developed mice (DRCD-associated microglia). Additionally, gene ontology term analysis revealed that pathways related to immune function, neuronal survival, and tissue repair were upregulated in OAL-microglia (**Supplementary Figure 4B**).

Quantitative RT-PCR was performed to distinguish representative neuroprotective genes from those fluctuating in OAL-microglia. As shown in **Figure 3D**, the following neuroprotective genes are significantly upregulated in OAL-microglia compared to DRCD-associated microglia: CSF1R, IL-10, IL-12B, prostaglandin-E_2 EP4 receptor (encoded by *Ptger4* gene), c-Jun, and heat shock protein (HSP) family (encoded by *Hsp90aa1*, *Hspb1*, *Dnaja4*, and *Dnajb4* genes). In addition, gene expression of IL-12B, EP4 receptor, and HSPβ1 was promoted in OAL-microglia compared to microglia of healthy mice. However, OAL did not affect the gene expression of inflammatory mediators in microglia. The gene expression of inflammatory mediators, such as IL-1β, IL-6, tumor necrosis factor (TNF)-α and nitric oxide synthase (NOS) 2, was not significantly different between OAL-microglia and DRCD-associated microglia (**Figure 3E**). These results indicate that OAL-microglia, which are characterized by high expression of neuroprotective genes, differ in gene expression from DRCD-associated microglia and microglia of healthy mice.

CSF1R Signaling Is Involved in the Transformation to Neuroprotective Microglia Through OAL

Ligands for CSF1R include CSF1 and IL-34. CSF1 is also expressed as two isoforms, the membrane-bound form (m-CSF1) and secretory form (s-CSF1) (23). Gene expression analysis of CSF1R ligands in peripheral leukocytes revealed that only m-CSF1 expression was promoted by OAL (**Figure 4A**). LPS stimulation promoted m-CSF1 gene expression in primary cultured bone marrow cells (**Figure 4B**). However, OAL did not alter the expression of s-CSF1 and IL-34 in peripheral leukocytes (**Figures 4A, C, D**). These results suggested that CSF1R activation by m-CSF1 of peripheral leukocytes induces transformation to neuroprotective OAL-microglia.

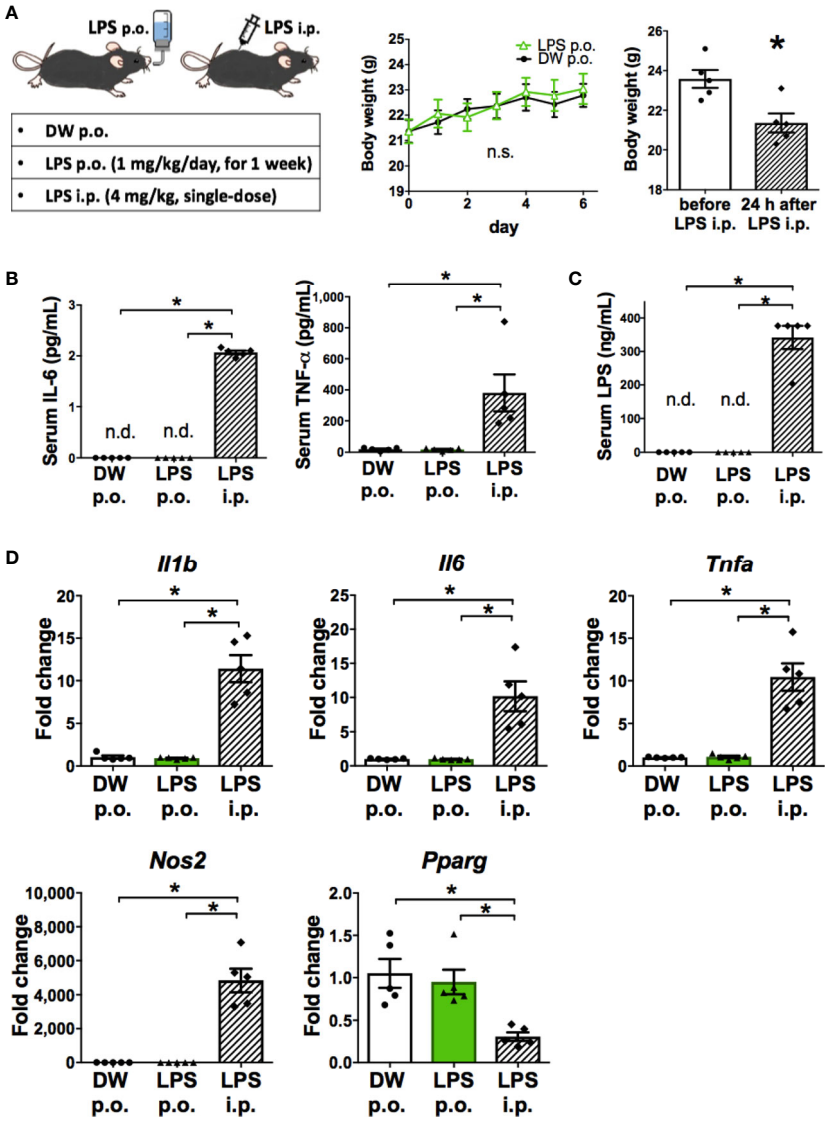

FIGURE 2 | OAL-microglia are distinct from inflammatory microglia transformed by intraperitoneal injection of LPS. **(A)** No weight loss by OAL in naïve mice without STZ i.c.v. (n = 5). **(B)** No increase in serum inflammatory cytokines by OAL. **(C)** Undetectable serum LPS by OAL. **(D)** OAL-microglia showed distinct gene expression patterns from inflammatory microglia transformed by LPS i.p. Means ± SE are presented. *$p < 0.05$ for Student's t test, one-way ANOVA with Tukey's multiple comparisons, or two-way ANOVA with Sidak multiple comparisons. n.s., not significant; n.d., not detected; i.p., intraperitoneal.

Thus, we examined whether neuroprotective transformations similar to OAL-microglia *in vivo* could be reproduced through CSF1R-stimulation of microglia *in vitro*. C8-B4 microglia, one of the most widely used *in vitro* assay systems, is a cell line whose homology with microglia *in vivo* has been sufficiently confirmed based on marker expression and immune responsiveness (**Figure 5A** and **Supplementary Figure 5**) (24–27). Therefore, the cell line was used to characterize CSF1R-stimulated microglia *in vitro*.

Consistent with OAL-microglia *in vivo*, CSF1R-stimulated microglia showed promotion of phagocytosis (**Figure 5B**). In addition, CSF1R-stimulated microglia also promoted gene expression of IL-10 and HSP40 (encoded by *Dnaja4* gene) (**Figure 5C**).

To investigate whether CSF1R-stimulated microglia prevent diabetes-induced neuropathy similar to OAL-microglia *in vivo*, STZ was applied to neurons treated with CSF1R-stimulated microglia culture supernatant (CSF1R-stimulated MCS). As shown in **Figure 5D**, it was demonstrated that CSF1-treated MCS suppressed STZ-induced neuronal cell death (**Figure 5D**). indicating the neuroprotective effect of CSF1R-stimulated microglia. These results demonstrate that neuroprotective transformations like OAL-microglia *in vivo* can be reproduced with CSF1R-stimulated microglia.

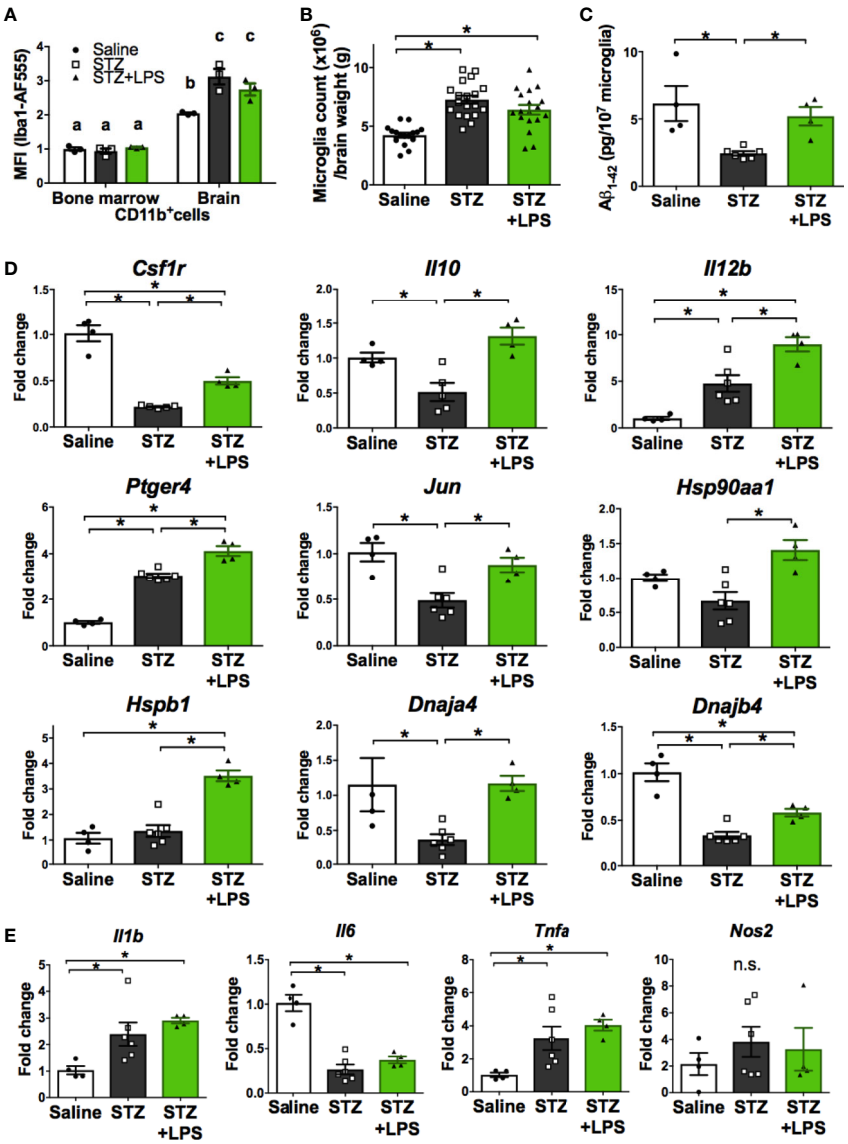

FIGURE 3 | Neuroprotective microglia are transformed through OAL. **(A)** High expression of Iba1 in isolated microglia (n = 3). **(B)** Number of isolated microglia (n = 17–19). **(C)** $A\beta_{1\text{-}42}$ levels in isolated microglia (n = 4–6). **(D, E)** Upregulation of neuroprotective genes and unchanged inflammatory genes in isolated microglia through OAL (n = 4–6). Means ± SE are presented. *p or $^{a,b}p < 0.05$ for one-way ANOVA with Tukey's multiple comparisons or two-way ANOVA with Sidak multiple comparisons. n.s., not significant. $^{a,b,c}p < 0.05$ for two-way ANOVA with Sidak multiple comparisons. The different letters (the symbols of a, b, c) indicate statistically significant difference between groups in multiple comparison test.

DISCUSSION

Our previous studies have revealed that OAL is effective in maintaining homeostasis (2, 12). We previously showed that the immunoprotective effect of OAL increases depending on the LPS dose. Phagocytosis of peritoneal macrophages induced by OAL is enhanced with higher LPS dose (10~1000 μg/kg/day) (28). In high-fat diet-fed apoE-deficient mice, the preventive effect of OAL to suppress weight gain and increasing blood glucose level is observed at higher LPS doses (1 mg > 0.3 mg/kg/day) (12). Similarly, in senescence-accelerated prone 8 mice fed a high-fat diet, the preventing effect of OAL on cognitive dysfunction is found at higher LPS doses (1 mg > 0.3 mg/kg/day) (2). Based on the above results, the LPS dose was set to 1 mg/kg/day in this study.

Here, we demonstrate the effect of OAL on preventing DRCD as MMM test showed that OAL prevented the loss of both learning (**Figure 1B**) and memory ability (**Figure 1C**) induced by diabetes. The preventing effect of OAL on high fat diet-induced cognitive dysfunction has also been demonstrated in our previous study, in which mice were individually bred to accurately control LPS intake (2). Because the preventing effect of OAL on cognitive dysfunction in this study is consistent with

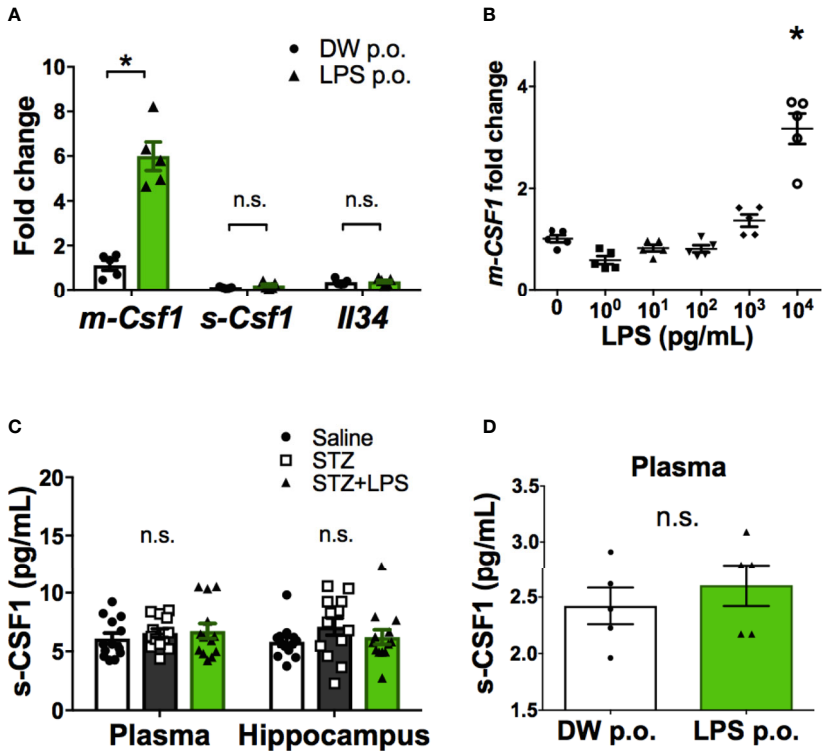

FIGURE 4 | Promotion of m-CSF1 on peripheral blood leukocytes by OAL. **(A)** Upregulated *m-Csf1* through OAL in peripheral blood leukocytes (n = 5). **(B)** Upregulated *m-Csf1* by LPS in primary bone marrow cells. **(C, D)** No increase in s-CSF1 levels through OAL in DRCD [**(C)**, n = 13] and naïve mice [**(D)**, n = 5]. Means ± SE are presented. *$p < 0.05$ for Student's t test or one-way ANOVA with Tukey's multiple comparisons. n.s., not significant.

the previous study, it is considered that there is almost no variation in the amount of water consumed among individuals. In addition, we previously reported that the phagocytic activity-enhancing effect of peritoneal macrophages induced by OAL was not observed in Toll-like receptor 4 (TLR4)-deficient mice (28). Therefore, the protective effects induced by OAL are considered to be TLR4 dependent. Furthermore, considering that the LPS derived from *P. agglomerans* used in this study has very low nucleic acid and protein contamination and activates macrophages in very small amounts (1.6 ng/ml) (11), it is reasonable to conclude that the effect obtained is due to LPS derived from *P. agglomerans*.

Microglia play a central role in the innate immune system and the maintenance of homeostasis in the central nervous system (CNS). Since our previous study suggested that OAL enhances phagocytosis of amyloid beta (Aβ) by microglia (2), we considered that microglia may also play an important role in the prevention of DRCD through OAL. According to our hypothesis, microglia depletion using PLX3397 revealed that microglia are necessary for DRCD prevention through OAL (**Figures 1D, E**).

Furthermore, microglial depletion did not reduce the spatial learning memory of saline-injected healthy controls, which was consistent with a previous study (20). Because PLX3397 does not affect the number of other CNS cell types and circulating leukocyte subsets (20, 21), these results indicate that microglia are indispensable for the prevention of DRCD through OAL, although they do not affect cognitive ability under physiological conditions.

Histological analysis showed that OAL prevented diabetes-induced cerebral atrophy and the accumulation of argyrophilic grains (**Figures 1F, G**), which are mainly composed of hyperphosphorylated tau protein and are frequently seen in association with neurodegeneration and cognitive decline (22). Therefore, it is indicated that suppression of cerebral atrophy and tau phosphorylation *via* microglia are the preventive mechanisms of DRCD through OAL.

Thus, while microglia are necessary to prevent DRCD through OAL, DRCD cannot be prevented without OAL, even in the presence of microglia. It was shown that the characteristics of OAL-microglia are distinct from those of DRCD-associated microglia. Therefore, transformation to the neuroprotective microglia induced by OAL is important for DRCD prevention.

Based on the above results, we next characterized the OAL-microglia. Generally, LPS is known to induce inflammation through transformation into inflammatory microglia when systemically injected (29, 30). Therefore, the characteristics of OAL-microglia in naïve mice were compared to that of inflammatory microglia.

As shown in **Figure 2**, unlike LPS i.p., OAL did not induce side effects such as weight loss and systemic inflammation (**Figures 2A, B**), or inflammatory microglia (**Figure 2D**). It has been reported that immune training (immune tolerance)

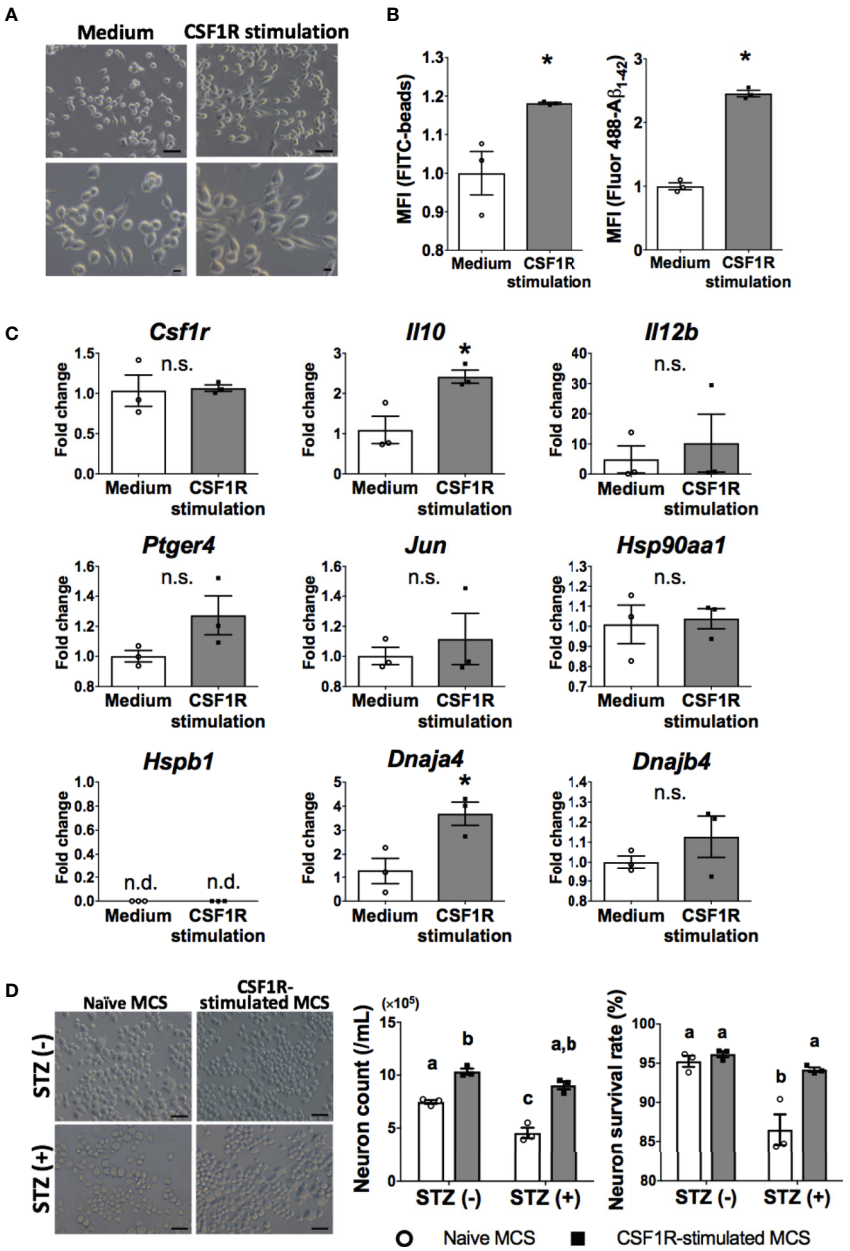

FIGURE 5 | Neuroprotective microglia are transformed by CSF1R signaling. **(A)** Dendrite protrusion of CSF1R-stimulated microglia. Bars, 50 (upper) and 10 μm (lower). **(B)** Promoted phagocytosis of CSF1R-stimulated microglia. **(C)** Upregulation of neuroprotective genes in CSF1R-stimulated microglia. **(D)** Prevention of diabetes-induced neuronal death by CSF1R-stimulated MCS. Bar, 50 μm. Means ± SE are presented. *p or $^{a,b}p < 0.05$ for Student's t test or two-way ANOVA with Sidak multiple comparisons. MCS, microglia culture supernatant. n.s., not significant; n.d., not detected. $^{a,b,c}p < 0.05$ for two-way ANOVA with Sidak multiple comparisons. The different letters (the symbols of a, b, c) indicate statistically significant difference between groups in multiple comparison test.

with repetitive low-dose LPS i.p. transforms microglia into a neuroprotective phenotype. However, mild sickness, weight loss, and systemic inflammation are often associated with LPS i.p. (31). In contrast, our results challenge the stereotype of LPS as an inflammation inducer by showing that the characteristics of OAL-microglia are fundamentally different from those of inflammatory microglia induced by systemic LPS injection. Additionally, LPS was not detected in the blood of mice that received OAL unlike LPS i.p. (**Figure 2C**), indicating that orally administrated LPS does not directly impact microglia.

Furthermore, it was revealed that characteristics of OAL-microglia were distinct form DRCD-associated microglia (**Figure 3**). Because the number of microglia was not significantly different between STZ-injected and LPS-treated mice (**Figure 3B**), we concluded that OAL induces qualitative rather than quantitative transformation of microglia. Consistent with our previous studies

which suggested that OAL-microglia contributed to the prevention of cognitive dysfunction by promoting the phagocytosis of Aβ (2, 28), the diabetes-induced suppression of Aβ phagocytosis by microglia was prevented by OAL (**Figure 3C**). This is considered a background mechanism for preventing tau phosphorylation by OAL (**Figure 1G**) since Aβ deposition triggers tau protein phosphorylation leading to neuropathy (32).

Gene analysis revealed that some neuroprotective genes are highly expressed in OAL-microglia compared to DRCD-associated microglia (**Figure 3D**). CSF1R regulates survival and proliferation of macrophages and its signal induces transformation into neuroprotective microglia (33–36). IL-10 is an anti-inflammatory cytokine and interestingly synergizes with IL-12B to regulate inflammation in tumor models (37). Activation of EP4 receptor suppresses brain inflammation (38–40), and also synergizes with CSF1 signaling (41). c-Jun forms activator protein 1 (AP-1), a transcription factor, which is activated downstream of CSF1 signal involving in transformation to anti-inflammatory macrophage (34, 42). AP-1 is also involved in the induction of IL-10, IL-12, HSP (43–46). *Hsp90aa1*, *Hspb1*, *Dnaja4*, and *Dnajb4* genes encode HSP family, and exogenous HSP promotes Aβ phagocytosis of microglia and induces neuroprotection (47). These results indicate that OAL-microglia are neuroprotective and qualitatively different from DRCD-associated microglia.

Considering our results above, we speculated that there must be a mediator that connects OAL and the transformation to neuroprotective microglia in the DRCD model. We focused on CSF1R as a potential mediator as it was one of the highly expressed genes in OAL-microglia. It has been reported that CSF1R signaling induces transformation to neuroprotective microglia *via* c-Jun (33–36, 42).

Furthermore, peripheral levels of CSF1, a CSF1R ligand, correlate with CSF1R levels in the CNS (48, 49), and peripheral administration of CSF1 improves neurological disorders (50–52). Therefore, we hypothesized that OAL increases expression of the peripheral CSF1R ligand, which activates the CSF1R signal to induce the transformation to neuroprotective microglia.

It was revealed that gene expression of m-CSF1, not s-CSF1 or IL-34, was promoted by OAL in peripheral leukocytes (**Figures 4A, C, D**), and that LPS stimulation promoted m-CSF1 gene expression in primary cultured bone marrow cells (**Figure 4B**). Therefore, it is suggested that m-CSF1, whose expression is promoted on peripheral leukocytes by OAL, is a mediator that induces transformation to neuroprotective OAL-microglia *via* CSF1R. It is yet unsolved mechanisms by which OAL promotes only m-CSF1, not s-CSF1. Concerning the point above, since *Csf1* gene is transcribed into m-CSF1 or s-CSF1 mRNA forms *via* alternative splicing (23), OAL is thought to influence the regulation of mRNA splicing of *Csf1* gene.

Since both m-CSF1 and s-CSF1 bind to CSF1R and induce transformation to homogeneous macrophages (53), the main difference between the two is assumed to be the mechanism of transmission. In other words, s-CSF1 acts systemically in an endocrine manner, whereas m-CSF1 acts locally in a juxtacrine or paracrine manner (23). Since CSF1R is specifically expressed in microglia in the brain, it is considered that m-CSF1, whose expression is promoted on peripheral leukocytes by OAL, may activate CSF1R signaling in microglia *via* the "just-in-time system" method.

Schwartz et al. reported that the cerebral choroid plexus functions as a location for crosstalk between CNS cells and the peripheral immune system (54). Under physiological conditions, peripheral immune cells regularly patrol to maintain CNS homeostasis in the choroid plexus. In contrast, under pathological conditions, peripheral immune cells sense the abnormality in the choroid plexus and prevent neuropathy through crosstalk with CNS cells by secreting neuroprotective molecules. Therefore, the cerebral choroid plexus is likely to act as a communication site for restrictive signaling between m-CSF1 of peripheral leukocytes and CSF1R on microglia.

In agreement with the theory of Schwartz et al., OAL had little effect on the expression of neuroprotective genes in the microglia of naïve mice (**Supplementary Figure 6**). Therefore, it is considered that CSF1R on microglia is activated by m-CSF1 of peripheral leukocyte only under pathological conditions such as CNS diabetes, which induces transformation to neuroprotective microglia to prevent DRCD. Assuming such an abnormality detection system, m-CSF1 is more plausible than s-CSF1.

Finally, we investigated whether CSF1R stimulation could reproduce the characteristics of OAL-microglia (**Figure 5**). It was shown that CSF1R-stimulated microglia promoted phagocytosis (**Figure 5B**) and gene expression of IL-10 and HSP40 (encoded by *Dnaja4* gene) (**Figure 5C**). Since the expression of the EP4 receptor and other HSPs is promoted downstream of IL-10 (55, 56), it can be said that CSF1R-stimulated microglia almost reproduces the characteristics of OAL-microglia *in vivo*, such as high phagocytosis and neuroprotective gene expression. Furthermore, since CSF1R-stimulated microglia prevented diabetes-induced neuronal death (**Figure 5D**), it is indicated that OAL-microglia *in vivo* can be reproduced with CSF1R-stimulated microglia. Therefore, it is strongly proposed that transformation to neuroprotective microglia *via* CSF1R activation is involved in the mechanism of DRCD prevention by OAL.

To prove our hypothesis that CSF1R signal mediates the transformation to neuroprotective OAL-microglia *in vivo*, we needed a system that functionally inhibits only the CSF1R signal without affecting the survival of microglia. However, the problem is that inhibition of CSF1R induces microglia death because the CSF1-CSF1R signal controls not only the function of microglia but also their survival and proliferation (20, 21). In fact, PLX3397 used for microglia depletion in this study is a CSF1R inhibitor. Therefore, the next task is to develop alternative approaches to test our hypothesis. Our discovery that the CSF1R activation by m-CSF1 is a key factor that mediates the transformation to neuroprotective OAL-microglia is a major step towards elucidating the DRCD prevention mechanism through OAL.

In conclusion, the present study demonstrates that OAL prevents DRCD by transforming microglia to a neuroprotective phenotype. In addition, activation of CSF1R on microglia mediated by m-CSF1 expressed on peripheral leukocytes strongly suggests that the CSFR1-mCSF1 interaction facilitates the mechanism of microglia transformation (**Figure 6**). Other groups also have reported that physiological mucosal exposure to

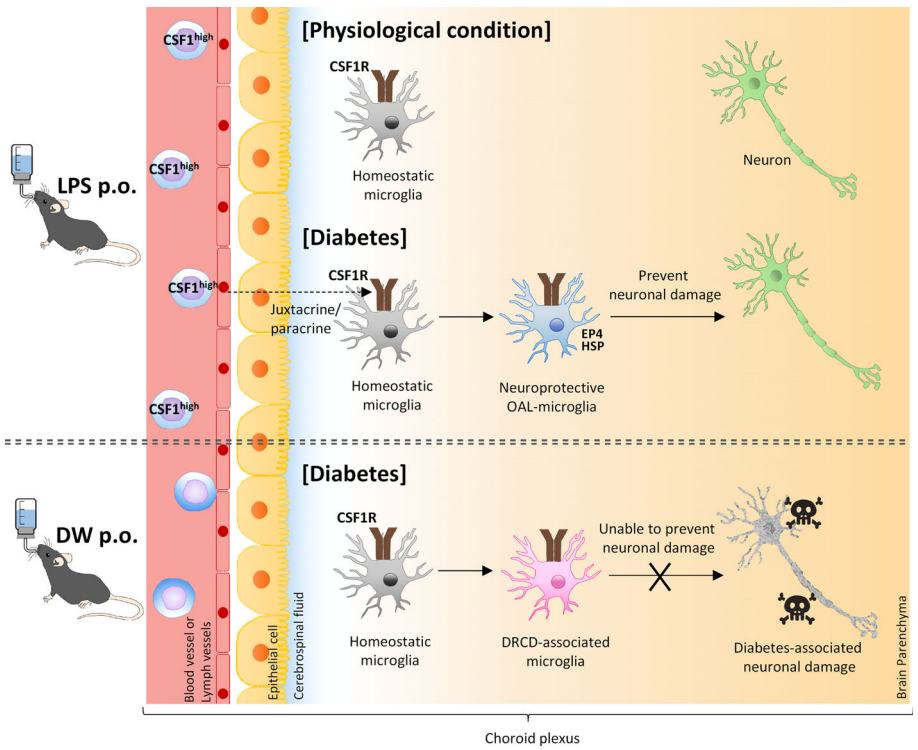

FIGURE 6 | A model of transformation into neural microglia through OAL. OAL induces m-CSF1 expressing leukocytes, which patrol and maintain CNS homeostasis under physiological conditions. Under diabetes-induced pathological conditions, microglia transform to a neuroprotective phenotype mediated by m-CSF1 in a juxtacrine/paracrine manner, and prevent neuronal damage.

LPS maintains homeostasis *via* tissue-resident macrophages (57, 58), which supports our findings.

Microglia depletion has been recently proposed as a new solution to neuropathy. Indeed, microglia shift to a pro-inflammatory phenotype in some neurological diseases, and therefore microglia depletion leads to anti-inflammatory and neuroprotective effects (21, 59). However, since microglia play diverse roles in CNS homeostasis, microglia depletion is an impractical strategy leading to collapse of the brain immune system and homeostasis (60, 61). However, it is an innovative method of preventing DRCD by controlling microglial transformation in a simple and safe way through OAL.

Previous study compared the biological activity of LPS from *P. agglomerans* with that of LPS from *Escherichia coli* and that of LPS from *Enterobacterium* (the rice symbiotic bacterium) at the cellular level, showing that there is not much difference in the biological activity of the three (62). However, LPS derived from *P. agglomerans* has been proven safe in animal studies when administered orally (no-observed adverse-effect level 4500 mg/kg/day) (5–7). Also in humans, it is confirmed that 10 μg/kg/day OAL does not induce systemic inflammation by measuring biomarkers such as white blood cell count, red blood cell count, aspartate aminotransferase, alanine aminotransferase, creatinine, C-reactive protein, and immunoglobulin A in human peripheral blood samples (63). Moreover, OAL at the dose improves hyperglycemia, hyperlipidemia (64), reduced bone density (65), and blood flow (63). In addition, because LPS from *P. agglomerans* is abundant in the organic foods we consume on a daily basis (6, 66–68), humans have a dietary experience of LPS from *P. agglomerans*. Therefore, although more careful safety studies will be required in the future, LPS from *P. agglomerans* is thought to be the suitable LPS considering the application of OAL to human therapy.

Based on the hygiene hypothesis (69), human beings used to intake LPS naturally from the organic environment. Accordingly, microglia used to be activated physiologically (6, 66, 67). However, the present age is described as the LPS-lost era, in which human beings live in an unnaturally clean and inorganic environment. In a sense, OAL is like a time machine that returns microglia back to the good old LPS-abundant era, as if *DeLorean* of "*Back to the Future*".

DATA AVAILABILITY STATEMENT

The original contributions presented in the study are included in the article/**Supplementary Material**. Further inquiries can be directed to the corresponding author.

ETHICS STATEMENT

The animal study was reviewed and approved by the Animal Care and Use Committee of the Control of Innate Immunity CIP.

AUTHOR CONTRIBUTIONS

HM, HI, and G-IS conceptualized the study and coordinated the experiments. HM, KY, and MY performed the experiments. HM performed data curation and formal analysis. YN and CK provided resource of LPS. HI and G-IS acquired the funding and administrated the project. HM wrote the manuscript supervised by G-IS, HI, CK, and YN with contribution from all authors. All authors contributed to the article and approved the submitted version.

FUNDING

This study was funded by the Control of Innate Immunity Collaborative Innovation Partnership. This study was also supported by a grant from the Cross-ministerial Strategic Innovation Promotion Program (SIP-No. 14533073) of the Council for Science from Technology and Innovation (CSTI) in the Cabinet Office of the Japanese Government and the National Agriculture and Food Research Organization (NARO). CSTI and NARO had no role in the study design, data collection and analysis, decision to publish, or preparation of the manuscript.

SUPPLEMENTARY MATERIAL

The Supplementary Material for this article can be found online at: https://www.frontiersin.org/articles/10.3389/fimmu.2021.650176/full#supplementary-material

REFERENCES

1. International Diabetes Federation. International Diabetes Federation. *IDF Diabetes Atlas*, *Ninth edition*, Vol. 2019. (2019).
2. Kobayashi Y, Inagawa H, Kohchi C, Kazumura K, Tsuchiya H, Miwa T, et al. Oral Administration of Pantoea Agglomerans-Derived Lipopolysaccharide Prevents Metabolic Dysfunction and Alzheimer's Disease-Related Memory Loss in Senescence-Accelerated Prone 8 (SAMP8) Mice Fed a High-Fat Diet. *PloS One* (2018) 13:e0198493. doi: 10.1371/journal.pone.0198493
3. Nunes C, Usall J, Teixidó N, Fons E, Viñas I. Post-Harvest Biological Control by Pantoea Agglomerans (CPA-2) on Golden Delicious Apples. *J Appl Microbiol* (2002) 92:247–55. doi: 10.1046/j.1365-2672.2002.01524.x
4. Usall J, Smilanick J, Palou L, Denis-Arrue N, Teixido N, Torres R, et al. Postharvest Biology and Technology Preventive and Curative Activity of Combined Treatments of Sodium Carbonates and Pantoea Agglomerans CPA-2 to Control Postharvest Green Mold of Citrus Fruit. *Postharvest Biol Technol* (2008) 50:1–7. doi: 10.1016/j.postharvbio.2008.03.001
5. Phipps KR, Sulaiman C, Simon R, Holalagoudar S, Kohchi C, Nakata Y. Subchronic (90-Day) Toxicity Assessment of Somacy-FP100, a Lipopolysaccharide-Containing Fermented Wheat Flour Extract From Pantoea Agglomerans. *J Appl Toxicol* (2020) 40:1342–52. doi: 10.1002/jat.3987
6. Taniguchi Y, Yoshioka N, Nishizawa T, Inagawa H, Kohchi C, Soma GI. Utility and Safety of LPS- Based Fermented Flour Extract as a Macrophage Activator. *Anticancer Res* (2009) 29:859–64.
7. Inagawa H, Kohchi C, Soma GI. Oral Administration of Lipopolysaccharides for the Prevention of Various Diseases: Benefit and Usefulness. *Anticancer Res* (2011) 31:2431–6.
8. Salkovic-Petrisic M, Hoyer S. Central Insulin Resistance as a Trigger for Sporadic Alzheimer-Like Pathology: An Experimental Approach. *J Neural Transm Suppl* (2007) 72:217–33. doi: 10.1007/978-3-211-73574-9-28
9. Kamat PK. Streptozotocin Induced Alzheimer's Disease Like Changes and the Underlying Neural Degeneration and Regeneration Mechanism. *Neural Regener Res* (2015) 10:1050–2. doi: 10.4103/1673-5374.160076
10. Biessels GJ, Despa F. Cognitive Decline and Dementia in Diabetes: Mechanisms and Clinical Implications. *Nat Rev Endocrinol* (2018) 14:591–604. doi: 10.1016/j.physbeh.2017.03.040
11. Taniguchi Y, Nishizawa T, Honda T, Yoshioka N, Inagawa H, Kohchi C, et al. Development and Potential Use of a Monoclonal Antibody to the Lipopolysaccharide of Pantoea Agglomerans (IP-PA1). *Anticancer Res* (2007) 27:3701–6.
12. Kobayashi Y, Inagawa H, Kohchi C, Kazumura K, Tsuchiya H, Miwa T, et al. Oral Administration of Pantoea Agglomeransderived Lipopolysaccharide Prevents Development of Atherosclerosis in High-Fat Diet-Fed apoE-Deficient Mice *via* Ameliorating Hyperlipidemia, Pro-Inflammatory Mediators and Oxidative Responses. *PloS One* (2018) 13:e0195008. doi: 10.1371/journal.pone.0195008
13. Gulyás M, Bencsik N, Pusztai S, Liliom H, Schlett K. AnimalTracker: An ImageJ-Based Tracking API to Create a Customized Behaviour Analyser Program. *Neuroinformatics* (2016) 14:479–81. doi: 10.1007/s12021-016-9303-z
14. Kobayashi Y, Inagawa H, Kohchi C, Okazaki K, Zhang R, Soma G. Effect of Lipopolysaccharide Derived From Pantoea Agglomerans on the Phagocytic Activity of Amyloid β by Primary Murine Microglial Cells. *Anticancer Res* (2016) 36:3693–8.
15. Quackenbush J. Microarray Data Normalization and Transformation. *Nat Genet* (2002) 32:496–501. doi: 10.1038/ng1032
16. Hiramoto T, Tahara M, Liao J, Soda Y, Miura Y, Kurita R, et al. Non-Transmissible MV Vector With Segmented RNA Genome Establishes Different Types of iPSCs From Hematopoietic Cells. *Mol Ther* (2020) 28:129–41. doi: 10.1016/j.ymthe.2019.09.007
17. Saeed AI, Sharov V, White J, Li J, Liang W, Bhagabati N, et al. TM4: A Free, Open-Source System for Microarray Data Management and Analysis. *Biotechniques* (2003) 34:374–8. doi: 10.2144/03342mt01
18. Saeed AI, Bhagabati NK, Braisted JC, Liang W, Sharov V, Howe EA, et al. TM4 Microarray Software Suite. *Methods Enzymol* (2006) 411:134–93. doi: 10.1016/S0076-6879(06)11009-5
19. He H, Xu J, Warren CM, Duan D, Li X, Wu L, et al. Endothelial Cells Provide an Instructive Niche for the Differentiation and Functional Polarization of M2-Like Macrophages. *Blood* (2012) 120:3152–62. doi: 10.1182/blood-2012-04-422758
20. Elmore MRP, Najafi AR, Koike MA, Dagher NN, Spangenberg EE, Rice RA, et al. Colony-Stimulating Factor 1 Receptor Signaling is Necessary for Microglia Viability, Unmasking a Microglia Progenitor Cell in the Adult Brain. *Neuron* (2014) 82:380–97. doi: 10.1016/j.neuron.2014.02.040
21. Spangenberg E, Severson PL, Hohsfield LA, Crapser J, Zhang J, Burton EA, et al. Sustained Microglial Depletion With CSF1R Inhibitor Impairs Parenchymal Plaque Development in an Alzheimer's Disease Model. *Nat Commun* (2019) 10:3758. doi: 10.1038/s41467-019-11674-z
22. Ferrer I, Santpere G, Van Leeuwen FW. Argyrophilic Grain Disease. *Brain* (2008) 131:1416–32. doi: 10.1093/brain/awm305
23. Douglass TG, Driggers L, Zhang JG, Hoa N, Delgado C, Williams CC, et al. Macrophage Colony Stimulating Factor: Not Just for Macrophages Anymore! A Gateway Into Complex Biologies. *Int Immunopharmacol* (2008) 8:1354–76. doi: 10.1016/j.intimp.2008.04.016
24. Moussaud S, Lamodière E, Savage C, Draheim HJ. Cellular Physiology Biochemistry and Biochemistr Y Characterisation of K + Currents in the C8-B4 Microglial Cell Line and Their Regulation by Microglia Activating Stimuli. *Cell Physiol Biochem* (2009) 24:141–52. doi: 10.1159/000233240
25. Moussaud S, Draheim H. A New Method to Isolate Microglia From Adult Mice and Culture Them for an Extended Period of Time. *J Neurosci Methods* (2010) 187:243–53. doi: 10.1016/j.jneumeth.2010.01.017
26. Beauvillain C, Donnou S, Jarry U, Scotet M, Gascan H, Delneste Y, et al. Neonatal and Adult Microglia Cross-Present Exogenous Antigens. *Glia* (2008) 56:69–77. doi: 10.1002/glia.20565

27. Sampaio NG, Yu W, Cox D, Wyckoff J, Condeelis J, Stanley ER, et al. Phosphorylation of CSF-1R Y721 Mediates its Association With PI3K to Regulate Macrophage Motility and Enhancement of Tumor Cell Invasion. *J Cell Sci* (2011) 124:2021–31. doi: 10.1242/jcs.075309
28. Inagawa H, Kobayashi Y, Kohchi C, Zhang R, Shibasaki Y, Soma GI. Primed Activation of Macrophages by Oral Administration of Lipopolysaccharide Derived From Pantoea Agglomerans. *In Vivo (Brooklyn)* (2016) 30:205–11.
29. Cazareth J, Guyon A, Heurteaux C, Chabry J, Petit-Paitel A. Molecular and Cellular Neuroinflammatory Status of Mouse Brain After Systemic Lipopolysaccharide Challenge: Importance of CCR2/CCL2 Signaling. *J Neuroinflamm* (2014) 11:132. doi: 10.1186/1742-2094-11-132
30. Zhao J, Bi W, Xiao S, Lan X, Cheng X, Zhang J, et al. Neuroinflammation Induced by Lipopolysaccharide Causes Cognitive Impairment in Mice. *Sci Rep* (2019) 9:5790. doi: 10.1038/s41598-019-42286-8
31. Wendeln AC, Degenhardt K, Kaurani L, Gertig M, Ulas T, Jain G, et al. Innate Immune Memory in the Brain Shapes Neurological Disease Hallmarks. *Nature* (2018) 556:332–8. doi: 10.1038/s41586-018-0023-4
32. Zhang F, Gannon M, Chen Y, Yan S, Zhang S, Feng W, et al. β-Amyloid Redirects Norepinephrine Signaling to Activate the Pathogenic GSK3β/Tau Cascade. *Sci Transl Med* (2020) 12:eaay6931. doi: 10.1126/scitranslmed.aay6931
33. Mitrasinovic OM, Grattan A, Robinson CC, Lapustea NB, Poon C, Ryan H, et al. Microglia Overexpressing the Macrophage Colony-Stimulating Factor Receptor Are Neuroprotective in a Microglial-Hippocampal Organotypic Coculture System. *J Neurosci* (2005) 25:4442–51. doi: 10.1523/JNEUROSCI.0514-05.2005
34. Yang Y, Qin J, Lan L, Li N, Wang C, He P, et al. M-CSF Cooperating With NFκB Induces Macrophage Transformation From M1 to M2 by Upregulating C-Jun. *Cancer Biol Ther* (2014) 15:99–107. doi: 10.4161/cbt.26718
35. Chu CH, Wang S, Li CL, Chen SH, Hu CF, Chung YL, et al. Neurons and Astroglia Govern Microglial Endotoxin Tolerance Through Macrophage Colony-Stimulating Factor Receptor-Mediated ERK1/2 Signals. *Brain Behav Immun* (2016) 55:260–72. doi: 10.1016/j.bbi.2016.04.015
36. Pepe G, De Maglie M, Minoli L, Villa A, Maggi A, Vegeto E. Selective Proliferative Response of Microglia to Alternative Polarization Signals. *J Neuroinflamm* (2017) 14:236. doi: 10.1186/s12974-017-1011-6
37. Lopez MV, Adris SK, Bravo AI, Chernajovsky Y, Podhajcer OL. IL-12 and IL-10 Expression Synergize to Induce the Immune-Mediated Eradication of Established Colon and Mammary Tumors and Lung Metastasis. *J Immunol* (2005) 175:5885–94. doi: 10.4049/jimmunol.175.9.5885
38. Woodling NS, Wang Q, Priyam PG, Larkin P, Shi J, Johansson JU, et al. Suppression of Alzheimer-Associated Inflammation by Microglial Prostaglandin-E2 EP4 Receptor Signaling. *J Neurosci* (2014) 34:5882–94. doi: 10.1523/JNEUROSCI.0410-14.2014
39. Pradhan SS, Salinas K, Garduno AC, Johansson JU, Wang Q, Manning-Bog A, et al. Anti-Inflammatory and Neuroprotective Effects of PGE2 EP4 Signaling in Models of Parkinson's Disease. *J Neuroimmune Pharmacol* (2017) 12:292–304. doi: 10.1016/j.physbeh.2017.03.040
40. Shi J, Johansson J, Woodling NS, Wang Q, Montine TJ, Andreasson K. The Prostaglandin E 2 E-Prostanoid 4 Receptor Exerts Anti-Inflammatory Effects in Brain Innate Immunity. *J Immunol* (2010) 184:7207–18. doi: 10.4049/jimmunol.0903487
41. Digiacomo G, Ziche M, Sbarba PD, Donnini S, Rovida E. Prostaglandin E2 Transactivates the Colony-Stimulating Factor-1 Receptor and Synergizes With Colony-Stimulating Factor-1 in the Induction of Macrophage Migration *via* the Mitogen-Activated Protein Kinase ERK1/2. *FASEB J* (2015) 29:2545–54. doi: 10.1096/fj.14-258939
42. Casals-Casas C, Álvarez E, Serra M, de la Torre C, Farrera C, Sánchez-Tilló E, et al. CREB and AP-1 Activation Regulates MKP-1 Induction by LPS or M-CSF and Their Kinetics Correlate With Macrophage Activation *Versus* Proliferation. *Eur J Immunol* (2009) 39:1902–13. doi: 10.1002/eji.200839037
43. Saraiva M, O'Garra A. The Regulation of IL-10 Production by Immune Cells. *Nat Rev Immunol* (2010) 10:170–81. doi: 10.1038/nri2711
44. Zhu C, Gagnidze K, Gemberling JHM, Plevy SE. Characterization of an Activation Protein-1-Binding Site in the Murine Interleukin-12 P40 Promoter: Demonstration of Novel Functional Elements by a Reductionist Approach. *J Biol Chem* (2001) 276:18519–28. doi: 10.1074/jbc.M100440200
45. Assimakopoulou M, Varakis J. AP-1 and Heat Shock Protein 27 Expression in Human Astrocytomas. *J Cancer Res Clin Oncol* (2001) 127:727–32. doi: 10.1007/s004320100280
46. Souza V, Escobar MDC, Gómez-Quiroz L, Bucio L, Hernández E, Cossio EC, et al. Acute Cadmium Exposure Enhances AP-1 DNA Binding and Induces Cytokines Expression and Heat Shock Protein 70 in HepG2 Cells. *Toxicology* (2004) 197:213–28. doi: 10.1016/j.tox.2004.01.006
47. Kakimura J-I, Kitamura Y, Takata K, Umeki M, Suzuki S, Shibagaki K, et al. Microglial Activation and Amyloid-β Clearance Induced by Exogenous Heat-Shock Proteins. *FASEB J* (2002) 16:601–3. doi: 10.1096/fj.01-0530fje
48. Guan Z, Kuhn JA, Wang X, Colquitt B, Solorzano C, Vaman S, et al. Injured Sensory Neuron-Derived CSF1 Induces Microglia Proliferation and DAP12-Dependent Pain. *Nat Neurosci* (2016) 19:94–101. doi: 10.1016/j.physbeh.2017.03.040
49. Knight AC, Brill SA, Queen SE, Tarwater PM, Mankowski JL. Increased Microglial CSF1R Expression in the SIV/macaque Model of HIV CNS Disease. *J Neuropathol Exp Neurol* (2018) 77:199–206. doi: 10.1093/jnen/nlx115
50. Boissonneault V, Filali M, Lessard M, Relton J, Wong G, Rivest S. Powerful Beneficial Effects of Macrophage Colony-Stimulating Factor on β-Amyloid Deposition and Cognitive Impairment in Alzheimers Disease. *Brain* (2009) 132:1078–92. doi: 10.1093/brain/awn331
51. Luo J, Elwood F, Britschgi M, Villeda S, Zhang H, Ding Z, et al. Colony-Stimulating Factor 1 Receptor (CSF1R) Signaling in Injured Neurons Facilitates Protection and Survival. *J Exp Med* (2013) 210:157–72. doi: 10.1084/jem.20120412
52. Laflamme N, Cisbani G, Préfontaine P, Srour Y, Bernier J, St-Pierre MK, et al. mCSF-Induced Microglial Activation Prevents Myelin Loss and Promotes its Repair in a Mouse Model of Multiple Sclerosis. *Front Cell Neurosci* (2018) 12:178. doi: 10.3389/fncel.2018.00178
53. Liao J, Feng W, Wang R, Ma S, Wang L, Yang X, et al. Diverse *In Vivo* Effects of Soluble and Membrane-Bound M-CSF on Tumor-Associated Macrophages in Lymphoma Xenograft Model. *Oncotarget* (2016) 7:1354–66. doi: 10.18632/oncotarget.6362
54. Shechter R, London A, Schwartz M. Orchestrated Leukocyte Recruitment to Immune-Privileged Sites: Absolute Barriers *Versus* Educational Gates. *Nat Rev Immunol* (2013) 13:206–18. doi: 10.1038/nri3391
55. Samiea A, Yoon JSJ, Cheung ST, Chamberlain TC, Mui ALF. Interleukin-10 Contributes to PGE2 Signalling Through Upregulation of EP4 *via* SHIP1 and STAT3. *PloS One* (2020) 15:e0230427. doi: 10.1371/journal.pone.0230427
56. Ripley BJM, Stephanou A, Isenberg DA, Latchman DS. Interleukin-10 Activates Heat-Shock Protein 90β Gene Expression. *Immunology* (1999) 97:226–31. doi: 10.1046/j.1365-2567.1999.00773.x
57. Muller PA, Koscsó B, Rajani GM, Stevanovic K, Berres ML, Hashimoto D, et al. Crosstalk Between Muscularis Macrophages and Enteric Neurons Regulates Gastrointestinal Motility. *Cell* (2014) 158:300–13. doi: 10.1016/j.cell.2014.04.050
58. Toda G, Soeda K, Okazaki Y, Kobayashi N, Masuda Y, Arakawa N, et al. Insulin- and Lipopolysaccharide-Mediated Signaling in Adipose Tissue Macrophages Regulates Postprandial Glycemia Through Akt-mTOR Activation. *Mol Cell* (2020) 79:43–53.e4. doi: 10.1016/j.molcel.2020.04.033
59. Shi Y, Manis M, Long J, Wang K, Sullivan PM, Remolina Serrano J, et al. Microglia Drive APOE-Dependent Neurodegeneration in a Tauopathy Mouse Model. *J Exp Med* (2019) 216:2546–61. doi: 10.1084/jem.20190980
60. Casali BT, MacPherson KP, Reed-Geaghan EG, Landreth GE. Microglia Depletion Rapidly and Reversibly Alters Amyloid Pathology by Modification of Plaque Compaction and Morphologies. *Neurobiol Dis* (2020) 142:104956. doi: 10.1016/j.nbd.2020.104956
61. Kempthorne L, Yoon H, Madore C, Smith S, Wszolek ZK, Rademakers R, et al. Loss of Homeostatic Microglial Phenotype in CSF1R-Related Leukoencephalopathy. *Acta Neuropathol Commun* (2020) 8:72. doi: 10.1186/s40478-020-00947-0
62. Kadowaki T, Inagawa H, Kohchi C, Hirashima M, Soma GI. Functional Characterization of Lipopolysaccharide Derived From Symbiotic Bacteria in Rice as a Macrophage-Activating Substance. *Anticancer Res* (2011) 31:2467–76.
63. Nakata Y, Kohchi C, Ogawa K, Nakamoto T, Yoshimura H, Soma GI. Effects of 3 Months Continuous Intake of Supplement Containing Pantoea Agglomerans LPS to Maintain Normal Bloodstream in Adults: Parallel Double-Blind Randomized Controlled Study. *Food Sci Nutr* (2017) 6:197–206. doi: 10.1002/fsn3.547
64. Nakata K, Taniguchi Y, Yoshioka N, Yoshida A, Inagawa H, Nakamoto T, et al. A Mixture of Salacia Oblonga Extract and IP-PA1 Reduces Fasting Plasma Glucose (FPG) and Low-Density Lipoprotein (LDL) Cholesterol Levels. *Nutr Res Pract* (2011) 5:435–42. doi: 10.4162/nrp.2011.5.5.435

65. Nakata K, Nakata Y, Inagawa H, Nakamoto T, Yoshimura H, Soma GI. Pantoea Agglomerans Lipopolysaccharide Maintains Bone Density in Premenopausal Women: A Randomized, Double-Blind, Placebo-Controlled Trial. *Food Sci Nutr* (2014) 2:638–46. doi: 10.1002/fsn3.145
66. Tamura Y, Inagawa H, Nakata Y, Kohchi C, Soma G-I. Effects of the Subaleurone Layer of Rice on Macrophage Activation and Protection of Pollen Allergy in a Murine Model. *Anticancer Res* (2015) 35:4467–72.
67. Inagawa H, Saika T, Nisizawa T, Kohchi C, Uenobe M, Soma GI. Dewaxed Brown Rice Contains a Significant Amount of Lipopolysaccharide Pointing to Macrophage Activation. *via TLRs Anticancer Res* (2016) 36:3599–605.
68. Mizobuchi H, Soma GI. Low-Dose Lipopolysaccharide as an Immune Regulator for Homeostasis Maintenance in the Central Nervous System Through Transformation to Neuroprotective Microglia. *Neural Regener Res* (2021) 16:1928–34. doi: 10.4103/1673-5374.308067
69. Braun-Fahrländer C, Riedler J, Herz U, Eder W, Waser M, Grize L, et al. Environmental Exposure to Endotoxin and Its Relation to Asthma in School-Age Children. *English J* (2002) 347:869–77. doi: 10.1056/NEJMoa020057

Conflict of Interest: HM, KY, MY, HI, and G-IS are employed by the Control of Innate Immunity, Collaborative Innovation Partnership. YN, HI, CK, and G-IS are employed by Macrophi Inc. This does not affect our adherence to journal policies on sharing data and materials.

frontiers in Immunology

BRIEF RESEARCH REPORT
published: 20 September 2021
doi: 10.3389/fimmu.2021.689453

Neuroimmune and Mu-Opioid Receptor Alterations in the Mesocorticolimbic System in a Sex-Dependent Inflammatory Pain-Induced Alcohol Relapse-Like Rat Model

Javier Cuitavi, Jesús David Lorente, Yolanda Campos-Jurado, Ana Polache and Lucía Hipólito *

Department of Pharmacy and Pharmaceutical Technology and Parasitology, University of Valencia, Burjassot, Spain

OPEN ACCESS

Edited by:
Michael D. Burton, The University of Texas at Dallas, United States

Reviewed by:
Subhas Das, Oklahoma State University, United States
Jorge Montesinos, Columbia University, United States
Elio Acquas, University of Cagliari, Italy
María José Sánchez-Catalán, University of Jaume I, Spain

***Correspondence:**
Lucía Hipólito
lucia.hipolito@uv.es

Specialty section:
This article was submitted to Multiple Sclerosis and Neuroimmunology, a section of the journal Frontiers in Immunology

Received: *31 March 2021*
Accepted: *26 August 2021*
Published: *20 September 2021*

Citation:
Cuitavi J, Lorente JD, Campos-Jurado Y, Polache A and Hipólito L (2021) Neuroimmune and Mu-Opioid Receptor Alterations in the Mesocorticolimbic System in a Sex-Dependent Inflammatory Pain-Induced Alcohol Relapse-Like Rat Model. Front. Immunol. 12:689453. doi: 10.3389/fimmu.2021.689453

Evidence concerning the role of alcohol-induced neuroinflammation in alcohol intake and relapse has increased in the last few years. It is also proven that mu-opioid receptors (MORs) mediate the reinforcing properties of alcohol and, interestingly, previous research suggests that neuroinflammation and MORs could be related. Our objective is to study neuroinflammatory states and microglial activation, together with adaptations on MOR expression in the mesocorticolimbic system (MCLS) during the abstinence and relapse phases. To do so, we have used a sex-dependent rat model of complete Freund's adjuvant (CFA)-induced alcohol deprivation effect (ADE). Firstly, our results confirm that only CFA-treated female rats, the only experimental group that showed relapse-like behavior, exhibited specific alterations in the expression of phosphorylated NFκB, iNOS, and COX2 in the PFC and VTA. More interestingly, the analysis of the IBA1 expression revealed a decrease of the microglial activation in PFC during abstinence and an increase of its expression in the relapse phase, together with an augmentation of this activation in the NAc in both phases that only occur in female CFA-treated rats. Additionally, the expression of IL1β also evidenced these dynamic changes through these two phases following similar expression patterns in both areas. Furthermore, the expression of the cytokine IL10 showed a different profile than that of IL1β, indicating anti-inflammatory processes occurring only during abstinence in the PFC of CFA-female rats but neither during the reintroduction phase in PFC nor in the NAc. These data indicate a downregulation of microglial activation and pro-inflammatory processes during abstinence in the PFC, whereas an upregulation can be observed in the NAc during abstinence that is maintained during the reintroduction phase only in CFA-female rats. Secondly, our data reveal a correlation between the alterations observed in IL1β, IBA1 levels, and MOR levels in the PFC and NAc of CFA-treated female rats. Although premature, our data suggest that neuroinflammatory processes, together with neural

adaptations involving MOR, might play an important role in alcohol relapse in female rats, so further investigations are warranted.

Keywords: mu-opioid receptor, alcohol, pain, alcohol deprivation effect, microglia, neuroinflammation

1 INTRODUCTION

Chronic alcohol intake is the third cause of death in developed countries (1, 2), and it is related to many medical conditions, since it is one of the most harmful drugs (3). Alcohol use disorder (AUD) is a recurrent pathological condition that is characterized by repeated relapse episodes after periods of prolonged abstinence (4). Nowadays, pharmacotherapeutic strategies to prevent alcohol relapse have not always shown a great rate of success, probably because there are different aspects (i.e., stress, co-occurrence of other pathologies) that can be developed during abstinence and might impact the efficacy of the anti-relapse pharmacological treatments (5–7). This point is crucial because a better knowledge of neurochemical adaptations occurring during the abstinence and the relapse phases in the presence of different factors (i.e., gender, genetic, contextual, environmental) might help us to develop better therapeutical strategies tailored to the characteristics of the patients.

Mu-opioid receptor (MOR) antagonists (naltrexone and nalmefene) are one of the selected anti-relapse treatments. These medications help reduce the risk of relapse and promote less hazardous drinking (8). Their use is based on the involvement of these receptors in the rewarding and reinforcing properties of alcohol. MORs located in different areas of the mesocorticolimbic system (MCLS) such as the ventral tegmental area (VTA), the nucleus accumbens (NAc), and the prefrontal cortex (PFC) are activated by alcohol-induced endorphin release (9) or alcohol metabolism derivatives (10) to indirectly increase dopaminergic neurons activity and, finally, drive some of the behavioral consequences of alcohol administration. Very interestingly, a variety of literature has revealed a relationship between MOR activation and neuroinflammatory events. On the one hand, MORs on microglia seem to enhance the release of neuroinflammatory mediators, cytokines, and chemokines after their activation (11, 12). On the other hand, pro-inflammatory cytokines such as IL1β, IL6, and TNFα can regulate MOR expression on some immune cells and neurons (13–16). Although this relationship is still not fully understood, cross talk between Toll-like receptor 4 (TLR4) and MORs at the intracellular level seems to participate, as has been recently explained in a revision (17, 18).

Alcohol has also shown to trigger neuroinflammatory events through the TLR4 pathway. In fact, Guerri's laboratory has shown in the last decade that alcohol intermittent administration induces proinflammatory cytokine release through the activation of TLR4, promoting neuronal adaptations (19–23). The reported results by this and other groups have shown that neuroinflammatory events appeared during alcohol administration and early abstinence but might also play an important role in alcohol relapse. In this sense, Ezquer and colleagues have shown very recently that the prevention of alcohol-induced oxidative stress and neuroinflammation in key brain areas of the MCLS through the intranasal administration of exosomes from human mesenquimal cells decreased alcohol intake and blunted alcohol relapse-like binge drinking in female rats bred as alcohol consumers (24).

We hypothesize that, during the abstinence and relapse phases, specific adaptations of the neuroinflammatory state and changes in MOR expression can be developed in selected brain areas of the MCLS of the rats showing relapse-like behavior. To further investigate this hypothesis, we selected a sex-dependent inflammatory pain-induced alcohol deprivation effect (ADE) rat model developed recently by our laboratory based on the complete Freund's adjuvant (CFA) (25). In this model, inflammatory pain could act as a risk factor toward alcohol relapse only in female rats, which were the only group that manifested the ADE (25). It is interesting to note that other animal models to investigate the relapse phenomenon induce alcohol-relapse-like behavior *per se* (i.e., four-bottle choice ADE paradigm), making the investigation of the biochemical adaptation occurring during abstinence in relapsing and non-relapsing individuals difficult. The use of the model proposed here allows us to do this since males and control females do not develop ADE, and the only group showing a significant increase of alcohol intake is the female rats suffering from inflammatory pain. Our objective here, by using this model, is to explore neuroinflammation (measuring phosphorylated NFkB, iNOS, COX2 expression), the activation of microglia (through the expression of IBA1), and cytokine (IL1β and IL10) expression in the abstinence and the reintroduction relapse phases in males and females with or without inflammatory pain in parallel to the expression of the MORs in selected areas of the MCLS.

2 METHODS

2.1 Animals

One hundred fourteen Sprague Dawley adult rats, females and males, were used (Envigo®, Barcelona, Spain). All the animals were kept in inverted light/dark (12/12 h, light on at 22:00) controlled cycles, temperature 23 ± 1°C, and 60% humidity. Each animal was individually housed in a standard plastic cage (42 × 27 × 18 cm^3) with food and tap water provided *ad libitum* throughout the experimental period. Rats were housed in the animal facilities of the University of Valencia. Animal protocols followed in this work were approved by the Animal Care Committee of University of Valencia and were strictly adhered to in compliance with the EEC Council Directive 63/2010 and Spanish laws (RD 53/2013).

2.2 Ethanol Intermittent Access Model and Pain Induction

In this procedure, 40 males and 52 females (total n = 92 rats) followed the classical ethanol intermittent access (IA) model (26) shown in **Figure 1A** in combination with a CFA-based inflammatory pain model (27–29), as we have previously described (25). Rats had free access to 20% ethanol solution and water on Monday, Wednesday, and Friday during 24 h for 8 weeks. After this acquisition period, alcohol was removed for 3 weeks to force a period of abstinence. On the first day of the third week of abstinence, animals received 0.1 ml of CFA (Calbiochem), or sterile saline, in the plantar surface of the hindpaw. The intraplantar injection was made alternately in the right or left hindpaw of the animals in a counterbalance fashion. At the end of 3 weeks of forced abstinence, alcohol was reintroduced following the same IA procedure for five more sessions. Twenty-four hours after the last alcohol session, animals were sacrificed by either isoflurane when the brain was freshly removed or pentobarbital overdose when animals were perfused with paraformaldehyde. Rats belonging to the abstinence groups were sacrificed in the same way after completing 3 weeks of abstinence, on the day when alcohol was supposed to be reintroduced. It is important to notice that brain tissue obtained from all males and 31 females following this protocol were obtained from rats used in a previous study (25). This decision was taken to reduce the number of animals used in this study in compliance with the 3Rs and animal care regulations. Nonetheless, to prove the reproducibility in the animal model first described by Lorente and collaborators (25), a new batch of 21 females was run. Therefore, we only include the alcohol consumption data from these females on this paper (see *Inflammatory Pain Induces Alcohol Relapse in Females* and **Figure 1**). The alcohol consumption data from the males and from the rest of the females can be found in Lorente et al. (2021) (25).

In addition to the rats that followed IA, a control group for the semiquantitative techniques (Western blot and immunofluorescence) composed of 10 females and 12 males

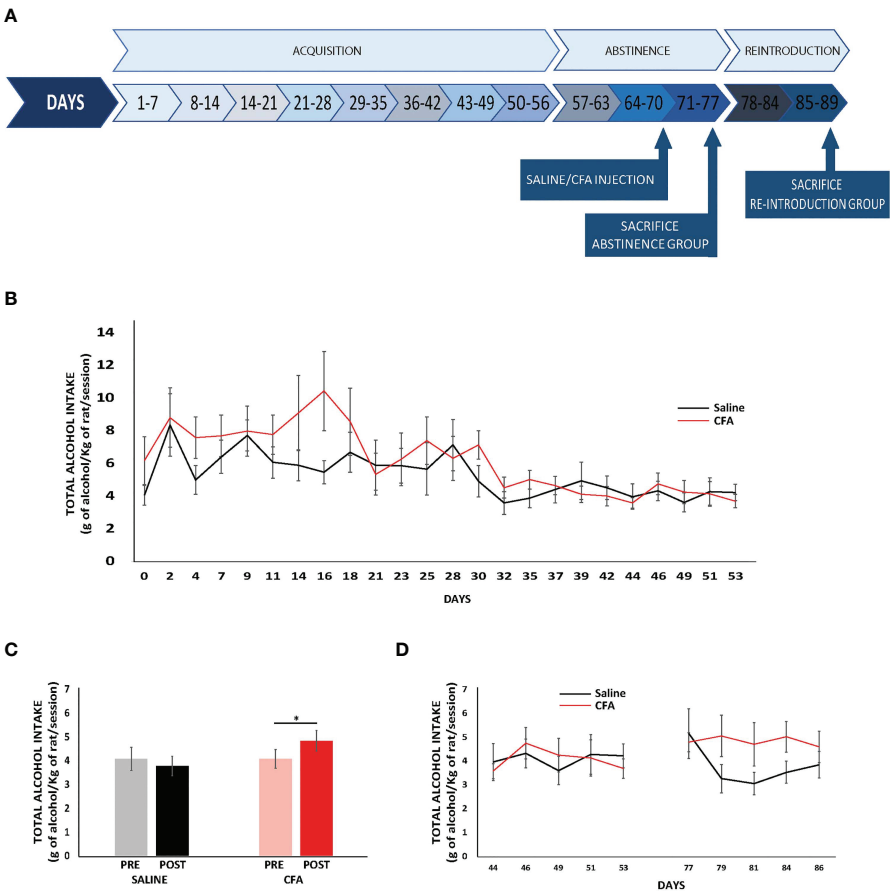

FIGURE 1 | Inflammatory pain induces alcohol relapse in female rats. **(A)** Schematic of the alcohol and inflammatory pain experimental design. **(B)** Alcohol intake during the acquisition period. Data are expressed as mean ± SEM of each consumption day (n = 10–11/group) (ANOVA for repeated measures, $p > 0.05$). **(C)** Mean ± SEM (left saline-female and right CFA-female) of total alcohol intake (g/kg/day) of the 5-day pre- (basal, lighter bar) and post-abstinence (darker bars) shown in gray/black for the saline-treated group (n = 10/group) and in pink/red for the CFA-treated group (n = 11/group) (ANOVA for repeated measures followed by Bonferroni multiple comparisons, *$p < 0.05$). **(D)** Mean ± SEM of total alcohol intake (g/kg/day) of the last 5 consumption days pre-abstinence and the 5 consumption days post-abstinence (n = 10–11/group); saline-females in black and CFA-females in red (ANOVA for repeated measures, $p > 0.05$).

(n = 22), only having access to water, was run at the same time. Half of the animals from this group were sacrificed by isoflurane when the brain was freshly removed whereas the other half were sacrificed by pentobarbital overdose when animals were perfused with paraformaldehyde.

Therefore, 10 experimental groups were organized by sex:

1. Male (n = 52): control group (rats that had access only to water) and four groups that followed the IA protocol, SAL-A (rats without pain, sacrificed during abstinence), SAL-R (rats without pain sacrificed after reintroduction), CFA-A (rats in pain sacrificed during abstinence), and CFA-R (rats in pain sacrificed after reintroduction);
2. Female (n = 62): control group and four groups that followed the IA protocol, SAL-A, SAL-R, CFA-A, and CFA-R.

2.3 Western Blot

This technique was used to measure the expression levels of phosphorylated-NFκB, iNOS, COX2, IL1β, IL10, and MOR, in different brain areas from control and IA animals sacrificed by isoflurane overdose. Freshly removed brains from 30 females (n = 6/condition) and 30 males (n = 6/condition) were immediately frozen in dry ice and stored at -80°C until the Western blot experiment was performed. Then, PFC, NAc, and VTA were dissected in both hemispheres, and the tissues were homogenized in cold lysis buffer (1% IGEPAL CA-630, 20 mM Tris–HCl pH 8, 130 mM NaCl, 10 mM NaF, and 1% protease inhibitor cocktail, Sigma, St. Louis), using 0.5 ml of lysis buffer each 250 mg of tissue. The homogenate extracts were kept in ice for 30 min. Afterward, samples were immediately centrifuged at 15,000 g for 15 min at 4°C; the supernatant was collected to determine the protein concentration by using a Bradford protein assay kit (Bio-Rad). This procedure was adapted from one previously used (30, 31).

Western blot was used to determine the expression levels of the abovementioned proteins in the homogenate extracts. To do so, we followed a previously used protocol described by Lorente and collaborators (25). The following primary antibodies were used: rabbit IgG anti-MOR (1:1000, Abcam ab134054) (32), rabbit IgG anti-phosphorylated-NFκB p65 (1:1000, Abcam ab86299) (33), rabbit IgG anti-iNOS (1:500, Abcam ab204017) (34), rabbit IgG anti-COX2 (1:1000, Abcam ab52237) (35), rabbit IgG anti-IL1β (1:2500, Invitrogen PA5-79485), and rabbit anti-IL10 (1:2500, Abcam ab9969) (36). Goat IgG anti-rabbit (1:1000, Bio-Rad 1706515) was used as a secondary antibody. Mouse IgG anti-GAPDH conjugated with HRP (1:1000, Invitrogen MA5-15738-HRP) (37) was used to detect GAPDH as a protein loading control. When the membranes were incubated with more than one primary antibody, before probing with the second or third antibody, they were treated with Restore™ Western Blot Stripping Buffer (Thermo Fisher) for 15 min. Finally, the intensity of the bands was expressed as arbitrary units and normalized to GAPDH band intensity. Relative protein levels to control were determined by setting the control group to 100% and calculating the respective percentages for each band. All samples (20 μg) were run in duplicate, obtaining an average of the % from control for each sample. A representative image obtained from each group included in the Western blot analysis is shown on **Supplementary Figure 1**.

2.4 Immunofluorescence

Microglial activation was assessed by measuring ionized calcium-binding adapter molecule 1 (IBA1) expression with an immunofluorescence assay (38). To do so, control and IA animals were used. Thirty-two females (control: n = 4; SAL-A, SAL-R, CFA-A, CFA_R: n = 7/condition) and 22 males (control: n = 6; SAL-A, SAL-R, CFA-A, CFA-R: n = 4/condition) were anesthetized by injecting pentobarbital and followed a procedure of cardiac perfusion with 200 ml paraformaldehyde 0.4% in phosphate buffer (PB) 0.1 M. Brains were extracted and kept in the same perfusion solution for 20 h at 4™C. After that, they were transferred to sucrose 30% in PB 0.1 M for 3 days. Following this, 40-μm brain slices were obtained in four series on a freezing microtome and were stored at -80°C in sucrose 30% in PB 0.1 M until their use. Immunofluorescence was performed as previously described (25). The rabbit IgG anti-IBA1 (1:2000, Wako 019-19741) primary antibody (39) and the donkey IgG anti-rabbit Alexa Fluor® 488 (1:1000, Invitrogen A32790) secondary antibody were used.

Images from PFC, NAc, and VTA were obtained with a ×20 objective (Leica Biosystems, Germany; images size 441 × 330 μm). We obtained six to eight images (from both hemispheres) per area, and mean gray intensity (MGI) was analyzed by means of FIJI software. Results were expressed in percentage of the control group. A representative microphotography of the DAPI and IBA1 staining is shown in **Supplementary Figures 1** and **2**.

2.5 Statistical Analysis

Results are shown as mean ± standard error of the mean (SEM). To perform the statistical analysis, the 26.0 version of the SPSS program was used. The Kolmogorov–Smirnov test and Levene's test were performed to assess the normality and the homogeneity of the variance of the data. When an experimental variable (i.e., alcohol consumption) was continuously measured (i.e., along the experimental procedure), an ANOVA for repeated measures was applied followed by Bonferroni multiple comparisons when appropriate. For Western blot and immunofluorescence, the control group (non-treated rats not exposed to alcohol) was used to allow us to compare the rest of the groups by normalizing them to control in a percentage. For these experiments, the two-way ANOVA test was performed followed by Bonferroni multiple comparisons when significant differences in the main effects (pain; abstinence) or in the interaction were detected. In all the statistical tests, a 95% confidence level was set.

3 RESULTS

3.1 Inflammatory Pain Induces Alcohol Relapse in Female Rats

Figure 1B shows the total alcohol intake rate (g/kg/session) of the new batch of 21 females run in this study along the days of

the acquisition period. Very importantly, no significant differences were found in alcohol consumption before the forced abstinence period between females that were afterward injected with CFA and the ones injected with saline (**Figure 1B**; ANOVA repeated measures, $F(1,19) = 1.048$ $p = 0.319$). **Figure 1C** shows the averages of the alcohol intake levels during the last 5 days of acquisition and the 5 days of reintroduction. Interestingly, the repeated-measure ANOVA showed significant differences ($F(1,19) = 4.615$ $p = 0.045$). In fact, the *post-hoc* test revealed that CFA-female rats significantly increased their consumption levels regarding the basal levels whereas animals injected with saline did not change their consumption levels (**Figure 1D** shows single-day data from the last 5 days of acquisition and the 5 days of reintroduction. Repeated-measure ANOVA showed that there are no differences in the ethanol intake between saline and CFA female rats through time ($F(1,19) = 0.858$ $p = 0.366$) but, as can be observed in the figure, CFA female rats presented higher levels of ethanol consumption than saline ones after reintroduction every testing day.

3.2 Biochemical Analysis of Neuroinflammatory Mediators, IBA-1, IL1β, IL10, and MOR Expression in PFC, NAc, and VTA of Saline and CFA-Treated Male and Female Rats in Abstinence and Reintroduction Phases

Statistical analysis and values of the F and p for the main effects *pain* and *abstinence/re-introduction* and the interaction are summarized in the table of the **Supplementary Material**.

3.2.1 Alcohol-Induced Neuroinflammation in PFC, NAc, and VTA of CFA-Treated Females Present Specific Alterations During Abstinence and Reintroduction Phases

As has previously been shown in the literature, during chronic alcohol administration and early abstinence (24 h), neuroinflammatory pathway is activated. Thereby, the levels of transcriptional factors (as pNFκB) and neuroinflammatory mediators (such as iNOS and COX2) are increased (20, 40). To investigate the neuroinflammatory pathway activation in NAc, PFC, and VTA of saline and CFA rats during abstinence and relapse, we measured by Western blot the levels of phosphorylated NFκB, iNOS, and COX2.

The two-way ANOVA performed found statistically significant differences in main variables and/or its interaction in PFC from saline- and CFA-treated females and males. On the one hand, regarding female rats, pNFκB levels were significantly increased after alcohol reintroduction regardless of the presence of inflammatory pain (**Figure 2A**: SAL_A *vs.* SAL_R, p= 0.03; CFA_A *vs.* CFA_R, $p = 0.0001$). When analyzing iNOS, we observe the opposite phenomenon since its levels were significantly decreased after alcohol reintroduction, regardless of the presence of inflammatory pain (**Figure 2D**: SAL_A *vs.* SAL_R, $p = 0.014$; CFA_A *vs.* CFA_R, $p = 0.036$). Very interestingly, COX2 was the only neuroinflammatory mediator that significantly increased after reintroduction only in CFA-females, indicating a specific change derived from the development of pain during abstinence (**Figure 2G**, CFA_A *vs.* CFA_R, $p = 0.0001$). On the other hand, regarding male rats, no significant differences were observed when analyzing the levels of pNFκB (**Figure 2J**). However, iNOS and COX2 show statistically significant alterations between groups. Interestingly, both proteins are altered only in CFA-males during abstinence since they have significantly higher levels of those proteins during abstinence than after reintroduction, which could be a direct consequence of the presence of inflammatory pain (**Figures 2M, P**).

We also observed significant alterations in VTA from females in our animal model when analyzing pNFκB and iNOS, but we did not observe any significant changes for COX2 (**Figure 2I**). Interestingly, inflammatory pain alters pNFκB levels in a different pattern during abstinence and after alcohol reintroduction in comparison with saline-females. Indeed, CFA-females have higher pNFκB levels than SAL-females during abstinence ($p = 0.0001$). Nonetheless, SAL-females increase their pNFκB levels after alcohol reintroduction ($p = 0.0001$), whereas CFA-females decrease them ($p = 0.007$) (**Figure 2C**). The two-way ANOVA also found differences for the main effect pain when analyzing iNOS expression in the VTA of female rats (**Figure 2F**). In this case, iNOS expression increased only in CFA-females after alcohol reintroduction which was only significant when compared with SAL-females ($p = 0.016$).

Finally, the two-way ANOVA tests performed failed to find any significant differences between groups in NAc for both females and males when analyzing pNFκB, iNOS, and COX2 (**Figure 2B**: pNFκB; **Figures 2E, N**: iNOS, **Figures 2H, Q**: COX2). Additionally, we found no significant differences when comparing groups in VTA from males (**Figures 2L, O, R**).

3.2.2 IBA1 Expression Is Decreased During Abstinence and Increased After Reintroduction of the Alcohol Beverages in the PFC Whereas Opposed Alterations Are Observed in the NAc of Only CFA-Treated Female Rats

Neuroinflammatory processes within the brain are partially regulated by glial cells. Microglia are the immune cells per excellence in the brain. Therefore, we assessed microglial activation with IBA1 immunofluorescence in brain areas of the mesocorticolimbic system, as shown in **Figure 3**.

The two-way ANOVA tests performed showed significant differences when comparing groups in female rats for PFC and NAc, but not for VTA IBA1 staining (**Figure 3E**). Regarding PFC, CFA-females show significantly lower levels during abstinence than after reintroduction ($p = 0.004$) and when compared to SAL-females ($p = 0.009$) during the same period (**Figure 3A**). Interestingly, alterations produced by pain in the NAc were not dependent on the abstinence or relapse-like phase, indicating a specific change for CFA-treated female rats (**Figure 3B**). In fact, inflammatory pain induces microglial activation in both periods since its expression is significantly

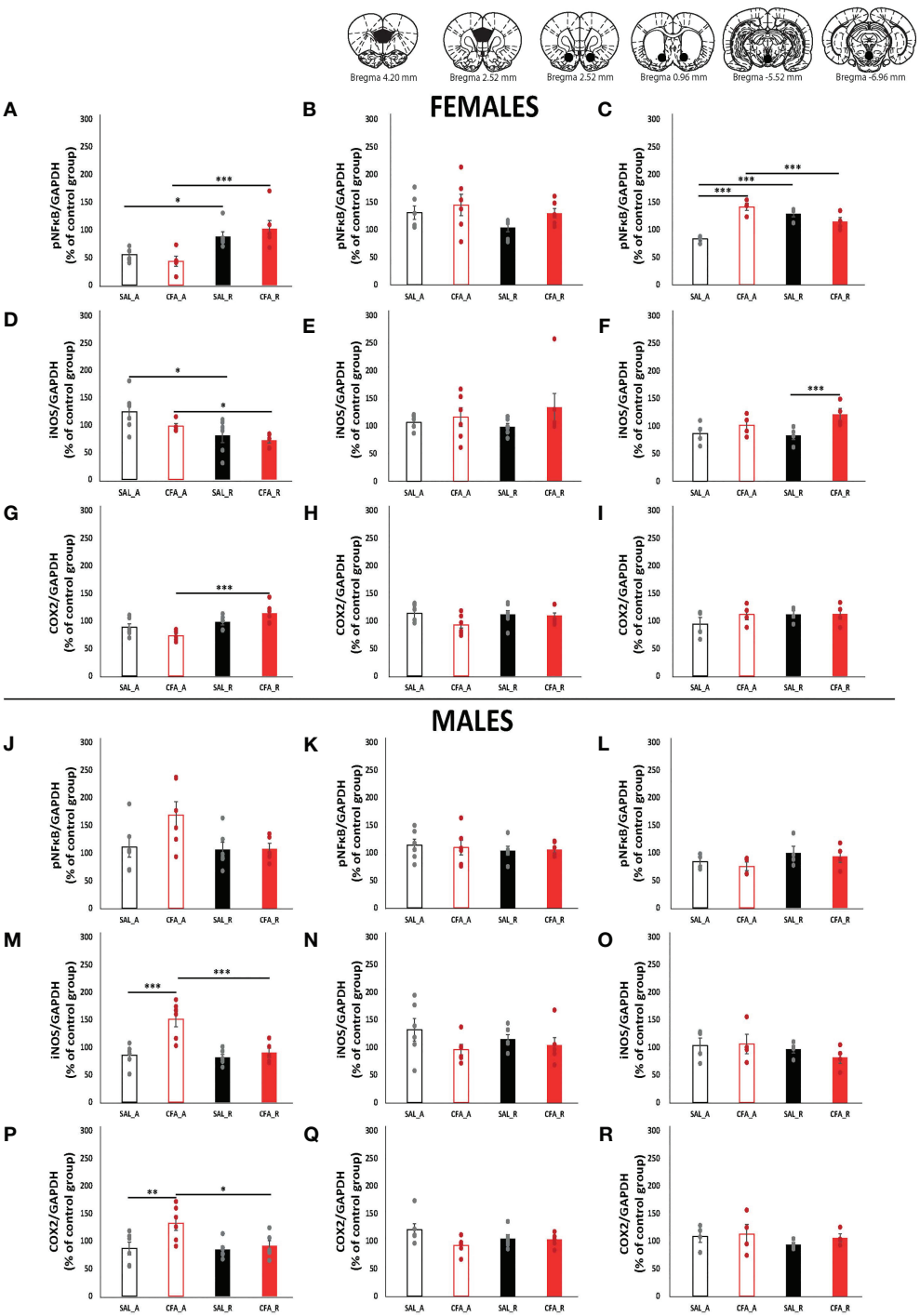

FIGURE 2 | Alterations of inflammatory mediators during the abstinence and the alcohol reintroduction periods in the presence or absence of inflammatory pain in female and male rats. Data are expressed as mean ± SEM of protein levels in % relative to control (n = 4–6/group). Black and red bars represent saline and CFA-females, respectively, during abstinence (empty bars) and after abstinence (filled bars) periods. Points represent the individual data from each animal from the group. On top, schematic representations of the punched brain areas harvested to perform the Western blots. Graphs **(A–I)** gather the protein analysis of female rats and graphs **(J–R)** those from male rats; PFC, NAc, and VTA protein analyses are represented in the following order, PFC: **(A**, **D**, **G**, **J**, **M**, **P)**; NAc: **(B**, **E**, **H**, **K**, **N**, **Q)**; VTA: **(C**, **F**, **I**, **L**, **O**, **R)**. The proteins analyzed are pNFκB **(A–C**, **J–L)**, iNOS **(D–F**, **M–O)**, and COX2 **(G–I**, **P–R)**. Asterisks mark statistically significant differences in the Bonferroni multiple-comparison test applied when the two-way ANOVA detected significant differences in the main effects or in the interaction (*$p < 0.05$, **$p < 0.01$, ***$p < 0.005$). CFA, complete Freund adjuvant; SAL, saline; A, abstinence period; R, reintroduction period; PRC, prefrontal cortex; NAc, nucleus accumbens; VTA, ventral tegmental area; pNFκB, phosphorylated nuclear factor κB; iNOS, inducible nitric oxide synthase and COX2, cyclooxygenase 2.

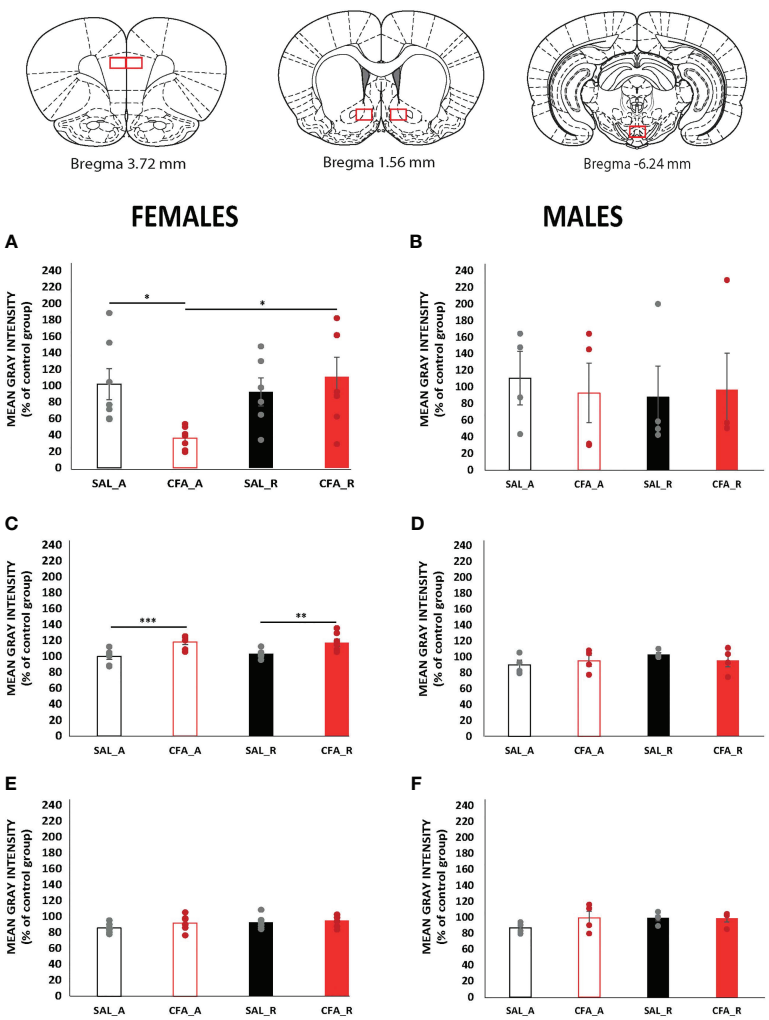

FIGURE 3 | Alterations of microglial activation measured as IBA1 staining during the abstinence and the alcohol reintroduction periods in the presence or absence of inflammatory pain in female and male rats. Data are expressed as mean ± SEM of IBA1 levels in % relative to control (n = 4–7/group). Black and red bars represent saline and CFA-females, respectively, during the abstinence (empty bars) and after abstinence (filled bars) periods. Points represent the individual data from each animal from the group. On the bottom, brain schematics representing the areas where the pictures were taken (Paxinos and Watson 2006). Graphs **(A, C, E)** gather the protein analysis of female rats, and graphs **(B, D, F)** those from male rats; PFC, NAc, and VTA protein analyses are represented in the following order, PFC: **(A, B)**; NAc: **(C, D)**; VTA: **(E, F)** Asterisks mark statistically significant differences in the Bonferroni multiple-comparison test applied when the two-way ANOVA detected significant differences in the main effects or in the interaction (*$p < 0.05$, **$p < 0.01$, ***$p < 0.005$). CFA, complete Freund adjuvant; SAL, saline; A, abstinence period; R, reintroduction period; PFC, prefrontal cortex; NAc, nucleus accumbens; VTA, ventral tegmental area; IBA1, ionized calcium-binding adapter molecule 1.

higher, about 20% higher, for CFA-females than for SAL-females in both abstinence ($p = 0.001$ and reintroduction ($p = 0.007$).

Very interestingly, no significant changes were observed when comparing groups in male rats for neither PFC (**Figure 3B**), NAc (**Figure 3D**), nor VTA (**Figure 3F**).

3.2.3 Downregulation and Upregulation of IL1β and IL10 in the NAc but Not in the PFC of CFA-Treated Female Rats Follow a Different Pattern Than That Observed in Saline-Treated Female Rats

Pro-inflammatory and anti-inflammatory cytokines mainly regulate the activity of several cells, above all immune cells, promoting cell communication. Since we observed alterations in microglial activation in PFC and NAc from female rats, we analyzed the levels of the pro-inflammatory cytokine IL1β and the anti-inflammatory one IL10 in those areas from females.

On the one hand, regarding PFC, the levels of IL1β were significantly lower during abstinence than after reintroduction regardless of the presence of inflammatory pain (**Figure 4A**. Bonferroni multiple comparison: SAL_A *vs.* SAL_R, $p = 0.001$; CFA_A *vs.* CFA_R, $p = 0.0001$). Interestingly, we observed the opposite changes in IL10, indicating a different regulation of pro- and anti-inflammatory events. The levels of IL10 suffered a decrease after reintroduction of the alcohol beverages

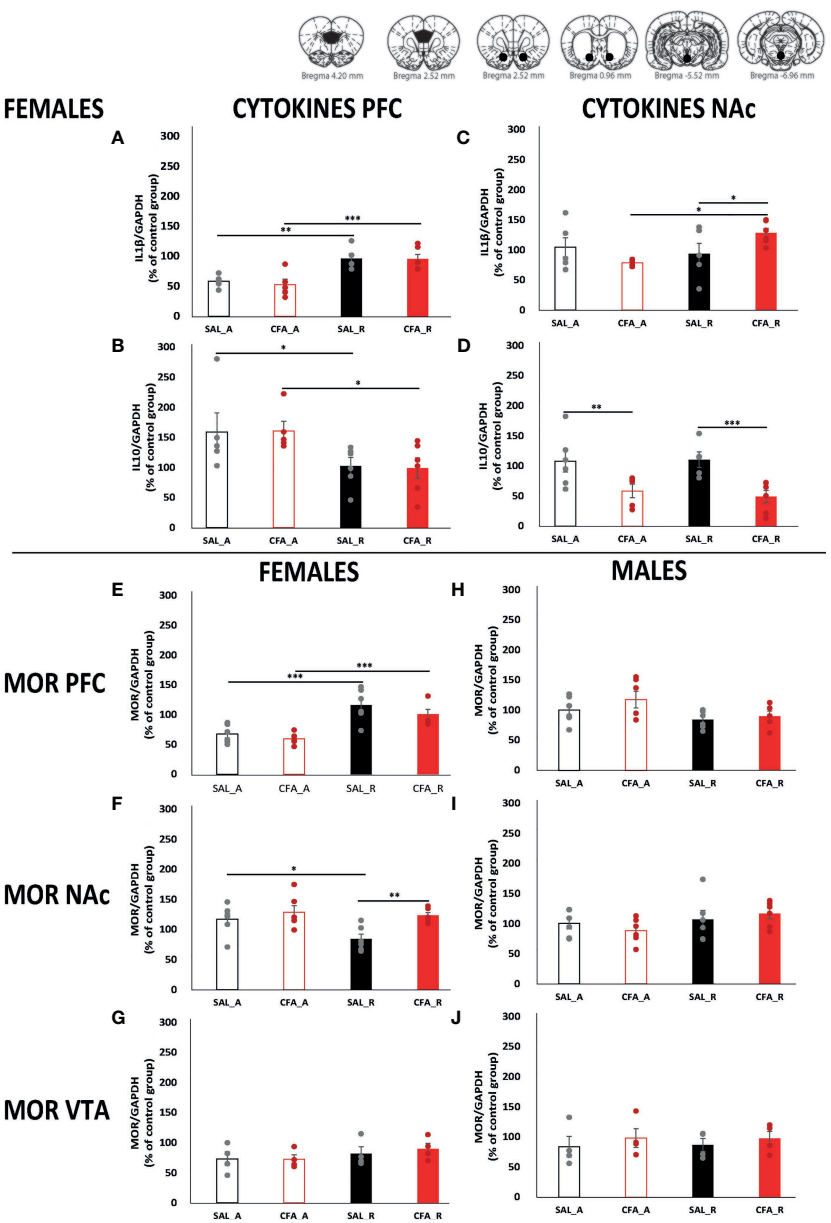

FIGURE 4 | Alterations of inflammatory mediators during the abstinence and the alcohol reintroduction periods in the presence or absence of inflammatory pain in female and male rats. Data are expressed as mean ± SEM of protein levels in % relative to control (n = 4–6/group). Black and red bars represent saline and CFA-females, respectively, during abstinence (empty bars) and after abstinence (filled bars) periods. Points represent the individual data from each animal from the group. On top, schematic representations of the punched brain areas harvested to perform the western blots. Graphs **(A–G)** gather the protein analysis of female rats and graphs **(H–J)** those from male rats; PFC, NAc, and VTA protein analyses are represented in the following order, PFC: **(A, B, E, H)**; NAc: **(C, D, F, I)**; VTA: **(G, J)**. The proteins analyzed are IL1β **(A, C)**, IL10 **(B, D)**, and MOR **(E–J)**. Asterisks mark statistically significant differences in the Bonferroni multiple-comparison test applied when the two-way ANOVA detected significant differences in the main effects or in the interaction (*p < 0.05, **p < 0.01, ***p < 0.005). CFA, complete Freund adjuvant; SAL, saline; A, abstinence period; R, reintroduction period; PFC, prefrontal cortex; NAc, nucleus accumbens; VTA, ventral tegmental area; IL1b, interleukin 1b; IL10, interleukin 10; MOR, mu-opioid receptor.

regardless of the presence of inflammatory pain (**Figure 4B**. Bonferroni multiple comparisons: SAL_A *vs*. SAL_R, p = 0.037; CFA_A *vs*. CFA_R, p = 0.025). On the other hand, in NAc of CFA-treated female rats, the levels of IL1β significantly increased after reintroduction (p = 0.006) and also when compared to SAL-animals (p = 0.045). Furthermore, when analyzing the levels of the anti-inflammatory cytokine IL10, the development of inflammatory pain significantly decreased the levels of IL10 during abstinence (0.011) and after reintroduction (p = 0.002) when compared to SAL-females (**Figure 4D**).

3.2.4 Alcohol and Inflammatory Pain Impacts MOR Expression Patterns in PFC and NAc During Abstinence and Reintroduction Phases in Female Rats: Specific Effect of the Presence of Pain in the NAc

MOR activation during reintroduction phases in areas of the MSCL has shown to play a crucial role in alcohol-relapse-like behavior (41). To investigate dynamic changes of MOR expression in the MSCL areas of interest in the abstinence and reintroduction phases of male and female rats in our model, we measured its relative expression levels by Western blot. **Figure 4** shows MOR expression in saline and CFA-treated female rats during abstinence and after alcohol reintroduction, and in control females in the same conditions. The two-way ANOVA tests performed confirmed that MOR levels were altered depending on the alcohol drinking period, the brain area studied, and the sex.

No changes were observed in the MOR expression of male rats in PFC (**Figure 4H**), NAc (**Figure 4I**), and VTA (**Figure 4J**). Moreover, the expression of MOR in VTA from female rats did not show any significant alterations between groups (**Figure 4G**).

Interestingly, MOR levels were significantly lower during abstinence than after reintroduction regardless of the presence of inflammatory pain in PFC from female rats (**Figure 4E**, Bonferroni multiple comparisons: SAL_A *vs*. SAL_R, $p = 0.0001$; CFA_A *vs*. CFA_R, $p = 0.001$). Finally, very interesting data show alterations in the pattern of MOR expression depending on the presence of pain in the NAc (**Figure 4F**). In the case of saline-treated female rats, MOR expression was reduced after the reintroduction of the alcohol beverages when compared to the abstinence period ($p = 0.018$). In addition, inflammatory pain significantly increases the levels of MORs by 50% in female rats after reintroduction when compared to saline-treated female rats ($p = 0.006$).

4 DISCUSSION

Our present results show dynamic alterations of microglial activation and neuroinflammatory mediator, cytokine, and MOR expression through the abstinence and reintroduction phases of a sex-dependent inflammatory pain-induced alcohol relapse rat model. Some of these alterations demonstrate to be dependent on the sex, abstinence, or reintroduction to alcohol drinking, the MCLS areas studied or their interaction providing new insights into neuroinflammatory properties of alcohol and its interaction with pain-induced alterations in these areas. Firstly, our drinking behavior results in female rats confirm that CFA-treated female rats show ADE, but the saline-treated ones do not as we have previously described in (25). Moreover, this group exhibited alterations in pNFκB and COX2, microglial activation (measured as IBA1 expression), and expression of IL1β and IL10 together with MOR in the PFC, NAc, and/or VTA, with those unique changes in NAc being of a special relevance. Indeed, these results showed a decrease of microglial activation in the PFC only during abstinence, and an augmentation of the microglial activation in the NAc of CFA-female rats in both abstinence and reintroduction phases. Additionally, the expression of pNFκB and IL1β also evidenced these dynamic changes through these two phases following similar expression patterns in both areas. As mentioned, these changes in NAc were observed in the presence of inflammatory pain only in female rats, which was the condition that triggered alcohol-relapse-like behavior in our animal model. Additionally, the expression of cytokine IL10 showed a different profile than the IL1β one, indicating anti-inflammatory processes occurring only during abstinence in the PFC of CFA-female rats, but not during the reintroduction phase in PFC or in the NAc. All in all, these data might indicate a downregulation of microglial activation and pro-inflammatory processes during abstinence in the PFC regardless of the presence of pain, whereas an upregulation can be observed in the NAc during abstinence that is maintained during the reintroduction phase only in CFA-treated females. Furthermore, we also investigated the expression of MORs in the same areas of the MCLS in the abstinence and reintroduction phases of our animal model. Notably, the same dynamics were also observed in the case of the MOR expression, suggesting that the already described interaction between MORs and neuroinflammation might also be underlying the adaptations developed during the abstinence and reintroduction phases.

To our knowledge, this is the first study analyzing neuroinflammatory mediators, microglial activation, and cytokines in the abstinence and alcohol relapse phases of a model that allows to compare sex-dependent behavior. Several reports have shown that chronic alcohol induces neuro inflammation, probably through TLR4, to produce release of diverse pro-inflammatory cytokines (21) and cause neural damage (22). These effects of alcohol exposure seem to be more intense in females than in males (42, 43), and, as shown in **Figure 2**, although the development of pain itself during abstinence altered some of these neuroinflammatory mediators in both male and female rats, our data failed to show increases in neuroinflammatory mediators in male rats. One plausible explanation might be related with the experimental protocol which allows free drinking, instead of forced alcohol intake shown in other studies (20, 44, 45), or the fact that sacrifices were carried out 24 h after the last alcohol consumption, allowing increased neuroinflammatory markers to return to normal levels. Very interestingly, the effect of inflammatory pain in neuroinflammation and microglial activation (see **Figures 2C, M, P**, **3C**) has recently captured the attention of researchers. Recent publications have shown that systemic inflammation leads also to the elevated presence of inflammatory mediators in the brain, which correlates with depressive-like behaviors in patients but also with negative affective state and alterations in neuronal excitability of neurons of NAc in mice (46–48). In line with these data, adaptations derived from the presence of pain might also account for the neuroinflammatory effects produced by alcohol, as is shown in our case for some studied proteins in CFA-treated female rats during abstinence and/or reintroduction phases.

Increasing evidence involves the innate immune system in alcohol drinking (49) and alcohol relapse behavior in female rats. Thus, in a very interesting set of studies, Ezquer and colleagues showed that administration of the secretome or exosomes from human mesenchymal cells prevented the increase in alcohol drinking after a period of abstinence in their female rat model (24, 50). In accordance with these results, our present data showed an increase of IBA1 staining in NAc of CFA-treated female rats during abstinence. Interestingly, in this same experimental group, IL10 expression in the NAc was downregulated, suggesting a pro-inflammatory state that might play a role in promoting ADE since we did not observe these changes in any of the non-relapsing groups. In addition to that, when alcohol was reintroduced, and presumably due to the presence of alcohol, the proinflammatory state was maintained as data of IBA1, pNFκB, and IL1β expression evidenced. Contrary to that, in PFC, CFA-treated female rats showed an anti-inflammatory state during abstinence that was reverted to pro-inflammatory state after alcohol reintroduction most likely as a consequence of alcohol intake and regardless of the presence of pain. In this case, IBA1 staining and the expression of pNFκB and IL1β were significantly lower, together with significantly higher levels of IL10 during abstinence. In line with these results, it has recently been shown that chronic intermittent access to ethanol and lipopolysaccharide exposure differentially alters PFC and NAc microglia soma volume 10 h after the end of the alcohol IA protocol, with microglia from PFC being more affected than that from NAc (51). These brain-region-dependent alterations might be a consequence of the presence of different subtypes of microglia populating in each area (52). It is also very interesting to observe that these alterations in the expression of IBA1 and IL1β in NAc of saline-treated females are different from those observed in CFA-treated females. Altogether, these significantly different alterations for CFA-treated female rats might be taken into consideration since they could potentially explain the inflammatory pain-induced alcohol relapse phenomenon that we observe in our model with only female rats.

Finally, abstinence and alcohol reintroduction did not increase microglial activation in VTA which is in accordance with previous results showing no effect of alcohol on microglial activation in VTA from postmortem human brains (53). From all the proteins studied, only pNFκB and iNOS after reintroduction of alcohol showed significant alterations in the VTA, but because of the involvement of this transcription factor in different physiological events, it is difficult to interpret its significance in the observed behavior. Moreover, we have not measured the levels of the non-phosphorylated form of NFκB, which is also a limitation of the study that makes even more difficult to interpret these results. Further studies should address the consequences of this increase in the pNFκB observed after alcohol reintroduction and its differences in saline versus CFA-treated females.

Interestingly, our results connect microglial activation and the expression of IL1β with MOR levels in relevant brain areas of MCLS. This correlation has already been described in a neonatal alcohol intake model in rats (12). In this report, the authors suggested that microglial MOR activation enhances the neuroinflammatory response, as other papers have also previously reported (11, 12, 54). In addition, the presence of neuroinflammation, and, more specifically, the increase of IL-1β, might influence MOR expression (13–16). In general, our results support these previous reports showing a bidirectional relationship between MORs and IL-1β. Nonetheless, it is interesting to mention that in the NAc, MOR expression remain unaltered during abstinence and after reintroduction to alcohol in CFA-female rats, whereas IL1β significantly increases only after the reintroduction of alcohol. Anyway, IL1β and MOR expressions are both significantly increased in CFA-treated females in the reintroduction phase (**Figures 4C, F**). This lack of correlation with IL1β in the abstinence period might be a consequence of different timelines in the expression patterns. In addition to this, MOR activation can also reduce the levels of anti-inflammatory cytokines such as IL10 (55, 56), and, as our results evidence, in NAc and PFC of females, MORs and IL10 expression levels are opposed along the different phases. The presence of neuroinflammation, and alterations of MCLS MOR expression, are suggested to underlie alcohol neurobiological effects and relapse-like behavior (23, 24, 57–60). All in all, these results point to neuroinflammation-MOR cross talk as a relevant piece in the abstinence and relapse neurobiological substrate puzzle.

Collectively, our results suggest that microglial activation and the resulting neuroinflammation, together with MOR level alterations in PFC and NAc, are likely to participate in an inflammatory pain-induced relapse-like behavior in female rats. Nonetheless, further research to clarify the role of the glial-neuron cross talk in alcohol relapse is warranted.

DATA AVAILABILITY STATEMENT

The raw data supporting the conclusions of this article will be made available by the authors, without undue reservation.

ETHICS STATEMENT

The animal study was reviewed and approved by the Ethics Committee in Experimentation and Animal Welfare of the University of Valencia and the local Goverment of Valencia (Conselleria d'Agricultura, Desenvolupament Rural, Emergéncia Climática i Transició Ecológica).

AUTHOR CONTRIBUTIONS

Conceptualization, LH and JC. Methodology, JC, JDL, YC-J, and LH. Formal analysis, JC and LH. Investigation, JC, JDL, and YC-J. Writing—original draft, JC. Resources, LH. Supervision, AP and LH. Writing—review and editing, JC, JDL, YC-J, AP, and LH. All authors contributed to the article and approved the submitted version.

FUNDING

This study has been supported by Spanish Ministerio de Ciencia e Innovación PID2019-109823RB-I00 (LH) and by Spanish Ministerio de Sanidad, Delegación del Gobierno para el Plan Nacional sobre Drogas PNSD2019I038 (LH). JC is supported by a Atracció de Talent PhD Fellowship from the University of Valencia (UV-INV-PREDOC-1327981).

ACKNOWLEDGMENTS

Firstly, we would like to acknowledge Dr. Carmen Agustín-Pavón for her kind provision of her valuable scientific input and for providing the microscope for immunofluorescence experiments. We would like to thank Mr. J.L. González-Romero for his assistance as lab technician and Ms. Pilar Laso, Mr. Clemente Bañuls, and Dr. Carmen Olmos for grant management. We would also thank Dr. Inmaculada Noguera, Chief Veterinarian Officer, and the personnel of the Animal facilities (SCSIE) at the University of Valencia for their help and effort in assuring animal welfare. We would also like to thank Mr. Darren Robinson for English Proofreading.

SUPPLEMENTARY MATERIAL

The Supplementary Material for this article can be found online at: https://www.frontiersin.org/articles/10.3389/fimmu.2021.689453/full#supplementary-material

Supplementary Figure 1 | Representative images of DAPI and IBA1 staining from each group in females taken with 20x objective. White scale bars represent 100 μm. Brain schematics represent the areas where the pictures were taken (Paxinos and Watson 2006). CFA, complete Freund Adjuvant; SAL, saline; C, control; A, abstinence period; R, re-introduction period; PFC, prefrontal cortex; NAc, nucleus accumbens; VTA, ventral tegmental area; IBA1, ionized calcium-binding adapter molecule 1; DAPI, 4′,6-diamidino-2-phenylindole.

Supplementary Figure 2 | Representative images of DAPI and IBA1staining from each group in males taken with 20x objective. White scale bars represent 100 μm. Brain schematics represent the areas where the pictures were taken (Paxinos and Watson 2006). CFA, Complete Freund Adjuvant; SAL, saline; C, control; A, abstinence period; R, re-introduction period; PFC, prefrontal cortex; NAc, nucleus accumbens; VTA, ventral tegmental area; IBA1, ionized calcium-binding adapter molecule 1; DAPI, 4′,6-diamidino-2-phenylindole.

Supplementary Figure 3 | Representative measured bands obtained in the western blot from each group and each analysed protein. CFA, Complete Freund Adjuvant; C, control; SAL, saline; A, abstinence period; R, reintroductionperiod; PFC, prefrontal cortex; NAc, nucleus accumbens; VTA, ventral tegmental area; pNF-kB, phosphorylated Nuclear Factor kB; iNOS, inducible Nitric Oxide Synthase; COX2, Cyclooxygenase 2; IL1b, Interleukin 1b; IL10, Interleukin 10; MOR, Mu-Opioid Receptor.

Supplementary Table 1 | Statistical analysis for **Figures 2**–**4** (Two-Way ANOVA, SPSS 26) Partial Eta2: proportion of explained variance, prefrontal cortex (PFC), nucleus accumbens (NAc), ventral tegmental area (VTA), phosphorylated Nuclear Factor κB (pNF-κB), inducible Nitric Oxide Synthase (iNOS), Cyclooxygenase 2 (COX2), Interleukin 1β (IL1β), Interleukin 10 (IL10), Mu Opioid Receptor (MOR) and ionized calcium-binding adapter molecule 1 (IBA1).

Supplementary Table 2 | Summary of the significant changes observed in the immunofluorescence and western blot analysis. In yellow we present significant effects in main variable abstinence and re-introduction periods, in blue significant effects in main effect saline-treated and CFA-treated rats, in green the significant effects for both and in red no differences. + and - simbols are used to indicate if the group presents higher (+) or lower (-) levels of the protein of analysis when compared to another group with the Bonferroni multiple comparisons. In green cell two simbols are provided, the first one to indicate differences between abstinence and re-introduction and the second one to indicate differences between saline- and CFA-treated rats. CFA, Complete Freund Adjuvant; SAL, saline; A, abstinence period; R, re-introduction period; PFC, prefrontal cortex; NAc, nucleus accumbens.

REFERENCES

1. World Health Organization. World Health Organization. Ageing, Life Course Unit. In: *WHO Global Report on Falls Prevention in Older Age*. Geneva: World Health Organization (2008).
2. Organization WH. *Global Status Report on Alcohol and Health 2018*. Geneva: World Health Organization (2019).
3. Nutt DJ, King LA, Phillips LD. Drug Harms in the UK: A Multicriteria Decision Analysis. *The Lancet* (2010) 376:1558–65. doi: 10.1016/S0140-6736(10)61462-6
4. Gilpin NW, Koob GF. Neurobiology of Alcohol Dependence: Focus on Motivational Mechanisms. *Alcohol Res Health* (2008) 31:185–95.
5. Drobes DJ, Anton RF, Thomas SE, Voronin K. A Clinical Laboratory Paradigm for Evaluating Medication Effects on Alcohol Consumption: Naltrexone and Nalmefene. *Neuropsychopharmacology* (2003) 28:755–64. doi: 10.1038/sj.npp.1300101
6. Fitzgerald N, Angus K, Elders A, Andrade M, Raistrick D, Heather N, et al. Weak Evidence on Nalmefene Creates Dilemmas for Clinicians and Poses Questions for Regulators and Researchers. *Addict (Abingdon England)* (2016) 111:1477–87. doi: 10.1111/add.13438
7. Palpacuer C, Laviolle B, Boussageon R, Reymann JM, Bellissant E, Naudet F. Risks and Benefits of Nalmefene in the Treatment of Adult Alcohol Dependence: A Systematic Literature Review and Meta-Analysis of Published and Unpublished Double-Blind Randomized Controlled Trials. *PloS Med* (2015) 12:e1001924. doi: 10.1371/journal.pmed.1001924
8. Niciu M, Arias A. Targeted Opioid Receptor Antagonists in the Treatment of Alcohol Use Disorders. *CNS Drugs* (2013) 27:777–87. doi: 10.1007/s40263-013-0096-4
9. Gianoulakis C. Alcohol-Seeking Behavior: The Roles of the Hypothalamic-Pituitary-Adrenal Axis and the Endogenous Opioid System. *Alcohol Health Res World* (1998) 22:202–10.
10. Peana AT, Sánchez-Catalán MJ, Hipólito L, Rosas M, Porru S, Bennardini F, et al. Mystic Acetaldehyde: The Never-Ending Story on Alcoholism. *Front Behav Neurosci* (2017) 11:81. doi: 10.3389/fnbeh.2017.00081
11. Merighi S, Gessi S, Varani K, Fazzi D, Stefanelli A, Borea PA. Morphine Mediates a Proinflammatory Phenotype *via* μ-Opioid Receptor–PKCε–Akt–ERK1/2 Signaling Pathway in Activated Microglial Cells. *Biochem Pharmacol* (2013) 86:487–96. doi: 10.1016/j.bcp.2013.05.027
12. Shrivastava P, Cabrera MA, Chastain LG, Boyadjieva NI, Jabbar S, Franklin T, et al. Mu-Opioid Receptor and Delta-Opioid Receptor Differentially Regulate Microglial Inflammatory Response to Control Proopiomelanocortin Neuronal Apoptosis in the Hypothalamus: Effects of Neonatal Alcohol. *J Neuroinflamm* (2017) 14:83. doi: 10.1186/s12974-017-0844-3
13. Kraus J, Börner C, Giannini E, Höllt V. The Role of Nuclear Factor κb in Tumor Necrosis Factor-Regulated Transcription of the Human μ-Opioid Receptor Gene. *Mol Pharmacol* (2003) 64:876–84. doi: 10.1124/mol.64.4.876
14. Börner C, Kraus J, Schröder H, Ammer H, Höllt V. Transcriptional Regulation of the Human μ-Opioid Receptor Gene by Interleukin-6. *Mol Pharmacol* (2004) 66:1719–26. doi: 10.1124/mol.104.003806
15. Langsdorf EF, Mao X, Chang SL. A Role for Reactive Oxygen Species in Endotoxin-Induced Elevation of MOR Expression in the Nervous and

Immune Systems. *J Neuroimmunol* (2011) 236:57–64. doi: 10.1016/j.jneuroim.2011.05.009
16. Byrne LS, Peng J, Sarkar S, Chang SL. Interleukin-1 Beta-Induced Up-Regulation of Opioid Receptors in the Untreated and Morphine-Desensitized U87 MG Human Astrocytoma Cells. *J Neuroinflamm* (2012) 9:252. doi: 10.1186/1742-2094-9-252
17. Eisenstein TK. The Role of Opioid Receptors in Immune System Function. *Front Immunol* (2019) 10:2904. doi: 10.3389/fimmu.2019.02904
18. Zhang P, Yang M, Chen C, Liu L, Wei X, Zeng S. Toll-Like Receptor 4 (TLR4)/Opioid Receptor Pathway Crosstalk and Impact on Opioid Analgesia, Immune Function, and Gastrointestinal Motility. *Front Immunol* (2020) 11:1455. doi: 10.3389/fimmu.2020.01455
19. Alfonso-Loeches S, Ureña-Peralta JR, Morillo-Bargues MJ, Oliver-De La Cruz J, Guerri C. Role of Mitochondria ROS Generation in Ethanol-Induced NLRP3 Inflammasome Activation and Cell Death in Astroglial Cells. *Front Cell Neurosci* (2014) 8:216. doi: 10.3389/fncel.2014.00216
20. Montesinos J, Pascual M, Pla A, Maldonado C, Rodríguez-Arias M, Miñarro J, et al. TLR4 Elimination Prevents Synaptic and Myelin Alterations and Long-Term Cognitive Dysfunctions in Adolescent Mice With Intermittent Ethanol Treatment. *Brain Behav Immun* (2014) 45:233–44. doi: 10.1016/j.bbi.2014.11.015
21. Pascual M, Baliño P, Aragón CMG, Guerri C. Cytokines and Chemokines as Biomarkers of Ethanol-Induced Neuroinflammation and Anxiety-Related Behavior: Role of TLR4 and TLR2. *Neuropharmacology* (2015) 89:352–9. doi: 10.1016/j.neuropharm.2014.10.014
22. Alfonso-Loeches S, Alfonso-Loeches S, Ureña-Peralta J, Ureña-Peralta J, Morillo-Bargues M, Morillo-Bargues M, et al. Ethanol-Induced TLR4/NLRP3 Neuroinflammatory Response in Microglial Cells Promotes Leukocyte Infiltration Across the BBB. *Neurochem Res* (2016) 41:193–209. doi: 10.1007/s11064-015-1760-5
23. Cantacorps L, Alfonso-Loeches S, Moscoso-Castro M, Cuitavi J, Gracia-Rubio I, López-Arnau R, et al. Maternal Alcohol Binge Drinking Induces Persistent Neuroinflammation Associated With Myelin Damage and Behavioural Dysfunctions in Offspring Mice. *Neuropharmacology* (2017) 123:368–84. doi: 10.1016/j.neuropharm.2017.05.034
24. Ezquer F, Quintanilla ME, Morales P, Santapau D, Ezquer M, Kogan MJ, et al. Intranasal Delivery of Mesenchymal Stem Cell-Derived Exosomes Reduces Oxidative Stress and Markedly Inhibits Ethanol Consumption and Post-Deprivation Relapse Drinking. *Addict Biol* (2019) 24:994–1007. doi: 10.1111/adb.12675
25. Lorente JD, Cuitavi J, Campos-Jurado Y, Montón-Molina R, González-Romero JL, Hipólito L. Kappa Opioid Receptor Blockade in NAc Shell Prevents Sex-Dependent Alcohol Deprivation Effect Induced by Inflammatory Pain. *Pain (Amsterdam)* (2021). doi: 10.1097/j.pain.0000000000002332
26. Carnicella S, Ron D, Barak S. Intermittent Ethanol Access Schedule in Rats as a Preclinical Model of Alcohol Abuse. *Alcohol (Fayetteville NY)* (2014) 48:243–52. doi: 10.1016/j.alcohol.2014.01.006
27. Parent AJ, Beaudet N, Beaudry H, Bergeron J, Bérubé P, Drolet G, et al. Increased Anxiety-Like Behaviors in Rats Experiencing Chronic Inflammatory Pain. *Behav Brain Res* (2012) 229:160–7. doi: 10.1016/j.bbr.2012.01.001
28. Hipólito L, Wilson-Poe A, Campos-Jurado Y, Zhong E, Gonzalez-Romero J, Virag L, et al. Inflammatory Pain Promotes Increased Opioid Self-Administration: Role of Dysregulated Ventral Tegmental Area μ Opioid Receptors. *J Neurosci* (2015) 35:12217–31. doi: 10.1523/JNEUROSCI.1053-15.2015
29. Campos-Jurado Y, Lorente JD, González-Romero JL, Granero L, Polache A, Hipólito L. Impaired Alcohol-Induced Dopamine Release in the Nucleus Accumbens in an Inflammatory Pain Model: Behavioural Implications in Male Rats. *Pain (Amsterdam)* (2020) 161:2203–11. doi: 10.1097/j.pain.0000000000001915
30. Sánchez-Catalán MJ, Hipólito, Guerri C, Granero, Polache A. Distribution and Differential Induction of CYP2E1 by Ethanol and Acetone in the Mesocorticolimbic System of Rat. *Alcalc* (2008) 43:401–7. doi: 10.1093/alcalc/agn012
31. Campos-Jurado Y, Martí-Prats L, Morón JA, Polache A, Granero L, Hipólito L. Dose-Dependent Induction of CPP or CPA by intra-pVTA Ethanol: Role of Mu Opioid Receptors and Effects on NMDA Receptors. *Prog Neuropsychopharmacol Biol Psychiatry* (2020) 100:109875. doi: 10.1016/j.pnpbp.2020.109875
32. Lupp A, Richter N, Doll C, Nagel F, Schulz S. UMB-3, a Novel Rabbit Monoclonal Antibody, for Assessing μ-Opioid Receptor Expression in Mouse, Rat and Human Formalin-Fixed and Paraffin-Embedded Tissues. *Regul Peptides* (2011) 167:9–13. doi: 10.1016/j.regpep.2010.09.004
33. Tang Y, Wang C, Wang Y, Zhang J, Wang F, Li L, et al. Isoliquiritigenin Attenuates LPS-Induced AKI by Suppression of Inflammation Involving NF-κb Pathway. *Am J Trans Res* (2018) 10:4141–51.
34. Yang B, Deng G, Zhao R, Dai C, Jiang C, Wang X, et al. Porous Se@SiO2 Nanosphere-Coated Catheter Accelerates Prostatic Urethra Wound Healing by Modulating Macrophage Polarization Through Reactive Oxygen Species-NF-κb Pathway Inhibition. *Acta Biomater* (2019) 88:392–405. doi: 10.1016/j.actbio.2019.02.006
35. Groenendyk J, Paskevicius T, Urra H, Viricel C, Wang K, Barakat K, et al. Cyclosporine A Binding to COX-2 Reveals a Novel Signaling Pathway That Activates the IRE1α Unfolded Protein Response Sensor. *Sci Rep* (2018) 8:16678–15. doi: 10.1038/s41598-018-34891-w
36. Zhao Y, Tian X, Liu G, Wang K, Xie Y, Qiu Y. Berberine Protects Myocardial Cells Against Anoxia-Reoxygenation Injury *via* P38 MAPK-Mediated NF-κb Signaling Pathways. *Exp Ther Med* (2019) 17:230–6. doi: 10.3892/etm.2018.6949
37. Bradley T, Peppa D, Pedroza-Pacheco I, Li D, Cain DW, Henao R, et al. RAB11FIP5 Expression and Altered Natural Killer Cell Function Are Associated With Induction of HIV Broadly Neutralizing Antibody Responses. *Cell (Cambridge)* (2018) 175:387–99.e17. doi: 10.1016/j.cell.2018.08.064
38. Hoogland ICM, Houbolt C, van Westerloo DJ, van Gool WA, van de Beek D. Systemic Inflammation and Microglial Activation: Systematic Review of Animal Experiments. *J Neuroinflamm* (2015) 12:114. doi: 10.1186/s12974-015-0332-6
39. Agustín-Pavón C, Mielcarek M, Garriga-Canut M, Isalan M. Deimmunization for Gene Therapy: Host Matching of Synthetic Zinc Finger Constructs Enables Long-Term Mutant Huntingtin Repression in Mice. *Mol Neurodegeneration* (2016) 11:64. doi: 10.1186/s13024-016-0128-x
40. Fernandez-Lizarbe S, Pascual M, Gascon MS, Blanco A, Guerri C. Lipid Rafts Regulate Ethanol-Induced Activation of TLR4 Signaling in Murine Macrophages. *Mol Immunol* (2008) 45:2007–16. doi: 10.1016/j.molimm.2007.10.025
41. Cuitavi J, Hipólito L, Canals M. The Life Cycle of the Mu-Opioid Receptor. *Trends Biochem Sci (Amsterdam Regular ed)* (2021) 46:315–28. doi: 10.1016/j.tibs.2020.10.002
42. Alfonso-Loeches S, Pascual M, Guerri C. Gender Differences in Alcohol-Induced Neurotoxicity and Brain Damage. *Toxicol (Amsterdam)* (2013) 311:27–34. doi: 10.1016/j.tox.2013.03.001
43. Barton EA, Baker C, Leasure JL. Investigation of Sex Differences in the Microglial Response to Binge Ethanol and Exercise. *Brain Sci* (2017) 7:139. doi: 10.3390/brainsci7100139
44. Pascual M, Blanco AM, Cauli O, Miñarro J, Guerri C. Intermittent Ethanol Exposure Induces Inflammatory Brain Damage and Causes Long-Term Behavioural Alterations in Adolescent Rats. *Eur J Neurosci* (2007) 25:541–50. doi: 10.1111/j.1460-9568.2006.05298.x
45. Montesinos J, Pascual M, Millán-Esteban D, Guerri C. Binge-Like Ethanol Treatment in Adolescence Impairs Autophagy and Hinders Synaptic Maturation: Role of TLR4. *Neurosci Lett* (2018) 682:85–91. doi: 10.1016/j.neulet.2018.05.049
46. Menard C, Pfau M, Hodes G, Kana V, Wang V, Bouchard S, et al. Social Stress Induces Neurovascular Pathology Promoting Depression. *Nat Neurosci* (2017) 20:1752–60. doi: 10.1038/s41593-017-0010-3
47. Dudek KA, Dion-Albert L, Lebel M, LeClair K, Labrecque S, Tuck E, et al. Molecular Adaptations of the Blood-Brain Barrier Promote Stress Resilience vs. Depression. *Proc Natl Acad Sci PNAS* (2020) 117:3326–36. doi: 10.1073/pnas.1914655117
48. Klawonn AM, Fritz M, Castany S, Pignatelli M, Canal C, Similä F, et al. Microglial Activation Elicits a Negative Affective State Through Prostaglandin-Mediated Modulation of Striatal Neurons. *Immun (Cambridge Mass)* (2021) 54:225–34.e6. doi: 10.1016/j.immuni.2020.12.016

49. Mayfield J, Ferguson L, Harris RA. Neuroimmune Signaling: A Key Component of Alcohol Abuse. *Curr Opin Neurobiol* (2013) 23:513–20. doi: 10.1016/j.conb.2013.01.024
50. Ezquer F, Morales P, Quintanilla ME, Santapau D, Lespay-Rebolledo C, Ezquer M, et al. Intravenous Administration of Anti-Inflammatory Mesenchymal Stem Cell Spheroids Reduces Chronic Alcohol Intake and Abolishes Binge-Drinking. *Sci Rep* (2018) 8:4325–15. doi: 10.1038/s41598-018-22750-7
51. Siemsen BM, Landin JD, McFaddin JA, Hooker KN, Chandler LJ, Scofield MD. Chronic Intermittent Ethanol and Lipopolysaccharide Exposure Differentially Alter Iba1-Derived Microglia Morphology in the Prelimbic Cortex and Nucleus Accumbens Core of Male Long-Evans Rats. *J Neurosci Res* (2020) 99:1922–39. doi: 10.1002/jnr.24683
52. Tan Y, Yuan Y, Tian L. Microglial Regional Heterogeneity and its Role in the Brain. *Mol Psychiatry* (2020) 25:351–67. doi: 10.1038/s41380-019-0609-8
53. He J, Crews FT. Increased MCP-1 and Microglia in Various Regions of the Human Alcoholic Brain. *Exp Neurol* (2008) 210:349–58. doi: 10.1016/j.expneurol.2007.11.017
54. Gessi S, Borea PA, Bencivenni S, Fazzi D, Varani K, Merighi S. The Activation of μ-Opioid Receptor Potentiates LPS-Induced NF-kB Promoting an Inflammatory Phenotype in Microglia. *FEBS Lett* (2016) 590:2813–26. doi: 10.1002/1873-3468.12313
55. Azuma Y, Ohura K. Endomorphins 1 and 2 Inhibit IL-10 and IL-12 Production and Innate Immune Functions, and Potentiate NF-kappaB DNA Binding in THP-1 Differentiated to Macrophage-Like Cells. *Scandinavian J Immunol* (2002) 56:260–9. doi: 10.1046/j.1365-3083.2002.01128.x
56. Duncker SC, Philippe D, Martin-Paschoud C, Moser M, Mercenier A, Nutten S. Nigella Sativa (Black Cumin) Seed Extract Alleviates Symptoms of Allergic Diarrhea in Mice, Involving Opioid Receptors. *PloS One* (2012) 7:e39841. doi: 10.1371/journal.pone.0039841
57. Mitchell JM, O'Neil JP, Janabi M, Marks SM, Jagust WJ, Fields HL. Alcohol Consumption Induces Endogenous Opioid Release in the Human Orbitofrontal Cortex and Nucleus Accumbens. *Sci Trans Med* (2012) 4:116ra6. doi: 10.1126/scitranslmed.3002902
58. Perry CJ, McNally GP. μ-Opioid Receptors in the Nucleus Accumbens Shell Mediate Context-Induced Reinstatement (Renewal) But Not Primed Reinstatement of Extinguished Alcohol Seeking. *Behav Neurosci* (2013) 127:535–43. doi: 10.1037/a0032981
59. Castro DC, Berridge KC. Advances in the Neurobiological Bases for Food 'Liking'versus 'Wanting'. *Physiol Behav* (2014) 136:22–30. doi: 10.1016/j.physbeh.2014.05.022
60. Richard JM, Fields HL. Mu-Opioid Receptor Activation in the Medial Shell of Nucleus Accumbens Promotes Alcohol Consumption, Self-Administration and Cue-Induced Reinstatement. *Neuropharmacology* (2016) 108:14–23. doi: 10.1016/j.neuropharm.2016.04.010

Conflict of Interest: The authors declare that the research was conducted in the absence of any commercial or financial relationships that could be construed as a potential conflict of interest.

Publisher's Note: All claims expressed in this article are solely those of the authors and do not necessarily represent those of their affiliated organizations, or those of the publisher, the editors and the reviewers. Any product that may be evaluated in this article, or claim that may be made by its manufacturer, is not guaranteed or endorsed by the publisher.

frontiers in Immunology

MINI REVIEW
published: 27 September 2021
doi: 10.3389/fimmu.2021.689344

A Focused Review of Neural Recording and Stimulation Techniques With Immune-Modulatory Targets

Lorenzo Carnevale[1]*, *Marialuisa Perrotta*[2] *and Giuseppe Lembo*[1,2]

[1] *Research Unit of Neuro and Cardiovascular Pathophysiology, IRCCS Neuromed, Department of Angiocardioneurology and Translational Medicine, Pozzilli (IS), Italy,* [2] *Department of Molecular Medicine, "Sapienza" University of Rome, Rome, Italy*

The complex interactions established between the nervous and immune systems have been investigated for a long time. With the advent of small and portable devices to record and stimulate nerve activity, researchers from many fields began to be interested in how nervous activity can elicit immune responses and whether this activity can be manipulated to trigger specific immune responses. Pioneering works demonstrated the existence of a cholinergic inflammatory reflex, capable of controlling the systemic inflammatory response through a vagus nerve-mediated modulation of the spleen. This work inspired many different areas of technological and conceptual advancement, which are here reviewed to provide a concise reference for the main works expanding the knowledge on vagus nerve immune-modulatory capabilities. In these works the enabling technologies of peripheral nervous activity recordings were implemented and embody the current efforts aimed at controlling neural activity with modulating functions in immune response, both in experimental and clinical contexts.

Keywords: immunity, bioelectronic medicine, inflammatory reflex, microneurography, neuro-immune interface

OPEN ACCESS

Edited by:
Michael D. Burton,
The University of Texas at Dallas,
United States

Reviewed by:
Anja Meissner,
Lund University, Sweden
Ishak Ozel Tekin,
Bülent Ecevit University, Turkey

***Correspondence:**
Lorenzo Carnevale
lorenzo.carnevale@neuromed.it

Specialty section:
This article was submitted to Molecular Innate Immunity, a section of the journal Frontiers in Immunology

Received: *31 March 2021*
Accepted: *09 September 2021*
Published: *27 September 2021*

Citation:
Carnevale L, Perrotta M and Lembo G (2021) A Focused Review of Neural Recording and Stimulation Techniques With Immune-Modulatory Targets. Front. Immunol. 12:689344. doi: 10.3389/fimmu.2021.689344

INTRODUCTION

How the central nervous system is able to communicate with all the other organs and systems across the living body has always represented an intriguing issue. On the technical side, the challenge has been similar, considering the complexity of the brain to body interactions under examination. While it was quite easy to measure the global neural activity in terms of brain cortical activity through electroencephalogram, or nervous activity directed to the skeletal muscle to control movement, measuring the nerve activity controlling visceral organs through autonomic nervous system (ANS) innervation was challenging. Hence, researchers often exploited the analysis of surrogate markers of nervous system activity, such as neurotransmitter spillover and tissue concentration, or the modulation of vital parameters which were tightly related to the ANS balance (heart rate, respiration rate, and intestinal motility). On this note, although the complexity and invasiveness of surgical approaches necessary to expose the multitude of peripheral nerves of interest make this approach possible in animal models, the translation to humans remains a challenging issue. The great technological improvements in material science and manufacturing, coupled with

miniaturization of electronic circuits and devices, gave researchers new tools to characterize, in a direct way, the activity of the nervous system in modulating the connections with peripheral tissues and organs (1, 2).

The investigation of ANS regulation of several physiological systems, such as the cardiovascular and renal districts, prompted the improvement of procedures and equipment necessary to perform microneurography. In this context, the straightforward accession to nerves projected to the organs of interest, like the renal nerve or the carotid baroceptors and the cervical trunk of the vagus nerve, allowed early breakthroughs, which shed light on the mechanisms underlying the interplay between blood pressure regulation, baroreflexes, and nerve activity (3, 4).

The immune system is one of the main regulators of body homeostasis. The first hints suggesting that the immune system is also tightly regulated by the nervous system go back to the beginning of the past century. The various mechanisms by which the neuro-immune interfaces are established in different physiological and diseases contexts are thoroughly described elsewhere (5–7). Connections and crosstalk between nervous and immune systems are established at every endpoint of the peripheral nervous system (PNS), with both somatosensory and ANS' afferent and efferent arms. For example, the somatosensory system allows receiving stimuli from the immunoinflammatory milieu and communicate them to the CNS through the nociceptors residing in the dorsal root or trigeminal ganglia. On the other hand, the ANS establishes routes of bidirectional communication between the CNS and peripheral organs mainly through noradrenergic and cholinergic nerves. Also, specific immune cells are able to respond to neurotransmitters and, at the same time, secrete them, acting as neural relays (8).

At the beginning of this century a solid body of works pivoting around the connections established between the nervous and immune systems demonstrated the existence of a direct neural control of immunity and inflammation (9, 10). These breakthrough findings paved the way for a new field of research centered on the existence of the neural control of immunity, which led researchers to investigate the existence of direct and/or indirect circuits elicited by the nervous system and capable of driving specific immune responses with a therapeutical and translational outlook. The scope of this review is to provide a concise overview of works focusing on neuro-immune modulation, by which it is possible to analyze and stimulate neural activity to obtain different effects on immune cells activation and possibly modulate inflammatory responses.

Investigating the role of the innervation reaching the immune system, which comprises primary, secondary, and tertiary lymphoid organs, involved in different stages of immune cells maturation and immune responses, is a complex challenge requiring the refinement of electronics, materials, and genetic tools to directly measure nerve activity during homeostasis and diseases. How these challenges were addressed to unravel the neuroimmune mechanisms underlying physiology and pathophysiology will be discussed in section 2 of the current review.

On the other hand, the demonstration of the existence of neuro-immune circuits opened the possibility to identify new therapeutic targets achievable by modulating these circuits with genetic or electronic tools, to control the immune response in a specific way, without the use of pharmacological system-wide modulators, often carrying several undesired and off-target effects. The branch of research aimed at translating these findings to human pathologies, called bioelectronic medicine, has been only recently implemented at the pre-clinical and clinical levels. As this field is only at the beginning of discovering its therapeutic application potential, several potentially interesting unexplored paths and contexts are emerging. The current technologies and results achieved with bioelectronic medicine and mechanistic findings obtained by stimulating nerves in a tightly controlled manner are presented in section 3 of the current review.

ANALYZING NERVOUS SYSTEM ACTIVITY TO UNDERSTAND ITS MODULATORY ACTION ON THE IMMUNE SYSTEM

The first efforts focused toward the direct measurement of the interplay established between neural activity and the immune system can be found in the first years of the nineties, when Nijima et al. demonstrated by direct renal, splenic, and adrenal nerve recording that the intravenous injection of IL-1β upregulated splenic nerve activity and suppressed renal nerve activity, while observing a fall in arterial pressure not affected by baroceptor denervation (11). These findings suggested that IL-1β induced a modulation of the splenic nerve activity, directly mediated by the brain, thus allowing them to propose a role of the central drive in eliciting peripheral immune responses. Subsequent works from the same group demonstrated that if IL-1β was injected into the portal vein, it increased the activity of the afferent branch of the hepatic vagus nerve. Also, an increase of splenic nerve activity mediated by a central reflex was observed and interestingly it was hampered by a resection of the hepatic branch of the vagus nerve (12, 13). These studies were hints to the breakthrough discoveries at the dawn of the new century, when Tracey and coworkers demonstrated the existence of the inflammatory reflex, whereby the nervous system was proved capable of regulating peripheral inflammatory responses through the efferent vagus nerve, in a similar way to the control exerted by the ANS on heart rate, respiration, and other vital functions (10). Their work paved the way for a completely new field of research, which shed light on the mechanisms by which the inflammatory reflex exerts its action, and proposed new concepts underlying the interplay between the two systems, demonstrating the existence of immune cells capable of synthetizing neurotransmitters, after being primed by neural signals (8, 14).

In subsequent years, the field of bioelectronic medicine exhibited a sharp increase in terms of applications and technological improvements. Even after acknowledging the initial challenges posed by the necessity of analyzing signals coming from peripheral nerves with high accuracy and fidelity (15), several solutions have been proposed to optimize surgical

procedures and set up, paving the way to the possibility of recording neural activity in a uniform manner (16–19).

This wave of technological evolution let researchers use reliable data to decode the neural circuits involved in immunomodulatory processes. Most of the attention has been focused on analyzing one of the main brain connections established with the rest of the body, the vagus nerve, achieving the goal of identifying a characteristic pattern of firing to discriminate whether the mouse under examination was exposed to IL-1β, TNF-α, or no cytokine (20). The vagus has also been investigated as a vector of neural signaling directed toward the gut, which has been shown as one of the fundamental regulators of systemic inflammatory and immune processes (21, 22).

Shifting the attention to other peripheral nerves, the main focus of investigation in the neuro-immune context has been the splenic nerve, identified as one of the modulators of the systemic inflammatory milieu (23). It has been demonstrated that hyperthermia upregulates inflammatory genes expression, and that this effect is mediated by splenic nerve activity (24). In the last ten years, our group demonstrated the fundamental role that the splenic nerve has in priming the immune response to angiotensin II, a hormone peptide which is capable of elevating blood pressure in experimental animals, priming T cells in the spleen and stimulating their egression toward target organs typically characterizing hypertensive damage, like in the vasculature and kidneys (25). An analogous circuit was identified in response to a different hypertensive stimulus, deoxycorticosterone-acetate salt that typically reproduces salt-sensitive hypertension (26). This response was primed by an elevated neural activity which recruited the splenic noradrenergic pathway (27) and was dependent on a direct interface between the celiac branch of the vagus nerve and the splenic nerve. Further investigation of this neural circuit showed that the splenic nerve activity increase was directly induced by an upregulation of the efferent branch of the celiac vagus nerve (28).

Since peripheral nerves are heterogeneous in terms of size, surgical approaches, and the types of activity which could be recorded, literature focused on a variety of approaches (**Figure 1**). To provide the reader with an example of the multitude of signals that are transmitted, in **Figure 2A** we show two different nerves and physiological variables recordings: boxed in blue there is an example of a two min recording of the celiac vagus nerve (raw signal in black, integrated signal in blue), characterized by rhythmic neural discharge well coupled with the blood pressure signal (green track). Boxed in green there is an example of a two min splenic nerve recording, characterized by isolated spikes non-synchronous with the blood pressure recordings.

ELICITING NERVOUS ACTIVITY THROUGH NERVE STIMULATION TO ALTER THE INFLAMMATION AND IMMUNE RESPONSE

In clinical practice, vagus nerve stimulation (VNS) has been proven as an invaluable tool to treat neurological conditions such as epilepsy or psychiatric disorders such as depression (29), whereas peripheral nerve stimulation has been used to directly evoke a muscle contraction in the rehabilitation context (30). These applications have the characteristic of leveraging a closed-loop design, providing immediate stimulation based on a physical readout suggesting the necessity of an action (i.e., a seizure onset in epilepsy or trajectory planning in rehabilitation) (2, 31), Moreover, the recent update in term of stimulatory devices gave clinicians the opportunity to test VNS strategies leveraging cutaneous auricular innervation, through the transcutaneous auricular VNS (tVNS), greatly reducing invasiveness and a series of drawback related to the invasive carotid VNS (32).

The exceptional efforts directed toward vagus nerve recording and signal decoding in animal models has the ultimate aim of delivering a translational approach to the neural control of immunity by means of VNS. In the preclinical research, the technical challenges raised by nerve recording procedures similarly apply to the electrodes designed to stimulate a specific peripheral neural district. A powerful addition to the availability of mouse models is the combination of optogenetic approaches and cre-loxP genetic engineering. In this way it is possible to generate mice in which the optogenetic stimulation selectively recruits specific nerve fibers of choice, making it possible to precisely identify the brain regions from which the neural circuits originated (33).

In animals, the bioelectronic VNS proved effective in downregulating the TNF-α increase observed in response to lipopolysaccharides (LPS) injection (9), providing the first proof of concept of a potential therapeutic strategy for inflammatory systemic diseases. A series of experiments, based on this model, thoroughly explained an immunomodulating mechanism in which LPS stimulated vagus nerve afferent activity, signaling danger to the brain. In the brain, specific areas are activated and recruit downstream nerve activity through the efferent arm of the vagus nerve and transduce this signal to the splenic nerve (33). Here the splenic nerve endings are capable of modulating and regulating lymphocyte functions: in this case they activate a specific T-cell niche which expresses choline acetyltransferase (ChAT). These cells are activated by bioelectronic stimulation of the vagus nerve by noradrenergic signaling and function as a neural relay, starting the biosynthesis of acetylcholine which in turn activates a population of anti-inflammatory macrophages (8).

Leveraging these anti-inflammatory properties, VNS has been tested as a treatment for food allergy (34) and intestinal inflammation (35). However, growing evidence suggests that the vagus nerve may not only be recruited in the context of an anti-inflammatory reflex, but also may be modulated as an inflammatory reflex. In fact, recent works showed that stimulating the celiac branch of the vagus nerve primes a splenic immune response, conveyed by the noradrenergic signaling in the spleen. This signaling recruits an α-adrenergic pathway, which upregulates Placental Growth Factor (PlGF), a key molecular player of the neuro-immune signal transduction (25), previously reported as capable of activating a specific subset of T cells, namely CD8 effector T cells, to promote their egression

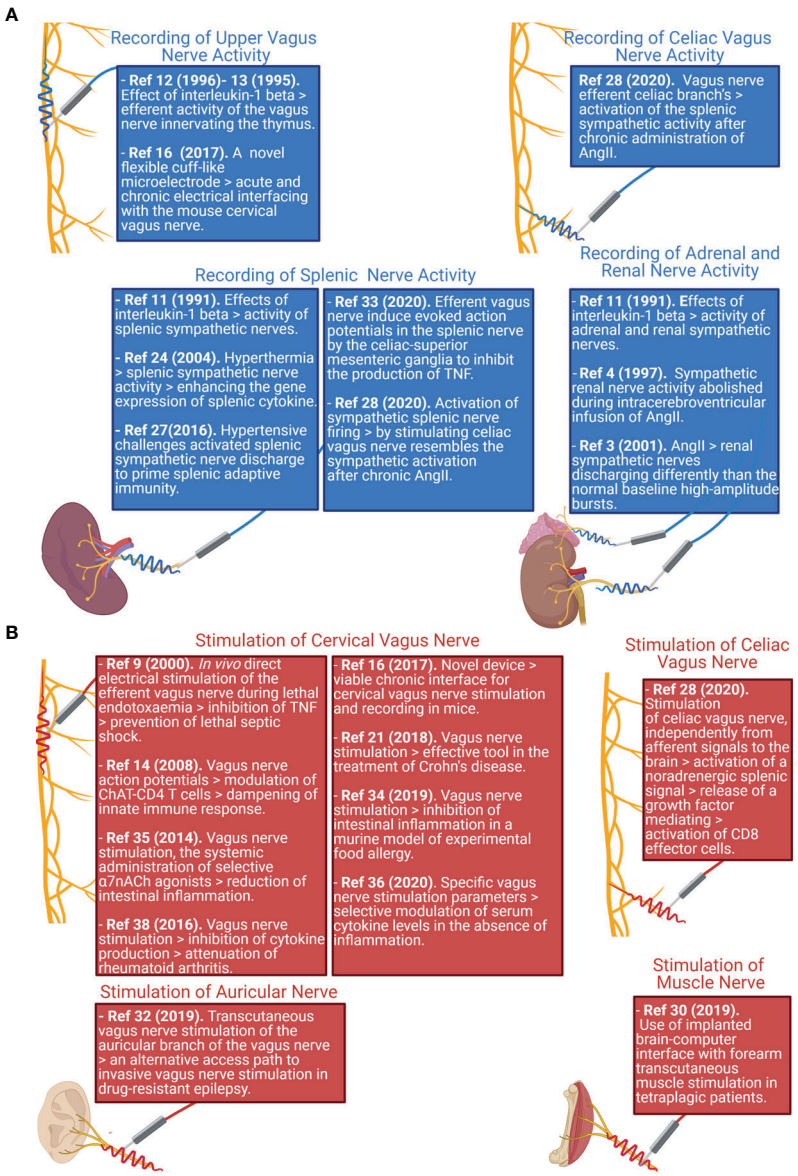

FIGURE 1 | Schematic representation reporting the main nerve recording **(A)** and stimulation **(B)** sites studied in literature, and the associated paper reporting findings on those nerve districts. Created with Biorender.com.

from the spleen (28). Overall, these data suggest that specific combinations of stimulation current and frequency can alter the cytokine landscape toward pro- or anti-inflammatory responses (36).

The current translation of immune modulation achieved by electronic medicine mainly focused on pathologies in which the recruited effect is anti-inflammatory, like Crohn's disease, Rheumatoid arthritis, and metabolic syndrome. In these contexts, VNS has been mainly tested in patients refractory to pharmacological therapies, showing promising results with the majority of patients reporting beneficial effects and reduced disease severity (37–39). Most of the clinical studies relying on VNS however face the major limitation of this technique: with the current technology they are not capable of selectively modulating one aspect of immunity and relying on the cervical VNS property of lowering circulating inflammatory cytokines like TNF-α, IL-6, and IL-17 (38), with the main clinical endpoint to lower pathology severity. For a comprehensive review of human studies involving nervous stimulation see (39).

The current body of literature and data available always focuses on the stimulation of the cervical vagus nerve (**Figure 1B**), since it is the easiest to be surgically accessed and is directed to most of the internal organs. As such, the cervical vagus nerve has been identified as an optimal target for bioelectronic stimulation. As an example of this procedure, **Figure 2B** shows, in the red box, a track recording of a

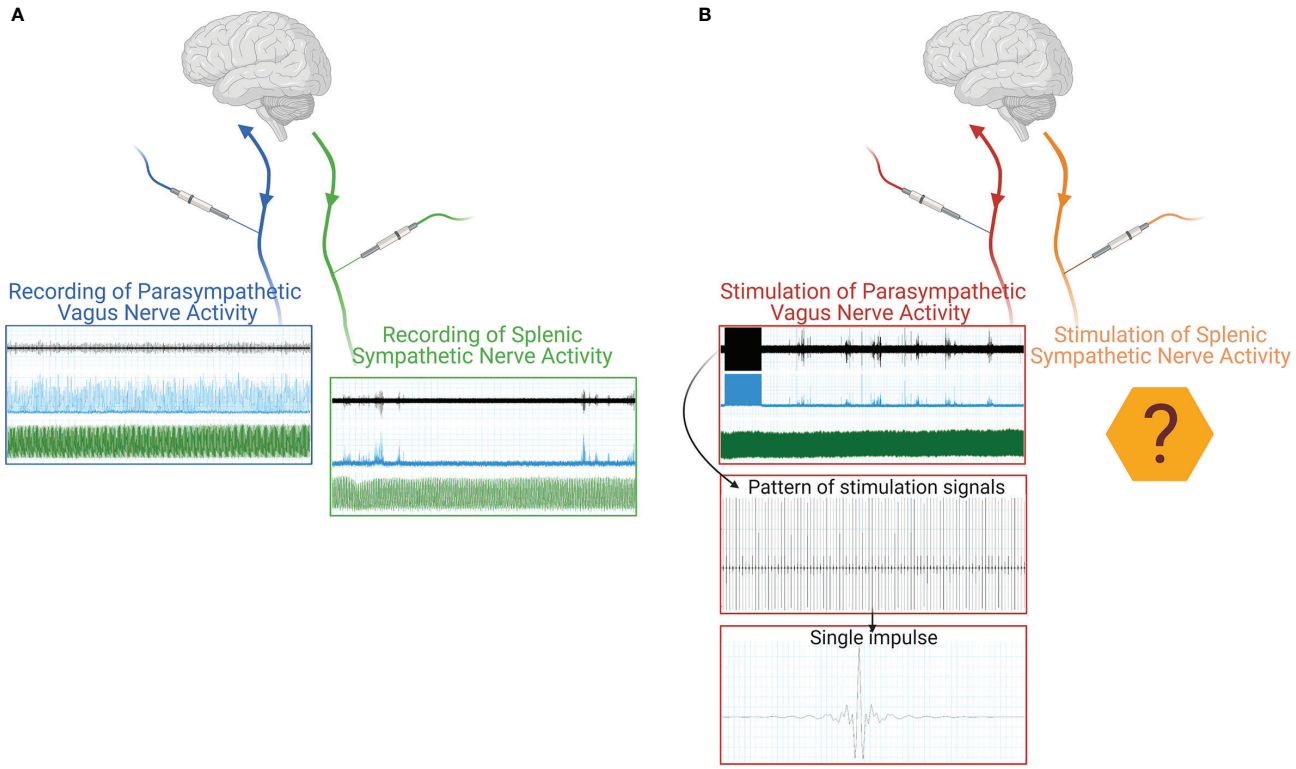

FIGURE 2 | Schematic representation of a neural signal recording **(A)** of both parasympathetic (blue box) and sympathetic nerve activity (green box). The raw neural traces are shown in black, the integrated signals in blue, and the blood pressure recordings in green. Schematic representation of a VNS stimulation **(B)**, the raw neural traces are shown in black, the integrated signals in blue, and the blood pressure recordings in green, with progressive detail on the electrical stimulus train and the single stimulus waveform. Created with Biorender.com.

stimulation procedure carried out on the celiac branch of the vagus nerve. The signal elicited on the splenic nerve (raw signal in black, integrated signal in blue, blood pressure in green) was concomitantly recorded, highlighting the impulse train and the single impulse provided to the nerve.

DISCUSSION

The current landscape of the research efforts directed toward the recording and interpretation of neural signals in the context of immune modulation is flourishing with net context and pathologies under scrutiny. Abundant and reliable evidence of the reflex-like regulation of inflammation has subverted the classical duality between sympathetic and parasympathetic autonomic regulation, pushing researchers to investigate the specific regulatory neural circuits driving the immunity in specific contexts. The heterogeneous cultural background of different specialties approaching nerve recording and signal interpretation results in a heterogeneity of procedures and lack of a standard approach. To hamper this problem, research groups, which discovered the inflammatory reflex, proposed methodology and procedures that could help in standardizing the recordings and analysis of the vagus nerve (40).

While preclinical bioelectronic medicine is in optimal shape and a fast-growing field, the translation of the findings to the clinical setting is slow. In fact, if VNS has been shown to be effective for autoimmune diseases such as rheumatoid arthritis and inflammatory diseases like Crohn's disease, it is not yet under consideration for pathologies where a fine modulation of immune responses could be necessary.

The current technologies let us record nervous activity on several nervous districts, such as the vagus or splenic nerve (**Figure 2A**), and also procedures stimulating the vagus nerve are consolidated. On the other hand, no stimulation has been tested on peripheral sympathetic nerves, except for the musculoskeletal nerves exploited to trigger muscle contraction and thus movement. In principle, it could be feasible to apply a similar concept to peripheral sympathetic nerves to obtain a targeted stimulation to internal organs without soliciting off-target effects due to a nonspecific nerve stimulation (like the one obtained on the cervical vagus nerve) (**Figure 2B**).

In the foreseeable future, the enabling technologies of nerve recording and stimulation, miniaturization of devices, and improved analytical capabilities, such as artificial intelligence, will allow researchers to overcome current limitations in this field and recommend it as a reliable and pervasive alternative to pharmacological treatments. On the clinical side, the main issue

is the lack of fast and precise readouts for the design of closed-loop immune-inflammatory control systems. If researchers will be able to provide such readouts, like seizure-onset in the context of epilepsy, it will be possible to fine tune the stimulation pattern and elicit the desired immuno-modulation (36), and a fundamental issue to be resolved in order to precisely target immune mechanisms in human pathologies. In addition, further studies will be needed to identify similar possibilities of modulation for the activation of specific immune cell subsets. In the experimental setting, nerve decoding and stimulation will become more and more prevalent not only as a valid therapeutic proof of concept, but also as an enabling technology to model specific patterns of immune cell activation (28) or inflammatory modulation (36).

Overall, bioelectronic medicine approaches have shown the potential to deeply impact the immune system and modulate it, while a growing number of researchers, both in the field of technology and life sciences, are contributing to expand the possibilities of investigation and combine knowledge in terms of how the nervous system can influence and modulate the immune system. If the different operators involved in this branch of research will be able to cooperate and collaborate to synthesize their findings, their final aim and product will be an atlas of the different nervous activation patterns corresponding to the desired immune system modulation and a series of stimulating devices and tools to directly evoke and elicit them.

AUTHOR CONTRIBUTIONS

LC wrote the manuscript. MP drafted figures and schematics. GL provided funding and supervised the work. All authors contributed to the article and approved the submitted version.

FUNDING

Italian Ministry of Health "Ricerca Corrente" and ERA-CVD (PLAQUEFIGHT) 01KL1808 to GL.

REFERENCES

1. Frank JA, Antonini MJ, Anikeeva P. Next-Generation Interfaces for Studying Neural Function. *Nat Biotechnol* (2019) 37(9):1013–23. doi: 10.1038/s41587-019-0198-8
2. Cho Y, Park J, Lee C, Lee S. Recent Progress on Peripheral Neural Interface Technology Towards Bioelectronic Medicine. *Bioelectron Med* (2020) 6(1):23. doi: 10.1186/s42234-020-00059-z
3. Ma X, Abboud FM, Chapleau MW. A Novel Effect of Angiotensin on Renal Sympathetic Nerve Activity in Mice. *J Hypertens* (2001) 19(3 Pt 2):609–18. doi: 10.1097/00004872-200103001-00014
4. May CN, McAllen RM. Baroreceptor-Independent Renal Nerve Inhibition by Intracerebroventricular Angiotensin II in Conscious Sheep. *Am J Physiol* (1997) 273(2 Pt 2):R560–7. doi: 10.1152/ajpregu.1997.273.2.R560
5. Ordovas-Montanes J, Rakoff-Nahoum S, Huang S, Riol-Blanco L, Barreiro O, von Andrian UH. The Regulation of Immunological Processes by Peripheral Neurons in Homeostasis and Disease. *Trends Immunol* (2015) 36(10):578–604. doi: 10.1016/j.it.2015.08.007
6. Huh JR, Veiga-Fernandes H. Neuroimmune Circuits in Inter-Organ Communication. *Nat Rev Immunol* (2020) 20(4):217–28. doi: 10.1038/s41577-019-0247-z
7. Chu C, Artis D, Chiu IM. Neuro-Immune Interactions in the Tissues. *Immunity* (2020) 52(3):464–74. doi: 10.1016/j.immuni.2020.02.017
8. Rosas-Ballina M, Olofsson PS, Ochani M, Valdés-Ferrer SI, Levine YA, Reardon C, et al. Acetylcholine-Synthesizing T Cells Relay Neural Signals in a Vagus Nerve Circuit. *Science* (2011) 334(6052):98–101. doi: 10.1126/science.1209985
9. Borovikova LV, Ivanova S, Zhang M, Yang H, Botchkina GI, Watkins LR, et al. Vagus Nerve Stimulation Attenuates the Systemic Inflammatory Response to Endotoxin. *Nature* (2000) 405(6785):458–62. doi: 10.1038/35013070
10. Tracey KJ. The Inflammatory Reflex. *Nature* (2002) 420(6917):853–9. doi: 10.1038/nature01321
11. Niijima A, Hori T, Aou S, Oomura Y. The Effects of Interleukin-1 Beta on the Activity of Adrenal, Splenic and Renal Sympathetic Nerves in the Rat. *J Auton Nerv Syst* (1991) 36(3):183–92. doi: 10.1016/0165-1838(91)90042-2
12. Niijima A. The Afferent Discharges From Sensors for Interleukin 1 Beta in the Hepatoportal System in the Anesthetized Rat. *J Auton Nerv Syst* (1996) 61(3):287–91. doi: 10.1016/S0165-1838(96)00098-7
13. Niijima A, Hori T, Katafuchi T, Ichijo T. The Effect of Interleukin-1 Beta on the Efferent Activity of the Vagus Nerve to the Thymus. *J Auton Nerv Syst* (1995) 54(2):137–44. doi: 10.1016/0165-1838(95)00003-G
14. Rosas-Ballina M, Ochani M, Parrish WR, Ochani K, Harris YT, Huston JM, et al. Splenic Nerve is Required for Cholinergic Antiinflammatory Pathway Control of TNF in Endotoxemia. *Proc Natl Acad Sci U S A* (2008) 105(31):11008–13. doi: 10.1073/pnas.0803237105
15. Grill WM, Norman SE, Bellamkonda RV. Implanted Neural Interfaces: Biochallenges and Engineered Solutions. *Annu Rev Biomed Eng* (2009) 11:1–24. doi: 10.1146/annurev-bioeng-061008-124927
16. Caravaca AS, Tsaava T, Goldman L, Silverman H, Riggott G, Chavan SS, et al. A Novel Flexible Cuff-Like Microelectrode for Dual Purpose, Acute and Chronic Electrical Interfacing With the Mouse Cervical Vagus Nerve. *J Neural Eng* (2017) 14(6):066005. doi: 10.1088/1741-2552/aa7a42
17. Falcone JD, Liu T, Goldman L, David DP, Rieth L, Bouton CE, et al. A Novel Microwire Interface for Small Diameter Peripheral Nerves in a Chronic, Awake Murine Model. *J Neural Eng* (2020) 17(4):046003. doi: 10.1088/1741-2552/ab9b6d
18. Giagka V, Serdijn WA. Realizing Flexible Bioelectronic Medicines for Accessing the Peripheral Nerves - Technology Considerations. *Bioelectron Med* (2018) 4:8. doi: 10.1186/s42234-018-0010-y
19. Lee S, Peh WYX, Wang J, Yang F, Ho JS, Thakor NV, et al. Toward Bioelectronic Medicine-Neuromodulation of Small Peripheral Nerves Using Flexible Neural Clip. *Adv Sci (Weinheim Baden-Wurttemberg Germany)* (2017) 4(11):1700149. doi: 10.1002/advs.201700149
20. Zanos TP, Silverman HA, Levy T, Tsaava T, Battinelli E, Lorraine PW, et al. Identification of Cytokine-Specific Sensory Neural Signals by Decoding Murine Vagus Nerve Activity. *Proc Natl Acad Sci U S A* (2018) 115(21):E4843–52. doi: 10.1073/pnas.1719083115
21. Bonaz B, Bazin T, Pellissier S. The Vagus Nerve at the Interface of the Microbiota-Gut-Brain Axis. *Front Neurosci* (2018) 12:49. doi: 10.3389/fnins.2018.00049
22. Matteoli G, Boeckxstaens GE. The Vagal Innervation of the Gut and Immune Homeostasis. *Gut* (2013) 62(8):1214–22. doi: 10.1136/gutjnl-2012-302550
23. Perrotta M, Lembo G, Carnevale D. The Interactions of the Immune System and the Brain in Hypertension. *Curr Hypertens Rep* (2018) 20(1):7. doi: 10.1007/s11906-018-0808-8
24. Ganta CK, Blecha F, Ganta RR, Helwig BG, Parimi S, Lu N, et al. Hyperthermia-Enhanced Splenic Cytokine Gene Expression Is Mediated by the Sympathetic Nervous System. *Physiol Genomics* (2004) 19(2):175–83. doi: 10.1152/physiolgenomics.00109.2004
25. Carnevale D, Pallante F, Fardella V, Fardella S, Iacobucci R, Federici M, et al. The Angiogenic Factor PlGF Mediates a Neuroimmune Interaction in the Spleen to Allow the Onset of Hypertension. *Immunity* (2014) 41(5):737–52. doi: 10.1016/j.immuni.2014.11.002

26. Perrotta M, Lori A, Carnevale L, Fardella S, Cifelli G, Iacobucci R, et al. Deoxycorticosterone Acetate-Salt Hypertension Activates Placental Growth Factor in the Spleen to Couple Sympathetic Drive and Immune System Activation. *Cardiovasc Res* (2018) 114(3):456–67. doi: 10.1093/cvr/cvy001
27. Carnevale D, Perrotta M, Pallante F, Fardella V, Iacobucci R, Fardella S, et al. A Cholinergic-Sympathetic Pathway Primes Immunity in Hypertension and Mediates Brain-to-Spleen Communication. *Nat Commun* (2016) 7:13035. doi: 10.1038/ncomms13035
28. Carnevale L, Pallante F, Perrotta M, Iodice D, Perrotta S, Fardella S, et al. Celiac Vagus Nerve Stimulation Recapitulates Angiotensin II-Induced Splenic Noradrenergic Activation, Driving Egress of CD8 Effector Cells. *Cell Rep* (2020) 33(11):108494. doi: 10.1016/j.celrep.2020.108494
29. Mertens A, Raedt R, Gadeyne S, Carrette E, Boon P, Vonck K. Recent Advances in Devices for Vagus Nerve Stimulation. *Expert Rev Med Devices* (2018) 15(8):527–39. doi: 10.1080/17434440.2018.1507732
30. Bockbrader M, Annetta N, Friedenberg D, Schwemmer M, Skomrock N, Colachis ST, et al. Clinically Significant Gains in Skillful Grasp Coordination by an Individual With Tetraplegia Using an Implanted Brain-Computer Interface With Forearm Transcutaneous Muscle Stimulation. *Arch Phys Med Rehabil* (2019) 100(7):1201–17. doi: 10.1016/j.apmr.2018.07.445
31. Ganzer PD, Sharma G. Opportunities and Challenges for Developing Closed-Loop Bioelectronic Medicines. *Neural Regen Res* (2019) 14(1):46–50. doi: 10.4103/1673-5374.243697
32. Ellrich J. Transcutaneous Auricular Vagus Nerve Stimulation. *J Clin Neurophysiol* (2019) 36(6):437–42. doi: 10.1097/WNP.0000000000000576
33. Kressel AM, Tsaava T, Levine YA, Chang EH, Addorisio ME, Chang Q, et al. Identification of a Brainstem Locus That Inhibits Tumor Necrosis Factor. *Proc Natl Acad Sci U S A* (2020) 117(47):29803–10. doi: 10.1073/pnas.2008213117
34. Bosmans G, Appeltans I, Stakenborg N, Gomez-Pinilla PJ, Florens MV, Aguilera-Lizarraga J, et al. Vagus Nerve Stimulation Dampens Intestinal Inflammation in a Murine Model of Experimental Food Allergy. *Allergy* (2019) 74(9):1748–59. doi: 10.1111/all.13790
35. Matteoli G, Gomez-Pinilla PJ, Nemethova A, Di Giovangiulio M, Cailotto C, van Bree SH, et al. A Distinct Vagal Anti-Inflammatory Pathway Modulates Intestinal Muscularis Resident Macrophages Independent of the Spleen. *Gut* (2014) 63(6):938–48. doi: 10.1136/gutjnl-2013-304676
36. Tsaava T, Datta-Chaudhuri T, Addorisio ME, Masi EB, Silverman HA, Newman JE, et al. Specific Vagus Nerve Stimulation Parameters Alter Serum Cytokine Levels in the Absence of Inflammation. *Bioelectron Med* (2020) 6:8. doi: 10.1186/s42234-020-00042-8
37. Bonaz B, Sinniger V, Hoffmann D, Clarençon D, Mathieu N, Dantzer C, et al. Chronic Vagus Nerve Stimulation in Crohn's Disease: A 6-Month Follow-Up Pilot Study. *Neurogastroenterol Motil* (2016) 28(6):948–53. doi: 10.1111/nmo.12792
38. Koopman FA, Chavan SS, Miljko S, Grazio S, Sokolovic S, Schuurman PR, et al. Vagus Nerve Stimulation Inhibits Cytokine Production and Attenuates Disease Severity in Rheumatoid Arthritis. *Proc Natl Acad Sci U S A* (2016) 113(29):8284–9. doi: 10.1073/pnas.1605635113
39. Johnson RL, Wilson CG. A Review of Vagus Nerve Stimulation as a Therapeutic Intervention. *J Inflamm Res* (2018) 11:203–13. doi: 10.2147/JIR.S163248
40. Silverman HA, Stiegler A, Tsaava T, Newman J, Steinberg BE, Masi EB, et al. Standardization of Methods to Record Vagus Nerve Activity in Mice. *Bioelectron Med* (2018) 4:3. doi: 10.1186/s42234-018-0002-y

Conflict of Interest: The authors declare that the research was conducted in the absence of any commercial or financial relationships that could be construed as a potential conflict of interest.

Publisher's Note: All claims expressed in this article are solely those of the authors and do not necessarily represent those of their affiliated organizations, or those of the publisher, the editors and the reviewers. Any product that may be evaluated in this article, or claim that may be made by its manufacturer, is not guaranteed or endorsed by the publisher.

frontiers in Immunology

ORIGINAL RESEARCH
published: 26 November 2021
doi: 10.3389/fimmu.2021.734349

Treatment With the CSF1R Antagonist GW2580, Sensitizes Microglia to Reactive Oxygen Species

*Katiria Soto-Diaz[1], Mario Vailati-Riboni[2], Allison Y. Louie[1], Daniel B. McKim[1,2,3], H. Rex Gaskins[2,3,4,5,6,7], Rodney W. Johnson[1,2,3] and Andrew J. Steelman[1,2,3,4]**

[1] Neuroscience Program, University of Illinois at Urbana-Champaign, Urbana, IL, United States, [2] Department of Animal Sciences, University of Illinois at Urbana-Champaign, Urbana, IL, United States, [3] Division of Nutritional Sciences, University of Illinois at Urbana-Champaign, Urbana, IL, United States, [4] Carl R. Woese Institute for Genomic Biology, University of Illinois at Urbana-Champaign, Urbana, IL, United States, [5] Cancer Center at Illinois, University of Illinois at Urbana-Champaign, Urbana, IL, United States, [6] Department of Pathobiology, University of Illinois at Urbana-Champaign, Urbana, IL, United States, [7] Department of Biomedical and Translational Sciences, University of Illinois at Urbana-Champaign, Urbana, IL, United States

OPEN ACCESS

Edited by:
Maureen Ann Cox,
University of Oklahoma Health Sciences Center, United States

Reviewed by:
Raymond B. Birge,
The State University of New Jersey, United States
Girdhari Lal,
National Centre for Cell Science, India

***Correspondence:**
Andrew J. Steelman
asteelma@illinois.edu

Specialty section:
This article was submitted to Molecular Innate Immunity, a section of the journal Frontiers in Immunology

Received: 01 July 2021
Accepted: 01 November 2021
Published: 26 November 2021

Citation:
Soto-Diaz K, Vailati-Riboni M, Louie AY, McKim DB, Gaskins HR, Johnson RW and Steelman AJ (2021) Treatment With the CSF1R Antagonist GW2580, Sensitizes Microglia to Reactive Oxygen Species. Front. Immunol. 12:734349. doi: 10.3389/fimmu.2021.734349

Microglia activation and proliferation are hallmarks of many neurodegenerative disorders and may contribute to disease pathogenesis. Neurons actively regulate microglia survival and function, in part by secreting the microglia mitogen interleukin (IL)-34. Both IL-34 and colony stimulating factor (CSF)-1 bind colony stimulating factor receptor (CSFR)1 expressed on microglia. Systemic treatment with central nervous system (CNS) penetrant, CSFR1 antagonists, results in microglia death in a dose dependent matter, while others, such as GW2580, suppress activation during disease states without altering viability. However, it is not known how treatment with non-penetrant CSF1R antagonists, such as GW2580, affect the normal physiology of microglia. To determine how GW2580 affects microglia function, C57BL/6J mice were orally gavaged with vehicle or GW2580 (80mg/kg/d) for 8 days. Body weights and burrowing behavior were measured throughout the experiment. The effects of GW2580 on circulating leukocyte populations, brain microglia morphology, and the transcriptome of magnetically isolated adult brain microglia were determined. Body weights, burrowing behavior, and circulating leukocytes were not affected by treatment. Analysis of Iba-1 stained brain microglia indicated that GW2580 treatment altered morphology, but not cell number. Analysis of RNA-sequencing data indicated that genes related to reactive oxygen species (ROS) regulation and survival were suppressed by treatment. Treatment of primary microglia cultures with GW2580 resulted in a dose-dependent reduction in viability only when the cells were concurrently treated with LPS, an inducer of ROS. Pre-treatment with the ROS inhibitor, YCG063, blocked treatment induced reductions in viability. Finally, GW2580 sensitized microglia to hydrogen peroxide induced cell death. Together, these data suggest that partial CSF1R antagonism may render microglia more susceptible to reactive oxygen and nitrogen species.

Keywords: microglia, Csf1r, GW2580, reactive oxygen species, *in vivo*, *in vitro*

INTRODUCTION

Microglia comprise 10-15% of total cells in the central nervous system (CNS) and are the recognized resident macrophages of this tissue. As such, microglia function to maintain homeostasis within the healthy brain and act as facilitators of immune responses within the CNS in response to damage or pathogenic challenge. For instance, microglia can clear cellular debris, non-functioning neuronal synapses (1) and dead neurons from the CNS through the process of phagocytosis (2). Upon activation by pathogen associated molecular patterns or by damage associated molecular patterns, microglia release cytokines, chemokines (3, 4) as well as cytotoxic substances including reactive oxygen species (ROS), and nitric oxide (NO) (4–6). While the production of inflammatory mediators by microglia may aid in the clearance of pathogens and/or facilitate repair, aberrant microglia activation is suspected to contribute to a plethora of neurological diseases and disorders including multiple sclerosis (7, 8), Alzheimer's disease (9), stroke (10), Parkinson's disease (11), amyotrophic lateral sclerosis (12) and autism spectrum disorder (13, 14). Moreover, pro-inflammatory cytokine production within the CNS is thought to contribute to sickness behavior (15, 16) and impaired cognitive function (15, 17–19).

Intriguingly, microglia viability within the adult brain has recently been shown to be dependent on constitutive colony-stimulating factor 1 receptor (CSF1R) signaling (20) which is needed for their survival, differentiation, proliferation and function (21). CSF1R binds to two ligands: CSF1 and interleukin-34 (IL-34) (22). While CSF1 is detectable in circulation, IL-34 is not circulated in blood (23). In the brain, CSF1 is expressed by astrocytes, oligodendrocytes and microglia, while IL-34 is primarily produced by neurons (24, 25). Ligand binding to CSF1R on microglia leads to tyrosine receptor kinase dimerization and autophosphorylation (26) and triggers activation of ERK and AKT pathways that regulate survival (27). Systemic administration of brain penetrant pharmacological inhibitors of CSF1R can suppress microglia reactivity and/or dramatically reduce viability by more than 90% (28). The use of these small molecules may prove to be clinically efficacious in curtailing the progression of neuroinflammatory and neurodegenerative disease states. Inhibitors of CSF1R include Pexidartinib/PLX-3397, BLZ945, and PLX5622 which eliminate microglia due to their strong affinity with the receptor and their ability to cross the blood brain barrier (28–34). Conversely, the inhibitors ARRY-382, Edicotinib, JTE-952 and GW2580 prevent cell proliferation without killing microglia (35–40). Notably, the consequence of systemic CSF1R antagonism on normal microglia physiology has not yet been fully elucidated. Some of these molecules such GW2580 are intriguing because they are brain penetrant, but do not appear to affect microglial cell survival.

Abbreviations: AST, Astrocytes; CNS, Central nervous system; CSF1, Colony stimulating factor 1; CSFR1, Colony stimulating factor 1 receptor; CTL, Control; DMEM, *Dulbecco's Modified Eagle Medium*; Endo, Endothelial cells; HBSS, Hanks Balanced Salt Solution; LDH, Lactate dehydrogenase; LPS, Lipopolysaccharide; MG, Microglia; Neu, Neuron; OL, Oligodendrocytes; ROS, Reactive oxygen species.

The small molecule GW2580 is an orally available selective inhibitor of the tyrosine kinase activity of CSF1R (39, 40). This molecule has been shown to affect both microglia and monocyte proliferation (40, 41). While GW2580 does not readily affect microglia viability, oral gavage has been used to successfully treat animal models of multiple sclerosis (42, 43), Alzheimer's disease (44), amyotrophic lateral sclerosis (45) and prion disease (46). Results from these studies suggest that treatment can decrease cell infiltration to the CNS (39, 41) and TNF production (40), however how this drug affects microglia physiology remains unknown.

Herein, we sought to determine the effect of GW2580 on microglia function in healthy mice. We found that treatment did not affect the percentage of circulating immune cell populations. However, our results revealed changes to microglia morphology as well as transcriptomic differences attributable to treatment, such as downregulation of genes related to reactive oxygen species regulation and survival. *In vitro* treatment of primary microglia cultures with GW2580 showed a dose-dependent reduction in viability only when concurrently treated with lipopolysaccharide (LPS). Notably, primary microglial cell cultures treated with either YCG0630, an inhibitor of ROS, or Nec-1, an inhibitor of necroptosis, abrogated the effects of GW2580 and LPS treatment on cell viability. Collectively, our data define the transcriptomic effects of systemic GW2580 treatment on normal microglia. Furthermore, our data suggest that CSF1R antagonism by GW2580 may render microglia more susceptible to reactive oxygen and nitrogen species.

MATERIALS AND METHODS

Animals

All experimental procedures were approved by the Institutional Animal Care and Use Committee at the University of Illinois Urbana–Champaign, under protocol #19068 and were performed in accordance with guidelines of the National Institute of Health. Male and female C57BL/6J (Jackson Laboratories No. 000664) mice aged 8-12 weeks old were used for all experiments. Breeders were group-housed in solid-bottom caging with standard bedding (Teklad 1/8" corncob) under temperature-controlled conditions (23 ± 1°C) with a 12-hour reversed light/dark cycles (10am-10pm). Rodent diet (Teklad No. 8640) and water were available *ad libitum*.

GW2580 Treatment by Oral Gavage

Oral treatment of rodents with GW2580 has been well characterized (40). Specifically, *in vitro* treatment with GW2580 at 5μM inhibited CSF1 mediated cell proliferation by nearly 100%, and an oral dose of 80mg/kg increased circulating plasma GW2580 concentrations to 5.6μM. Oral treatment was subsequently shown to inhibit disease progression in rodent models of multiple sclerosis [40mg/kg/d (42)], amyotrophic lateral sclerosis [75mg/kg/d; (45)] Alzheimer's disease [75mg/kg/d; (44)] and to attenuate depression-like behavior in MRL/lpr mice [100mg/kg/d; Chalmers et al. (47)]. As such, in the current study, mice were orally gavaged with either 80 mg/kg of GW2580

(LC Labs, Cat No. G-5903) diluted in 200µl of 0.1% Tween 80, 0.5% hydroxymethyl propyl-cellulose or vehicle alone (44) using 18G needles (Instech, Cat No. FTP-18-30-50) for a total of eight days (40). Animal weight and food disappearance were record daily. Burrowing activity, an indicator of sickness behavior, was measured every 48h (48). On day 8 post treatment, mice were euthanized by CO_2 asphyxiation, blood was collected *via* cardiac puncture and the mice were perfused with 20-30 mL of sterile phosphate buffered saline (PBS; pH=7.4).

Flow Cytometry

Following euthanasia blood samples were collected by cardiac puncture with EDTA-coated syringes. Whole blood (100µl) was added to ammonium chloride potassium (500µl) solution for 10 min. at room temperature in order to lyse the red blood cells. The cells were subsequently washed then suspended in ice-cold flow cytometry staining buffer (sterile PBS containing 2% FBS) and counted using an automated cell counter (Nexcelom Bioscience). Next, $1x10^6$ cells were labeled on ice with fluorophore conjugated antibodies to CD4 (Pacific Blue; clone RM4-5; BioLegend, Cat. No. 116008), CD8a (APC-Cy7; Clone 53-6.7; BioLegend, Cat. No. 100714), CD11b (APC; Clone M1/70; BioLegend, Cat. No. 101212), B220 (PE-Cy7; Clone RA3-682; BioLegend, Cat. No. 103224), Ly6G (FITC; Clone 1A8; BioLegend, Cat. No. 127608), Ly6C (PE; Clone HK1.4; BioLegend Cat. No. 128044), and FCblock (CD16/32) for 20 min. Cell were washed, suspended in flow buffer and data were acquired on a LSRII Flow cytometer (BD). Gates were determined using unstained and single-stained samples obtained from the same tissue of origin. Results were analyzed using FlowJo version 10.6.2 flow cytometry software (BD).

Adult brains were collected from mice, minced with a sterile razor blade and an enzymatic digestion for 45 min. in 5ml of StemPro Accutase (Gibco, Cat No. A1110501) at 37°C. Then the brain homogenate was filtered through a 70µm filter using a 3ml syringe plunger, then pelleted by centrifuging at 400x*g* for 5 min. Red cells were removed with a red blood cell lysis buffer (Biolegend, Cat No. 420302) followed by another centrifugation at 400xg for 5 min. Next, cells were suspended in 5ml of PBS solution containing 35% Percoll (VWR, Cat. No. 899428-524), underlay with 3ml of PBS containing 70% Percoll, then centrifuged for 20 min. at 2000x*g* with no brake. The cells at the 35/70% Percoll interface were collected and in some cases these cells were washed with magnetic activated cell sorting (MACS) buffer (PBS with 3% FBS and 10mM EDTA) to enrich for CD11b positive cells following the manufacturer's instructions (ThermoFisher Scientific, Cat No. 8802-6860-74). Flow cytometry was also used to confirm the purity of microglia subjected to MACS cell enrichment. Here, microglia from non-enriched and enriched populations were stained with antibodies for CD45 (APC; clone 30-F11) (eBioscience, Cat No. 17-0451-82), CD11b (FITC; clone M1/70) (eBioscience, Cat No. 11-0112-82) and viability dye (eFlour 780) (eBioscience, Cat No. 65-0865-14) as markers.

Immunohistochemistry

Brains were collected and placed in fixation buffer (PBS containing 4% paraformaldehyde, pH 7.4) at 4°C for 24h. The tissue was then cryoprotected by replacing the fixation buffer with PBS containing 30% sucrose (w/v) until the tissue sank. The brain tissue was frozen in optimal cutting temperature compound (O.C.T.) with dry ice, then stored at -80°C. Next, 15µm coronal sections were collected using a cryostat (Leica CM3050 S). Tissue sections were then blocked and permeabilized with PBS containing 5% goat serum and 0.3% Triton X-100, then incubated with an anti-Iba-1 specific antibody derived from rabbit (diluted 1/200; Rabbit; Wako Inc. Richmont, VA, Cat No. 019-19741). After washing with PBS three times for 5 min. the tissues were incubated with an Alexa Fluor 488 conjugated goat anti-rabbit antibody (Invitrogen, Cat No. A11034) diluted in 1/1000 in blocking buffer for 1h at room temperature. After washing, the tissue was coverslipped. Sections were imaged and morphological changes were determined by Imaris surface analysis. Specifically, for the Imaris three-dimensional (3D) modeling and analysis sets of 50 serial images for Iba-1^+ cells in the cortex at 500 nm steps in the Z direction, 1 µm per pixel in the X, Y-plane, and 4.92 µsec pixel dwell time were acquired with the Zeiss LSM 710 Confocal Microscope and 10x objective with 2.0 zoom, resulting in whole datasets of 425 µm x 425 µm in the X, Y-plane and 25 µm in the Z direction. The images were rendered into 3D with Imaris software (version 9.3.1; Bitplane, Oxford Instruments) and analyzed with the software's automated Filament Tracer module. Seed point and starting point thresholds were manually adjusted to fit each data set and local contrast threshold was set to three for all data sets. The number of Iba-1^+ cells from the medial prefrontal cortex, cortex and hippocampus were counted using ImageJ (NIH).

Isolation of Adult Microglia and RNA Sequencing

Brains were immediately extracted following perfusion with cold PBS and kept on ice in Hanks Balanced Salt Solution (HBSS) buffer (Fisher, Cat No. SH3058801) until further processing. They were minced using as sterile razor blade and enzymatically dissociated for 45 min. in 5ml of StemPro Accutase (Gibco, Cat No. A1110501) at 37°C. The brain homogenate was filtered through a 70µm filter using a 3ml syringe plunger, then pelleted by centrifuging at 400x*g* for 5 min. Red cells were lysed by osmotic shock (red blood cell lysis buffer; Biolegend, Cat No. 420302) then the cells were washed in sterile PBS by centrifugation at 400x*g* for 5 min. Cells were suspended in 5ml of PBS solution containing 35% Percoll (VWR, Cat. No. 899428-524), underlaid with 3ml of PBS containing 70% Percoll, then centrifuged for 20 min. at 2000x*g* with no brake. The cells at the 35/70% Percoll interface were collected and washed with magnetic activated cell sorting (MACS) buffer (PBS with 3% FBS and 10mM EDTA). Microglia were enriched by positive selection using antibodies directed towards CD11b, as previously described. RNA was isolated using the GeneJET™ RNA Purification kit (ThermoFisher Scientific, Cat No. 0732) by following the manufacturer's instructions. SMART-Seq v4 PLUS Kit (Takara, Cat No. 634888) was used to generate high-quality cDNA libraries from ultra-low amounts of total RNA (10pg–10 ng). Subsequently high-quality Illumina sequencing-

ready libraries were prepared and sequencing was performed using with Illumina Hi-seqlane. The fastq read files were generated and demultiplexed with the bcl2fastq v2.20 Conversion Software (Illumina, San Diego, CA, USA). The quality of the resulting fastq files was evaluated with the FastQC software, which generates reports with the quality scores, base composition, k-mer, GC and N contents, sequence duplication levels and overrepresented sequences. On average 47.9 million 150nt paired-end reads per sample were obtained, with a minimum FastQC score of 34. Alignments and counts were performed on the Carl R. Woese Institute for Genomic Biology Biocluster of the University of Illinois High-Performance Biological Computing. Pair-end reads were first filtered using Trimmomatic 0.33 (49) with a minimum quality score of 28 (i.e., base call accuracy of 99.84%) leading and trailing with a minimum length of 30 bp long and subsequently checked using FastQC 0.11.6 (Babraham Institute, Cambridge, UK). No reads were filtered as all had scores greater than 28. Reads were then mapped to the *Mus musculus* reference genome (GRCm38 e! Ensembl, downloaded in September 2019) using default settings of STAR 2.6.0 (50). Uniquely aligned reads were quantified using feature Counts (51) in the Subread package (v1.5.2) based on the Refseq gene annotation.

Further data analysis was conducted using R. 3.5.1 (R Core Team, 2018). Reads uniquely assigned to a gene were used for subsequent analysis. Genes were filtered if 3 samples did not have > 1 count per million mapped reads. A TMM (trimmed mean of M-values) normalization was applied to all samples using edgeR (52). After data were log2-transformed, edgeR was used to conduct differential expression analyses. The applied statistical model included treatment (GW2580 vs Control) as fixed effect.

The genome index was prepared using STAR and the *Mus musculus* DNA FASTA file from e!Ensembl. The reads were aligned to the reference genome to both reads. Reads were counted using a FeatureCount in STAR. Statistical analysis of differentially expressed genes (DEG) was performed using R studio. Gene ontology was determined by DAVID Functional AnnotationBioinformatics Microarray Analysis (v6.8). Data is publically available through Gene Expression Omnibus (GEO) from NCBI at (https://www.ncbi.nlm.nih.gov/geo/query/acc.cgi?acc=GSE185564) and can be accessed using the accession no. GSE185564

Primary Microglia Cultures

Glial cultures were prepared from the brains of 4-10 C57BL/6 neonatal mice per experiment using the differential attachment method as described previously (3, 53). In brief, P1–2 mouse pups were decapitated with scissors, brains dissected and meninges removed under a dissection microscope (Leica). Brain tissue was disassociated in Accutase at 37°C for 45 min., passed through a 70μm filter, washed with Dulbecco's Modified Eagle Medium (DMEM), seeded onto poly-d-lysine-coated T75-flasks, and grown to confluence (7–10 days) in a humidified incubator at 37°C and 5% CO_2. Microglia were isolated by shaking the T-flasks at 37°C for 1h at 177rpm in an orbital shaker (ThermoScientific Max Q 4000).

Effect of GW2580 Treatment on Microglia Proliferation

Primary microglia were seeded at a density of $1x10^5$ cells per well in a 96-well plate in DMEM supplemented with 10% FBS, 100U pen/strep and glutamax. To determine the effect of CSF1 and GW2580 on cell proliferation, microglia were treated with recombinant mouse CSF1 (0-30ng/ml; R&D Systems; Cat No. 416-ML-10) for 48h with increasing concentrations of GW2580 (0-5μM). After treatment, cells were fixed with 4% paraformaldehyde for 20 min. at room temperature, washed with PBS then blocked and permeabilized in PBS containing 0.3% Triton-X 100 (PBST) and 5% goat serum for 1h at room temperature. Next, the cells were incubated with a rabbit anti-Ki-67 antibody (Dilution 1:200; Cell Signaling; Cat No. 9129S) overnight at 4°C. After washing with PBS, cells were incubated with Alexa Fluor 488 conjugated goat anti-rabbit IgG diluted 1/1000 in PBST for 1h. (ThermoScientific). After washing with PBS, proliferation was determined by counting the number of microglia per well, as well as the number of Ki-67^+ cells per well using ImageJ (NIH).

Gene Expression Analysis by qRT-PCR

To validate the effect of GW2580 on the expression of select genes involved in the regulation of ROS, qRT-PCR was used. Here, primary microglia were stimulated with 5μM of GW2580 or media alone for 72h in a humidified incubator at 37°C and 5% CO_2. RNA was isolated using TRIzol protocol (Ambion by Life Technologies, Cat No., 15596018) and further purified using the GeneJET RNA Purification Kit (Thermo Scientific, Cat No., K0731). cDNA was created using the reverse transcription system (Promega Corporation, Cat No., A3500), and amplified using Sybr Green qPCR master mix (Applied Biosystems, Cat No., A25742), and primers specific for *Ndufs8* (Fwd-CGCAGCACTTCAAGATGTATCG; Rev-TCTTGGCTCAGCCTCAATGG), *Prdx2* (Fwd-CAACCACCGCCAGAATTGC; Rev-AACATTGTGGATGGCTTGGC), *Prdx5* (Fwd-AGGGTACCCAACCCTGTTCT; Rev-GCACAGTAGTACACAGCCGA), *Gpx4* (Fwd-CGCCAAAGTCCTAGGAAACG; Rev-TATCGGGCATGCAGATCGAC), and *Actb* (Fwd-GATTACTGCTCTGGCTCCTAG; Rev-GACTCATCGTACTCCTGCTTG) in a 7300 Real-Time PCR System (Applied Biosystems, ABI) at 95°C for 10min, followed by 40 cycles of 95°C for 15secs and 60°C for 1min. Expression was normalized to *Actb* expression and control samples. Fold change was calculated using the formula $2^{-\Delta\Delta Ct}$.

Detection of Reactive Oxygen Species (ROS) in Cultured Microglia

Primary microglia ($1x10^6$ per condition) were stimulated with 100ng/ml of LPS for 0, 6 or 24h in a 1.5ml tube in complete RPMI media at 37°C and 5% CO_2. Cells stimulated with media containing 75μM hydrogen peroxide were used as a positive control. After the stimulation, light-protected cells were stained with 5μM of CellROX Green Reagent (ThermoFisher Scientific, Cat No. C10444) for 30 min. at 37°C and 5% CO_2. The cells were washed twice with 1ml of cold flow buffer (PBS, 2% FBS) then suspended in

100µl of flow buffer. The cells were stained with viability dye (APC Alexa Flour 780, Invitrogen, Cat No. 50-112-9035) for 20 min on ice, washed, then suspended in 500µl of flow buffer and analyzed using flow cytometer. Gates were determined using a complete unstained sample.

Microglia Susceptibility to ROS

To assess the effect of GW2580 on cell viability, microglia were incubated with or without GW2580 at a concentration of 5µM for 45 min. prior to stimulation with vehicle (medium) or lipopolysaccharide from *Escherichia coli* O111:B4 (100ng/ml) for 48h. TNF production was measured by ELISA (ThermoFisher Scientific, Cat No. 88-7324-88) following the manufacturer's instructions. For some experiments, microglia were pre-treated with the ROS inhibitor YCG063 (10µM, Sigma Aldrich, Cat No. 557354). Specifically, cells were pre-treated with either YCG063 or YCG063 plus GW2580 for 45 min. prior to LPS stimulation for 48h. To determine if GW2580 treatment of microglia increased sensitivity to ROS, cells were pretreated with GW2580 (5µM) for 48h then challenged with 0-100µM of hydrogen peroxide (H_2O_2; Fisher Scientific, Cat No. H325-100) for 4h. Cell death was assessed by measuring supernatant lactate dehydrogenase (LDH) levels as indicated by manufactures instructions (Sigma Aldrich, Cat No. 4744926001) as well as by counting the number of cells per field.

Treatment of Primary Microglia With Nec-1

Primary microglia ($1x10^5$ per condition) were pre-treated with either Nec-1 (30nM) or Nec-1 plus GW2580 for 45 min. prior to LPS (100ng/ml) stimulation for 48h in a 96 well plate. After treatment, cells were fixed with 4% paraformaldehyde for 20 min. at room temperature, washed with PBS then blocked and permeabilized with PBS containing 0.3% Triton-X 100 (PBST) and 5% goat serum for 1h at room temperature. Next, the cells were incubated with a rabbit anti-Iba-1 antibody (diluted 1/200; Rabbit; Wako Inc. Richmond, VA, Cat No. 019-19741) overnight at 4°C. After washing with PBS, cells were incubated with Alexa Fluor 488 conjugated goat anti-rabbit IgG diluted 1/1000 in PBST for 1h. (ThermoScientific). Cell death was assessed by measuring supernatant lactate dehydrogenase (LDH) levels as indicated by manufacturer's instructions (Sigma Aldrich, Cat No. 4744926001).

Statistics

Data are expressed as means ± standard error (S.E.). For the RNA-seq experiment differentially expressed genes (DEG) across time points were determined with a combination of fold-change (> 2.0 or < -2.0) and *P*-value (< 0.05) thresholds to balance for reproducibility, sensitivity, and specificity or results (54, 55). Statistical analysis of all other data was performed using GraphPad Prism (version 8.0 or higher) software. Student's *t*-tests were used to compare differences between two groups. Analysis of variance (ANOVA) followed by Bonferroni's *post hoc* test was used to compare differences between more than two groups. Statistical significance was determined by p-value <0.05. Data are expressed as means ± standard error (S.E.).

RESULTS

Effect of GW2580 Treatment on Indices of Sickness and Circulating Immune Cell Populations

Treatment with GW2580 neither reduced body weight nor the degree of food disappearance (**Figures 1A, B**). Furthermore, GW2580 did not alter burrowing behavior (**Figure 1C**). No effect of gender was found for weight, food intake or burrowing behavior (**Supplemental Figure 1**). Because macrophages and monocytes also express *Csf1r* (56), we questioned whether treatment affected the percentages of circulating immune cells. Flow cytometry analysis performed on blood samples indicated that treatment did not alter percentages of circulating B cells, T cells, monocytes or granulocytes (**Figure 2**). Together, these data indicate that treatment with GW2580 does not overtly affect behavior or hematopoiesis, nor does it decrease blood leukocyte viability.

Treatment With GW2580 Caused Morphological and Transcriptomic Alterations to Microglia

We next questioned whether treatment with GW2580 altered microglia morphology, a commonly used proxy for activation. Imaris™ software was used to non-subjectively determine effects of

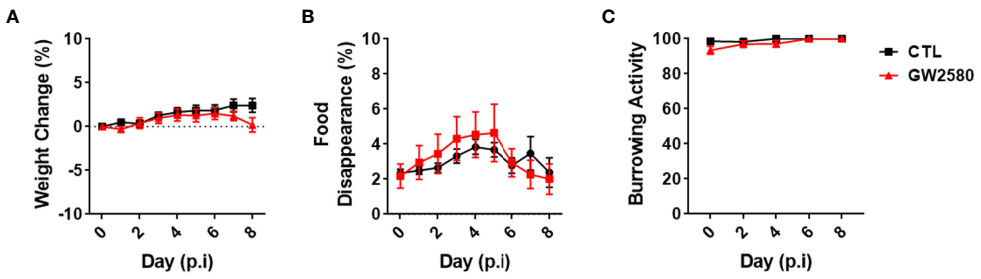

FIGURE 1 | Effect of GW2580 treatment on mouse weight and behavior. **(A–C)** Mice were treated with GW2580 at a dose of 80mg/kg/d by oral gavage for 8 days. The effect of treatment on weight **(A)**, food disappearance **(B)**, and burrowing activity **(C)** is shown. Data are expressed as means ± standard error (S.E.). Each group is composed by n=30 per group from four independent experiments for weight change, n=6 per group from a single experiment for food disappearance, and n=15 per group from three independent experiments for the burrowing activity.

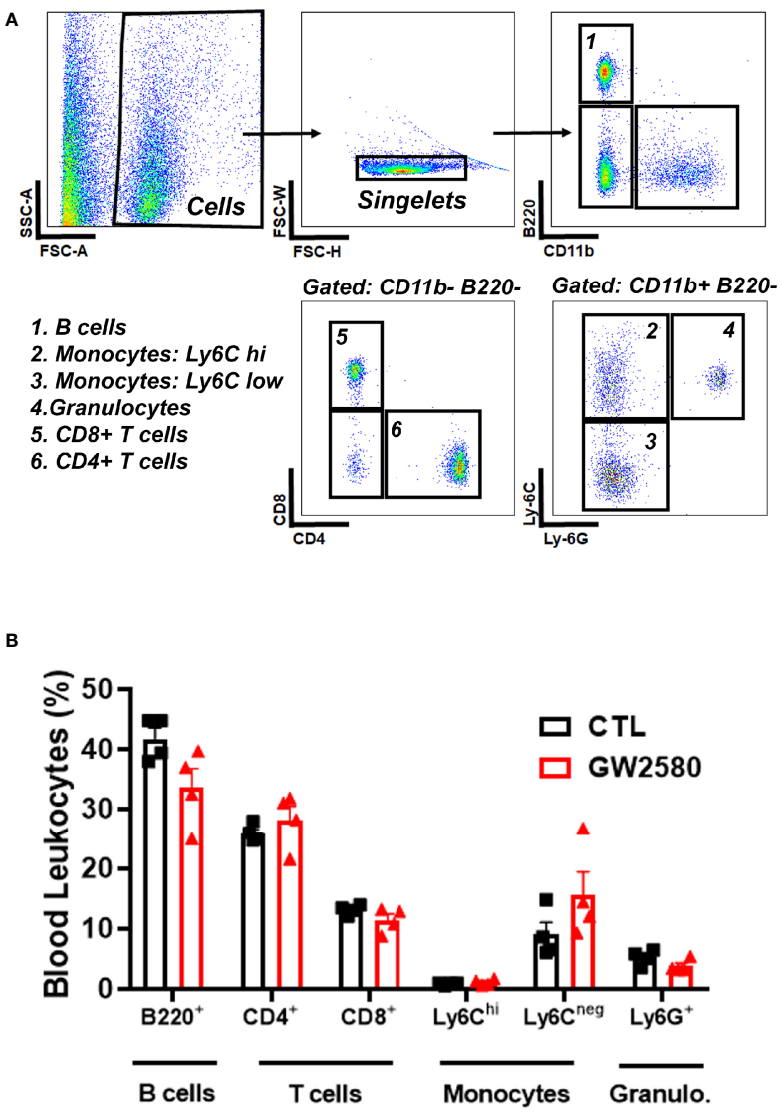

FIGURE 2 | Effect of GW2580 treatment on blood leukocytes. **(A, B)** Mice were treated with vehicle or GW2580 by oral gavage for 8 days and the effect of treatment on circulating leukocytes determined by flow cytometry. **(A)** Representative gating strategy used to determine the percentage of B cell, T cell, monocyte and granulocyte subsets. **(B)** Cell percentages of blood leukocytes from vehicle and treated mice are shown. Data are expressed as means ± standard error (S.E.), n=4 per group.

GW2580 on various morphological characteristics of Iba-1 labeled microglia in 20x images including: mean filament area, filament length, filament diameter, filament volume, mean number of branches, mean number of branch points, mean number of segments and mean number of terminal points (**Figure 3A** and **Supplemental Table 1**). The cortex was chosen as a representative region of morphological changes after GW2580 treatment (57). We found that GW2580 treatment altered morphological characteristics of brain microglia in the cortex. Specifically, the filament length was increased, but filament diameter, number of branches, number of branch points, the number of segments and the mean number of terminal points were decreased as a result of GW2580 treatment (**Figure 3B**). Interestingly, morphological analysis of Iba-1$^+$ microglia in 40x images showed similar results, where the number of branch points were decreased in the treated mice, as well as the number of segments (**Supplemental Figure 2**). However, as in previous studies (40), GW2580 treatment for 8 days did not change the number of microglia in medial prefrontal cortex, cortex or cerebellum (**Figure 3C**).

To access the *in vivo* effects of CSF1R inhibition, we performed RNA sequencing on freshly isolated microglia from GW2580 treated mice. Microglia were enriched by MACS using CD11b microbeads. This produced greater than 95% enrichment of cells phenotypically characterized as being CD11b$^+$CD45^{int} by flow cytometry (**Figures 4A, B**). The majority of the contaminating cells (5%) were found to be CD11b$^+$CD45^{hi} monocytes/granulocytes (**Figures 4A, B**). To validate the purity of microglia

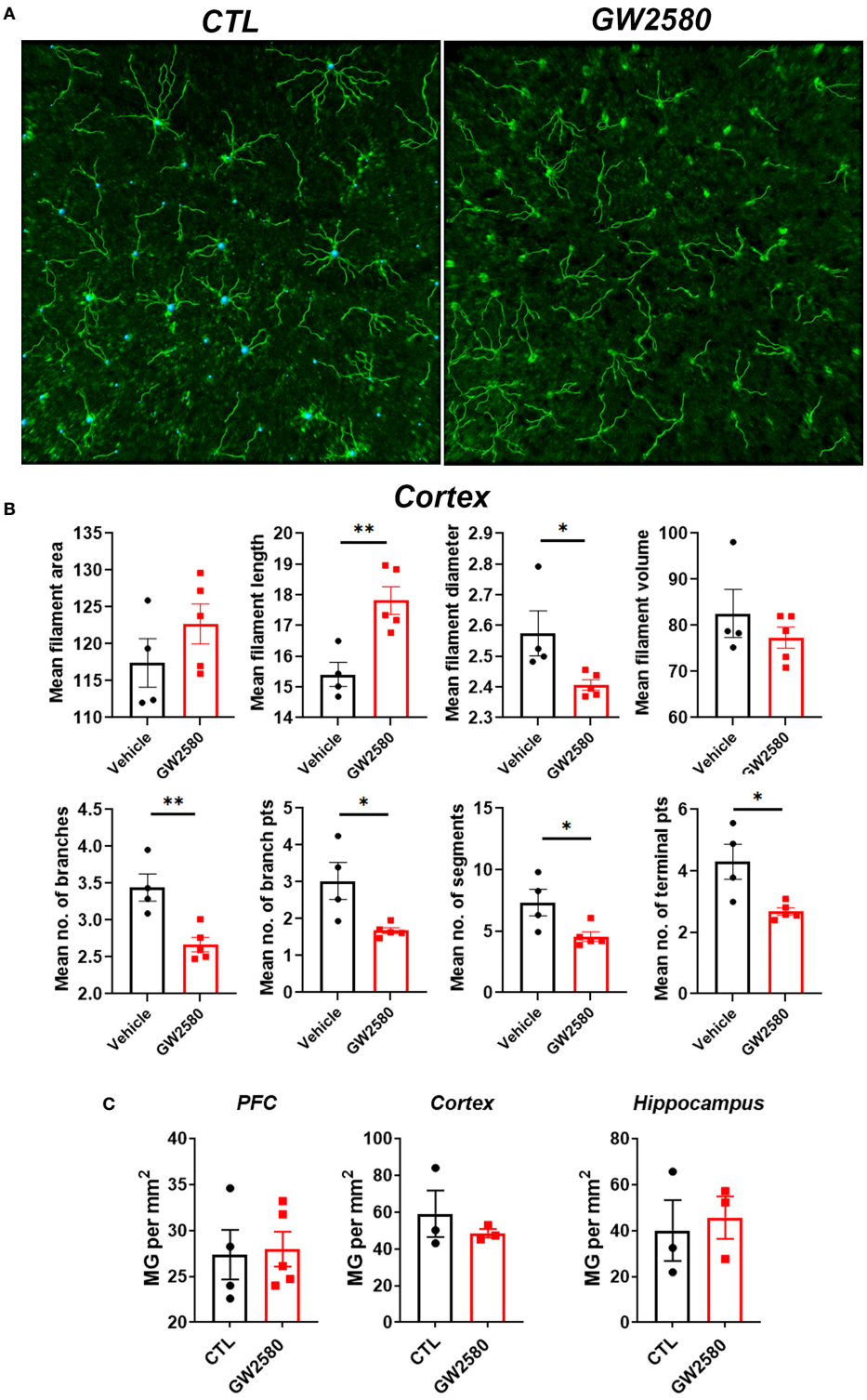

FIGURE 3 | Effect of GW2580 treatment on changes to microglia morphology. **(A–C)** Mice were treated with GW2580 by oral gavage for 8 days and the effect of treatment on microglia morphology and viability examined. **(A)** Representative three dimensional reconstruction of a microglia cell in the cortex of vehicle and GW2580 treated mice from a 20x picture. Scale bar is 50µm. **(B)** Results from Imaris analysis. Each point represents an average of three cells per mouse (n=4-5 animals per group), average of three 20x z-stacks of 25µm and 500nm steps per animal. **(C)** Microglia counts per mm^2 in the prefrontal cortex, cortex and hippocampus. Each point represents an average of three pictures. Data shown are expressed as means ± standard error (SE). Statistical significance is represented by p-value < 0.05 (*), and p-value < 0.01 (**).

after RNA-seq was performed, we examined the expression of genes specific for microglia (*Tmem119*, *Hexb*, *Fcrls*, *Siglech*), astrocytes (*Gfap*, *Aldh1l1*, *Aqp4*), oligodendrocytes (*Olig2*, *Plp1*, *Sox10*), endothelial cells (*Pecam1*, *Cldn5*, *Tie2*) and neurons (*Sp9*, *Reln*) (**Supplemental Table 2**). This analysis revealed that the RNA was enriched for microglia specific genes, confirming that the sequenced cells were microglia (**Figure 4C** and **Supplemental Table 2**). In total, we identified 577 differentially expressed genes (DEGs), of which 144 were upregulated and 433 were downregulated. Since GW2580 is a CSF1R antagonist we hypothesized that genes involved in the CSF1/CSF1R signaling pathway may be affected by treatment. Therefore, we examined the expression values of the CSF1R ligands *Csf1* and *Il34* as well as the expression of *Csf1r* itself. The RNA sequencing analysis showed that *Csf1* was upregulated in the GW2580 treated group. Furthermore, while the mean expression value for *Csf1r* trended towards being higher in the treated group, the effect did not reach statistical significance (p-value of 0.08). Consistent with the fact that *Il34* is predominantly expressed by pericytes and neurons (Tabula Muris Consortium, 2018) but not microglia, we found the expression values for *Il34* were low. There was no difference in the level of *Il34* expression. Analysis of the gene ontology terms indicated that genes encoding proteins involved in glutathione metabolic process, response to oxidative stress, removal of superoxide radicals and response to estradiol were decreased by treatment (**Figure 4D** and **Supplemental Table 3**). Additionally, ontology analysis of the upregulated genes showed that GW2580 affects expression of genes involved in G-protein coupled receptor signaling pathway and sensory perception of smell (**Supplemental Table 4**).

In Vitro Effects of Inhibiting Csfr1 From Primary Microglia After GW2580 Treatment

We sought to determine if GW2580 treatment affected microglia in culture. Unlike microglial cell lines, such as BV-2 cells, primary mouse microglia monocultures do not readily proliferate in culture. However, as reported by others (58, 59) we found that CSF1 treatment for 48h increased cell number as well as the number of Ki-67$^+$ cells per well in a dose-dependent fashion without affecting cell viability (**Figures 5A, B**). These data indicate that primary microglia are responsive to CSF1. To establish the dose at which GW2580 affects microglial function, primary cultures were pretreated with increasing concentration of GW2580 then stimulated with either media or CSF1. As before, CSF1 treatment increased the number of Ki-67$^+$ cells. However, concurrent treatment with GW2580 ameliorated this effect, without affecting cell viability (**Figures 5C, D**). These findings indicate that cultured primary microglia proliferate in response to CSF1 and confirm that treatment with GW2580 at a concentration of 5μM is sufficient to inhibit the effects of CSF1 signaling.

To confirm the effects of GW2580 on cultured microglia, we examined the expression levels of select genes that comprised the gene ontology term "response to oxidative stress" (*Ndufs8, Prdx5*), "removal of superoxide radicals" (*Prdx2*), and "glutathione metabolic process" (*Gpx4*), identified by our RNA-seq analysis.

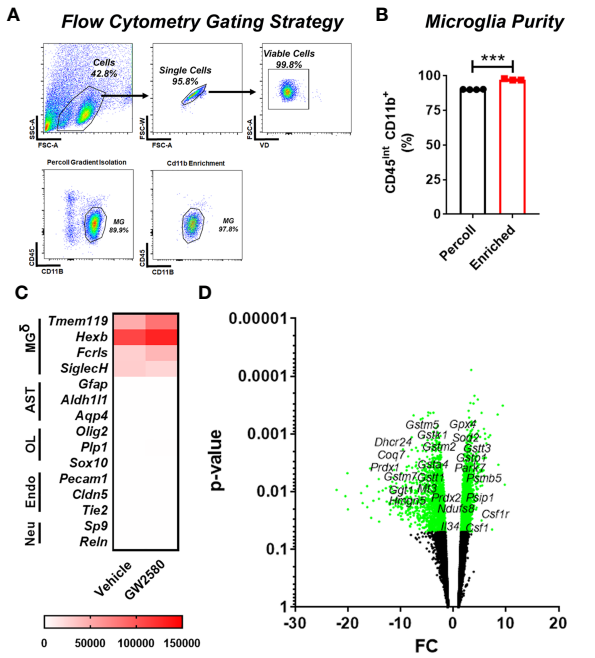

FIGURE 4 | Microglia transcriptional changes induced by GW2580 treatment. **(A–D)** Mice were gavaged with vehicle or GW2580 for 8 days then brains were collected, and microglia were isolated by Percoll gradient centrifugation, enriched by positive selection by magnetic associated cellular sorting (MACS) using antibodies specific for CD11b and changes to the transcriptome assessed by RNA-seq. **(A, B)** Microglia purity was determined before (Percoll) and after (enriched) MACS enrichment by flow cytometry. Representative flow cytometry gates **(A)** and cell purity following Percoll gradient centrifugation and positive selection **(B)**. **(B)** n=3-4 mice per condition. **(C)** Mean expression values of select microglia, astrocyte, oligodendrocyte, endothelial and neuron specific cell lineage genes following transcriptomic analysis of microglia isolated from vehicle (*left*) and treated (*right*) mice (n=5 per condition). Scale bar is gene expression level (RMPK). δ= Genes for microglia were enriched. **(D)** Volcano plot representing all the genes detected with the RNA sequencing experiment, significant genes are represented in green, including *Csf1, Csf1r* and *Tspo*, as well as the ROS related genes. Data are expressed as means ± standard error (S.E.). Statistical significance is represented by p-value < 0.001 (***).

Treatment of primary microglia cultures with GW2580 suppressed the expression of *Ndufs8*, *Prdx2*, *Prdx5* and *Gpx4* without affecting viability (**Supplemental Figure 3**).

Treatment With GW2580 Sensitizes Microglia to ROS Toxicity

Stimulation with LPS upregulates ROS production in BV-2 cells (60) and primary microglia (61). In order to validate ROS production by primary microglia after LPS stimulation, we analyzed ROS production by flow cytometry using CellRox. For these experiments treatment with H_2O_2 served as a positive control. As reported by others, we found that both LPS and H_2O_2 treated microglia displayed increased fluorescence after 24h (**Figures 6A, B**). Since our RNA-seq data suggested that GW2580 suppressed genes associated with regulation of ROS, we questioned the effects of treatment on primary cultures

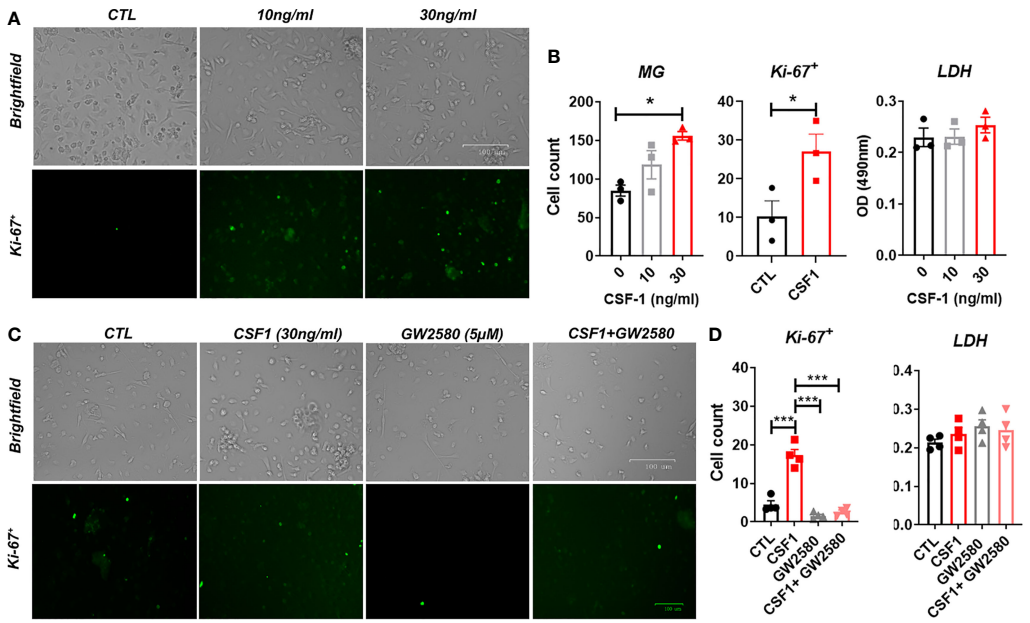

FIGURE 5 | Effect of GW2580 treatment on microglia cell proliferation. **(A, B)** Primary mouse microglia were stimulated with 0, 10 or 30ng/ml of CSF1 and then stained with 30μg/ml of Ki-67. Cell death was assessed by measuring supernatant levels of LDH. Cells were manually count and represented by the graphs. Data are expressed as means ± standard error (S.E.), n=3 independent experiments per group. **(C, D)** Cells were treated with either media, with CSF1 (30ng/ml), GW2580 (5μM), or CSF1 and GW2580, then Ki-67. The number of Ki-67$^+$ cells determined by immunohistochemistry were manually counted and represented by the graphs. Data are expressed as means ± standard error (S.E.), n=4 independent cultures per group. Statistical significance is represented by p-value < 0.05 (*), and p-value < 0.001 (***).

stimulated with LPS. For these experiments microglia cultures were stimulated with either media, LPS, GW2580 or LPS and GW2580 together. Treatment with GW2580 or LPS alone had minimal effects on cell viability. In contrast, when microglia were concurrently treated with LPS and GW2580 we observed a marked decrease in cell viability which was validated by increased levels of LDH in the supernatant (**Figures 6C, D**). Notably, this effect was dependent on the concentration of GW2580 added to the culture (**Figure 6D**). As reported for primary peritoneal macrophages treatment did not affect the acute production of TNF from stimulated cultures (**Figure 6E**) (40). Taken together, these data indicate that LPS induces ROS in primary microglia and that CSF1R antagonism decreases viability when microglia are activated by LPS.

Next, we sought to examine a potential relationship between cell death resulting from treatment with LPS and GW2580 and ROS production. To determine if ROS was responsible for microglia death, we replicated the experimental design from previous experiments and pretreated cultures with or without YCG063, a ROS scavenger (62–64). As in previous experiments, microglial cell viability was decreased only when they were cultured in the presence of GW2580 and LPS. This effect was prevented in the presence of the ROS inhibitor YCG063 (**Figures 7A, B**), indicating that ROS was involved in the reduction of cell viability observed when microglia were treated with GW2580 and LPS.

To determine if pretreatment with GW2580 increased the sensitivity of microglia to ROS, cultures were challenged with increasing concentration of H_2O_2 in the presence or absence of drug treatment. Microglia pretreated with GW2580 had increased supernatant levels of LDH when stimulated with 50μM, 75μM and 100μM concentrations of H_2O_2 compared to control cultures (**Figures 7C, D**), indicating that GW2580 increased susceptibility of cells to a direct ROS challenge. Taken together, these data indicate that CSF1 antagonism by GW2580 suppresses the capacity for microglia to respond to oxidative stressors and sensitizes them to ROS when they become reactive.

Treatment With the RIP1 Inhibitor Nec-1 Prevented GW2580-Mediated Toxicity

Treatment mediated dysregulation of ROS may promote cell death by either apoptosis or necroptosis (65–67). However, a time course experiment showed that treatment did not cause appreciable changes in the number of cells positively stained for cleaved caspase-3, indicating apoptosis is not likely to be the mechanism of cell death (data not shown). It was recently shown that Toll-like receptor activation in the context of caspase-8 inhibition caused microglia cell death by necroptosis in a manner contingent upon activation of RIP1/RIP3 complex and ROS production (66). CSF1R ligation by CSF1 also promotes caspase-8 activation (68), which may function to inhibit RIP1/RIP3 mediated necroptosis. To test whether necroptosis was involved in cell death resulting from co-treatment with LPS and GW2580, primary microglia were stimulated as before in the presence or absence of Nec-1, a RIP1 antagonist and potent necroptosis inhibitor (**Figure 8A**). Our data

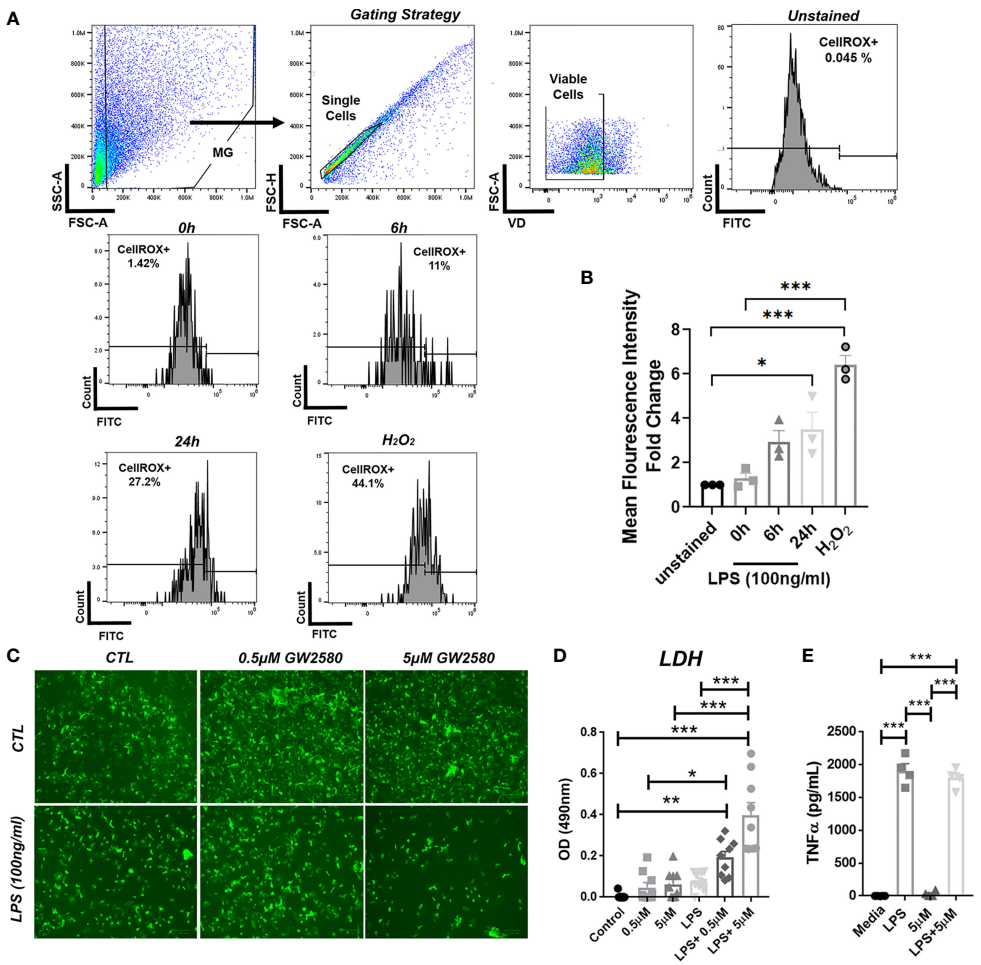

FIGURE 6 | Combined treatment of primary microglia with GW2580 and LPS decreased viability *in vitro*. **(A, B)**, Primary microglia were stimulated with LPS (100ng/ml) for 0, 6 or 24h or with 75μM of H_2O_2, for 24h. **(A)** Microglia were stained for ROS using CellROX and then analyzed by flow cytometry to detect changes in fluorescence intensity. Gating strategy for the experiment. **(B)** Mean fluorescent intensity for ROS production after primary microglia stimulation. **(C–E)** Cells were treated with either media, LPS (100ng/ml), GW2580 (0-5μM), or LPS and GW2580 for 48h. **(C)** Representative images. **(D)** Cell death was measured by LDH assay. **(E)** TNF production by stimulated microglia. Data shown are expressed as means ± standard error (S.E.), n=3 per group for **(A)**, n=9 per group for **(B)** and n=4 per group for **(C)**. Statistical significance is represented by p-value < 0.05 (*), p-value < 0.01 (**) and p-value < 0.001 (***).

show that treatment with Nec-1 inhibited cell death in LPS and GW2580 stimulated cells (**Figure 8B**), indicating an involvement of necroptosis in treatment mediated cell death.

DISCUSSION

In the current study we characterized the effects of GW2580, a CSF1R antagonist, on microglia. Herein, we report that treatment does not affect weight, food disappearance or burrowing activity. However, GW2580 induced morphological changes to microglia and altered their transcriptome without affecting viability. Ontology analysis of down regulated genes indicated glutathione metabolic processes and response to oxidative stress may be dysregulated in microglia isolated from treated mice. Indeed, our culture experiments revealed that primary microglia produce ROS after stimulation with LPS, and that cell viability was only reduced under culture conditions in which cells were concurrently treated with GW2580 and LPS, an effect that was ameliorated in the presence of an ROS inhibitor. In addition, we found that GW2580 treated microglia were more sensitive to hydrogen peroxide treatment. In addition, we observed that this effect was abolished in the presence of the necroptosis inhibitor, Nec-1. These data collectively indicate that CSF1R antagonism alters the ability of microglia to regulate oxidative stress, and that concurrent treatment with LPS and GW2580 promotes cell death in a manner contingent on activation of necroptosis.

Our results indicate that eight days of treatment with GW2580 does not affect microglia cell number, burrowing behavior or food disappearance, but evokes subtle changes to microglia morphology. The effects of GW2580 on animal behavior are similar to those reported previously with PLX3397 (37, 44, 69). In fact, previous studies using the

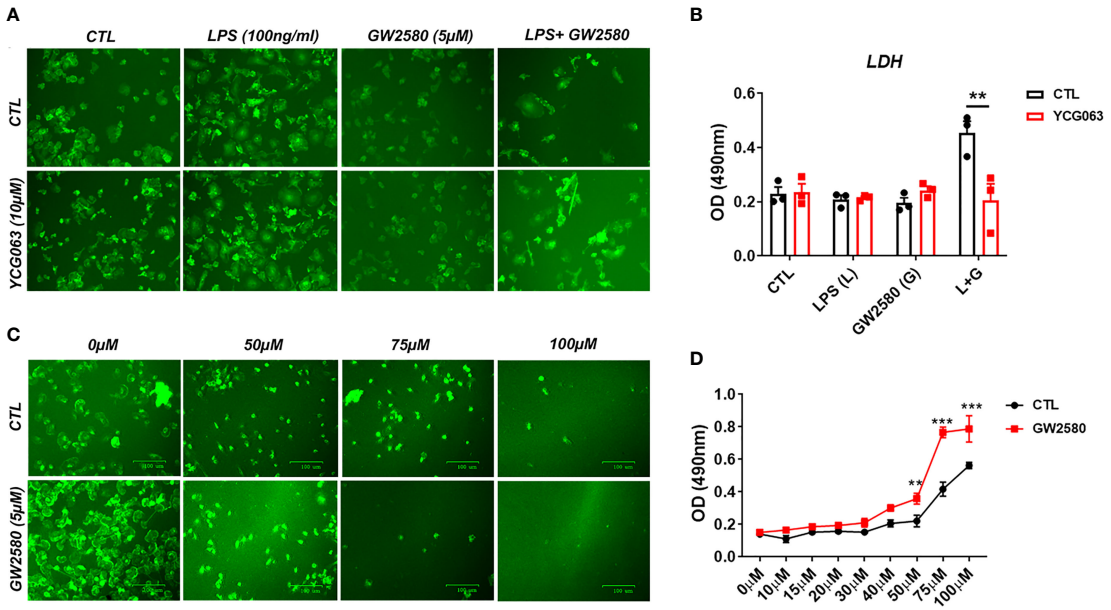

FIGURE 7 | Treatment with the ROS inhibitor YCG063 inhibits cell death in GW2580 and LPS treated cultures. **(A)** Microglia treatment with YCG063, a ROS inhibitor, was used to inhibit cell death. **(B)** LDH results for both conditions. **(C)** Primary microglia were stimulated with hydrogen peroxide (from 0μM- 100μM) with and without 5μM of GW2580. **(D)** LDH results for these conditions. Four independent cultures, represented by a total 19 neonatal pups were used for **(A, B)**. **(C, D)** Three independent experiments, in at least duplicate for each condition in **(C, D)**, represented by 17 neonatal pups. Data shown are expressed as means ± standard error (SE). Statistical significance is represented by p-value < 0.01 (**) and p-value < 0.001 (***).

microglia depleting CSF1R antagonist PLX3397, demonstrated that treatment does not alter animal behavior in otherwise healthy animals (28, 57). In addition to this, CSF1R inhibition using PLX5622 did not alter body weights (70, 71). Furthermore PLX5622 mediated microglia depletion only altered food intake when fed a diet high in saturated fatty acids, but did not impact food intake under normal conditions (72). In terms of morphological changes, few studies have investigated the effects of systemic treatment with non-depleting CSF1R agonists on microglia morphology. Elmore et al., showed that treatment with PLX3397 depletes microglia and that microglia are only morphologically distinct from controls during the repopulation period (57). Treatment with the same antagonist caused morphological changes after 2 days of treatment (73). Similar effects were observed following PLX5622 treatment (74–76). Given that PLX3397 and PLX5622 both rapidly induce microglial cell death, the finding that these drugs alter morphology might be anticipated. Of relevance, treatment with ki20227 is similar to GW2580 in that it does not alter microglial cell numbers. However, as in our study treatment with ki20227 altered the number of microglial segments and branch endpoints (77). Finally, two additional studies have shown that GW2580 is capable of altering microglial morphology (28, 39). Taken together these data indicate that CSF1R inhibition impacts microglia morphology, and indicate that even the non-toxic molecules affect normal microglial physiology.

To better understand how GW2580 treatment affected microglial physiology, we performed an RNA-sequencing experiment on microglia isolated from the brains of control and GW2580 treated mice. Our findings revealed that treatment caused transcriptomic changes to microglia. Unsurprisingly, our data show that *Csf1* was upregulated in the GW2580 treated group, and that *Csf1r* expression exhibits a trend towards being increased. The upregulation of *Csf1* likely reflects an attempt by microglia to increase CSF1R signaling, and indicates that treatment may perturb the CSF1/CSF1R pathway. While many studies have recently utilized pharmacological inhibition of CSFR1 to delete microglia, the effects of CSF1R inhibition on the microglia transcriptome has not been completely elucidated. Similar to our results, data obtained from an RNA sequencing experiment performed on microglia isolated from wild-type and *Csf1r*$^{-/-}$ zebrafish, indicated that *Csf1r* expression was increased (78). Additionally, in this zebrafish model, upregulation of genes involved in chemotaxis and migration was observed in *Csf1r*-deficient microglia compared to wild-type controls (78). Ontology terms from our upregulated genes associated with treatment showed genes related to G-coupled receptor signaling pathway and sensory perception of smell. However, the RMPK level of the genes associated with these ontology terms was low in the control group. Oosterhof and coworkers also observed downregulation of genes related to central nervous system development and ion transportation (78), consistent with the findings from our current study. Transcriptomic analyses performed on metastatic tumors from mice treated with AZD7507, another CSF1R pharmacological inhibitor, showed alterations in tumor microenvironment composition and function (79). This does not imply any significance in terms of direct changes in the macrophage population but it suggests that macrophages present in the tumor

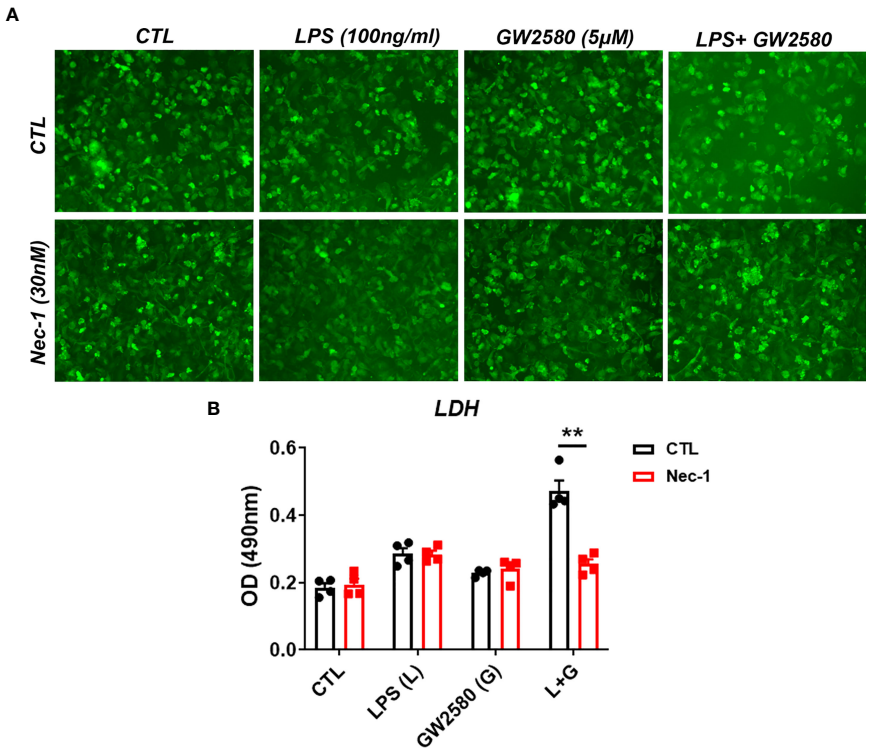

FIGURE 8 | Treatment with the RIP1 inhibitor Nec-1 inhibits cell death in GW2580 and LPS treated cultures. **(A, B)** Primary microglia were treated with either media, LPS (100ng/ml), GW2580 (5μM), or LPS and GW2580 with and without Nec-1 (30nM) for 48h. **(A)** Microglia treatment with Nec-1, inhibitor of necroptosis, was used to inhibit cell death. **(B)** Cell death was addressed by LDH measurement. Data shown is expressed as means ± standard error (SE). Statistical significance is represented by p-value < 0.01 (**).

responded to treatment and altered their relationship with the tumor, because they express CSF1R. Of relevance, human glioblastoma cells also produce CSF1 (80) and treatment with GW2580 inhibits tumor growth following implantation (81).

Transcriptomic analysis of our RNA-sequencing data showed that treatment with GW2580 decreased expression of genes involved in glutathione metabolism and regulation of ROS. We are not aware of other studies that have reported this effect of GW2580 on murine microglia. However, RNA sequencing from *Csf1r*-deficient microglia obtained from zebrafish also showed downregulation of ROS-related genes. These include *Gpx4a* (glutathione peroxidase 4a- down 516), *Mgst2* (microsomal glutathione S-transferase 2), *Gstt1a* (glutathione S-transferase theta 1a), *Gstp1* (glutathione S-transferase pi 1), *Gpx1a* (glutathione peroxidase 1a), *Nrros* (negative regulator of reactive oxygen species), and *Romo1* (reactive oxygen species modulator 1) (78) which are related to glutathione metabolism. Intriguingly, $Mac2^{+}$ microglia that repopulate the brain after PLX5622 mediated deletion upregulate genes related to the ROS pathway (82). This finding is interesting given that intracellular ROS production appears to control the fate of common myeloid progenitors (CMP) in bone marrow. Specifically, CMP cells expressing low levels of ROS differentiate into megakaryocyte-erythrocyte progenitors and those expressing high levels of ROS upregulate CSFR1 and are likely to differentiate into granulocytes or monocytes (83). Continual stimulation of CSF1R by CSF1 inhibits receptor activator of nuclear factor-κB ligand (RANKL), activation of Nox1 and Nox4 protein expression and subsequent osteoclast generation (84). In addition to this, it has been previously proposed that CSF1 increase ROS production *via* NADPH oxidase inducing the expression of RANK (85, 86). Increased intracellular ROS activates both Akt1 and p38 MAPK pathways to regulate monocyte survival (86). Stimulation with TNF seem to upregulate CSF1 production, but in the absence of it, classical monocyte survival factors, including CSF1, GM-CSF and IL-34 seem to not contribute to cell survival (87). In addition, RNA-sequencing performed on microglia isolated from brain and spinal cords of mice treated with the CSF1R inhibitor BLZ945 show that treatment downregulated *Gstm1* (glutathione S-transferase, mu 1) and *Gsto1* (glutathione S-transferase omega 1) (88). Together these data implicate a yet to be established connection between CSF1R signaling, ROS production, detoxification, microglia differentiation and survival.

Since ROS plays an important role in microglia activation and CNS damage this provides a potential mechanism of how CSF1R inhibition, specifically GW2580, works. This becomes very relevant because it was previously found that CSF1 signaling may contribute to the pathology of neurological disorders due to the altered microglia (89). For example, a large-scale RNA-sequencing from spinal cord tissue identified CSF1R as a key node of disease progression in a model of progressive multiple sclerosis (58). They generated a selective CNS-penetrant CSF1R inhibitor molecule and observed

attenuation of the inflammatory response in microglia and macrophages and significant reduction of symptoms in the animal model for multiple sclerosis (58). Similar findings have been reported with other CSF1R inhibitors to treat models of multiple sclerosis (42, 70, 90) demyelination (91–94), Alzheimer's disease (36, 44, 91, 95, 96) neuroinflammation and neurodegeneration (36, 37, 44).

While it is established that CSF1R inhibition readily causes microglia cell death, the mechanism by which the cells die is not clearly established and may be context dependent. For instance, caspase-3^+ microglia have been detected in naïve mice treated with the CSF1R inhibitor PLX3397 (28). Our data suggest that TLR4 activation *via* LPS stimulation in the presence of GW2580, promotes necroptosis, at least in culture. While growth factor withdrawal is known to promote apoptosis, it has also been shown that interactions between CSF1 and its receptor CSF1R leads to caspase-8 activation *via* activation of phosphatidylinosol-3 and AKT (68). Caspase 8 is an established inhibitor of the RIP1/RIP3 complex and thus reductions in caspase 8 promote cell death by necroptosis. For instance, TLR4 activation induced microglial necroptosis in a TNF/TNFR1 independent manner that was instead dependent on TRIF and RIP3 signaling (66). TLR4 activation recruits the adaptor molecules TRIF and MyD88, TRIF interacts with RIP1 and RIP3 *via* receptor-interacting protein homotypic interaction motif leading to RIPK1 ubiquitination and the formation of RIP1/RIP3 complex directing necrosome formation and necroptosis (66, 97). It is notable that LPS-activated microglia are capable of producing ROS, and that activation of the RIP1/RIP3 complex can also lead to ROS production (66). ROS can activate the necrosome causing necroptosis. As such, inhibition of ROS may prevent necroptosis (66), which relate to our findings as well. In contrast, multiple studies have shown CSF1R inhibition promotes cell death *via* apoptosis (28, 58, 75). However, our data suggest that inhibition of CSF1R signaling during a state of activation may lead to necroptosis, an effect that should be investigated further.

In summary, we have characterized the effects of systemic GW2580 treatment, a CSF1R antagonist, on microglia isolated from healthy mice. While treatment did not alter behavior or microglial cell viability, the data reveal that it suppressed expression of genes involved in regulating ROS. Culture experiments indicate that CSF1R inhibition sensitizes microglia to ROS-mediated cell death. These data indicate a yet to be established link between CSF1R signaling, redox status and microglial cell viability.

DATA AVAILABILITY STATEMENT

The data presented in the study are deposited in the Gene Expression Omnibus repository, accession number GSE185564.

ETHICS STATEMENT

The animal study was reviewed and approved by Institutional Animal Care and Use Committee at the University of Illinois Urbana–Champaign.

AUTHOR CONTRIBUTIONS

KS-D, DBM, RWJ, HRG and AJS designed and coordinated the experiments. KS-D performed the experiments. MV-R performed bioinformatics statistical analysis. AYL performed the imaging and analysis. KS-D and AJS drafted the manuscript with inputs from all authors. All authors contributed to the article and approved the submitted version.

FUNDING

This research was funded by grants from the National Multiple Sclerosis Society (RG 1807-32053; AJS), the NIH (RF1AG059622; RWJ), the USDA National Institute of Food and Agriculture, Hatch project ILLU-538-941 and by Division of Nutritional Sciences-Vision 20/20 (DBM).

ACKNOWLEDGMENTS

We would like to thank Victoria Fisher, for her excellent instruction on how to perform oral gavage.

SUPPLEMENTARY MATERIAL

The Supplementary Material for this article can be found online at: https://www.frontiersin.org/articles/10.3389/fimmu.2021.734349/full#supplementary-material

Supplementary Figure 1 | Effect of GW2580 treatment on mouse weight and behavior per gender. **(A–C)** Mice were treated with GW2580 at a dose of 80mg/kg/d by oral gavage for 8 days. The effects of treatment on weight **(A)**, food disappearance **(B)**, and burrowing activity **(C)** are shown. Data are expressed as means ± standard error (S.E.). Each group is composed of n=12-15 mice per group from four independent experiments for weight change, n=3 per group from a single experiment for food disappearance, and n=3 per group from three independent experiments for the burrowing activity.

Supplementary Figure 2 | Effect of GW2580 treatment in microglia morphology. **(A–E)** Mice were treated with GW2580 by oral gavage for 8 days and the effect of treatment on microglia morphology and viability examined. **(A, B)** Representative three dimensional reconstruction of a microglia cell in the cortex of vehicle **(A)** and GW2580 treated **(B)** mice from a 40x picture. Scale bar is 10μm. **(C)** Results from Imaris analysis. Each point represents an average of three cells per mouse. Each point represents an average of three pictures. Data shown is expressed as means ± standard error (SE). *p-value < 0.05.

Supplementary Figure 3 | Effect of GW2580 treatment on expression of select genes by RT-qPCR. **(A–E)**, Primary microglia were cultured from brains of neonatal mice and plated at a density of $5x10^5$ cells per well in 24-well plates. Cells were treated with GW2580 (5μM) or medium for 72h, then the expression of select genes determined by qRT-PCR. The effect of treatment on expression of *Ndufs8* **(A)**, *Prdx2* **(B)**, *Prdx5* **(C)**, and *Gpx4* **(D)** is shown. **(E)** Cell death from the treated samples was addressed by LDH measurement. Data are combined means ± standard error (S.E.) and are from 4-6 independent cultures. ### means that the gene was undetectable. Statistical significance is represented by p-value, p-value < 0.01 (**) and p-value < 0.001 (***).

REFERENCES

1. Paolicelli RC, Jawaid A, Henstridge CM, Valeri A, Merlini M, Robinson JL, et al. TDP-43 Depletion in Microglia Promotes Amyloid Clearance But Also Induces Synapse Loss. *Neuron* (2017) 95:297–308.e6. doi: 10.1016/j.neuron.2017.05.037
2. Marin-Teva JL, Dusart I, Colin C, Gervais A, van Rooijen N, Mallat M. Microglia Promote the Death of Developing Purkinje Cells. *Neuron* (2004) 41:535–47. doi: 10.1016/S0896-6273(04)00069-8
3. Soto-Diaz K, Juda MB, Blackmore S, Walsh C, Steelman AJ. TAK1 Inhibition in Mouse Astrocyte Cultures Ameliorates Cytokine-Induced Chemokine Production and Neutrophil Migration. *J Neurochem* (2020) 152:697–709. doi: 10.1111/jnc.14930
4. von Bernhardi R, Eugenin-von Bernhardi L, Eugenin J. Microglial Cell Dysregulation in Brain Aging and Neurodegeneration. *Front Aging Neurosci* (2015) 7:124. doi: 10.3389/fnagi.2015.00124
5. Guevara CA, Del Valle P, Mercedes CR. Microglia and Reactive Oxygen Species Are Required for Behavioral Susceptibility to Chronic Social Defeat Stress. *J Neurosci* (2020) 40:1370–2. doi: 10.1523/JNEUROSCI.2175-19.2019
6. Simpson DSA, Oliver PL. ROS Generation in Microglia: Understanding Oxidative Stress and Inflammation in Neurodegenerative Disease. *Antioxidants (Basel)* (2020) 9:743–70. doi: 10.3390/antiox9080743
7. Bogie JF, Stinissen P, Hendriks JJ. Macrophage Subsets and Microglia in Multiple Sclerosis. *Acta Neuropathol* (2014) 128:191–213. doi: 10.1007/s00401-014-1310-2
8. Giunti D, Parodi B, Cordano C, Uccelli A, Kerlero de Rosbo N. Can We Switch Microglia's Phenotype to Foster Neuroprotection? *Focus Multiple Sclerosis Immunol* (2014) 141:328–39. doi: 10.1111/imm.12177
9. Heppner FL, Ransohoff RM, Becher B. Immune Attack: The Role of Inflammation in Alzheimer Disease. *Nat Rev Neurosci* (2015) 16:358–72. doi: 10.1038/nrn3880
10. Benakis C, Garcia-Bonilla L, Iadecola C, Anrather J. The Role of Microglia and Myeloid Immune Cells in Acute Cerebral Ischemia. *Front Cell Neurosci* (2014) 8:461. doi: 10.1016/B978-0-12-803058-5.00027-8
11. Machado V, Zoller T, Attaai A, Spittau B. Microglia-Mediated Neuroinflammation and Neurotrophic Factor-Induced Protection in the MPTP Mouse Model of Parkinson's Disease-Lessons From Transgenic Mice. *Int J Mol Sci* (2016) 17:151–75. doi: 10.3390/ijms17020151
12. Radford RA, Morsch M, Rayner SL, Cole NJ, Pountney DL, Chung RS. The Established and Emerging Roles of Astrocytes and Microglia in Amyotrophic Lateral Sclerosis and Frontotemporal Dementia. *Front Cell Neurosci* (2015) 9:414. doi: 10.3389/fncel.2015.00414
13. Petrelli F, Pucci L, Bezzi P. Astrocytes and Microglia and Their Potential Link With Autism Spectrum Disorders. *Front Cell Neurosci* (2016) 10:21. doi: 10.3389/fncel.2016.00021
14. Estes ML, McAllister AK. Immune Mediators in the Brain and Peripheral Tissues in Autism Spectrum Disorder. *Nat Rev Neurosci* (2015) 16:469–86. doi: 10.1038/nrn3978
15. Menza M, Dobkin RD, Marin H, Mark MH, Gara M, Bienfait K, et al. The Role of Inflammatory Cytokines in Cognition and Other Non-Motor Symptoms of Parkinson's Disease. *Psychosomatics* (2010) 51:474–9. doi: 10.1371/journal.pone.0047387
16. Dantzer R. Cytokine, Sickness Behavior, and Depression. *Immunol Allergy Clin North Am* (2009) 29:247–64. doi: 10.1016/j.iac.2009.02.002
17. Wang WY, Tan MS, Yu JT, Tan L. Role of Pro-Inflammatory Cytokines Released From Microglia in Alzheimer's Disease. *Ann Transl Med* (2015) 3:136. doi: 10.3978/j.issn.2305-5839.2015.03.49
18. Dik MG, Jonker C, Hack CE, Smit JH, Comijs HC, Eikelenboom P. Serum Inflammatory Proteins and Cognitive Decline in Older Persons. *Neurology* (2005) 64:1371–7. doi: 10.1212/01.WNL.0000158281.08946.68
19. Mrak RE, Griffin WS. Potential Inflammatory Biomarkers in Alzheimer's Disease. *J Alzheimers Dis* (2005) 8:369–75. doi: 10.3233/JAD-2005-8406
20. Erblich B, Zhu L, Etgen AM, Dobrenis K, Pollard JW. Absence of Colony Stimulation Factor-1 Receptor Results in Loss of Microglia, Disrupted Brain Development and Olfactory Deficits. *PLoS One* (2011) 6:e26317. doi: 10.1371/journal.pone.0026317
21. Patel S, Player MR. Colony-Stimulating Factor-1 Receptor Inhibitors for the Treatment of Cancer and Inflammatory Disease. *Curr Top Med Chem* (2009) 9:599–610. doi: 10.2174/156802609789007327
22. Lin H, Lee E, Hestir K, Leo C, Huang M, Bosch E, et al. Discovery of a Cytokine and Its Receptor by Functional Screening of the Extracellular Proteome. *Science* (2008) 320:807–11. doi: 10.1126/science.1154370
23. Mun SH, Park PSU, Park-Min KH. The M-CSF Receptor in Osteoclasts and Beyond. *Exp Mol Med* (2020) 52:1239–54. doi: 10.1038/s12276-020-0484-z
24. Zeisel A, Munoz-Manchado AB, Codeluppi S, Lonnerberg P, La Manno G, Jureus A, et al. Brain Structure. Cell Types in the Mouse Cortex and Hippocampus Revealed by Single-Cell RNA-Seq. *Science* (2015) 347:1138–42. doi: 10.1126/science.aaa1934
25. Cahoy JD, Emery B, Kaushal A, Foo LC, Zamanian JL, Christopherson KS, et al. A Transcriptome Database for Astrocytes, Neurons, and Oligodendrocytes: A New Resource for Understanding Brain Development and Function. *J Neurosci* (2008) 28:264–78. doi: 10.1523/JNEUROSCI.4178-07.2008
26. Lemmon MA, Schlessinger J. Cell Signaling by Receptor Tyrosine Kinases. *Cell* (2010) 141:1117–34. doi: 10.1016/j.cell.2010.06.011
27. Luo J, Elwood F, Britschgi M, Villeda S, Zhang H, Ding Z, et al. Colony-Stimulating Factor 1 Receptor (CSF1R) Signaling in Injured Neurons Facilitates Protection and Survival. *J Exp Med* (2013) 210:157–72. doi: 10.1084/jem.20120412
28. Elmore MR, Najafi AR, Koike MA, Dagher NN, Spangenberg EE, Rice RA, et al. Colony-Stimulating Factor 1 Receptor Signaling Is Necessary for Microglia Viability, Unmasking a Microglia Progenitor Cell in the Adult Brain. *Neuron* (2014) 82:380–97. doi: 10.1016/j.neuron.2014.02.040
29. Ye T, Wang D, Cai Z, Tong L, Chen Z, Lu J, et al. Antidepressive Properties of Macrophage-Colony Stimulating Factor in a Mouse Model of Depression Induced by Chronic Unpredictable Stress. *Neuropharmacology* (2020) 172:108132. doi: 10.1016/j.neuropharm.2020.108132
30. Hagemeyer N, Hanft KM, Akriditou MA, Unger N, Park ES, Stanley ER, et al. Microglia Contribute to Normal Myelinogenesis and to Oligodendrocyte Progenitor Maintenance During Adulthood. *Acta Neuropathol* (2017) 134:441–58. doi: 10.1007/s00401-017-1747-1
31. Han J, Harris RA, Zhang XM. An Updated Assessment of Microglia Depletion: Current Concepts and Future Directions. *Mol Brain* (2017) 10:25. doi: 10.1186/s13041-017-0307-x
32. Yan D, Kowal J, Akkari L, Schuhmacher AJ, Huse JT, West BL, et al. Inhibition of Colony Stimulating Factor-1 Receptor Abrogates Microenvironment-Mediated Therapeutic Resistance in Gliomas. *Oncogene* (2017) 36:6049–58. doi: 10.1038/onc.2017.261
33. Mok S, Koya RC, Tsui C, Xu J, Robert L, Wu L, et al. Inhibition of CSF-1 Receptor Improves the Antitumor Efficacy of Adoptive Cell Transfer Immunotherapy. *Cancer Res* (2014) 74:153–61. doi: 10.1158/0008-5472.CAN-13-1816
34. Pyonteck SM, Akkari L, Schuhmacher AJ, Bowman RL, Sevenich L, Quail DF, et al. CSF-1R Inhibition Alters Macrophage Polarization and Blocks Glioma Progression. *Nat Med* (2013) 19:1264–72. doi: 10.1038/nm.3337
35. Ikegashira K, Ikenogami T, Yamasaki T, Oka T, Hase Y, Miyagawa N, et al. Optimization of an Azetidine Series as Inhibitors of Colony Stimulating Factor-1 Receptor (CSF-1r) Type II to Lead to the Clinical Candidate JTE-952. *Bioorg Med Chem Lett* (2019) 29:873–7. doi: 10.1016/j.bmcl.2019.02.006
36. Mancuso R, Fryatt G, Cleal M, Obst J, Pipi E, Monzon-Sandoval J, et al. CSF1R Inhibitor JNJ-40346527 Attenuates Microglial Proliferation and Neurodegeneration in P301S Mice. *Brain* (2019) 142:3243–64. doi: 10.1093/brain/awz241
37. Neal ML, Fleming SM, Budge KM, Boyle AM, Kim C, Alam G, et al. Pharmacological Inhibition of CSF1R by GW2580 Reduces Microglial Proliferation and Is Protective Against Neuroinflammation and Dopaminergic Neurodegeneration. *FASEB J* (2020) 34:1679–94. doi: 10.1096/fj.201900567RR
38. Edwards VD, Sweeney DT, Ho H, Eide CA, Rofelty A, Agarwal A, et al. Targeting of Colony-Stimulating Factor 1 Receptor (CSF1R) in the CLL Microenvironment Yields Antineoplastic Activity in Primary Patient Samples. *Oncotarget* (2018) 9:24576–89. doi: 10.18632/oncotarget.25191
39. Gerber YN, Saint-Martin GP, Bringuier CM, Bartolami S, Goze-Bac C, Noristani HN, et al. CSF1R Inhibition Reduces Microglia Proliferation, Promotes Tissue Preservation and Improves Motor Recovery After Spinal Cord Injury. *Front Cell Neurosci* (2018) 12:368. doi: 10.3389/fncel.2018.00368
40. Conway JG, McDonald B, Parham J, Keith B, Rusnak DW, Shaw E, et al. Inhibition of Colony-Stimulating-Factor-1 Signaling *In Vivo* With the Orally

Bioavailable cFMS Kinase Inhibitor GW2580. *Proc Natl Acad Sci USA* (2005) 102:16078–83. doi: 10.1073/pnas.0502000102
41. Moughon DL, He H, Schokrpur S, Jiang ZK, Yaqoob M, David J, et al. Macrophage Blockade Using CSF1R Inhibitors Reverses the Vascular Leakage Underlying Malignant Ascites in Late-Stage Epithelial Ovarian Cancer. *Cancer Res* (2015) 75:4742–52. doi: 10.1158/0008-5472.CAN-14-3373
42. Borjini N, Fernandez M, Giardino L, Calza L. Cytokine and Chemokine Alterations in Tissue, CSF, and Plasma in Early Presymptomatic Phase of Experimental Allergic Encephalomyelitis (EAE), in a Rat Model of Multiple Sclerosis. *J Neuroinflamm* (2016) 13:291. doi: 10.1186/s12974-016-0757-6
43. Crespo O, Kang SC, Daneman R, Lindstrom TM, Ho PP, Sobel RA, et al. Tyrosine Kinase Inhibitors Ameliorate Autoimmune Encephalomyelitis in a Mouse Model of Multiple Sclerosis. *J Clin Immunol* (2011) 31:1010–20. doi: 10.1007/s10875-011-9579-6
44. Olmos-Alonso A, Schetters ST, Sri S, Askew K, Mancuso R, Vargas-Caballero M, et al. Pharmacological Targeting of CSF1R Inhibits Microglial Proliferation and Prevents the Progression of Alzheimer's-Like Pathology. *Brain* (2016) 139:891–907. doi: 10.1093/brain/awv379
45. Martinez-Muriana A, Mancuso R, Francos-Quijorna I, Olmos-Alonso A, Osta R, Perry VH, et al. CSF1R Blockade Slows the Progression of Amyotrophic Lateral Sclerosis by Reducing Microgliosis and Invasion of Macrophages Into Peripheral Nerves. *Sci Rep* (2016) 6:25663. doi: 10.1038/srep25663
46. Gomez-Nicola D, Fransen NL, Suzzi S, Perry VH. Regulation of Microglial Proliferation During Chronic Neurodegeneration. *J Neurosci* (2013) 33:2481–93. doi: 10.1523/JNEUROSCI.4440-12.2013
47. Chalmers SA, Wen J, Shum J, Doerner J, Herlitz L, Putterman C. CSF-1R Inhibition Attenuates Renal and Neuropsychiatric Disease in Murine Lupus. *Clin Immunol* (2017) 185:100–8. doi: 10.1016/j.clim.2016.08.019
48. Jirkof P, Cesarovic N, Rettich A, Nicholls F, Seifert B, Arras M. Burrowing Behavior as an Indicator of Post-Laparotomy Pain in Mice. *Front Behav Neurosci* (2010) 4:165. doi: 10.3389/fnbeh.2010.00165
49. Bolger AM, Lohse M, Usadel B. Trimmomatic: A Flexible Trimmer for Illumina Sequence Data. *Bioinformatics* (2014) 30:2114–20. doi: 10.1093/bioinformatics/btu170
50. Dobin A, Davis CA, Schlesinger F, Drenkow J, Zaleski C, Jha S, et al. STAR: Ultrafast Universal RNA-Seq Aligner. *Bioinformatics* (2013) 29:15–21. doi: 10.1093/bioinformatics/bts635
51. Liao Y, Smyth GK, Shi W. Featurecounts: An Efficient General Purpose Program for Assigning Sequence Reads to Genomic Features. *Bioinformatics* (2014) 30:923–30. doi: 10.1093/bioinformatics/btt656
52. Robinson MD, Oshlack A. A Scaling Normalization Method for Differential Expression Analysis of RNA-Seq Data. *Genome Biol* (2010) 11:R25. doi: 10.1186/gb-2010-11-3-r25
53. Steelman AJ, Zhou Y, Koito H, Kim S, Payne HR, Lu QR, et al. Activation of Oligodendroglial Stat3 Is Required for Efficient Remyelination. *Neurobiol Dis* (2016) 91:336–46. doi: 10.1016/j.nbd.2016.03.023
54. Shi L, Jones WD, Jensen RV, Harris SC, Perkins RG, Goodsaid FM, et al. The Balance of Reproducibility, Sensitivity, and Specificity of Lists of Differentially Expressed Genes in Microarray Studies. *BMC Bioinf* (2008) 9 Suppl 9:S10. doi: 10.1186/1471-2105-9-S9-S10
55. Guo L, Lobenhofer EK, Wang C, Shippy R, Harris SC, Zhang L, et al. Rat Toxicogenomic Study Reveals Analytical Consistency Across Microarray Platforms. *Nat Biotechnol* (2006) 24:1162–9. doi: 10.1038/nbt1238
56. Tabula Muris C. C. Overall, C. Logistical, C. Organ, Processing, P. Library, Sequencing, a. Computational Data, a. Cell Type, G. Writing, G. Supplemental Text Writing, and I. Principal, Single-Cell Transcriptomics of 20 Mouse Organs Creates a Tabula Muris. *Nature* (2018) 562:367–72. doi: 10.1038/s41586-018-0590-4
57. Elmore MR, Lee RJ, West BL, Green KN. Characterizing Newly Repopulated Microglia in the Adult Mouse: Impacts on Animal Behavior, Cell Morphology, and Neuroinflammation. *PLoS One* (2015) 10:e0122912. doi: 10.1371/journal.pone.0122912
58. Hagan N, Kane JL, Grover D, Woodworth L, Madore C, Saleh J, et al. CSF1R Signaling Is a Regulator of Pathogenesis in Progressive MS. *Cell Death Dis* (2020) 11:904. doi: 10.1038/s41419-020-03084-7
59. Smith AM, Gibbons HM, Oldfield RL, Bergin PM, Mee EW, Curtis MA, et al. M-CSF Increases Proliferation and Phagocytosis While Modulating Receptor and Transcription Factor Expression in Adult Human Microglia. *J Neuroinflamm* (2013) 10:85. doi: 10.1186/1742-2094-10-85
60. Sun GY, Li R, Cui J, Hannink M, Gu Z, Fritsche KL, et al. Withania Somnifera and Its Withanolides Attenuate Oxidative and Inflammatory Responses and Up-Regulate Antioxidant Responses in BV-2 Microglial Cells. *Neuromolecular Med* (2016) 18:241–52. doi: 10.1007/s12017-016-8411-0
61. Yauger YJ, Bermudez S, Moritz KE, Glaser E, Stoica B, Byrnes KR. Iron Accentuated Reactive Oxygen Species Release by NADPH Oxidase in Activated Microglia Contributes to Oxidative Stress In Vitro. *J Neuroinflamm* (2019) 16:41. doi: 10.1186/s12974-019-1430-7
62. Paeng SH, Park WS, Jung WK, Lee DS, Kim GY, Choi YH, et al. YCG063 Inhibits Pseudomonas Aeruginosa LPS-Induced Inflammation in Human Retinal Pigment Epithelial Cells Through the TLR2-Mediated AKT/NF-kappaB Pathway and ROS-Independent Pathways. *Int J Mol Med* (2015) 36:808–16. doi: 10.3892/ijmm.2015.2266
63. Locatelli SL, Cleris L, Stirparo GG, Tartari S, Saba E, Pierdominici M, et al. BIM Upregulation and ROS-Dependent Necroptosis Mediate the Antitumor Effects of the HDACi Givinostat and Sorafenib in Hodgkin Lymphoma Cell Line Xenografts. *Leukemia* (2014) 28:1861–71. doi: 10.1038/leu.2014.81
64. Kim KH, Park JY, Jung HJ, Kwon HJ. Identification and Biological Activities of a New Antiangiogenic Small Molecule That Suppresses Mitochondrial Reactive Oxygen Species. *Biochem Biophys Res Commun* (2011) 404:541–5. doi: 10.1016/j.bbrc.2010.12.022
65. Redza-Dutordoir M, Averill-Bates DA. Activation of Apoptosis Signalling Pathways by Reactive Oxygen Species. *Biochim Biophys Acta* (2016) 1863:2977–92. doi: 10.1016/j.bbamcr.2016.09.012
66. Kim SJ, Li J. Caspase Blockade Induces RIP3-Mediated Programmed Necrosis in Toll-Like Receptor-Activated Microglia. *Cell Death Dis* (2013) 4:e716. doi: 10.1038/cddis.2013.238
67. Ryter SW, Kim HP, Hoetzel A, Park JW, Nakahira K, Wang X, et al. Mechanisms of Cell Death in Oxidative Stress. *Antioxid Redox Signal* (2007) 9:49–89. doi: 10.1089/ars.2007.9.49
68. Jacquel A, Benikhlef N, Paggetti J, Lalaoui N, Guery L, Dufour EK, et al. Colony-Stimulating Factor-1-Induced Oscillations in Phosphatidylinositol-3 Kinase/AKT Are Required for Caspase Activation in Monocytes Undergoing Differentiation Into Macrophages. *Blood* (2009) 114:3633–41. doi: 10.1182/blood-2009-03-208843
69. Shaposhnik Z, Wang X, Lusis AJ. Arterial Colony Stimulating Factor-1 Influences Atherosclerotic Lesions by Regulating Monocyte Migration and Apoptosis. *J Lipid Res* (2010) 51:1962–70. doi: 10.1194/jlr.M005215
70. Nissen JC, Thompson KK, West BL, Tsirka SE. Csf1R Inhibition Attenuates Experimental Autoimmune Encephalomyelitis and Promotes Recovery. *Exp Neurol* (2018) 307:24–36. doi: 10.1016/j.expneurol.2018.05.021
71. Seitz S, Clarke P, Tyler KL. Pharmacologic Depletion of Microglia Increases Viral Load in the Brain and Enhances Mortality in Murine Models of Flavivirus-Induced Encephalitis. *J Virol* (2018) 92:JVI.00525-18–48. doi: 10.1128/JVI.00525-18
72. Valdearcos M, Robblee MM, Benjamin DI, Nomura DK, Xu AW, Koliwad SK. Microglia Dictate the Impact of Saturated Fat Consumption on Hypothalamic Inflammation and Neuronal Function. *Cell Rep* (2014) 9:2124–38. doi: 10.1016/j.celrep.2014.11.018
73. De I, Nikodemova M, Steffen MD, Sokn E, Maklakova VI, Watters JJ, et al. CSF1 Overexpression has Pleiotropic Effects on Microglia In Vivo. *Glia* (2014) 62:1955–67. doi: 10.1002/glia.22717
74. Ali S, Mansour AG, Huang W, Queen NJ, Mo X, Anderson JM, et al. CSF1R Inhibitor PLX5622 and Environmental Enrichment Additively Improve Metabolic Outcomes in Middle-Aged Female Mice. *Aging (Albany NY)* (2020) 12:2101–22. doi: 10.18632/aging.102724
75. Henry RJ, Ritzel RM, Barrett JP, Doran SJ, Jiao Y, Leach JB, et al. Microglial Depletion With CSF1R Inhibitor During Chronic Phase of Experimental Traumatic Brain Injury Reduces Neurodegeneration and Neurological Deficits. *J Neurosci* (2020) 40:2960–74. doi: 10.1523/JNEUROSCI.2402-19.2020
76. Yang X, Zhao L, Campos MM, Abu-Asab M, Ortolan D, Hotaling N, et al. CSF1R Blockade Induces Macrophage Ablation and Results in Mouse Choroidal Vascular Atrophy and RPE Disorganization. *Elife* (2020) 9:1–30. doi: 10.7554/eLife.55564

77. Hou B, Jiang C, Wang D, Wang G, Wang Z, Zhu M, et al. Pharmacological Targeting of CSF1R Inhibits Microglial Proliferation and Aggravates the Progression of Cerebral Ischemic Pathology. *Front Cell Neurosci* (2020) 14:267. doi: 10.3389/fncel.2020.00267
78. Oosterhof N, Kuil LE, van der Linde HC, Burm SM, Berdowski W, van Ijcken WFJ, et al. Colony-Stimulating Factor 1 Receptor (CSF1R) Regulates Microglia Density and Distribution, But Not Microglia Differentiation In Vivo. *Cell Rep* (2018) 24:1203–17.e6. doi: 10.1016/j.celrep.2018.06.113
79. Candido JB, Morton JP, Bailey P, Campbell AD, Karim SA, Jamieson T, et al. CSF1R(+) Macrophages Sustain Pancreatic Tumor Growth Through T Cell Suppression and Maintenance of Key Gene Programs That Define the Squamous Subtype. *Cell Rep* (2018) 23:1448–60. doi: 10.1016/j.celrep.2018.03.131
80. De I, Steffen MD, Clark PA, Patros CJ, Sokn E, Bishop SM, et al. CSF1 Overexpression Promotes High-Grade Glioma Formation Without Impacting the Polarization Status of Glioma-Associated Microglia and Macrophages. *Cancer Res* (2016) 76:2552–60. doi: 10.1158/0008-5472.CAN-15-2386
81. Achyut BR, Shankar A, Iskander AS, Ara R, Angara K, Zeng P, et al. Bone Marrow Derived Myeloid Cells Orchestrate Antiangiogenic Resistance in Glioblastoma Through Coordinated Molecular Networks. *Cancer Lett* (2015) 369:416–26. doi: 10.1016/j.canlet.2015.09.004
82. Zhan L, Fan L, Kodama L, Sohn PD, Wong MY, Mousa GA, et al. A MAC2-Positive Progenitor-Like Microglial Population is Resistant to CSF1R Inhibition in Adult Mouse Brain. *Elife* (2020) 9:1–22. doi: 10.7554/eLife.51796
83. Shinohara A, Imai Y, Nakagawa M, Takahashi T, Ichikawa M, Kurokawa M. Intracellular Reactive Oxygen Species Mark and Influence the Megakaryocyte-Erythrocyte Progenitor Fate of Common Myeloid Progenitors. *Stem Cells* (2014) 32:548–57. doi: 10.1002/stem.1588
84. Wittrant Y, Gorin Y, Mohan S, Wagner B, Abboud-Werner SL. Colony-Stimulating Factor-1 (CSF-1) Directly Inhibits Receptor Activator of Nuclear Factor-{Kappa}B Ligand (RANKL) Expression by Osteoblasts. *Endocrinology* (2009) 150:4977–88. doi: 10.1210/en.2009-0248
85. Nakanishi A, Hie M, Iitsuka N, Tsukamoto I. A Crucial Role for Reactive Oxygen Species in Macrophage Colony-Stimulating Factor-Induced RANK Expression in Osteoclastic Differentiation. *Int J Mol Med* (2013) 31:874–80. doi: 10.3892/ijmm.2013.1258
86. Wang Y, Zeigler MM, Lam GK, Hunter MG, Eubank TD, Khramtsov VV, et al. The Role of the NADPH Oxidase Complex, P38 MAPK, and Akt in Regulating Human Monocyte/Macrophage Survival. *Am J Respir Cell Mol Biol* (2007) 36:68–77. doi: 10.1165/rcmb.2006-0165OC
87. Darrieutort-Laffite C, Boutet MA, Chatelais M, Brion R, Blanchard F, Heymann D, et al. IL-1beta and TNFalpha Promote Monocyte Viability Through the Induction of GM-CSF Expression by Rheumatoid Arthritis Synovial Fibroblasts. *Mediators Inflamm* (2014) 2014:241840. doi: 10.1155/2014/241840
88. Giorgetti E, Panesar M, Zhang Y, Joller S, Ronco M, Obrecht M, et al. Modulation of Microglia by Voluntary Exercise or CSF1R Inhibition Prevents Age-Related Loss of Functional Motor Units. *Cell Rep* (2019) 29:1539–54.e7. doi: 10.1016/j.celrep.2019.10.003
89. Chitu V, Biundo F, Shlager GGL, Park ES, Wang P, Gulinello ME, et al. Microglial Homeostasis Requires Balanced CSF-1/CSF-2 Receptor Signaling. *Cell Rep* (2020) 30:3004–19.e5. doi: 10.1016/j.celrep.2020.02.028
90. Wlodarczyk A, Benmamar-Badel A, Cedile O, Jensen KN, Kramer I, Elsborg NB, et al. CSF1R Stimulation Promotes Increased Neuroprotection by CD11c+ Microglia in EAE. *Front Cell Neurosci* (2018) 12:523. doi: 10.3389/fncel.2018.00523
91. Pons V, Levesque P, Plante MM, Rivest S. Conditional Genetic Deletion of CSF1 Receptor in Microglia Ameliorates the Physiopathology of Alzheimer's Disease. *Alzheimers Res Ther* (2021) 13:8. doi: 10.1186/s13195-020-00747-7
92. Liu Y, Given KS, Dickson EL, Owens GP, Macklin WB, Bennett JL. Concentration-Dependent Effects of CSF1R Inhibitors on Oligodendrocyte Progenitor Cells Ex Vivo and In Vivo. *Exp Neurol* (2019) 318:32–41. doi: 10.1016/j.expneurol.2019.04.011
93. Tahmasebi F, Pasbakhsh P, Mortezaee K, Madadi S, Barati S, Kashani IR. Effect of the CSF1R Inhibitor PLX3397 on Remyelination of Corpus Callosum in a Cuprizone-Induced Demyelination Mouse Model. *J Cell Biochem* (2019) 120:10576–86. doi: 10.1002/jcb.28344
94. Beckmann N, Giorgetti E, Neuhaus A, Zurbruegg S, Accart N, Smith P, et al. Brain Region-Specific Enhancement of Remyelination and Prevention of Demyelination by the CSF1R Kinase Inhibitor BLZ945. *Acta Neuropathol Commun* (2018) 6:9. doi: 10.1186/s40478-018-0510-8
95. Martin-Estebane M, Gomez-Nicola D. Targeting Microglial Population Dynamics in Alzheimer's Disease: Are We Ready for a Potential Impact on Immune Function? *Front Cell Neurosci* (2020) 14:149. doi: 10.3389/fncel.2020.00149
96. Sosna J, Philipp S, Albay R3rd, Reyes-Ruiz JM, Baglietto-Vargas D, LaFerla FM, et al. Early Long-Term Administration of the CSF1R Inhibitor PLX3397 Ablates Microglia and Reduces Accumulation of Intraneuronal Amyloid, Neuritic Plaque Deposition and Pre-Fibrillar Oligomers in 5XFAD Mouse Model of Alzheimer's Disease. *Mol Neurodegener* (2018) 13:11. doi: 10.1186/s13024-018-0244-x
97. Seo J, Nam YW, Kim S, Oh DB, Song J. Necroptosis Molecular Mechanisms: Recent Findings Regarding Novel Necroptosis Regulators. *Exp Mol Med* (2021) 53:1007–17. doi: 10.1038/s12276-021-00634-7

Conflict of Interest: The authors declare that the research was conducted in the absence of any commercial or financial relationships that could be construed as a potential conflict of interest.

Frontiers in Immunology

Explores novel approaches and diagnoses to treat immune disorders.

The official journal of the International Union of Immunological Societies (IUIS) and the most cited in its field, leading the way for research across basic, translational and clinical immunology.

Discover the latest Research Topics

See more →

Frontiers

Avenue du Tribunal-Fédéral 34
1005 Lausanne, Switzerland
frontiersin.org

Contact us

+41 (0)21 510 17 00
frontiersin.org/about/contact